WAVE UPLIFT PRESSURES ON HORIZONTAL PLATFORMS

Thesis by

Jonathan Akin French

In Partial Fulfillment of the Requirements

For the Degree of

Doctor of Philosophy

California Institute of Technology

Pasadena, California

1970

(Submitted June 26, 1969)

ACKNOWLEDGEMENTS

The writer wishes to express overdue thanks to his exacting but extremely helpful and patient thesis adviser, Professor Fredric Raichlen. The advice and encouragement of Professors Vito A. Vanoni and Norman H. Brooks are also deeply appreciated.

The writer encountered and became interested in the problem of wave uplift while employed by Moffatt and Nichol, Consulting Engineers, Long Beach, California.

In his studies at the California Institute of Technology, the writer has received financial support from the Alfred P. Sloan Foundation (1963-64), from the Title Insurance and Trust Company (1964-67), and from the California Institute of Technology. Financial support for the experimental research was received from the Sloan Fund for Basic Research and from the National Science Foundation (Grant No. GK-1729). The experiments were performed in the W. M. Keck Laboratory of Hydraulics and Water Resources, California Institute of Technology.

Assisting the writer in preparing the thesis were Messrs. Robert Bellue, Tom Bicknell, Jiin-jen Lee, James Perry, Dennis Pocekay, and Claude Vidal, who contributed many tedious but necessary hours of data reduction. Mr. Robert Logan contributed his skills at computer programming, and Mr. Yoshiaki Daimon unflinchingly devoted several megahours to mathematical and numerical computation, as well as to data reduction. Mrs. Peggy Paxson typed much of the copy in the early stages of writing.

The drawings were prepared by Carl A. Green, Jr., and by the Caltech Graphic Arts Facilities. The final manuscript was typed by

Mrs. Patricia A. Rankin, Mrs. Catherine Musso, Mrs. Yvonne Vedder, and Mrs. Joyce Lundstedt.

The writer wishes to thank Mr. Elton F. Daly, who supervised the construction of much of the laboratory equipment, for his instruction and advice in designing and building much of the experimental equipment; Mr. Robert L. Greenway, for his ready cooperation and assistance in building the experimental apparatus; and Mr. Carl Eastvedt, for taking and developing the photographs and for reducing the drawings.

In addition, the writer wishes to express his thanks and appreciation to his parents, Mr. and Mrs. Howard B. French, for their assistance in preparing the drawings as well as for their comforting support during some of the whirlwind weeks of final preparation, and to Mr. and Mrs. Lee A. Tinder, for their neighborly assistance in preparing the final manuscript. The writer also expresses loving gratitude to his patient bride, Sarah, who having offered considerable assistance in the preparation of many parts of the thesis, as well as showing a remarkable willingness to prepare breakfast at 5 a.m., has done her part to Put Husband Through.

ABSTRACT

The major objective of the study has been to investigate in detail the rapidly-varying peak uplift pressure and the slowly-varying positive and negative uplift pressures that are known to be exerted by waves against the underside of a horizontal pier or platform located above the still water level, but not higher than the crests of the incident waves.

In a "two-dimensional" laboratory study conducted in a 100-ft long by 15-in. -wide by 2-ft-deep wave tank with a horizontal smooth bottom, individually generated solitary waves struck a rigid, fixed, horizontal platform extending the width of the tank. Pressure transducers were mounted flush with the smooth soffit, or underside, of the platform. The location of the transducers could be varied.

The problem of adequate dynamic and spatial response of the transducers was investigated in detail. It was found that unless the radius of the sensitive area of a pressure transducer is smaller than about one-third of the characteristic width of the pressure distribution, the peak pressure and the rise-time will not be recorded accurately. A procedure was devised to correct peak pressures and rise-times for this transducer defect.

The hydrodynamics of the flow beneath the platform are described qualitatively by a simple analysis, which relates peak pressure and positive slowly-varying pressure to the celerity of the wave front propagating beneath the platform, and relates negative slowly-varying pressure to the process by which fluid recedes from the platform after the wave has passed. As the wave front propagates beneath the

platform, its celerity increases to a maximum, then decreases. The peak pressure similarly increases with distance from the seaward edge of the platform, then decreases.

Measured peak pressure head, always found to be less than five times the incident wave height above still water level, is an order of magnitude less than reported shock pressures due to waves breaking against vertical walls; the product of peak pressure and rise-time, considered as peak impulse, is of the order of 20% of reported shock impulse due to waves breaking against vertical walls. The maximum measured slowly-varying uplift pressure head is approximately equal to the incident wave height less the soffit clearance above still water level. The normalized magnitude and duration of negative pressure appears to depend principally on the ratio of soffit clearance to still water depth and on the ratio of platform length to still water depth.

CONTENTS

CONTENTS (Continued)

CONTENTS (Continued)

LIST OF FIGURES

LIST OF FIGURES (continued)

LIST OF FIGURES (continued)

LIST OF FIGURES (continued)

LIST OF FIGURES (continued)

LIST OF FIGURES (continued)

LIST OF FIGURES (continued)

LIST OF FIGURES (continued)

LIST OF FIGURES (continued)

LIST OF FIGURES (continued)

LIST OF FIGURES (continued)

LIST OF FIGURES (continued)

Photographs are catalogued in the W. M. Keck Laboratory of Hydraulics and Water Resources negative file, according to the number indicated at the lower right-hand corners of the photographs.

LIST OF TABLES

CHAPTER 1

INTRODUCTION

In a storm, a maritime structure such as a pier or an offshore platform may be subject to significant uplift pressures when incident waves propagate beneath the platform and in contact with it. On a platform whose horizontal underside, or soffit, is situated above the still water level, studies by El Ghamry (1963) and by Wang (1967) indicate that uplift pressures are characterized by an initial peak pressure of considerable magnitude but of short duration, followed by a slowly-varying uplift pressure of less magnitude but of considerable duration, and which typically is first positive, then negative.

The slowly-varying pressure may be of concern to an engineer considering the structural strength of the platform as a unit. The rapidly-varying peak pressure, shown in this study to be distributed over only a very narrow portion of the soffit at any given time, may be of concern when the strength of individual members of the structure is considered, such as the deck timbers in a wooden pier.

Previous studies, while demonstrating the existence of the peak pressure, provided no clear definition of the basic nature, magnitude, duration, or spatial extent of the peak pressure, nor of its functional dependence on such variables as incident wave height or platform geometry. The major aim of the present study has therefore been to investigate in basic detail the hydrodynamics associated with the uplift pressures on the platform, in particular the peak pressure.

The experimental conditions were designed to be simple, to enable the uplift process to be observed most clearly and to simplify the

analysis of the hydrodynamics of uplift. Therefore the experimental study was "two-dimensional," i.e. dependence on the transverse coordinate was eliminated. Tests were conducted in a relatively narrow wave tank with a rigid, fixed, model platform extending the full width of the tank. The platform had a smooth, horizontal underside, or soffit, and a smooth, vertical front face. Uplift pressures on the soffit were measured at numerous locations.

Previous studies had shown that the peak pressure was a quantity subject to considerable variance. Therefore it was required that the incident wave be as reproducible as possible, in order to reduce as much as possible the experimental variance in peak pressure. Other requirements were that the incident wave be conveniently representable mathematically, and that it be a relevant model of ocean waves in shoal water in which piers or platforms are likely to be situated. Therefore, the incident wave form chosen was that of the solitary wave propagating into still water, for which there are several mathematical theories, and which may be considered a relevant model of an ocean wave propagating through shoal water. Solitary wave generators designed and constructed for this study were capable of a high degree of reproducibility of wave height.

In Chapter 2 previous studies of uplift forces on platforms and related phenomena are surveyed. In Chapter 3 an analysis is presented by which one may predict peak pressures, slowly-varying pressures, and related phenomena. In Chapter 4 the experimental equipment and procedure are discussed, with particular attention given to the subject of dynamic response of the pressure measurement system. In Chapter 5 a question of spatial response of the pressure transducers is in-

vestigated in detail, with a procedure proposed for correcting peak pressure data. In Chapter 6 experimental results, including photographs of the wave profile, are presented, compared with analytical predictions, and discussed. Conclusions and suggestions for future study are presented in Chapter 7.

Appendix A contains a list of the notation used. Experimental data are tabulated in Appendix B. Appendix C contains a derivation of the natural frequency of oscillation of the modified pressure transducer used in the experiments.

CHAPTER 2

LITERATURE SURVEY

2.1 Theoretical Analysis of Uplift Forces on Platforms with Zero Soffit Clearance.

There is a considerable body of literature concerning water waves propagating towards a rigid, plane shore having a slope ϖ. When $0<\varpi<\pi/2$, the problem is one of waves breaking on a beach; for $\varpi \geq \pi/2$, the waves can be considered to be striking a cliff, vertical or overhanging; when $\varpi=\pi$, there is what has been called the "dock problem."

This family of problems has been collectively treated for the two-dimensional case by Friedrichs (1948), Friedrichs and Lewy (1948), John (1948), and Isaacson (1948); the work has been summarized by Stoker (1957). A paper from this collection by Friedrichs and Lewy (1948) on the dock problem presents solutions for the flow (and hence the pressure) beneath a flat, horizontal, semi-infinite dock situated at still water level, against which sinusoidal waves of small amplitude propagate from $x=+\infty$. As in all other cases in this family of problems, it is shown that there are two standing wave solutions. One solution predicts finite amplitude waves at the seaward edge of the dock (or the shoreline, for the beach and cliff problems) and small cosinusoidal waves at $x=+\infty$; the other, with logarithmic singularity at the dock edge (or shoreline), predicts waves of infinite height there and small sinusoidal waves at $x=+\infty$. At $x=+\infty$ the solutions are out of phase by 90°; the problem is linear and homogeneous, so that the solutions may be combined to represent waves progressing towards the dock (or the shore). Physically, the singularity may be considered an energy-dissipating device (Stoker, 1957, p. 71), and one may note that no progres-

sive waves bearing energy shoreward are predictable without use of the singular solution.

Heins (1948) treated the problem of a dock of infinite width and semi-infinite length, where the water was of finite depth and the waves not necessarily normally incident on the dock. In this case, too, there is a regular solution, and a solution with a logarithmic singularity at the dock edge, obtained by differentiating the bounded solution. The solutions are presented as infinite series, the terms of which must be computed to provide useful results.

Stoker (1957) discusses the problem of a rigid board of finite length and of infinite width freely floating or rigidly fixed on the water surface. The channel is of finite constant depth, and small sinusoidal waves approach the board normally. The shallow-water approximation is applied, so that variations of flow quantities with depth are neglected.

For the case of the rigidly fixed board, the flow beneath the board is uniformly horizontal and sinusoidally dependent on time. The resultant pressure on the board at any given position is sinusoidally dependent on time, and at any given time is linearly dependent on distance.

2.2 Related Flow Phenomena.

The mathematical treatments discussed above all deal with a platform with zero soffit clearance. A positive soffit clearance changes the character of the flow in that there is now a line of intersection of the free surface with the rigid platform soffit, propagating beneath the platform with the wave. A sharp upward pressure is imparted to the platform at this line, as observed by the writer as well as by El Ghamry (1963) and Wang (1967) (see Section 2.3). In the mathe-

matical treatments discussed in the previous section a free surface beneath the platform was not considered, and high peak pressures propagating beneath the platform were not predicted. To study the peak pressure, then, one may turn to analysis of other flows which in some way resemble the flow beneath a platform, at least in the region where peak pressures are generated.

2.2.1 Pressures on planing bodies.

In his studies on the planing of water craft, Wagner (1932, 1948) described the ideal fluid flow near an infinitely wide flat plate planing on the water surface at high Froude number. To an observer moving with the plate, the steady flow appears to have a stagnation point on the underside of the plate which approaches the front edge as the angle of inclination of the plate with respect to the still water surface approaches zero. Forward of the stagnation point the flow shoots forward as spray. If one is able to determine the velocity distribution beneath the plate, the pressure distribution follows from Bernoulli's equation, with the gravitational term negligible because of the high Froude number. Qualitatively, the distribution has a sharp peak at the stagnation point, with the peak pressure simply equal to $\rho U^2/2$, where U is the velocity of the flow at infinity, and ρ is the fluid density. The width of the pressure peak increases with the angle of inclination of the plate with the still water surface. The pressure distribution with its peak is reminiscent of the distribution on a platform with a wave beneath it, and suggests that the pressure peak measured on the platform may be considered a stagnation pressure.

2.2.2 Forces on a vertical wall.

Occasionally when a water wave breaks against a vertical wall, it generates an intense pressure of short duration, which has often been called "shock pressure," "impact pressure," or, in French, "gifle." There is always a slowly-varying pressure, or "bourrage," upon which the impact pressure is superposed, if it occurs. There has been considerable study of this problem, in theory and in laboratory and prototype experiments (Bagnold, 1939; Minikin, 1950; Denny, 1951; Ross, 1954; Rundgren, 1958; Nagai, 1960; Garcia, 1968). The problem of waves breaking against walls is not directly related to that of wave uplift on platforms, but it is true that both problems deal with wave action on coastal structures, and that a prominent feature in both cases is the intense pressure peak.

The first recent work on the wall problem is by Bagnold (1939), who in laboratory experiments observed that shock pressures occurred only if the wave struck the wall at its precise moment of breaking. If the wave never broke or if it broke before striking the wall, there was no shock, but only the slowly-varying bourrage.

At breaking, the front surface of the wave was found to lie very nearly in a forward-moving vertical plane; it was when this near-vertical front surface struck the solid wall that shock pressures were generated. It happened that the wave would also trap a thin cushion of air against the wall.

Bagnold concluded that (1) the "shock pressures occur only when the shape of the advancing wavefront is such as to enclose an air cushion between it and the wall . . . they increase in intensity with decreasing thickness of the air cushion"; (2) the great variation in

peak pressure observed from wave to wave was due to variation in the air cushion thickness, in turn due to random irregularities on the water surface; (3) although the peak pressures varied greatly from wave to wave, the integral of the pressure-time curve tended to approach and not exceed a definite value; (4) the pressure peaks and the maximum pressure-time areas were measured only in the part of the wall where the air-cushion was formed; (5) in the model experiments, peak pressure values never exceeded one-sixth of the theoretical "water-hammer" value. The duration was at least ten times the duration time predicted for "water-hammer"; thus the impact energy was apparently absorbed in compression of the air rather than of the water.

Denny (1951) made a statistical analysis of impact pressures and impulses. Whereas the pressures appeared to be randomly distributed, Denny, like Bagnold, observed that the impulses tended to approach but never exceed a definite maximum value. The ranges of values of impulse measured by Denny (1951), by Ross (1954), and by Garcia (1968) are compared with uplift impulse in Section 6.6.

2.2.3 Velocity of, and pressures related to, a propagating air cavity.

In a theoretical treatment of various aspects of gravity currents, Benjamin (1968) chose as a convenient fundamental formulation of gravity-current problems the case of a void or air-filled cavity propagating along the upper horizontal boundary of a liquid-filled region of finite depth. This case is approximated by that in which a solitary wave has struck a platform, and the liquid is in the process of receding from the platform. The expression obtained by Benjamin for the celerity of propagation of the cavity is equivalent to Equation 3.49 in Section 3.2 for the celerity of the wave of recession beneath the

platform. Benjamin's expression for the negative pressure on the upper boundary is equivalent to Equation 3.51 in Section 3.2 for negative pressure related to the flow at the wave of recession.

2.3 Experimental Studies of Wave Uplift Forces on Docks and Quay Aprons.

El Ghamry's work (1963) is to the writer's knowledge the first experimental uplift study. The main objectives were: "(1) to study the nature of forces acting on a horizontal deck under the action of breaking and non-breaking periodic waves and for certain geometric conditions, (2) to determine the feasibility of using the existing theories in predicting the magnitude of these forces, (3) to correlate these forces with measurable wave parameters, (4) to study the instantaneous pressures at some points along the deck and (5) to provide information about the effect of some geometric parameters on the relationships between the induced forces and the wave characteristics." (El Ghamry, 1963, p. 7).

The experiments were performed in a wave tank 3 ft deep, 1 ft wide and 100 ft long. The dock was 4 ft long and nearly as wide as the tank. For the "non-breaking waves" case, the tank bottom was horizontal beneath the dock, and there was no beach. Ample space for air to escape from beneath the dock ahead of the advancing wave was provided between the dock edges and the tank walls. For all tests the mean water depth was 2.00 ft. The soffit clearance was varied between 0 and 0.20 ft above the mean water level.

To sample local pressures, pressure transducers were installed 2.00 ft and 4.00 ft from the seaward edge of the dock. A force-

meter system built into the two supports from which the dock was suspended enabled total uplift force and moments to be measured.

For the "breaking waves" case a rigid, smooth beach was installed, the toe of which was offshore of the front of the dock. The dock extended back to meet the beach. For one series of runs ample space was again provided at the dock edges; for another series, the spaces between the dock edges and the walls and beach were caulked to trap the air.

For the case of no beach and non-breaking waves, the data from six consecutive waves were averaged for each test. In comparing his results with those of the Stoker analysis already described, El Ghamry found the force F(t) to be not a simple sine function but a complicated periodic function dependent on the wave period and the soffit clearance. Neither the maximum positive and negative pressures nor the durations of positive and negative pressures were equal, even for zero soffit clearance. He also determined the center of force for the positive and negative uplifts, finding them dependent on wave height and on the ratio of wave length to platform length.

With the passage of each wave, the pressure records showed a high pulse of short duration, reminiscent of the impact pressure exerted on vertical walls. A slowly-varying pressure of much less amplitude, sometimes positive and sometimes negative, followed the impulse, or peak pressure. There was much variation in the peak pressure even when there was little variation in generating conditions. The peak pressure head rarely exceeded 2.5 times the trough-to-crest waveheight.

From examining the waves transmitted shoreward past the dock,

El Ghamry concluded that such a dock can be an efficient breakwater if of sufficient length and at the proper soffit clearance. For the case of breaking waves, statistical analysis of six consecutive waves showed a Gaussian distribution of pressure maxima, whether the air was trapped or was allowed to escape. The mean peak pressure when air was trapped was about twice as high as when air was not trapped, but in either case the standard deviation was about half the mean value. The maximum recorded pressure head was 17.5 times the incident wave height. The maximum uplifts had approximately a Rayleigh distribution. Where there was complete air entrapment, the pressure and force records showed only a single impulsive shock for each wave, with little or no slowly-varying part.

The pressure transducers were modified versions of the Statham Model 264 TC, with the sensitive diaphragms mounted flush with the dock soffit. According to the manufacturer, this model has a sensitive diaphragm 1/2 inch in diameter.

El Ghamry made several suggestions for future studies. For the two-dimensional, or wide-dock, case he suggested further tests with a variety of dock lengths, different beach slopes between 1:10 and 1:2, and different shapes of bulkheads in different water depths. He also suggested that the instantaneous pressure distribution on the dock be measured, and that motion pictures be used to aid flow visualization. Furthermore, he suggested that three-dimensional studies would show the effects of dock width, different angles of wave approach, and the effect of shape of dock or platform on uplift pressure. El Ghamry also suggested the evaluation of a wave force spectrum induced on a dock by

incident irregular wind waves, and prototype pressure measurements. For purposes of comparison, El Ghamry's uplift force and peak pressure data are presented in Sections 6.5 and 6.6.

Wang (1967), noting the presence of peak pressures and positive and negative uplift pressures as observed in El Ghamry and in his own experiments, derived simple theoretical values for peak pressures and slowly-varying pressures generated by standing waves, periodic progressive waves, and dispersive wave trains.

To determine the peak pressure he adapted an approximate analysis for the transient force on an immersing wedge, derived by von Karman (1929), in relating peak pressure to the celerity of the wave front and to the vertical fluid element velocity in the wave near the wave front.

The slowly-varying pressure head he simply took as the pressure in the undeformed wave at elevation s; near the breaker zone, where vertical accelerations contribute to the pressure but never exceed the acceleration of gravity, g, the pressure head is therefore equal to one to two times the local water surface elevation, less the soffit clearance (i.e., the elevation of the platform above still water level). These theories predict that the slowly-varying pressure depends strongly on the soffit clearance, whereas the peak pressure does so to a much lesser extent.

These theories for peak pressure and slowly-varying pressure are applied in the analysis of standing waves, periodic progressive waves and dispersive waves striking a narrow dock. (It may be noted that Wang's is the only study discussed here that has dealt with a "three-dimensional" case, where the dock was not considered to be

infinitely wide.) Wang was not able to compare his predicted pressures with experimental results for the standing-wave case, since he knew of no such data; for the periodic-progressive wave case he compared his theory for peak pressures with El Ghamry's data, and for the dispersive wave case he compared his theory with his own data.

For peak pressures due to periodic waves, the agreement with the El Ghamry data was fairly good, considering the large variation inherent in peak pressure measurements. The slowly-varying pressure maxima due to dispersive waves showed a wide range of scatter, but for the most part fell within the predicted range.

The peak pressures associated with dispersive waves from his own experiments correlated poorly with analytical values. Evidently, individual data were plotted; if Wang had been able to average pressures due to several identical waves, the correlation might well be better.

Wang made only cursory examination of the details of the pressure pulse. For 15 waves, the pulse was recorded on an oscilloscope at a sweep speed of 10 msec./div. The traces are described as "single- or dual-peaked, . . . [existing] for a period of 6 to 16 msec." With incident waveheights of about 0.16 ft., Wang proposed the range-relationship

$$t = (15 \text{ to } 40)\sqrt{H},$$

where t is the pulse duration in milliseconds and H is the waveheight in feet.

Two transducers were used: Consolidated Electrodynamics Corporation resistance-type transducers with a natural frequency of 4 kc, and a Susqehanna ST-2 piezoelectric transducer with a natural

frequency of 250 kc. The signals from the CEC transducer were displayed on an oscillograph, whereas the signal from the Susquehanna transducer, used to measure the high-frequency components, was displayed on an oscilloscope. The sizes of the transducers were not indicated.

The CEC transducer output was susceptible to temperature shift, presenting a problem similar to that encountered by the writer (see Section 4.4). Wang's solution was to build a shallow manifold on the upper side of the dock so that water pumped from the basin could be circulated around the housing of each transducer. A small clearance between transducer and dock allowed the coolant to leak down to the transducer face as well. Before an experiment was begun, the water was circulated continuously around the pier for at least two hours to bring pier and instruments to the same temperature as the water in the basin. Despite this precaution there was still a small temperature shift in the record which was minimized by an appropriate data reduction procedure.

Wang's peak-pressure data are compared with the writer's data in Section 6.6.

Furudoi and Murota (1966) studied experimentally the total uplift force on a horizontal platform extending seaward from a vertical wall. It is notable that only sharp impulses and no slowly-varying forces were measured, similar to what El Ghamry observed for breaking waves with complete air entrapment beneath a platform. Indeed, the major difference between the two experiments was that Furudoi and Murota had a vertical wall adjoining the platform, whereas El Ghamry

had a sloping beach. The average pressure head on the platform was from 1 to 8 times the incident wave height.

An empirical formula derived from the laboratory data relating uplift force to incident wave height and soffit clearance was found to be in fair agreement with some hindcasted prototype data.

2.4 The Solitary Wave.

Lamb (1945, p. 423) defines the solitary wave as "a wave consisting of a single elevation, of height not necessarily small compared with the depth of the fluid, which, if properly started, may travel for a considerable distance along a uniform canal, with little or no change of type." Stoker (1957, p. 342) adds the condition that the form be symmetric.

The history of experimental and theoretical study of the solitary wave is given by Ippen and Kulin (1955) and by Laitone (1963), and so will be only briefly discussed here. Study of the solitary wave began in 1834 when J. Scott Russell (1844) observed a single intumescence propagating with constant form along a canal, generated when a volume of water impounded by a lock was suddenly released to the canal. Of the many theoretical studies of the solitary wave, three are mentioned here, and are compared with experimental results in Section 6.1. The analysis of Boussinesq (1872) is the earliest known to the writer. McCowan's analysis (1891) has been adapted by Munk (1948) and applied to the analysis of surf. Laitone's study (1963) is one of the most recent. He obtained the first and second approximations to solitary waves and cnoidal waves by carrying out to fourth order the shallow-water expansion method of Friedrichs (1948) and Keller (1948). The

first approximation to the solitary wave is identical to the expression developed by Boussinesq (1872); the second approximation is that presented in Table 6.1.

Keulegan (1948) developed a theoretical expression for the decrease of amplitude of a solitary wave due to energy dissipation in the boundary layer. In Section 6.1, the expression is compared with experimental values of amplitude decay measured in a study by Ippen, Kulin, and Raza (1955), and in the present study.

Daily and Stephan (1952) studied the solitary wave experimentally, using a $16\frac{1}{2}$ in. wide channel with a horizontal smooth bottom, with undisturbed water depths between 0.2 and 0.4 ft. They concluded that the celerity relationship derived empirically by Russell (1844) and analytically by Boussinesq (1872), Rayleigh (1876), Korteweg and de Vries (1895), and others is adequate for practical applications, but that the theoretical celerity is somewhat greater than the observed celerity. They found the experimental profile to be closely approximated by the formula of Boussinesq (1872). The data of Daily and Stephan for celerity and wave profile are presented in comparison with data from the present study in Section 6.1.

Perroud (1957) measured profiles of waves in a uniform channel, finding them well represented by the profile derived by Boussinesq (1872). However, waves in a channel with converging side walls had profiles that were relatively wider than the Boussinesq profile, and no longer symmetric.

Ippen, Kulin, and Raza (1955), in their study of damping characteristics of the solitary wave, found that the formula for amplitude decay derived by Keulegan (1948) accurately predicted amplitude decay

only for a ratio of wave height to still water depth of about 0.4. For lesser values, the formula predicted lower rates of decay than measured; for greater values, the formula predicted a greater rate of decay than was measured. The data of Ippen, Kulin, and Raza (1955), along with that of the present study, are compared with the Keulegan formula in Section 6.1.

In Chapter 1, a reason stated for the choice of the solitary wave as the experimental incident wave was that the solitary wave is a relevant model of an ocean wave in shoal water. Munk (1948) reasoned that the solitary wave would be a suitable model for the theoretical study of surf problems. He noted that whereas periodic waves in deep water can be characterized by the ratio of wavelength to water depth and by wave steepness, waves in shallow water have narrow crests separated by wide troughs, where, as with solitary waves, the character of the isolated crests depends strongly on the ratio of wave height to water depth, rather than on wave length.

Use of the solitary wave theory was further prompted by "an obvious resemblence between the theoretically derived wave profile and the observed profile in the region just outside the breaker zone" (Munk, 1948).

Munk applied the solitary wave theory, as developed by McCowan (1891), to the forecasting of breaker characteristics, wave refraction, longshore currents, and rise in the sea surface caused by onshore wave momentum. Laboratory and field observations, while showing considerable scatter, gave "the overall impression . . . that the solitary wave theory provides a useful tool for the study of various surf phenomena" (Munk, 1948).

2.5 Solitary Wave Generators.

In the literature there are several different methods described for generating solitary waves, but all designs may be classified as being of either the "plunger type" or the "piston type." "Plunger type" wave generation usually consists of a body of finite displacement being driven down through the free water surface, then kept in an immersed or partly-immersed position. "Piston type" generation usually consists of a flat vertical plate being driven along the tank in a single finite stroke, then kept in its advanced position. In either case, a finite volume of water is displaced at one end of the tank, and there results a solitary wave travelling away from the generator, transporting a volume of water equal to the volume originally displaced by the generator.

The ideal wave generator would displace water in precisely the same manner as a fully-developed solitary wave does as it propagates along a channel. Several methods have been used to move the piston or plunger in as ideal way as possible. Usually the best design efforts fall short of perfection, however, in that the wave generated, while in itself possessing most of the symmetry, form, and permanence attributed to the ideal wave, is followed by a train of parasitic wavelets. Often a cut-off gate is installed near the generator to remove the parasitic wavelets: the gate is raised to let the major wave pass, then quickly lowered to cut off the following wavelet train.

Caldwell (1949) used plunger type generator consisting of a rectangular floating body hinged along one side to the end wall of the tank. The other side of the body could be pulled downward by a chain, connected by pulleys to a cam follower. The accompanying motor-

driven cam was cut so that the rate of displacement of water by the body approximated the rate of horizontal displacement in a fully-formed solitary wave. A cut-off gate was used to remove the parasitic wavelets. Romita (1954) evidently generated satisfactory solitary waves simply by pushing a piston by hand, and by using a cut-off gate. Because of the human factor, one could obviously not expect a high degree of reproducibility. Hall and Watts (1953) used a piston driven by a falling weight, acting through a mechanical linkage. A fair degree of reproducibility was claimed. Perroud (1957) used a piston driven by an electrically released falling weight. The weight and stroke were adjustable. Reproducibility of wave height was within 4%.

A procedure followed by Daily and Stephan (1952), Ippen and Kulin (1955), and Ippen, Kulin, and Raza (1955) was to drive a piston by impounding a quantity of water in a reservoir behind it, then suddenly releasing it to surge against the piston and drive it forward.

A more sophisticated device is an hydraulically driven piston controlled by an electric servosystem. Such a system provides for greater reproducibility than is available with manual or water-driven systems, yet there is no constraint on the form of the input displacement function, and the stroke amplitude may be varied. In the wind, water-wave research facility at Stanford University (Hsu, 1965), the electrohydraulic system is programmed to drive the piston as $x = \tanh\omega t$, in close approximation to the water particle displacement as predicted by the Boussinesq solitary wave theory.

CHAPTER 3

ANALYSIS

In Chapter 3 a first-order analysis is presented to predict and explain the transient hydrodynamics of a solitary wave striking a horizontal platform. Simplifying assumptions and the conditions necessary for valid application of each part of the analysis are set forth here. In Chapter 6, where the analysis is compared with experimental results, the validity of each simplifying assumption is examined.

The two-dimensional case studied consists of a fluid-filled region above which is suspended a rigid platform. The plane $y = 0$ represents the rigid, horizontal bottom of the channel. The fluid-filled region extends from $x = -\infty$ to $x = +\infty$ and has a local depth $d + \eta$, where d is the still water depth and η is the local elevation above still water level. The platform, whose flat horizontal soffit has a clearance s above the still-water level, or $d + s$ above the tank bottom, extends from $x = 0$ at its seaward end to $x = +\infty$. (The effect of the shoreward end of the platform is thus not to be considered.)

Initially, a solitary wave approaches from $x = -\infty$ (Figure 3. 1a). If the wave has a height H greater than the soffit clearance s, the wave will strike the platform at its seaward end, i. e. at $x = 0$ (Figure 3. 1b). A transmitted wave disturbance then continues to propagate beneath the platform in the $+x$ direction, and a reflected wave train propagates in the $-x$ direction from $x = 0$ (Figure 3. 1c).

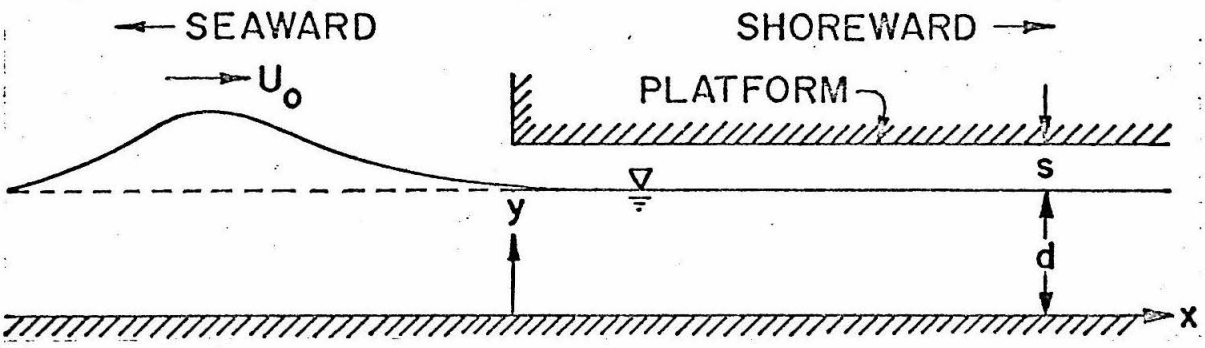

Figure 3.1a. Solitary wave approaching the platform.

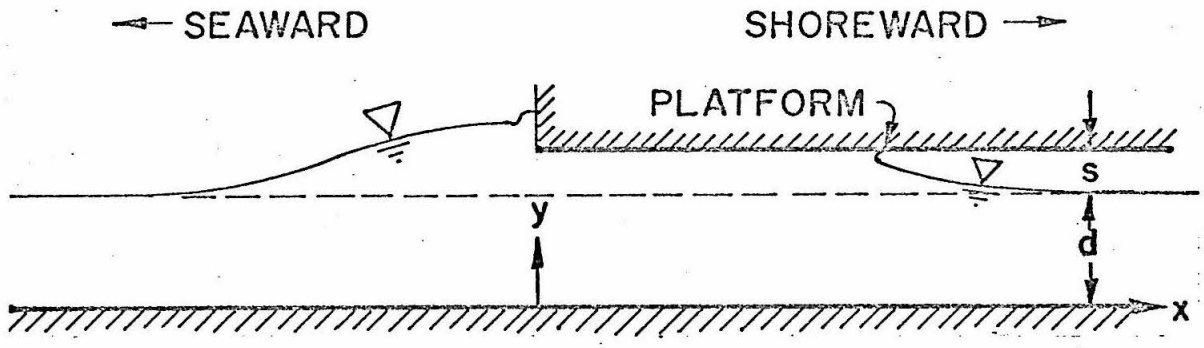

Figure 3.1b. Wave striking the platform.

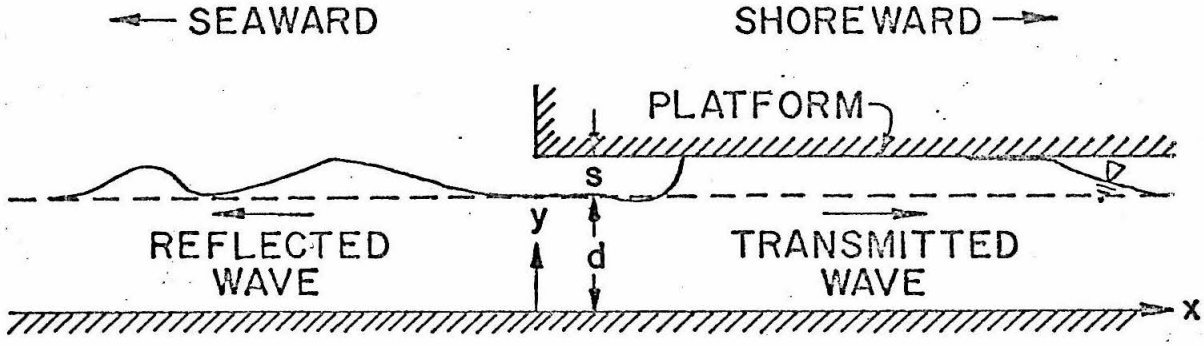

Figure 3.1c. Reflected and transmitted waves.

3.1. General Considerations

The analysis that follows may depend on one or more of the following assumptions:

1. The form of a free surface wave profile remains approximately constant, i.e. the propagation celerity is the same for all locations on the profile at a given instant, although the celerity may change with time. A mathematical expression of this assumption is:

$$\frac{\partial U(t)}{\partial x} = 0, \tag{3.1}$$

where U is the wave celerity.

2. The effects of surface tension, air entrainment, and viscous boundary shear stress are negligible. Vorticity is negligible, except in areas of concentrated energy dissipation, such as an hydraulic jump.

3. The horizontal fluid velocity beneath the seaward edge of the platform, and the water surface elevation at the seaward edge, are approximately the same as for the case when there is no platform present.

The surface elevation may be expressed as $\eta = \eta(x-Ut)$, indicating that a water wave is propagating in the $+x$ direction with celerity U. The total time derivative is zero:

$$\frac{d\eta}{dt} = \frac{\partial \eta}{\partial t} + U\frac{\partial \eta}{\partial x} = 0. \tag{3.2}$$

It should be stated with reference to Equation 3. 2 (and to Equation 3. 18 which is to appear later) that the operation $\frac{d}{dt} = \frac{\partial}{\partial t} + U\frac{\partial}{\partial x}$ denotes the time rate of change of a quantity measured at a position fixed with respect to an observer moving with the wave at celerity U.

In the following analysis, the familiar hydrodynamic differential equations are used. The equation of continuity is:

$$\frac{\partial u}{\partial x} + \frac{\partial v}{\partial y} = 0; \tag{3. 3}$$

the equation of motion in the x-direction is:

$$\frac{\partial u}{\partial t} + u\frac{\partial u}{\partial x} + v\frac{\partial u}{\partial y} + \frac{1}{\rho}\frac{\partial P}{\partial x} = 0; \tag{3. 4a}$$

the equation of motion in the y-direction is:

$$\frac{\partial v}{\partial t} + u\frac{\partial v}{\partial x} + v\frac{\partial v}{\partial y} + \frac{1}{\rho}\frac{\partial P}{\partial y} + g = 0; \tag{3. 4b}$$

and the equation of vorticity is:

$$\frac{\partial u}{\partial y} - \frac{\partial v}{\partial x} = 0. \tag{3. 5}$$

Equations 3. 4 and 3. 5 are subject to the assumption that the effects of viscosity, surface tension, and air entrainment are negligible. Equation 3. 5 violates this assumption in areas of concentrated energy dissipation, such as an hydraulic jump. The pressure at the free surface is taken to be equal to zero.

When Equation 3.5 is substituted into Equations 3.4, the latter may be integrated to give the familiar Bernoulli equation:

$$\frac{P}{\rho} + \frac{u^2+v^2}{2} + g\,y + \frac{\partial \varphi}{\partial t} = F(t), \tag{3.6}$$

where φ is the velocity potential and F is a function dependent on t alone. The Bernoulli equation is applicable only where Equation 3.5 is valid; i.e. for irrotational flows.

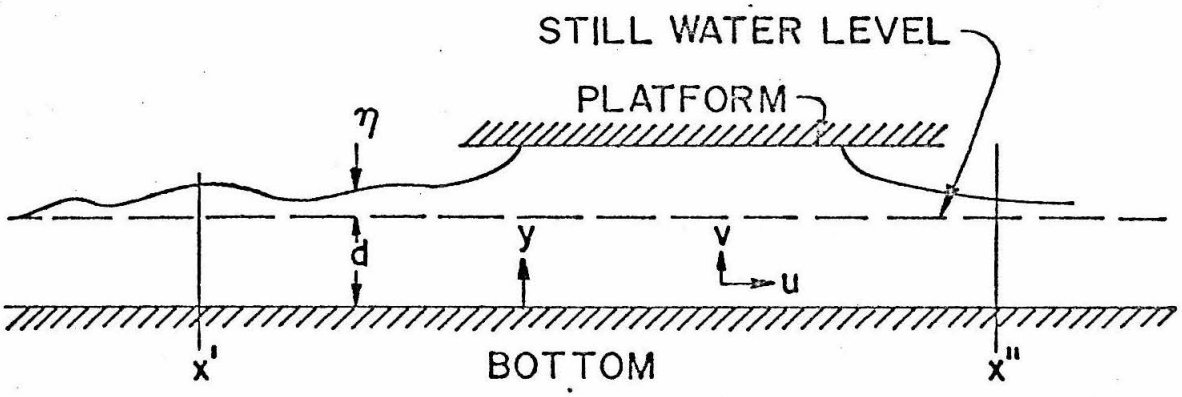

Figure 3.2. Generalized region of integration.

It will be convenient to use an integrated form of the equation of continuity. If Equation 3.3 is integrated over the region shown in Figure 3.2 bounded by vertical planes at x' and x'', by the horizontal bottom at $y = 0$, and by the free or bounded upper surface at $y = d + \eta$, one has:

$$\int_{x'}^{x''}\int_{o}^{d+\eta}\left(\frac{\partial u}{\partial x}+\frac{\partial v}{\partial y}\right)dy\,dx = 0. \tag{3.7}$$

Leibnitz' formula for the differentiation of integrals (see Bronwell, 1953, p. 110 or other mathematics texts) is:

$$\frac{dF(\alpha,u)}{du} = \frac{d}{du}\int_{\alpha_1}^{\alpha_2} f(x,u)\,dx =$$

$$f(\alpha_2,u)\frac{d\alpha_2}{du} - f(\alpha_1,u)\frac{d\alpha_1}{du} + \int_{\alpha_1(u)}^{\alpha_2(u)} \frac{\partial f(x,u)}{\partial u}\,dx, \tag{3.8}$$

where $F(\alpha,u)$ is differentiable and where the limits α_1, α_2 are functions of u. When the formula is applied to the first term in Equation 3.7, and when the second term is integrated, Equation 3.7 becomes:

$$\int_{x'}^{x''}\left[\frac{\partial}{\partial x}\int_{o}^{d+\eta} u\,dy - u_s\frac{\partial \eta}{\partial x} + v_s\right]dx = 0, \tag{3.9}$$

where the subscript $(\,)_s$ indicates a value on the upper surface. The kinematic free surface condition (Milne-Thomson, 1960, p. 390) is

$$v_s = u_s\frac{\partial \eta}{\partial x} + \frac{\partial \eta}{\partial t}. \tag{3.10}$$

When Equations 3. 10, and then 3. 2, are substituted into Equation 3. 8, one obtains:

$$\int_{x'}^{x''} \left[- U \frac{\partial \eta}{\partial x} + \frac{\partial}{\partial x} \int_{o}^{d+\eta} u \, dy \right] dx = 0. \tag{3. 11}$$

Since it is assumed that at a given instant U is independent of x in the region of integration, Equation 3. 11 may be integrated to:

$$\left[\int_{o}^{d+\eta} u \, dy - U\eta \right]_{x'}^{x''} = 0, \tag{3. 12}$$

or:

$$\int_{o}^{d+\eta} u \, dy - U\eta = \text{Const.} \tag{3. 13}$$

In the present study, the constant is zero, because far ahead of any disturbance, $u = 0$ and $\eta = 0$. Thus the continuity equation becomes

$$\int_{o}^{d+\eta} u \, dy = U\eta, \tag{3. 14}$$

subject to the assumption that the wave form is constant. For the case where fluid velocity u is not a function of depth y at $x = x'$ and $x = x''$, the left-hand side of Equation 3. 14 may be easily evaluated:

$$u(d+\eta) = U\eta \,. \tag{3.15}$$

Similarly, it is convenient to use Equation 3.4a, the equation of horizontal motion, after it has been integrated over a region such as that shown in Figure 3.2:

$$\int_{x'}^{x''} \int_{o}^{d+\eta} \left[\frac{\partial u}{\partial t} + u\frac{\partial u}{\partial x} + v\frac{\partial u}{\partial y} + \frac{1}{\rho}\frac{\partial P}{\partial x}\right] dy\, dx = 0. \tag{3.16}$$

Rearrangement of the third term and introduction of the equation of continuity (Equation 3.3) gives:

$$\int_{x'}^{x''} \int_{o}^{d+\eta} \left[\frac{\partial u}{\partial t} + 2\,u\frac{\partial u}{\partial x} + \frac{\partial (uv)}{\partial y} + \frac{1}{\rho}\frac{\partial P}{\partial x}\right] dy\, dx = 0. \tag{3.17}$$

Now:

$$\frac{du}{dt} = \frac{\partial u}{\partial t} + U\frac{\partial u}{\partial x} \tag{3.18}$$

(see the paragraph following Equation 3.2).

The quantity $\frac{du}{dt}$ is not, in general, equal to zero; rather, it is proportional to $\frac{dU}{dt}$, as may be seen by differentiating Equation 3.14 with respect to t:

$$\int_{o}^{d+\eta} \frac{du}{dt}\, dy = \eta \frac{dU}{dt}. \tag{3.19}$$

Introduction of Equation 3.18 into Equation 3.17 gives:

$$\int_{x'}^{x''} \int_{o}^{d+\eta} \left[- U \frac{\partial u}{\partial x} + 2u \frac{\partial u}{\partial x} + \frac{1}{\rho} \frac{\partial P}{\partial x} + \frac{du}{dt} + \frac{\partial (uv)}{\partial y} \right] dy\, dx = 0 \tag{3.20}$$

With the application of Leibnitz' formula, Equation 3.20 becomes:

$$\int_{x'}^{x''} \left[\frac{\partial}{\partial x} \int_{o}^{d+\eta} \left[\frac{P}{\rho} + u^2 - U u \right] dy - \eta_x \left[\frac{P_s}{\rho} + u_s^2 - U u_s \right] + u_s v_s + \int_{o}^{d+\eta} \frac{du}{dt} dy \right] dx = 0, \tag{3.21}$$

where again the subscript $(\,)_s$ indicates that the quantity is to be evaluated on the surface.

Now $\frac{\partial \eta}{\partial x} \frac{P_s}{\rho} = 0$ everywhere on the surface. When the kinematic surface condition (Equation 3.10) and Equation 3.2 are applied to the second bracketed term in Equation 3.21, and when the first bracketed term of Equation 3.21 is integrated with respect to x, one obtains:

$$\int_0^{d+\eta} \left[\frac{P}{\rho} + u^2 - U u\right] dy \Bigg|_{x'}^{x''} + \int_{x'}^{x''} \int_0^{d+\eta} \frac{du}{dt}\, dy\, dx = 0 \qquad (3.22)$$

The momentum equation at this point is subject to the assumptions of constant wave form, negligible viscosity, surface tension, and air entrainment.

For the case where horizontal flow is uniform and vertical velocity is zero for $x = x'$ and for $x = x''$, the first bracketed term of Equation 3.22 may be evaluated as follows: the equation of vertical motion, Equation 3.4b, becomes:

$$\frac{1}{\rho} \frac{\partial P}{\partial y} + g = 0; \qquad (3.23)$$

i.e., the pressure is hydrostatically distributed. Integration with respect to y and evaluation of the integration constant in terms of the surface pressure P_s gives:

$$\int_0^{d+\eta} \frac{P}{\rho}\, dy = \left(\frac{P_s}{\rho} + \frac{g(d+\eta)}{2}\right)(d+\eta). \qquad (3.24)$$

Since in this case u is assumed to be independent of y at $x = x'$ and $x = x''$, the velocity terms in the first bracketed term of Equation 3.22 are easily integrated. When the integrated equation of continuity (Equation 3.15) is applied, Equation 3.22 becomes:

$$\left(\frac{P_s}{\rho} + \frac{g(d+\eta)}{2} - \frac{U^2 \eta d}{(d+\eta)^2}\right)(d+\eta)\Bigg|_{x'}^{x''} + \int_{x'}^{x''}\int_{o}^{d+\eta} \frac{du}{dt}\, dy\, dx = 0. \qquad (3.25)$$

This form of the equation of motion is subject to the assumption that $\frac{\partial u}{\partial x} = 0$ and the assumption that effects of surface tension and viscosity are negligible, and is restricted to the case where at $x = x'$ and $x = x''$ pressure is hydrostatic and horizontal velocity is independent of depth.

3.2 Application of the Analysis.

3.2.1. Conditions at x = 0.

In the third assumption listed at the beginning of the section, it was supposed that as the wave strikes and propagates beneath the platform, as in Figure 3.1b, the horizontal fluid velocity beneath the seaward edge of the platform and the surface elevation at the seaward edge of the platform are approximately the same as would be found if the platform were not present.

This assumption is somewhat similar to one made by Wiegel (1960, 1964): the power being transmitted by a wave in the range of depth between the bottom of a thin, rigid, vertical barrier and the ocean bottom, is the same as the power transmitted by the wave in that range of depth if the barrier were not there. Wiegel used his assumption to develop a theory to predict the height of waves transmitted past the barrier. Comparing measured heights of waves produced in the laboratory with the theoretical wave heights, Wiegel concluded that the theory is "useful to the engineer", although "improvements in the theory are needed".

The assumption made in the present study takes no account of the presence of the vertical front face of the platform and is thus equally applicable to the case of a "thin" horizontal platform with no front face.

The horizontal fluid element velocity in a solitary wave (with no platform present) is given by Boussinesq (1872) as:

$$u = \sqrt{\frac{g}{d}}\left[\eta - \frac{\eta^2}{4d} + \left(\frac{d^2}{3} - \frac{y^2}{2}\right) \frac{d^2\eta}{dx^2} \right], \tag{3.26}$$

where η is the elevation of the surface above still water level, d is the still water depth, and x is the horizontal coordinate. The surface elevation η is given by Boussinesq as:

$$\eta = H \operatorname{sech}^2 \sqrt{\frac{3}{4}\frac{H}{d}}\frac{x}{d}, \tag{3.27}$$

where H is the wave height. By differentiating Equation 3.27 twice with respect to x, and substituting Equation 3.27 into the result, one obtains the relationship:

$$\frac{d^2\eta}{dx^2} = \frac{3H\eta}{2d^3}\left(2 - \frac{3\eta}{H}\right). \tag{3.28}$$

Substituting Equation 3.28 into Equation 3.26, one obtains an expression for normalized horizontal fluid velocity $u/\sqrt{gd}$ in terms of the normalized quantities η/d, H/d:

$$\frac{u}{\sqrt{gd}} = \frac{\eta}{d} - \frac{1}{4}\left(\frac{\eta}{d}\right)^2 + \frac{\eta}{d}\left[\frac{1}{3} - \frac{1}{2}\left(\frac{y}{d}\right)^2\right]\left[\frac{3H}{d} - \frac{9}{2}\left(\frac{\eta}{d}\right)\right]. \tag{3.29}$$

Equation 3.27 is an expression for the surface profile as viewed by an observer moving with the wave at its celerity of propagation U_o. To a fixed observer, the time history of the surface elevation may be expressed by replacing x with the quantity $U_o\ (t + t_o)$, where t_o is a constant:

$$\frac{\eta}{d} = \frac{H}{d}\ \text{sech}^2 \left[\sqrt{\frac{3}{4}\frac{H}{d}}\ \frac{U_o(t + t_o)}{d} \right] . \qquad (3.30)$$

As the wave approaches the point of observation, values of $t + t_o$ are negative. When the crest passes the observer, $t + t_o = 0$; after the wave has passed, $t + t_o$ is positive.

In this study, $t = 0$ is defined as the time when the approaching wave first makes contact with the soffit at $x = 0$, at an elevation s above still water level. Therefore, still considering the case where no platform is present, one must assign to the constant t_o a value such that when $t = 0$, $\eta = s$:

$$s = H\ \text{sech}^2 \left[\sqrt{\frac{3}{4}\frac{H}{d}} \left(\frac{U_o\ t_o}{d} \right) \right] . \qquad (3.31)$$

The value of t_o should be negative, since the wave crest is still approaching the point of observation at $t = 0$. (It may be pointed out that the absolute value of t_o is the time needed for the wave crest to arrive at the point of observation, measured from the time when $\eta = s$ at the point of observation.)

Therefore at the point of observation $x = 0$, with no platform present, the theory of Boussinesq (1872) predicts the fluid velocity u as given by Equation 3.29, and surface elevation η as given by

Equation 3.30, where t_o is defined in Equation 3.31; in the assumption made, it is supposed that even with the platform present, values of u and η at x = 0 are approximately as given by Equations 3.29 and 3.30, respectively, with t_o defined in Equation 3.31. The time t_a when the fluid level η, after having reached a maximum, again descends to the soffit elevation s, is equal to $2t_o$.

An observation may be made concerning the surface elevation and the fluid velocity u at x = 0 after the wave has passed. The amount of energy in the system considered is finite, and is initially equal to the sum of potential and kinetic energy in the approaching solitary wave. After the solitary wave reaches the seaward end of the platform at x = 0, a train of reflected waves and a train of transmitted waves radiate from x = 0 towards $x = -\infty$ and $x = +\infty$, respectively. These wave trains, like the incident solitary wave, have finite energy, and therefore must leave the fluid behind them at rest. After the solitary wave has arrived at the seaward edge of the platform and the last components of the reflected and transmitted waves have propagated away, a zone of rest propagates outward in both directions from the seaward edge of the platform. In the zone of rest, the surface elevation η and the fluid velocity u regain the value of zero that they had before the arrival of the solitary wave.

This result, obtained independently of the assumption discussed previously, is also predicted by Equations 3.29 and 3.30: for sufficiently large t, η tends to zero, and therefore u tends to zero.

3.2.2. Flow conditions beneath the platform.

Figures 3.3 show schematically the two fundamental flow regimes that are observed to exist beneath the platform (as will be shown in Section 6.2). In Figure 3.3a the seaward edge of the platform (at x = 0) is immersed. The principal feature of this flow is the wavefront advancing shoreward with celerity U_d beneath the platform. Figure 3.3b shows the conditions that follow those of 3.3a: the fluid has receded from the seaward edge of the platform, and the principal feature of the flow is the wave of recession that is propagating shoreward with celerity U_e. Throughout this study, the subscript $(\ )_d$ will be used to denote reference to the wave front shown in Figure 3.3a, and the subscript $(\ )_e$ will be used to denote reference to the wave of recession shown in Figure 3.3b. An expression with no subscript may refer to either the wavefront or to the wave of recession.

In each of Figures 3.3 there are points on the upper surface labelled 1, 2, and 3. Beneath Points 1 the flow completely fills the region between the tank bottom and platform; $\eta_1 = s$ (where the numerical subscript indicates the point at which a quantity is to be evaluated). In each case depicted, Point 1 is to be taken far enough away from the wave front or wave of recession so that the flow beneath that point is uniform, and the pressure hydrostatically distributed. Equation 3.15 can therefore be applied to relate local fluid velocity to wave celerity:

$$u_1 (d+s) = U_d s \qquad \text{(Figure 3.3a);} \qquad (3.32a)$$

$$u_1 (d+s) = U_e s \qquad \text{(Figure 3.3b).} \qquad (3.32b)$$

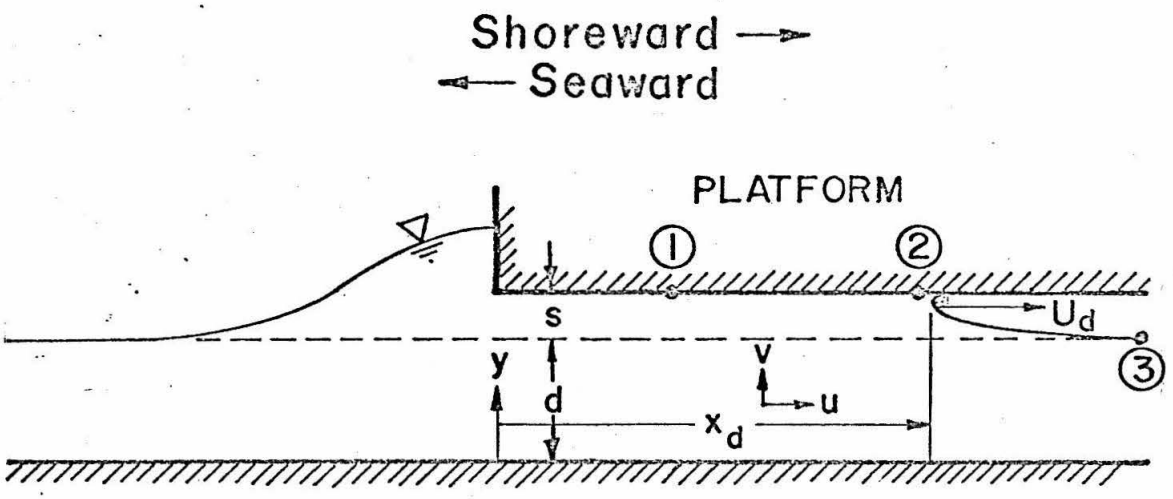

Figure 3.3a. Observed form of free surface with wave front.

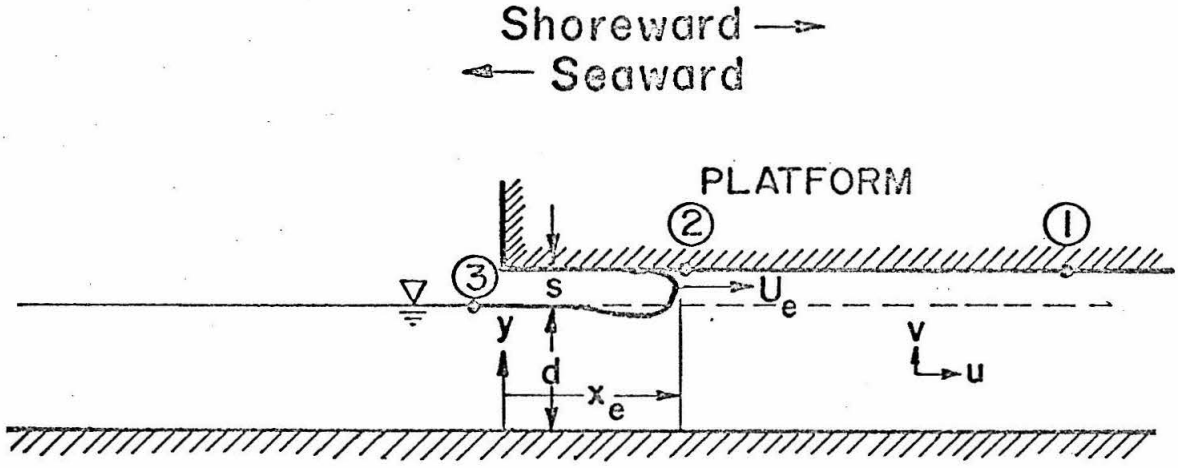

Figure 3.3b. Observed form of free surface with wave of recession.

At Points 2, located near the wavefront in Figure 3.3a and near the principal wave of recession in Figure 3.3b, the fluid has a horizontal velocity equal to the wave celerity U_d or U_e. (If either flow is viewed from a moving frame of reference such that the flow in the wave appears steady, Points 2 appear as stagnation points.) Since Points 2 are on the soffit, $\eta_2 = s$.

In Figure 3.3a, Point 3 is far ahead of any disturbance, and the water depth has the still water value d; therefore $u_3 = 0$ and $\eta_3 = 0$. In Figure 3.3b, the conditions $u = 0$ and $\eta = 0$ are realized in a region near $x = 0$, according to the reasoning presented in Subsection 3.2.1. Thus if Point 3 is chosen to be on the free surface sufficiently near $x = 0$, the conditions $u_3 = 0$ and $\eta_3 = 0$ may be obtained.

The wavefront celerity U_d is obtained as follows: in the assumption discussed in Subsection 3.2.1, it is supposed that the values of fluid velocity u at $x = 0$ are given approximately by the solitary wave theory of Boussinesq (1872), i.e., Equation 3.29, where η is a time-dependent function defined in Equation 3.30, in which t_o is a negative constant defined in Equation 3.31.

In the fluid-filled region beneath the platform, which in Figure 3.3a extends from the seaward end of the platform at $x = 0$ to the wavefront location (Point 2) at $x = x_d$, the surface elevation η equals the soffit clearance s. Thus Equation 3.14 becomes:

$$\int_o^{d+s} u \, dy = U_d s, \tag{3.33}$$

where the subscript $()_d$ has been added to indicate that specifically the wavefront is being considered.

When Equation 3.29 is substituted into Equation 3.33 and integrated, one obtains the result:

$$\frac{U_d}{\sqrt{gd}} = \frac{\eta}{d}\left(\frac{1+\frac{s}{d}}{\frac{s}{d}}\right)\left(\left[1+\frac{H}{d}-\frac{H}{d}\frac{\left(1+\frac{s}{d}\right)^2}{2}\right]+\frac{\eta}{d}\left[\frac{3}{4}\left(1+\frac{s}{d}\right)^2-\frac{7}{4}\right]\right), \qquad (3.34)$$

where H is the incident wave height, d is the still water depth, and where η is to be considered simply as a time-dependent function defined in Equations 3.30 and 3.31, not in this case the water surface elevation beneath the platform.

The analytical wave front celerity expressed in Equation 3.34 is dependent on the assumption of constant form of the wave front, and on the assumption that fluid velocity at the seaward edge of the platform due to an incident solitary wave is approximately equal to the velocity to be found if the platform were not present. Examination of Equation 3.34 indicates that since $U_d/\sqrt{gd}$ is proportional to first and second powers of η/d, and since Equation 3.30 indicates that for $t > 0$, η/d will first increase and then decrease one may expect $U_d/\sqrt{gd}$ also to increase, attain a maximum value, then decrease. It is also evident that as the ratio s/d of soffit clearance to still water depth becomes small, predicted values of normalized wave front celerity $U_d/\sqrt{gd}$ become very large.

The position x_d of the wave front at any given time t_d may be obtained by integrating U_d with respect to t:

$$x_d = \int_0^{t_d} U_d dt \, . \qquad (3.35)$$

The slowly-varying pressures are to be studied next. At Points 1 and 3, in either the wave front case depicted in Figure 3.3a or the wave of recession case depicted in Figure 3.3b, the pressure is assumed to be hydrostatically distributed and the horizontal velocity is assumed to be independent of depth. Thus the distances x_1 and x_3 may be substituted for x' and x'', respectively, in Equation 3.25:

$$\left[\left(\frac{P_s}{\rho} + \frac{g(d+\eta)}{2} - \frac{U^2 \eta d}{(d+\eta)^2}\right)(d+\eta)\right]_{x_1}^{x_3} + \int_{x_1}^{x_3}\int_{o}^{d+\eta} \frac{du}{dt}\, dy\, dx = 0. \qquad (3.36)$$

At Point 1, $\eta_1 = s$ and $P_s = P_1$. At Point 3, $P_s = 0$ and $\eta_3 = 0$. Therefore, when normalized, and rearranged, Equation 3.36 becomes:

$$\frac{P_1}{\gamma d} = \frac{U^2}{gd}\frac{\frac{s}{d}}{(1+\frac{s}{d})^2} - \frac{s}{d}\frac{(2+\frac{s}{d})}{2(1+\frac{s}{d})} + \left[\frac{1}{gd^2(1+\frac{s}{d})}\int_{x_1}^{x_3}\int_{o}^{d+\eta}\frac{du}{dt}\, dy\, dx\right]. \qquad (3.37)$$

To evaluate the integral on the right-hand side, one must know or assume the functions U(x) and $\eta(x)$ for $x_1 \le x \le x_3$. A simple assumed approximation is a step-form wave:

$$\eta = s, \quad u = \frac{Us}{d+s} \qquad \text{for } x_1 \le x \le x_2, \qquad (3.38)$$

$$\eta = 0, \quad u = 0 \qquad \text{for } x_2 \le x \le x_3, \qquad (3.39)$$

for which Equation 3.37 becomes:

$$\frac{P_1}{\gamma d} = \frac{U^2}{gd}\frac{\frac{s}{d}}{(1+\frac{s}{d})^2} - \frac{s}{d}\frac{(2+\frac{s}{d})}{2(1+\frac{s}{d})} + \frac{(x_3-x_1)}{d}\frac{\frac{s}{d}}{(1+\frac{s}{d})}\frac{1}{g}\frac{dU}{dt}. \qquad (3.40)$$

For irrotational flows, the Bernoulli integral (Equation 3.6) may be applied between Points 1 and 3 of Figures 3.3:

$$\frac{P_1}{\rho} = -\frac{1}{2}u_1^2 - gs + \frac{\partial \varphi}{\partial t}\bigg|_3 - \frac{\partial \varphi}{\partial t}\bigg|_1 , \tag{3.41}$$

where $\partial\varphi/\partial x = u$, therefore:

$$\frac{\partial \varphi}{\partial t}\bigg|_3 - \frac{\partial \varphi}{\partial t}\bigg|_1 = \int_{x_1}^{x_3} \frac{\partial}{\partial x}\left(\frac{\partial \varphi}{\partial t}\right)dx = \int_{x_1}^{x_3} \frac{\partial}{\partial t}\left(\frac{\partial \varphi}{\partial x}\right)dx = \int_{x_1}^{x_3} \frac{\partial u}{\partial t}dx =$$

$$- U\int_{x_1}^{x_3} \frac{\partial u}{\partial x}dx + \int_{x_1}^{x_3} \frac{du}{dt}dx = Uu_1 + \int_{x_1}^{x_3} \frac{du}{dt}dx . \tag{3.42}$$

Thus when normalized, with respect to gd, Equation 3.41 becomes:

$$\frac{P_1}{\gamma d} = \frac{U^2}{gd}\,\frac{\frac{s}{d}\left(2+\frac{s}{d}\right)}{2\left(1+\frac{s}{d}\right)^2} - \frac{s}{d} + \frac{1}{gd}\int_{x_1}^{x_3} \frac{du}{dt}dx . \tag{3.43}$$

When Equations 3.37 and 3.43 are combined and the pressure is eliminated, one finds that:

$$\frac{U^2}{gd} = \left(1+\frac{s}{d}\right) + \left[\frac{2\left(1+\frac{s}{d}\right)}{gd\left(\frac{s}{d}\right)^2}\int_{x_1}^{x_3}\left(\frac{1}{d}\int_0^{d+\eta}\frac{du}{dt}dy - \left(1+\frac{s}{d}\right)\frac{du}{dt}\right)dx\right]. \tag{3.44}$$

The integral on the right-hand side will vanish, if $dU/dt = 0$, since from Equation 3.19 the quantity du/dt is proportional to dU/dt. Thus for constant U, Equation 3.44 reduces to:

$$\frac{U^2}{gd} = 1 + \frac{s}{d} . \tag{3.45}$$

The Bernoulli integral (Equation 3.41), and thus Equation 3.44 are valid if and only if the flow in the region of integration is irrotational and energy-conserving. Therefore the only non-dissipative wave that can propagate beneath the platform is one whose celerity is given by Equation 3.44. The only possible constant celerity for an energy-conserving wave is given by Equation 3.45; to first order, this is the celerity of a solitary wave of height s propagating through water of depth d (Boussinesq, 1872). To be sure, such a wave, just grazing the platform soffit, would not be disturbed by the platform, and would not suffer energy dissipation other than by boundary shear stress.

In the general case where U^2/gd is different from $1 + s/d$ or the value given in Equation 3.44, Equations 3.37 and 3.43 will be inconsistent unless a negative term representing energy dissipation is added to the right-hand side of Equation 3.43. The major energy dissipation, such as is observed in an hydraulic jump, may be expected in the neighborhood of the wave front (Point 2 in Figure 3.3a), or, according to Benjamin (1968), behind or seaward of the wave of recession (between Points 2 and 3 in Figure 3.3b).

(It may be noted that for the conditions described in this study, it is impossible for the wave to propagate indefinitely beneath the platform and in contact with it, such as shown in Figures 3.1b and 3.3a. The incident solitary wave has a finite amount of energy per unit width, and therefore cannot indefinitely sustain the condition of energy dissipation at the wave front. After propagating a distance $x_{d_{max}}$, the wave front will cease to be defined, and the wave will continue to propagate beneath the platform at a diminished height H which is less than the soffit clearance s, so that no further contact with the soffit

is made. It is reasonable to expect that $x_{d_{max}}$ will increase with an increase in the amount of energy available for dissipation. Therefore, the normalized maximum distance $x_{d_{max}}/d$ may be expected to increase with relative wave height H/d, since the energy per unit width of a wave is proportional to the square of the wave height (Wiegel, 1964).)

In the case depicted in Figure 3.3a, the two unknown flow quantities u_1 and P_1 may be determined using the integrated equations of continuity (Equation 3.32) and of momentum (Equation 3.40), and values of $U_d(t)$ determined experimentally or from Equation 3.34. Therefore, the general inapplicability of the Bernoulli integral (Equation 3.41) is not a hindrance.

In the case depicted in Figure 3.3b, one need not even know the values of U_e a priori. Since the energy dissipation is concentrated between Points 2 and 3, the Bernoulli integral may be applied between Points 1 and 2:

$$\frac{P_1}{\rho} = -\frac{1}{2}U_e^2 - \frac{1}{2}u_1^2 + \frac{\partial \varphi}{\partial t}\bigg|_2 - \frac{\partial \varphi}{\partial t}\bigg|_1 , \qquad (3.46)$$

or:

$$\frac{P_1}{\gamma d} = -\frac{1}{2}\frac{U_e^2}{gd}\left(\frac{1}{1+\frac{s}{d}}\right)^2 + \frac{1}{gd}\int_{x_1}^{x_2}\frac{du}{dt}\,dx, \qquad (3.47)$$

where Equations 3.32b and 3.42 and Leibnitz' formula have been applied, and the equation normalized with respect to gd. When Equation 3.47 is combined with Equation 3.37 the result is:

$$\frac{U_e^2}{gd} = \frac{s}{d}\left(1 + \frac{s}{d}\right)\frac{\left(2+\frac{s}{d}\right)}{\left(2\frac{s}{d}+1\right)}$$

$$- \frac{2\left(1+\frac{s}{d}\right)}{gd\left(1+2\frac{s}{d}\right)}\left(\frac{1}{d}\int_{x_1}^{x_3}\int_{o}^{d+\eta}\frac{du}{dt}\,dy\,dx - \left(1+\frac{s}{d}\right)\int_{x_1}^{x_2}\frac{du}{dt}\,dx\right). \quad (3.48)$$

When U_e is constant or when the approximation of a step-form wave (Equation 3.39) is applied, Equation 3.48 reduces to:

$$\frac{U_e^2}{gd} = \frac{s}{d}\left(1+\frac{s}{d}\right)\frac{\left(2+\frac{s}{d}\right)}{\left(2\frac{s}{d}+1\right)}. \quad (3.49)$$

Equation 3.48 substituted into Equation 3.47 gives:

$$\frac{P_1}{\gamma d} = -\frac{1}{2}\frac{s}{d}\frac{\left(2+\frac{s}{d}\right)}{\left(2\frac{s}{d}+1\right)\left(1+\frac{s}{d}\right)}$$

$$+\frac{1}{gd\left(1+2\frac{s}{d}\right)}\left(\frac{1}{d\left(1+\frac{s}{d}\right)}\int_{x_1}^{x_3}\int_{o}^{d+\eta}\frac{du}{dt}\,dy\,dx + 2\frac{s}{d}\int_{x_1}^{x_2}\frac{du}{dt}\,dx\right). \quad (3.50)$$

When the approximation of a step-form wave is applied, U_e assumes the constant value given by Equation 3.49 and the time-dependent integral terms in Equation 3.50 vanish, leaving:

$$\frac{P_1}{\gamma d} = -\frac{1}{2}\frac{s}{d}\frac{\left(2+\frac{s}{d}\right)}{\left(1+\frac{s}{d}\right)\left(1+2\frac{s}{d}\right)}. \quad (3.51)$$

For the case in which no energy is dissipated, U_e is given by Equation 3.45, which when combined with Equation 3.49, shows that s = d. This is the result obtained by Benjamin (1968). This case is not of practical importance in the present study, since the maximum possible height of a solitary wave is H = 0.78d (McCowan, 1891), and such a wave would not strike a platform for which s = d.

The time t_e at which the wave of recession may be expected at a particular location x_e is given by the formula:

$$t_e = t_a + x_e/U_e, \tag{3.52}$$

where t_a is the time of initial formation of the wave of recession, and, as shown in subsection 3.2.1, is equal to twice the value of t_o defined in Equation 3.31; and where the celerity of the wave of recession U_e is given by Equation 3.49.

To summarize the analysis for slowly-varying pressure, the normalized pressure head $P_1/\gamma d$ may be related to the celerity of the wave front or the celerity of the wave of recession by Equation 3.40, subject to the assumption that the wave form is unchanging, the assumption that the effects of surface tension and viscosity are negligible, the condition that at the position of measurement, Point 1, the pressure is hydrostatically distributed and the fluid velocity is independent of depth, and the assumption that the flow may be approximated by a simple step-form as expressed by Equations 3.38 and 3.39. The quantities U, x_2, and dU/dt may be either measured experimentally or derived by Equations 3.34 and 3.35. The celerity of the wave of recession is expressed by Equation 3.49, subject to the same assumptions as Equation 3.40; and where pressure is related to flow

conditions at the wave of recession, as depicted in Figure 3.3b, the expression for pressure reduces to a function of the ratio of soffit clearance to still water depth s/d shown in Equation 3.51. Where the wave front is considered, as in Figure 3.3a, the quantity U becomes U_d, and x_2 becomes x_d. Where the wave of recession is considered, U becomes U_e, and x_2 becomes x_e.

Equation 3.40 may be integrated with respect to x to give the total uplift force per unit width F, normalized with respect to γd^2:

$$\frac{F}{\gamma d^2} = \frac{1}{d}\int_o^{x_d} \frac{P_1}{\gamma d}\, dx = \frac{x_d}{d}\left[\frac{U_d^2}{gd}\,\frac{\frac{s}{d}}{(1+\frac{s}{d})^2} - \frac{s}{d}\,\frac{(2+\frac{s}{d})}{2(1+\frac{s}{d})} + \frac{x_d}{d}\,\frac{\frac{s}{d}}{2(1+\frac{s}{d})}\,\frac{1}{g}\,\frac{dU_d}{dt}\right]. \tag{3.53}$$

The average pressure P_{av} is simply the total uplift force per unit width divided by the wetted length x_d. In normalized form:

$$\frac{P_{av}}{\gamma d} = \frac{F}{\gamma d x_d}. \tag{3.54}$$

The center of uplift pressure x_{cp} is the first moment of the pressure distribution:

$$\frac{x_{cp}}{d} = \frac{\int_o^{x_d} \frac{P_1}{\gamma d}\,\frac{x}{d}\, dx}{\int_o^{x_d} \frac{P_1}{\gamma d}\, dx} = \frac{x_d}{2d}\left[1 - \frac{\frac{x_d}{3}\,\frac{dU_d}{dt}}{\frac{2U_d^2}{(1+\frac{s}{d})} - gd(2+\frac{s}{d}) + x_d\frac{dU_d}{dt}}\right]. \tag{3.55}$$

In cases where pressure is determined from Equation 3.51 from consideration of flow at the wave of recession, the average normalized pressure head $P_{av}/\gamma d$ is simply equal to the constant value of pressure

$P_1/\gamma d$ given by Equation 3.51. The normalized (negative) uplift force per unit width in this case is the normalized pressure head $P_1/\gamma d$ given by Equation 3.51 multiplied by the relative length of the portion of platform that is in contact with the wave. If the secondary wave of recession is not considered and it is assumed that fluid is in contact with the platform from the location of the principal wave of recession x_e to the location of the shoreward end of the platform L, the normalized force per unit width is:

$$\frac{F}{\gamma d^2} = \frac{P_1}{\gamma d}\left(\frac{L-x_e}{d}\right), \tag{3.56}$$

where $P_1/\gamma d$ is given by Equation 3.51, and x_e as a function of time t_e may be determined from Equation 3.52. Since by Equation 3.51 the pressure is distributed uniformly on the platform, the location of the center of uplift pressure is simply the centroid of the portion of platform in contact with the wave:

$$\frac{x_{cp}}{d} = \frac{1}{2}\left(\frac{L+x_e}{d}\right). \tag{3.57}$$

The peak pressure that is observed at the wave front, at Point 2 in Figure 3.3a, may be analyzed by considering separately the flow in the neighborhood of the wave front. Figures 6.13 through 6.16 (to be presented in Section 6.2) show that at the wave front, spume is driven ahead of the main body of fluid, and air is entrained in the fluid in the wave, in action reminiscent of an hydraulic jump. In this section it was concluded that for wave front celerities other than that given by Equation 3.44, there must be energy dissipation, most likely at the

wave front, so that a term representing energy loss may be introduced into Equation 3.43 to make it consistent with Equation 3.37.

It has been stated that Point 2 in Figure 3.3a may be considered a stagnation point. Potential flow considerations indicate that the stagnation point, where fluid velocity relative to the wave front celerity is zero, cannot in general lie on the free surface, although it must lie on some fluid boundary. A flow configuration in which a thin jet of spray shoots forward from the stagnation point, as shown in Figure 3.4, satisfies the condition just described. Furthermore, by considering the mass flux and momentum flux in the thin jet one may modify the horizontal equation of motion (Equation 3.37) so that it may be made consistent with the Bernoulli integral as expressed in Equation 3.43, i.e., without an additional term representing energy dissipation. The droplets of spume observed in Figures 6.13 through 6.16 may be considered the real-fluid version of the idealized jet, whose complete formation is hindered by effects of surface tension and viscosity.

In ideal flow with the thin jet formed as in Figure 3.4, the pressure at Point 2 may be obtained by applying the Bernoulli integral (Equation 3.6) between 2 and 3:

$$\frac{P_2}{\rho} = -\frac{1}{2}u_2^2 - gs + \left.\frac{\partial \varphi}{\partial t}\right|_3 - \left.\frac{\partial \varphi}{\partial t}\right|_2 . \tag{3.58}$$

When the last two terms are treated in a manner corresponding to that shown in Equation 3.42, Equation 3.58 becomes:

$$\frac{P_2}{\rho} = U_d u_2 - \frac{1}{2}u_2^2 - gs + \int_{x_2}^{x_3} \frac{du}{dt}\, dx . \tag{3.59}$$

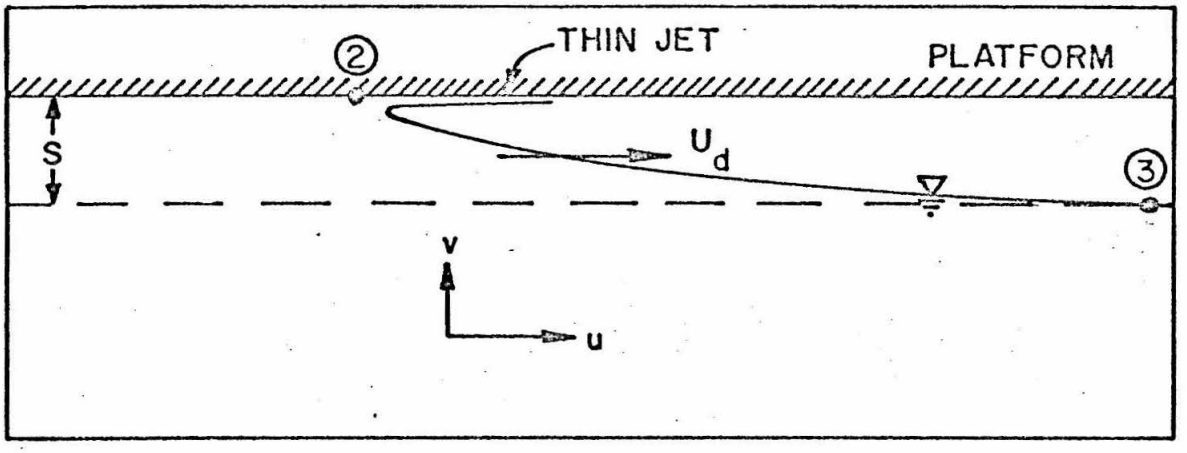

Figure 3.4. Idealized flow at wave front with thin jet of spray.

Point 2 has been defined as a stagnation point such that $u_2 = U_d$. By Equation 3.19, subject to the assumption that the wave form is constant, du/dt is proportional to dU_d/dt, the wave front acceleration; and for $\eta > 0$, is of the same sign as dU_d/dt. Therefore, one may write:

$$\frac{P_2}{\rho} = \frac{1}{2} U_d^2 - gs + K \frac{dU_d}{dt} , \qquad (3.60)$$

where K is a positive coefficient depending on the wave profile form and the velocity distribution between Points 2 and 3. For values of dU_d/dt sufficiently small compared to other terms, or for constant

celerity U_d, the last term in Equation 3.60 may be neglected, leaving:

$$\frac{P_2}{\rho} = \frac{1}{2} U_d^2 - gs \,. \tag{3.61}$$

Equation 3.61, subject to the assumption that flow is irrotational in the neighborhood of the wave front, that the wave form is constant, and that the acceleration term is negligible, may be used to determine the amplitude of the peak pressure.

The foregoing analysis, and indeed most of the present study, has been devoted to the case where the soffit clearance is greater than zero. The flow situation is considerably different when $s = 0$, primarily because there is no wave front advancing beneath the platform such as shown in Figure 3.3a. Because the peak pressure phenomenon is associated with the advancing wave front when $s > 0$, there is no peak pressure when $s = 0$.

For predicting slowly-varying pressure, the analysis developed in this chapter is of limited usefulness when $s = 0$, since it provides a relation between pressure and the celerity and acceleration of the wave front found with positive soffit clearance. Furthermore, the analysis does not take into consideration the total platform length L. For $s > 0$, the length of platform that need be considered is just $x_d(t)$, the distance from the seaward edge to the advancing wave front; but for $s = 0$, the fluid beneath the entire platform is set in motion simultaneously, and L becomes an important parameter.

Considering the limitations of the present analysis when $s = 0$, it seems best to formulate a different analysis, with a different set of assumptions, for the case of zero soffit clearance; this problem, treated by others as discussed in Section 2.1, will not be treated herein.

3.3. Discussion of the Assumptions.

The assumption that the free surface profile is of constant form has permitted development of much of the analysis without the need for detailed knowledge of the form of the wave profile and its change with time. In general, without such detailed knowledge of the wave form, one cannot calculate the error introduced by the assumption. However, by comparing photographs or wave gauge records of the profile made at successive time intervals, one may determine simply whether or not any change with respect to time in profile form can be observed. If no change is observed, no error is introduced by the assumption.

The assumption that viscosity has negligible effect on pressure may be examined by analysis of boundary-layer growth. With respect to Figure 3.3a, one would expect that in a real fluid, viscous boundary layers would develop along the platform soffit and the channel bottom. According to the Prandtl boundary-layer theory (Schlichting, 1960, pp. 107 et seq.) the presence of the boundary layer has negligible effect on the boundary pressure, providing that the thickness δ of the boundary layer is much less than a characteristic length dimension of the body such as the platform length L. In laminar flow past a flat plate, the ratio of boundary layer thickness δ to the distance x from the leading edge is $\delta/x = 5/R_e^{\frac{1}{2}} = 5/(ux/\nu)^{\frac{1}{2}}$ Rouse, 1950, p. 106), where R_e is the Reynolds number, u is a characteristic fluid velocity, and ν is the kinematic viscosity. In a turbulent boundary layer, $\delta/x = 0.38/R_e^{1/5}$ (ibid.). Therefore, to estimate the order of magnitude of the ratio δ/L of boundary layer thickness to body length, one may replace x with L in the expressions presented. For sufficiently large R_e, therefore sufficiently small δ/L, the pressure will not be affected by viscosity.

At the wave front, viscosity may indirectly affect the peak pressure by inhibiting the formation of the thin jet of spray shown in Figure 3.4, as postulated for an ideal flow. The peak pressure, described as occurring at a stagnation point in the region of the wave front, may be considered as resulting partly from the acceleration given the fluid in the thin jet. Therefore if acceleration of the fluid is inhibited by viscosity, the peak pressure will be reduced.

The component of pressure added to the fluid by surface tension is directly proportional to the curvature of the free surface. The Bernoulli integral (Equation 3.6), when applied to the free surface, may be expanded to include a term representing surface tension:

$$\frac{P}{\rho} + \frac{1}{2}(u^2+v^2) + gy + \frac{\partial \varphi}{\partial t} + \frac{\sigma}{\rho r} = F(t), \tag{3.62}$$

where σ is the surface tension per unit length and r is the local radius of curvature. (The expression just given is for two-dimensional flow; where there is variation in the transverse direction, $\frac{1}{r}$ may be replaced by $(\frac{1}{r_1} + \frac{1}{r_2})$, where r_1 and r_2 are the principal radii of surface curvature (Lamb, 1945, p. 456).). If the value of σ is known, the importance of the surface tension term relative to the other terms in Equation 3.62 may be evaluated for a given value of r.

The relative importance of surface tension is often expressed by the Weber number $W_e = \frac{U}{\sqrt{\sigma/\rho r}}$. When normalized with respect to U^2, Equation 3.62 may be written:

$$\frac{P}{\rho U^2} + \frac{1}{2}\left(\frac{u^2+v^2}{U^2}\right) + \frac{gy}{U^2} + \frac{1}{U^2}\frac{\partial \varphi}{\partial t} + \frac{1}{W_e^2} = F(t) . \tag{3.63}$$

Equation 3.63 shows that as W_e becomes large, the relative importance of surface tension becomes very small. Equation 3.63 will be applied in Section 6.6 to estimate the importance of surface tension. The effect of surface tension is to minimize the ratio of surface area to volume of fluid. Therefore, at the wave front, surface tension tends to inhibit formation of the thin jet postulated for ideal flow.

In the real case where formation of the thin jet is inhibited, there must be energy dissipation at the wave front, as in an hydraulic jump, where the principal mechanism of energy dissipation is turbulence. In turbulent flow near the free surface there may be sufficiently severe perturbation of the free surface that air is entrained in the main body of fluid. Air bubbles entrained in the flow act to reduce the average density of the fluid. Since hydrostatic and hydrodynamic pressure are directly proportional to fluid density, a decrease in density will result in a proportional decrease in pressure.

An increase in geometric length scale increases the Reynolds number R_e and reduces any relative effect of viscosity; an increase in scale increases the Weber number W_e and thereby reduces the direct importance of surface tension, as shown in Equation 3.63. However, it is likely that an increase in scale will be accompanied by an increase in the relative amount of air entrained. Turbulence is inhibited at sufficiently small Reynolds number, and deformation of the free surface is inhibited at small Weber number. Therefore, with increasing scale and correspondingly increasing R_e and W_e the forces inhibiting air entrainment become weaker, and a relative increase in air entrainment may be expected.

The assumption that the fluid element velocity beneath the seaward end of the platform at $x = 0$ is approximately the velocity at $x = 0$ if no platform were present incurs little error if the incident wave is deformed only slightly, i.e., if $(H-s)/d << 1$, where H is the wave height, s is the soffit clearance, and d is the still water depth. With increasing (H-s)/d, the distortion of the incident wave becomes greater, and the assumption becomes less valid.

Equation 3.40 for the slowly-varying pressure P_1 is dependent on the condition that at Point 1, where pressure is to be evaluated, the pressure is hydrostatically distributed and the horizontal velocity is independent of depth. Such a condition is obtained in irrotational flow between parallel plates of infinite extent, or between plates whose length is great compared with the distance between them. The flow beneath the platform shown in Figures 3.3 increasingly resembles the flow between parallel plates as the distance x_d or x_e increases with respect to the total depth d+s. The main body of the fluid can be considered to be irrotational at all times since the fluid is initially at rest, and vorticity is introduced by viscosity only at the boundaries and in regions of concentrated energy dissipation. For small values of $x_d/(d+s)$ the condition of uniform flow may not be approximated well and error may be introduced into Equation 3.40; yet with increasing $x_d/(d+s)$, the flow should become more uniform, and the error introduced should become less.

The assumptions will be re-examined in Chapter 6, where the analysis is compared with the experimental results.

A chronology of the process of solitary wave impact is now presented, with corresponding illustrations shown in Figure 3.5:

$t = 0$ The wave first strikes the platform.

$t = t_a$ The fluid level at $x = 0$, having risen from $\eta = s$ at $t = 0$ to a maximum, has again descended to the value $\eta = s$. The wave of recession begins to form at this time.

$t = t_b$ The advancing wave front ceases to be defined, because the celerity U_d has decreased to the extent that the transmitted wave henceforward propagates beneath the platform with a height less than s. (To recognize the effect of finite platform length, t_b may be defined as the time when the wave front reaches the shoreward end of the platform, if at that time the wave is still propagating in contact with the platform.) The wetted length of the platform may be defined as $x_{d_{max}} = \int_o^{t_b} U_d dt$.

$t = t_c$ The wave is no longer in contact with the platform anywhere. A conservatively large value of t_c is the time at which the principal wave of recession reaches the point $x_{d_{max}}$ attained by the wave front at time t_b:

$$\int_{t_a}^{t_c} U_e \, dt = x_{d_{max}} = \int_o^{t_b} U_d \, dt,$$

The wave first strikes the platform.

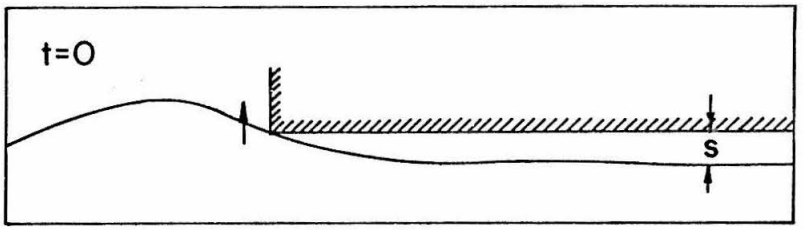

$\eta = s$ for second time; principal wave of recession begins to form.

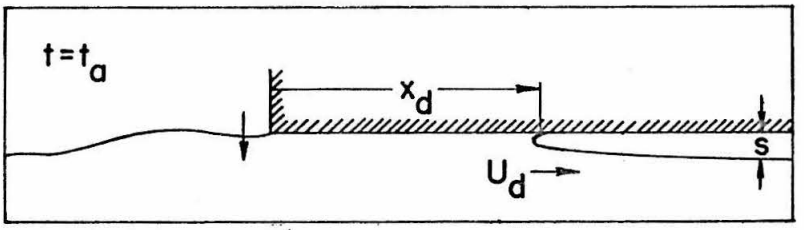

The wave front ceases to be defined.

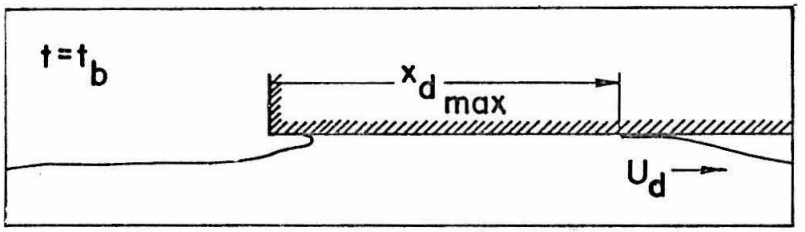

The platform ceases to be in contact with the fluid in the wave.

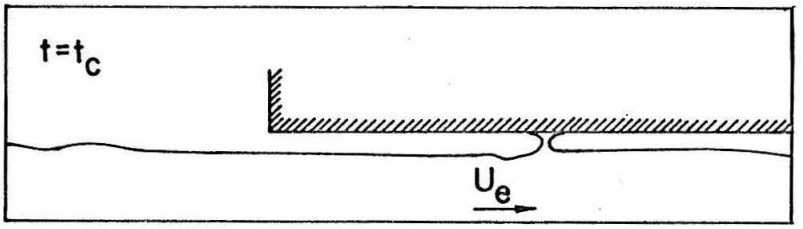

The wave front reaches the point x. (Note that $0 < t_d < t_b$.)

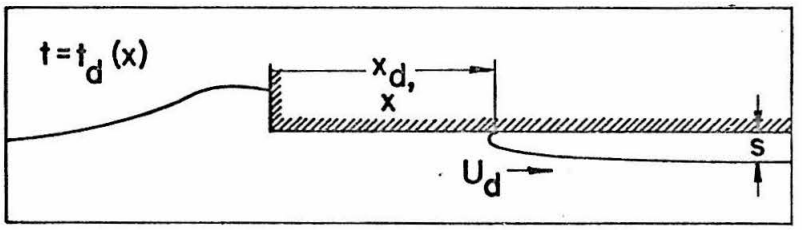

The principal wave of recession reaches the point x. (Note that $t_a < t_e < t_c$.)

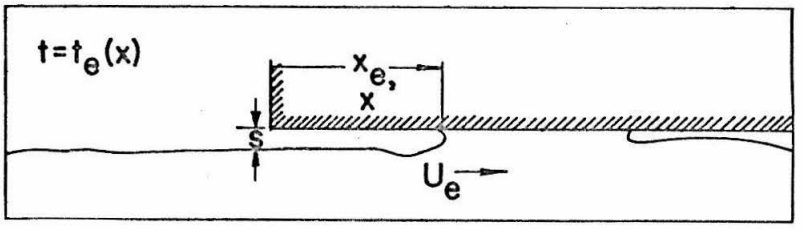

Figure 3.5. Chronology of wave impact on the platform.

where U_e is the celerity of the wave of recession. Usually a secondary wave of recession propagates seaward from $x_{d_{max}}$ to meet the principal wave of recession, making t_c less than that implicit in the equation just given.

$t = t_d(x)$ The advancing wave front reaches the point x:

$$x = x_d = \int_o^{t_d} U_d \, dt \, .$$

Note that $0 < t_d < t_b$.

$t = t_e(x)$ The principal wave of recession reaches the point x:

$$x = x_e = \int_{t_a}^{t_e} U_e \, dt \, .$$

Note that $t_a < t_e < t_c$.

The period during which each part of the analysis may be validly applied is now examined. Equation 3.34 for wave front celerity U_d may be applied as long as the soffit at x = 0 is submerged, i.e. for $0 < t < t_a$. As stated in subsection 3.2.1, an analytical value for t_a is simply $2\,t_o$, where t_o is implicitly defined in Equation 3.31. Equation 3.40 for slowly-varying pressure P_1 (when applied with respect to wave-front celerity) and Equation 3.61 for peak pressure P_2 may be applied during the period for which the wave front celerity U_d is defined. If the celerity is computed from Equation 3.34, pressure may be computed for $0 < t < t_a$, since U_d is defined for $0 < t < t_a$; if the celerity is measured directly, pressure may be computed for

$0 < t < t_b$, since U_d is defined for $0 < t < t_b$. Equation 3.49 for celerity U_e of the wave of recession and Equation 3.51 for slowly-varying pressure related to conditions at the wave of recession may be applied whenever the wave of recession exists, i.e. for $t_a < t < t_c$.

CHAPTER 4

EXPERIMENTAL EQUIPMENT AND PROCEDURE

4.1. The Wave Tanks.

The preliminary experiments were conducted in a channel 10 in. deep x 10-1/2 in. wide x 40 ft long, shown in Figure 4.1, normally used as a tilting flume but modified to serve as a wave tank. The modifications consisted of blocking the recirculation pipe, installing a gravel beach at one end to absorb wave energy, and installing a wave generator at the other end. The flume was adjusted to give the bottom zero slope.

The tank walls were of steel except at the 5-ft test section, where they were of glass. The test section was located about 5 ft from the toe of the beach, and about 25 ft from the wave generator. The beach, with approximately a 1:4 slope, was constructed of 3/4-in. plywood covered with 3/4-in. gravel.

The major part of the experimental program was performed in a horizontal channel 24 in. deep x 15-1/2 in. wide x 100 ft long, shown in Figures 4.2 through 4.4. As shown in Figures 4.3 and 4.4, the tank is composed of ten 10-ft modules. The side wall panels are of glass. At each junction between two modules the legs are supported on two 1/2-in. bolts, in turn supported by a flat steel bar bolted to the laboratory floor. The 1/2-in. bolts provide a means of making minor adjustments in elevation.

In construction, the welded modules were bolted one to another at the desired location. With careful surveying, the bottom was

Figure 4.1. The 40-ft tilting flume modified for use as a wave tank.

Figure 4.2. The 100-ft wave tank.

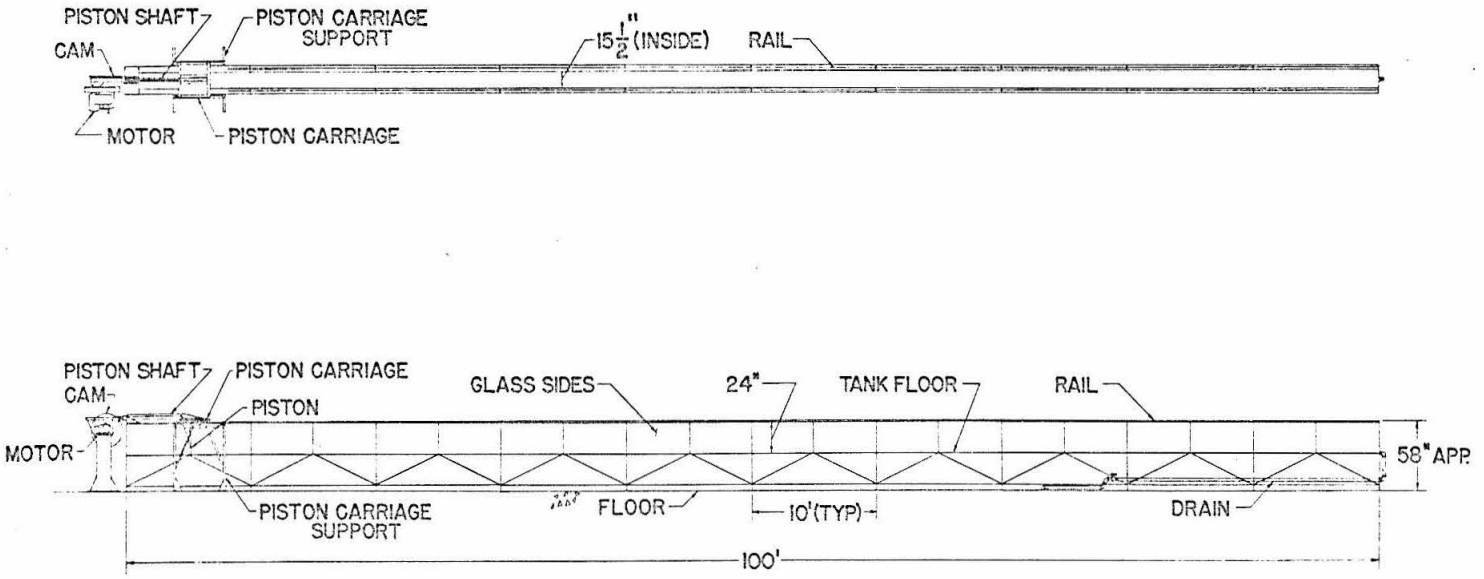

Figure 4.3. Drawing of the 100-ft wave tank.

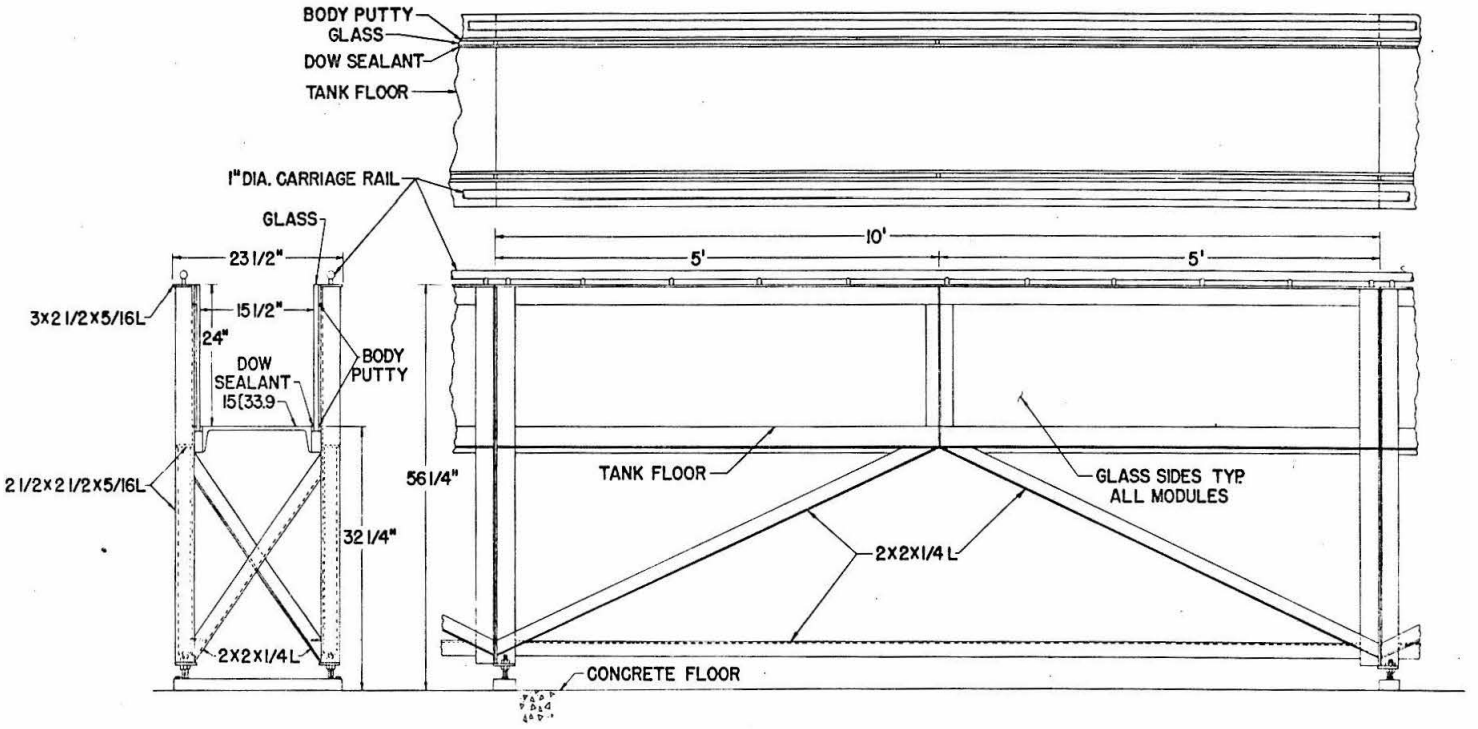

Figure 4.4. A typical module of the 100-ft wave tank.

adjusted to within 1/32 in. of constant elevation. The modules were then welded together permanently.

The glass window panes, each measuring 1/2 in. x 25 in. x 5 ft, were mounted using the techniques described by Daly (1965), using body putty and Dow Corning 780 building sealant. The floor of the tank was painted with a 5-coat Pittsburgh Aquapon epoxy-paint system.

The instrument carriage rails, made of 1-in. stainless steel round stock, were mounted above the top flanges of the tank walls with 3/8-in. bolts spaced at intervals of 2 ft. Considered part of a precision-measurement system, the rails were made level with respect to a stillwater surface to within 0.001 ft.

Mounted at one end of the tank was the wave generator, to be discussed in the next section. At the other end was a 3/4-in. plywood beach of 1:4 slope covered with 1-1/2-in. gravel. The test platform was mounted approximately 75 ft from the wave generator and 7 ft from the toe of the beach.

4.2. The Wave Generators.

Two design requirements for the wave generators were that a generator be able to produce a single wave of translation, unbroken and of unchanging form, whose characteristics are described approximately by the "solitary wave" theories, and which may itself be called a "solitary wave"; and that the generated waves be reproducible, so that a series of experiments could be performed with waves of nearly identical size and form.

In order to insure the formation of a solitary wave at a minimum distance from the generator, the piston of a wave generator should, at any given depth, have nearly the same motion as that of a fluid particle at that depth in a solitary wave. To a fixed observer the fluid velocity u is expressed approximately by Equation 3.29 (See Chapter 3) where the elevation η of the free surface above still water level is expressed by Equation 3.30, in which U_o is the wave celerity and t_o remains an arbitrary constant (not, in general, as defined in Equation 3.31).

If only first-order terms are retained, Equation 3.29, combined with Equation 3.30, becomes:

$$\frac{u}{\sqrt{gd}} = \frac{\eta}{d}\left[1+\frac{H}{d}\right] = \frac{H}{d}\left[1+\frac{H}{d}\right]\operatorname{sech}^2\left[\sqrt{\frac{3}{4}\frac{H}{d}}\,\frac{U_o(t+t_o)}{d}\right], \qquad (4.1)$$

where H is the wave height and d is the still water depth. According to the theory of Boussinesq (1872):

$$\frac{U_o}{\sqrt{gd}} = \sqrt{1+\frac{H}{d}}\ , \qquad (4.2)$$

a relationship which may be substituted into Equation 4.1.

The piston velocity u_p may be substituted for u in Equation 4.1, which may then be integrated with respect to time to give the piston displacement x_p:

$$x_p = \int_o^t u_p dt = \sqrt{\frac{4Hd}{3}\left(1+\frac{H}{d}\right)}\tanh\left[\sqrt{\frac{3Hg}{4d^2}\left(1+\frac{H}{d}\right)}\left(t+t_o\right)\right]. \qquad (4.3)$$

Therefore, it is desirable to move the generator piston with the velocity u_p expressed in Equation 4.1, so that its displacement is of the form:

$$x_p = \frac{D}{2} \tanh \Omega \left(t + t_o \right), \qquad (4.4)$$

where $D = 4\sqrt{\frac{Hd}{3}\left(1 + \frac{H}{d}\right)}$ is the total stroke, and $\Omega = \sqrt{\frac{3Hg}{4d^2}\left(1 + \frac{H}{d}\right)}$ is a measure of piston velocity. The arbitrary constant Ωt_o may be set equal to zero, so that at $t = 0$, $x_p = 0$ and the piston is midway through its stroke. (This definition of $t_o = 0$ should be considered separate from, and is not to be confused with, the definition expressed by Equation 3.31.)

After examination of several solitary-wave generator designs reported in the literature (described in Section 2.5), it was decided that a cam-driven piston type of generator would best satisfy requirements of reproducibility and form. Although the electronically-programmed, hydraulically-driven piston system was deemed the most versatile and potentially accurate, a cam-driven piston system was seen to be far less costly and more readily built. Furthermore, the cam-driven piston system with its positive action was thought to offer better reproducibility than the system where a piston would be driven by a released impoundment of water, in which stroke length and piston speed could easily be affected by bearing friction.

The system actually developed and used is now to be described. In each tank, the piston was a vertical plate nearly filling the tank cross-section, fixed to the underside of a carriage mounted on four ball bushings running on stainless steel rails. The piston was driven by a shaft connected directly to a cam follower. The accompanying cam was cut to give the cam follower and the piston the motion described by Equation 4.4.

The wave generator built for the 40-ft tank is shown in Figure 4.5. The cam wheel was 12 in. in overall diameter. The cam groove, 3/8-in. wide, had a maximum radius of 5 in. and provided for a stroke of 8 in. The wheel was composed of a 1/8-in. aluminum disc and a 1/4-in. steel disc bolted to a 4-in. hub mounted on the motor axle. The aluminum disc served as a backing for the 1/4-in. steel disc, through which the groove was cut. A round-headed brad put in the hub at an appropriate position served as a trip for a microswitch, mounted on the motor casing. The Bodine 1/4-hp electric motor was regulated by a Minarik speed control. The range of cam wheel speeds was 30 to 70 rpm. The piston arm, made of 2-1/4-in. aluminum channel, was fastened directly to the piston carriage. With this generator, the forces involved were small enough that the piston arm needed no support beyond being bolted securely to the carriage. The piston-carriage rails were simply clamped parallel to the instrument carriage rails.

The generator for the 100-ft tank, similar to the one for the 40-ft tank, is shown in Figure 4.6, with a dimensioned drawing presented in Figure 4.7. The cam was powered by SpeedTrol Infinite Variable Speed power unit, manufactured by Sterling Electric Motors, Inc. The 30-in. diameter cam wheel was composed of a 1/4-in. steel disc bolted to a 3/4-in. plywood disc, mounted on a steel hub on the drive shaft of the power unit. The plywood disc served as a backing for the steel disc, through which the cam groove was cut. Again, a brad on the hub served as a trip for a microswitch. The cam groove had a maximum radius of 12-1/2 in. and provided for a stroke of 20 in.

The cam follower was a 1/2-in. steel pin 2 in. long, housed in a brass sleeve mounted at the end of the piston shaft. Figure 4.8 shows

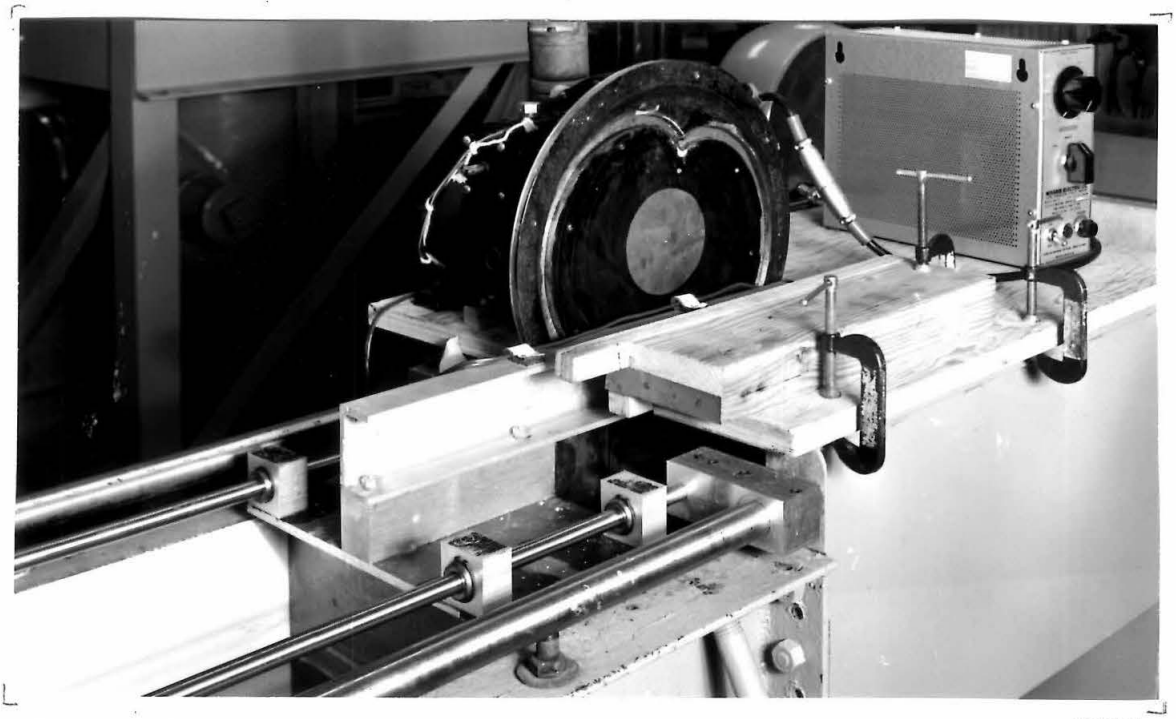

Figure 4.5. The wave generator for the 40-ft tank. 9093

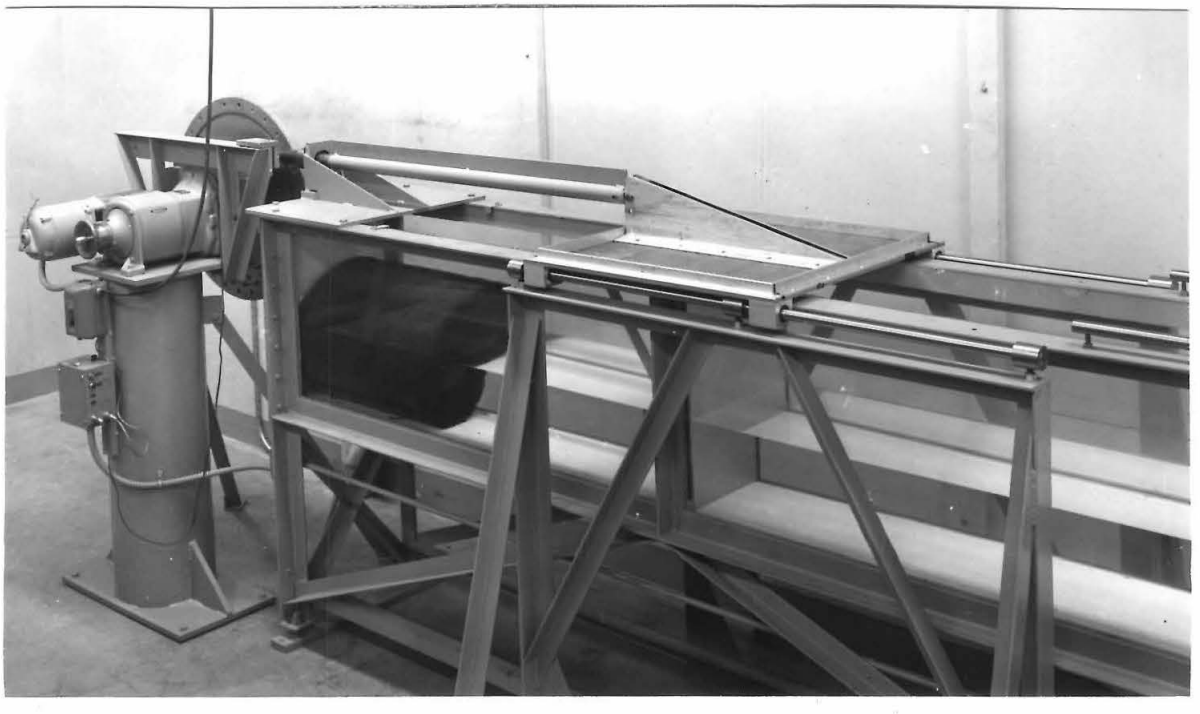

Figure 4.6. The wave generator for the 100-ft tank. 9445

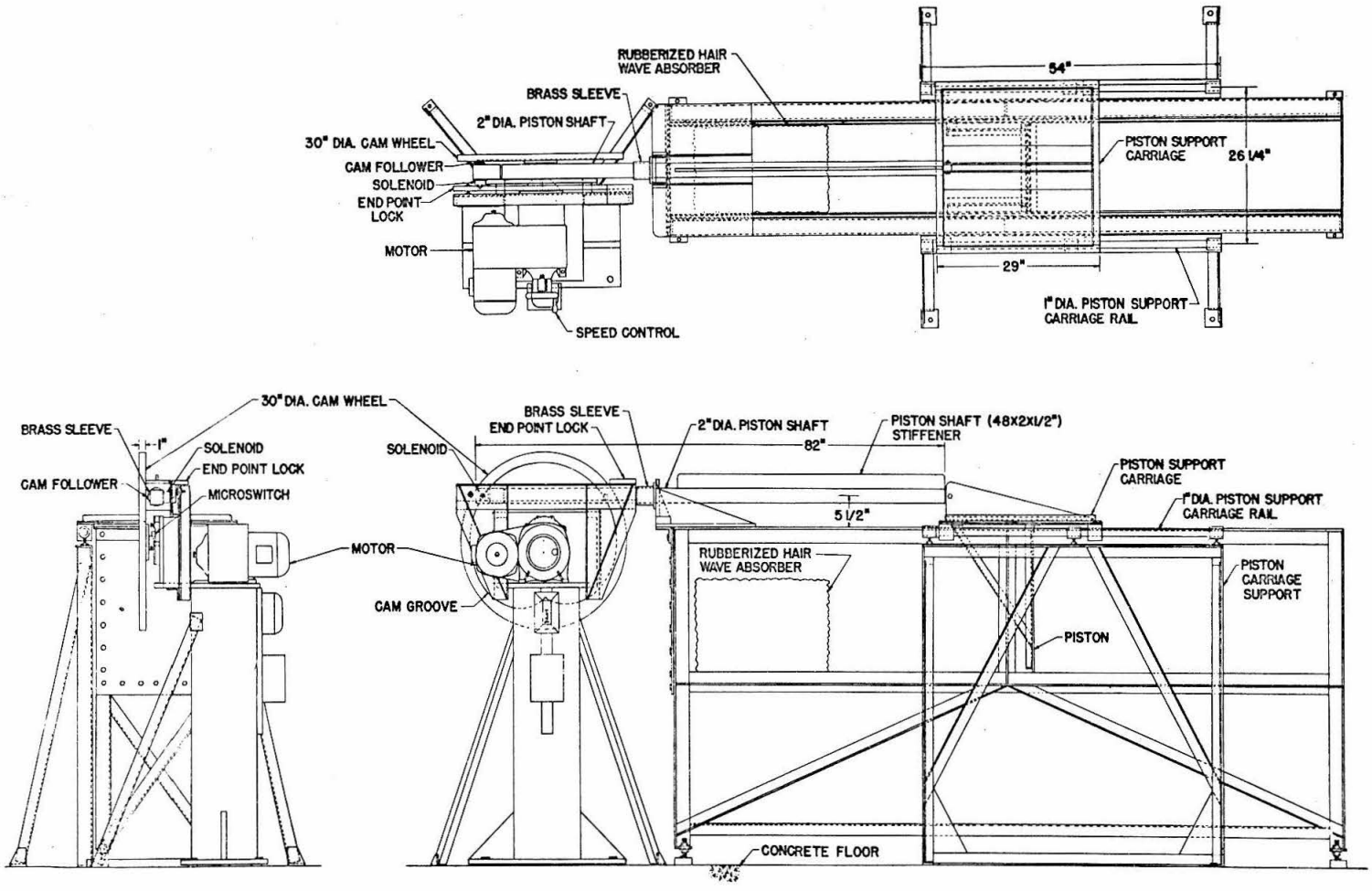

Figure 4.7. The wave generator for the 100-ft tank.

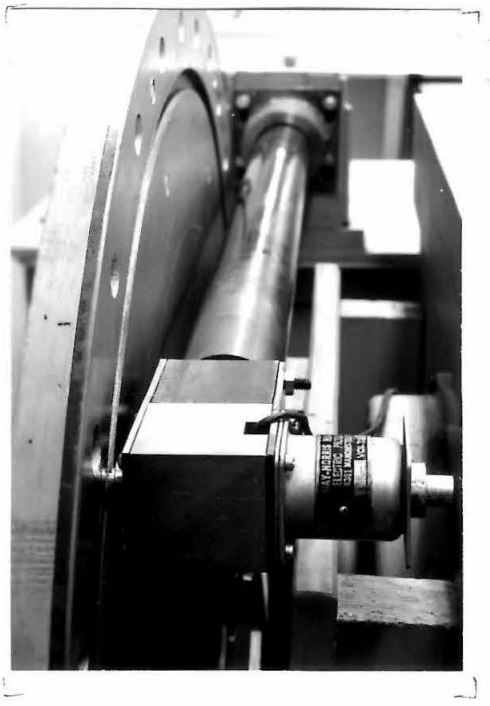

'9475

Figure 4.8. End view of the piston shaft (100-ft tank), showing cam wheel, cam follower sleeve, and solenoid. (End point lock has been removed).

the end of the piston shaft, with the cam follower sleeve appearing as a rectangular block. The solenoid is seen mounted on the sleeve on the side opposite the cam wheel. A portion of the cam follower may be seen inserted in the cam groove. The function of the end point lock (indicated in Figure 4.7 but not shown in Figure 4.8) will be described in the discussion of wave generator operation, to follow presently.

In the 100-ft tank, the forces of wave generation were large enough to require refinements in design not necessary in the 40-ft tank generator. The piston shaft was not rigidly bolted to the carriage but was pinned to it, and supported and constrained by a 4-in. brass sleeve fixed to the end of the wave tank. The shaft was a 2-in. steel tube with 1/8-in. wall thickness, 6-1/2 ft long. A 2-in. x 1/2-in. x 4-ft rib was welded to the shaft to reduce deflection. It was necessary to gusset the brass sleeve securely, to prevent binding and chatter. Proper alignment of the sleeve and lubrication of the shaft were also required for smooth operation.

The piston carriage travelled along 1-in. diameter stainless steel rails, mounted on steel supports which stood independent of the wave tank in order to reduce the amount of vibration transmitted to the tank. A roll of rubberized hair obtained from an upholsterer was placed at the end of the tank behind the piston, as shown in Figure 4.7. The roll did an excellent job of absorbing the disturbance behind the piston that occurred whenever a wave was generated.

The cam design was in part dictated by the range of values of still water depth d and wave height H to be studied, since the piston stroke for optimal wave form $D = 4\sqrt{\frac{Hd}{3}\left(1+\frac{H}{d}\right)}$ is dependent on d and H. In the 100-ft tank, for example, it was desired to generate waves

with a still-water depth d of 1.25 ft, and a height H ranging from 0.12 ft to 0.50 ft. A median wave height of 0.33 ft was chosen for design purposes. The stroke then required was D = 1.67 ft = 20 in.

In a normal cam system, such as that shown in Figure 4.9a, the cam follower moves along a line passing through the cam's center of rotation. To accomodate a total length of travel D, the cam must have a maximum radius R greater than D. In the 100-ft tank a cam of 20 in. radius seemed unwieldly. Therefore, a "chordal cam" was devised, where the cam follower moves not along the radius of a circle centered at the center of rotation, but along a chord or secant of that circle. As shown in Figure 4.9b, the maximum radius R of the cam groove can be substantially less than D (although not less than D/2). The form of the "heart-shaped" groove, characteristic of a chordal cam and evident in Figure 4.9b, is discussed further at the end of this subsection.

The essential parts of the wave generator are the piston, the piston shaft, the solenoid, the cam follower, the end-point lock, the cam wheel, the variable-speed motor, a microswitch, a double-pole - single-throw relay, and the trigger. The piston shaft is constrained to move only along its axis, and may not rotate about its axis. The solenoid, mounted on the end of the piston shaft, is of the type that both ends of the armature are exposed. The end of the armature called the "head" is used to lock the piston shaft at its initial and final positions. The other end of the armature, called the "toe", is connected directly to the cam follower.

The cam wheel, end point lock, and solenoid are shown schematically in Figures 4.10. The cam wheel and solenoid are shown in the photographs in Figure 4.11, with the end point lock removed for clarity.

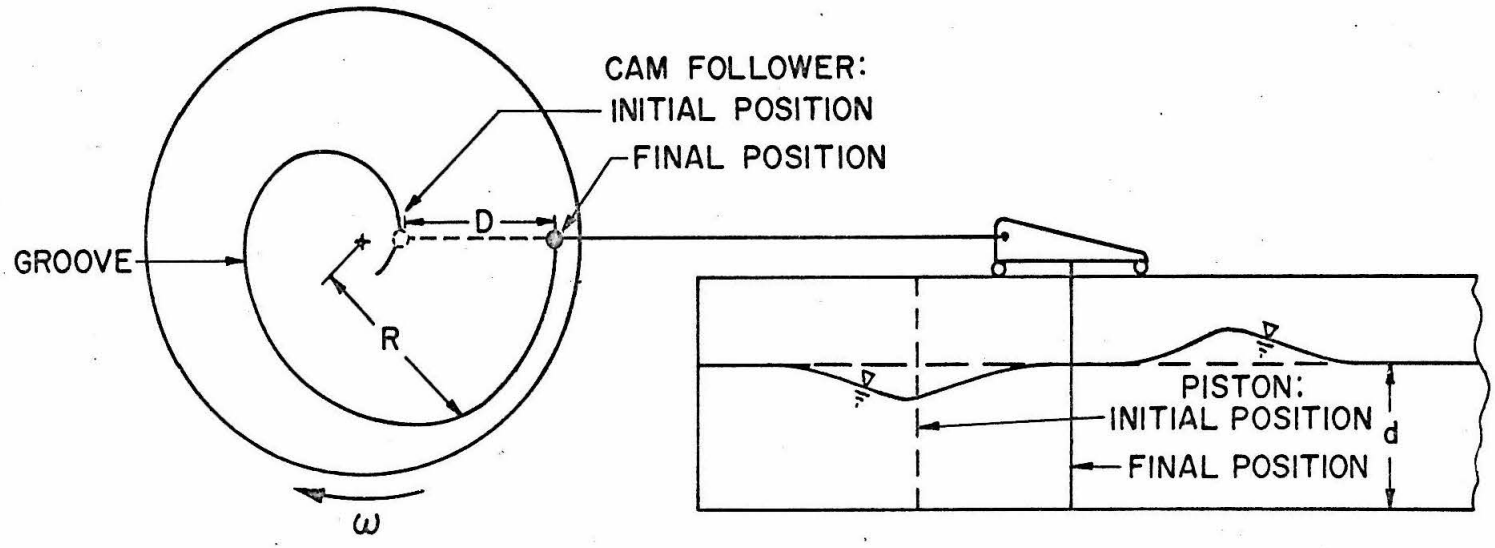

Figure 4.9a. A normal cam arrangement.

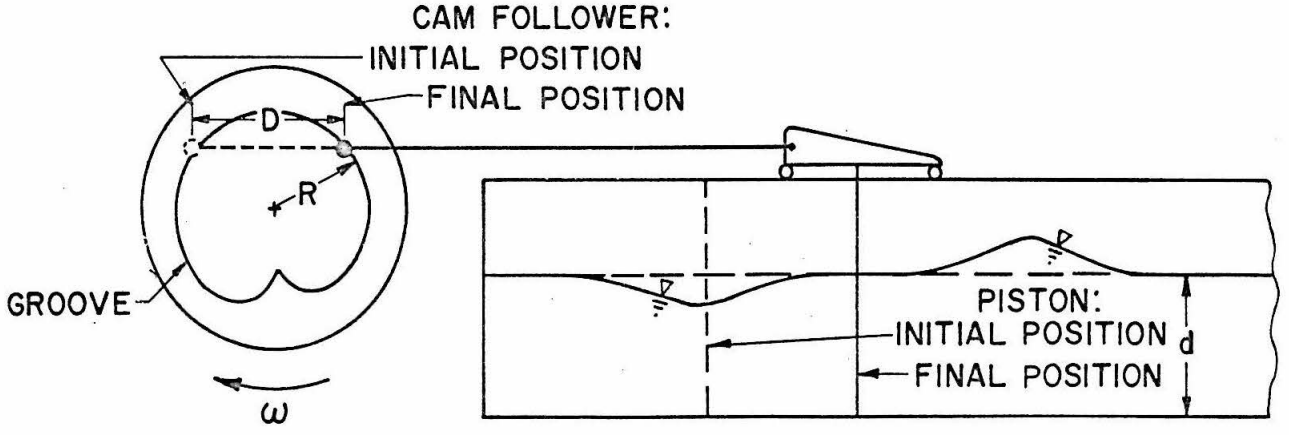

Figure 4.9b. A chordal cam arrangement.

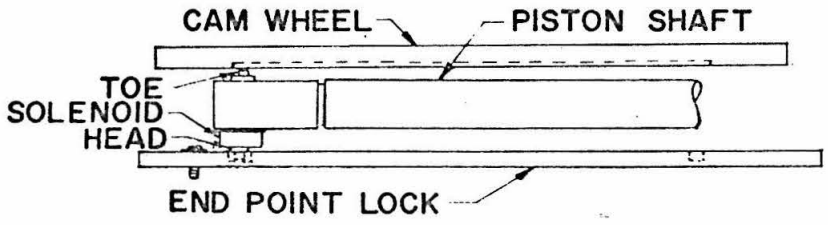

a. Beginning of stroke.

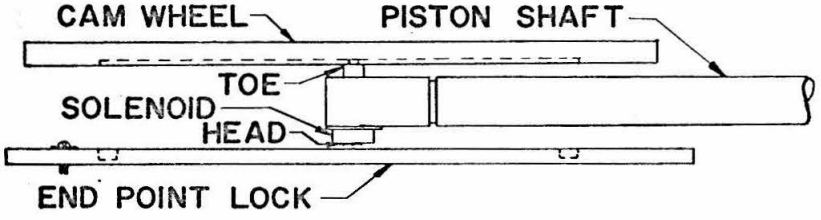

b. Midway through stroke.

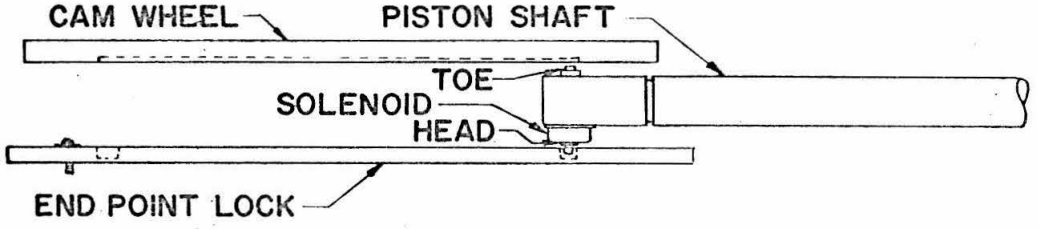

c. End of stroke.

Figures 4.10. Schematic diagrams of position of the piston shaft and solenoid with respect to the cam wheel and the end point lock.

9467

Figure 4.11a.
Beginning of stroke.

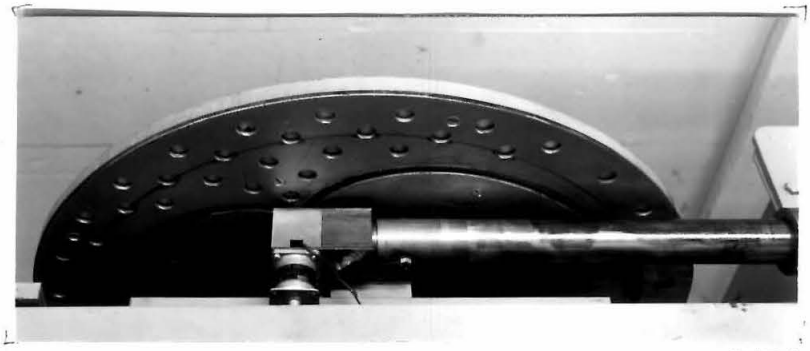

9470

Figure 4.11b.
During stroke.

9471

Figure 4.11c.
During stroke.

9472

Figure 4.11d.
End of stroke.

When no wave is yet to be generated, the solenoid is at rest. As shown in Figures 4.10a and 4.11a, the armature head protrudes into the end point lock, keeping the piston at its initial position, and the armature toe is retracted, keeping the cam follower retracted from the cam groove. The cam is free to turn unloaded at a constant velocity.

When a wave is to be generated, the solenoid is activated. The head is retracted, unlocking the piston shaft, and the toe is thrust out, driving the cam follower into its groove, as shown in Figures 4.10b, 4.11b, and 4.11c. The rotating cam wheel drives the piston shaft and piston through its stroke, at the end of which the solenoid circuit is broken. The spring-loaded armature then returns to its inactivated position, retracting the cam follower from the cam groove and inserting the head into the end point lock to keep the piston in its final position, shown in Figures 4.10c and 4.11d.

A double-throw microswitch and a relay are included in the solenoid circuit, shown in Figure 4.12, to ensure that the solenoid is switched on and off at the proper orientation of the cam wheel. A brad on the cam wheel trips the microswitch every cam revolution, when the cam wheel is in the position shown in Figures 4.9b, 4.11a, and 4.11d. When no wave is to be generated, the tripping of the microswitch has no effect.

When a wave is to be generated, the trigger is held closed until the next tripping of the microswitch, at which a circuit is completed: the relay and the solenoid are powered, the solenoid head is retracted from the end-point lock, and the cam follower passes into the cam groove. The relay keeps the solenoid circuit closed after the trigger is opened. The second tripping of the microswitch opens the relay

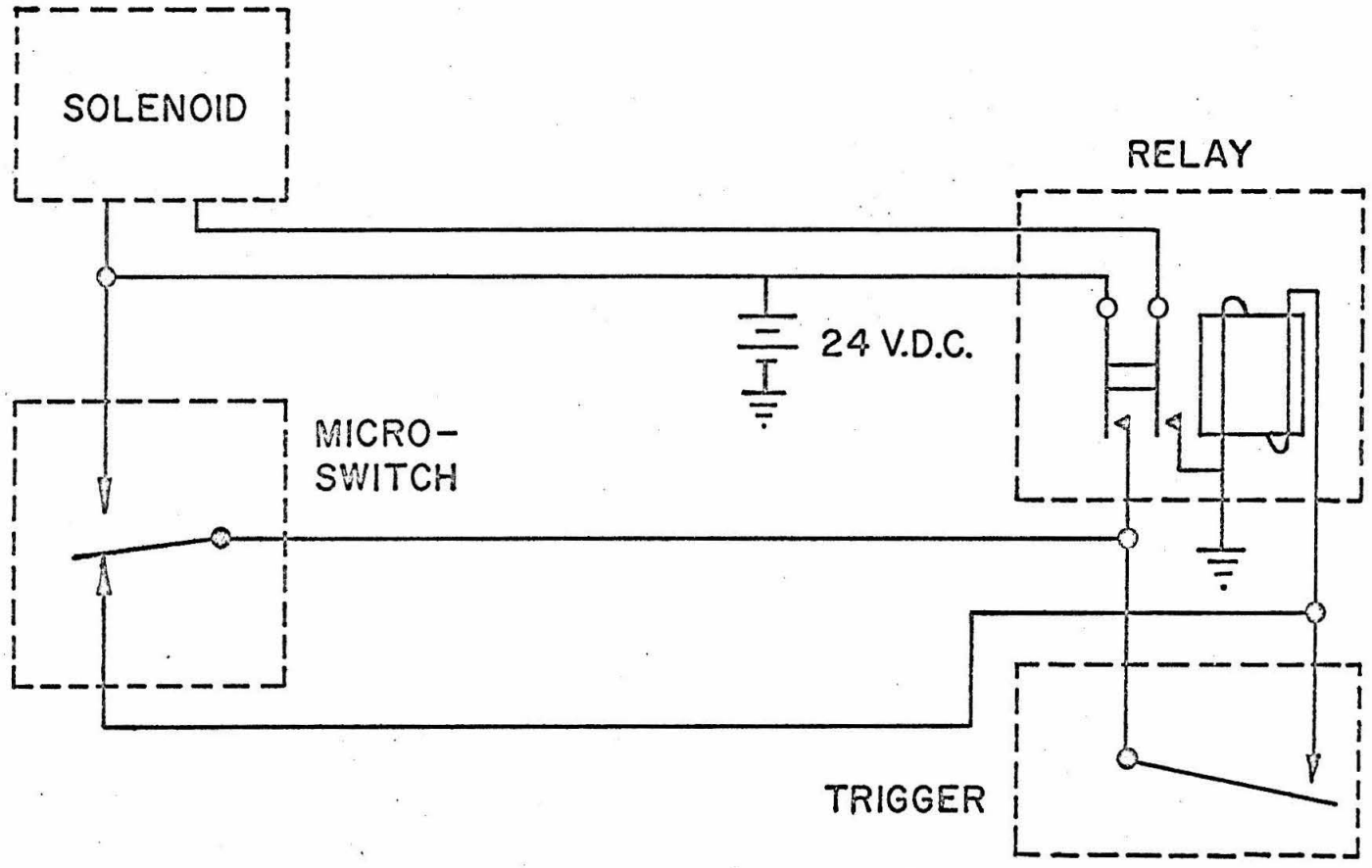

Figure 4.12. Solenoid circuit for the wave generator in the 100-ft tank. (Microswitch is in normal, or "untripped," position.)

circuit, thence the solenoid circuit. The cam follower, not at its final position, retracts from the cam groove, and the armature head protrudes into the end-point lock, preventing further motion of the piston. Before another wave can be generated, the piston must be returned to its original position by hand.

Discussion now returns to the cam groove, designed to give the cam follower the linear motion of Equation 4.4 when the cam wheel is rotating with constant angular velocity ω. The groove function $r = r(\theta)$, where r is the distance of a point on the groove from the center of the wheel and θ is its angular coordinate measured with respect to a particular radius turning with the wheel, is plotted in Figure 4.13a and is calculated as follows:

Within a fixed circle of radius R, the path of the cam follower is along a chord of length D, as shown in Figure 4.13b. The center of the chord is a distance c from the center of the circle. A point on the chord whose distance from the chord center is x_p and whose distance from the center of the circle is r may be considered to represent the position of the cam follower. The angle θ_o is the angular coordinate of this position of the cam follower measured with respect to the vertical radius of the fixed circle. It may be noted that $r^2 = x_p^2 + c^2$ and that $\theta_o = (\cos^{-1} c/r)\ \mathrm{sgn}\ (x)$.

From Equation 4.4, it is required that $x_p = D/2 \tanh \Omega (t + t_o)$ where Ωt_o has been set equal to zero, or that:

$$t = \frac{1}{\Omega} \tanh^{-1} \left[\left(\frac{2}{D} \right) \sqrt{r^2 - c^2} \right] \mathrm{sgn}(x_p). \qquad (4.5)$$

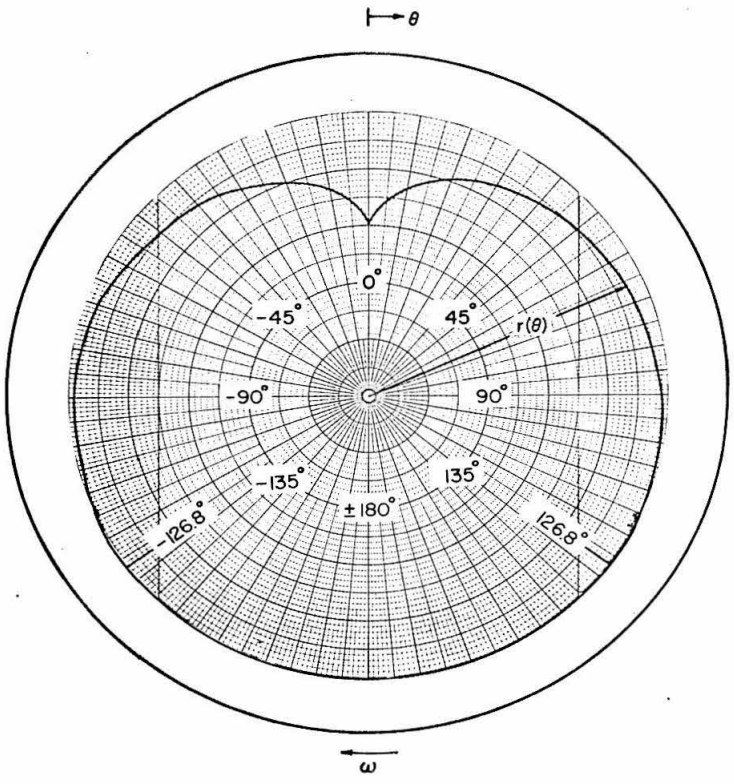

Figure 4. 13a. The cam groove function $r(\theta)$.

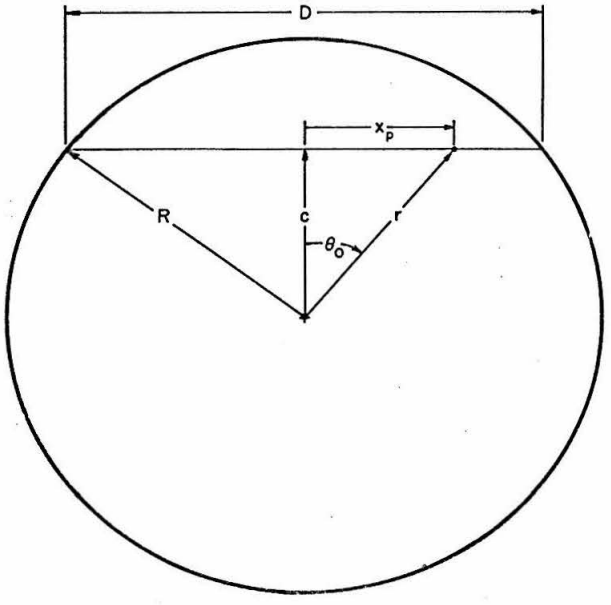

Figure 4. 13b. Path of cam follower shown with respect to center of cam wheel.

If the cam wheel is considered to be concentric and coplanar with the circle and to be rotating clockwise with constant circular frequency ω, the angular coordinate of the cam follower measured with respect to a particular radius rotating with the wheel will be:

$$\theta = \theta_o - \omega t. \tag{4.6}$$

The radial coordinate will still be r. By combining Equations 4.5 and 4.6 to eliminate t, one finds that:

$$\theta = \cos^{-1}\left[\frac{c}{r}\right] \operatorname{sgn}(x_p) - \frac{\omega}{\Omega} \tanh^{-1}\left[\frac{2c}{D}\sqrt{\left(\frac{r}{c}\right)^2 - 1}\right]\operatorname{sgn}(x_p). \tag{4.7}$$

One may note that $\theta = \theta_o = 0$ and $x_p = 0$ when $t = 0$.

Thus as the cam follower moves according to Equation 4.4 and as the cam wheel rotates, Equation 4.7 relates the radial coordinate r of the cam follower to the angular coordinate θ measured with respect to the wheel. Conversely, when the cam groove is cut according to Equation 4.7 and the wheel rotates at a circular frequency, ω, the cam follower is constrained to move according to Equation 4.4.

Equation 4.7, a form of the groove function $r = r(\theta)$, is plotted on polar coordinate paper in Figure 4.13a for $c/D = 3/8$ and $\omega/\Omega = 4/3$, which were the values used in building the generators. Only the portion of the groove for which $-126.8^\circ < \theta < +126.8^\circ$ was utilized; at these limits the groove is nearly tangent to the circle of radius R. The groove shape was taken directly from the shape of the plotted curve; for the generator in the 40-ft tank, D = 8 in.; for the generator in the 100-ft tank, D = 20 in.

The choice of values of ω/Ω and c/D strongly influences the shape of the groove function near $\theta = 0$. For small θ, Equation 4.7 may be approximated as:

$$\theta = \frac{x}{c}\left(1 - \frac{\omega}{\Omega}\,\frac{2c}{D}\right). \tag{4.8}$$

For $(1-2\,\omega c/\Omega D) < 0$, the groove function is smooth, resembling a circle with a "dimple" in it at $\theta = 0$. When $(1-2\omega c/\Omega D) = 0$, the "dimple" becomes the cusp shown in Figure 4.13a. For $(1-2\omega/\Omega D) > 0$, the cusp becomes a "nodule" similar to that of a prolate cycloid. Of these three configurations the only one practically applicable as a cam is the cusped one; hence it was required that $\frac{\omega}{\Omega} = \frac{D}{2c}$. The quantity c/D was chosen so that D would be within the range $R < D < 2R$. (In operation, the cusp caused an unavoidable roughness in piston motion. However, as will be shown in Section 6.1, the quality of the generated wave appeared to be not at all affected by the irregular motion that resulted when the cam follower passed the cusp.

Properly, each size of solitary wave demands its own values of D and ω. For a given cam wheel, D is obviously not variable. However, as will be shown in Section 6.1, it was found that by merely changing ω a satisfactory range of wave heights, with waves of consistently good form, could be produced.

A problem did arise in the 100-ft tank when operating at a depth d of 0.64 ft, a still water depth that was considerably less than that for which the cam wheel was designed. At the slowest possible motor speed the waves, although of good form, were much higher than desired. The solution was to insert the cam follower in the groove, and turn the cam wheel by hand through part of a cycle to about the position shown in

Figure 4.11b. When a wave was desired, the motor was switched on, the cam wheel would complete its cycle, and the piston would move through its shortened stroke. The initial form of waves thus generated was not as good as for full-stroke generation, but the tank was long enough to allow the waves to stabilize into satisfactory form by the time they reached the test section, as shown by profiles presented in Section 6.1. Fortunately the acceleration characteristics of the motor remained sufficiently constant from test to test so that with a constant reduced stroke length, the waves were as reproducible as with full-stroke generation.

4.3. The Platforms.

In each tank, the platform had a flat, horizontal underside (hereinafter termed the "soffit"), spanning the entire width of the tank. The soffit was made and kept as smooth as possible. Each platform had a flat, vertical front face high enough to prevent incident waves from splashing over the top of the structure.

The platform in the 40-ft tank was constructed of 10-in. wide anodized aluminum channel with a 1/2-in. web. This channel was cut in two 2-1/2-ft lengths, and was supported by a 5-ft steel frame. One could thus use a single section as a 2-1/2-ft platform, or both sections together as a 5-ft platform. The steel frame was suspended from three large C-clamps, supported by angles laid across the top of the tank. The narrow spaces between the platform and tank wall were caulked with plasticene, scraped smooth on the bottom so that the horizontal plane of the soffit was continued uniformly out to the vertical wall. The weight of the structure and the viscosity of the plasticene resisted

upward movement of the structure due to wave forces; no upward movement was observed.

Five pairs of holes were drilled in one section so that the transducers could be mounted at different locations. The holes were arranged in pairs so that the two transducers could sample the "two-dimensional" wave simultaneously at the same distance from the seaward end of the platform, i.e. the end closer to the wave generator. Where there were no transducers mounted, the holes were securely plugged. The flush-mounted transducers and plugs kept the platform soffit a smooth, plane surface.

In the 100-ft tank the platform was a 1/2-in. thick x 15-in. wide x 5-ft long anodized aluminum plate, shown in a dimensioned drawing in Figure 4.14. Two longitudinal ribs were attached to the upper side to give the plate stiffness. A 1/2-in. thick aluminum plate formed the vertical front face. Sponge rubber adhesive stripping was used to caulk the 1/8-in. space between the platform and the tank walls to prevent the passage of water or air. The structure was suspended by three 3/4-in. threaded bars suspended from two pieces of structural steel channel clamped across the top of the tank. Two struts bolted to the rear of the platform and to the top edge of the tank prevented the platform from moving longitudinally.

As with the platform in the 40-ft tank, the holes in which transducers could be mounted were arranged in pairs so that two transducers could sample pressure simultaneously at the same distance from the seaward end of the platform. Seven pairs of holes were drilled one inch either side of the platform centerline. The distances from the centerlines of the seven pairs of holes to the seaward end of the

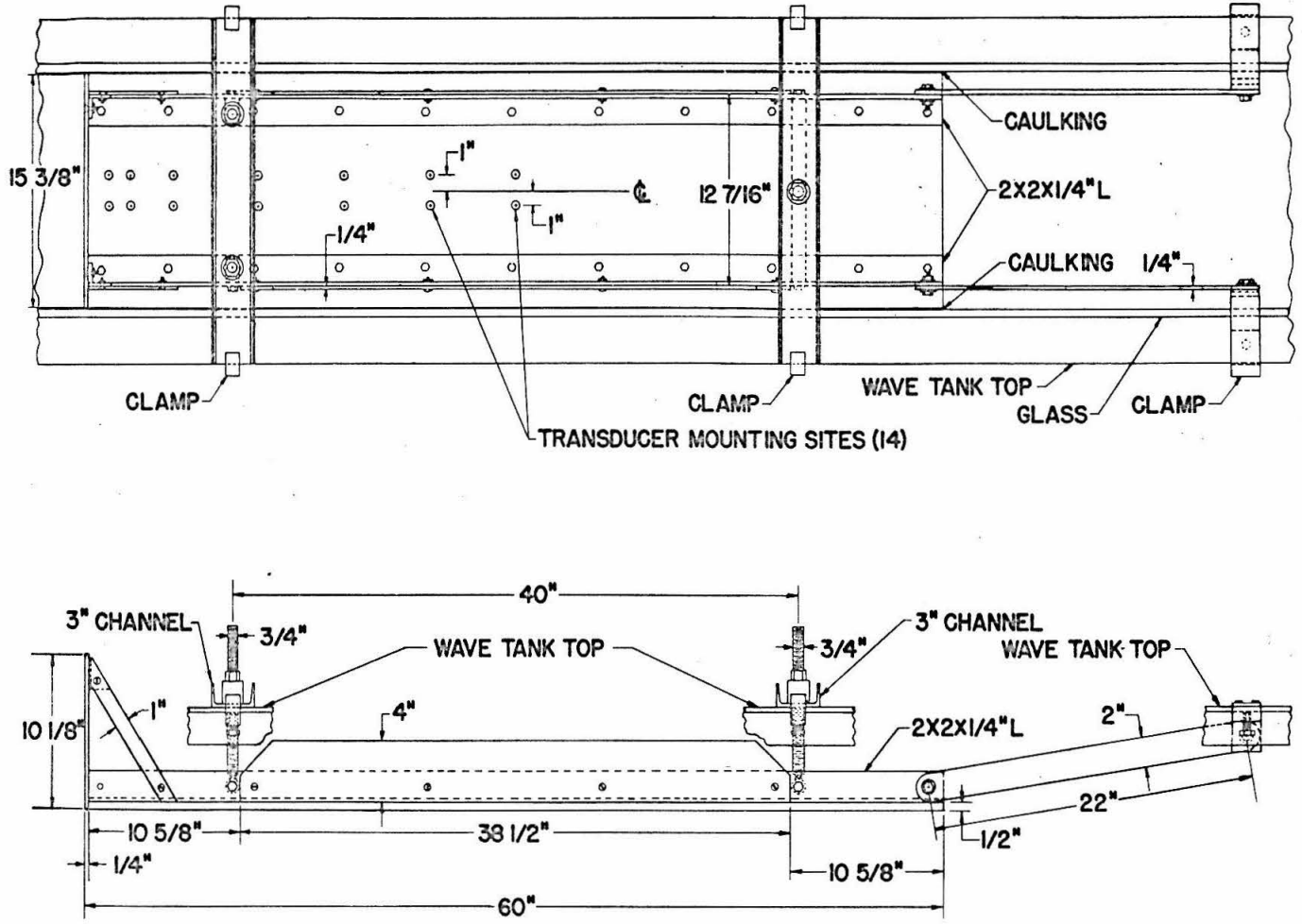

Figure 4.14. Drawing of test platform (100-ft tank).

platform are listed in Section 6.3. As in the 40-ft tank, each hole not occupied by a transducer was fitted with a plug, so that the soffit retained a smooth plane surface.

As it was desired to keep the soffit as smooth as possible, the number of holes was minimized by drilling no holes at a distance from the leading edge greater than half the platform length. The structure was designed so that the supporting bars, the struts, and the vertical front plate could be attached to either end of the basic plate. To measure pressures on the rear half of the platform, therefore, the unit could be removed from the tank, and the basic 1/2-in. plate (but not the front plate, the supporting bars, or the struts) could be turned through 180°, and the unit reassembled and returned to the tank.

The platform was levelled by measuring the soffit clearance along the front and rear edges with a hook gauge on a vernier scale accurate to ± 0.0005 ft.

4.4. Apparatus and Techniques of Measurement.

The parallel-wire resistance gauge shown in Figure 4.15 was used for continuous measurement of the water surface elevation at a given point. The wave gauge was composed of two 0.010-in.-diameter stainless steel wires 9 in. long, stretched taut and parallel between the arms of a stainless steel C-frame. The wires were electrically insulated from each other, except that current could pass from one wire to the other through the water in which the gauge was immersed. The recorder output signal was proportional to probe conductance, which in turn was proportional to the depth of immersion of the wires. (A typical wave gauge trace is shown in Figure 4.18b, to be discussed presently.) The gauge, mounted on a rack-and-pinion graduated in

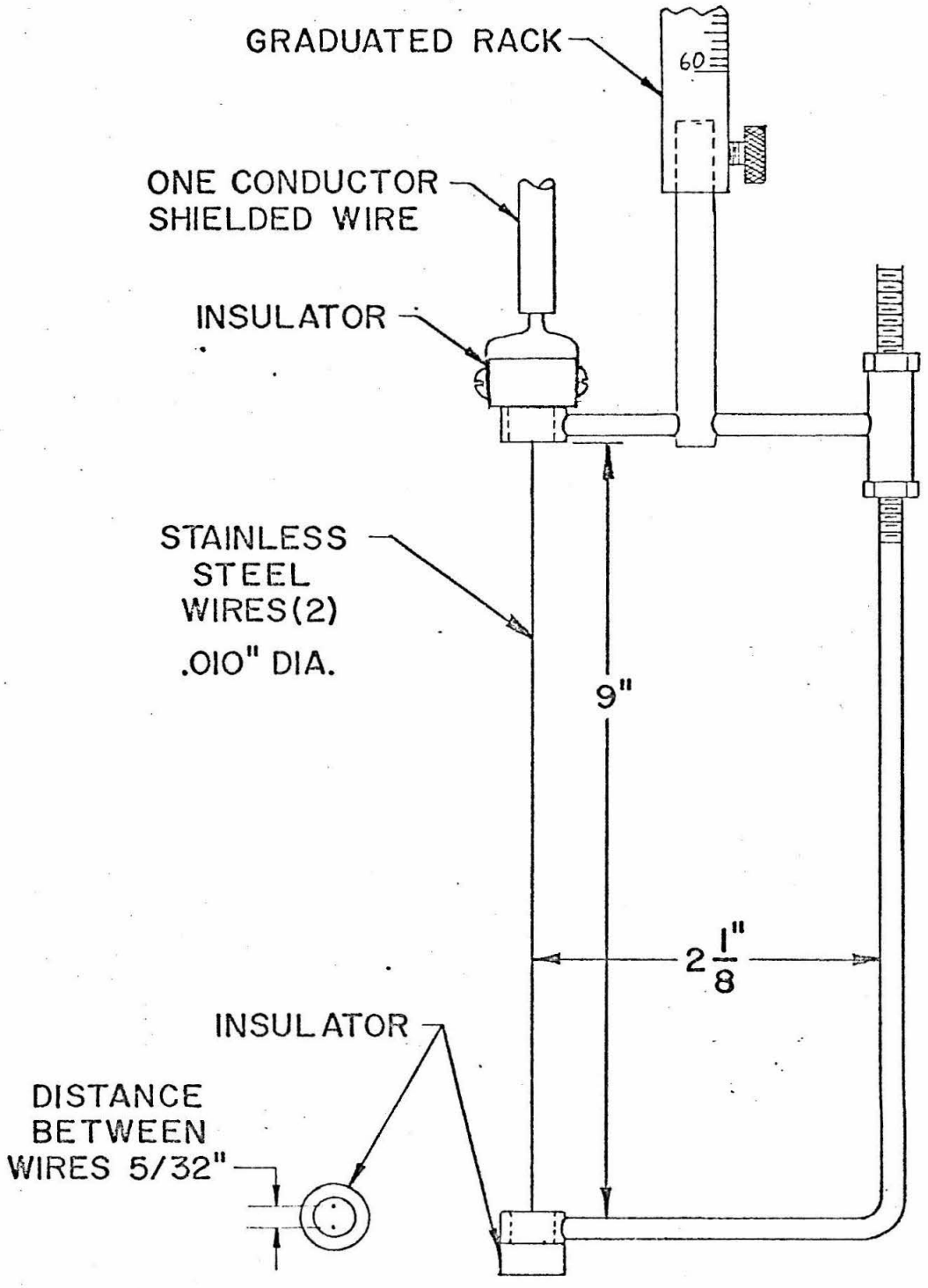

Figure 4.15. A parallel-wire resistance wave gauge.

feet, was calibrated by immersing it into still water a known amount and then retracting it. Typical wave gauge calibration curves are shown in Figure 4.16 for calibration approximately one hour apart.

Three point gauges were used to measure wave front celerity. Each point gauge was wired to one channel of a recorder so that when the point was grounded by contact with water, the recorder pen would make a simple deflection.

The signal from the wave gauge and the three point gauges was recorded simultaneously by a four-channel Sanborn Series 150 recording system. The circuitry consisted essentially of a Wheatstone Bridge circuit excited by 2400 cps alternating current at 4.5 volts. The AC supply and half of the bridge elements were contained in the Sanborn Model 150-1100AS Carrier Preamplifier. The external half of the bridge was constructed of precision wirewound resistors.

As shown in Figure 4.17, the probe formed part of one arm of the external half-bridge. The wave gauge was connected to terminals A and B, and the point gauges simply to terminals B in their respective channels.

The use of an alternating excitation current prevented electrolysis on the wires of the wave gauge.

To measure the celerity of the solitary wave, the three point gauges were mounted along the tank centerline, separated by known distances x_1 and x_2, as shown in Figure 4.18a. The points were raised above the stillwater level a common distance δ, roughly 1/3 to 2/3 the height of the waves to be generated. Using a multi-channel recorder, it was easy to measure the time interval between initial deflections on two adjacent channels, as shown in Figure 4.18b.

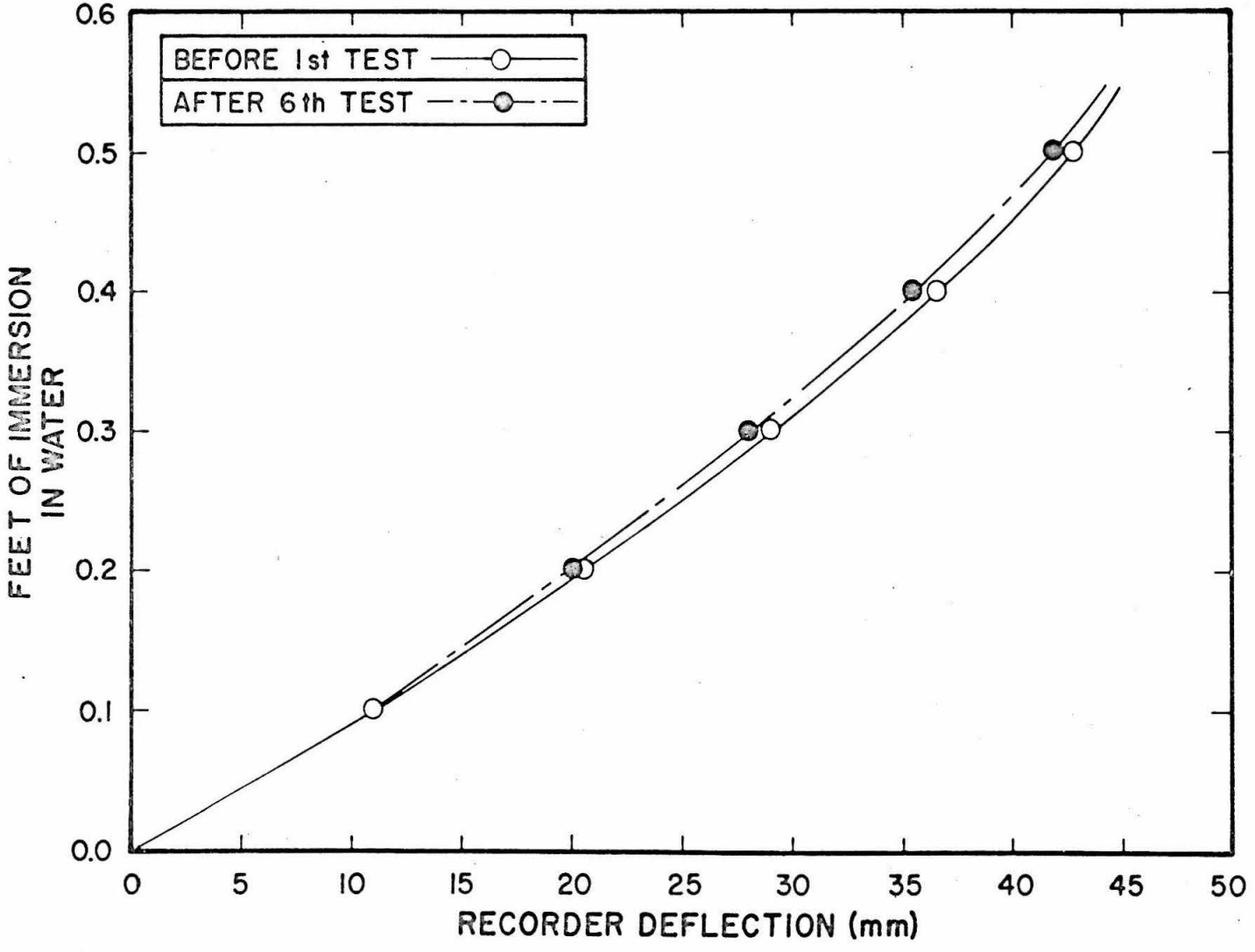

Figure 4.16. Typical calibration curves for the wave gauge.

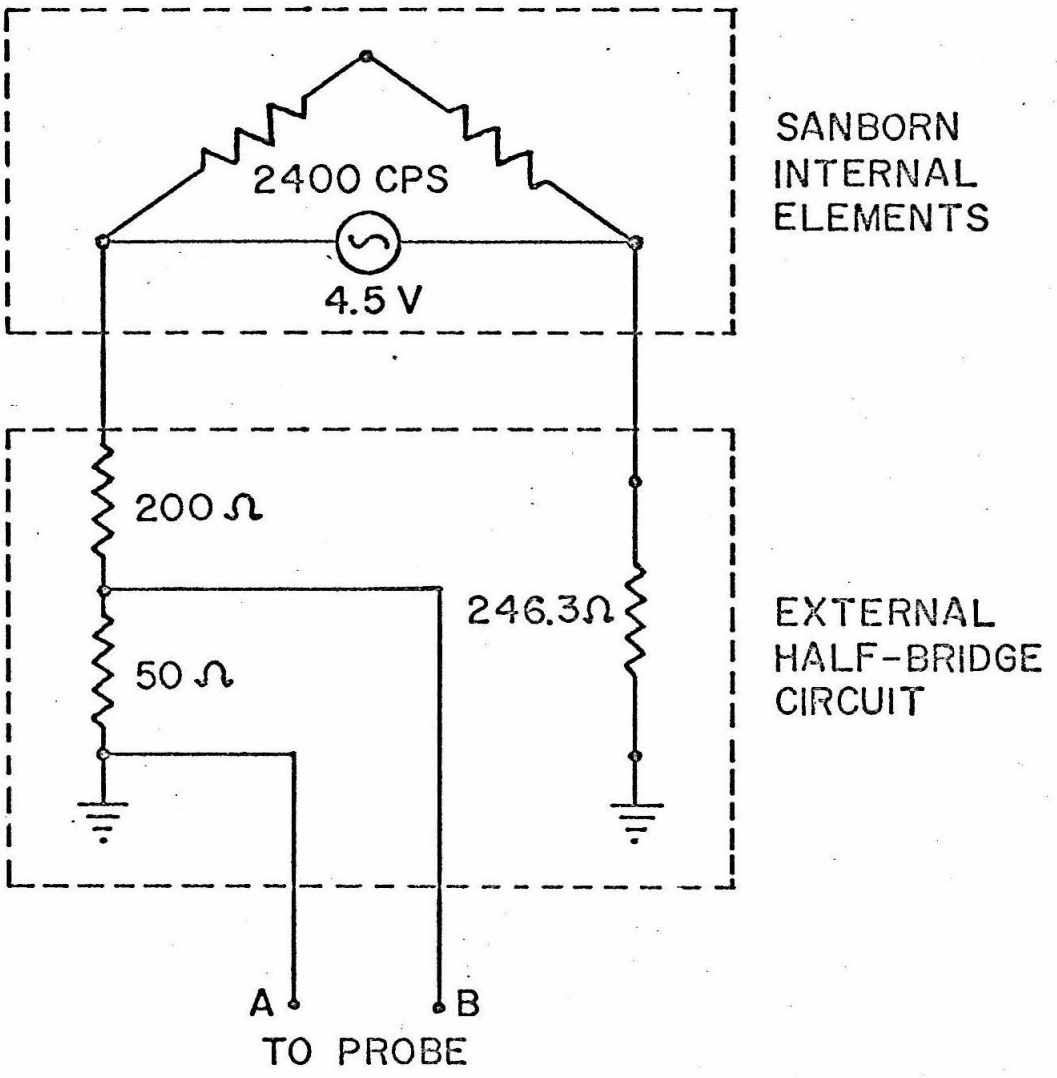

Figure 4.17. Schematic diagram of wave gauge circuit.

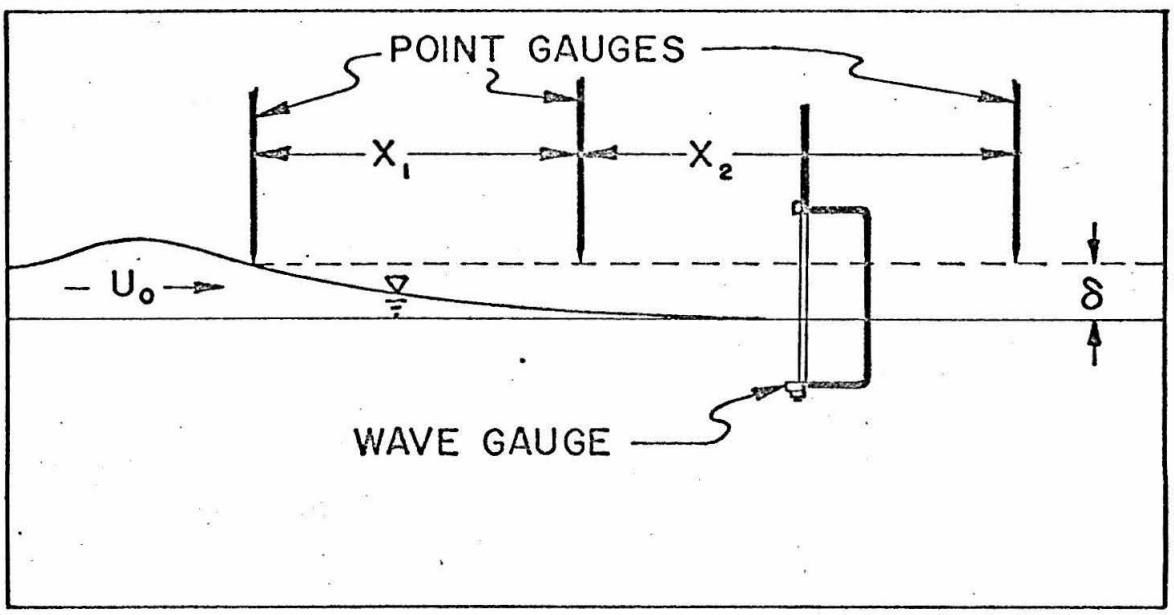

Figure 4.18a. Diagram of the wave measurement system.

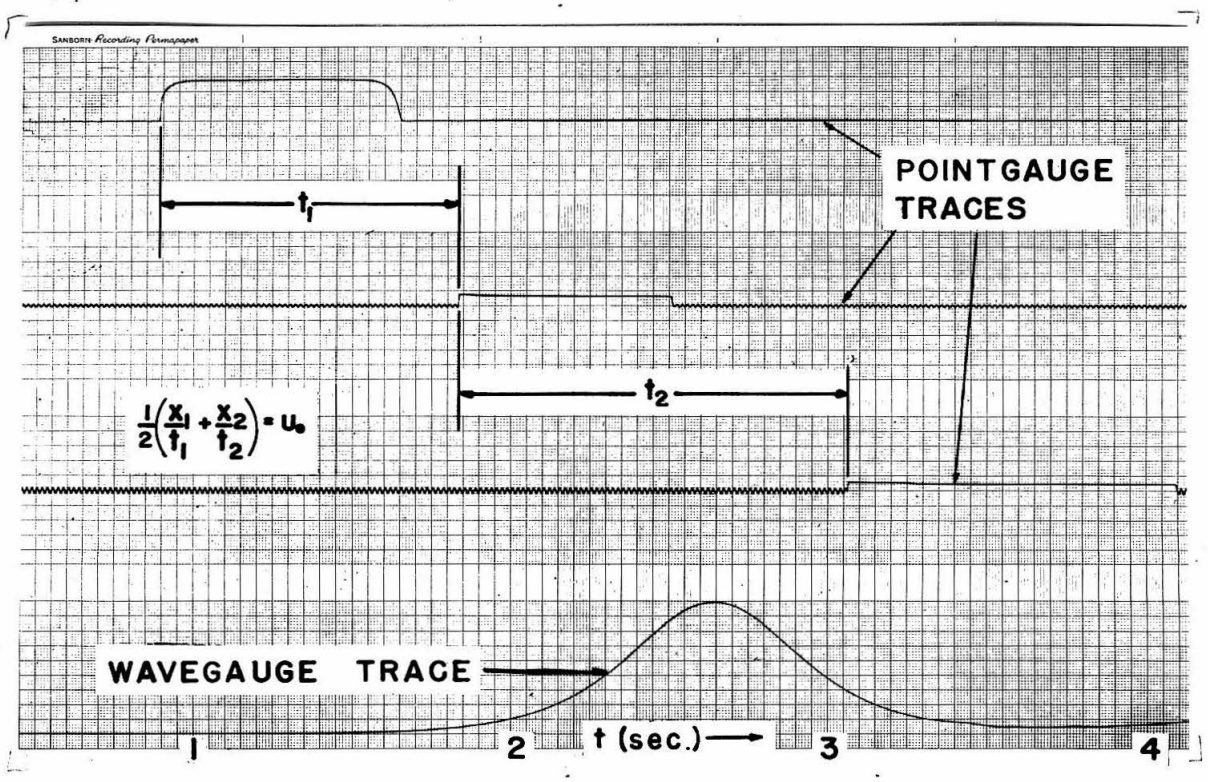

Figure 4.18b. A typical record for wave profile and celerity.

This time interval divided into the distance separating the corresponding gauges is the average wave celerity between the gauges.

The pressure measuring system is shown schematically in Figure 4.19 and in Figures 4.20 and 4.21. Two strain-gauge type pressure transducers shown in Figure 4.20, each excited by a D. C. voltage source, were mounted in the test platform so that their external sensitive diaphragms were flush with the platform soffit. One transducer was a Statham Model PM 131 TC, in which an unbonded strain gauge containing all four arms of a Wheatstone Bridge circuit was connected to the center of a thin, circular stainless steel diaphragm of 1/2-in. external diameter. The excitation voltage used was 12 V. From this transducer the signal was amplified 1000-fold by a Dynamics Model 6450 differential D. C. amplifier, and recorded on a multi-channel Consolidated Electrodynamics Corporation Model 5-124A recording oscillograph, equipped with two model 7-362 fluid-damped galvanometers and with a flash timer. According to the manufacturer's specifications, the Model 7-362 galvanometer has an undamped natural frequency of 4150 cps. An external resistance of 200Ω was connected in series with each galvanometer, as recommended by the manufacturer, to provide a damping ratio of 0.64. The timer, consisting essentially of a mercury discharge lamp in a resistance-capacitance circuit, marked the moving recorder paper at intervals of 0.01 ± 0.0003 sec. (A warm-up period of about 20 minutes was necessary to ensure a constant flash rate.) The other transducer was a Schaevitz-Bytrex Model HFD-2, enclosed in a special adapter for reasons to be discussed presently. Two Wheatstone Bridge elements, composed of semiconductor filaments, were in the probe itself, and the other

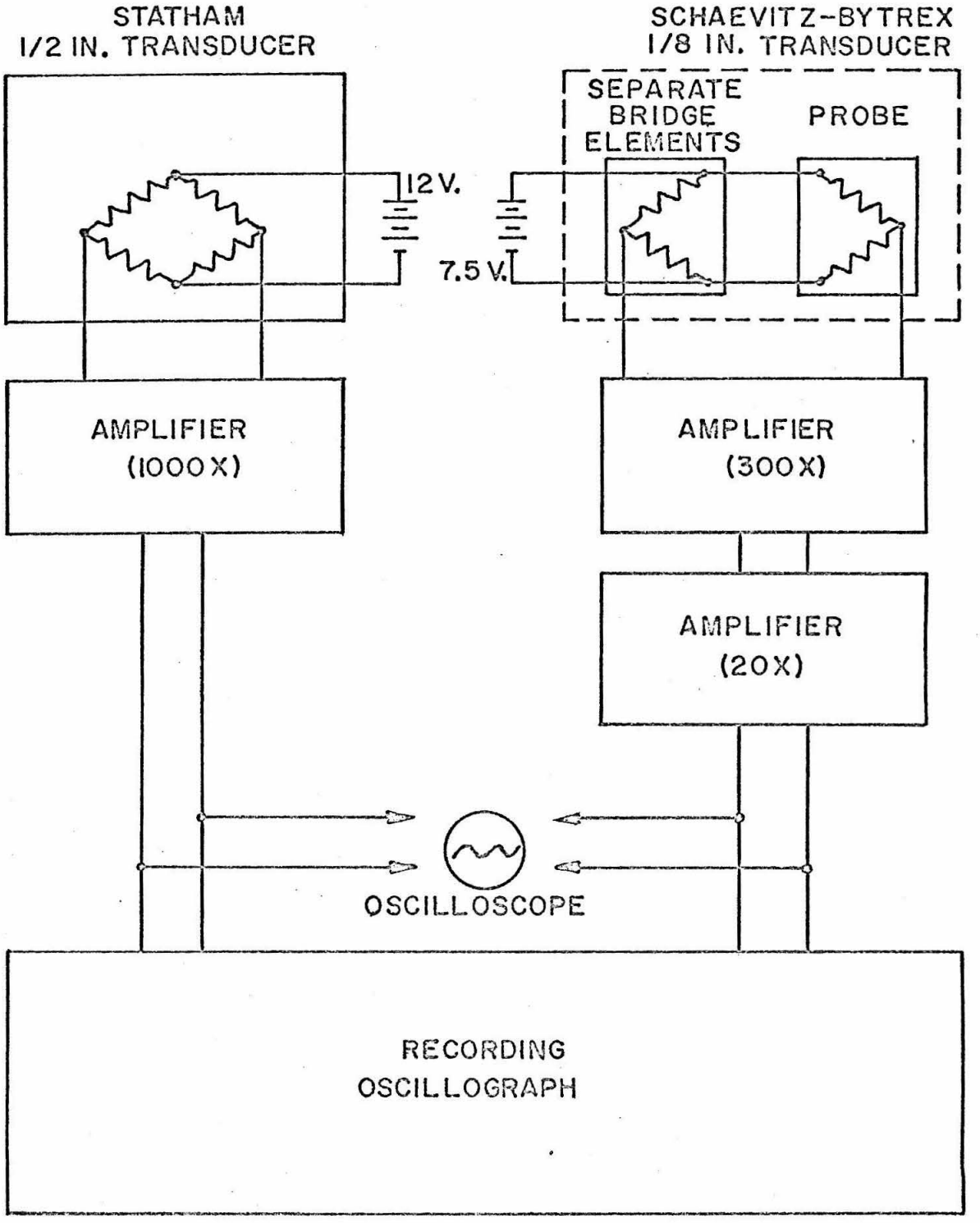

Figure 4.19. Schematic diagram of the pressure measurement system.

Figure 4.20. (right). the 1/2-in. Statham transducer (left) and the 1/8-in. Schaevitz-Bytrex transducer in adapter, with outer diaphragm and oil removed.

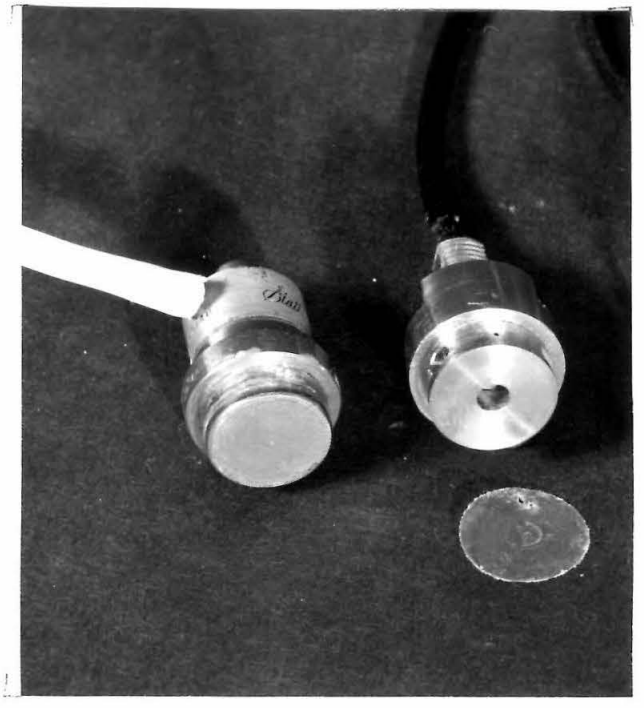

9633

Figure 4.21. (below). From left to right: the Kintel amplifier, two Dynamics amplifiers, CEC recording oscillograph.

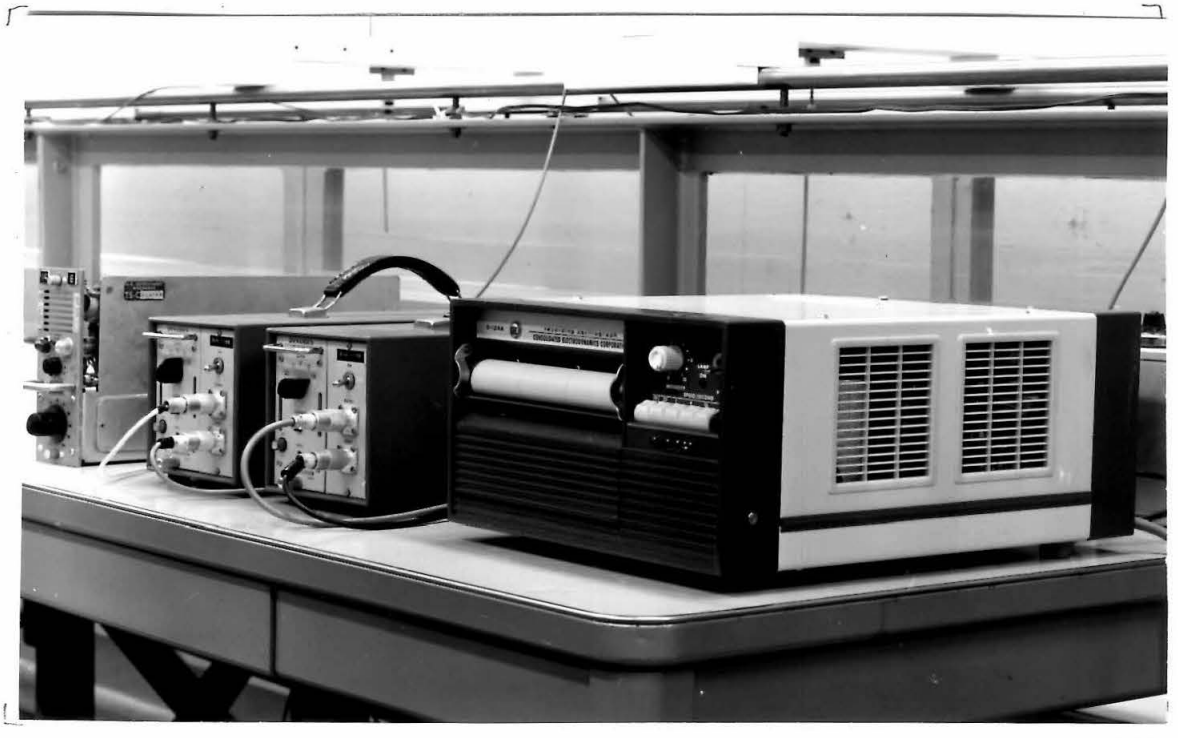

9446

elements were in a separate unit. The excitation voltage used was 7.5 V. The output signal was amplified 300-fold through a Dynamics 6450 amplifier and 20-fold through a Kintel Model 111 BF D. C. amplifier, thence recorded on the CEC oscillograph. Occasionally a Tektronix Model 310A cathode-ray oscilloscope was connected in parallel with the oscillograph on one or the other of the transducer channels.

As will be explained in Chapter 5, analysis of spatial transducer resolution requires knowledge of internal transducer structure. According to a publication of the manufacturer (Stedman, 1967), the sensitive diaphragm of the Statham Model PM 131 TC is machined in one piece, with a reinforcing boss in the center and a stiff ring around the outside, as shown in Figure 4.22a. Therefore, while the external diameter of the diaphragm is 1/2 in. (i.e. the radius is 1/4 in. or 0.0208 ft), the radius of the sensitive area is somewhat less than 0.0208 ft, due to the thick outer ring providing reinforcement. The effective radius, or radius of the sensitive area of the diaphragm, is estimated to be 0.016 ft, based on the diagram accompanying the manufacturer's notes (Stedman, 1967). The reinforcing boss in the center is connected to the unbonded strain gauge containing all four arms of the Wheatstone Bridge circuit.

The 1/8-in. Schaevitz-Bytrex pressure transducer was employed because its smaller size provided improved spatial resolution, as will be explained in Chapter 5. Yet as originally mounted, with its sensitive diaphragm exposed directly to the air or water beneath the test platform, it suffered a significant shift in output signal due to changes in temperature. The silicon semiconductor transducing element

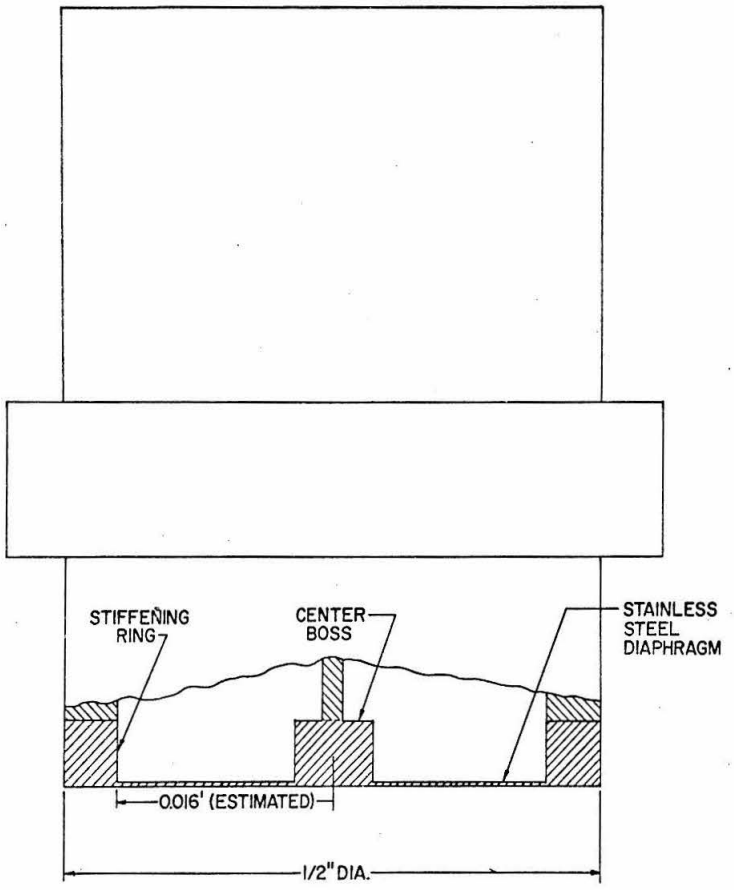

4.22a. A cutaway view of the Statham 1/2-in. transducer.

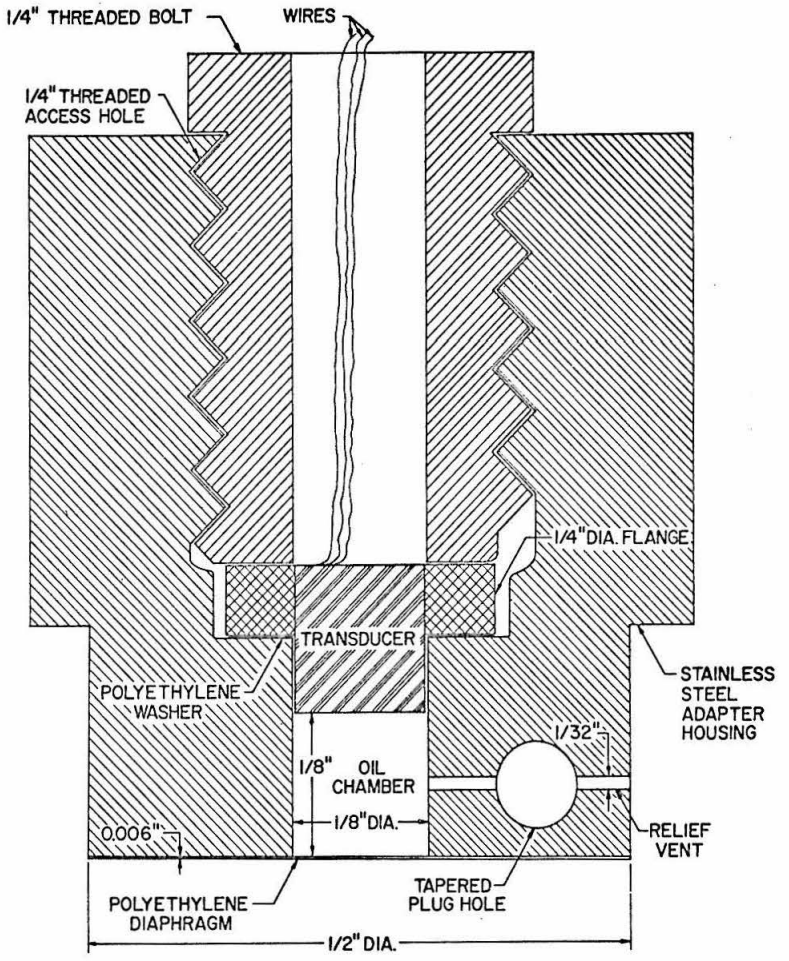

4.22b. A sectional view of the 1/8-in. Schaevitz-Bytrex transducer in its 1/2-in. adapter.

carried an electric current when operating and was thus a source of heat, which was conducted away to the metal of the platform and to the air beneath the platform. When water in a wave touched and flowed past the transducer diaphragm, the rate of heat conduction was increased and the sensitive element was cooled significantly, causing a shift in output obscuring any pressure signal which should have been recorded.

To solve or at least ameliorate the temperature-shift problem, three tactics were tried. The first was to reduce the excitation voltage, to reduce the amount of heat generated; the second was to cool the transducer, or heat the water in the wave tank; the third was to insulate the transducer thermally from the water in the wave.

Reduction of the excitation voltage from the rated value of 25 V to 1.5 V reduced the temperature shift considerably with respect to the recorded pressure function. However, reduction of the excitation voltage led to a small output voltage, so that the signal-to-noise ratio was reduced.

It was found that by heating the water in the tank a few degrees Celsius, the zero shift could be nullified or reversed. However, it was evident that to heat the tank water above room temperature would introduce unwanted problems of temperature control, and convection and stratification of the fluid. As an alternative it was attempted to cool the transducer by enclosing it in a brass jacket through which ice-water was circulated. Here, too, the zero shift could be nullified or reversed, but again it was impracticably difficult to determine the flow of coolant necessary for consistent nullification of the zero shift.

The problem was eventually solved to an acceptable degree by mounting the transducer in an adapter, so that the sensitive diaphragm was recessed behind a 1/8-in. x 1/8-in. oil-filled chamber sealed with an external diaphragm of polyethylene, as shown in Figures 4.20 and 4.22b. The adapter housing was machined out of stainless steel, with external dimensions equal to those of the Statham 1/2-in. transducer so that holes drilled in the platform could accommodate either the 1/2-in. transducer or the 1/8-in. transducer in its adapter. The 1/8-in. diameter, 1/8-in. long chamber was drilled from the plane, circular end of the adapter, and connected with a 1/4-in. threaded access hole drilled from the other end of the adapter. A 1/32-in. relief vent was drilled from the side of the adapter to the chamber, and a tapered hole for a plug to close the relief vent was drilled through the adapter, intersecting the relief vent perpendicularly. A diaphragm of adhesive polyethylene tape, 1/2-in. in diameter and 0.006 in. thick, was attached to the plane, circular end of the adapter. Since the transducer as provided by the manufacturer was cylindrical, a 1/16-in. thick by 1/4-in. outer-diameter ring was cemented to it to provide a flange for purposes of mounting.

The transducer was mounted in the adapter as follows: the adapter, with polyethylene diaphragm attached, was immersed in a bath of oil deep enough to insure that the chamber, relief vent, and tapered plug hole were completely filled with oil, with no air bubbles remaining. The oil used was Dow Corning "200 Fluid" silicone oil with a dynamic viscosity of 1 centipoise at 250C. The transducer was set in place, with a washer of polyethylene between the transducer flange and the end of the access hole; and then secured firmly by a

threaded bolt screwed into the access hole. (The core of the threaded bolt was drilled out to accommodate the wires leading from the transducer). With the adapter containing the mounted transducer still immersed in oil, a smooth, tapered teflon plug was driven firmly into the plug hole to seal the relief vent, thereby completing the assembly procedure.

(The unit as shown in Figure 4.20 is partially disassembled. The polyethylene diagram, shown lying separate from the unit, has been removed, and the oil has been drained, permitting a view into the oil chamber. The diaphragm of the transducer itself is partially visible at the inner end of the chamber. As the unit lies on the table, the outer end of the relief vent is visible on the top of the adapter. Both ends of the tapered plug hole are visible, indicating that the plug hole passes through the adapter above the oil chamber, intersecting the relief vent.)

The diameter of the sensitive area of the external polyethylene diaphragm was 1/8-in., as was that of the unmodified transducer. Pressure was satisfactorily transmitted through the polyethylene diaphragm and silicon oil to the transducer, yet the thermal insulation provided by the oil reduced the temperature shift to a small fraction of its former value. Using an excitation voltage of 7.5 V, less than one third the rated voltage of 25 V, also helped reduce the temperature shift.

To determine the extent of amplitude distortion and phase shift introduced by the pressure measurement system, the dynamic properties of the pressure transducers, the amplifiers, and the recording oscillograph were analyzed. It was assumed that the transducers and

galvanometers could be treated as damped single-degree-of-freedom harmonic oscillators, for which the equation of motion is (White, 1948):

$$j(t) = K'y(t) + B\frac{dy}{dt} + M\frac{d^2y}{dt^2}, \tag{4.9}$$

where j(t) is the applied forcing function, y is the resultant displacement or output, K' is the static proportionality constant of input force to output displacement, B is the damping coefficient, and M is the mass. The undamped natural frequency of such a system is $f_n = \sqrt{K'}/(2\pi\sqrt{M})$, and the damping ratio is $\zeta = B/(4\pi f_n M)$. For a sinusoidal input function $j = j_o \sin\left[(2\pi f)\right]$, the output will be $y = y_o \sin\left[(2\pi f)t - \epsilon\right]$, where the ratio of output to input amplitudes is given by:

$$\frac{K'y_o}{j_o} = \frac{1}{\sqrt{\left[1 - (f/f_n)^2\right]^2 + \left[2\zeta f/f_n\right]^2}}, \tag{4.10}$$

and the phase shift is:

$$\epsilon = \tan^{-1}\left[\frac{2\zeta f/f_n}{1 - (f/f_n)^2}\right]. \tag{4.11}$$

Equation 4.10 may be rewritten as:

$$\frac{K'y_o}{j_o} = \frac{1}{1 - (f/f_n)^2}\sqrt{\frac{1}{1 + \tan^2\epsilon}}. \tag{4.12}$$

The natural frequency f_n and the damping ratio ζ of the two transducers were determined experimentally by lightly tapping the transducer housing with a sharp object in order to excite free oscillations at the natural frequency of the instrument. The output, after amplification, was displayed on the cathode-ray oscilloscope, where

the trace was photographed. Tests were made with each transducer in air, and with the sensitive diaphragm immersed in water to simulate operating conditions. Figure 4.23a shows a typical output trace from the 1/2-in. transducer in air; Figure 4.23b shows a typical output trace from the 1/8-in. transducer with oil-filled chamber, with the outer diaphragm of the unit in contact with water.

The free damped oscillations of the instrument may be described by Equation 4.9 with the forcing function j set equal to zero. A solution to the equation is:

$$y = y_o \exp\left[\left(-\frac{B}{2M} \pm 1/2 \sqrt{\left(\frac{B}{M}\right)^2 - \frac{4K'}{M}}\right)t\right]. \tag{4.13}$$

When $(B/M)^2$ is less than $4K'/M$, the second term in the exponent is imaginary, and gives the function y(t) the form of a sine wave whose amplitude is $y = y_o \exp(-Bt/2M)$, and whose diminished frequency is:

$$f_d = \frac{1}{2\pi} \sqrt{\frac{K'}{M} - \frac{1}{4}\left(\frac{B}{M}\right)^2} \ . \tag{4.14}$$

The damped natural frequency f_d was obtained directly from the photographs of the oscilloscope traces by dividing the number of cycles shown per screen division by the oscilloscope beam sweep rate, measured in seconds per division. The ratio B/2M was computed by comparing the amplitudes of oscillation $Y = y_o \exp(-Bt/2M)$ measured at two different times t_1 and t_2:

$$\frac{Y_1}{Y_2} = \frac{y_o \exp(-Bt_1/2M)}{y_o \exp(-Bt_2/2M)}, \tag{4.15}$$

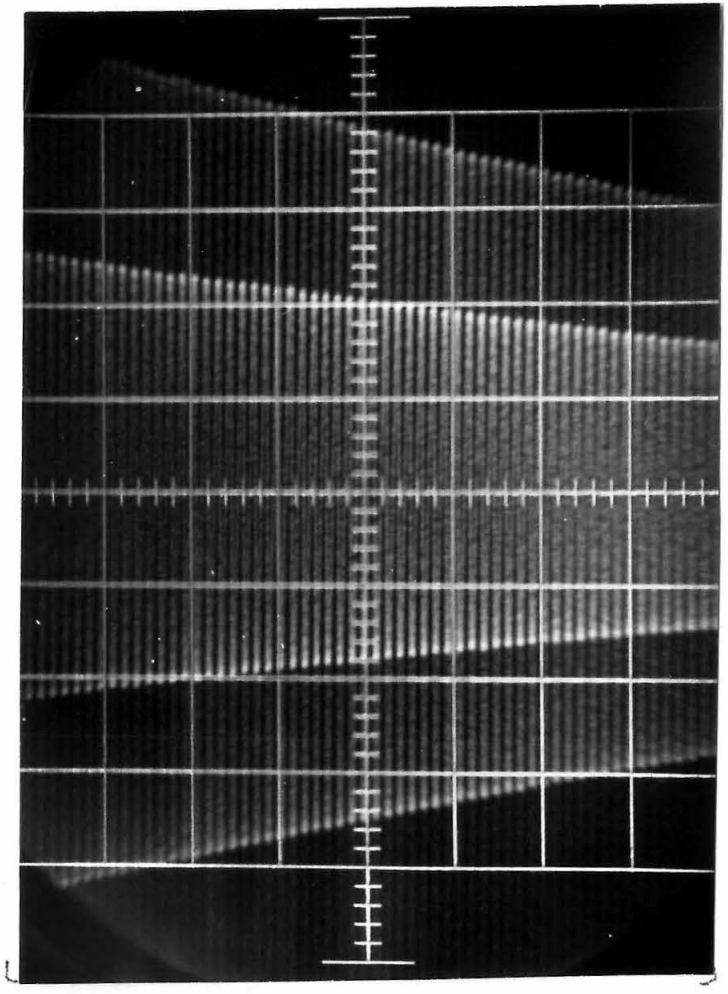

9008

Figure 4.23a. Damped free oscillations of the 1/2-in. Statham transducer in air. (Horizontal scale: 2 millisec/div.)

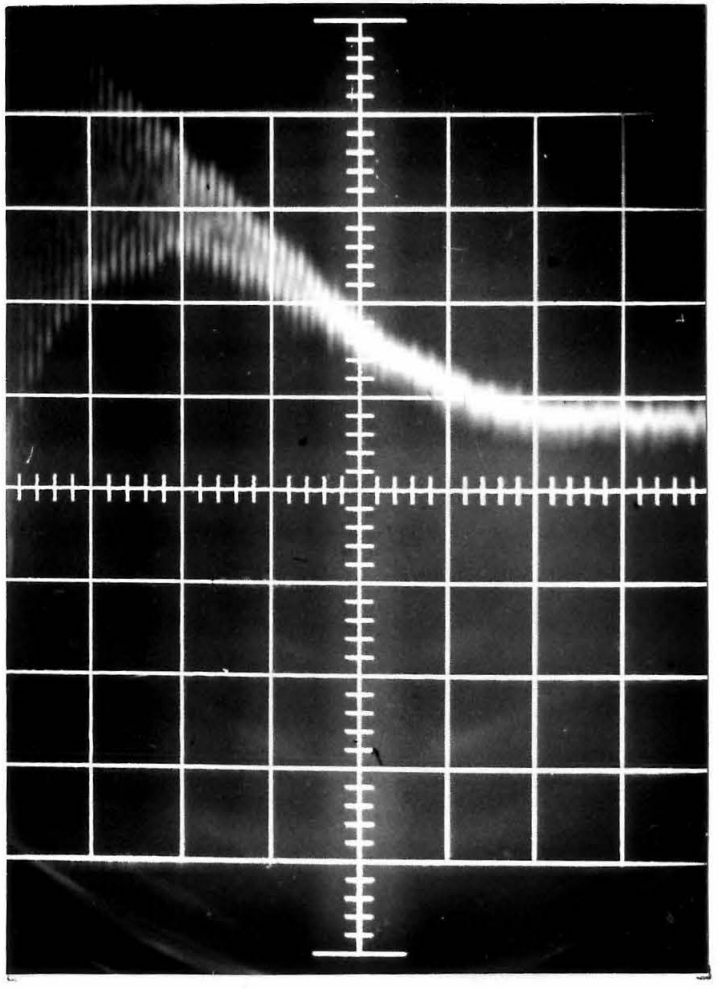

8996

Figure 4.23b. Damped free oscillations of the 1/8-in. Schaevitz-Bytrex transducer with oil chamber, in water. (Horizontal scale: 500 microsec/div.)

which when rearranged becomes:

$$\frac{\ell_n (Y_1 / Y_2)}{t_2 - t_1} = \frac{B}{2M} . \tag{4.16}$$

With f_d and B/2M known, the undamped natural frequency $f_n = \sqrt{K'}/(2\pi\sqrt{M})$ and the damping ratio $\zeta = B/(4\pi f_n M)$ were computed. The two sets of measured values for the 1/6-in. Schaevitz-Bytrex transducer with oil chamber were obtained before and after the testing program, a time interval of approximately one year.

The measured values of f_n and ζ for the two transducers in air and in water are presented in Table 4.1. Also presented is the rated natural frequency of the 1/2 in. transducer, supplied by the manufacturer. A value of natural frequency for the 1/8-in. transducer with the oil chamber, computed from known characteristics of the unmodified transducer, considering the mass of oil, but neglecting the stiffness of the external polyethylene diaphragm, is also included. (Details of the computation are provided in Appendix C.) Manufacturer's rated values of f_n and ζ for the CEC 7-362 galvanometer are also included.

The amplitude response of the two types of amplifiers used were tested by exciting each amplifier with a sine wave of variable frequency, and displaying the result on the oscilloscope screen. The displayed amplitude was measured for frequencies ranging from 1 kilocyc/sec to 16 kilocyc/sec. To eliminate the effect of amplitude variation in the sine-wave generator, amplitude of the generated wave displayed directly on the oscilloscope without amplifiers was measured over the same range of frequencies. At each frequency tested, the

Table 4.1. Dynamic characteristics of components in the pressure-measurement system.

COMPONENT	EXPERIMENTS				PREDICTED OR RATED	
	IN AIR		IN WATER			
	f_n (kilocyc/sec)	ζ	f_n (kilocyc/sec)	ζ	f_n (kilocyc/sec)	ζ
CEC 7-362 galvanometer (with 200 Ω in series)					4.15[a]	0.64[a]
1/2-in. Statham transducer	3.61	0.00090	3.50	0.00122	3.50[a] (in air)	
1/8-in. Schaevitz-Bytrex transducer with oil chamber	24.3[b] 24.1[c]	0.00808	20.3	0.01904	20.8[d]	

Notes: a) Manufacturer's rating.
b) Measured before testing program was begun.
c) Measured after testing program was completed.
d) Calculated value, with mass and stiffness of outer diaphragm neglected (see Appendix C).

ratio of amplifier output amplitude to signal generator input amplitude was normalized with respect to the ratio obtained at a frequency of 1 kilocyc/sec.

In Figure 4.24, the amplitude response $K'y_o/j_o$, determined from Equation 4.10, is plotted as a function of frequency f for the 1/8-in. transducer and the 1/2-in. transducer (using measured values of f_n and ζ from tests in water) and for the CEC 7-362 galvanometer (using rated values of f_n and ζ). The measured amplitude response, or normalized ratio of output to input amplitudes, is also included for two models of amplifier used.

It should be noted here that the Tektronix 310A oscilloscope used to determine the curves presented in Figure 4.24 is rated as having a frequency range of zero to 4000 kilocyc/sec., with an accuracy of $\pm 3\%$. Since the frequency range examined is well within the range of capability of the oscilloscope, the measurements should be free of error introduced by that instrument.

For accurate measurement, amplification, and recording of the pressure signal, it is necessary to have constant amplitude response over the range of frequencies represented in the input pressure function. Figure 4.24 shows that all system components except the 1/2-in. Statham transducer have an amplitude response of $1.00 \pm .05$ up to a frequency of 3 kilocyc/sec, above which the galvanometer response decreases steadily. The amplitude response of the 1/8-in. Schaevitz-Bytrex transducer with its oil chamber, and the response of the two amplifier models, is $1.00 \pm .05$ up to 4.5 kilocyc/sec. (It is of interest to note that the amplitude response of the sub-system consisting of the 1/8-in. transducer, the Dynamics 6450 amplifier, and the

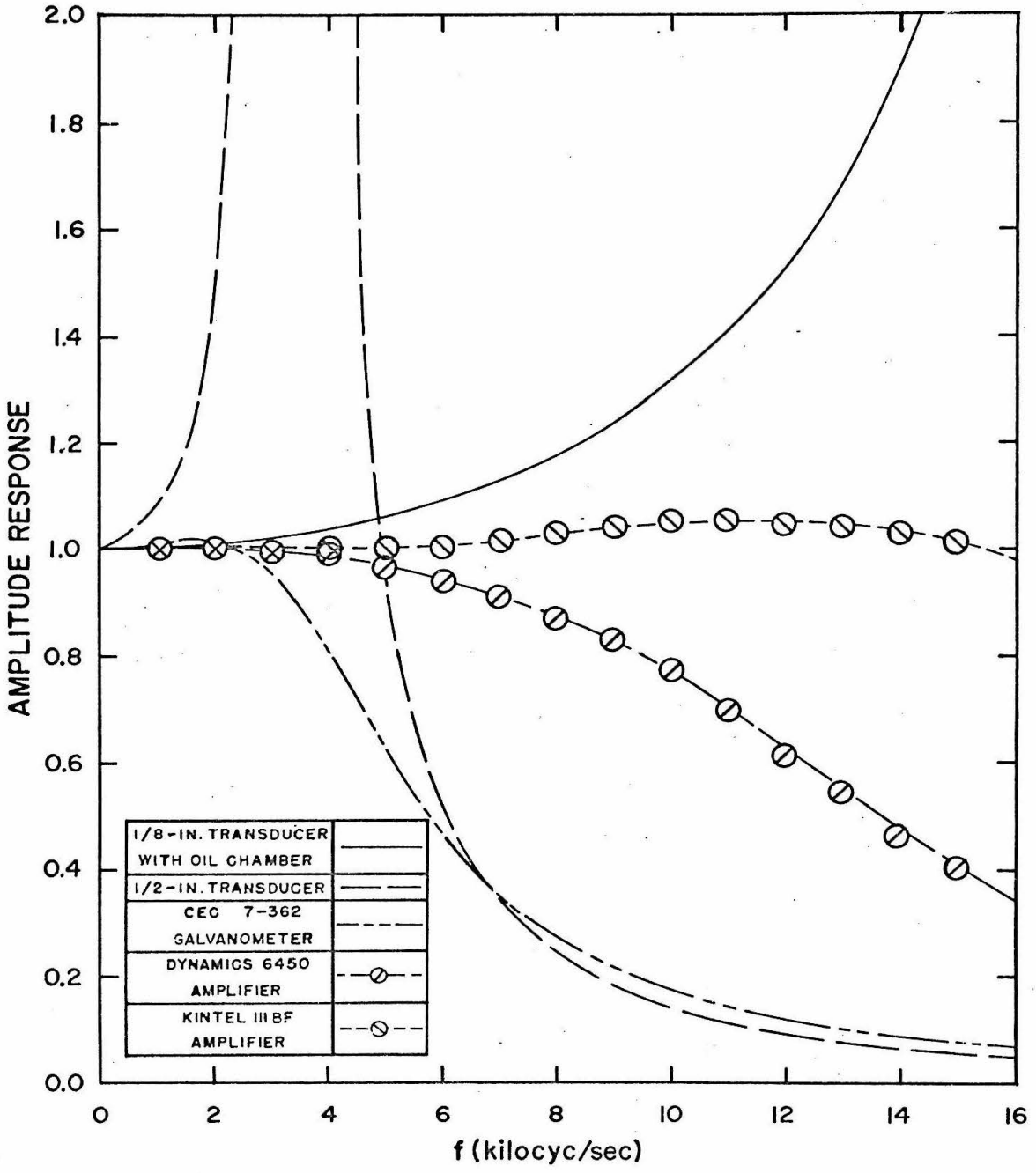

Figure 4.24. Dynamic amplitude response as a function of input frequency, for each component of the pressure-measuring system.

Kintel 111 BF amplifier will, at a given frequency, be the product of the amplitude responses of the three components at that frequency. Thus computed, the amplitude response of the subsystem is $1.00 \pm .07$ for frequencies up to 14 kilocyc/sec.)

Therefore, for recorded measurements obtained with the 1/2-in. transducer, the Dynamics 6450 amplifier, and the CEC 7-362 galvanometer, the upper limit of the range of useful frequencies is set by the transducer. On the other hand, for measurements obtained with the 1/8-in. transducer with the oil chamber, the Dynamics 6450 and Kintel 111 BF amplifiers, and the CEC 7-362 galvanometer, the upper limit of the range of useful frequencies is set by the galvanometer.

The phase shift inherent in an harmonic oscillator, as expressed in Equation 4.11, may cause a distortion in recorded rise-time of the peak-pressure function. The phase shift ϵ has been plotted as a function of input frequency f in Figure 4.25 for the CEC 7-362 galvanometer and for both transducers, using values of f_n and ζ obtained as described previously. It is evident that for frequencies ranging from zero to 3 kilocyc/sec, ϵ is the greatest for the CEC galvanometer.

To determine whether the measurement system was capable of measuring peak pressures adequately, several typical uplift experiments were conducted, with pressures measured by the 1/8-in. transducer. The signal was amplified by the Dynamics and Kintel amplifiers, and displayed simultaneously on the oscilloscope and on the recording oscillograph with the 7-362 galvanometer. A calibration (using the oscilloscope) of the recording oscillograph was made to determine the rate of static galvanometer trace deflection per millivolt excitation of the galvanometer. For the oscilloscope, it was assumed

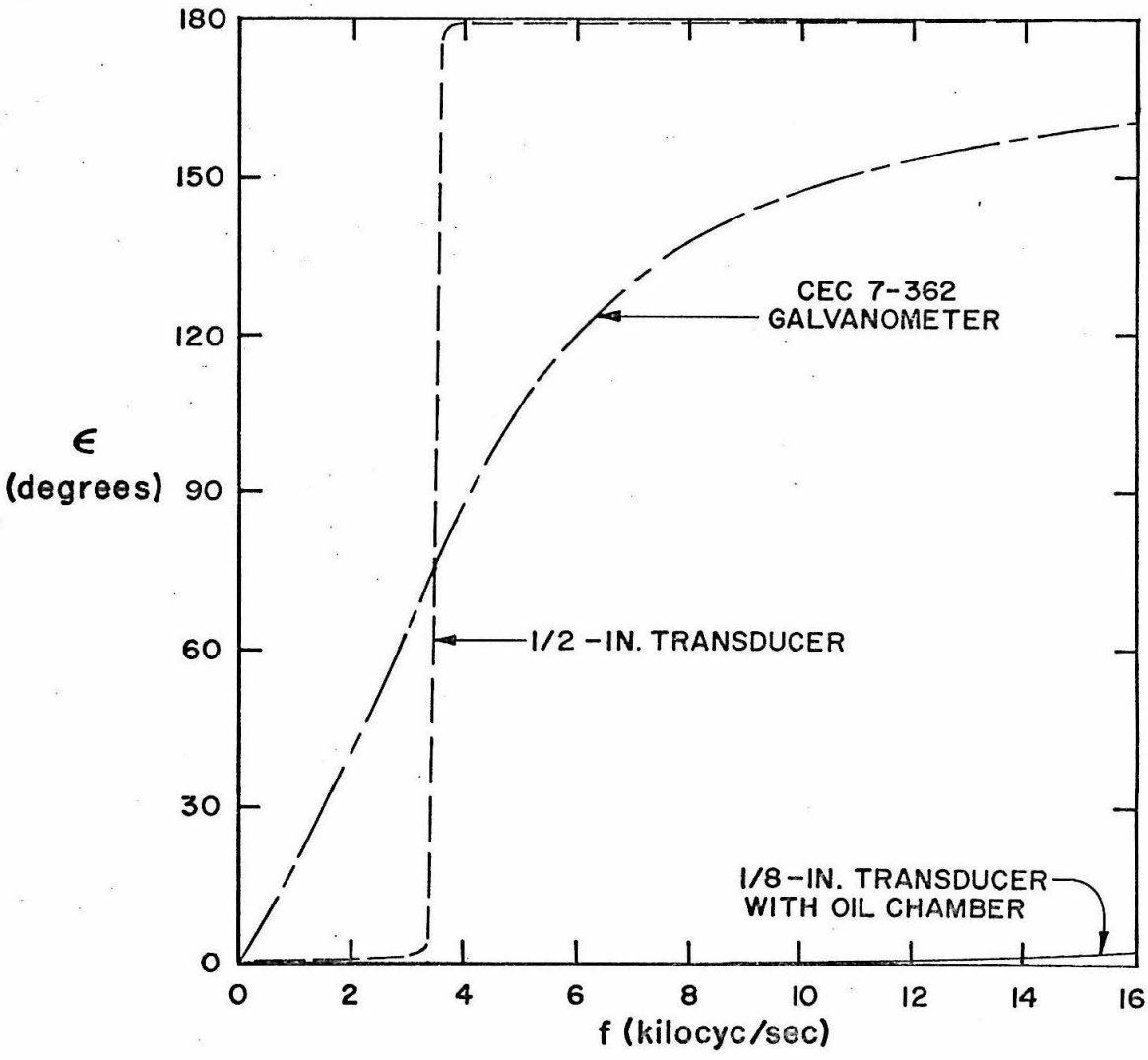

Figure 4.25. Phase shift ε as a function of input frequency, for the pressure transducers and the recorder galvanometer.

that the rate of trace deflection per millivolt excitation was accurately indicated by a dial setting. For each test, the peak pressure was measured in terms of trace deflection of both the oscillograph galvanometer and of the oscilloscope, and converted to an equivalent pair of values of millivolt static excitation of the oscillograph galvanometer and of the oscilloscope. Peak pressure in terms of equivalent millivolt excitation is plotted against corresponding peak pressure values recorded by the oscilloscope in Figure 4.26a, to determine the amplitude response of the galvanometer to the generated and amplified peak pressure signal (it again being assumed that the oscilloscope introduced no error). As shown in Figure 4.26a, the amplitude response of the galvanometer was approximately 0.98 for the typical pressure input functions.

As shown in Figure 4.24, the galvanometer amplitude response is 0.98 or greater for frequencies less than 3 kilocyc/sec but decreases rapidly above this frequency; therefore, one may conclude that components of the pressure pulse whose frequency is greater than 3 kilocyc/sec are of negligible amplitude. One may also conclude that within the range of important component frequencies, i.e. frequencies less than 3 kilocyc/sec, that the amplitude response of the 1/8-in. transducer will be within two percent of unity and that of each of the amplifiers will be within one percent of unity, so that for the measuring system consisting of the 1/8-in. transducer, the Dynamics and Kintel amplifiers, and the CEC 7-362 galvanometer, the overall amplitude response will be within six percent of unity. The measurement system containing the 1/2-in. transducer, on the other hand, may have an overall amplitude response far in excess of unity.

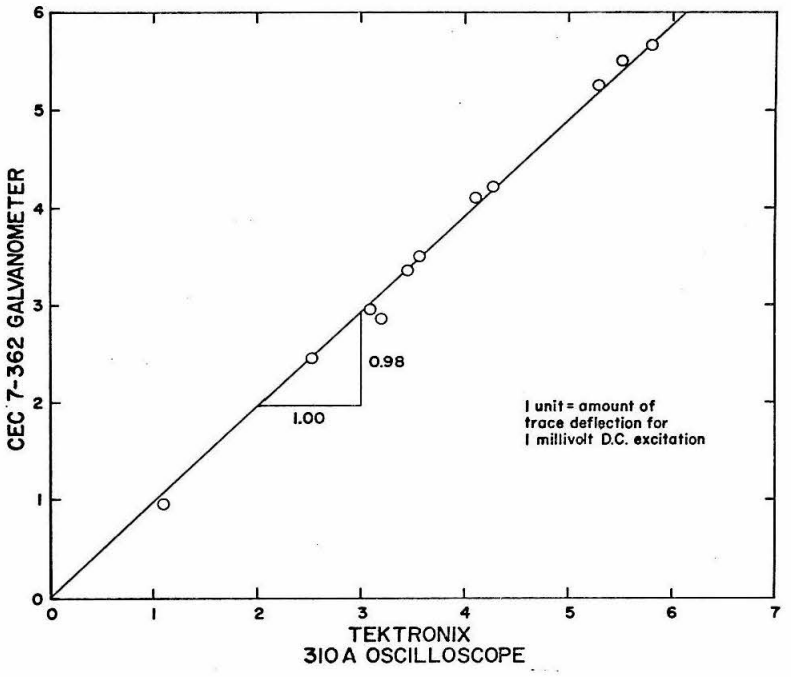

Figure 4.26a. Comparison of peak pressures recorded by oscillograph and by oscilloscope to test oscillograph response.

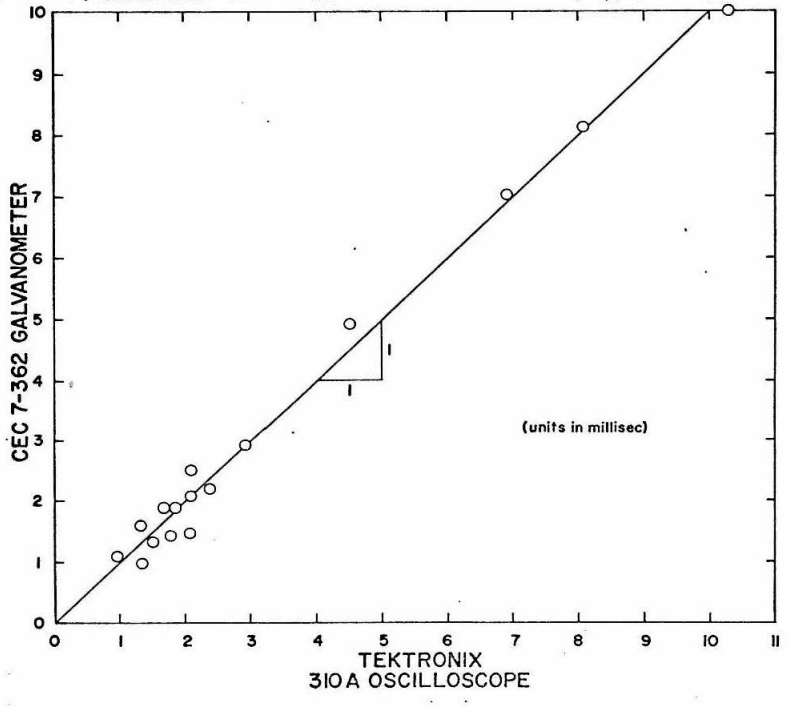

Figure 4.26b. Comparison of rise-times recorded by oscillograph and by oscilloscope to test oscillograph response.

On the same records of peak pressure obtained in the amplitude response tests, the rise-time t_r was measured, and comparisons made between values obtained with the CEC galvanometer and the oscilloscope, as shown in Figure 4.26b. ("Rise-time" is defined as the interval between the time of first major deflection of the record and the time of peak deflection; see Section 6.3.) Aside from a small amount of scatter there is no measurable difference between rise-times as recorded by the two instruments. Therefore, there is no measurable error introduced by galvanometer phase shift. Since the range of important component frequencies includes only frequencies less than 3 kilocyc/sec, and since for the 1/8-in. transducer the phase shift, ϵ, is much less than that for the galvanometer, one may conclude that no error in rise-time measurement is introduced by the 1/8-in. transducer. For frequencies less than 3 kilocyc/sec the amplifiers show an amplitude response deviating from unity by 0.01 or less. If in Equation 4.12 all deviation of $K'y_o/j_o$ from unity is attributed to the phase shift ϵ, the maximum possible value of ϵ is about 0.01 radians, or about half a degree, which is much less than values obtained for the galvanometer, as shown in Figure 4.26b. One may then conclude that the amplifiers introduce no rise-time error.

With no measurable error in rise-time, and with amplitude response within six percent of unity when the pressure-measurement system using the 1/8-in. transducer is excited by a typical peak-pressure distribution, it appears that measurements of peak pressure obtained with the 1/8-in. transducer are free of distortion due to dynamic characteristics of the measurement system. Measurements of peak pressure obtained with the 1/2-in. transducer, however, are

subject to considerable distortion due to the previously mentioned fact that amplitude response may be much greater than unity. The smaller 1/8-in. transducer therefore has a dynamic advantage over the 1/2-in. transducer as far as measuring peak pressure is concerned, in addition to the advantage of spatial resolution to be discussed in Chapter 5.

The pressure transducers were calibrated in place before and after each series of tests. The reference pressure was applied uniformly and statically to the sensitive diaphragm. The calibration apparatus, shown schematically in Figure 4.27, consisted of a water reservoir, a manometer, and a tube connecting the manometer to a gasketed cup, which could be raised into position beneath the transducer mounted in the platform. Valves A and B connected the manometer with the reservoir and with a drain, respectively.

To calibrate, the cup and jack were placed in the tank beneath the transducer. Valve B was closed; valve A was opened slightly to permit a small bleed from the reservoir to the cup and over the rim of the cup, to ensure that air would not be trapped between the transducer diaphragm and the cup. The cup was then raised and firmly seated against the soffit around the transducer, thus connecting the transducer hydraulically with the manometer. With the recorder running slowly, the valves were operated to stepwise increase and decrease the head on the system, by amounts read on the manometer to 0.002 ft. After calibration, the cup and jack were removed from the tank.

Typical calibration curves for the two transducers are shown in Figure 4.28 for a time interval of approximately two hours between calibrations.

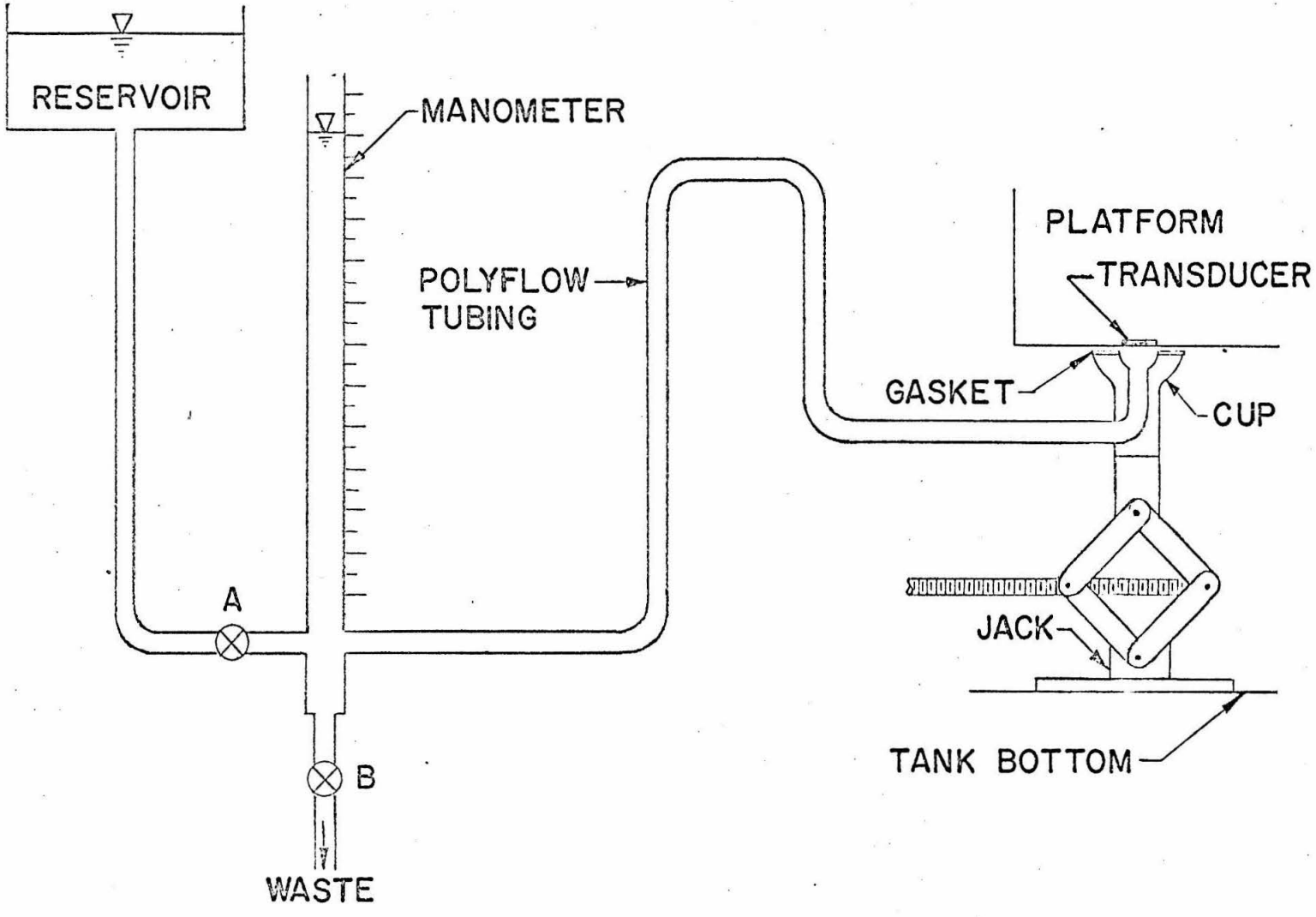

Figure 4.27. Schematic diagram of the pressure calibration apparatus.

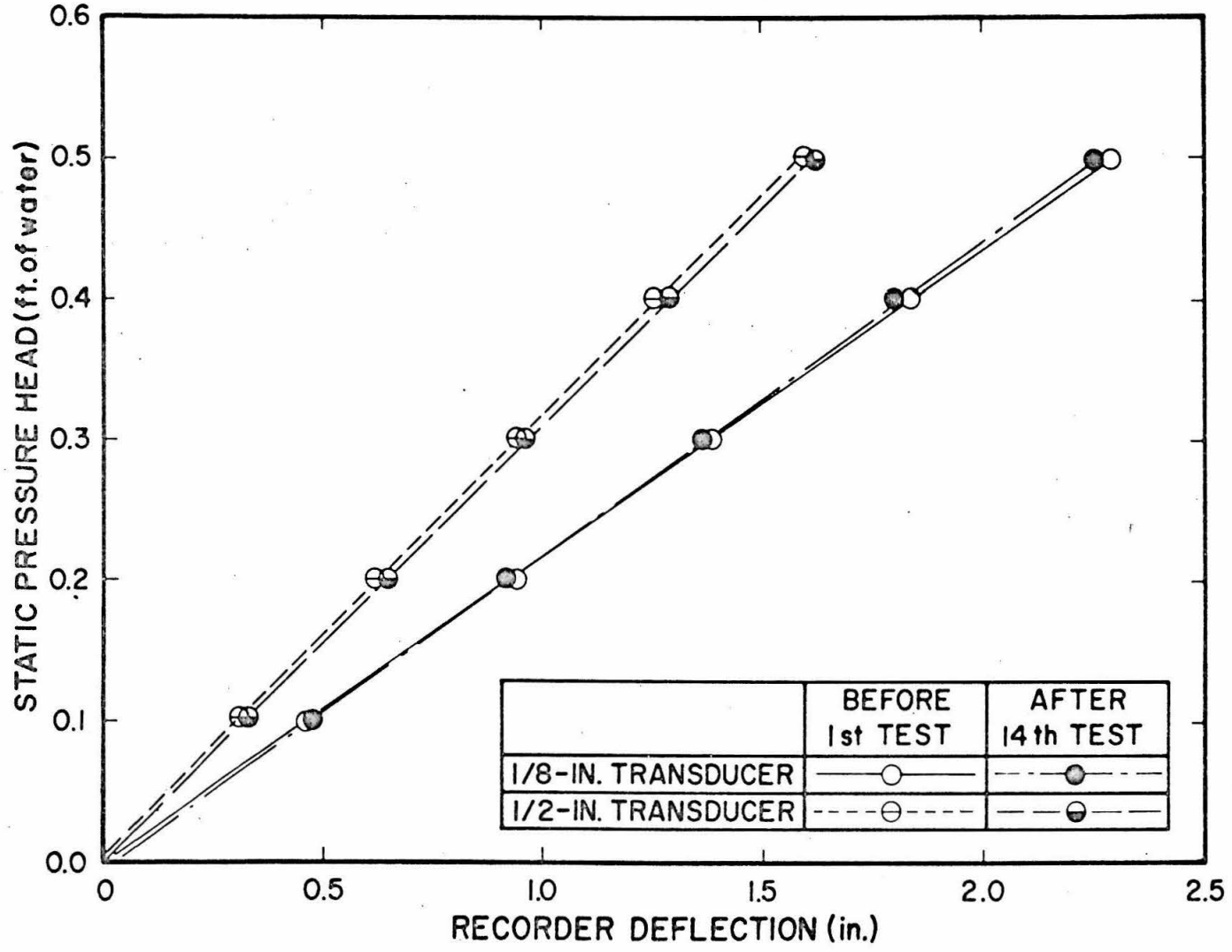

Figure 4.28. Typical calibration curves for the two pressure transducers.

Single-image photographs of the wave profile, such as those shown in Section 6.2, were obtained by setting two Edgerton high-voltage flash-tube lamps behind the 100-ft tank at the test section as shown in Figure 4.29. The outside of two panes of the far glass wall was covered with translucent paper, and the flash lamps adjusted to illuminate the papered panes as evenly as possible. With the laboratory darkened, the 4-in. x 5-in. Calumet camera with a wide-angle lens, set in front of the tank, was kept on open shutter as a wave approached the test section. At the desired instant, the flash lamps were triggered manually, after which the camera shutter was closed.

A number of multiple-image photographs were made to study visually the progress of the wave beneath the platform and to measure the wave front celerity, as described in Section 6.4. Most such photographs, such as that shown in Figure 4.30, were taken at the 40-ft. tank; a few, such as that shown in Figure 6.21a, were taken at the 100-ft tank. The two xenon helical flash tubes providing illumination, positioned as shown in Figure 4.29, were driven by a 4-kilovolt power supply and regulated by a variable-frequency oscillator and variable-duration timer. The flashes could be triggered electrically. Thus, a burst of flashes, at 10 flashes per second lasting 1 second, say, or 100 flashes per second lasting 0.2 seconds, could be triggered when a wave made contact with a sensitized point gauge mounted in the tank near the test section.

The 4 in. x 5 in. Graflex Crown Graphic camera was kept on open shutter. The lens cap was removed when the wave approached the test section, and replaced soon after the lights had flashed.

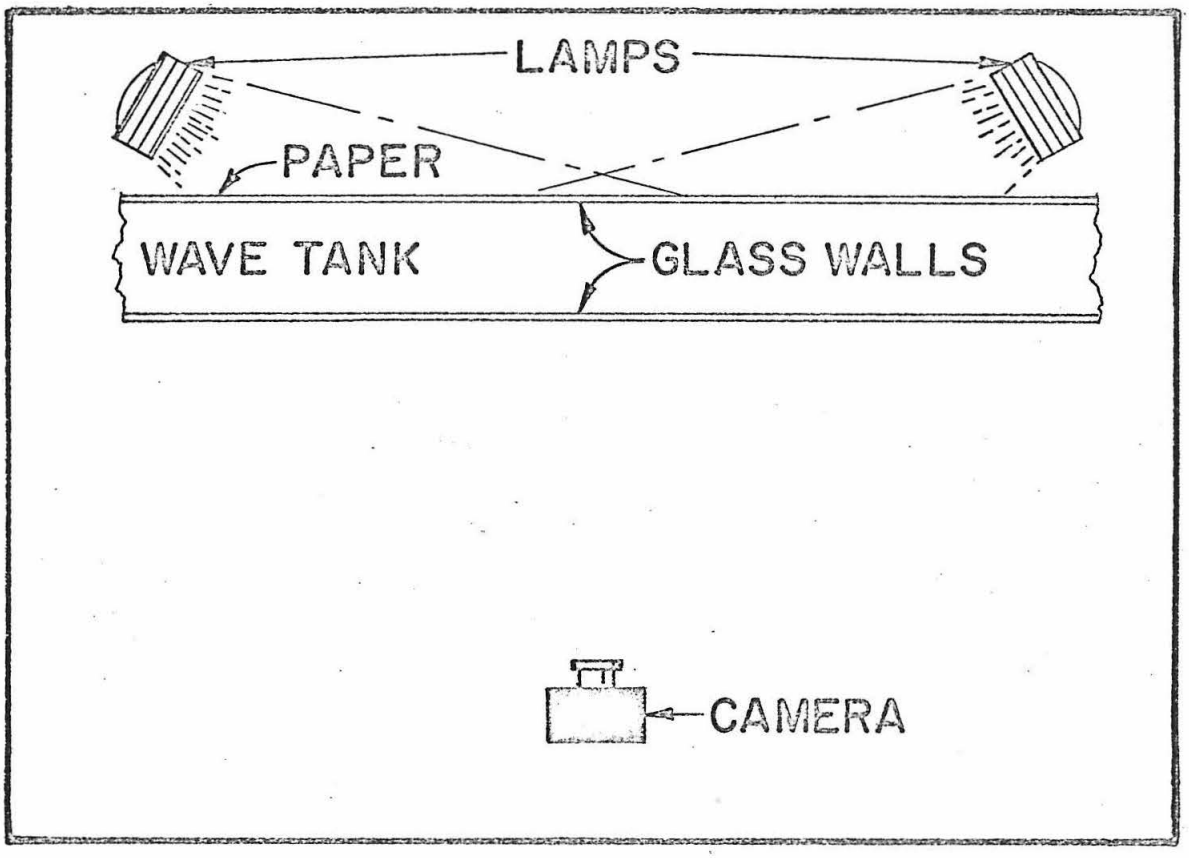

Figure 4.29. Plan view of the photographic set-up.

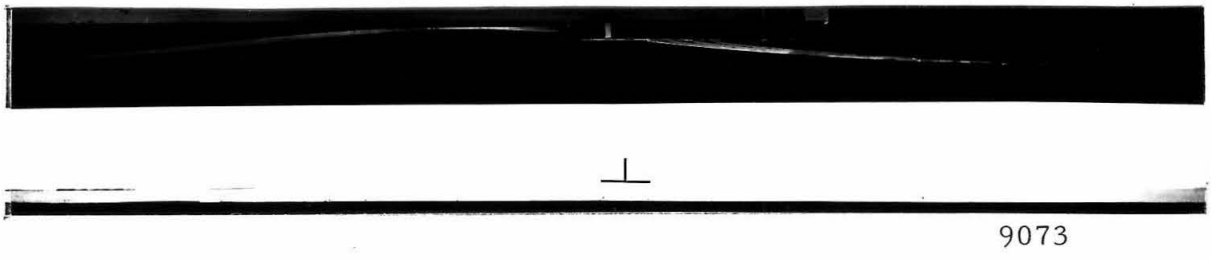

Figure 4.30. A typical multiple-image photograph (40-ft tank). (Wave is propagating from left to right; flash rate is 100/sec.)

To photograph a wave profile in a glass-walled tank is actually to photograph the meniscus at the intersection of the air-water interface and the near glass wall. As described previously, it was possible to photograph a single image by covering the far wall with translucent paper and backlighting it. The profile appeared dark on a light background. For a multiple-image photograph, however, it was necessary to produce light profiles on a dark background, to avoid exposing the entire frame of film on the first flash. Experimentation showed that the best technique for this was to have the tank bottom painted white, to cover the top half of the far wall with black, opaque paper and the bottom half with white, translucent paper, and to backlight the white paper as evenly as possible. It was necessary that the still water level be above the boundary of black and white paper. Light reflected from the bottom and from the lower wall reflected in the meniscus, illuminating the wave profile in contrast to the dark background of black paper, as shown in Figure 4.30.

4.5 Operating Procedure.

Each experiment consisted of the generation of a solitary wave, and the recorded observation of the wave and its resultant effects on the platform.

Experiments were conducted in groups of six or more, for which geometric parameters such as the still-water depth, the soffit clearance, and the transducer location were unchanged, and the wave height H was kept as constant as possible. The large number of repetitive experiments was made necessary by the large deviation inherent in the measured peak pressure.

The "universal mean" m' of a variable quantity z_i (such as the peak pressure) is defined as the mean of a sample of infinite size (Parratt, 1961, p. 76). The mean m of a sample of finite size n provides an estimate of the universal mean. A measure of the deviation of the measured quantity z_i is the experimental standard deviation S, defined in this study as:

$$S = \left(\frac{\sum_{i=1}^{n} (Z_i - m)^2}{n} \right)^{1/2} . \qquad (4.17)$$

Corresponding to the experimental standard deviation S is the "universal" standard deviation S', defined as the standard deviation of a sample of infinite size. A measure of the reliability of the experimental mean m as an estimator of the universal mean m' is the experimental standard deviation in the mean S_m, defined in this study as $S_m = S/\sqrt{n}$, and the corresponding "universal" standard deviation in the mean $S'_m = S'/\sqrt{n}$.

The standard deviation in the mean S_m may be interpreted as follows: for a quantity that is normally distributed, there is 68% probability that the universal mean m' lies within the confidence interval $m \pm S'_m$. There is 95% probability that m' lies within the confidence interval $m \pm 2\, S'_m$ (Parratt, 1961, pp. 94, 174), where the "universal" value S'_m may be approximated by the experimented value S_m.

For a given confidence limit such as 68% or 95%, the experimental mean M becomes a more reliable estimate of the universal mean m' as the sample size n increases. However, there is a

diminishing return in accuracy with increasing sample size n. For example, when n is increased from one to four, the interval within which one may expect m with 95% probability is reduced from a half-width of 2S to S; yet to achieve another two-fold increase in accuracy would require a further increase in sample-size to n = 16.

Since the wave-testing procedure was time-consuming and thus did not allow for large sample sizes to be obtained throughout the program, a value of n = 6 was chosen for most of the experiments, while for selected cases n was equal to or greater than 30. As will be shown in Section 6.6, the ratio S/m of experimental standard deviation to mean peak pressure was usually less than 25%. For S/m = 25%, there is therefore 95% probability that the sample mean m is within $2S/(m\sqrt{n}) = 20.4\%$ of the universal mean m for n = 6, and within $2S/(m\sqrt{n}) = 9.1\%$ of m for n = 30.

In preparation for a group of experiments, the water level in the tank was adjusted to its proper elevation within $\pm$ 0.001 ft, and the water surface was wiped clean. To wipe the surface a piece of unglazed paper nearly the width of the tank was gently laid on the surface and slowly towed the length of the tank. A considerable amount of dust, oil film, and algal growth could be so collected.

The electronic apparatus was allowed time to warm up, after which pressure and wave transducer calibrations were taken. The flash frequency of the CEC recording oscillograph timer was checked with the oscilloscope. The wave generator motor was turned on, causing the cam to rotate unloaded at a constant velocity, adjusted for generation of waves of desired height. After water disturbances

caused in calibration and other preparation died out and the water was sensibly still, the first wave was generated.

The wave and pressure recorders were engaged as the wave approached the test section, and disengaged as soon as the wave had passed completely beneath the platform. The wave generator was then immediately reset and the water was allowed to become still again.

The time needed for the water to become still was found to be 5 minutes in the 40-ft tank and 8 minutes in the 100-ft tank. When the required stilling time had elapsed, the next wave was generated.

After every 4th experiment the wave gauge was calibrated; a pressure transducer calibration was performed after every 16th wave. Occasionally calibrations were more frequent. At the end of the day's operation, the wave gauge was raised out of the water and wiped clean with methyl alcohol.

In the hydraulics laboratory, situated in an air-conditioned building, the air temperature was maintained between 70°F and 75°F.

CHAPTER 5

DEFECT IN PEAK PRESSURE MEASUREMENT DUE TO TRANSDUCER AREA

In Chapter 1 the recorded pressure function was described as having an initial peak of short duration, followed by a more slowly-varying part, usually of lesser amplitude. In Chapter 3 such a pressure peak was predicted at the advancing wavefront where the rising water surface makes initial contact with the platform soffit; in Section 6.3 it will be shown that the pressure peak is indeed sustained at the advancing wavefront. Moving along the soffit with the celerity U_d of the wave front, the pressure distribution may be expressed as $P_{ac}(x-U_d t)$ as shown in Figure 5.1a, if changes in form and amplitude are neglected. A pressure transducer mounted in the soffit, having been calibrated with a reference pressure applied uniformly, i.e., without spatial variation, to the sensitive transducer surface, generates an output displayed on the recorder. The recorded output function may be mapped point-by-point into a pressure function $P_r(t)$ shown in Figure 5.1b by multiplication by the calibration factor. The recorded pressure function $P_r(t)$ therefore indicates the time-dependent pressure P_{ac} exerted on the transducer, providing the pressure is exerted uniformly, as in the calibration.

With respect to the actual non-uniform pressure distribution, $P_{ac}(x-U_d t)$, shown in Figure 5.1a, the rise-length b is defined as the distance between the region of zero pressure and the locus of maximum pressure. Correspondingly, the rise-time t_r of the recorded pressure function $P_r(t)$ is defined as the time interval between the

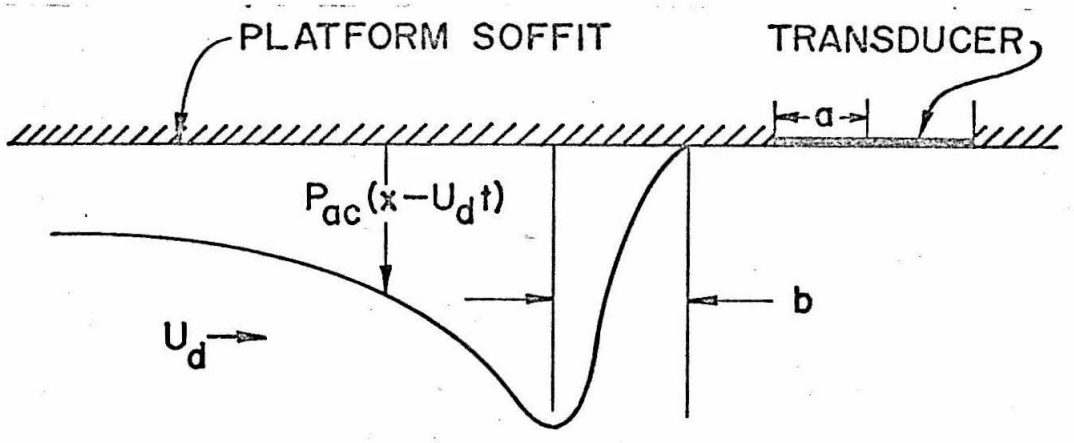

Figure 5.1a. A travelling pressure distribution approaching a transducer.

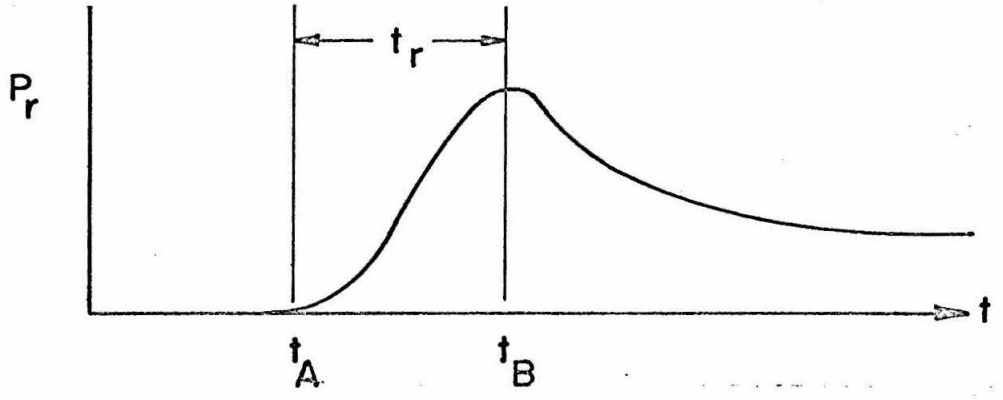

Figure 5.1b. The recorded pressure function.

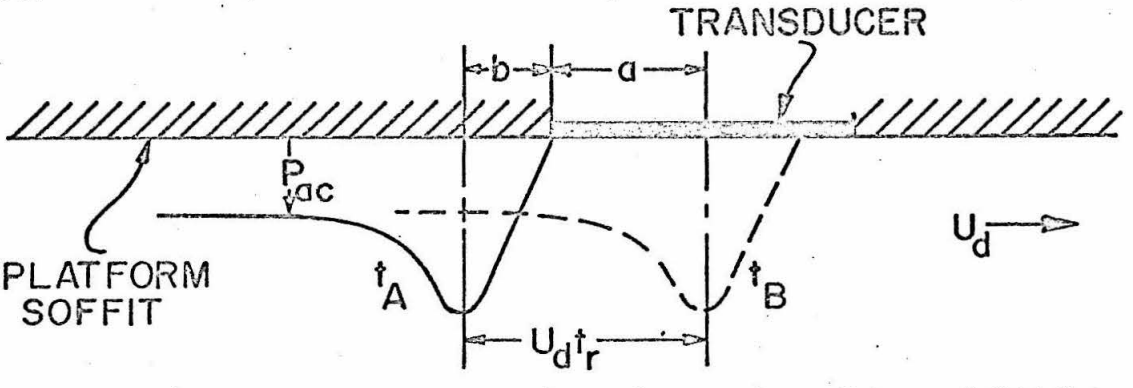

Figure 5.1c. Increase in recorded rise-time due to finite transducer area.

initial condition of zero recorder deflection and the condition of maximum recorder deflection as shown in Figure 5.1b. If pressure is measured at one point, i.e. if the transducer radius a is vanishingly small, the rise-time t_r will be equal to the time needed for the pressure wave to travel a distance equal to the rise-length b: $t_r = b/U_d$. Therefore if one is interested in measuring the rise-length b, one need merely measure t_r and U_d: $b = U_d\, t_r$.

Early in the experimental program, however, it was noticed that the rise-time t_r multiplied by the wave front celerity U_d resulted in a length quantity that was usually of the same order of magnitude as the transducer radius a; and it was recognized that a "delta-function" pressure distribution, i.e. one with vanishingly small rise-length b, would be recorded as having a rise-time t_r equal to the time needed for the narrow pressure peak to travel from the edge of the sensitive transducer area to the point where the transducer is most sensitive to the pressure peak, i.e. the transducer center. In such a case it would be wrong to believe that the product $U_d\, t_r$ was equal to the rise-length b, when in fact it would merely be a measurement of the transducer radius a.

For a pressure distribution where b is not vanishingly small, it is reasonable to assume that the product $U_d\, t_r$ is equal to the sum of the rise length b and the transducer radius a, as shown in Figure 5.1c. At time t_A, the toe of the moving pressure distribution has just reached the edge of the sensitive transducer area, causing initial recorder trace deflection. At a later time t_B, the peak of the distribution is at the transducer center. If it is assumed that peak transducer output occurs when the peak of the distribution is at the transducer

center, then the rise-time $t_r = t_B - t_A$ is equal to the distance propagated b + a divided by the rate of propagation U_d:

$$t_r = \frac{b + a}{U_d} . \qquad (5.1)$$

Equation 5.1 shows that unless a<<b, derivation of b from U_d and t_r will be affected by transducer size. As will be discussed in Section 5.1, measurement of the peak pressure P_2 will also be affected by transducer size if a is not much smaller than b.

This problem of transducer size was recognized during preliminary tests with the 1/2-in. transducer. To improve spatial resolution, i.e. to reduce the transducer radius, a, the 1/8-in. transducer was procured. (As described in Section 4.4, the 1/8-in. transducer had dynamic response characteristics that made it a much more suitable instrument than the 1/2-in. transducer for measuring peak pressures, from the point of view of dynamics as well as of spatial resolution.) With the 1/8-in. transducer too, however, the product of rise-time t_r and wave front celerity U_d was of the order of magnitude of the transducer radius a, indicating that the problem of spatial resolution had not yet been completely obviated and still had to be taken into consideration.

5.1 Mathematical Formulation of the Problem.

One may consider a spatially varying distribution of pressure exerted on a plane surface, and the problem of measuring the pressure magnitude at any given point on that surface. As shown in Figure 5.2, any real pressure transducer, mounted in the surface

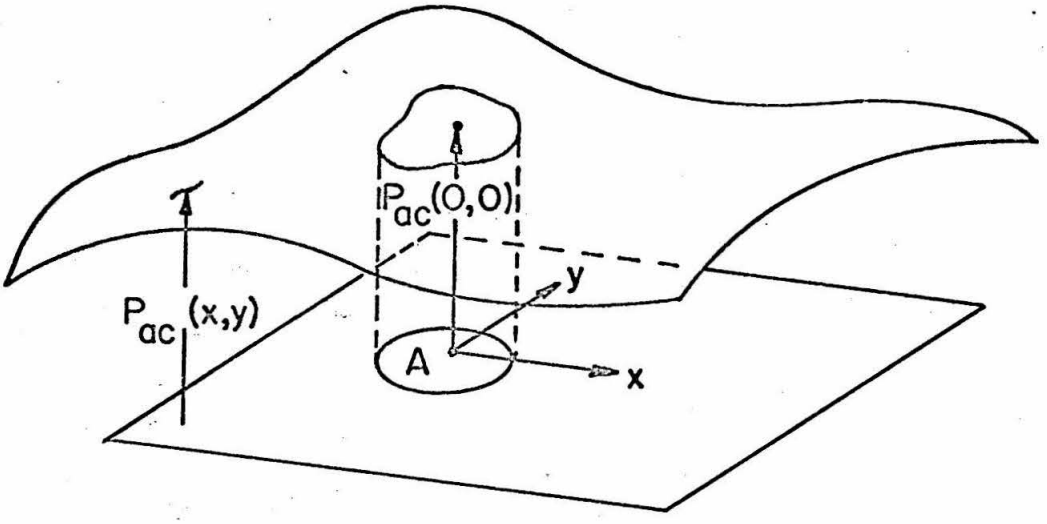

Figure 5.2. Diagram showing how a spatially-varying pressure distribution is averaged over the sensitive transducer area A.

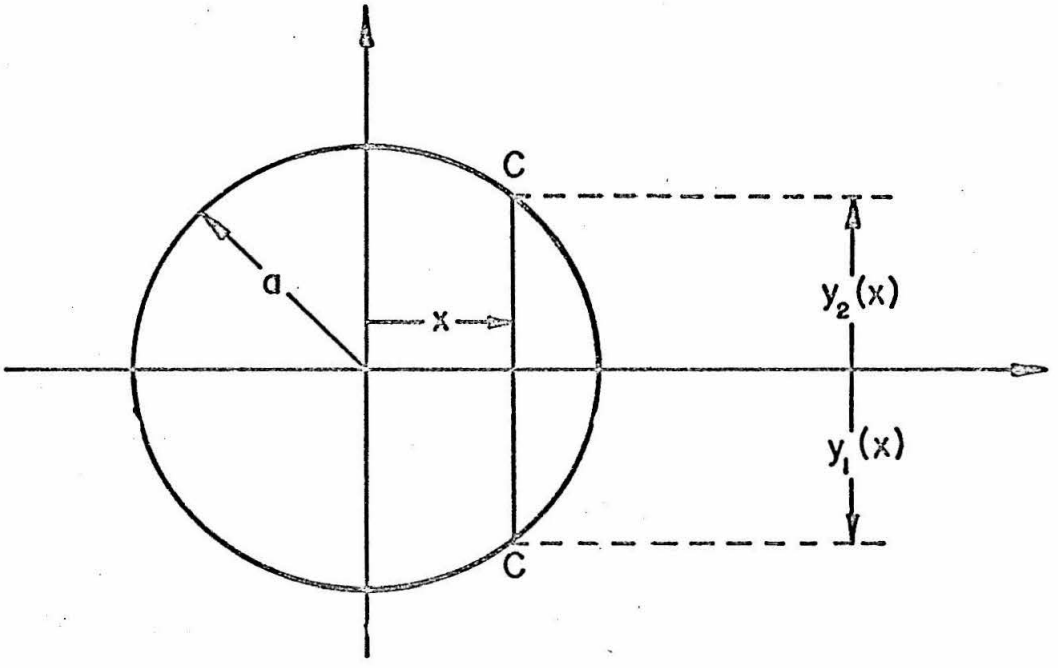

Figure 5.3. Definition sketch of the limits of integration for Equation 5.4.

and centered at the given point, will sample pressure over a finite area of the surface; and thus report an average pressure for the finite, although perhaps small, area surrounding the desired point of measurement, rather than report the pressure at just the point.

In the analysis that follows, the dynamic response characteristics of the transducer are not considered. (This has been justified by the discussion of Section 4.4.) Deflection of the sensitive transducer surface by a pressure distribution is assumed to be independent of the time rate of change of the pressure distribution, i.e. it is assumed that analytical expressions for static deflection are adequate for expressing the deflection at any instant due to the pressure distribution on the transducer surface at that instant. Furthermore, it is assumed that transducer output may be considered equal to a linear superposition of outputs due to unit forces applied at points distributed over the sensitive transducer surface.

The recorded pressure function $P_r(t)$ may be related to the actual pressure distribution $P_{ac}(x, y, t)$ by an integral equation of the form:

$$\int\int_A G_1(x, y)\, P_{ac}(x, y, t)\, dx\, dy = P_r(t). \tag{5.2}$$

As shown in Figure 5.2 the (x, y) plane is that of the surface, with the transducer centered at the origin; $P_{ac}(x, y, t)$ is the pressure distribution; the region of integration is the sensitive area A of the transducer; and the spatial response function $G_1(x, y)$ describes the relative sensitivity of various parts of the transducer surface. The condition that the recorded pressure P_r equal the actual pressure P_{ac} when the

latter is distributed uniformly over the transducer area A, i.e., P_{ac} is independent of x and y, is satisfied if:

$$\iint_A G_1(x, y)dx\ dy = 1. \tag{5.3}$$

Now if pressure distributions varying in one direction only are considered, such as $P_{ac}(x, y, t) = P_{ac}(x, t)$, the left-hand side of Equation 5.2 may be expressed as:

$$\iint_A G_1(x, y)P_{ac}(x, t)\,dx\ dy = \int_{-a}^{a} \left[P_{ac}(x, t) \int_{y_1(x)}^{y_2(x)} G_1(x, y)\,dy \right] dx, \tag{5.4}$$

where the notation is defined as shown in Figure 5.3. If:

$$\int_{y_1(x)}^{y_2(x)} G_1(x, y)\,dy = G(x),$$

where now:

$$\int_{-a}^{a} G(x)\,dx = 1,$$

Equation 5.2 becomes:

$$\int_{-a}^{a} G(x)\,P_{ac}(x, t)\,dx = P_r(t). \tag{5.5}$$

When the pressure distribution moves across the transducer surface as a wave of unchanging form, as in Figure 5.1a, or Figure 5.1c, Equation 5.5 has the particular form:

$$\int_{-a}^{a} G(x) P_{ac}(x - U_d t)\,dx = P_r(t), \tag{5.6}$$

where U_d is the wave celerity.

The spatial response function $G_1(x, y)$ describing the sensitivity of various parts of the transducer surface may be considered proportional to the static transducer output due to a unit force applied at the point (x, y) on the transducer surface. The integrated spatial response function $G(x) = \int_{y_1(x)}^{y_2(x)} G_1(x, y)\,dy$ may be considered to be proportional to the static transducer output due to a unit line load applied along a chord of the sensitive transducer area, perpendicular to the x-axis, situated a distance x from the center of the transducer, such as the line C-C in Figure 5.3. The actual pressure $P_{ac}(x, t)$ may be considered a weighting function, indicating at a given time t the amplitude of the line loads at every value of x. The total transducer response $P_r(t)$ is then the summation of component responses to the line loads distributed over the sensitive surface area of the transducer.

The integrated spatial response function G(x) may be derived as follows: $G_1(x, y) = QF_1(x, y)$, where $F_1(x, y)$ is proportional to the calibrated transducer output due to a unit force applied at the point (x, y). The constant Q is determined by Equation 5.3:

$$\iint_A G_1(x, y)\,dx\,dy = Q \iint_A F_1(x, y)\,dx\,dy \equiv 1. \tag{5.8}$$

Similarly, $G(x) = QF(x)$, where $F(x)$ is proportional to the calibrated transducer output due to a unit line load applied along a chord a

distance x from the transducer center, and where Q is determined by the relationship:

$$\int_{-a}^{a} G(x)dx = Q \int_{-a}^{a} F(x)\,dx \equiv 1. \tag{5.8}$$

The relationship between F_1 and F is the same as that between G_1 and G:

$$F(x) = \int_{y_1(x)}^{y_2(x)} F_1(x, y)\,dy\ . \tag{5.9}$$

The spatial response functions G(x) are derived for five different transducer configurations in Table 5.1. The first two cases presented in Table 5.1 are for transducers with spatially uniform sensitivity, in which the transducer output due to a unit force is independent of the location on the sensitive surface at which the force is applied. Case 1) is for a square surface; Case 2) is for a circular surface. Case 3) is for a transducer whose sensitive surface is a circular membrane, resisting deformation by a resistance to stretching; where the transducer output is proportional to the average deflection to the membrane. Cases 4) and 5) are for transducers whose sensitive surfaces are circular diaphragms, resisting deformation by a resistance to bending, with the slope of the diaphragm surface at the periphery constrained to be zero. In Case 4) transducer output is proportional to average diaphragm deflection; in Case 5) transducer output is proportional to deflection at the center of the diaphragm.

Table 5.1

Derivation of spatial response functions G(x)

1. Square piston or piezometer tap, sides of length 2a, sides aligned with x, y axes. Output independent of location of applied force.

   a) The output due to a unit point force exerted at (x, y) is proportional to: $F_1(x, y) = 1$ (or any other constant);

   b) $F = \int_{-a}^{a} F_1 \, dy = 2a$;

   c) $\int_{-a}^{a} G(x)dx = Q \int_{-a}^{a} F \, dx = 4a^2Q \equiv 1; \; Q = \frac{1}{4a^2}$;

   d) $G(x) = \frac{1}{2a}$.

2. Circular piston or piezometer tap of radius a. Output independent of location of applied force.

   a) The output due to a unit point force exerted at (x, y) is proportional to: $F_1(x, y) = 1$ (or any other constant)

   b) $F = \int_{-\sqrt{a^2-x^2}}^{+\sqrt{a^2-x^2}} F_1 \, dy = 2\sqrt{a^2-x^2}$;

   c) $\int_{-a}^{a} G(x)dx = Q \int_{-a}^{a} F \, dx = \pi a^2 Q \equiv 1; \qquad Q = \frac{1}{\pi a^2}$;

   d) $G(x) = \frac{2}{\pi a} \sqrt{1 - (\frac{x}{a})^2}$.

Table 5.1 (continued)

3. Circular membrane of radius a. Output proportional to average deflection of entire membrane.

a) The deflection at point (r_o, θ_o) due to a unit point load exerted at (r, θ) is proportional to:

$$F_2 = 2\left[\ell n\left(\frac{r_o}{a}\right) - \sum_{n=1}^{\infty} \frac{1}{n} \left\{\left(\frac{r}{r_o}\right)^n - \left(\frac{r_o r}{a^2}\right)^n\right\} \cos n(\theta - \theta_o)\right]$$

for $r < r_o < a$;

$$F_2 = 2\left[-\ell n\left(\frac{r}{a}\right) - \sum_{n=1}^{\infty} \frac{1}{n} \left\{\left(\frac{r}{r_o}\right)^n - \left(\frac{a^2}{r_o r}\right)^n\right\} \cos n(\theta - \theta_o)\right]$$

for $r_o < r$.

(Morse and Feshbach, 1953, p. 1189.)

The average deflection of the entire membrane due to the unit point load is proportional to:

$$F_1(x, y) = \frac{1}{\pi a^2} \int_0^a \int_0^{2\pi} F_2 \, r_o \, d\theta_o \, dr_o =$$

$$4\left[-\left(\frac{r}{a}\right)^2 \ell n\left(\frac{r}{a}\right) + \frac{3}{4} - \frac{2}{3}\left(\frac{r}{a}\right) + \frac{1}{4}\left(\frac{r}{a}\right)^2 - \frac{1}{3}\left(\frac{r}{a}\right)^4\right];$$

Table 5.1 (continued)

b) $$F(x) = \int_{-\sqrt{a^2-x^2}}^{+\sqrt{a^2-x^2}} F_1(x, y)dy =$$

$$-\frac{\pi}{3}\left(\frac{x}{a}\right)^3 + \frac{2}{3}\left(\frac{x}{a}\right)^3 \arcsin\left(\frac{x}{a}\right) - \frac{1}{3}\left(\frac{x}{a}\right)^2 \ell n \left(\frac{1+\sqrt{1-\left(\frac{x}{a}\right)^2}}{\left|\frac{x}{a}\right|}\right)$$

$$+\sqrt{1-\left(\frac{x}{a}\right)^2}\left[-\frac{8}{45}\left(\frac{x}{a}\right)^4 + \frac{19}{30}\left(\frac{x}{a}\right)^2 + \frac{49}{90}\right].$$

c) $$\int_{-a}^{a} G(x)dx = Q\int_{-a}^{a} F(x)dx = \frac{2\pi}{9} Q \equiv 1; \qquad Q = \frac{9}{2\pi}.$$

d) $$G(x) = \frac{3}{2\pi a}\left[-\pi\left(\frac{x}{a}\right)^3 + 2\left(\frac{x}{a}\right)^3 \arcsin\left(\frac{x}{a}\right)\right.$$

$$-\left(\frac{x}{a}\right)^2 \ell n \left(\frac{1+\sqrt{1-\left(\frac{x}{a}\right)^2}}{|x/a|}\right)$$

$$\left. +\sqrt{1-\left(\frac{x}{a}\right)^2}\left\{-\frac{8}{15}\left(\frac{x}{a}\right)^4 + \frac{19}{10}\left(\frac{x}{a}\right)^2 + \frac{49}{30}\right\}\right].$$

4. Circular diaphragm of radius a, edges clamped. Output proportional to average deflection of diaphragm.

a) The deflection at point (r_o, θ_o) due to a unit point load exerted at (r, θ) is proportional to:

$$F_2 = \left[(r_o^2 + r^2)\ell n\left(\frac{r_o}{a}\right) + \frac{(a^2+r^2)(a^2 - r_o^2)}{2a^2}\right] + \theta\text{-dependent terms}$$

for $r_o < r < a$;

Table 5.1 (continued)

$$F_2 = \left[(r_o^2 + r^2) \ell n \left(\frac{r}{a}\right) + \frac{(a^2+r_o^2)(a^2-r^2)}{2a^2} \right] + \theta\text{-dependent terms}$$

for $0 < r < r_o$

(Timoshenko and Woinowsky-Krieger, 1959, p. 290.)

The average deflection of the diaphragm due to the unit point load is proportional to:

$$\frac{1}{\pi a^2} \int_0^a \int_0^{2\pi} F_2 \, r d\theta dr = F_1 = \frac{a^2}{64\pi} \left[1 - \left(\frac{r}{a}\right)^2 \right]^2$$

b) $$F(x) = \int_{-\sqrt{a^2-x^2}}^{+\sqrt{a^2-x^2}} F_1(x, y) dy = \frac{a^3}{60\pi} \left[1 - \left(\frac{x}{a}\right)^2 \right]^{5/2}$$

c) $$\int_{-a}^{a} G(x) dx = Q \int_{-a}^{a} F(x) dx = \frac{Qa^4}{60\pi} \frac{5\pi}{16} \equiv 1; \; Q = \frac{192}{a^4}$$

d) $$G(x) = \frac{16}{5\pi a} \left[1 - \left(\frac{x}{a}\right)^2 \right]^{5/2}.$$

5. Circular diaphragm of radius a, edges clamped. Output proportional to deflection of center of diaphragm.

a) The deflection at point (r_o, θ_o) due to a unit point load exerted at (r, θ) is proportional to:

$$F_2 = \left[(r_o^2 + r^2) \ell n \left(\frac{r}{a}\right) + \frac{(a^2+r_o^2)(a^2-r^2)}{2a^2} \right] + \theta\text{-dependent terms proportional to } r_o$$

for $0 < r < r_o$

(Timoshenko and Woinowsky-Krieger, 1959, p. 290.)

Table 5.1 (continued)

The deflection at the center of the diaphragm is proportional to F_2 when $r_o = 0$:

$$F_1 = r^2 \ell n\left(\frac{r}{a}\right) + \frac{a^2 - r^2}{2} .$$

b) $$F = \int_{-\sqrt{a^2-x^2}}^{+\sqrt{a^2-x^2}} F_1(x, y)dy =$$

$$= \frac{2a^2}{3}\left[\pi\left(\frac{x}{a}\right)^3 - 2\left(\frac{x}{a}\right)^3 \text{arc sin}\left(\frac{x}{a}\right)\right.$$

$$\left. - \frac{2}{3}\sqrt{1 - \left(\frac{x}{a}\right)^2}\left\{4\left(\frac{x}{a}\right)^2 - 1\right\}\right];$$

c) $$\int_{-a}^{a} G(x)dx = Q\int_{-a}^{a} F(x)dx = Q\,\frac{\pi a^3}{8} \equiv 1; \quad Q = \frac{8}{\pi a^3};$$

d) $$G(x) = \frac{16}{3\pi a}\left[\pi\left(\frac{x}{a}\right)^3 - 2\left(\frac{x}{a}\right)^3 \text{arc sin}\left(\frac{x}{a}\right)\right.$$

$$\left. - \frac{2}{3}\sqrt{1 - \left(\frac{x}{a}\right)^2}\left\{4\left(\frac{x}{a}\right)^2 - 1\right\}\right].$$

For each case, the function $F_1(x, y)$ is derived in Step (a); the result is integrated with respect to y to yield F(x) in Step (b); the proportionality constant Q is evaluated in Step (c); and the integrated spatial response function $G(x) = QF(x)$ is presented in Step (d).

5.2 Mathematical Solution of the Integral Equation.

If the recorded function $P_r(t)$, the spatial response function G(x), the transducer radius a, and the wave celerity U_d are known, it is theoretically possible to solve Equation 5.6 for the actual travelling pressure distribution $P_{ac}(x-U_dt)$. The mathematical procedure is outlined in this section for interest. However, it should be noted that the procedure was not applicable to the present study, for reasons to be shown presently.

As in Section 5.1, dynamic response characteristics of the transducer are not considered, and it is assumed that analytical expressions for static deflection of the transducer diaphragm are adequate for expressing the deflection at any instant due to the pressure distribution at that instant. As in Section 5.1, it is assumed that principles of linear superposition may be applied.

The Fourier transform of Equation 5.6 is:

$$\int_{-\infty}^{\infty} \left[\int_{-a}^{a} G(x)\, P_{ac}(x-U_dt)\, dx \right] e^{i\omega t} dt = \int_{-\infty}^{\infty} P_r(t)\, e^{i\omega t} dt. \qquad (5.10)$$

When the left-hand side is multiplied and divided by $e^{i\omega x/U_d}$, and when factors are rearranged, Equation 5.10 takes the form:

$$\int_{-a}^{a} G(x)\, e^{i\omega \frac{x}{U_d}} \left[\int_{-\infty}^{\infty} P_{ac}(t-\tfrac{x}{U_d}) e^{i\omega(t-\frac{x}{U_d})}\, dt \right] dx$$

$$= \int_{-\infty}^{\infty} P_r(t) e^{i\omega t}\, dt. \qquad (5.11)$$

In the bracketed factor on the left-hand side of Equation 5.11, the argument $(t-x/U_d)$ may be replaced by the symbol ξ, where $d\xi=dt$ and the range of integration may be expressed as $-\infty < \xi < \infty$. The bracketed factor, after integration, is therefore a function of ω alone, and therefore independent of t and x. The bracketed factor is simply the Fourier transform of $P_{ac}(\xi)$, and may be labelled $\pi_{ac}(\omega)$.

The right-hand side of Equation 5.11 is the Fourier transform of $P_r(t)$, and may be labelled $\pi_r(\omega)$. The integral $\int_{-a}^{a} G(x) e^{i\omega \frac{x}{U_d}} dx$ on the left-hand side may be labelled $I(\omega, a, U_d)$. Therefore, Equation 5.11 may be written in abbreviated form as:

$$I(\omega, a, U_d)\, \pi_{ac}(\omega) = \pi_r(\omega). \qquad (5.12)$$

With complete knowledge of $P_r(t)$, one may determine $\pi_r(\omega)$; with knowledge of the transducer radius a, the wave celerity U_d, and the spatial response function G(x), one may determine $I(\omega, a, U_d)$. The function $\pi_{ac}(\omega)$ is then simply the ratio π_r/I, and the actual pressure distribution $P_{ac}(x-U_d t)$ is the inverse transform of $\pi_{ac}(\omega)$.

However, it should be noted that the integral $I(\omega, a, U_d) = \int_{-a}^{a} G(x)\, e^{i\omega x/U_d}\, dx$ may become zero for certain values of ω.

For instance, in the fourth case listed in Table 5.1, where

$G(x) = \frac{16}{5\pi a}\left[1 - \left(\frac{x}{a}\right)^2\right]^{5/2}$, the integral I becomes zero for

$\omega a/U_d = 8.92$ and for certain greater values. When I = 0, information is lost concerning the value of $\pi_{ac}(\omega)$ at the corresponding value of ω, i.e., there is no way to learn the value of $\pi_{ac}(\omega)$ from $\pi_r(\omega)$ at that value of ω. Thus there is an obstacle to complete retrieval of the input pressure function P_{ac}. Only if it is known that the Fourier transform $\pi_{ac}(\omega)$ of the actual pressure input is itself zero for values of ω at which $I(\omega, a, U_d)$ equals zero can the function $\pi_{ac}(\omega)$ be retrieved from the transform $\pi_r(\omega)$ of the recorded function $P_r(t)$.

It was attempted to apply the correction procedure so described to the recorded pressure function obtained with the 1/8-in. Schaevitz-Bytrex transducer described in Section 4.4. For this transducer, the radius, a, was 0.0052 ft (or 1/16-in.). It was assumed that the polyethylene tape covering the exposed end of the modified transducer assembly acted as a diaphragm, in which there is resistance to deflection by bending; rather than as a membrane, in which there is a resistance to deflection by stretching. Pressure causing deflection of the outer polyethylene diaphragm was transmitted through the oil to the recessed transducer. Transducer output was therefore proportional to average deflection of the outer diaphragm, indicating that the appropriate spatial response function was the fourth one listed in Table 5.1: $G(x) = \frac{16}{5\pi a}\left[1 - \left(\frac{x}{a}\right)^2\right]^{5/2}$.

The wave front celerity U_d, corresponding to the pressure function $P_r(t)$ examined, was measured experimentally. The continuous recorded function $P_r(t)$ was put into digital form. With the aid of an IBM 7040/7094 high-speed digital computer, the integral $I(\omega, a, U_d)$ and the Fourier transform $\pi_r(\omega)$ of $P_r(t)$ were computed. Next, the inverse transform of the ratio π_r/I was computed to give $P_{ac}(x-U_d t)$.

An application of the correction procedure is illustrated in Figure 5.4a, for a transducer radius, a, of 0.0052 ft, and a wave front celerity U_d of 6.0 ft/sec. In the top panel, it is seen that values of both the real and imaginary parts of $\pi_r(\omega)$ are relatively small for $\omega > 3000$ sec $^{-1}$ compared to values for $\omega < 1000$ sec^{-1}. Therefore for purposes of computation it has been possible to limit ω to the range $0 < \omega < 4500$ sec^{-1} with only negligible loss of information in π_r for $\omega > 4500$ sec^{-1}. For $0 < \omega < 4500$ sec^{-1}, the integral $I(\omega, a, U_d)$ is positive, ranging from unity to about 0.35. In the second panel, the real and imaginary parts of $\pi_{ac}(\omega) = \pi_r(\omega)/I(\omega, a, U_d)$ are qualitatively similar to $\pi_r(\omega)$. In the bottom panel, the inverse transform of $\pi_{ac}(\omega)$ results in a predicted pressure function $P_{ac}(t)$ that is quite similar to the recorded function $P_r(t)$, except for slightly increased peak pressure and slightly reduced rise-time.

The application of the correction procedure illustrated in Figure 5.4a is "successful" in that a coherent pressure distribution $P_{ac}(t)$ is obtained, yet since the difference between P_{ac} and P_r is quite small, it would seem that the correction needed in this particular case was not great to begin with, i.e. the rise-length b may be

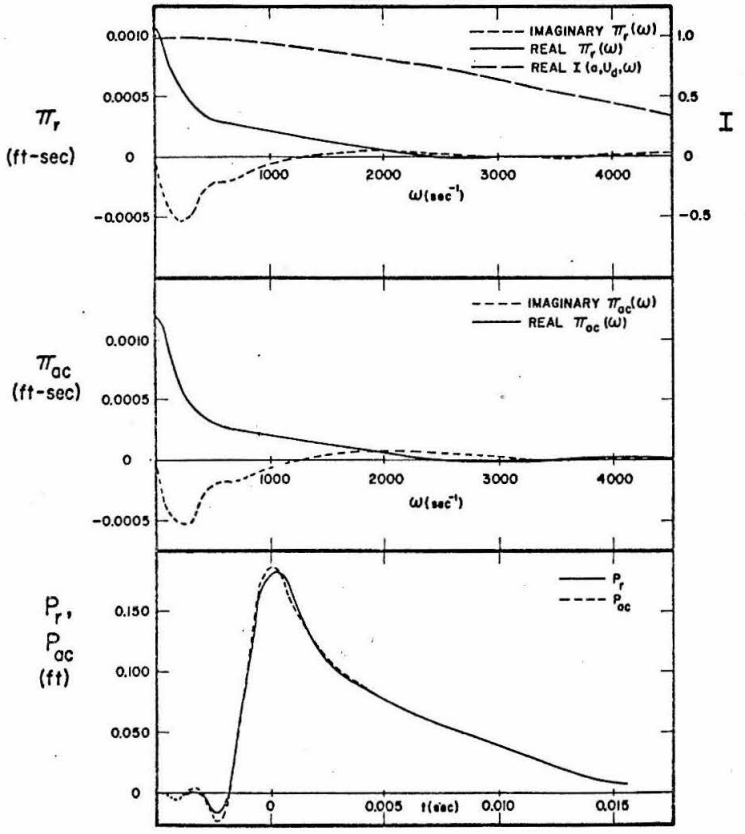

a) U_d = 6.0 ft/sec, a = 0.0052 ft, t_r = 0.0019 sec.

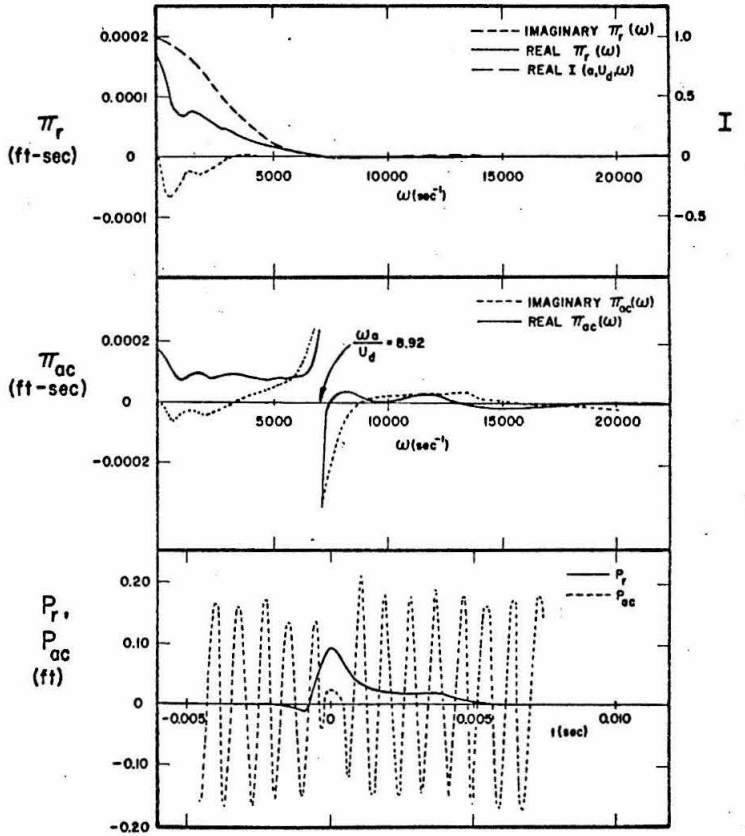

b) U_d = 4.1 ft/sec, a = 0.0052 ft, t_r = 0.0008 sec.

Figures 5.4. Application of the Fourier transformation correction procedure.

sufficiently greater than the transducer radius a that the error introduced by finite transducer size is small.

Another, less successful, application of the correction procedure is illustrated in Figure 5.4b, for a transducer radius, a, of 0.0052 ft and a wave front celerity U_d of 4.1 ft/sec. In the bottom panel it is seen that in this case the rise=time t_r of the recorded function P_r is about 0.0008 sec, considerably less than in the case illustrated in Figure 5.4a, where the rise-time is about 0.0019 sec. Correspondingly, the range of values of ω for which $\pi_r(\omega)$ is of significant amplitude is greater in Figure 5.4b than in Figure 5.4a: for example, at $\omega = 4500$ sec^{-1} the real part of π_r is of significant amplitude in Figure 5.4b, whereas it is of negligible amplitude in Figure 5.4a. For purposes of computation it is therefore necessary to extend the range of ω, so that all significant values of π_r are included.

However, the extended range of ω now includes the value $\omega = 7040$ sec^{-1} $= 8.92\ U_d/a$, where $I(\omega, a, U_d)$ becomes zero but where the real and imaginary parts of $\pi_r(\omega)$ have positive, albeit small, values. In the second panel of Figure 5.4b, the function $\pi_{ac}(\omega) = \pi_r(\omega)/I(\omega, a, U_d)$ is dominated by the very great values that result for ω near 7040 sec^{-1}. The appearance of both real and imaginary parts of $\pi_{ac}(\omega)$ is not unlike that of the Dirac delta function $\delta(\omega-\omega_o)$, where $\omega_o = 7040$ sec^{-1}. The resultant inverse transform $P_{ac}(t)$ resembles more the inverse transform of a delta function, i.e. a cosine function of angular frequency $\omega_o = 7040$ sec^{-1}, than it resembles a corrected pressure function qualitatively similar to the recorded function $P_r(t)$.

Therefore, the correction procedure derived in this section either provides a coherent but not particularly informative result, as in Figure 5.4a, or its produces an incoherent result, as in Figure 5.4b. For this reason another correction procedure was developed, as will be discussed in Section 5.3.

Several studies concerning the loss of signal resolution due to transducer size have been reported in the literature. All studies known to the writer (Uberoi and Kovasznay, 1953; Liepmann, 1952; Willmarth and Roos, 1965) have been concerned with the measurement of stochastic properties of a random field, rather than of a particular pressure distribution as in the present study.

The work of Uberoi and Kovasznay (1953) and of Liepmann (1952) showed that if the properties of the recorded stochastic function and of the transducer are completely known, the properties of the original stochastic function can be recovered. The mathematical formulation of the problem by Uberoi and Kovasznay is essentially similar to that presented in this section: the recorded function is assumed to be related to the actual function through a convolution integral, as in Equation 5.2, where the kernel represents the spatial response characteristics of the transducer. The convolution integral equation is solved by the use of Fourier integrals, as in Equations 5.10 to 5.12.

Willmarth and Roos (1965), in measuring fluctuations of pressure on a flow boundary beneath a turbulent boundary layer, attempted to correct measurements made with finite-sized transducers by the method of Uberoi and Kovasznay. As in the present study, difficulties arose in applying the correction procedure to any but low spectral frequencies, because of zeroes in the transform of the function

representing transducer characteristics (corresponsing to the function $I(\omega, a, U_d)$ in Equation 5.12).

5.3 Correction of Rise-Time and Peak Pressure.

Since the correction procedure described in Section 5.2, which was to provide a corrected time-dependent pressure function, was not capable of producing useful results, an attempt was made to devise a procedure to provide corrected values for at least the peak pressure P_2 and the rise-time t_r, the two parameters which describe in a fundamental way the pressure distribution near the wave front.

To gain fundamental understanding of the defect process, Equation 5.6 was evaluated for several mathematical models of actual pressure distribution $P_{ac}(x-U_d t)$. Three of the models chosen were of the form of single, symmetric pulses of unit amplitude and width 2b, viewed at the time t when the pulses are centered at the transducer center:

$$P_{ac}(x) = 1 - \left(\frac{x}{b}\right)^n \qquad \text{for } x \le b, \tag{5.13a}$$

$$P_{ac}(x) = 0 \qquad \text{for } x > b. \tag{5.13b}$$

Three values of n were examined: n = 1 (for triangular distribution), n = 2 (for a parabolic distribution), and $n = \infty$ (for a top-hat distribution). A fourth model distribution was a cosine function with a wave length, 4b:

$$P_{ac}(x) = \cos \frac{\pi x}{2b}. \tag{5.14}$$

If it is assumed that peak transducer output occurs when the peak of the pressure distribution is at the transducer center, a pressure distribution with its maximum situated at the transducer center may be considered a model of the pressure distribution at the instant when the recorded pressure is a maximum. The "defect ratio" R is now defined as the ratio of recorded peak pressure P_{2r} to actual peak pressure P_{2ac}:

$$\int_{-a}^{a} G(x)\, P_{ac}\, dx = P_{2r} = RP_{2ac} , \qquad (5.15)$$

when the recorded pressure is a maximum.

Figure 5.5 shows the dependence of the defect ratio R upon the form of the pressure distribution, and upon its width b normalized with respect to the transducer radius a, for the four models of pressure distribution described by Equations 5.13 and 5.14. The normalized width parameter b/a varies from 0 to 3. Each of the three single symmetric pulse functions (top-hat, parabolic, and triangular) is integrated with each of the last three spatial response functions listed in Table 5.1 (for a membrane, output proportional to average deflection; for a diaphragm, output proportional to average deflection; for a diaphragm, output proportional to deflection at the center). The cosine distribution is integrated with the fourth function listed in Table 5.1, for the case of a diaphragm whose average deflection is proportional to transducer output.

Figure 5.5 shows that for the single-pulse distributions, R increases monotonically from zero at b/a = 0, and approaches unity as b/a increases. The defect ratio R sometimes has negative values for the cosine distribution for small b/a, but again R approaches unity as b/a increases. It is apparent that for a given value of b/a, the defect

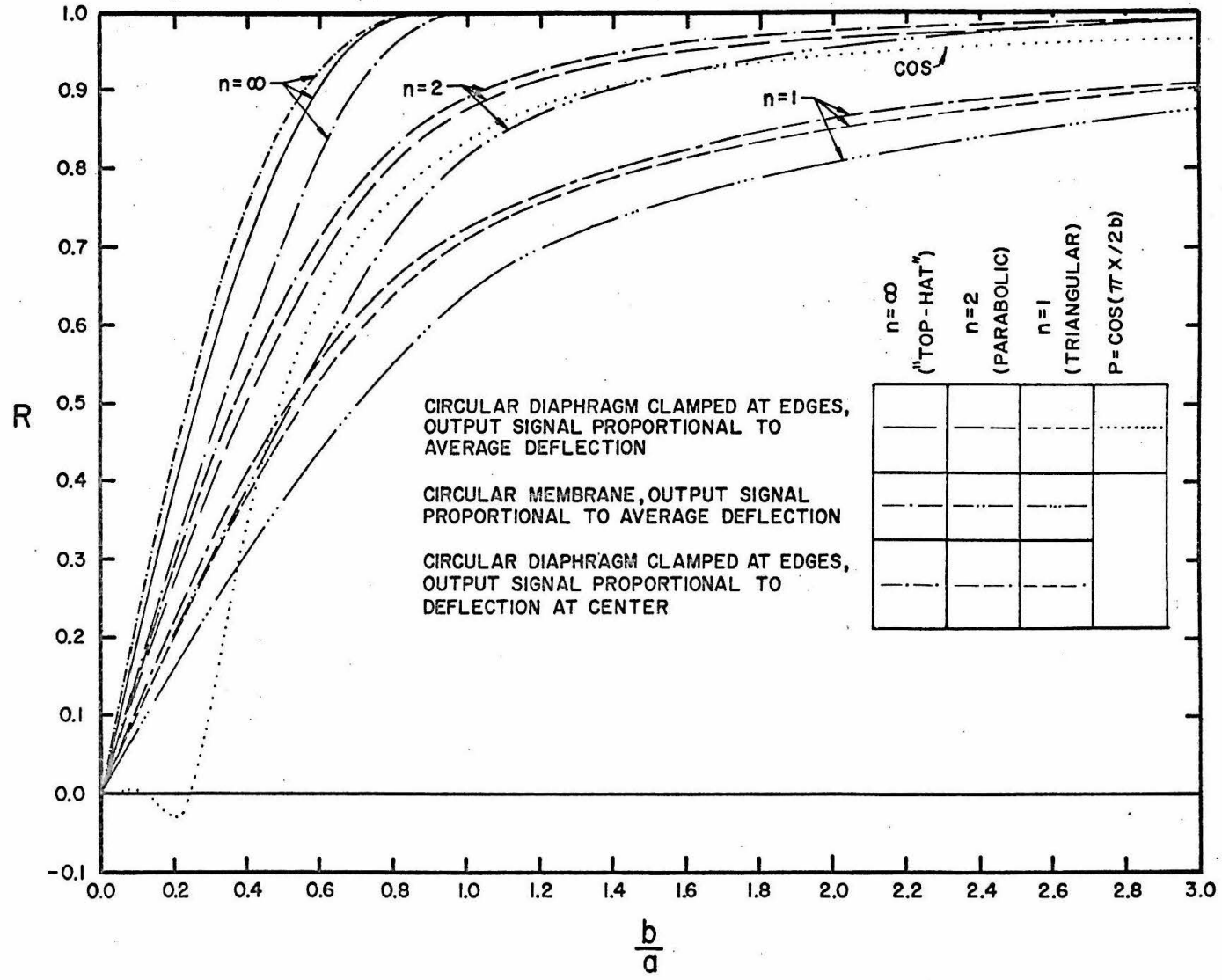

Figure 5.5. The defect ratio R as a function of pressure distribution, and transducer spatial response.

ratio R depends more strongly on the form of the pressure distribution (top-hat, parabolic, triangular, or cosinusoidal) than it does on transducer structure. (For $b/a > 0.5$, the defect ratio for the cosinusoidal pressure distribution is in close agreement with values of R for the parabolic distribution, $P_{ac} = 1 - \left(\frac{x}{b}\right)^2$, a result that is not surprising when it is remembered that the first two terms of a Taylor's series expansion about $x = 0$ for $\cos\left(\frac{\pi x}{2b}\right)$ are $P_{ac} = 1 - \frac{1}{2}\left(\frac{\pi x}{2b}\right)^2$, similar to the parabolic distribution).

The effect of finite transducer area on measured rise-time was hypothesized at the beginning of the section, assuming that peak transducer output P_{2_r} occurs when the peak of the actual distribution is located at the transducer center: as shown in Figure 5.1c, the recorded rise-time t_r, the time interval between the time of zero deflection, is the time interval between the time t_A when the pressure distribution first arrives at the edge of the transducer diaphragm, causing initial deflection, and the time t_B when the peak of the pressure distribution arrives at the transducer center causing maximum deflection: $t_r = t_B - t_A$. The distance travelled in the time interval t_r is the rise-length b plus the transducer radius a, i.e., $t_r = (a + b)/U_d$, where U_d is the celerity of the pressure distribution (Equation 5.1). Correspondingly, the rise-length b may be derived in terms of the recorded rise-time t_r:

$$b = U_d t_r - a. \tag{5.16}$$

The effect of finite transducer size may therefore be summarized as follows: the recorded peak pressure P_{2_r} will be less than

the actual peak pressure $P_{2\,ac}$ by a factor R, and the recorded rise-time t_r will be greater than the actual rise-time (i.e. the rise-time that would be recorded by an ideal, infinitesimal transducer) by an amount a/U_d, where a is the transducer radius and U_d is the celerity of the pressure distribution.

The correction procedure described next, which was applied to peak pressure and rise time data in the present study, does not depend on a particular spatial response function G(x), as did the correction procedure described in Section 5.2. It is actually an extrapolation procedure using peak pressure and rise time data obtained with a transducer of finite size to predict values that would be obtained with an infinitesimal transducer, i.e. one for which a = 0. The procedure is based on qualitative considerations of peak pressure defect and rise time increment as expressed in Equations 5.15 and 5.1.

The following assumptions were made: 1) the celerity U_d of the wave front (and of the pressure distribution) is approximately constant for the time taken for the wave front to cross the transducer, i.e $\frac{dU_d}{dx}\,\frac{a}{U_d}$ is much less than unity; 2) the wave form does not vary in the transverse direction over the transducer width; 3) pressure distributions at the wave front are similar for all experimental conditions, and are time-dependent only as a propagating wave form, i.e.:

$$P_{ac} = P_{2\,ac}\,\varphi\left(\frac{x - U_d t}{b}\right), \tag{5.17}$$

where $P_{2\,ac}$ and b may vary, but the form function φ depends solely on the value of the argument $(x - U_d t)/b$; 4) the greatest transducer

output P_{2_r} occurs when the actual pressure peak is centered on the transducer center; 5) the defect ratio R increases monotonically with the ratio of rise-length to transducer radius b/a, from a value of zero at b/a = 0 to a value asymptotically approaching unity as b/a becomes large (as shown in Figure 5.5); 6) hydrodynamic models of different absolute size that are geometrically similar exhibit kinematic and dynamic similarity according to the Froude modelling law, i.e. scale effects due to viscosity or surface tension are assumed to be negligible; and 7) dynamic properties of the transducer may be neglected in the analysis. These assumptions are re-examined in the light of experimental data in Section 6.6

With the wave celerity U_d, the measured rise-time t_r, and the transducer radius, a, known, the rise-length b is obtained directly from Equation 5.16. The corrected rise-time is then the ratio b/U_d, or $t_r - a/U_d$.

To correct the recorded peak pressure P_{2_r}, it is necessary to construct empirically the function R=R(b/a) such as shown for several mathematical models in Figure 5.5. The ratio R of recorded peak pressure to actual peak pressure cannot be determined directly, but ratios of R at two different values of b/a may be obtained by conducting two experiments, similar in every respect except for the value of b/a. Such a pair of experiments could be performed with two transducers of differing radius, a, operating simultaneously and side-by-side, sampling pressures generated by a single wave; or the pair of experiments could be performed with one transducer operating at two different model scales maintaining complete geometric, kinematic,

and dynamic similitude except for the ratio b/a, which would be proportional to the absolute length scale.

For purposes of discussion (and because it was the procedure actually used, as will be described in Section 6.6), it may be supposed that data obtained from a pair of similar experiments, with a single transducer operating at two model scales, are to be compared. The subscript $(\ )_M$ will be used to denote the larger model scale, and the subscript $(\ )_m$ will be used to denote the smaller model scale.

Since it is assumed that there is dynamic similarity between scales, the actual normalized peak pressure obtained in the two experiments will be the same at both scales:

$$\left(\frac{P_2 ac}{\gamma d}\right)_M = \left(\frac{P_2 ac}{\gamma d}\right)_m , \tag{5.18}$$

where γ is the unit weight of water and where the still water depth d is used as a measure of scale size. There will also be equality of normalized rise-length:

$$\left(\frac{b}{d}\right)_M = \left(\frac{b}{d}\right)_m . \tag{5.19}$$

The only systematic difference between these experiments would be in the ratio of characteristic lengths to the transducer radius, such as b/a:

$$\left(\frac{b}{a}\right)_M = \left(\frac{d_M}{d_m}\right)\left(\frac{b}{a}\right)_m . \tag{5.20}$$

The defect ratio R is assumed to be a function of b/a that is common to both model scales. Therefore, since from Equation 5.20:

$$\left(\frac{b}{a}\right)_M > \left(\frac{b}{a}\right)_m , \tag{5.21}$$

it is expected that:

$$R_M > R_m, \tag{5.22}$$

for a given set of experimental conditions.

From Equations 5.15 and 5.18:

$$\frac{\left(P_{2r}/\gamma d\right)_M}{\left(P_{2r}/\gamma d\right)_m} = \frac{R_M\left(P_{2ac}/\gamma d\right)_M}{R_m\left(P_{2ac}/\gamma d\right)_m} = \frac{R_M}{R_m}. \tag{5.23}$$

At this point the functions $\Gamma = \log_{10} R$, $\beta = \log_{10}(b/a)$, and $\Gamma' = d\Gamma/d\beta$ are introduced. (The choice of ten as a logarithm base is arbitrary.) The unknown function $R = R(b/a)$ is sketched schematically in Figure 5.6a, its form derived from the assumption that R increases monotonically with b/a from zero at $b/a = 0$ to values approaching unity, as shown by curves in Figure 5.5. The function $\Gamma = \Gamma(\beta)$ is sketched schematically in Figure 5.6b. From the general form of $R = R(b/a)$, one may infer that Γ will have negative values that asymptotically approach zero as β increases. The function $\Gamma' = d\Gamma/d\beta$ is sketched schematically in Figure 5.6c. Figure 5.5 shows that as b/a increases, the rate of change of R with b/a decreases. Similarly, the rate of change $d\Gamma/d\beta$ will decrease with increasing β.

The subscript notation may be extended to Γ and β:

$$\log_{10} R_M = \Gamma_M, \quad \log_{10} R_m = \Gamma_m,$$
$$\log_{10}(b/a)_M = \beta_M, \quad \log_{10}(b/a)_m = \beta_m. \tag{5.24}$$

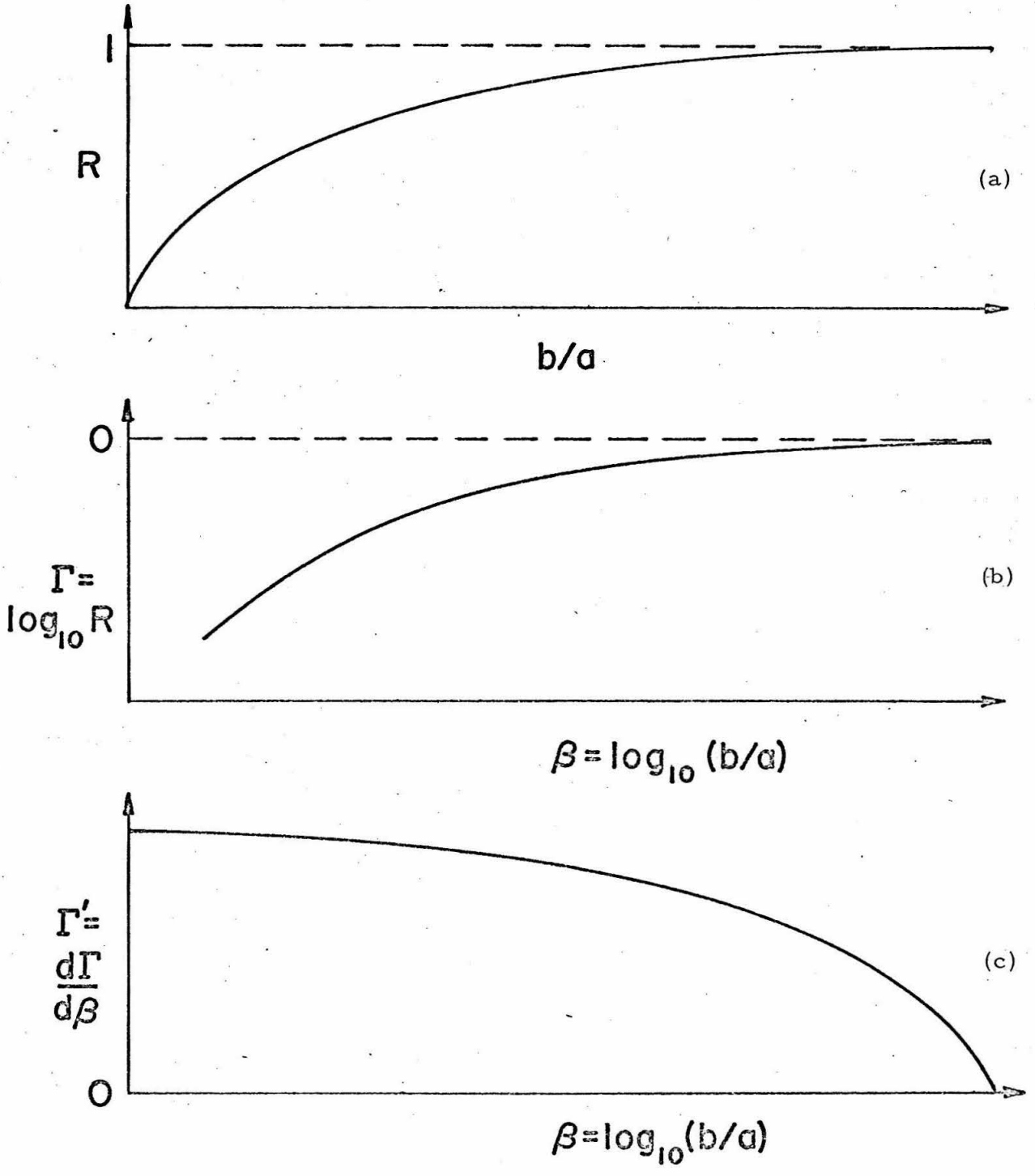

Figures 5.6. The defect ratio R = R(b/a) and the associated functions $\Gamma = \Gamma(\beta)$ and $\Gamma' = \Gamma'(\beta)$ used to determine R = R(b/a) from experimental data.

Now from Equations 5.20, 5.23, and 5.24:

$$\frac{\log_{10}\left[\frac{(P_{2_r}/\gamma d)_M}{(P_{2_r}/\gamma d)_m}\right]}{\log_{10}\left[\frac{(b/a)_M}{(b/a)_m}\right]} = \frac{\log_{10}\left[\frac{R_M}{R_m}\right]}{\log_{10}\left[\frac{d_M}{d_m}\right]} = \frac{\Gamma_M - \Gamma_m}{\beta_M - \beta_m} \qquad (5.25)$$

The ratio of differences on the far right-hand side of Equation 5.25 may be approximated as a differential:

$$\frac{\Gamma_M - \Gamma_m}{\beta_M - \beta_m} \cong \frac{d\Gamma}{d\beta} = \Gamma'. \qquad (5.26)$$

The differential Γ' may be supplied with an argument β equal to the arithmetic average of β_M and β_m:

$$\beta = \frac{\beta_M + \beta_m}{2} = \log_{10}\left[(b/a)_M (b/a)_m\right]^{1/2} \qquad (5.27)$$

Since $(b/a)_M = (b/d)d_M/a$ and $(b/a)_m = (b/d)\,d_m/a$:

$$\beta = \log_{10}\left[(b/d)\sqrt{d_M d_m}/a\right]. \qquad (5.28)$$

From each pair of experiments performed at the two model scales, values of P_{2_r}, b, d, and a may be obtained so that Γ' and a corresponding value β may be computed. Experimental conditions are then varied in each model to generate as wide a range of values of $P_{2_r}/\gamma d$ and b/a as possible, so that a range of values of Γ' and β as wide as possible may be obtained. The differential Γ' is then

plotted against β as in Figure 5.6c, and a curve is fitted to the data. The function is then integrated numerically to give $\Gamma(\beta)$. As an integration condition, it is assumed that since R approaches unity as dR/d(b/a) approaches zero, as shown in Figures 5.5 and 5.6a, then $\Gamma(\beta)$ should become zero at that value of β where $\Gamma'(\beta)=d\Gamma/d\beta$ equals zero. The final step is to transform $\Gamma(\beta) = \log_{10}R$ to $R = R(b/a)$.

Now each recorded peak pressure P_2 may be corrected by the appropriate value of R. Two values of $P_{2_r}/\gamma d$ obtained for similar experimental conditions at the two model scales, after each value has been corrected, should yield the same value of $P_{2_{ac}}/\gamma d$, as indicated by Equation 5.18.

The logarithmic correction procedure just described was applied to the rise-time and peak pressure data obtained in the present study. The details and discussion of the results of the procedure as actually applied are presented in Section 6.6.

An extrapolation procedure that was simpler and more direct than the logarithmic extrapolation procedure just described was used by Willmarth and Roos (1965). After attempting to correct measurements made with finite-sized transducers by the method of Uberoi and Kovasznay (1953), Willmarth and Roos compared data taken with transducers having four different diameters, and were able to extrapolate the results linearly to estimate the function which would be recorded by an infinitesimal transducer. The measured power spectrum of pressure fluctuations on a flow boundary beneath a turbulent boundary layer varied approximately linearly with transducer radius as the radius approached zero. The extrapolation procedure "was not difficult, not did it appear uncertain" (Willmarth and Roos, 1965,

p. 88, footnote). The measured power spectrum function integrated with respect to frequency, that is the measured root mean square wall pressure, also varied linearly with transducer radius, and a value for zero radius could apparently be obtained by linear extrapolation.

Correction of the peak pressure data by linear extrapolation, as suggested by Willmarth and Roos, is presented in Section 6.6, and is compared with the corrections made by the logarithmic extrapolation method outlined in this section.

CHAPTER 6

RESULTS

As indicated by the Table of Contents, the measurements of profile, celerity, and decay rate for the incident wave are presented and discussed in Section 6.1. In Section 6.2 the observed flow in the neighborhood of the platform is discussed, accompanied by several series of photographs showing generated waves striking the platform. Measurements of water surface elevation at the seaward edge of the platform are also presented.

In Section 6.3, the pressure records and methods of data reduction are discussed, in light of the discussion of operating procedure presented in Section 4.5.

In Section 6.4 the elapsed travel times and celerities of the advancing wave fronts and the waves of recession are presented and discussed. In Section 6.5 the functional form and the amplitude of the slowly-varying pressure is presented, and in Section 6.6 the peak pressure is corrected for transducer area defect, and its functional dependence on other parameters is examined.

Except where indicated, all data are derived from experiments made in the 100-ft wave tank.

6.1 The Incident Wave.

In Chapter 1, it was stated that the requirements for the incident wave were that the wave be a single intumescence (or at least the first of a train of waves) propagating into still water; that the wave form be subject to accurate mathematical representation; and that it be a relevant model of finite-amplitude ocean waves propagating through shoal water.

As stated in Chapter 1, the so-called solitary wave was chosen as the incident wave. The definitive solitary wave characteristics set forth by Lamb (1945) and by Stoker (1957), mentioned in Section 2.4, were that the solitary wave has a single, symmetric elevation, propagates without change of form, and may be of finite amplitude-to-depth ratio. The profile, celerity, and other characteristics of the solitary wave have been theoretically analyzed by Boussinesq (1872), McCowan (1891), Laitone (1963), and others. Munk (1948) has argued that the solitary wave may be used as an approximate model for a finite-amplitude ocean wave propagating into shoal water. The solitary wave therefore satisfies the requirements that the incident wave be a single elevation, mathematically describable, and a relevant model of a wave in shoal water. As described in Section 4.2, the wave generators in the present study were designed according to the solitary wave theory of Boussinesq (1872).

However, it should be borne in mind that precisely speaking, the solitary wave is an ideal wave whose exact form is unknown. On the one hand, all the theoretical expressions for the profile and celerity of the solitary wave are to some degree approximate. On the other hand, "solitary" waves generated in the laboratory are generally accompanied by a following train of parasitic wavelets, albeit often of relatively small amplitude. Therefore, when theoretical profiles and celerities for the solitary wave are compared with profiles and celerities of the generated waves, it is fruitless to attempt to judge how well the generated wave represents a "solitary wave", since the precise form of the solitary wave is unknown. Rather, it is more pertinent to judge how well the generated wave is

described mathematically by the approximate solitary wave theories, and to judge which solitary wave theory describes the generated wave best.

In Section 4.4, a typical wave gauge trace was presented in Figure 4.18b. Other wave gauge traces shown in Figure 6.1 show more clearly the time history of water surface elevation at four locations before and after passage of the principal intumescence.

The record of four wave gauge traces shown in Figure 6.1 was obtained in a test to determine amplitude decay of the generated wave, to be discussed later in this section. Four wave gauges of the type described in Section 4.4 were mounted along the wave tank centerline at 10-ft intervals. The order of the recorded traces in Figure 6.1 corresponds to the spatial order of the corresponding wave gauges. The lowest trace was produced by a gauge mounted 45 ft from the generator. The uppermost trace was produced by a gauge mounted 75 ft from the generator, at the section of the wave tank where the test platform was normally located (the platform was removed for the tests described in this section). The uppermost trace therefore indicates the form of the waves incident on the platform.

Before the arrival of the principal wave, the wave gauge at each location records no disturbance, since before the generation of the wave all disturbances of the fluid have been allowed to die out. After the principal wave, the train of waves of small amplitude arrives at the wave gauge, as shown most clearly in the lower two traces in Figure 6.1. However, the amplitude of the following waves is generally only of the order of 5 per cent of the height of the principal wave.

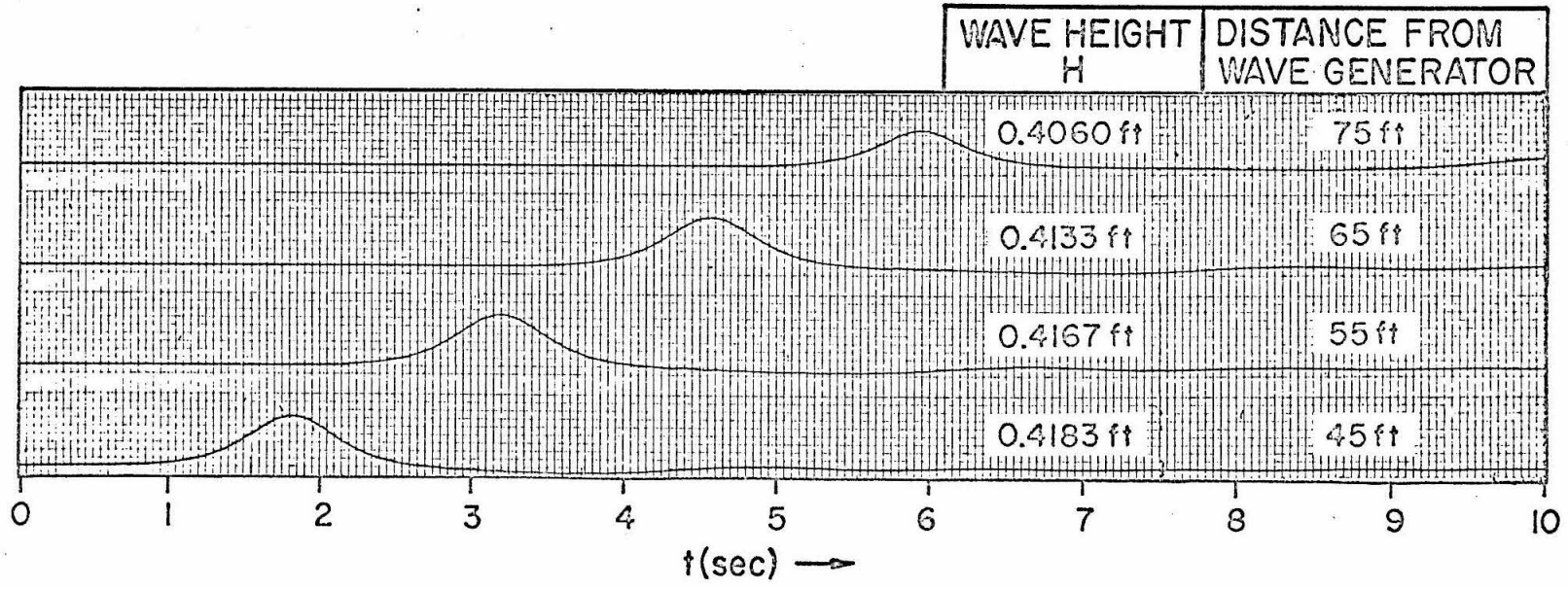

Figure 6.1. Profiles of a wave recorded simultaneously by four wave gauges mounted 45 ft to 75 ft from the wave generator. (Still water depth d = 1.25 ft; generator stroke length D = 1.67 ft).

The theoretical expressions for solitary wave profile and celerity as derived by Boussinesq (1872), McCowan (1891), and Laitone (1963) are presented in Table 6.1. (The expressions for profile by McCowan (1891) are as arranged by Munk (1948).) The expressions for the free-surface profile are given in terms of the surface elevation above still water level $\eta = \eta(x)$, and thus describe the profile as viewed by an observer moving with the wave at its celerity of propagation U_o. To a fixed observer, the time history of the surface elevation may be expressed by replacing x with the quantity $U_o(t+t_o)$, where t_o is a constant, as was done in Equation 3.30 in Chapter 3. The value of $U_o t_o$ is equal to the distance between the location of the fixed observer and the location of the wavecrest at t = 0. If one defines t = 0 to be the time when the wave crest arrives at a wave gauge, then $U_o t_o = 0$, and throughout Table 6.1 one may replace x with $(U_o t)$ to obtain analytical expressions for profiles observed at the location of the wave gauge as the wave propagates past.

In each of the figures in this section indicating experimental and theoretical wave profiles, the surface elevation η has been normalized with respect to its maximum value, the wave height H. The argument $(U_o t)$ has been multiplied by the normalizing factor $\sqrt{\frac{3}{4}\frac{H}{d}}\frac{1}{d}$. Thus normalized, the theoretical profiles by McCowan and by Laitone are still dependent on the ratio of wave height to still water depth H/d; but the profile by Boussinesq assumes the simple form: (ordinate) = sech^2 (abscissa), where the ordinate is η/H and the abscissa is $\sqrt{\frac{3}{4}\frac{H}{d}}\frac{U_o t}{d}$. Thus normalized, the profile by Boussinesq is not dependent on H/d in the same way as the other theories presented.

Table 6.1. Summary of theoretical solitary wave profiles and celerities.

INVESTIGATOR	PROFILE	CELERITY
Boussinesq (1872)	$\frac{\eta}{d} = \frac{H}{d} \operatorname{sech}^2 \sqrt{\frac{3}{4}\frac{H}{d}\frac{x}{d}}$	$\frac{U_o}{\sqrt{gd}} = \sqrt{1 + \frac{H}{d}}$
McCowan (1891) [M is a function of $\frac{H}{d}$ (Munk, 1948)]	$\frac{\eta}{d} = \frac{\sin M\left(1 + \frac{\eta}{d}\right)}{\cos M\left(1 + \frac{\eta}{d}\right) + \cosh M\left(\frac{x}{d}\right)}$ [as presented by Munk, 1948]	$\frac{U_o}{\sqrt{gd}} = \sqrt{\frac{\tan M}{M}}$
Laitone (1963)	$\frac{\eta}{d} = \frac{H}{d} \operatorname{sech}^2 \alpha x - \frac{3}{4}\left(\frac{H}{d}\right)^2 (\operatorname{sech}^2 \alpha x - \operatorname{sech}^4 \alpha x)$ $\left[\alpha x = \sqrt{\frac{3}{4}\frac{H}{d}\left(1 - \frac{5}{8}\frac{H}{d}\right)\frac{x}{d}}\right]$	$\frac{U_o}{\sqrt{gd}} = 1 + \frac{1}{2}\frac{H}{d} - \frac{3}{20}\left(\frac{H}{d}\right)^2$

The three theoretical profiles presented in Table 6.1 are compared with an experimental profile for a ratio of waveheight to still water depth H/d = 0.241 in Figure 6.2, for H/d = 0.386 in Figure 6.3, and for H/d = 0.620 in Figure 6.4. (In each figure there is only one experimental profile from the present study, because rarely do two experimental profiles have exactly the same value of H/d, and since the normalized profiles by McCowan and by Laitone are not independent of H/d, a separate profile must be plotted for each value of H/d.) Figures 6.2 through 6.4 show that at each value of H/d, no theoretical profile fits the data better than that of Boussinesq in the region of the crest (i.e. for $\eta/H > 0.5$); although far from the crest the McCowan profile provides the best fit, and may be judged the best over-all representation of the wave-profile data thus far examined. The Laitone profile gives consistently poorer agreement with data than either of the other two profiles, predicting greater values of η/H than those measured, everywhere except for the trivial cases of large t and zero t.

In Figure 6.4, four experimental profiles obtained by other workers are included. Two profiles by Daily and Stephan (1952), one for H/d = 0.232 and one for H/d = 0.610, are in good agreement with the writer's data. The water depth was reported to be 0.4 ft. A wave profile by Perroud (1957) for H/d = 0.57, obtained in a uniform rectangular channel, agrees well with the data of Daily and Stephan and of the present study. The data from a profile by Perroud for H/d = 0.62, obtained in a channel whose width was decreasing in the direction of propagation, lie well above the data obtained from waves in uniform channels, and exhibit marked asymmetry with respect to the crest.

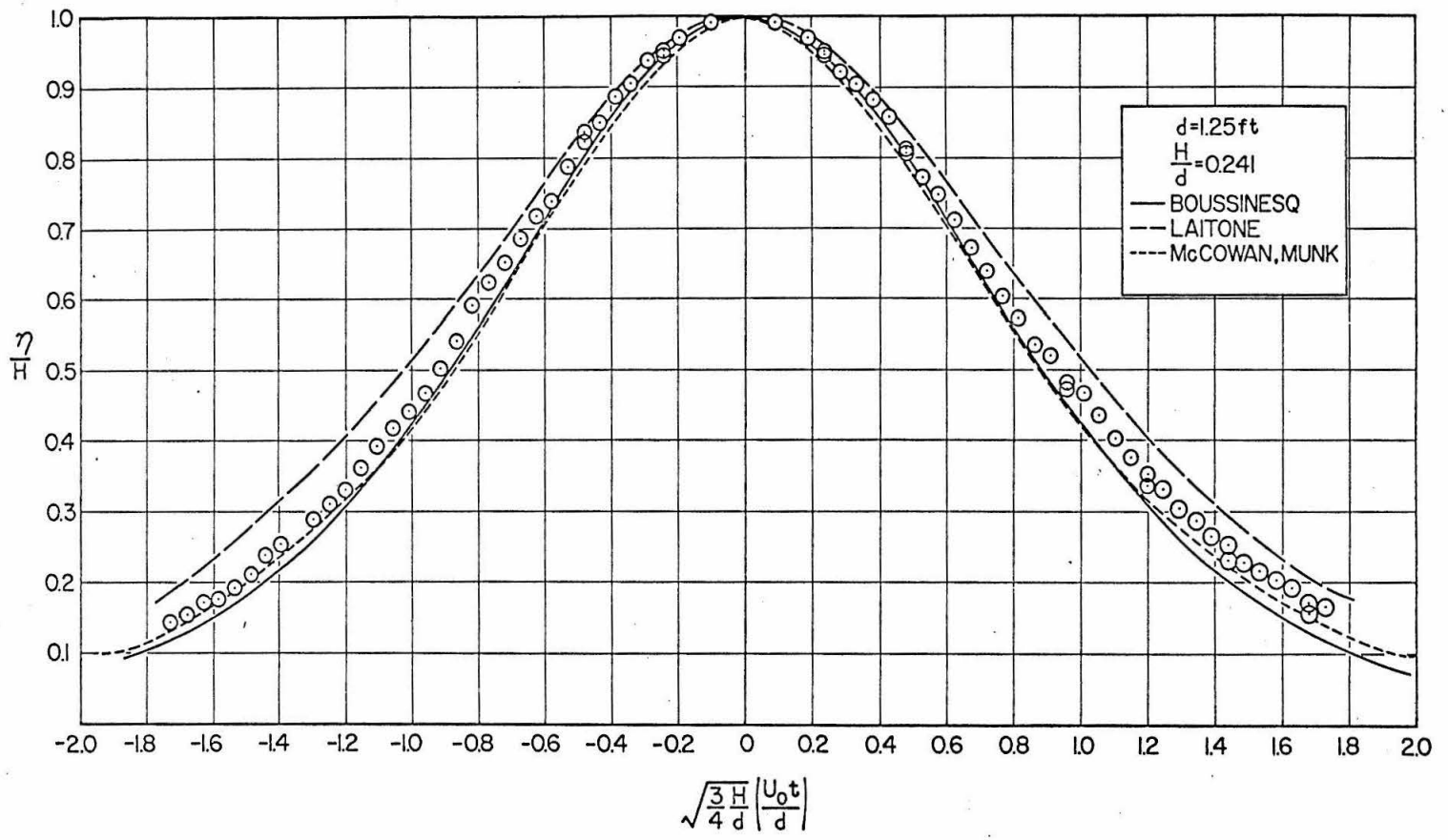

Figure 6.2. Theoretical solitary wave profiles compared with an experimental wave profile. Generator stroke length D = 1.67 ft.

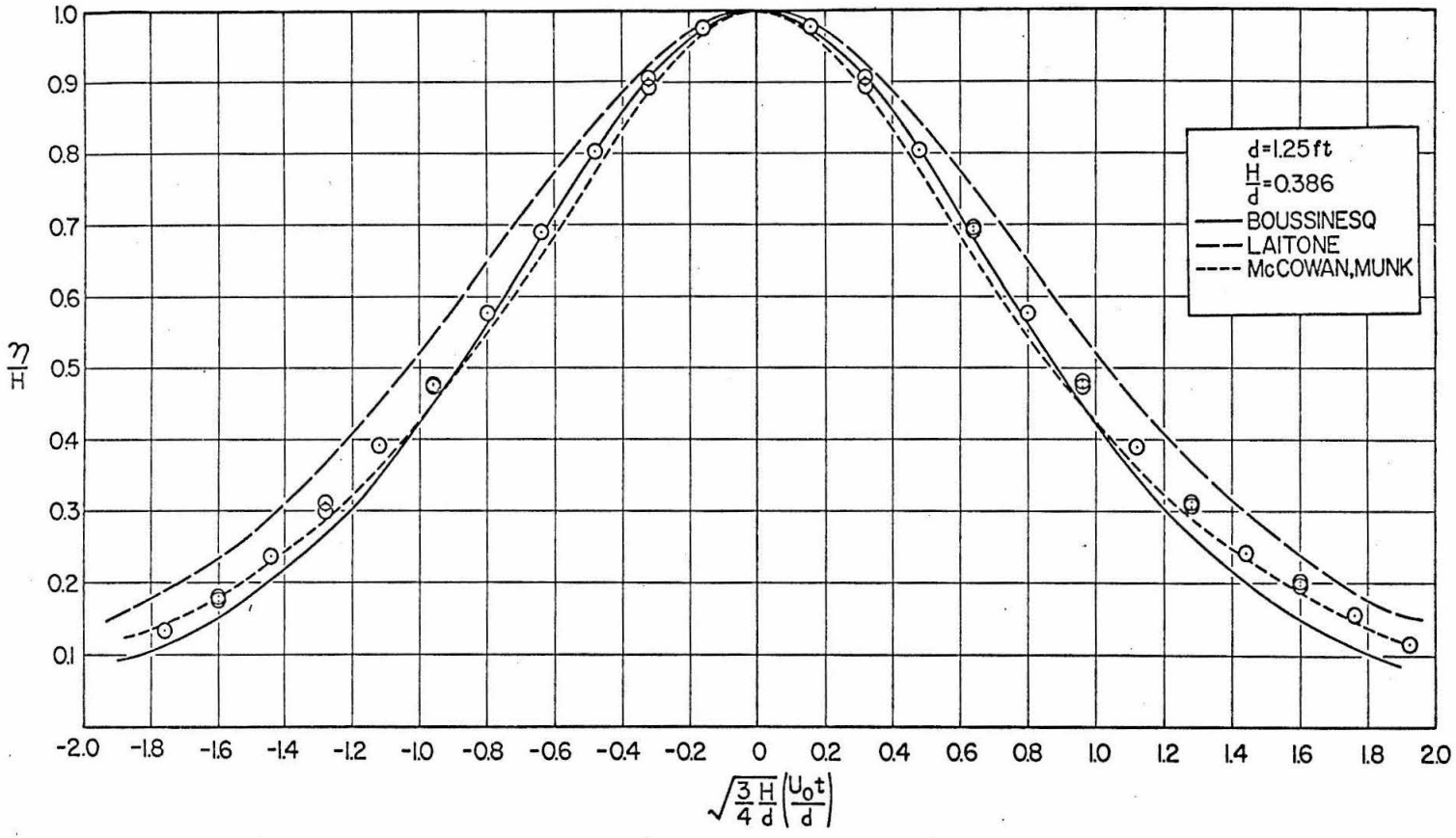

Figure 6.3. Theoretical solitary wave profiles compared with an experimental wave profile. Generator stroke length D = 1.67 ft.

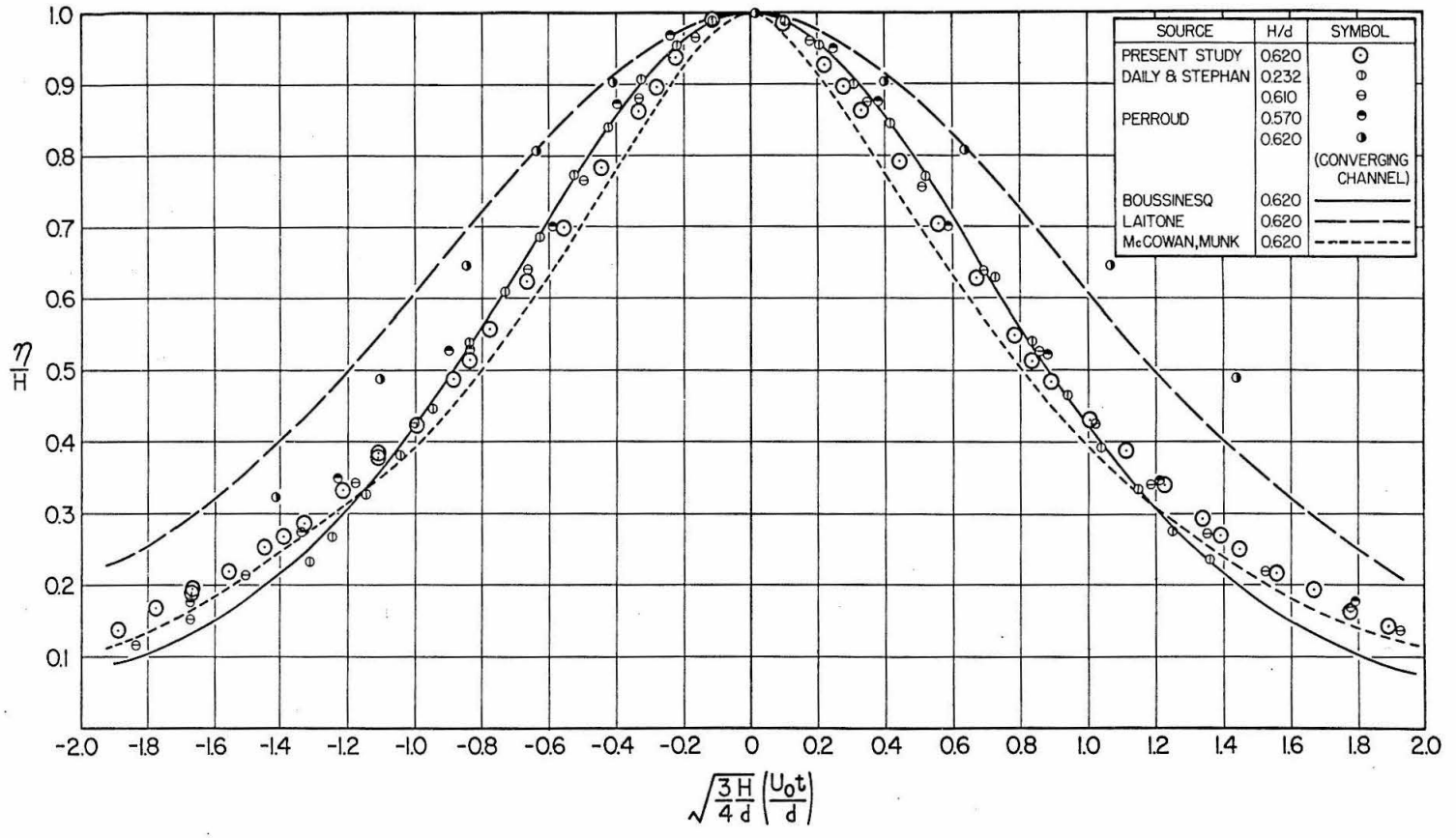

Figure 6.4. Theoretical solitary wave profiles and experimental profiles by other workers compared with an experimental profile from the present study (for which d = 0.75 ft). Generator stroke length D = 1.67 ft.

The profiles obtained by Daily and Stephan (1952), and by Perroud (1957) for a wave in a uniform channel, are best represented by the profile of Boussinesq (1872) in the region near the crest. Despite the overall agreement of the profile of McCowan (1891) with the data shown in Figures 6.2 through 6.4, the Boussinesq profile has been used in this study as the basis of some of the analysis of Chapter 3. Because much of the study involves impact of the wave on a platform with a finite soffit clearance, great accuracy far from the crest is not needed, and close to the crest the Boussinesq profile is as good or better than that of McCowan. Furthermore, the simpler form of the normalized Boussinesq expression does not change with H/d. Use of the proper normalization parameters as employed in Figures 6.2 through 6.4 permits meaningful superposition of several experimental profiles of different H/d onto one graph where they may be compared with a single theoretical profile.

With the Boussinesq theory singled out as the most convenient, and most accurate in the important region near the wave crest, 20 additional experimental profiles are shown in comparison with the Boussinesq profile in Figures 6.5 through 6.8. The data represent different values of H/d, of water depth d, and of wave generator stroke length D. In Figures 6.5, 6.6 and 6.7, the data are from experiments where d = 1.25 ft, 1.00 ft, 0.75 ft, and 0.50 ft, and the wave generator stroke was 1.67 ft (20 in.). The normalized profiles show no measurable dependence upon either relative wave height H/d, relative generator stroke-length D/d, or absolute water depth d. As in Figures 6.2 through 6.4, the experimental profiles are well represented by the theoretical profile of Boussinesq (1872) in the region

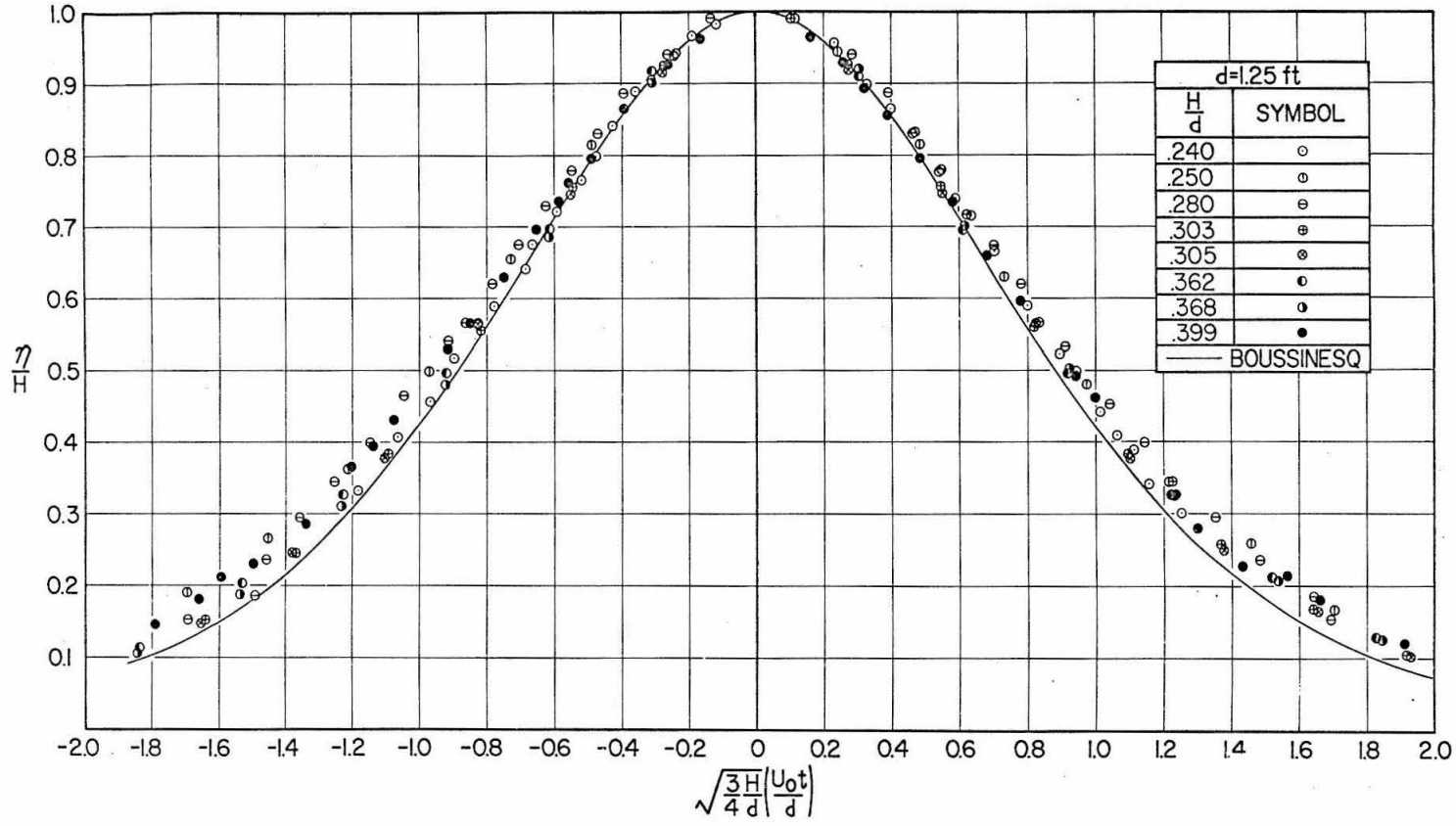

Figure 6.5. Profiles of generated waves, compared with the Boussinesq profile, for d = 1.25 ft and D = 1.67 ft.

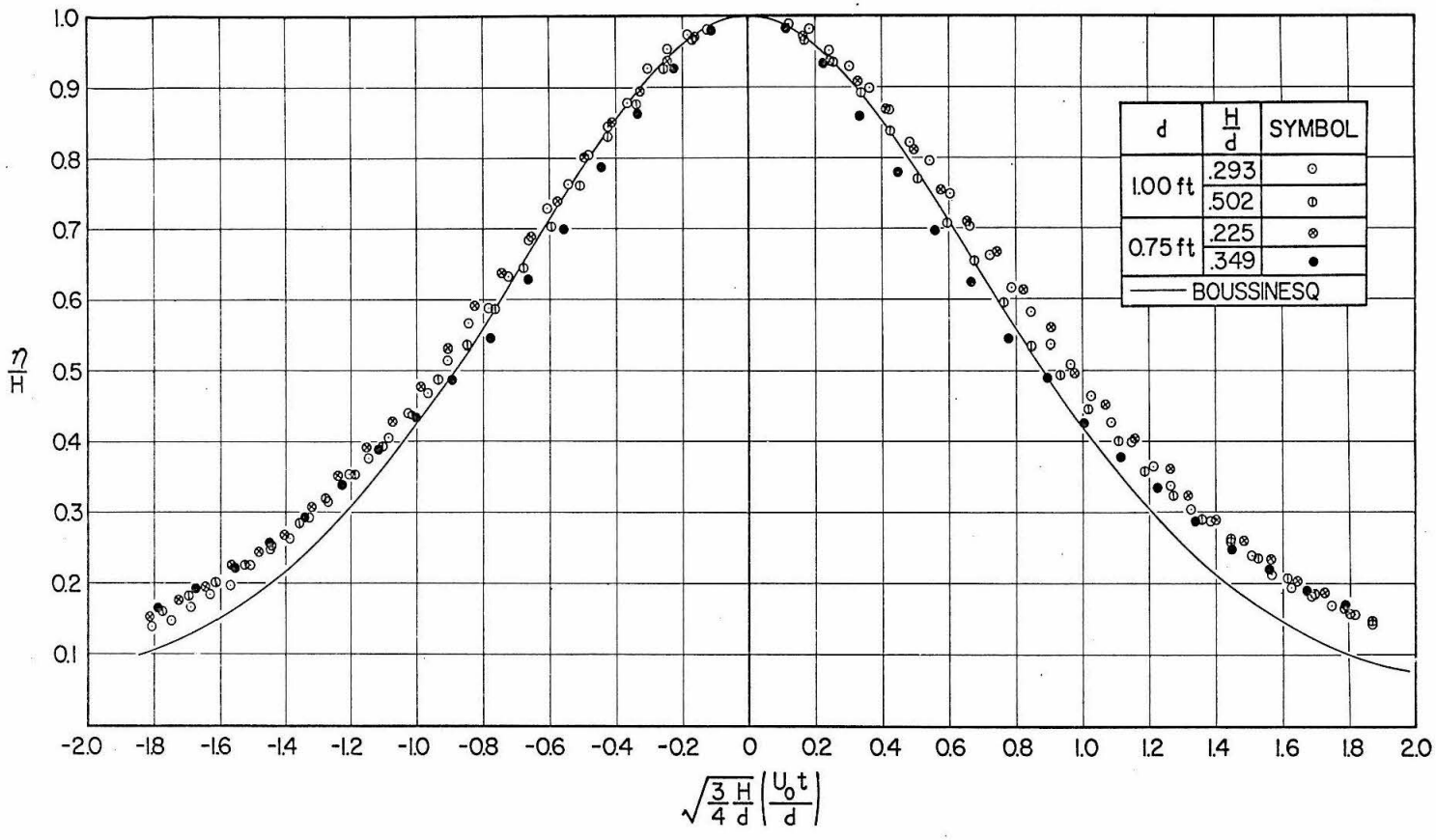

Figure 6.6. Profiles of generated waves, compared with the Boussinesq profile, for d = 1.00 ft and d = 0.75 ft, and D = 1.67 ft.

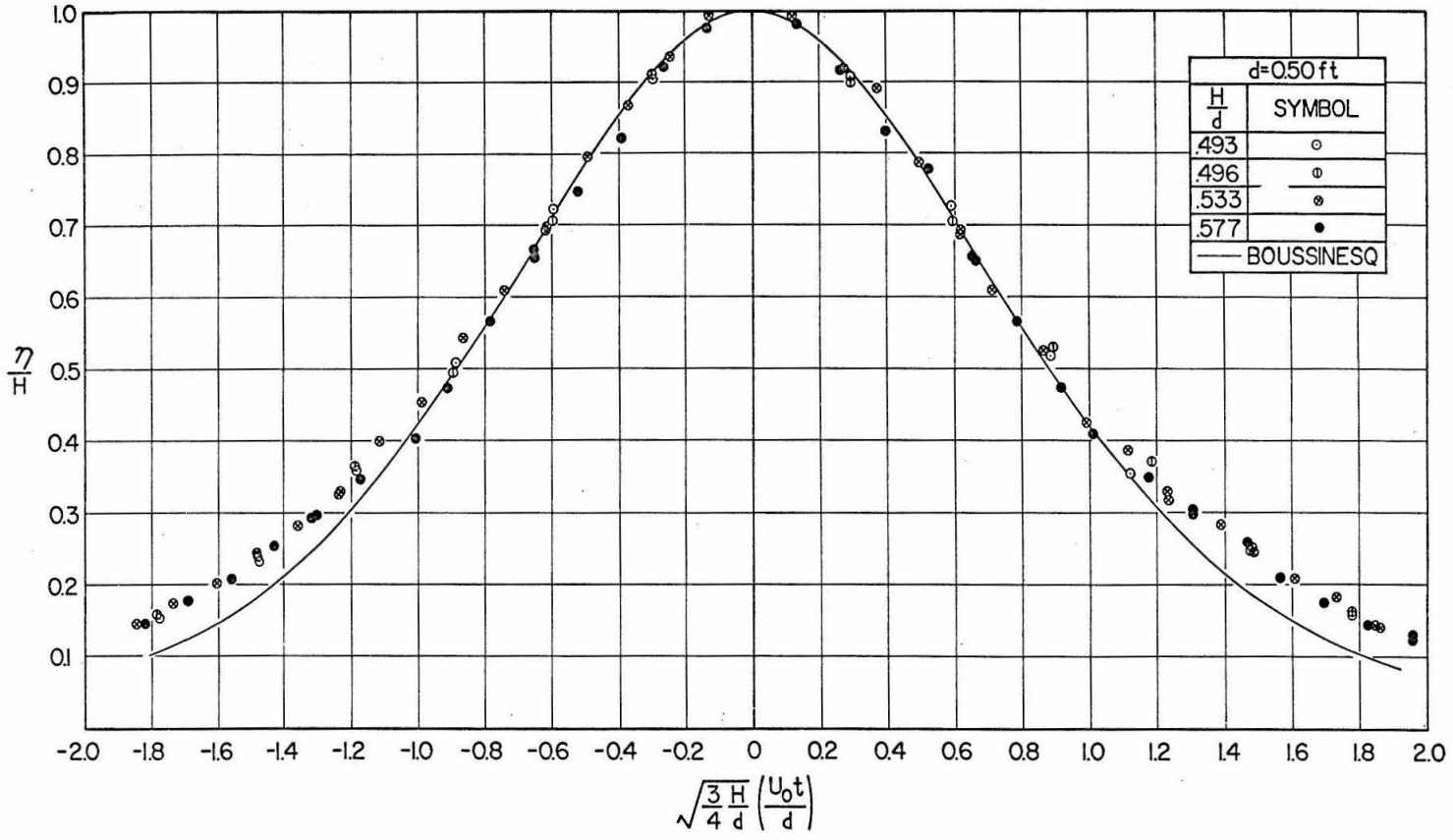

Figure 6.7. Profiles of generated waves, compared with the Boussinesq profile, for d = 0.50 ft and D = 1.67 ft.

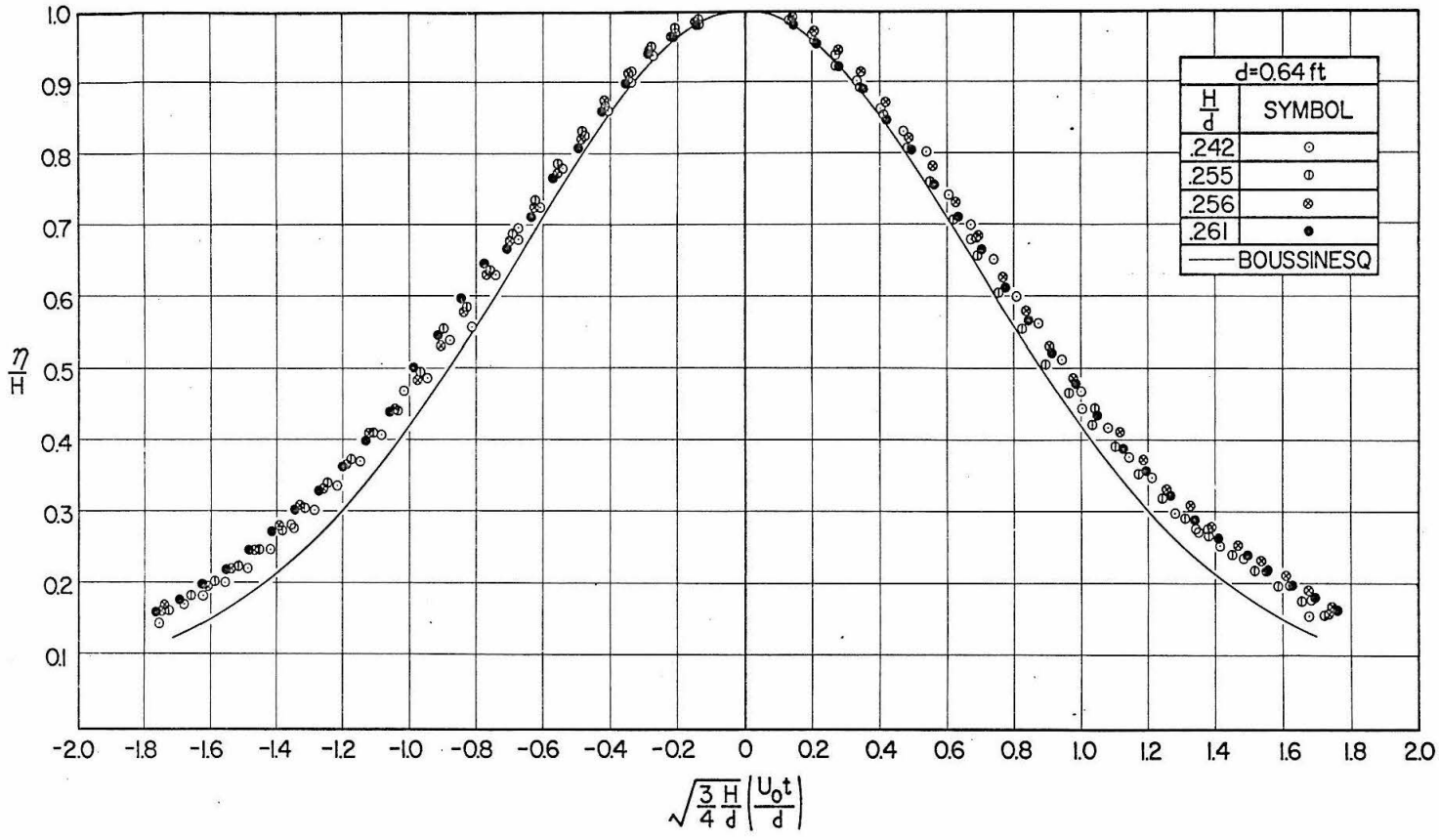

Figure 6.8. Profiles of generated waves, compared with the Boussinesq profile, for d = 0.64 ft and D = 0.83 ft (half-stroke arrangement).

near the crest, while farther from the crest the experimental values of η are greater than the theoretical values.

The wave generator was designed to operate for a depth d of 1.00 ft to 1.25 ft: for lesser depths it was necessary to operate the generator at a shorter stroke in an improvised manner described in Section 4.2. Figure 6.8 shows four profiles from experiments where d = 0.64 ft and the stroke was 0.83 ft (10 in.). The normalized experimental profiles are very nearly the same as those presented in Figures 6.2 through 6.7, demonstrating that operating the wave generator with a shortened stroke did not cause the normalized wave profiles to be appreciably different from normalized profiles obtained with full-stroke operation.

That the normalized profiles obtained in the present study are the same whether generated by full-stroke or by shortened-stroke operation of the generator, and that they agree with profiles obtained by other experimenters studying waves in uniform channels, indicates that the form of laboratory-generated approximations to the ideal solitary wave is relatively independent of the method of generation. (The wave generators used by Daily and Stephan (1952) and by Perroud (1957) are described briefly in Section 2.5.) Similitude between profiles obtained by Daily and Stephan (1952) at a water depth 0.4 ft and those obtained in the present study at a depth of 1.25 ft indicates that scale effects are negligible, and that the predominant forces in the wave are gravity forces and inertial forces.

The measured celerity U_o of the generated waves, normalized by division by $\sqrt{g\,d}$, is plotted against relative waveheight H/d in Figure 6.9. In instances where large samples of waves (16 to 32

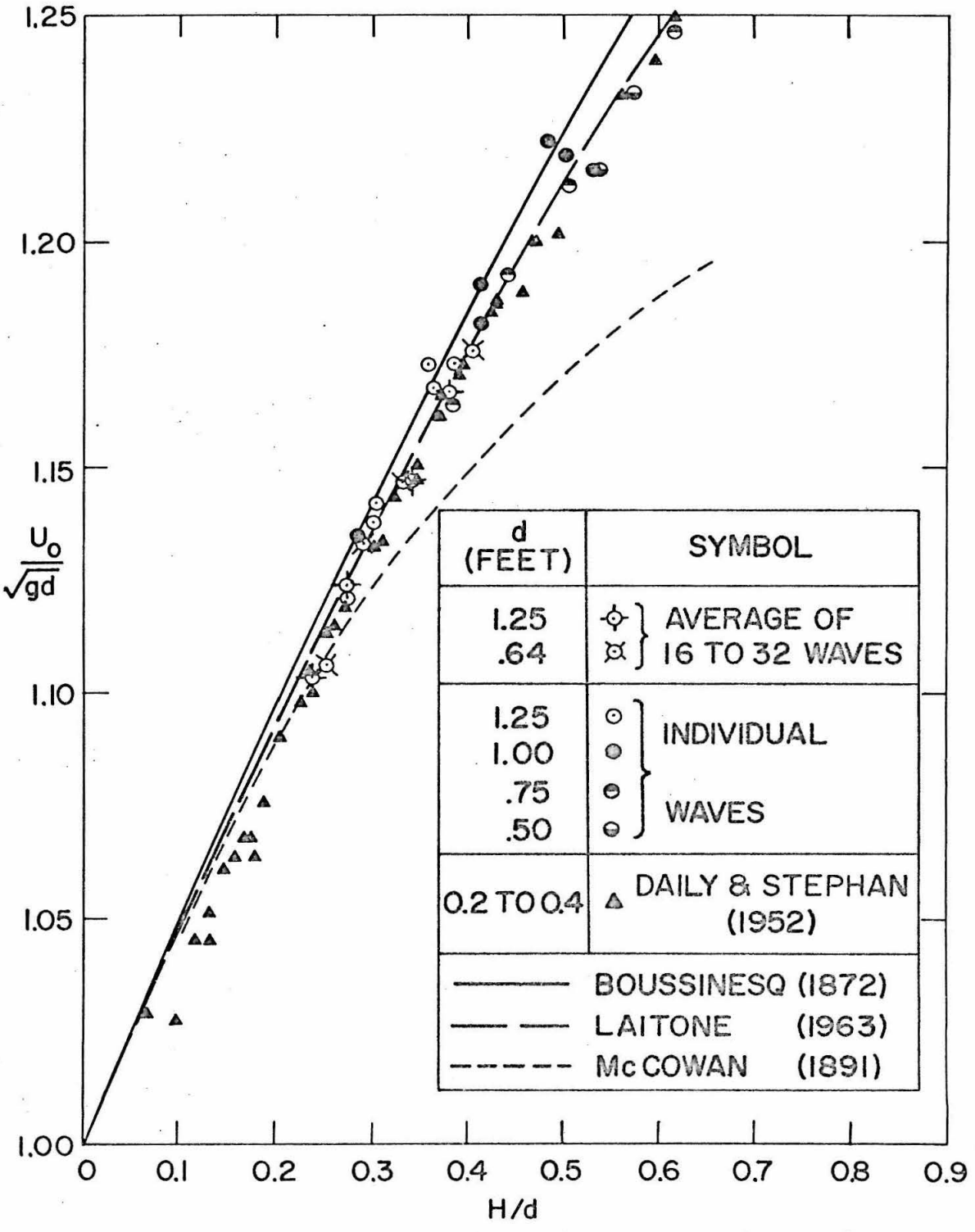

Figure 6.9. Celerity of the solitary wave.

waves) were generated at waveheights held as constant as possible, mean celerity is plotted as a function of mean wave height. Data from individual waves are also plotted. The theoretical celerities by Boussinesq (1872), McCowan (1891), and Laitone (1963), and data by Daily and Stephan (1952), are plotted for comparison.

Data from the present study agree well with those by Daily and Stephan. Of the theoretical curves, that of Boussinesq provides fair agreement with data, that of Laitone is in very good agreement, and that of McCowan shows very poor agreement with the data. The writer has not investigated why Laitone's theory predicts celerity so well, when it is inferior at predicting wave profile; nor why the McCowan analysis, in predicting the profile best, should be inadequate in predicting celerity.

The rate of gradual deformation of the generated wave was examined by mounting four wave gauges along the centerline of the 100- ft tank, spaced at 10-ft intervals as described previously. Waves were generated in water depths d of 1.25 ft, 1.00 ft, 0.75 ft, and 0.50 ft. The change of amplitude and profile of a wave could be studied by comparing the records of the 4 gauges, as shown in Figure 6.1.

Figures 6.10a and 6.10b each show two profiles of a single wave measured by wave gauges mounted 30 ft apart. One gauge was mounted approximately 45 ft from the wave generator; the other was mounted 75 ft from the wave generator. In Figure 6.10a, the water depth d is 1.25 ft; in Figure 6.10b, the depth d is 0.50 ft. Each wave profile was normalized with respect to the local wave height H, and with respect to the local celerity U_o determined from the local wave

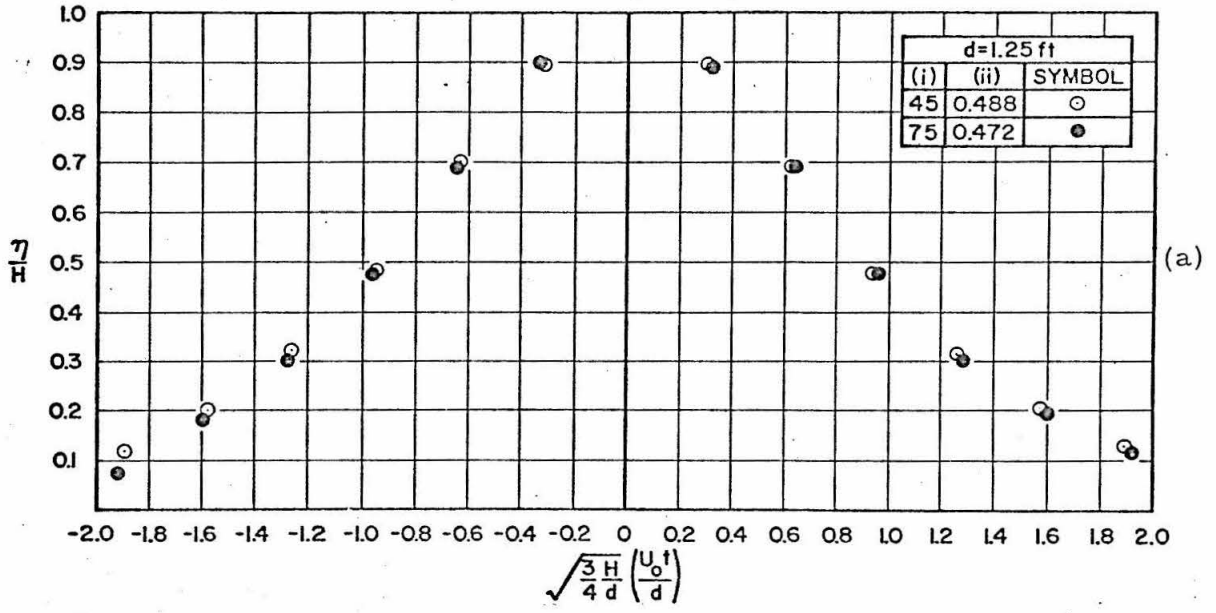

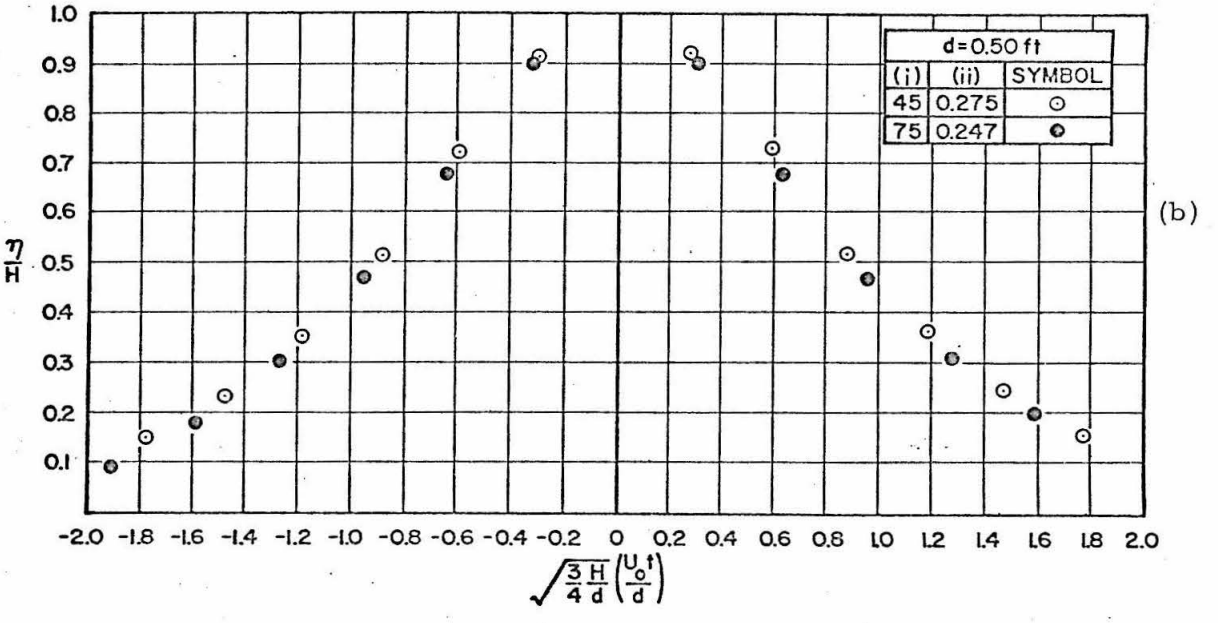

Figures 6.10. Comparison of normalized profiles of a wave as measured at two stations 30 ft apart. (a) d = 1.25 ft; (b) d = 0.50 ft. (Legend: (i) Distance of wave gauge from generator (ft); (ii) local wave height (ft).)

height H and the still water depth d by the Laitone (1963) expression for celerity. In neither Figure 6.10a nor 6.10b is there an appreciable change evident in the shape of the normalized profile. However, the figure legends indicate that there is a decay of wave height with distance travelled; the wave height measured 75 ft from the generator is several per cent less than the height of the same wave measured 45 ft from the generator.

The measured rate of amplitude decay, as a function of distance travelled Δx, still water depth d, relative wave height H_o/d, channel width B, kinematic viscosity ν, and gravitational acceleration g, is plotted in Figure 6.11. The ordinate of the graph is H/H_o, where H_o is a measured wave height, and H is the height of the same wave, measured at a later time, at a distance Δx from the place of the first measurement. (On the right-hand margin of the graph the quantity $\frac{\Delta H}{H_o} = \frac{H_o - H}{H_o}$ is also presented as an ordinate.) The abscissa is merely the right-hand side of a version of Keulegan's (1948) equation for amplitude decrement due to energy dissipation (see Section 2.4):

$$\left(\frac{H}{H_o}\right)^{-\frac{1}{4}} - 1 = \frac{\Delta x}{d}\left(\frac{H_o}{d}\right)^{\frac{1}{4}} \frac{1}{12}\left(1 + \frac{2d}{B}\right)\left(\frac{\nu^2}{gd^3}\right)^{\frac{1}{4}}. \qquad (6.1)$$

In the present study, the abscissa of Figure 6.11 was evaluated as follows: the tank width B was 1.29 ft; laboratory ambient temperature was always about 70°F, from which one may infer a kinematic viscosity ν of 10^{-5} ft^2/sec for water (Rouse, 1950); and the gravitational acceleration g was 32.2 ft/sec.^{2} The still water depth was d, the heights H_o and H were measured by any two of the four wave gauges mounted at 10-ft intervals; the separation distance Δx was therefore 10 ft, 20 ft, or 30 ft.

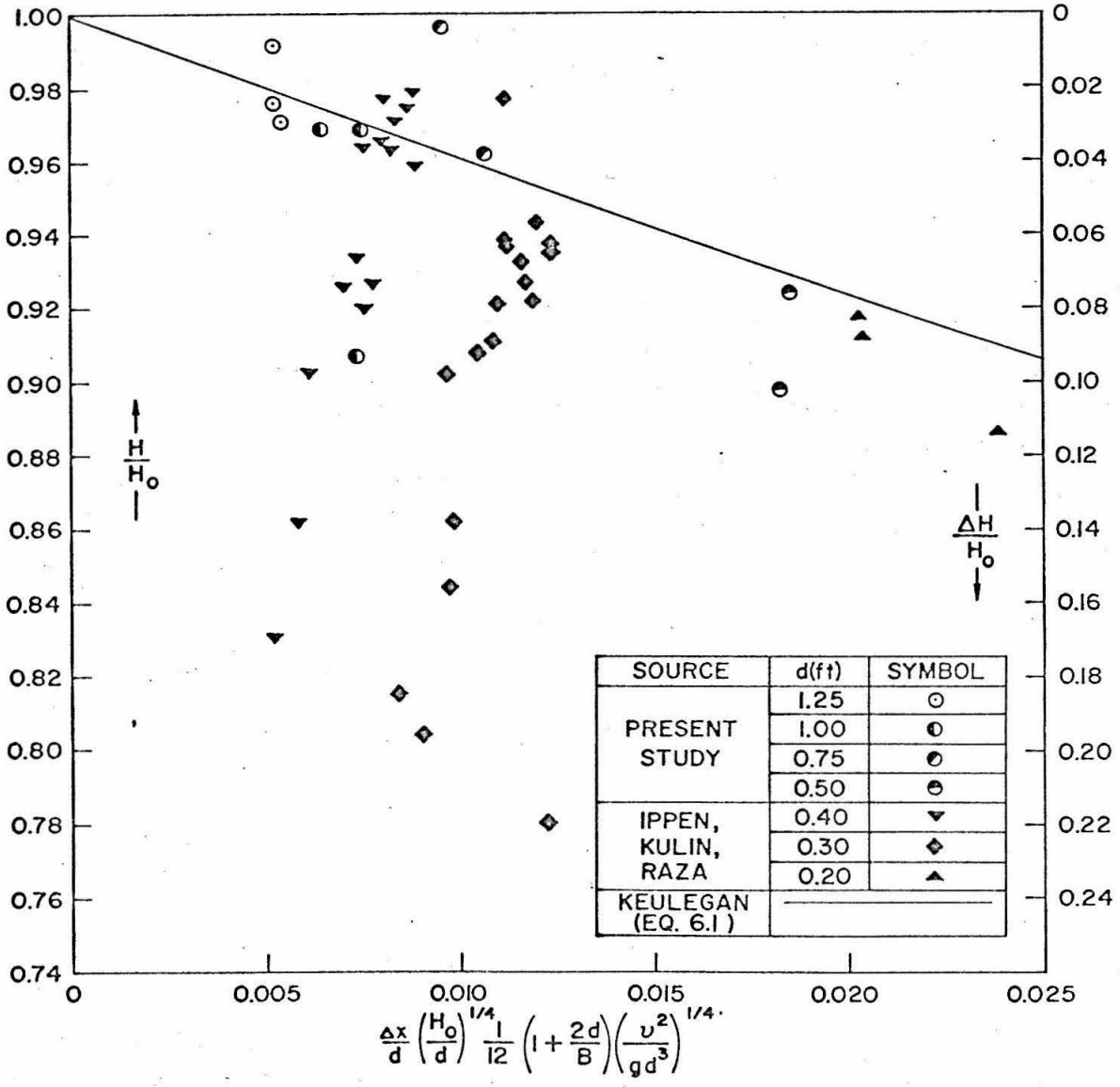

Figure 6.11. Decay of solitary wave height.

In Figure 6.11, data from the present study are compared with data by Ippen, Kulin, and Raza (1955), and with a curve representing Equation 6.1. The data from the present study show considerable scatter, falling to either side of the theoretical curve. Data obtained by Ippen, Kulin, and Raza, while scattered throughout the same regions in which data from the present study are found, also are scattered in regions indicating greater decay rates $\Delta H/H_o$ than indicated by Equation 6.1 or by the data from the present study.

For the present study, it is of interest to know the extent of amplitude decay that prevailed in the uplift tests between the point of measurement of the incident wave and the seaward edge of the platform. The distance Δx between the edge of the platform and the wave gauge was approximately five ft. Thus for a still-water depth d of 0.64 ft and a relative waveheight H_o/d of 0.40, and for B, ν, and g evaluated as described earlier, the right hand side of Equation 6.1 takes the value 0.0019. For an abscissal value of 0.0019, Equation 6.1 indicates a fractional decay $\Delta H/H_o$ of 0.0076, implying an error of 0.0076 or approximately one per cent in the measurement of the height of the wave incident on the platform.

When designing the wave generator, as described in Section 4.2, it was deemed important to be able to generate waves reproducibly, so that a wave would be as nearly as possible identical to its predecessor, for constant water depth, generator cam speed, and generator stroke length.

For the pressure measurement experiments, waves were generated in samples of five, six, or as many as 32 waves of nearly

constant height. The mean height and standard deviation were computed for each sample (see Table B2 in Appendix B).

In Figure 6.12, eight cumulative frequency diagrams show the frequency distribution of the wave height H normalized with respect to the sample mean wave height $\overline{H}$. The two still water depths represented are d = 1.25 ft and d = 0.64 ft. The sample sizes range from 16 to 32. Plotted on arithmetic probability paper, the distributions may in most cases be fitted by a straight line, indicating an approximately normal distribution. The ratio of sample standard deviation to sample mean, which is equal to the slope of a straight line fitted to the data in each sample, appears to be independent of the mean relative wave height $\overline{H}/d$.

Of all the samples of wave height data obtained during the study, the arithmetic mean of the ratio of sample standard deviation to sample mean wave height was 0.0074 for a water depth d of 1.25 ft; 0.0096 for d = 1.00 ft; and 0.0115 for d = 0.64 ft. As the wave generator was therefore capable of generating a sample of waves whose standard deviation in wave height was approximately one per cent of the sample mean wave height, it may be considered as having successfully fulfilled the requirement of reproducibility.

Section 6.1 may be summarized as follows: the profile of the generated wave is well approximated by the Boussinesq representation for a solitary wave, except far from the crest. The wave form is not measurably different from experimental profiles measured by other workers using other laboratory channels of constant rectangular corss-section, and using other methods of wave generation. The celerity is best represented by Laitone's theory, and is in general

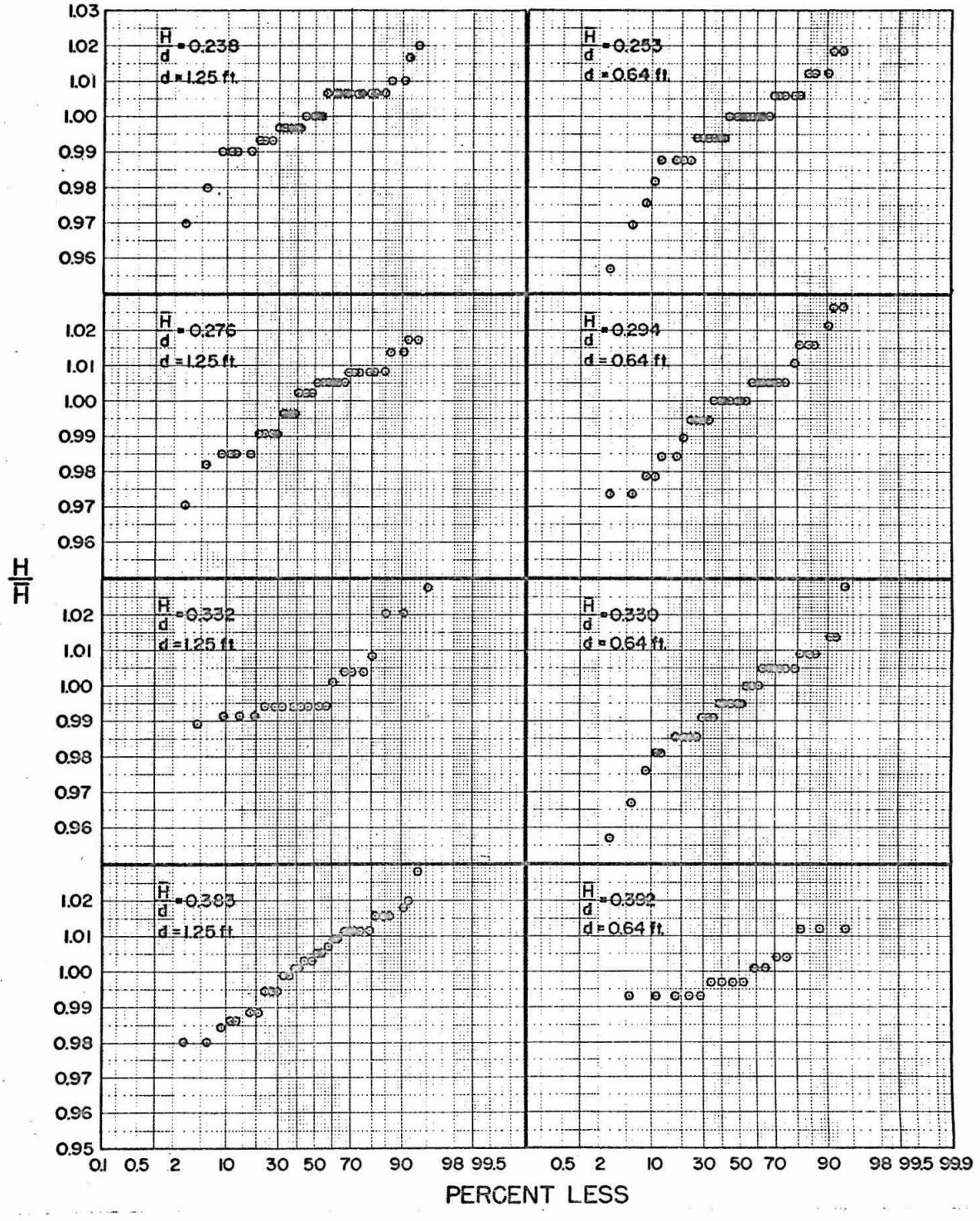

Figure 6.12. Cumulative frequency diagrams of $H/\overline{H}$ for eight samples of 16 to 32 waves each.

agreement with the data of Daily and Stephan. As the wave propagates along the channel, it is subject to a decrease or decay of amplitude, but its form does not change when normalized with respect to local amplitude and celerity as shown in Figures 6.10. The measured rate of amplitude decay indicates that there is a decay of approximately one per cent in amplitude in the five-ft distance between the wave gauge and the seaward end of the platform. Reproducibility of wave height, measured as the ratio of standard deviation to mean value, is about one per cent.

6.2 Flow Beneath the Platform: Photographic Description.

In this section the flow beneath the platform will be described qualitatively, illustrated by sequences of photographs. In Sections 6.3 through 6.6 quantitative measurements of the flow are discussed.

The photographs presented on the following pages are grouped in series, each series being given a figure number. Each series contains several photographs of waves of a common height H, taken at different times during the impact process. Viewed in sequence, the photographs of a series help one visualize the progress of a wave as it approaches, strikes, propagates beneath, and recedes from the platform. (It should be stated that a fresh wave was generated for each photograph; operating conditions did not permit more than one photo to be taken of each wave.)

Each figure, or series of photographs, represents one value of relative wave height H/d and one value of relative soffit clearance s/d. Figures in this section represent two or more values of H/d at each of the three values of relative soffit clearance at which uplift pressure experiments were made: s/d = 0.2, 0.1, and 0.0. The range of

conditions represented by the photographs in this section is approximately the same as the range of conditions at which uplift measurement experiments were performed.

For convenience, the distance of the platform d + s above the channel bottom was held constant at 0.77 ft for all photographs presented in this section. Thus for s/d = 0.2, the still water depth d was 0.64 ft, one of the two depths at which uplift pressure tests were performed. For s/d = 0.1, d was 0.70 ft, not the depth at which experiments were performed; however, the appearance of the flow is similar to the appearance of the flow for d = 1.00 ft, the depth at which uplift experiments were performed, except that the ratio of platform length L to still water depth d was greater in the photographs than in the uplift experiments. For s/d = 0.0, the depth d was 0.77, the depth at which uplift experiments were performed.

In the descriptive text that accompanies the photographs that are to follow, reference is often made to the chronology presented in Figure 3.5, Section 3.3. Below each photograph is indicated the chronological time interval within which the photograph was taken.

The waves in Figures 6.13, for which H/d = 0.450 and s/d = 0.2, are somewhat larger than those studied extensively, yet some of the interesting phenomena are more evident in this series than in photos of smaller waves. In Figure 6.13a the undisturbed wave propagates shoreward approaching the platform. In Figure 6.13b the wavefront propagates beneath the platform, while the high vertical front face of the platform causes a jet of fluid to shoot upwards. At the wavefront there appears to be a turbulent condition, with spume driven ahead of the wave front and with air being entrained in the fluid behind the wave

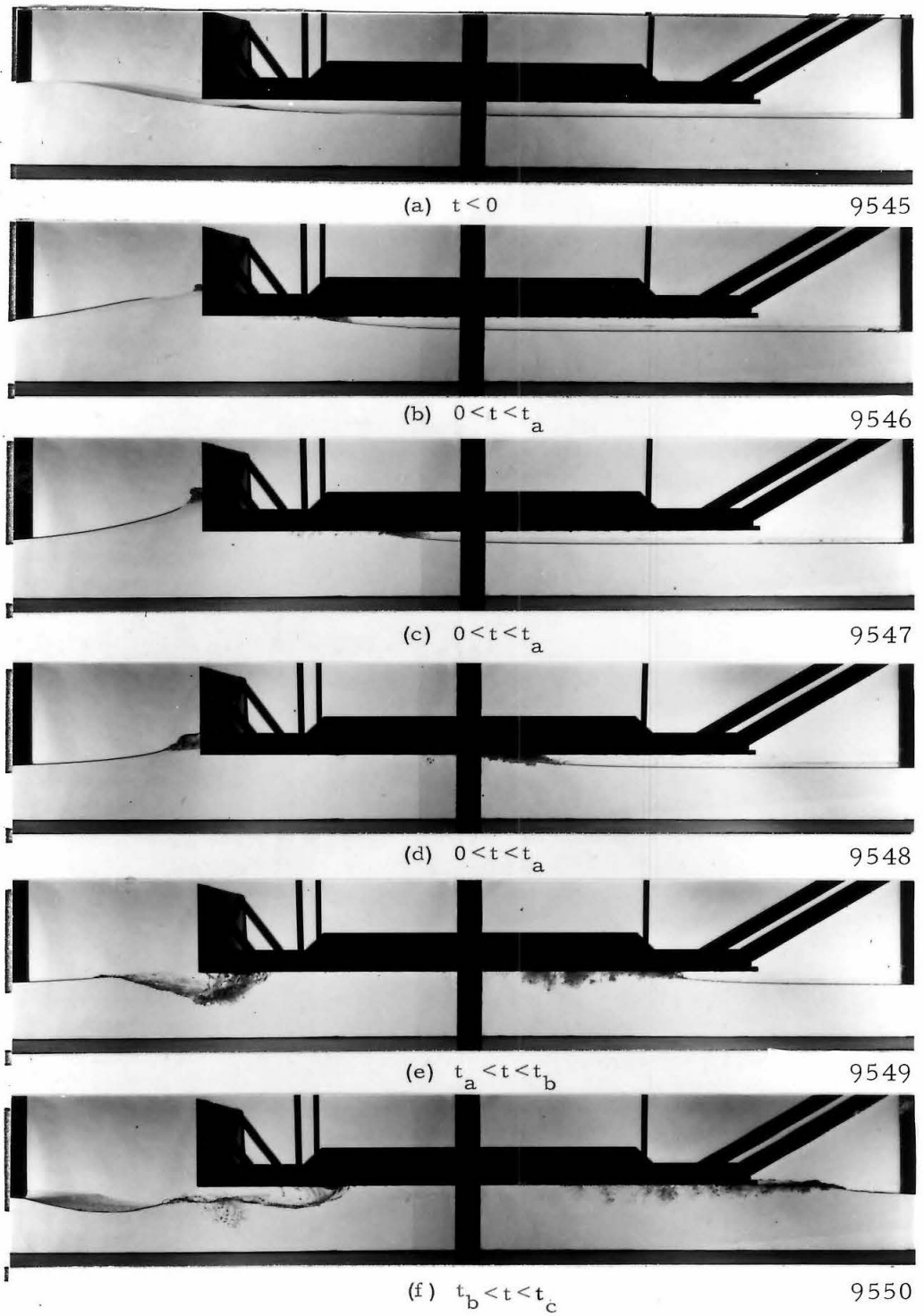

Figure 6.13. Waves striking the platform, d = 0.64 ft, s/d = 0.2, H/d = 0.450.

front, in action reminiscent of an hydraulic jump. In Figure 6.13c the wave front has advanced further; the amount of spume created appears to have increased with distance from the seaward edge of the platform. The jet on the front face has also grown wider with vertical distance from the platform edge. In Figure 6.13d the wave front has continued to propagate and grow more turbulent; the vertical jet grows no taller but descends to form part of a reflected wave train. In Figure 6.13e the seaward edge of the platform is again exposed to air, and the wave of recession has begun; $t > t_a$, the time at which the fluid recedes from the seaward edge of the platform. At this instant the water depth at $x = 0$ is considerably less than d. In Figure 6.13f the wave front has moved past the end of the platform; $t > t_b$, the time after which the wave front is no longer defined. At $x = 0$, the water depth has almost completely returned to its original value d.

In Figures 6.14 the value of s/d is again 0.2, but H/d has been reduced to 0.250. In Figure 6.14a, the undisturbed wave approaches the platform. In Figure 6.14b the wavefront propagates beneath the platform with much less spume and air entrainment than in Figures 6.13. A modest upward jet of fluid is visible at the front face. In Figure 6.14c the time t_a has passed, and the wave of recession has begun. Somewhat more air is being entrained now than in Figure 6.14b. In Figure 6.14d the flow is slightly more advanced. In neither Figure 6.14c nor Figure 6.14d has the wave of recession developed into its final form; the wavefront is still definable in both pictures. In Figure 6.14e, the time t_b has passed; the wave propagates without wetting more of the platform. A small secondary wave of recession may be seen propagating seaward to meet the first wave, which is

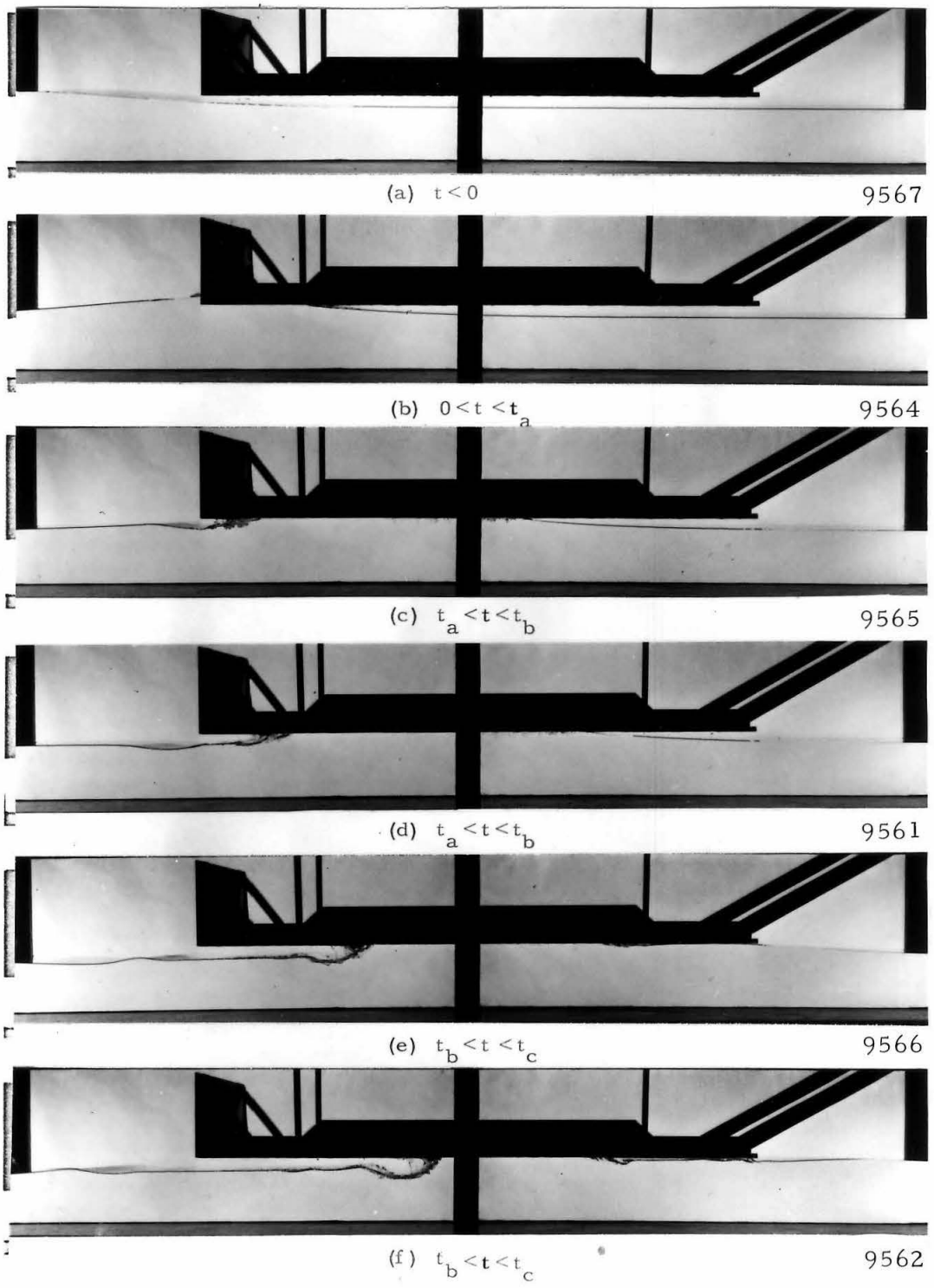

Figures 6.14. Waves striking the platform, d = 0.64 ft, s/d = 0.2, H/d = 0.250.

now fully developed. Figure 6.14f shows the progress of the waves of recession. In Figures 6.14e and 6.14f the fluid at $x = 0$ is quite still, and the depth is again equal to the still water depth.

When Figure 6.14e or Figure 6.14f is viewed inverted, the waves of recession, with characteristic head formation, resemble the gravity currents reported by Keulegan (1958), Middleton (1966), and others. As Benjamin (1968) points out, the present case of a light fluid or cavity propagating into a heavier fluid along the upper boundary may itself be classed as a gravity current.

Figures 6.15, for which $s/d = 0.2$ and $H/d = 0.203$, illustrate the case of a wave just high enough to make contact with the soffit. Figure 6.15f shows flow conditions at $t = t_c$, when the last of the fluid in the wave recedes from the soffit. To the right in Figure 6.15f the transmitted wave may be clearly seen propagating beneath the soffit, resembling the undeformed waves shown in Figures 6.15a and 6.15b, but of diminished height.

Figures 6.16 and 6.17 for $s/d = 0.1$ show behavior qualitatively similar to that described for $s/d = 0.2$. In Figures 6.16, $H/d = 0.436$, a relative height comparable to the value in Figures 6.13 for $s/d = 0.2$. One may note that for similar values of H/d, there will be more distortion of the wave at the lesser value of s/d. The vertical jet is higher and thicker in Figures 6.16 compared to that shown in Figures 6.13.

In Figures 6.16 it happens that t_b is less than t_a: the wave front reaches the shoreward end of the platform before fluid recedes from the seaward end. Whether or not t_b is greater than t_a depends on the

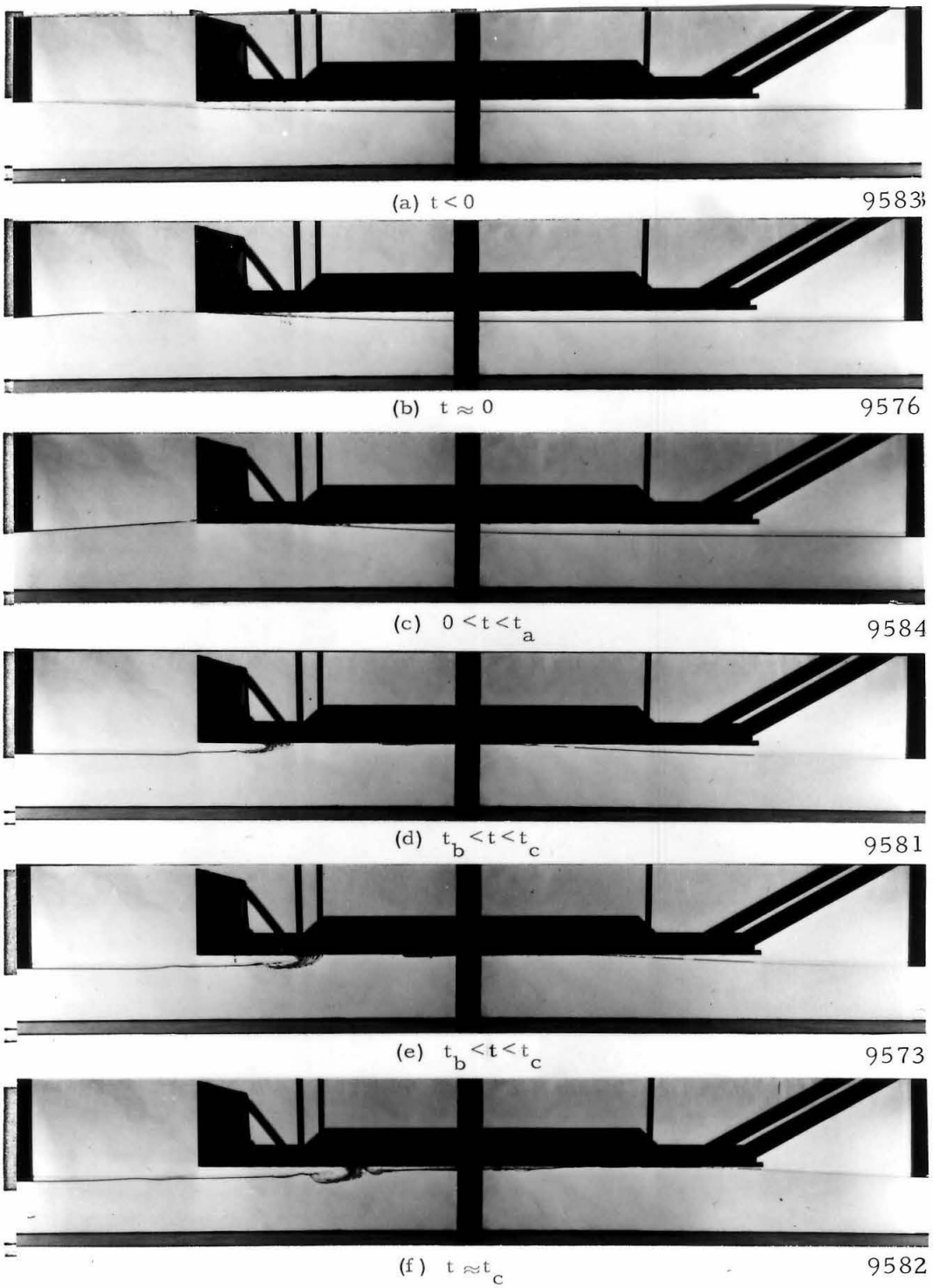

Figure 6.15. Waves striking the platform, d = 0.64 ft, s/d = 0.2, H/d = 0.203.

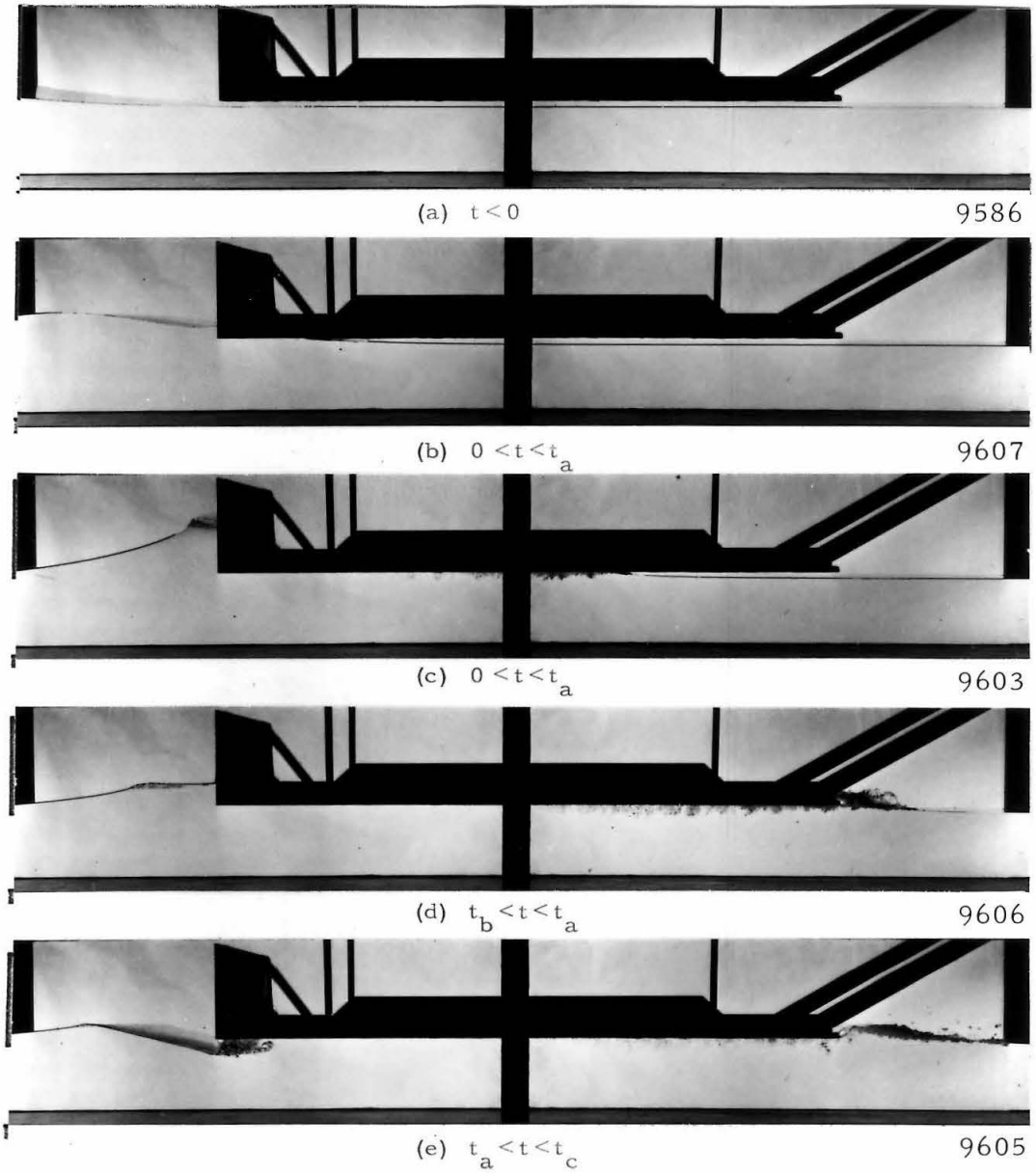

Figure 6.16. Waves striking the platform, d = 0.70 ft, s/d = 0.1, H/d = 0.436.

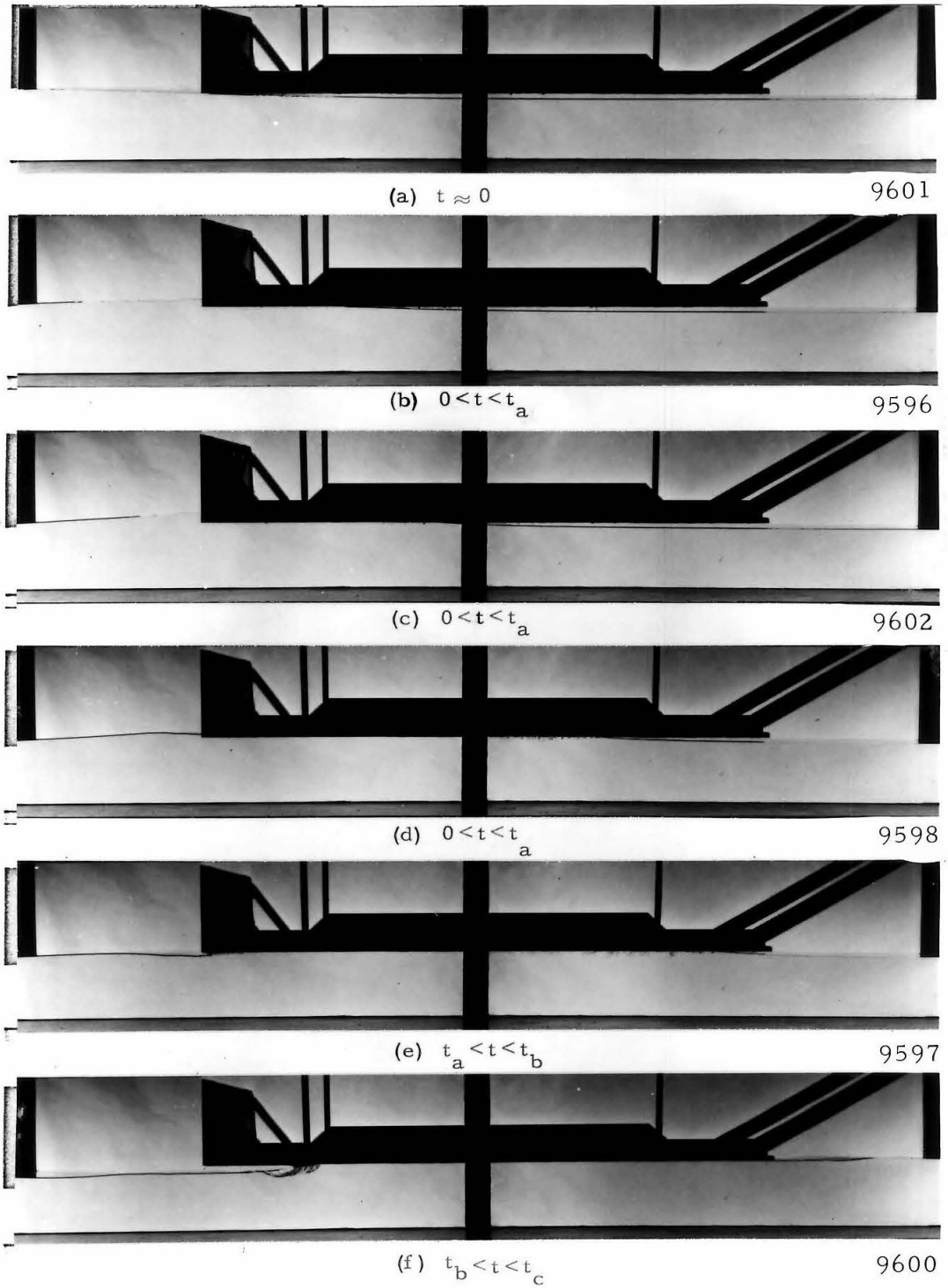

Figures 6.17. Waves striking the platform, d = 0.70 ft, s/d = 0.1, H/d = 0.157.

relative soffit clearance s/d, the relative waveheight H/d, and the relative platform length L/d.

Figures 6.17 illustrate the case for s/d = 0.1, H/d = 0.157.

In Chapter 3, one of the assumptions underlying the analysis was that the form of the free surface profile near the wave front and near the wave of recession did not change appreciably with time. The assumption may be tested by examining and comparing the profiles shown in Figures 6.13 through 6.17. For example, if the profile near the wave front shown in Figure 6.13b is traced onto vellum, and the tracing is laid over the profiles shown at different locations (and hence times) in Figures 6.13c, d, and e, no change in profile shape with respect to distance travelled is detectable, except for an increase in the amount of spume driven forward of the main body of fluid, and in the amount of air entrained. With no change in form detectable, one may conclude that the assumption of constant form introduces no error into the analysis as far as the wave front is concerned.

For the wave of recession, however, there is obviously a change of form when the wave is initially formed, as shown in Figures 6.13 through 6.17. Therefore, one may expect error introduced into the analysis by the assumption of constant form for the time following t_a during which the wave of recession is initially developing.

Figures 6.18, for which s/d = 0.0 and H/d = 0.426, show that as the wave arrives at the platform there is an immediate increase in water level shoreward of the platform. With no soffit clearance, there is obviously no wave front beneath the platform. At the front

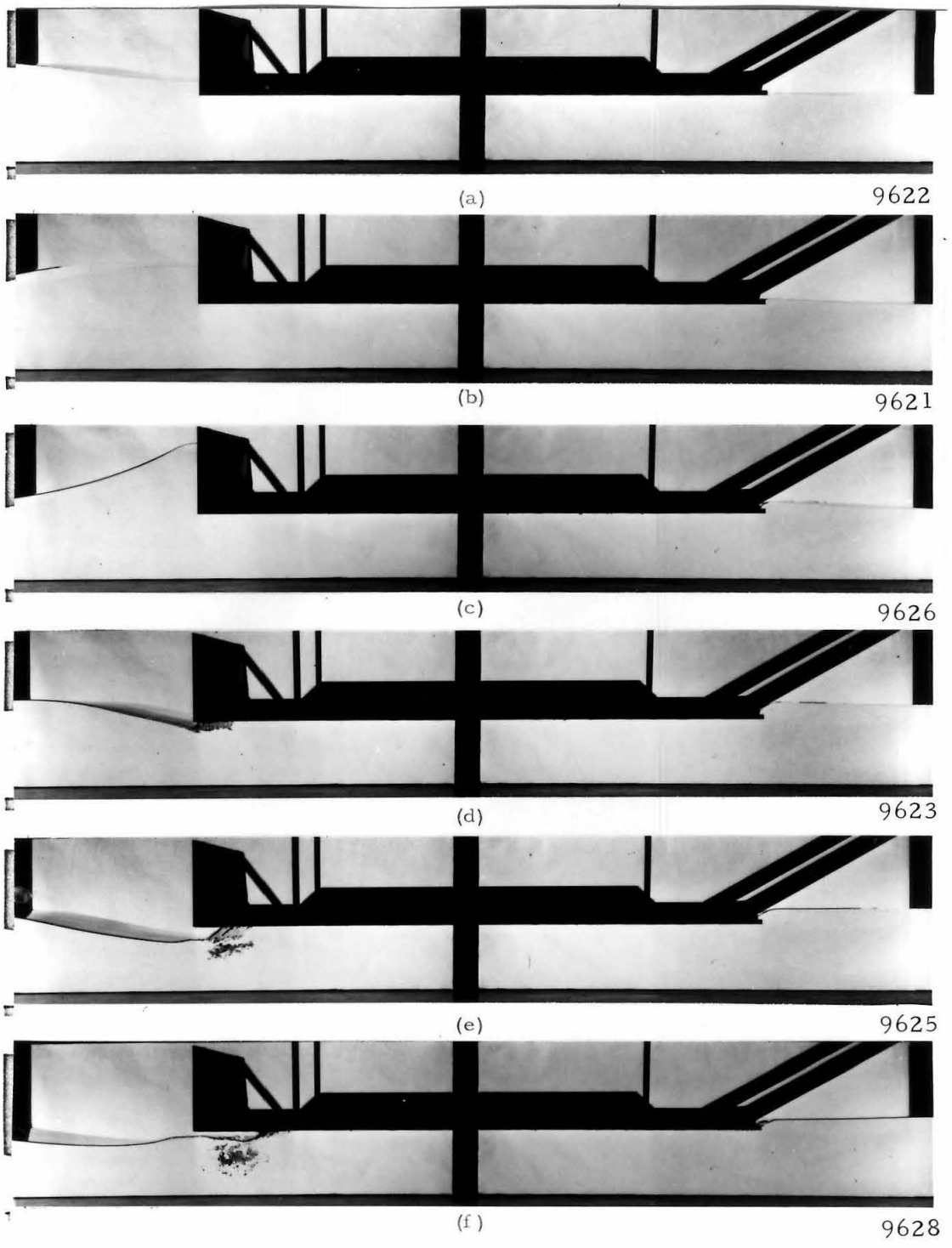

Figures 6.18. Waves striking the platform, d = 0.77 ft, s/d = 0.0, H/d = 0.426.

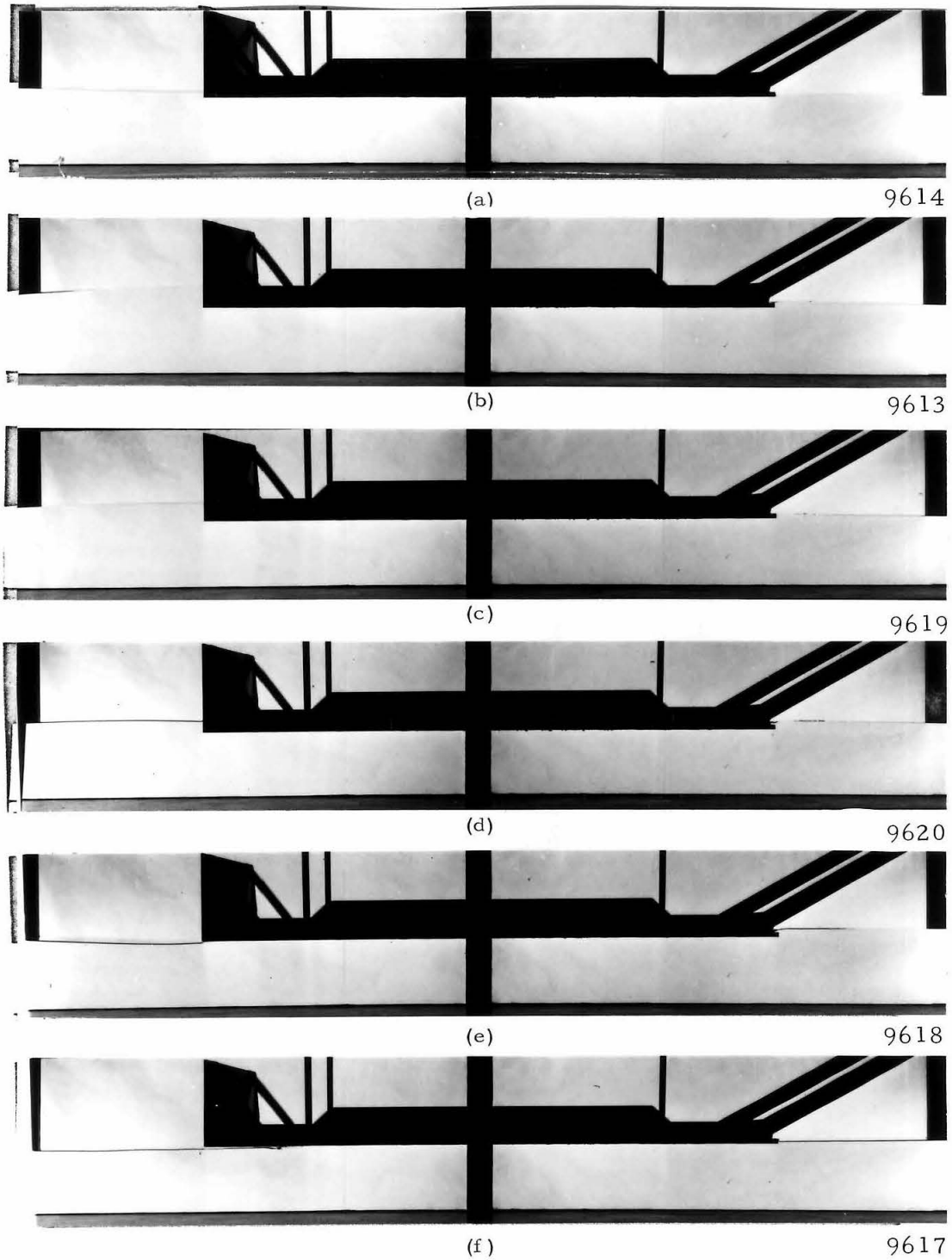

Figures 6.19. Waves striking the platform, d - 0.77 ft, s/d = 0.0, H/d = 0.172.

face the reflecting wave shows fewer characteristics of the upward-shooting jet, and resembles more a clapotis created by a vertical wall extending to the tank bottom. At x=0 the water level drops to less than d, in Figure 6.18d. In Figure 6.18f the depth at x = 0 is again approaching its original value d. Figures 6.19 show the process for s/d = 0.0, H/d = 0.172. In Figures 6.18f and 6.19f, air-filled cavities following waves of recession are visible. The air is eventually driven back to x = 0 as the system returns to rest.

For s/d = 0.0, chronological times have not been listed on the photographs for the simple reason that the times t = 0, t_a, and t_c cannot be defined when s/d = 0.0. As stated in Section 3.3, study of the case for s/d = 0.0 demands an approach fundamentally different from the approach used in the present study for finite soffit clearance, which has been to relate flow conditions to the position and celerity of the wave front and of the wave of recession.

6.3 Pressure Recording Procedure; Qualitative Discussion of the Records.

Sections 6.4 through 6.6 are devoted to quantitative measurements of the flow beneath the platform. All such measurements, including those of uplift pressures, and of times of arrival and celerities of the wave front and of the wave of recession, were reduced from pressure-time records obtained with the 1/2-in. transducer and the 1/8-in. transducer with oil chamber, described in Section 4.4, mounted flush with the platform soffit. Except for pressure measurements made for zero soffit clearance (s/d = 0.0), which were recorded with the Sanborn recorder, all pressures were

recorded with the Consolidated Electrodynamics Corporation Model 5-124A high-speed oscillograph described in Section 4.4.

The flow quantities measured were: the slowly-varying pressure P_1, the peak pressure P_2, the rise-time t_r (that is, the time interval between zero deflection and maximum deflection on the record at the pressure peak), the time t_d needed for the wave front to travel from the seaward edge of the platform to the transducer, and the time t_e at which the transducer became free of the fluid in the wave, as the fluid fell away from the platform. The quantities may be found in Tables B1 and B2 of Appendix B. The wave front celerity U_d and the celerity U_e of the wave of recession are quantities derived from t_d and t_e, respectively.

The conditions under which uplift experiments were performed are listed in Table 6.2. As stated in Section 6.2, there were three values of relative soffit clearance studied: $s/d = 0.2$, 0.1, and 0.0. For each value of s/d, the relative wave height H/d ranged from approximately 0.2 to 0.4.

Holes in which transducers could be mounted were drilled in the platform at seven locations, x, ranging from 0.148 ft to 2.520 ft., the latter value being approximately equal to half the platform length L. To obtain measurements at $x > L/2$, the platform was turned end-for-end, as described in Section 4.3. Values of x for which the platform was turned end-for-end from its normal position are indicated in Table 6.2 by the superscript $(\ )^a$. To ensure that flow conditions were not altered when the platform was turned end-for-end, pressures recorded at $x = 2.525$ ft with the platform turned were compared with pressures recorded at $x = 2.520$ ft with the platform in its normal

Table 6.2. Summary of transducer locations, relative soffit clearances, and relative platform lengths. (Arrows relate comparable values of x/d at two model scales.)

	s/d = 0.2		s/d = 0.1	s/d = 0.0
RANGE OF H/d:	0.23-0.46		0.15-0.38	0.16-0.42
d(ft)	1.25	0.64	1.00	0.77
x(ft)	x/d	x/d	x/d	x/d
0.148	0.118	→0.231		
0.270	0.216 ←	→0.422	0.270[d]	
0.522	0.418 ←	→0.816	0.522	
1.020	0.816 ←	→1.594	1.020[d]	
1.520	1.216	→2.374	1.520[d]	
2.020	1.616 ←	→3.156		
2.520	2.016	→3.938	2.520[d]	
2.523[a,b]	2.020			
3.025[a]	2.420 ←			3.940
3.525[a]		5.510[c]		
4.025[a]	3.220 ←			
4.525[a]		7.070	4.525	
4.900[a]	3.920 ←			6.380
Relative platform length L/d (L = 5 ft)	4.00	7.81	5.00	6.50

a) Plate turned end-for-end.
b) Data obtained limited to peak pressure P_2.
c) Slowly-varying pressure P_1, rise-time t_r, not obtained.
d) Data obtained limited to t_d.

position. Comparison of the peak pressures thus obtained indicated no difference in flow conditions for the two cases. (For that test, the relative soffit clearance s/d was 0.2, and the still water depth d was 1.25 ft.)

For s/d = 0.2, the case most exhaustively studied, two complete series of experiments were performed at different model scales in order to apply the correction procedure for measured peak pressure described in Section 5.3. At the larger scale, the still water depth d was 1.25 ft; at the smaller scale, d was 0.64 ft, thereby providing a scale ratio of approximately two to one. In Table 6.2 the ratios s/d of transducer location to still water depth are listed for each value of the still water depth d. As shown by the arrows, there are seven instances in which a value of x/d for d = 1.25 ft is approximately equal to a value of x/d for d = 0.64 ft. Therefore data obtained for d = 1.25 ft at one of a matching pair of values of x/d may be compared with data obtained for d = 0.64 ft at the comparable value of x/d, thus providing geometric similarity between the two scales.

The platform had a constant length L of five ft, so that the relative platform length L/d varied with the still water depth d, as shown in Table 6.2. At d = 1.25 ft, L/d = 4.0; at d = 0.64 ft, L/d = 7.8. The difference in L/d generally caused a difference in flow pattern between the two model scales, as will be shown in Section 6.5, but only after the wave front had propagated from the seaward end of the platform a relative distance x/d greater than 4.0, the relative platform length at the larger scale. When the wave front was at relative locations x/d less than 4.0, there was no effective geometric difference between scales. Since the purpose of performing experiments

at two scales was to measure peak pressure and rise-time at two scales, and since peak pressure and rise-time were measured as the wave front propagated past the transducer, it was unimportant whether geometric similarity was lost after the wave front had passed the transducer. Therefore, despite dissimilarities in relative platform length L/d, there was otherwise adequate similarity in conditions at the two scales for obtaining information to correct measurements of rise-time and peak pressure.

For s/d = 0.1, the water depth d was 1.00 ft. Pressures were recorded at distances x = 0.522 ft and 4.525 ft from the seaward edge of the platform. Elapsed travel times t_d were measured at x = 0.270 ft, 0.522 ft, 1.020 ft, 1.520 ft, and 2.520 ft. For s/d = 0.0, transducers were mounted at x = 3.025 ft and 4.900 ft. The still water depth was 0.77 ft.

It was the practice at each value of x/d and s/d to generate waves at only a limited number of wave heights (usually 4), but at each wave height to generate a reasonably large sample of waves. Generally the sample size was five or six, but in selected instances it was as great as 32. For each sample, the mean, standard deviation, and deviation of the mean were computed for the wave height H, the peak pressure P_2 as recorded by both transducers, the rise-time t_r as recorded by both transducers, and the wave front travel time t_d, as measured by the 1/8-in. transducer. As discussed in Section 4.5, a sample size larger than one or two was needed to obtain meaningful average values for the peak pressure P_2, which was subject to considerable scatter. The slowly-varying pressure P_1 and the time of arrival t_e of the wave of recession, judged to be much less variable than the peak pressure

P_2, were obtained from only one or two records of each sample, and treated as individual data, not averaged.

Two typical pressure records are shown in Figures 6.20. The record shown in Figure 6.20a is characteristic of records obtained at s/d = 0.2 and 0.1. The CEC Model 5-124A recording oscillograph was operated at a paper speed of 64 in./sec, in order to give as much recorded resolution as possible to the pressure peak. The vertical grid lines indicate intervals of 0.01 sec. The two traces on the record, representing the outputs of the 1/2-in. transducer and the 1/8-in. transducer, are characterized by a short train of preliminary oscillations followed by a high deflection of short duration (the "pressure peak"); followed by a slowly-varying deflection, at first positive and then negative; followed by a return to zero deflection. At approximately the point where the slowly-varying deflection passes from positive to negative, there are superimposed on it a series of oscillations which may be termed "secondary oscillations" in order to distinguish them from the preliminary oscillations mentioned earlier.

For positive soffit clearance, i.e. for s/d = 0.2 and 0.1, the 1/2-in. pressure transducer and the 1/8-in. pressure transducer with the oil chamber described in Section 4.4 were mounted side-by-side in the platform at the same distance x from the seaward edge. The side-by-side arrangement was necessary for recording the peak pressure accurately: the 1/8-in. transducer more accurately resolved the peak pressure function, as stated in Chapter 5, but suffered a troublesome drift in zero-pressure output due to a temperature shift, in spite of ameliorative measures. The record of the 1/2-in. transducer, which suffered negligible temperature shift, was used to

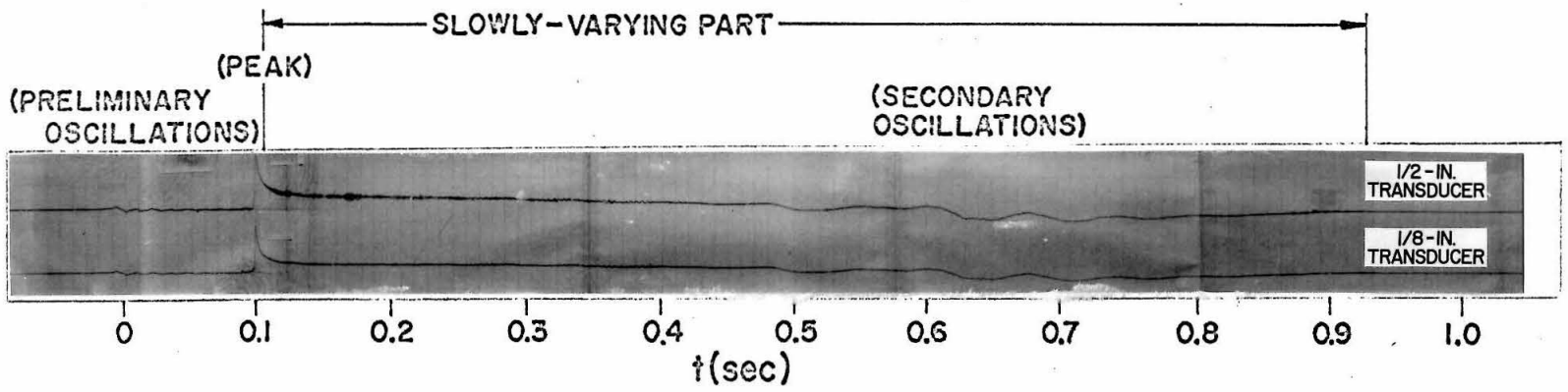

Figure 6.20a. Typical pressure record for s/d = 0.2 or 0.1. CEC oscillograph used. (For record shown, d = 1.25 ft, s/d = 0.2, x/d = 0.816, H/d = 0.388.)

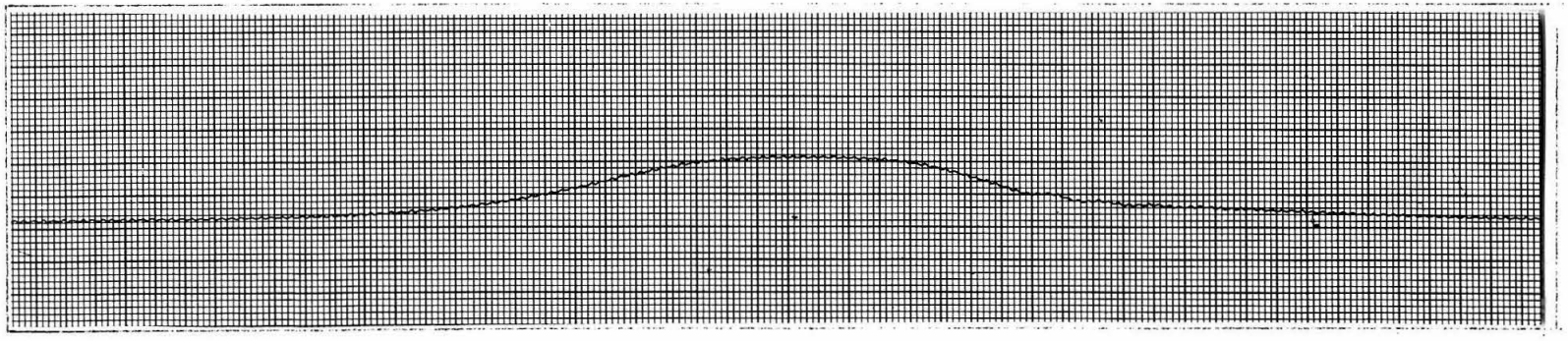

Figure 6.20b. Typical pressure record for s/d = 0.0. Sanborn recorder used. (For record shown, d = 0.77, s/d = 0.0, x/d = 3.940, H/d = 0.231. Time scale is 0.05 sec per major paper division.)

re-define the zero-pressure or baseline deflection for the 1/8-in. transducer at the time of peak pressure, as follows:

On the trace representing the output of the 1/2-in. transducer, at a time about 0.02 sec after the pressure peak, the pressure deflection is slowly-varying, and the transducer may be considered to be functioning accurately. It is assumed that the pressure measured at that time by the 1/2-in. transducer is simultaneously exerted by the fluid on the 1/8-in. transducer. By subtracting the deflection that would be due to the known pressure from the actual deflection of the 1/8-in. transducer's output trace, the zero-pressure or baseline deflection for the 1/8-in. transducer is obtained for that time. A straight line is drawn connecting the trace before the pressure peak with the derived zero-pressure point. The straight line, visible in Figure 6.20a (and in Figures 6.22, to be discussed presently), is used as the zero-pressure line or baseline, from which the peak pressure is measured. Due to the heat-insulating properties of the oil chamber, described in Section 4.4, the baseline correction necessary is only a small fraction of the peak pressure deflection.

The slowly-varying pressure P_1 was obtained from the 1/2-in. transducer output trace, since for slowly-varying pressure no problem of area defect was considered to exist, and the 1/2-in. transducer was free of temperature shift.

For a relative soffit clearance s/d of 0.0, there was no observed pressure peak, as shown in Figure 6.20b. The single slowly-varying positive deflection is nearly symmetric. Since a high-speed

recorder was not needed for this case, the Sanborn recorder was used, operating at a speed of 100 mm per sec. With water in contact with the platform and the transducers at all times, the problem of transient temperature shift in the 1/8-in. transducer did not exist. With no pressure peak, the problem of spatial and dynamic response did not exist for either transducer. Therefore, at $s/d = 0.0$, both transducers could be used.

The preliminary oscillations, visible in Figures 6.20a and 6.22a, while originally unexpected, fortuitously provided a means of determining a zero point for the time coordinate. It may be shown that the oscillations are not caused by vibration of the platform: if the transducers are mounted in the platform but not exposed to the air space beneath the platform, no oscillations are recorded. The oscillations may rather be attributed to vibrations in the air chamber formed by the water surface, tank walls, and the five-ft platform, where the air chamber is closed at the seaward end and open at the shoreward end of the platform. This conjecture is supported by agreement between the measured period of oscillation, 0.0176 sec, and the computed natural period of a five-ft organ pipe closed at one end, 0.0177 sec (where the velocity of sound in air is taken as 1130 ft/sec). The oscillations are thus not to be expected in model or prototype pressure measurements on a narrow pier without side walls to confine an air chamber.

Although not created intentionally, the preliminary oscillations did indicate on the pressure record the time at which the wave first

struck the platform, thus providing an origin for the time variable t. With the aid of Figures 6.21a and 6.21b, the oscillations may be shown to occur when the wave first strikes the platform. (The wave propagates from left to right.) Figure 6.21a is a multiple-exposure photograph of the wave front as it makes initial contact with the platform. For each image in Figure 6.21a there is a corresponding pulse in the record shown in Figure 6.21b. (The pulses actually are "noise" in the pressure transducer circuit, caused by high-voltage electrical discharge to the lamps as they flashed to form each image.) There are six images and seven pulses; it was found that generally no image appeared at the first pulse. Therefore the six images in Figure 6.21a correspond to pulses 1 through 6 in Figure 6.21b, with no image for the 0th pulse.

Figure 6.21a shows that the wave made initial contact with the seaward edge of the platform shortly before the second image was recorded on the film. In Figure 6.21b, correspondingly, the first and greatest maximum of the trace oscillations occurs shortly before the second pulse. One may therefore conclude that the wave makes initial contact with the platform when the first maximum of the train of preliminary oscillations is recorded; that time is taken to be $t = 0$.

To have available a time scale with an origin common to experiments of all values of H/d and x/d has proved most valuable, in that it has allowed the results of many experiments to be combined to construct such functions as the celerity of the wave front U_d and the celerity of the wave of recession U_e, and to observe functional rela-

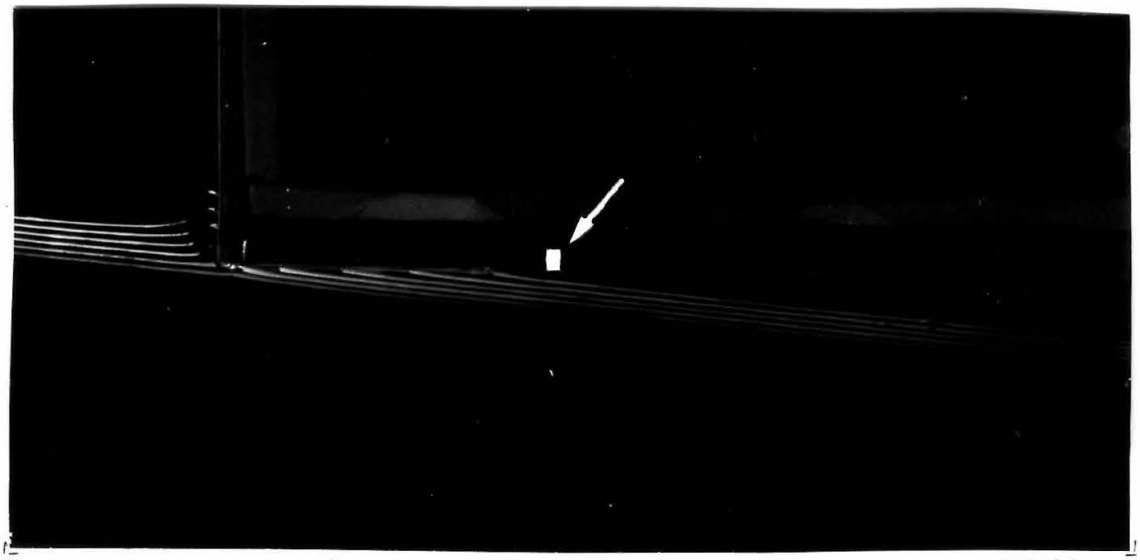

Figure 6.21a. Multiple image photograph of wave first striking the platform. (Transducer location marked in white, indicated by arrow, 100 ft. tank, d = 1.25 ft., s/d = 0.2, x/d = 0.270, H/d = 0.302.)

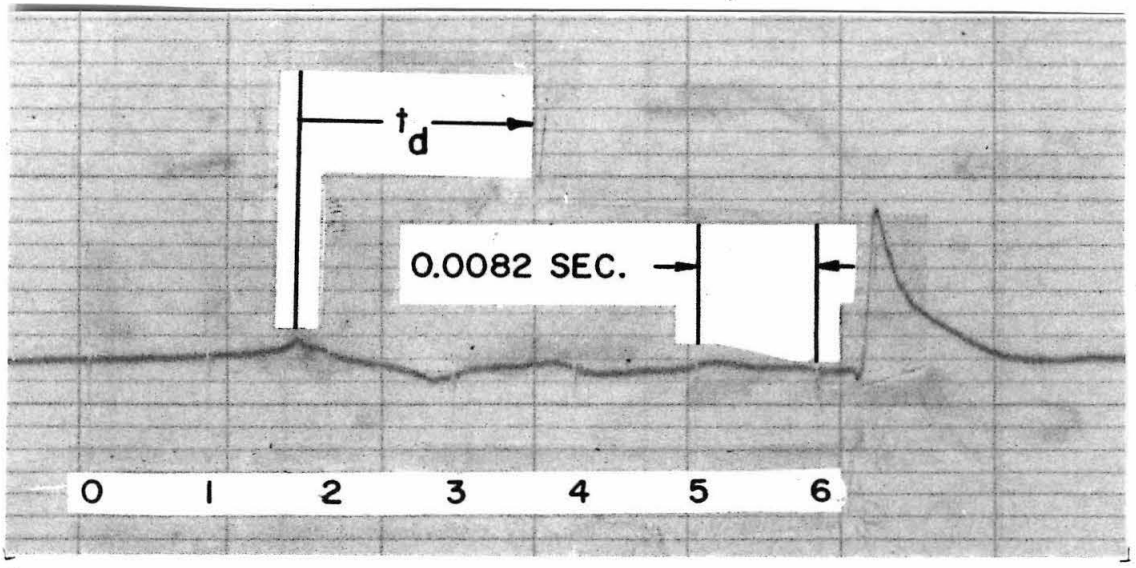

Figure 6.21b. Pressure record from 1/8 in. transducer mounted at x/d = 0.270, as shown in Figure 6.21a. (Pulse marks (1) to (6) correspond to the six images in the photograph.)

tionships between the slowly-varying pressure P_1 and distance x. To obtain these functions and functional relationships otherwise would require several transducers operating simultaneously at different values of x/d.

Figures 6.21 also support the prediction derived in Section 3.2 that peak pressure occurs when the wave front arrives at the transducer. The sixth pulse in Figure 6.21b is seen to occur less than a pulse interval before the pressure peak is recorded. Correspondingly, the transducer location indicated in Figure 6.21a is less than an image interval distant from the sixth image. It thus appears likely that if by chance one of the strobe flashes were to occur at the instant that maximum pressure was being recorded, then not only would a pulse mark be superimposed on the pressure peak in Figure 6.21b, but there would also be an image in Figure 6.21a of the wave front intersecting the soffit at the transducer location. Hence, the wave front may be defined as the location of the peak pressure.

Figures 6.22 show 3 samples of peak-pressure records produced by the 1/8-in. transducer. Often the records show a simple deflection, as in Figure 6.22a, but occasionally, especially at large x/d, the records show random fluctuations superimposed on the principal deflection, as shown in Figure 6.22c. Such fluctuations, which may be attributed to the condition of turbulence and air entrainment at the wavefront indicated in Section 6.2, made measurement of peak pressure and rise-time difficult and somewhat subjective. Rise-time was taken as the interval between the time of first major deflection of

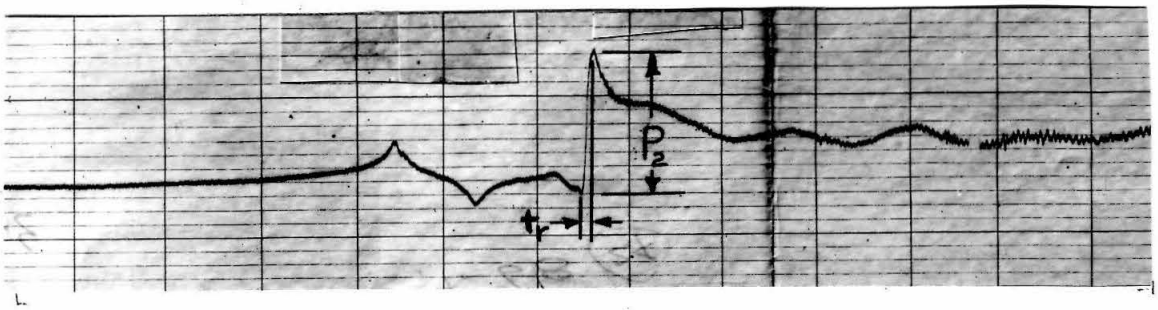

a) x/d = 0.118, H/d = 0.379, $P_2/\gamma d$ = 0.340

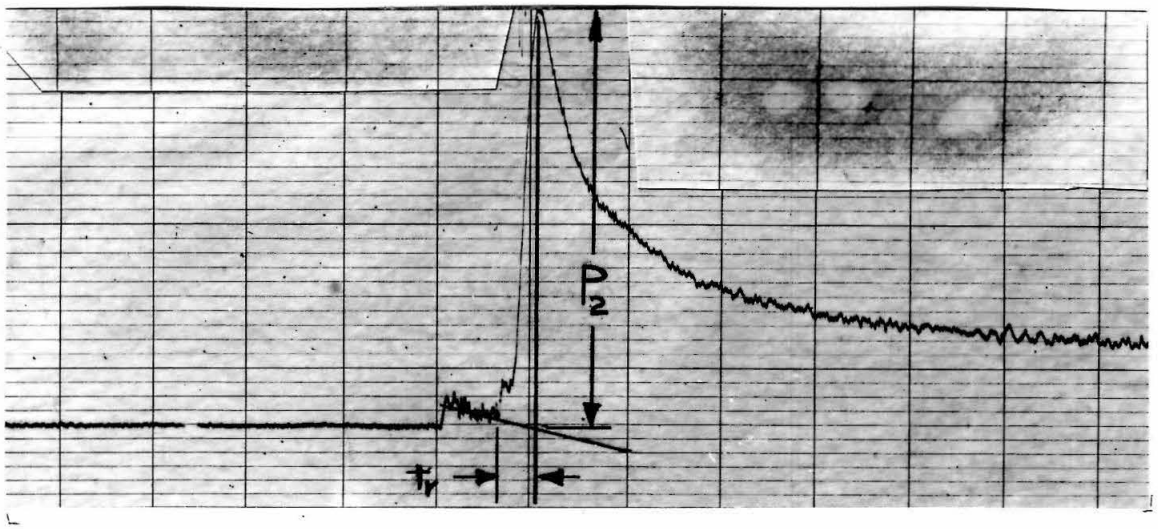

b) x/d = 1.616, H/d = 0.373, $P_2/\gamma d$ = 0.865

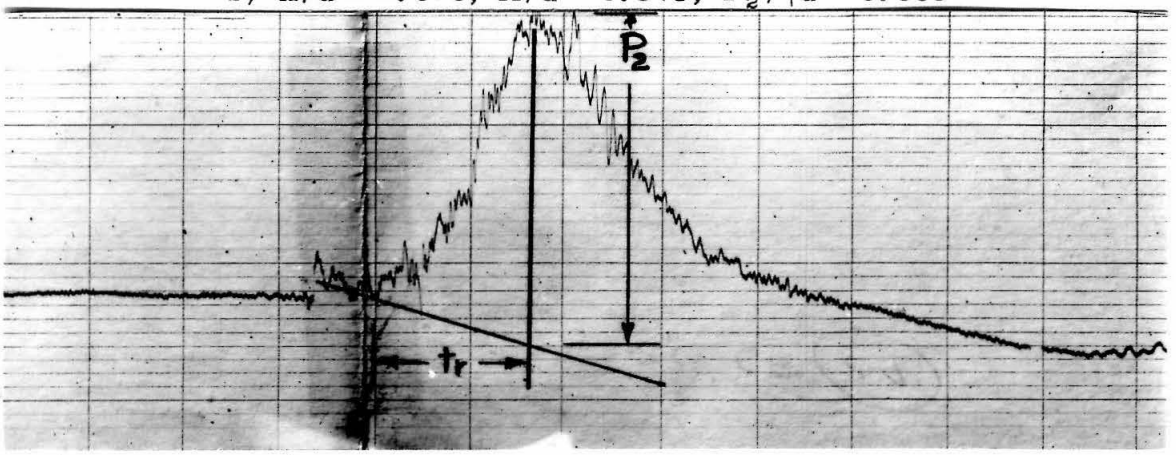

c) x/d = 3.92, H/d = 0.376, $P_2/\gamma d$ = 0.516

Figures 6.22. Examples of recorded pressure peaks. (For each case, s/d = 0.2 and d = 1.25 ft. Ordinates are not to a common scale. Vertical lines indicate intervals of 0.01 sec.)

the record and the time of peak deflection, as indicated in Figures 6.22. Peak pressure amplitude was measured from the corrected zero-level to the maximum deflection of the principal pulse, exclusive of high-frequency fluctuations, as indicated in Figures 6.22.

The secondary oscillations indicated in Figure 6.20a were not investigated extensively. Whereas the preliminary oscillations have been shown to occur when the wave first makes contact with the platform, before the transducers are in contact with the fluid in the wave, the secondary oscillations occur when the fluid in the wave is in contact with much of the platform soffit, including the pressure transducers. The secondary oscillations will be discussed again briefly in Section 6.5.

Figure 6.23 summarizes schematically the data obtained from the pressure records. From the trace representing the 1/2-in. transducer's output, values of peak pressure P_2, rise-time t_r, and recession time t_e are measured. The slowly-varying pressure P_1 is sampled frequently (at 0.02 sec or 0.05 sec intervals) for times t greater than t_d but less than t_e. The 1/2-in. transducer's output trace is used to make a baseline correction of the 1/8-in. transducer's trace, from which values of P_2, t_r, and wave front time of arrival t_d are measured.

6.4 The Advancing Wave Front and the Wave of Recession: Times of Arrival and Celerity.

The time of arrival of the wave front t_d is defined as the time needed for the wave front to propagate from the seaward end of the

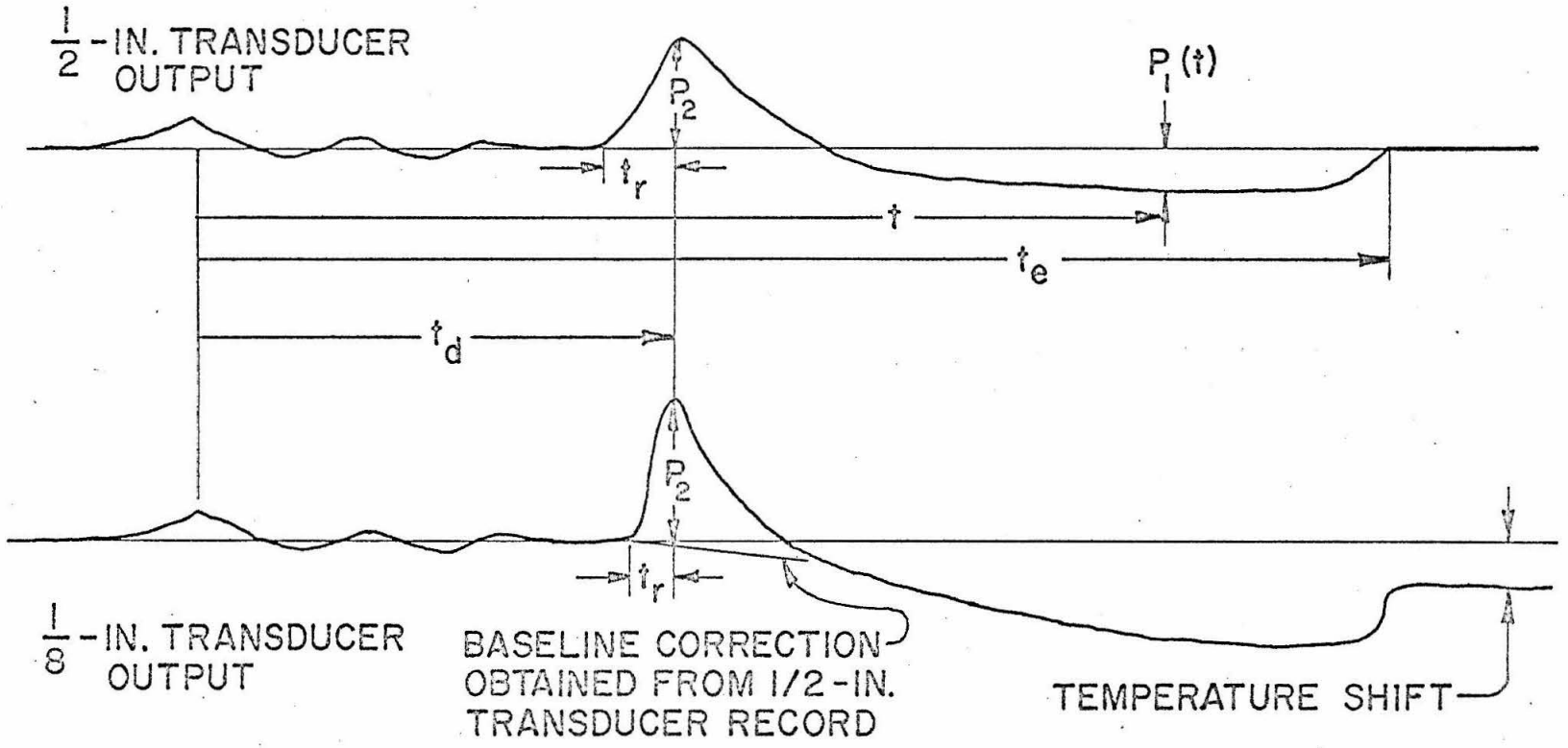

Figure 6.23. Summary of quantities obtained from each pressure record.

platform, at $x = 0$, to a given position $x = x_d$. In Section 6.3 it was indicated that t_d is taken to be the time between the recording of the first maximum of the preliminary oscillations and the recording of the peak pressure maximum, as shown in Figure 6.23.

The function t_d, multiplied by the normalizing factor $\sqrt{g/d}$, is plotted against the relative wave height H/d for a number of relative distances x_d/d; for $s/d = 0.2$ in Figure 6.24, and for $s/d = 0.1$ in Figure 6.25. Each value of t_d and H represented is a sample mean value.

In Figure 6.24, for which $s/d = 0.2$, data from both model scales $d = 1.25$ ft. and $d = 0.64$ ft are included. Comparison of data from the two scales at the same or nearly the same value of x_d/d shows generally good agreement between scales, and no consistent difference in measurement due to scale size, except for the effect of relative platform length L/d. Obviously, there can be no data for $x_d/d > L/d$. For $d = 1.25$ ft, $L/d = 4.00$; the greatest value of x_d/d for which there are data is 3.92. For $d = 0.64$ ft, $L/d = 7.81$, and there are data for as large a value of x_d/d as 7.07.

Figure 6.24 shows most, but not all, of the measured data. The purpose of the figure has been to indicate functional form, comparison of data from two experimental scales, and comparison of analytical results with data. For the sake of clarity, data for which $d = 1.25$ ft, $x_d/d = .118$, 1.216, and 2.016 have not been included in the figure but may be found tabulated in Tables B1 and B2 of Appendix B.

The data in Figures 6.24 and 6.25 indicate a monotonic increase

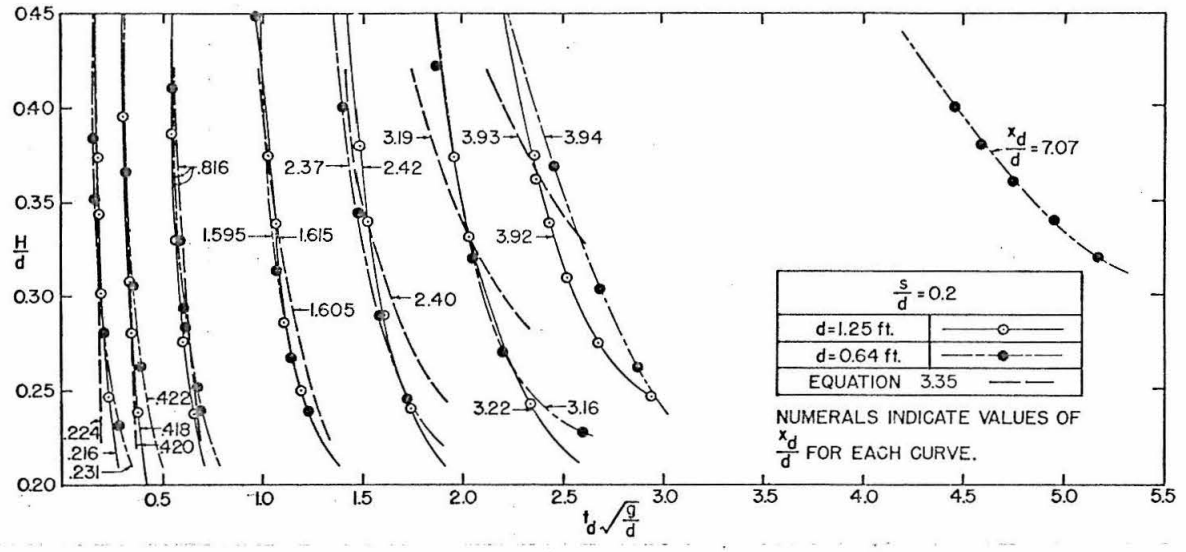

Figure 6.24. Normalized time of wave front arrival $t_d\sqrt{g/d}$, for s/d = 0.2.

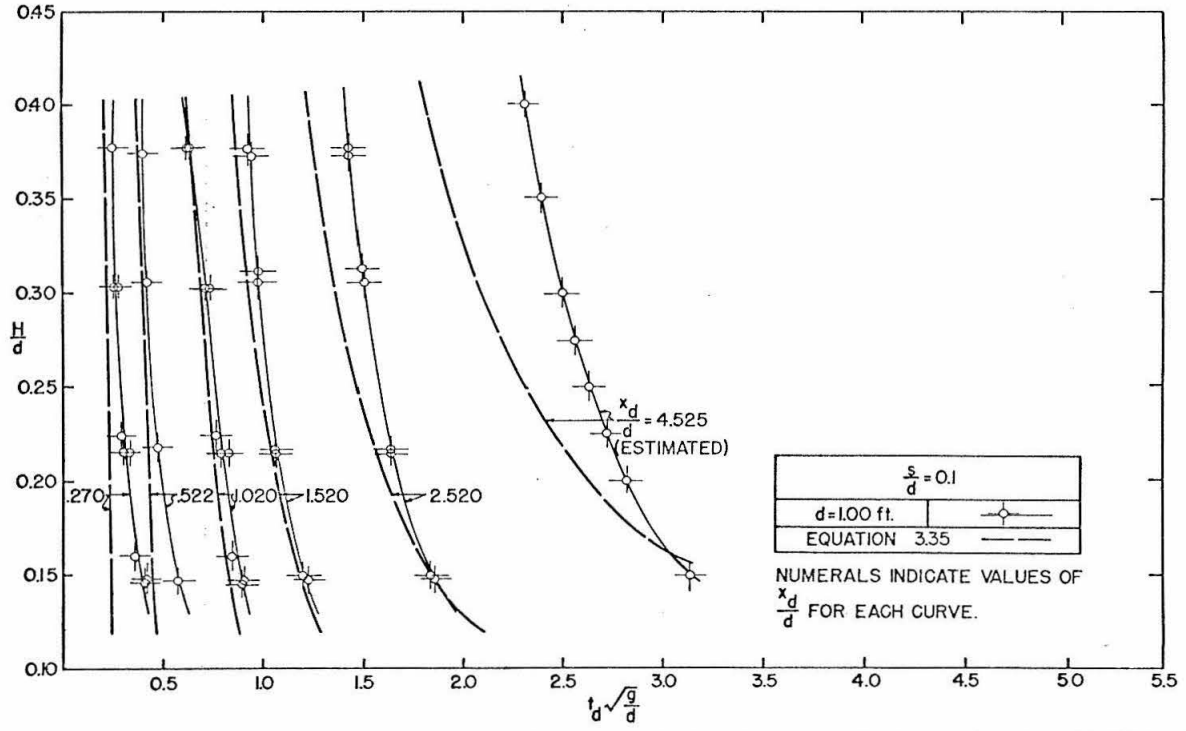

Figure 6.25. Normalized time of wave front arrival $t_d\sqrt{g/d}$, for s/d = 0.1.

of $t_d\sqrt{g/d}$ with x_d/d for constant H/d, and a decrease of $t_d\sqrt{g/d}$ with increasing H/d for constant x_d/d. This behavior is to be expected when it is considered that the relative wave front celerity $U_d/\sqrt{gd}$ (to be discussed presently) increases with relative wave height H/d. At constant H/d, greater relative distances x_d/d require greater travel times $t_d\sqrt{g/d}$; and at constant relative distance x_d/d, an increased relative wave height H/d, causing an increased relative celerity $U_d\sqrt{g\,d}$, will result in reduced travel time $t_d\sqrt{g/d}$.

In Section 3.2, Equation 3.34 expresses the relative wave front celerity $U_d/\sqrt{g\,d}$ in terms of the relative wave height H/d, the relative soffit clearance s/d, and a function η/d whose dependence on time t is expressed by Equation 3.30 (in which t_0 is defined in Equation 3.31). As shown in Equation 3.35, the wave front location x_d is simply the integral of U_d with respect to t from t=0 to $t=t_d$, the time of arrival of the wave front at x_d. By combining Equations 3.30, 3.31, 3.34, and 3.35, it is possible to determine functional relationships between t_d, U_d, and x_d for all values of s/d and H/d considered. Since Equation 3.34 is considered valid only for the range $0<t<t_a$, where t_a is the time at which fluid begins to recede from the platform soffit at the seaward end of the platform (see Section 3.3), values of U_d and x_d may be computed only within the range $0<t_d<t_a$.

Values of $t_d\sqrt{g/d}$ thus derived are plotted as functions of x_d/d and H/d in Figures 6.24 and 6.25. In Figure 6.24, for

s/d=0.2, there is generally good agreement with the data, except that predicted values of $t_d\sqrt{g/d}$ are less than the experimental values for large H/d, and are greater than the experimental values for small H/d. Agreement is best for small x_d/d. In Figure 6.25 for s/d=0.1, analytical values are in fair agreement with experimental values for x_d/d less than or equal to 1.520. For greater values of x_d/d, the analytical values of $t_d\sqrt{g/d}$ are in fair agreement with data for H/d less than 0.2, but are significantly less than measured values for H/d greater than 0.2. Since the analysis relating t_d to x_d is intimately related to the analysis for U_d, further discussion of the analysis is deferred to the discussion of wave front celerity, to follow presently.

The variation in measured values of t_d is examined first in Figure 6.26, where t_d is plotted in cumulative frequency diagrams on arithmetic probability paper for the samples of 16 to 32 experiments made at $x_d/d=0.816$. In each sample, the values of t_d are normalized with respect to $\overline{t}_d$, the sample mean value of t_d. In most cases, the data appear to be approximately normally distributed. With respect to the entire study, the ratios of sample standard deviation in t_d to sample mean were generally less than one percent. (Standard deviation in measured values of t_d will be referred to later in the discussion of standard deviation in U_d.)

The wavefront celerity U_d is derived from experimental data as follows: each curve fitted to experimental data in Figures 6.24 and 6.25 indicates the travel time $\left(t_d\right)_i$ taken by the wavefront to propagate a particular distance $\left(x_d\right)_i$ from the seaward edge of the

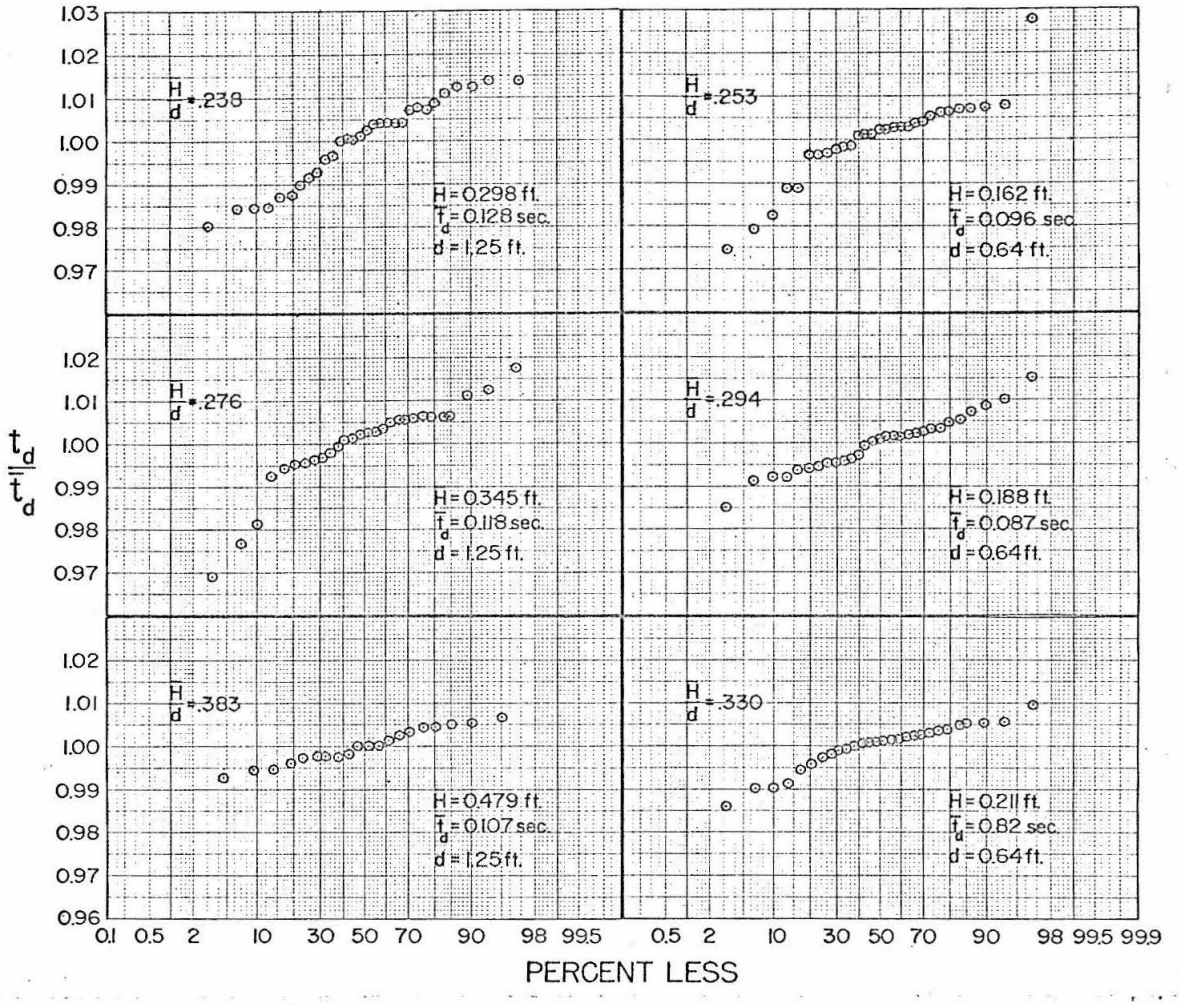

Figure 6.26. Cumulative frequency diagrams for normalized time of arrival $t_d/\bar{t}_d$ of the wave front ($x/d = 0.816$, $s/d = 0.2$).

platform. At a particular relative wave height H/d, the normalized time interval

$$\left[\left(t_d\right)_{i+1} - \left(t_d\right)_i\right]\sqrt{g/d}$$

between adjacent curves corresponding to transducer locations

$$\frac{(x_d)_{i+1}}{d} \text{ and } \frac{(x_d)_i}{d}$$

was evaluated. In the region of the platform between the locations, the average wave front celerity is simply:

$$U_{d_{av}} = \frac{\left[(x_d)_{i+1} - (x_d)_i\right]}{\left[(t_d)_{i+1} - (t_d)_i\right]} . \qquad (6.2)$$

This value of celerity is expressed as a function of the average value of x_d/d in the region:

$$\left(\frac{x_d}{d}\right)_{av} = \frac{1}{2d}\left[(x_d)_{i+1} + (x_d)_i\right] . \qquad (6.3)$$

The function

$$\left(\frac{U_d}{\sqrt{gd}}\right)_{av} = \frac{U_d}{\sqrt{gd}} = f\left(\frac{x_d}{d}\right)_{av}$$

is thus computed for the intervals between all adjacent curves (including those which were omitted from Figure 6.25 for clarity) for several values of H/d; for s/d = 0.2 at both d = 1.25 ft and d = 0.64 ft; and for s/d = 0.1.

Figures 6.27 show $(U_d/\sqrt{gd})_{av}$ for s/d = 0.2. Included also are data from the 40-ft wave tank, for which d = 0.50 ft, obtained both by the method just described, and from multiple-image photographs.

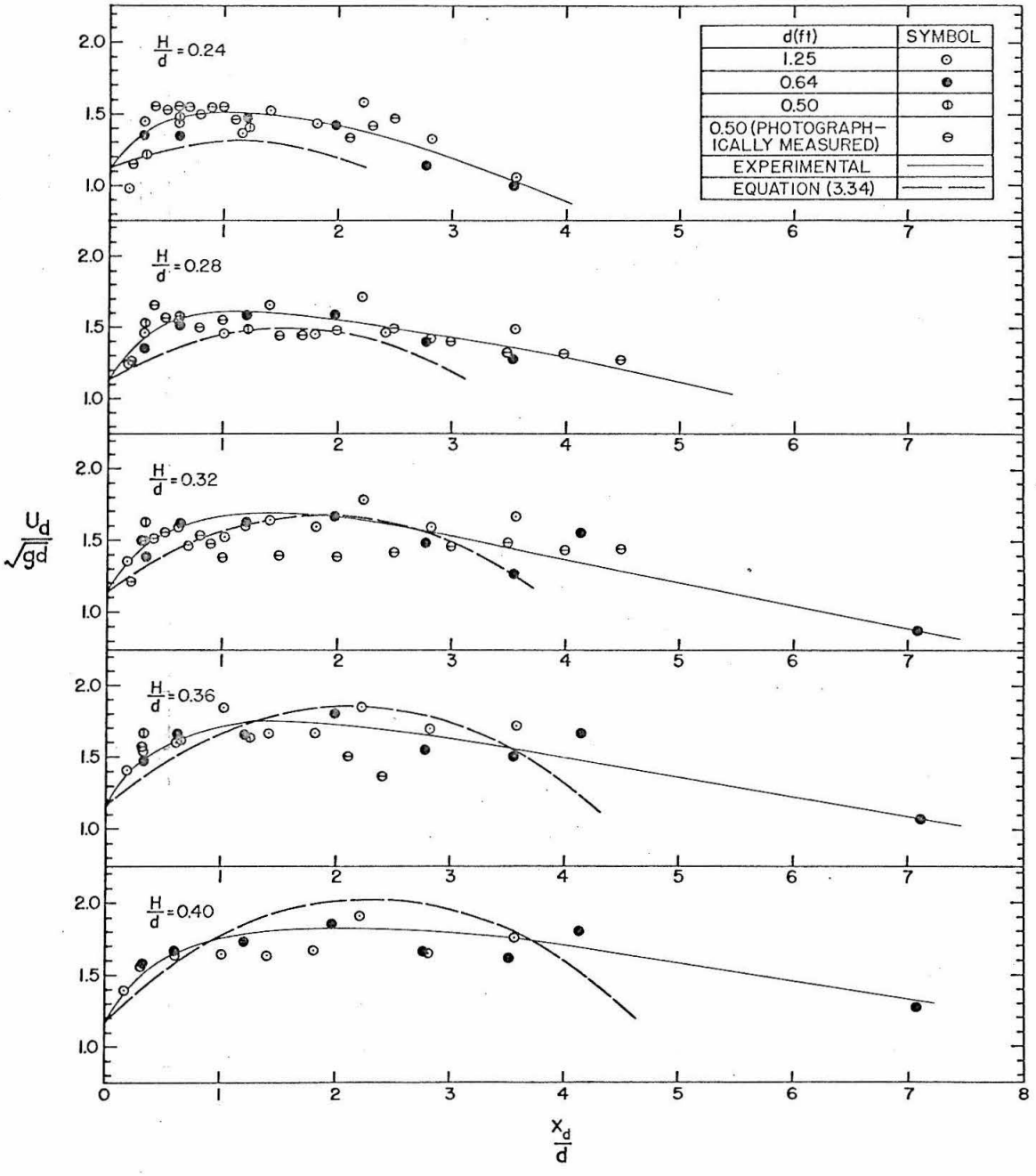

Figures 6.27. Normalized wave front celerity $U_d/\sqrt{gd}$ for s/d = 0.2.

In experiments made in the 40-ft tank a large number of multiple-image photographs (such as those shown in Figures 4.30 and 6.21a) were taken of the wave front as it progressed beneath the platform. The distance x of each wave front image from the seaward edge of the platform was measured directly from the photograph. The spacing

$$\left[(x_d)_{i+1} - (x_d)_i\right]$$

of two adjacent images, when divided by the time interval between light flashes, gave the average wave celerity as a function of the mean image position

$$\frac{1}{2}\left[(x_d)_{i+1} + (x_d)_i\right] .$$

There is considerable scatter among the measured values of $U_d / \sqrt{gd}$, yet within the range of scatter there is no observable difference in measured celerity with respect to scale size. The data obtained photographically from the 40-ft tank are in fair agreement with those obtained from the pressure records in experiments in both the 40-ft tank and the 100-ft tank.

Figures 6.28 show the corresponding variation of $U_d / \sqrt{gd}$ with x_d / d for several relative wave heights H/d for s/d = 0.1. Solid curves have been fitted to the data points in Figures 6.27 and 6.28 so that interpolated values of $U_d / \sqrt{gd}$ may be obtained for any desired value of x_d/d.

As described earlier, a combination of Equations 3.30, 3.31, 3.34, and 3.35 provided the analytical functional relationship between

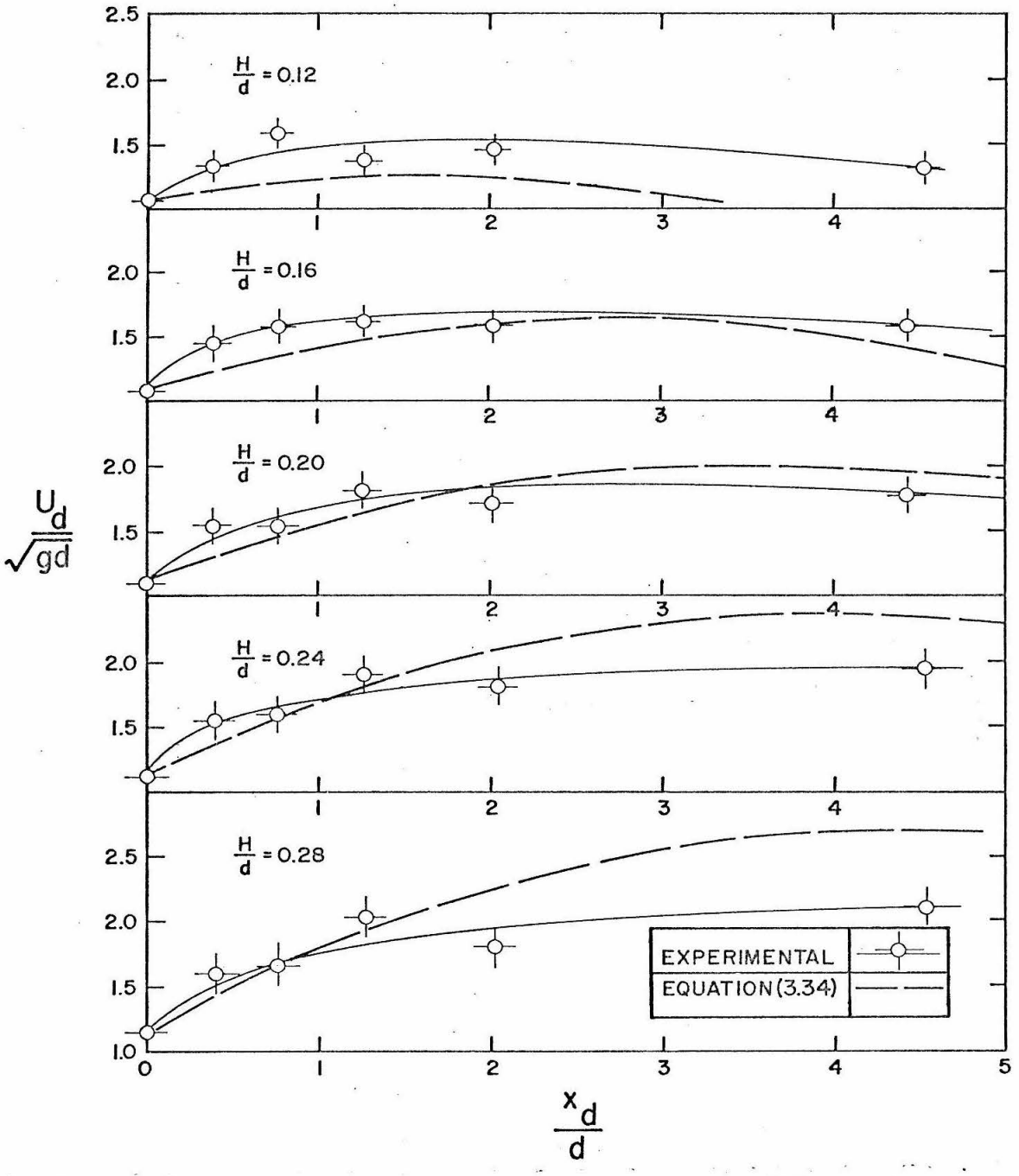

Figures 6.28. Normalized wave front celerity $U_d/\sqrt{gd}$ for s/d = 0.01.

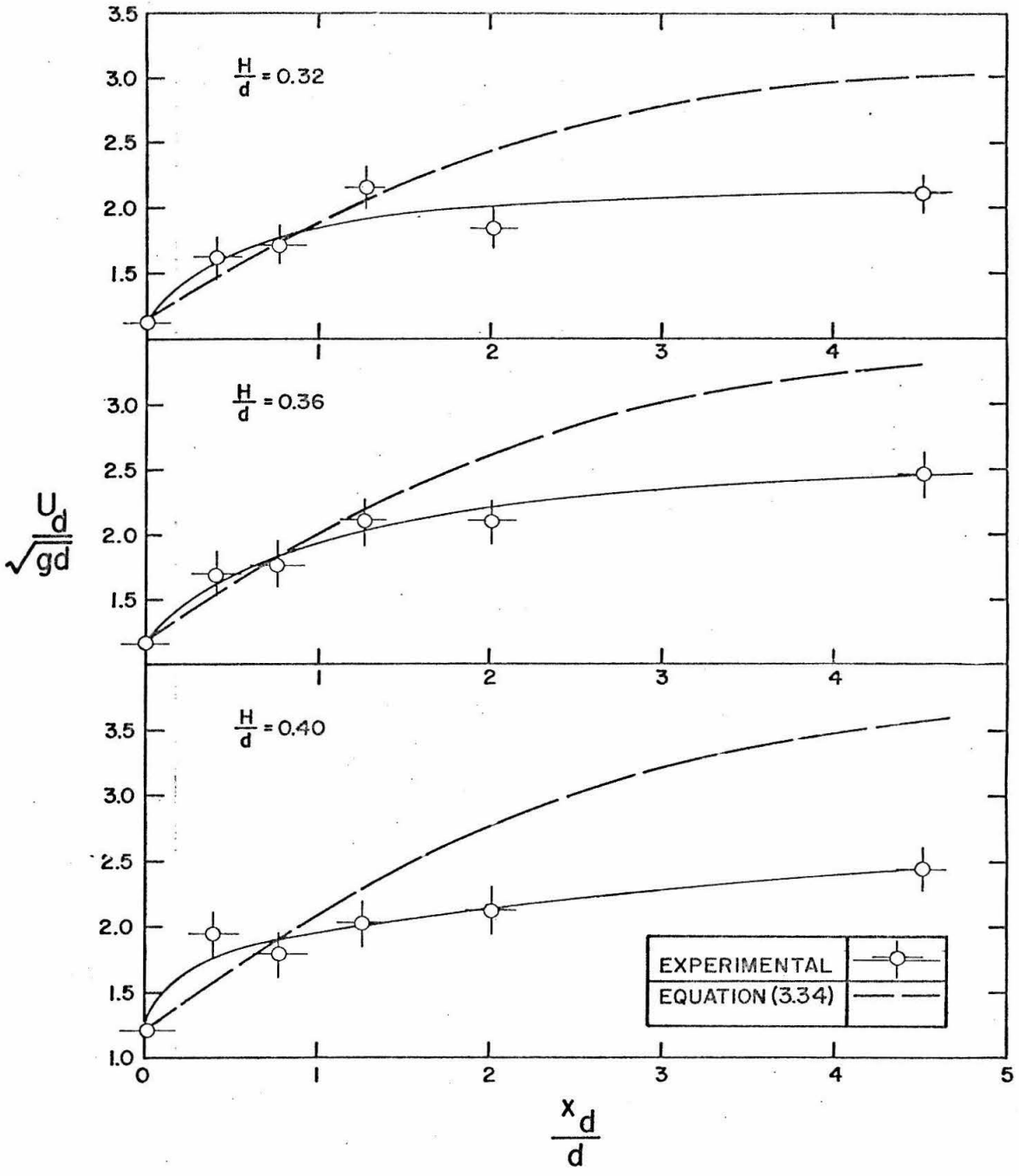

Figure 6.28. Normalized wave front celerity $U_d/\sqrt{gd}$ for s/d = 0.1.

normalized wave front celerity $U_d / \sqrt{gd}$ and relative wave front location x_d/d. Values of $U_d / \sqrt{gd}$ predicted by the analysis are shown by dashed curves in Figures 6.27 and 6.28. Again, the analysis is limited to values of x_d/d coresponding to the range $0 < t_d < t_a$.

At $x = 0$ the wave front celerity is simply the celerity U_o of the undeformed incident wave. For both $s/d = 0.2$ and $s/d = 0.1$, both the predicted and measured celerity values show that with increasing x_d/d, the wave front celerity increases to a maximum value, then decreases again. However, the analytical function attains its maximum value at a greater value of x/d than does the measured function, and thereafter it decreases more rapidly with respect to distance x/d than does the measured function. For $s/d = 0.2$, the best agreement is found when $H/d = 0.36$. For $s/d = 0.1$, the best agreement between predicted and measured values is found when $H/d = 0.20$. The degree to which anaytical values of t_d agree with experimental values in Figures 6.24 and 6.25 may be directly related to the degree to which anaytical values of U_d agree with experimental values in Figures 6.27 and 6.28. Figures 6.27 and 6.28 show predicted values of U_d less than experimental values for small relative wave height H/d, which in Figures 6.24 and 6.25 is generally reflected in predicted times of arrival $t_d\sqrt{g/d}$ which are greater than measured values. Conversely, for larger H/d, predicted values of U_d are generally greater than measured values, corresponding to predicted t_d less than measured t_d at larger values of H/d.

To determine the cause of disagreement between predicted and experimental values of U_d (and therefore of t_d), the assumptions underlying the analysis must be re-examined. The two assumptions involved were that the form of the free surface wave remains approximately constant, although the wave celerity may change with time; and that the horizontal fluid velocity beneath the seaward edge of the platform and the water surface elevation at the seaward edge are approximately the same as for the case when there is no platform present. The photographs of the surface profile near the wave front, presented in Section 6.2, showed no discernible change of profile with time, indicating that little error is introduced into the analysis by the assumption of constant wave form. On the other hand, as stated in Section 3.3, the assumption that fluid velocity at $x = 0$ (the seaward end of the platform) is the same as that found when no platform is present, introduces little error for $(H-s)/d << 1$, but becomes less valid as $(H-s)/d$ increases. Figures 6.27 and 6.28 show that generally as H/d increases, i.e., as $(H-s)/d$ increases, agreement between predicted and measured U_d decreases. For $s/d = 0.1$ the disagreement is more severe than for $s/d = 0.2$, because $(H-s)/d$ is greater for the same value of H/d. In general, at $s/d = 0.1$ the wave is more perturbed by the platform than at $s/d = 0.2$. The photographs in Figure 6.2 show that indeed the presence of the platform causes a significant perturbation of the flow in the incident wave, as indicated by the formation of the vertical jet on the front face of the platform, and by other features not characteristic of an

undisturbed solitary wave. Therefore the discrepancy between analytical and experimental values of U_d and of t_d may be ascribed chiefly to the assumption that the fluid velocity at $x = 0$ is that which would be found if the platform were not there.

The standard deviation in the measured value of $U_d/\sqrt{gd}$ may be estimated from the standard deviation of $t_d\sqrt{g/d}$, following the procedure outlined by Parratt (1961) in a discussion of the propagation of errors. If a quantity u is a function of n independent variables t_i, which have known standard deviation $(S_t)_i$, then the standard deviation of u is:

$$S_u \left[\sum_{i=1}^{n} \left(\frac{\partial u}{\partial t_i} \right)^2 (S_t)_i^2 \right]^{\frac{1}{2}} . \qquad (6.4)$$

In the present case, the derived quantity is U_d, and the independent variables are $(t_d)_i$ and $(t_d)_{i+1}$. The partial derivatives may be determined by differentiating Equation 6.2 first with respect to $(t_d)_i$ and then with respect to $(t_d)_{i+1}$:

$$\frac{\partial U_d}{\partial (t_d)_i} = - \frac{\partial U_d}{\partial (t_d)_{i+1}} \cong \frac{U_d}{\left[(t_d)_{i+1} - (t_d)_i \right]} . \qquad (6.5)$$

Thus the standard deviation becomes:

$$S_u = \frac{U_d \sqrt{(S_t)_i^2 + (S_t)_{i+1}^2}}{\left[(t_d)_{i+1} - (t_d)_i \right]}, \qquad (6.6)$$

and the ratio of standard deviation in celerity to mean celerity S_u/U is:

$$\frac{S_u}{U_d} = \frac{\sqrt{(S_t)_i^2 + (S_t)_{i+1}^2}}{\left[(t_d)_{i+1} - (t_d)_i\right]}, \qquad (6.7)$$

Equation 6.7 indicates that the ratio S_u/U_d of standard deviation to mean celerity is directly proportional to the magnitude of deviation in $t_d\sqrt{g/d}$, and inversely proportional to the difference in values of $t_d\sqrt{g/d}$ from which $U_d/\sqrt{gd}$ is computed. In other terms, for a given deviation in t_d, U_d computed from small differences in t_d will have a much larger deviation than the deviation in t_d.

Values of S_u/U_d are plotted in Figure 6.29, where they may be compared with values of the ratio of standard deviation to mean for t_d. That the fractional standard deviation of celerity U_d thus estimated is considerably greater than the fractional standard deviation of travel time t_d is due to large values of the partial derivatives in Equation 6.5. This explains why there is considerable scatter appearing in Figures 6.27 and 6.28 in values of $U_d/\sqrt{gd}$ computed from measured values of $t_d\sqrt{g/d}$, when there is little scatter apparent in measured values of $t_d\sqrt{g/d}$ plottted in Figures 6.24 and 6.25.

The time of arrival t_e is defined as the time that elapses between $t = 0$, when the incident wave makes initial contact with the seaward end of the platform, and the time when fluid recedes from a given position x_e on the platform soffit. As indicated in Figure 6.23, t_e is taken to be the time between the recording of the first maximum of the preliminary oscillations and the final return of the recorded trace to zero deflection.

Figure 6.30a shows t_e, normalized by multiplication by $\sqrt{g/d}$, plotted as a function of H/d for various values of x_e/d, for

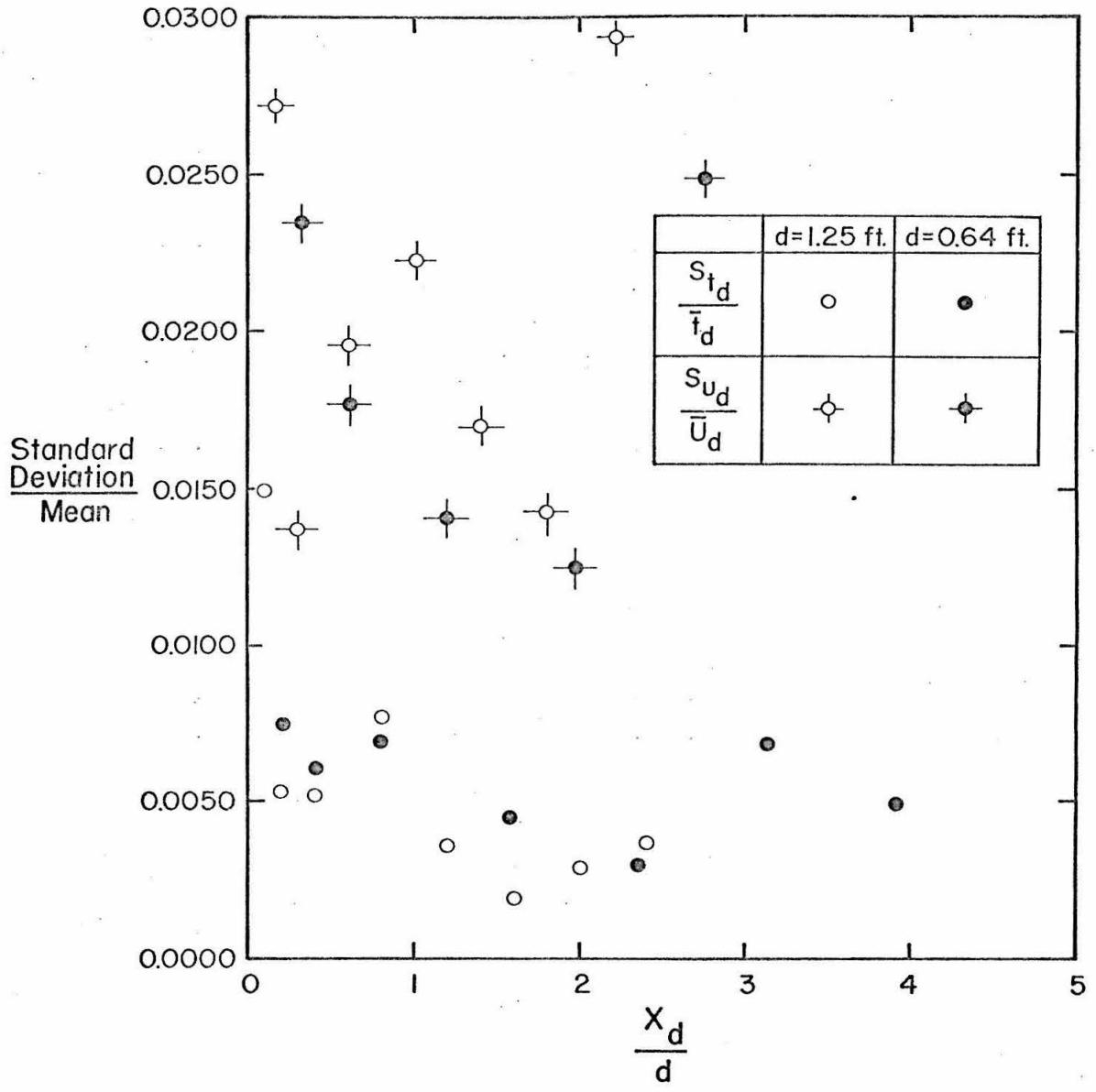

Figure 6.29. Ratio of standard deviation to sample mean, measured for t_d, estimated for U_d.

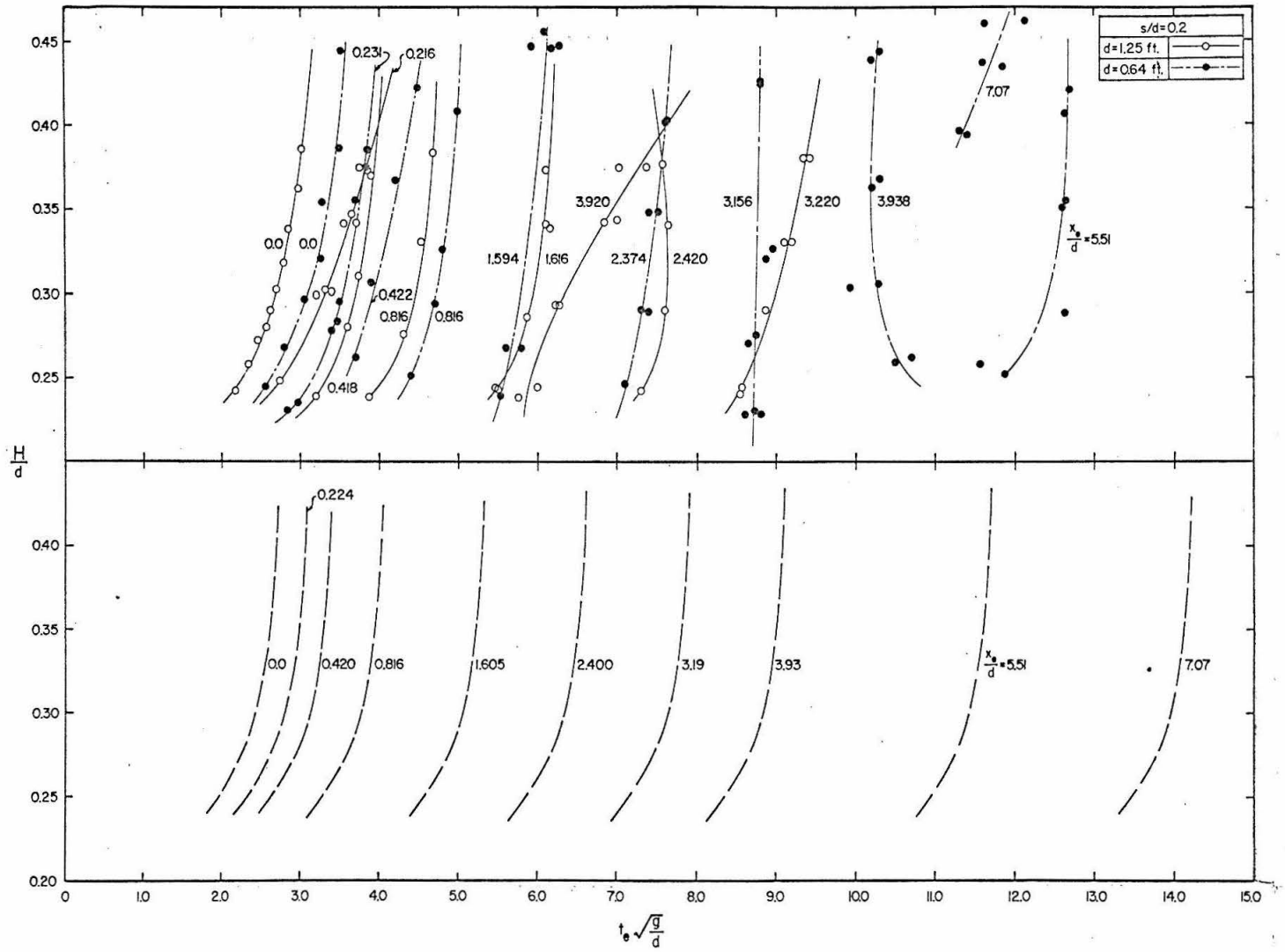

Figures 6.30. Normalized time of arrival $t_e\sqrt{g/d}$ of the wave of recession for s/d = 0.2. (a) Experimental data; (b) predicted values.

$s/d = 0.2$. (The number adjacent to each curve indicates the value of x_e/d.) Data from both scales, $d = 1.25$ ft and $d = 0.64$ ft, are included. Unless otherwise indicated, the plotted points represent not sample means, but data from individual wave records. Curves have been fitted through the data points for purposes of interpolating $t_e\sqrt{g/d}$ for any value of H/d.

The curves labelled "0.0" actually indicate values of t_a, the time at which fluid recedes from the seaward end of the platform. The values of $(t_e)_{x=0} = t_a$ were obtained with a parallel-wire wave gauge mounted 1/4-in. seaward of the seaward end of the platform. The water level indicated by the gauge showed an increase from still water level to the soffit elevation s, then to a maximum value, followed by a decrease again to s and to the still water level. The recorded interval between the time when the rising water level was equal to the soffit clearance s and when the falling water level was equal to s was taken as the value of t_a.

The dashed curves in Figure 6.30b represent analytical values of t_e predicted by Equation 3.52. For clarity, the analytical curves have been presented separately in Figure 6.30b, rather than superimposed on the experimental data in Figure 6.30a.

In Figure 6.30a, comparison of data from the two model scales indicates that for x_e/d less than about 1.0, values of $t_e\sqrt{g/d}$ for $d = 1.25$ ft are consistently less than for $d = 0.64$ ft. The cause of the difference is not understood; apparently it is not due to error in measurement, since the difference between scales exists for

$x_e/d = 0.0$, where data were obtained with a wave gauge, as well as for $x_e/d = 0.2$, 0.4, and 0.8, where data were obtained in independent measurements with the pressure transducers.

There is fair agreement between scales for values of $t_e\sqrt{g/d}$ measured at $x_e/d = 1.6$, 2.4, and 3.2. For $x_e/d > 3.2$, there appears a very large difference between scales: for $d = 0.64$ ft, $t_e\sqrt{g/d}$ continues to increase with x_e/d, whereas for $d = 1.25$ ft, $t_e\sqrt{g/d}$ appears to decrease with increasing x_e/d. This difference is most likely due to the difference in relative platform length L/d. For $d = 1.25$ ft, $L/d = 4.0$, and the portion of the soffit for which $3.2 < x/d < 4.0$ is affected not by the principal wave of recession but by the secondary wave of recession, shown in several figures in Section 6.2. For $d = 0.64$ ft, where $L/d = 7.68$, the principal wave of recession propagates over the approximate region $0 < x/d < 5.5$; the secondary wave propagates over the region $5.5 < x/d < 7.68$. (The behavior of the secondary wave of recession will be illustrated more clearly in Section 6.5.)

Comparison of Figure 6.30b with Figure 6.30a shows predicted values of $t_e\sqrt{g/d}$ to be consistently less than measured values. The curves for $x_e/d = 7.07$ are an exception: the position is affected by the secondary wave of recession, whereas the predicted value is computed as if it were subject to the principal wave of recession, giving a value of $t_e\sqrt{g/d}$ much greater than actually measured. The analysis clearly cannot be expected to predict accurate values of t_e in regions of x_e/d which are subject to the secondary wave of recession, since

the secondary wave is not considered at all in the analysis.

In Figures 6.30, the difference between measured and predicted values of $t_e\sqrt{g/d}$ for $0 < x_e/d < 5.51$ is everywhere approximately equal to the difference between measured and predicted values of $t_a\sqrt{g/d}$ indicating that the error in the analysis lies mainly in the first term in Equation 3.52, which is $t_a\sqrt{g/d}$, and less in the second term, which is proportional to the reciprocal of the predicted value of celerity U_e.

Figure 6.31 shows measured and predicted values of $t_e\sqrt{g/d}$ for $s/d = 0.1$, for the two values of x_e/d at which measurements of t_e were obtained. There is close agreement between measured and predicted values of $t_e\sqrt{g/d}$ for $x_e/d = 0.522$, but for $x_e/d = 4.525$ the predicted value is much greater than the measured value, from which one may infer that $x_e/d = 4.525$ lies within a region subject to the secondary wave of recession, rather than the principal wave.

As explained in Section 6.3, the travel time t_e of the wave of recession, as well as the slowly-varying pressure head P_1/γ, were in most cases obtained from only one or two wave records of each sample of five or six records. However, for the samples of 16 to 32 waves generated at $x/d = 0.816$, t_e was obtained for each record so that several large samples of t_e would be available for statistical analysis. For each sample the ratio of t_e to sample mean $\bar{t}_e$ is presented in cumulative frequency diagrams in Figure 6.32, similar to those for $t_d/\bar{t}_d$ presented in Figure 6.26. Like t_d, the travel time t_e appears to be normally distributed. For these samples, the average ratio of

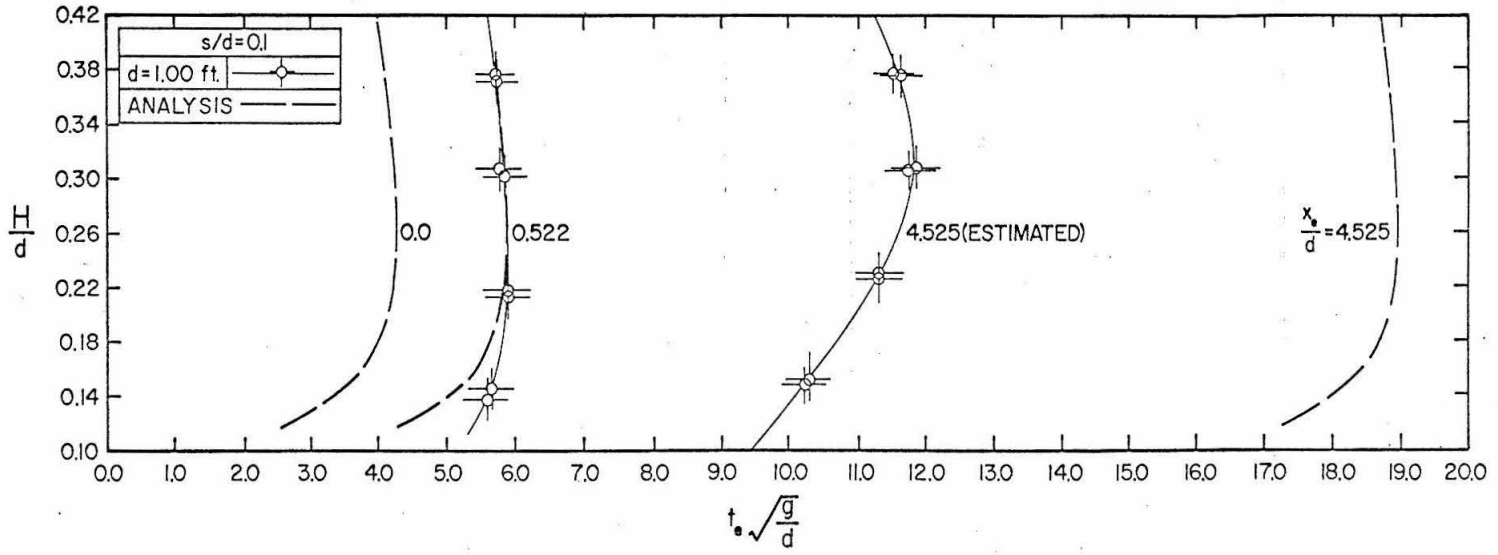

Figures 6.31. Normalized time of arrival $t_e\sqrt{g/d}$ of the wave of recession for s/d = 0.1.

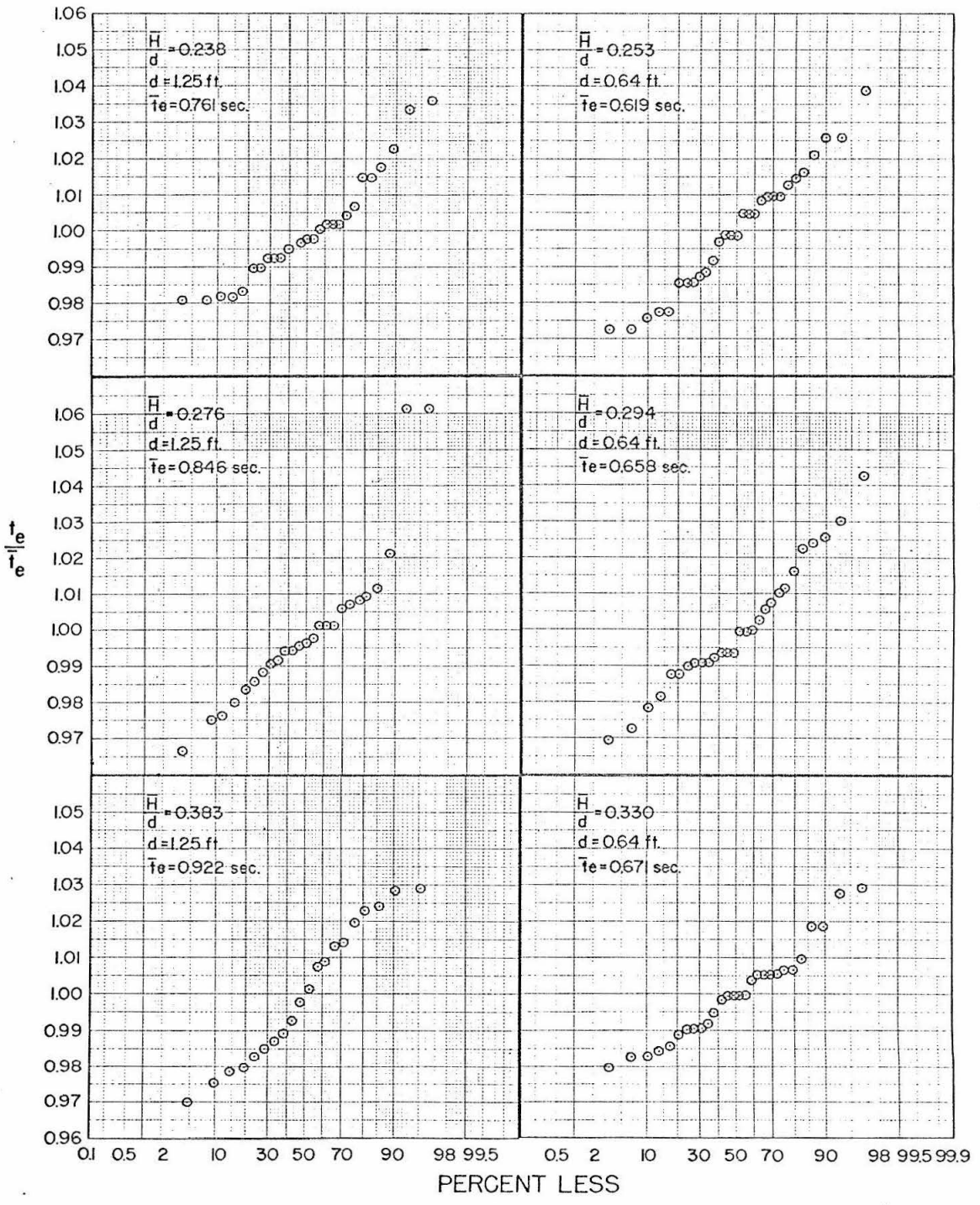

Figure 6.32. Cumulative frequency diagrams for normalized time of arrival $t_e/\bar{t}_e$ of the wave of recession ($x/d = 0.816$, $s/d = 0.2$).

standard deviation to mean is 0.015.

The celerity U_e of the principal wave of recession is computed from measured values of t_e in the same manner in which the advancing wave front celerity U_d was computed from t_d. For $s/d = 0.2$, the normalized celerity $U_e/\sqrt{gd}$ is shown in Figure 6.33 as a function of distance x_e/d, with the relative wave height H/d indicated. The constant value $U_e/\sqrt{gd} = 0.615$ predicted by the analysis for $s/d = 0.2$ (Equation 3.49) is also shown. The experimental data vary with x/d and H/d, but show no consistent trend dependent upon these parameters. The analytical value of 0.615 is close to the value of the average celerity in the range $0.5 \leq x_e/d \leq 5.0$. The values representing one scale are not consistently greater or less than the values from the other scale.

Equation 3.49 is based upon the following assumptions:

1. that there is a location shoreward of the wave of recession (Point 1 in Figure 3.3b) at which the horizontal fluid velocity does not depend on depth;

2. that the surface profile of the wave of recession is of unchanging form;

3. that effects of viscosity, surface tension, and air entrainment are negligible.

These assumptions are among those upon which the analysis for slowly-varying pressure is based. Detailed discussion of the assumptions is deferred to Subsection 6.5.4 in the discussion of slowly-varying pressure, rather than presented in this section, because for this study,

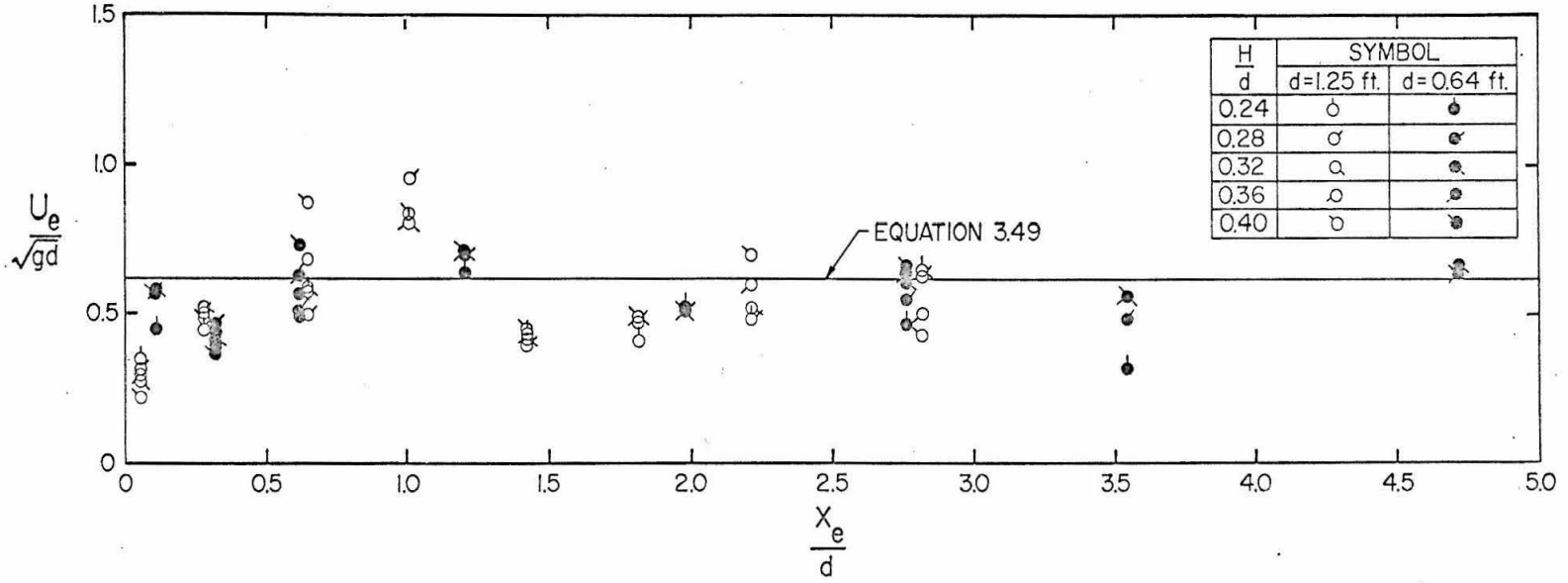

Figure 6.33. Normalized celerity $U_e/\sqrt{gd}$ of the wave of recession for s/d = 0.2.

slowly-varying pressure is considered to be a more important topic than is the celerity of the wave of recession. As expressed in Subsection 6.5.4, the assumption of velocity constant with depth is most valid for large x_d/d. A comparison of Figures 6.30a and 6.31 with Figures 6.24 and 6.25 show that for times when the wave of recession exists ($t > t_a$), x_d/d is greater than 2. However, it has not been possible to measure quantitatively how well the condition of uniform flow has been met. As stated in Subsection 6.5.4, photographs in Section 6.2 show distinctly that the assumption of constant wave profile is not valid for the wave of recession for the time immediately following t_a when the wave is beginning to form. (For times sufficiently greater than t_a, however, the assumption may be valid.) From the discussion presented in Subsection 6.5.4, the effects of viscosity and of surface tension may safely be neglected in the analysis for the celerity of the wave recession. The photographs in Figures 6.13 through 6.17 in Section 6.2 show practically no air entrained at the wave of recession, except perhaps during initial formation of the wave (see Figures 6.13e, 6.13f and 6.16e); hence the entrained air will not affect the analysis for U_e. It is interesting to note that despite the questionable validity of the assumptions of uniform velocity at Point 1 (see Figure 3.3b) and of constant profile, and despite variations in measured U_e, Equation 3.49 predicts well an average value of the celerity U_e of the wave of recession, as shown in Figure 6.33.

For $s/d = 0.1$, where $t_e\sqrt{g/d}$ has been measured at only two values of x_e/d, it appears that the location $x_e = 0.522$ is subject to

the principal wave of recession, whereas the location x/d = 4.525 is subject to the secondary wave of recession, as stated earlier. In such a case, it is meaningless to try to derive a wave celerity U_e from the two measurements of t_e, since there are in fact two independent waves of recession propagating in opposite directions with different celerities. Therefore, with no other data for s/d = 0.1 available, no measurement of U_e is possible. (The matter is discussed further in Section 6.5.)

The magnitude of the standard deviation in "measured" U_e may be estimated by the same procedure used for the wave front celerity U_d. Adapted for the variables t_e and U_e, Equation 6.7 becomes:

$$\frac{S_u}{U_e} = \frac{\sqrt{(S_t)_i^2 + (S_t)_{i+1}^2}}{(t_e)_{i+1} - (t_e)_i} \quad . \tag{6.8}$$

The standard deviations S_t of the six samples of t_e plotted in Figure 6.32, normalized by multiplication by $\sqrt{g/d}$, have a mean value of 0.076. If one assumes that this average normalized value of standard deviation represents the order of magnitude of the standard deviation in $t_e\sqrt{g/d}$ at all values of x_e/d, then the ratio of standard deviation to mean celerity

U_e of the wave of recession is of the order of:

$$\frac{S_u}{U_e} = \frac{\sqrt{(0.076)^2 + (0.076)^2}}{(t_e\sqrt{g/d})_{i+1} - (t_e\sqrt{g/d})_i} \quad . \tag{6.9}$$

Again, the ratio of standard deviation to mean celerity is inversely proportional to the difference in values of $t_e\sqrt{g/d}$ from which $U_e/\sqrt{gd}$ is computed. Figures 6.30 show that for $x_e/d < 0.42$, the difference $(t_e\sqrt{g/d})_{i+1} - (t_e\sqrt{g/d})_i$ is about 0.4; therefore, by Equation 6.9, S_u/U_e is approximately 0.27. For $0.4 < x_e/d < 3.9$, the difference is about unity; therefore S_u/U_e is approximately 0.11 for this range.

6.5 The Slowly-Varying Pressure.

In this section measurements of slowly-varying pressure, obtained with the 1/2-in. transducer, are presented and discussed. The total uplift force, the average pressure, and the center of pressure, derived from the distribution of measured pressure, are also presented and discussed. The data which correspond to the slowly-varying pressure are tabulated in Table B1 of Appendix B.

6.5.1 Statistical considerations.

To estimate the deviation inherent in measurements of the slowly-varying pressure head, P_1/γ, one measurement of P_1/γ was obtained from each of the pressure records obtained at $x/d = 0.816$ for various ratios of wave height to still water depth, H/d, and for a time t which was constant for all records in a sample. (At this location between 16 and 32 experiments were conducted for each wave height. For $d = 1.25$ ft, the time t was 0.14 sec, so that $t\sqrt{g/d}$ was 0.712; for $d = 0.64$ ft, the time t was 0.12 sec, so that $t\sqrt{g/d} = 0.852$. At each each scale the choice of t was arbitrary, it being necessary only to choose a value sufficiently greater than t_d to ensure that slowly-varying pressure rather than peak pressure was being measured.)

Cumulative frequency diagrams for six samples, shown in Figure 6.34, indicate an approximately normal distribution. The average ratio of measured standard deviation of slowly-varying pressure to incident mean wave height is 0.029.

6.5.2 Pressure.

Figures 6.35 through 6.40 represent an attempt to aid visualization of the functional pattern of pressure, in its dependence on time, t, and distance, x. The ordinate of each graph is the normalized time coordinate $t\sqrt{g/d}$, and the abscissa is normalized distance x/d. The graphs are similar to the characteristics diagrams commonly used in the one-dimensional analysis of shock waves or shallow-water waves. The plotted values which define the

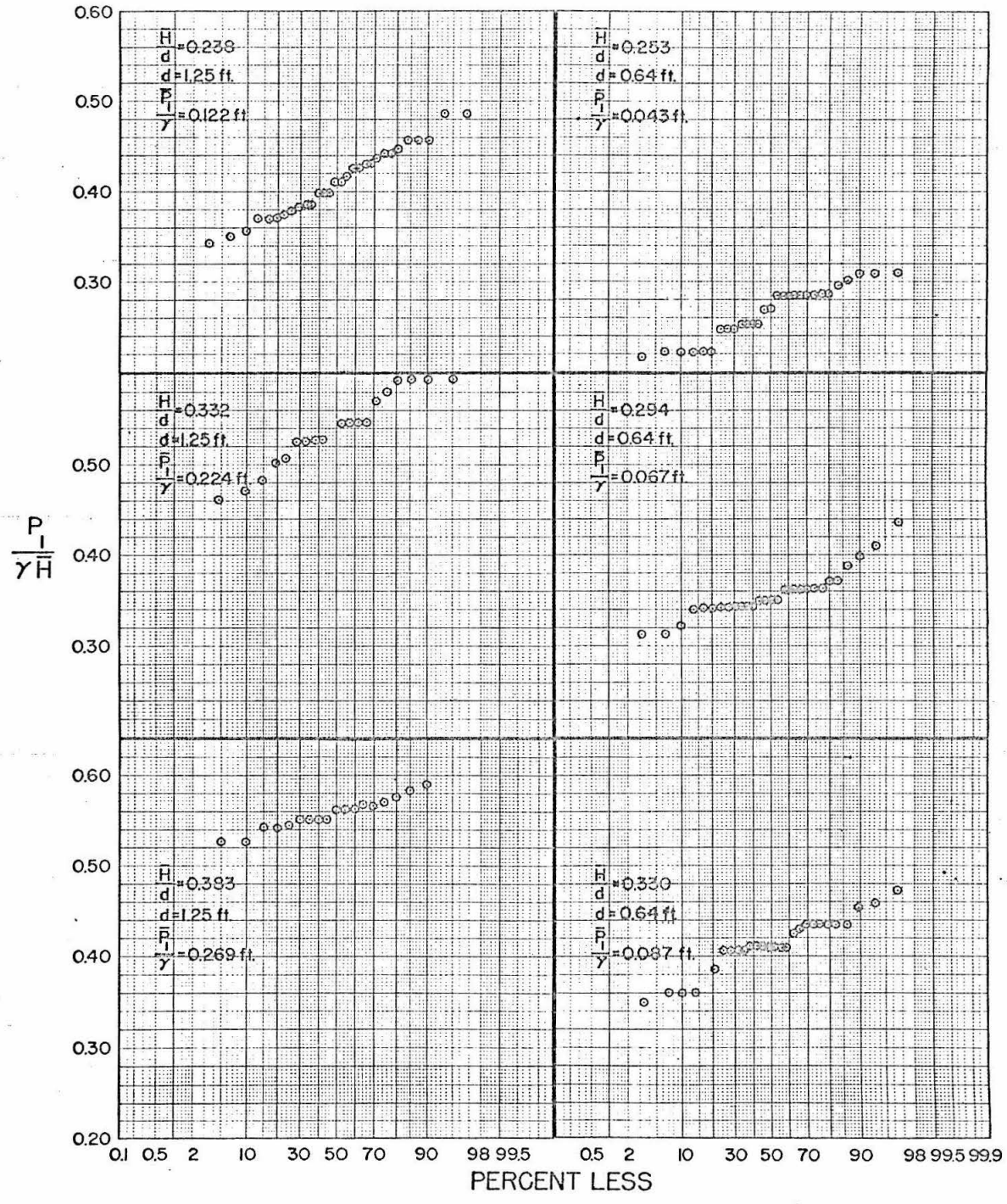

Figure 6.34. Cumulative frequency diagrams for normalized slowly-varying pressure $P_1/\gamma H$.

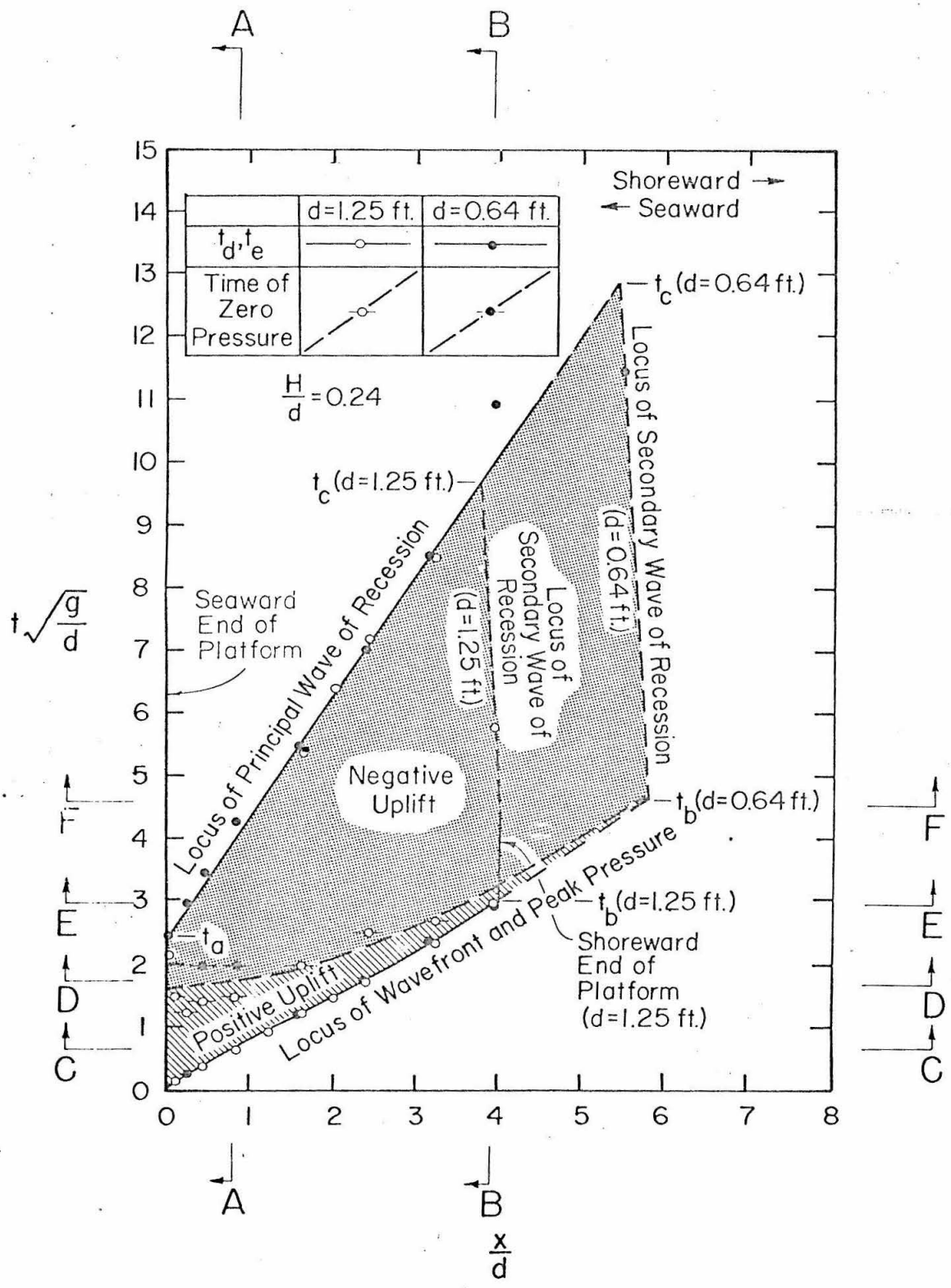

Figure 6.35. Time-distance diagram for s/d = 0.2, H/d = 0.24.

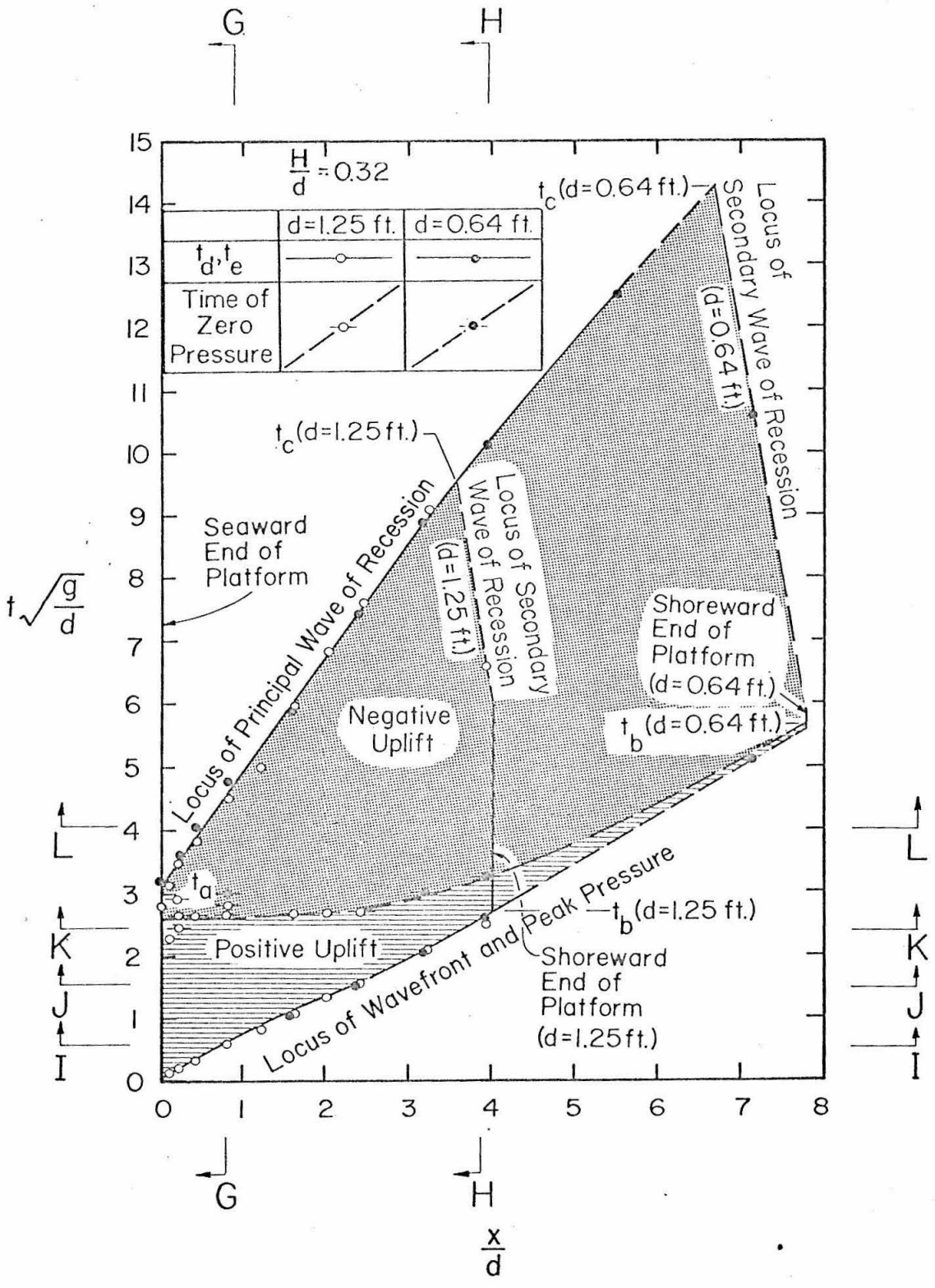

Figure 6.36. Time-distance diagram for s/d = 0.2, H/d = 0.32.

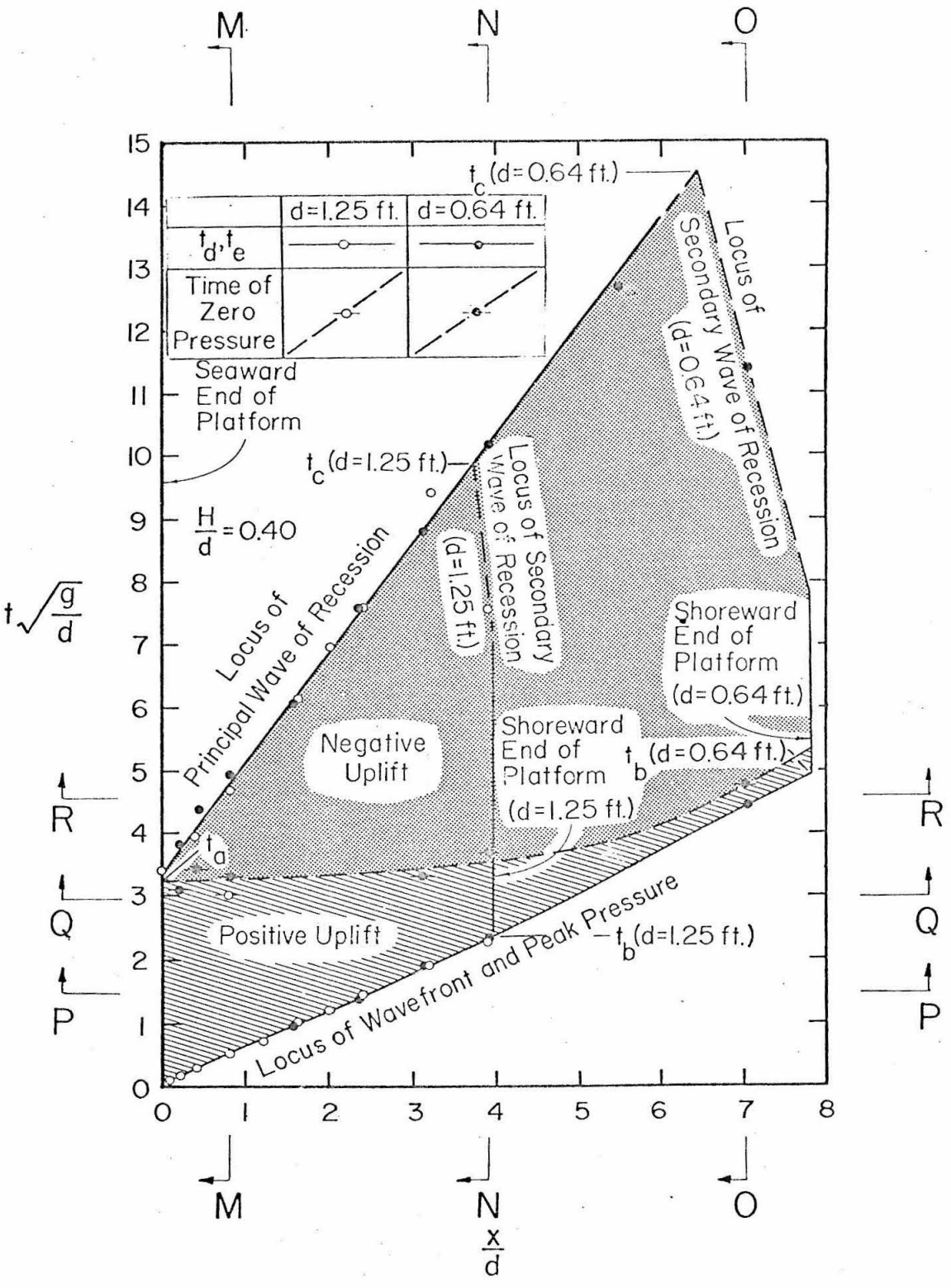

Figure 6.37. Time-distance diagram for s/d = 0.2, H/d = 0.40.

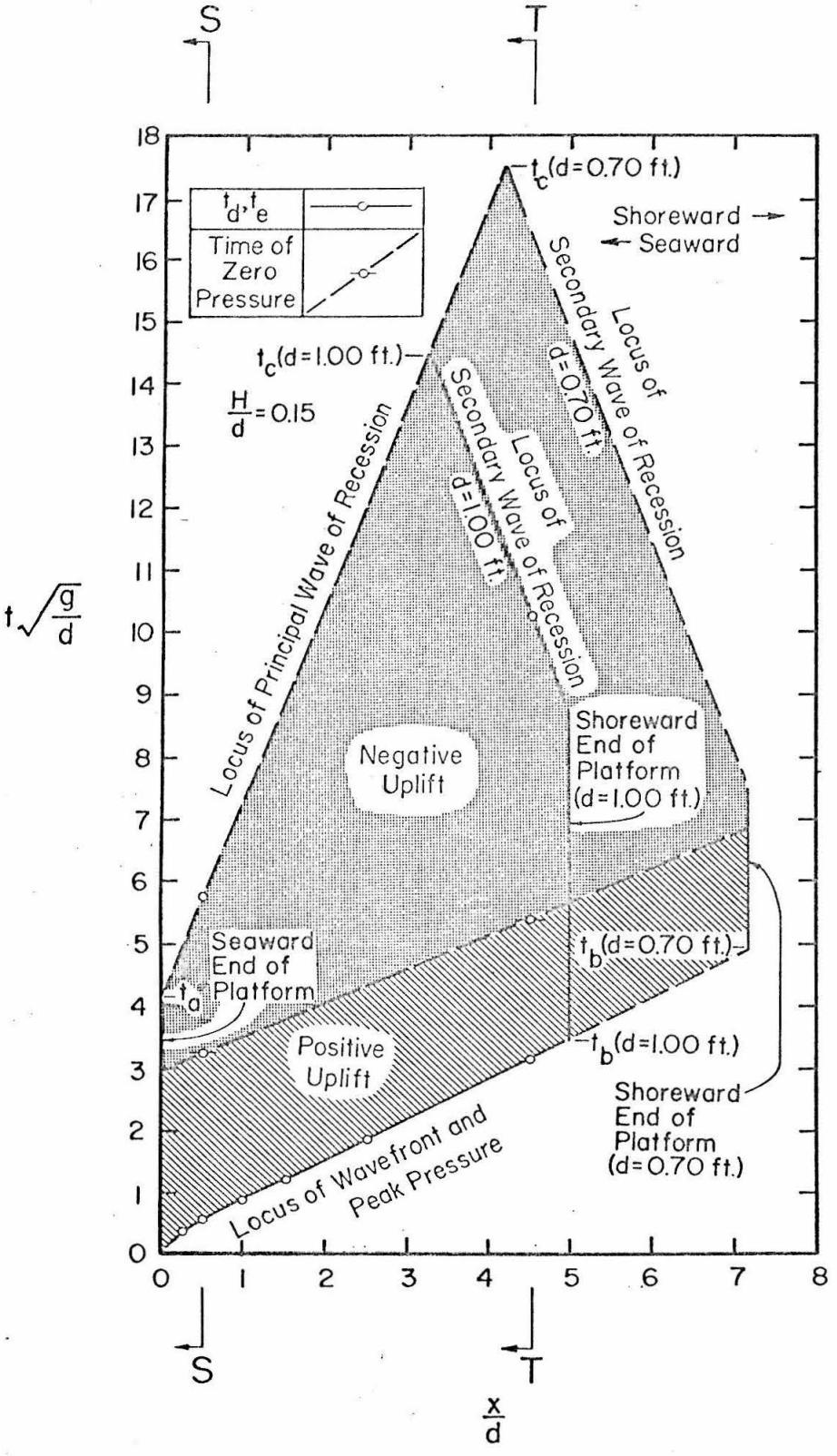

Figure 6.38. Time-distance diagram for s/d = 0.1, H/d = 0.15.

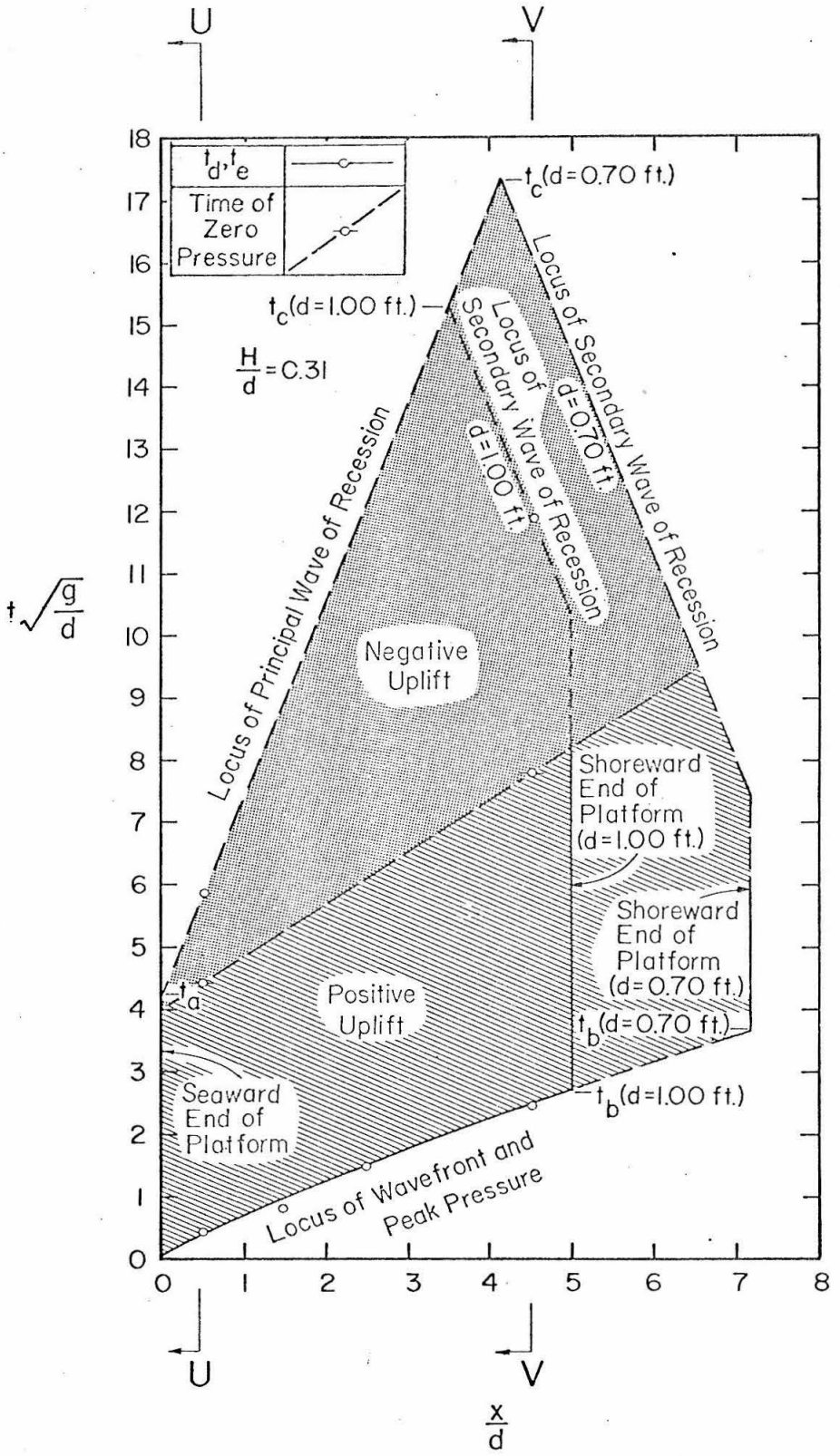

Figure 6.39. Time-distance diagram for s/d = 0.1, H/d = 0.31.

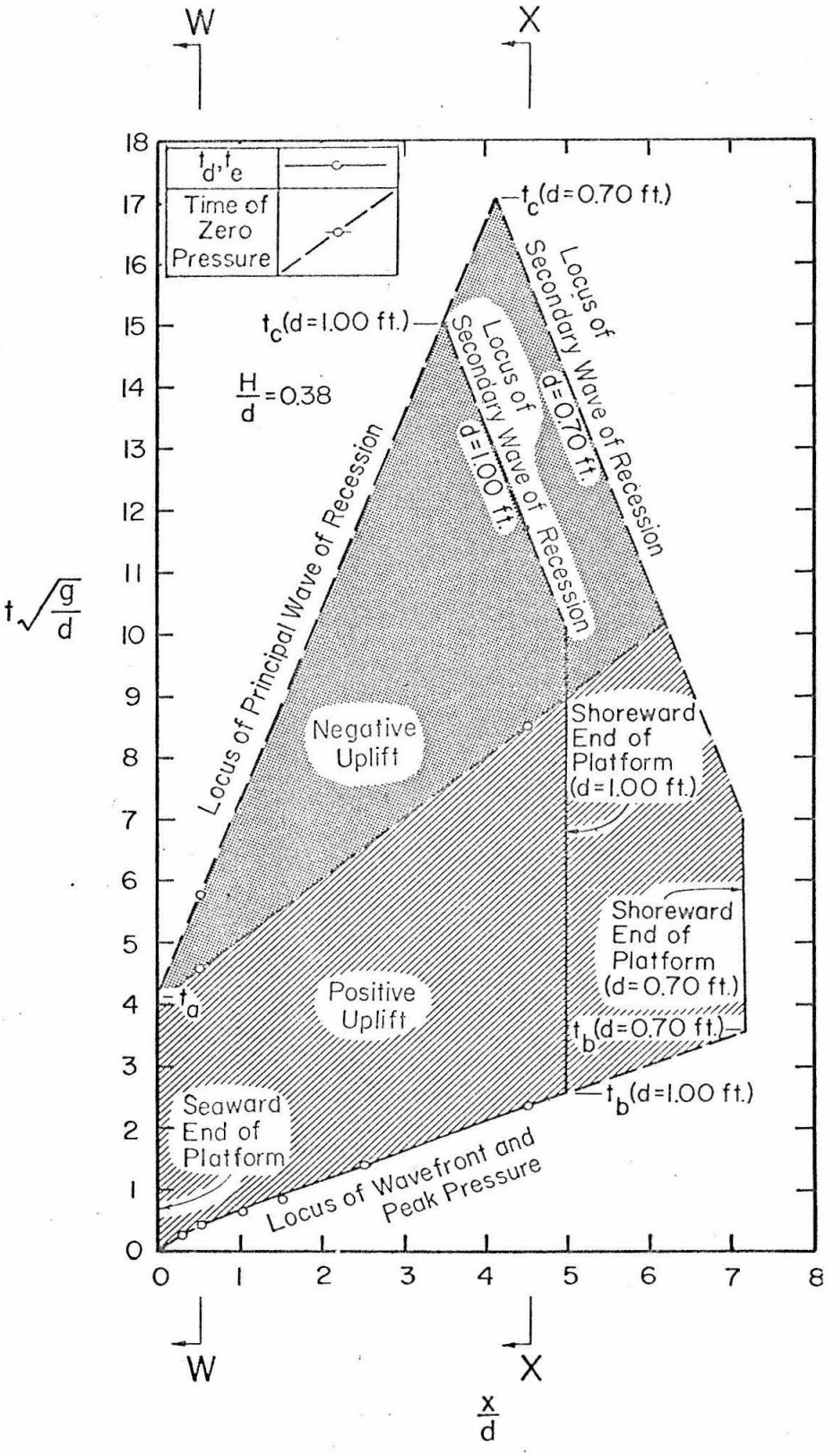

Figure 6.40. Time-distance diagram for s/d = 0.1, H/d = 0.38.

locus of the wave front are obtained from the experimental curves presented in Figures 6.24 and 6.25; plotted values defining the locus of the waves of recession are obtained from the experimental curves presented in Figures 6.27 and 6.28. Determination of the loci is aided by interpretation of photographs of the wave beneath the platform, such as shown in Section 6.2. The data which define the line separating the regions of positive and negative uplift are determined from the pressure data presented in Table B1 of Appendix B. Solid curves are fitted to the data; dashed curves represent estimated or extrapolated values. Theoretical curves are not included in these figures, since a comparison of theoretical and experimental values of t_d and t_e has been presented in Figures 6.24, 6.25, 6.30, and 6.31 in Section 6.4.

Figures 6.35 through 6.40 may be interpreted as follows: at $x/d = 0$, $t\sqrt{g/d} = 0$, the wave first makes contact with the platform. The wave front, defined in Section 6.3 as the location of the pressure peak, propagates along the platform as shown by the curved labeled, "locus of wave front and peak pressure". The platform used in all experiments was 5 ft long; hence for $s/d = 0.2$ and for a depth $d = 1.25$ ft, the wave front curve terminates at $x/d = 4$, whereas for $d = 0.64$ ft, the curve continues to $x/d = 7.8$ (except in Figures 6.35, as will be noted presently). For $s/d = 0.1$, pressure tests were made at a depth of $d = 1.00$ ft, for which the maximum value of x/d is 5.00; photographs presented in Figures 6.16 and 6.17 were made at $d = 0.70$ ft, for which the platform extends to $x/d = 7.16$. The length

of each vertical line labeled, "shoreward end of the platform" indicates the length of time for which the shoreward end of the platform is submerged. The time at which the vertical lines intersect the wave front curve is t_b, the time beyond which the advancing wave front is no longer defined (Table 3.1).

At $x/d = 0$, $t\sqrt{g/d} = t_a\sqrt{g/d}$, the principal wave of recession begins to form and propagate shoreward, as shown by the curve labeled "locus of principal wave of recession". Similarly, from the shoreward end of the platform, the secondary wave of recession propagates seaward, as shown, meeting the principal wave of recession at $t\sqrt{g/d} = t_c\sqrt{g/d}$. In each figure a curve which defines a secondary wave of recession is indicated for each model scale, in the same manner as the shoreward end of the platform was indicated for each model scale.

In Section 3.2 it was noted that the normalized distance $x_{d\,max}/d$ in which the wave propagates beneath and in contact with the platform may be expected to increase with increasing relative wave height H/d. In Figures 6.36 and 6.37 for $s/d = 0.2$, and in Figures 6.38, 6.39, and 6.40 for $s/d = 0.1$, H/d is great enough so that the normalized maximum distance $x_{d\,max}/d$ is greater than the relative platform length L/d; i.e., the wave front is in contact with the platform over the whole length of the platform, as in the cases illustrated in Figures 6.13 and 6.16 in Section 6.2. However, for Figure 6.35, H/d is sufficiently small that the wave front is not defined for a relative location x/d greater than about 5.8, which for

$d = 0.64$ ft is less than the relative platform length $L/d = 7.81$. The condition is shown in Figures 6.14 in Section 6.2: the wave front that may be seen in Figure 6.14d is no longer defined in Figure 6.14e, in which the wave crest (which is seen approaching the shoreward end of the platform) propagates without wetting more of the platform. At $t\sqrt{g/d} = t_b\sqrt{g/d}$, which in this case is the time when the wave front can no longer remain in contact with the platform, the secondary wave of recession immediately forms and propagates seaward.

In each of Figures 6.35 through 6.40, the polygon enclosed by the curves is subdivided into shaded areas labeled, "positive uplift" and"negative uplift". At any given value of relative time $t\sqrt{g/d}$, values of x/d within the polygon represent the portion of the platform soffit in contact with, or wetted by, the wave. For any given value of x/d, the polygon and its shaded areas indicate the relative time of wave front arrival, the subsequent duration of positive and negative pressures, and the relative time of arrival of the principal or secondary wave of recession.

The chronological events t_a, t_b, and t_c, defined in Table 3.1 of Section 3.3, are indicated in each of Figures 6.35 through 6.40. In Section 6.2, each of the photographs in Figures 6.13 through 6.17 shows the flow within a particular time range (such as $0 < t < t_a$). By reference to photographs taken at comparable values of s/d and H/d, one may visualize the flow conditions at corresponding times plotted in Figures 6.35 through 6.40.

Since the primary concerns of the present study were the peak pressure (to be discussed in Section 6.6) and the positive slowly-varying pressure, there was no attempt made to measure either the celerity of the secondary wave of recession or the value of t_c, the time at which the principal and secondary waves of recession meet. Yet photographs such as shown in Figures 6.14e, 614.f, 6.15e, and 6.15f clearly indicate the existence of the secondary wave of recession, and its representation in Figures 6.35 through 6.40, even if its position is only estimated, permits one to make several observations about pressure as a function of time t and distance x.

It is of interest to study the curve which separates the regions of positive and negative uplift in Figures 6.35 through 6.37. The points defining the curve were obtained for several values of x/d by determining the time at which pressure records, after indicating positive pressures, indicated zero pressure before indicating negative values. It was often difficult to determine meaningful values of time of zero pressure because of severe oscillations in the record which almost always occurred at the time of zero pressure. (These oscillations, the "secondary oscillations" indicated in Figure 6.20a, of interest in themselves, will be discussed presently.) On each record examined for time of zero pressure, a curve was fitted through the region of oscillation to represent the mean value about which pressure varied. The curve connected smoothly with the pressure trace in the regions before and after the regions of oscillation. The time at which the fitted curve indicated zero pressure was

taken as the time of zero pressure, separating regions of positive and negative pressure.

It may be noted that the curve separating the regions of positive and negative uplift in Figures 6.35 through 6.37, when extrapolated to $x/d = 0$, tends to a value of $t\sqrt{g/d}$ approximately equal to $t_a\sqrt{g/d}$, the time when the water level at $x/d = 0$ has decreased to the elevation of the platform soffit. From hydrostatic considerations, it is very reasonable that at $x/d = 0$ the uplift pressure should be zero at the nondimensional time $t_a\sqrt{g/d}$ when the elevation of the nearby water surface is equal to the elevation of the point of pressure measurement.

For $x/d = 0.2$, in Figures 6.35 through 6.37, it is notable that the time of zero pressure does not vary significantly with increasing x/d, except at larger values of x/d where the curve approaches the curve which describes the wave front. With the time of zero pressure remaining relatively constant with x/d compared to the time of arrival of the wave front or of the wave of recession, Figures 6.35 through 6.37 show clearly that the ratio of duration of positive uplift to duration of negative uplift at any given point on the platform decreases with increasing x/d.

Use of the same absolute platform length (five ft) at the two model scales ($d = 1.25$ ft and $d = 0.64$ ft) provides information on the pressure-time-distance distribution on platforms of different relative lengths L/d for similar values of relative soffit clearance s/d and relative wave height H/d. To extend the obervation just mentioned,

that the ratio of positive uplift duration to negative uplift duration decreases with increasing x/d, the principal effect of increased relative platform length L/d is to increase considerably the duration of time for which portions of the platform are subjected to negative uplift, with little increase in the duration of time for which the platform is subjected to positive uplift.

For relative soffit clearance $s/d = 0.1$, Figures 6.38 through 6.40 show that the time of zero pressure increases with x/d; yet in this case also the ratio of the durations of positive and negative uplift apparently decreases with increasing x/d, and an increase in platform length L/d increases the duration of negative uplift more than it increases the duration of positive uplift.

Figures 6.35 through 6.40 show that for all x/d the ratio of the duration of the positive uplift pressure to that of the negative uplift pressure increases with relative wave height H/d, for both $s/d = 0.2$ and $s/d = 0.1$. Comparison of Figures 6.35 through 6.37 for $x/d = 0.2$ with Figures 6.38 through 6.40 for $s/d = 0.1$ indicates that for any value of x/d the ratio of the duration of the positive to the negative uplift pressures increases with decreasing relative soffit clearance s/d. (It should be kept in mind that these results were obtained for a platform as wide as the wave tank, where air was not permitted to flow between the platform edges and the tank walls to relieve negative pressures. For a narrow pier without confining side walls, the qualitative picture may be different.)

In Section 6.4, Figure 6.30a for $s/d = 0.2$ showed that the

time of arrival of the wave of recession t_e, after initially increasing with x/d, decreased markedly with increasing x/d. In particular, for d = 1.25 ft the value of $t_e \sqrt{g/d}$ for x/d = 3.920 was considerably less than for x/d = 3.220; and for d = 0.64 ft the value of $t_e \sqrt{g/d}$ for x/d = 7.070 was less than for x/d = 5.510. It was suggested in Section 6.4 that this behavior could be attributed to the presence of the secondary wave of recession, as is now shown in Figures 6.35 through 6.37 for s/d = 0.2. For d = 1.25, values of $t_e \sqrt{g/d}$ obtained at all transducer locations except x/d = 3.920 lie on the curve representing the principal wave of recession and increase with increasing x/d. The transducer location x/d = 3.920 is subject to the secondary wave, where values of $t_e \sqrt{g/d}$ decrease with the increasing x/d; the value of $t_e \sqrt{g/d}$ at x/d = 3.920 may therefore be less than at x/d = 3.220. For d = 0.64, the transducer location x/d = 7.070 is subject to the secondary wave of recession, and the value of $t_e \sqrt{g/d}$ may therefore be less than at x/d = 5.510. (One may note that at d = 0.64 ft, the location x/d = 3.938 is subject to the principal wave of recession and there is hence a great difference in values of $t_e \sqrt{g/d}$ for this location and the corresponding location x/d = 3.920 at d = 1.25 ft, which was subjected to the secondary wave of recession. Other differences between pressure values obtained at these two corresponding locations will be discussed presently.)

In Figure 6.31 for s/d = 0.1, it was shown that despite good agreement between theoretical and experimental values for $t_e \sqrt{g/d}$ for x/d = 0.522, there was very poor agreement between theory and

experiment for $x/d = 4.525$; because, it was suggested, the location $x/d = 4.525$ is subjected to the secondary wave of recession rather than the principal wave of recession, as assumed in the analysis. Figures 6.38 through 6.40 for $x/d = 0.1$ for $d = 1.00$ ft show an experimental value of $t_e\sqrt{g/d}$ at $x/d = 4.525$ on the curve for the secondary wave of recession, as suggested. The slope of the curve which represents the principal wave of recession in Figures 6.38 through 6.40 (defined as $d(x/d)/d(t\sqrt{g/d})$) is the normalized celerity $U_e/\sqrt{gd} = 0.318$, where the numerical value is obtained from Equation 3.45. There are at least two observations which can be made to support the use of estimated curves of the loci of the principal and secondary waves of recession as constructed in Figures 6.38 through 6.40, as opposed to simply passing a straight line through measured values of $t_e\sqrt{g/d}$ at both $x/d = 0.522$ and $x/d = 4.525$. Such a line would result in a normalized celerity $U_e/\sqrt{gd}$ of about 0.7. First, it may be pointed out that in Figures 6.35 through 6.37 for $s/d = 0.2$, the slope of the curves for the principal wave of recession is in excellent agreement with the value $U_e/\sqrt{gd} = 0.615$ predicted by Equation 3.49, giving one confidence in the analysis resulting in Equation 3.45, and hence in using the value $U_e/\sqrt{gd} = 0.318$ predicted from Equation 3.45 for $s/d = 0.1$. Second, as stated earlier with respect to $s/d = 0.2$, it is reasonable to expect that $x/d = 0$ the time of occurrence of zero pressure should coincide with $t_a\sqrt{g/d}$, the time at which the water level has decreased to equal the soffit elevation. In Figures 6.38 through 6.40, the curve for the principal wave of

recession, extrapolated to $x/d = 0$, is in closer agreement with the time of zero pressure (also extrapolated to $x/d = 0$) than it would be if a curve had simply been placed through the two plotted values of $t_e\sqrt{g/d}$ shown.

The values of the slowly-varying pressure which correspond to locations and times shown in Figures 6.35 through 6.40 will now be presented and discussed. In Figures 6.35 through 6.40, where time is the ordinate and distance is the abscissa, the relative pressure head $P_1/\gamma d$ may be considered to be plotted with respect to an axis normal to the plane of the paper. Figures 6.41 through 6.47, showing relative pressure head as a function of time, and Figures 6.48 through 6.50, showing relative pressure head as a function of distance, may be considered sectional views of the function plotted in Figures 6.35 through 6.40. For instance, Section A-A indicated in Figure 6.35 is shown as Figure 6.41a, and Section C-C in Figure 6.35 is shown as Figure 6.48a.

The data presented in Figures 6.41 through 6.47 are obtained directly from the pressure records such as shown in Figures 6.20 and as tabulated in Table B1 of Appendix B. Because it was difficult to control precisely the values of H/d at which waves were generated, the relative wave height H/d associated with each pressure record is only approximately equal to the value of H/d association with the entire figure. For instance, in Figure 6.41, associated with $H/d = 0.24$, the relative wave heights H/d for the records plotted range from 0.240 to 0.252. However, the values obtained are

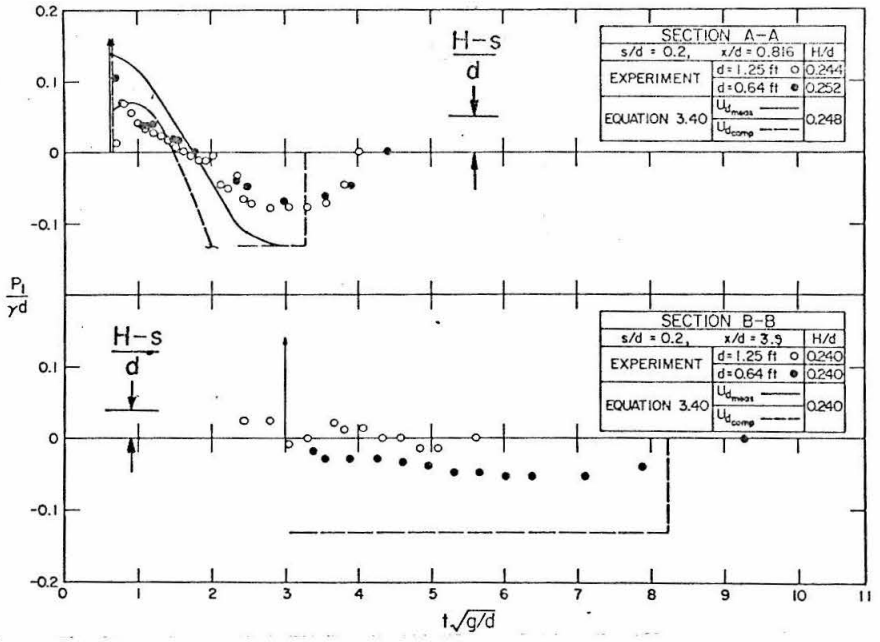

Figure 6.41. Pressure as a function of time for s/d = 0.2, H/d = 0.24.

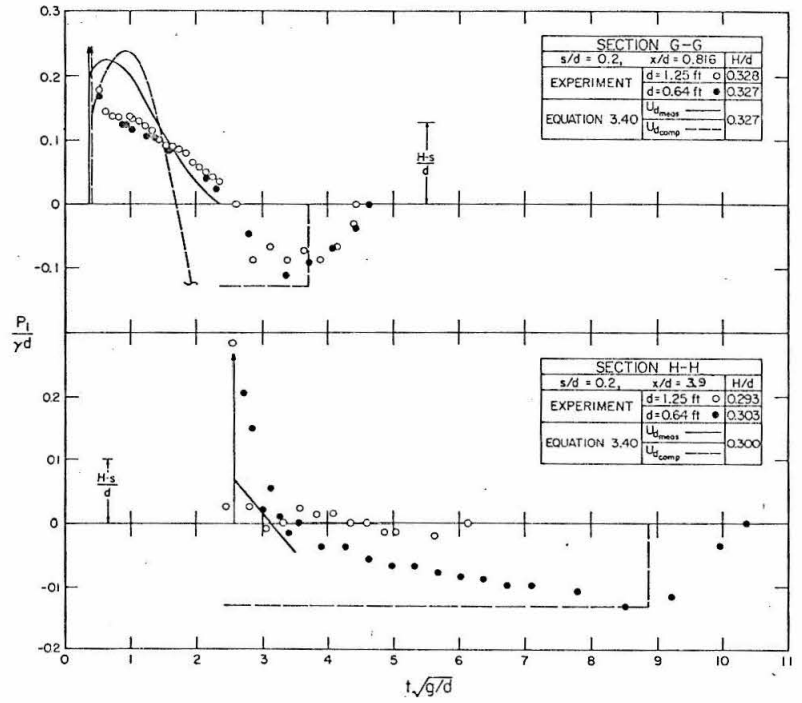

Figure 6.42. Pressure as a function of time for s/d = 0.2, H/d = 0.32.

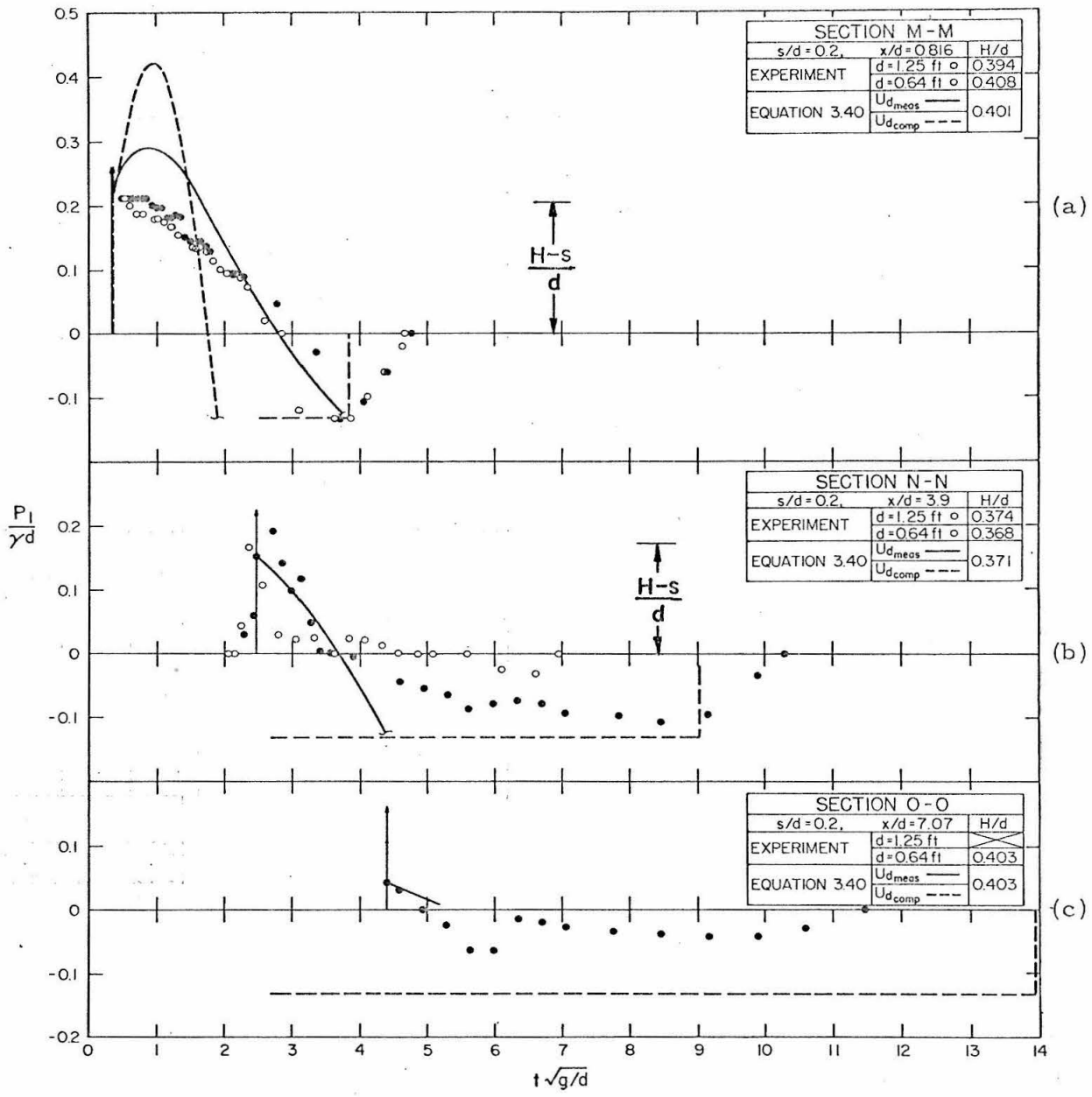

Figure 6.43. Pressure as a function of time for s/d = 0.2, H/d = 0.40.

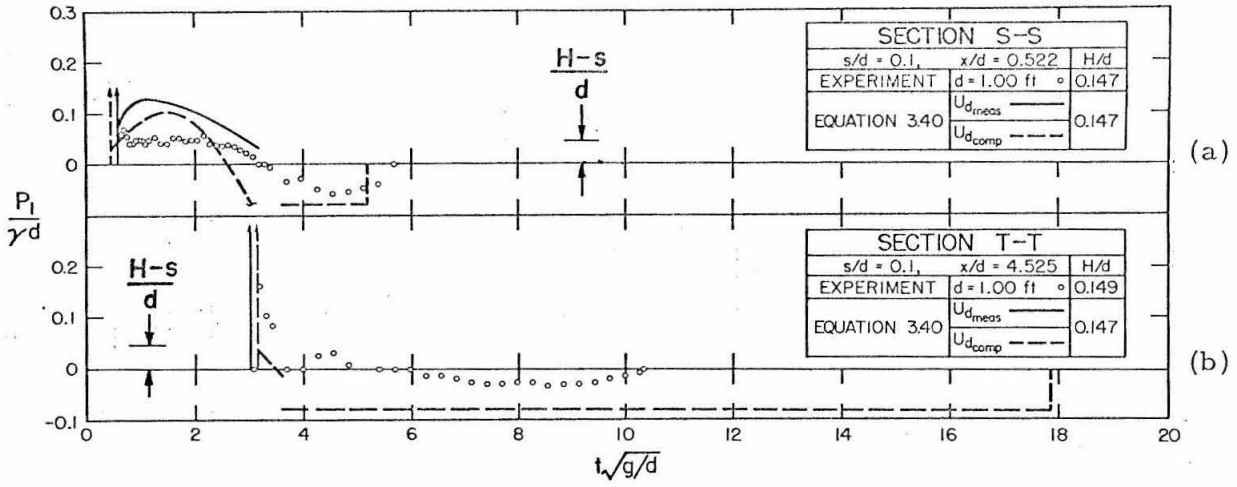

Figure 6.44. Pressure as a function of time for s/d = 0.1, H/d = 0.15.

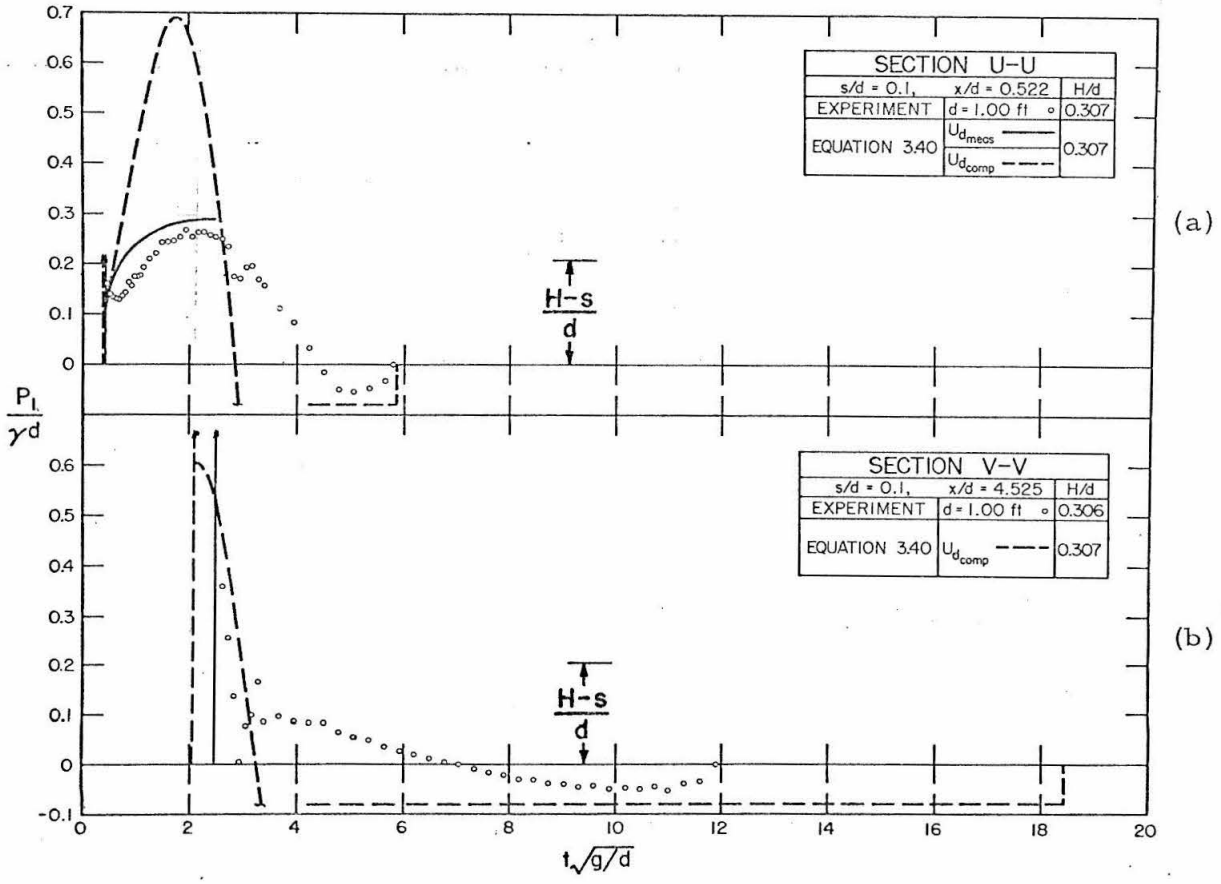

Figure 6.45. Pressure as a function of time for s/d = 0.1, H/d = 0.31.

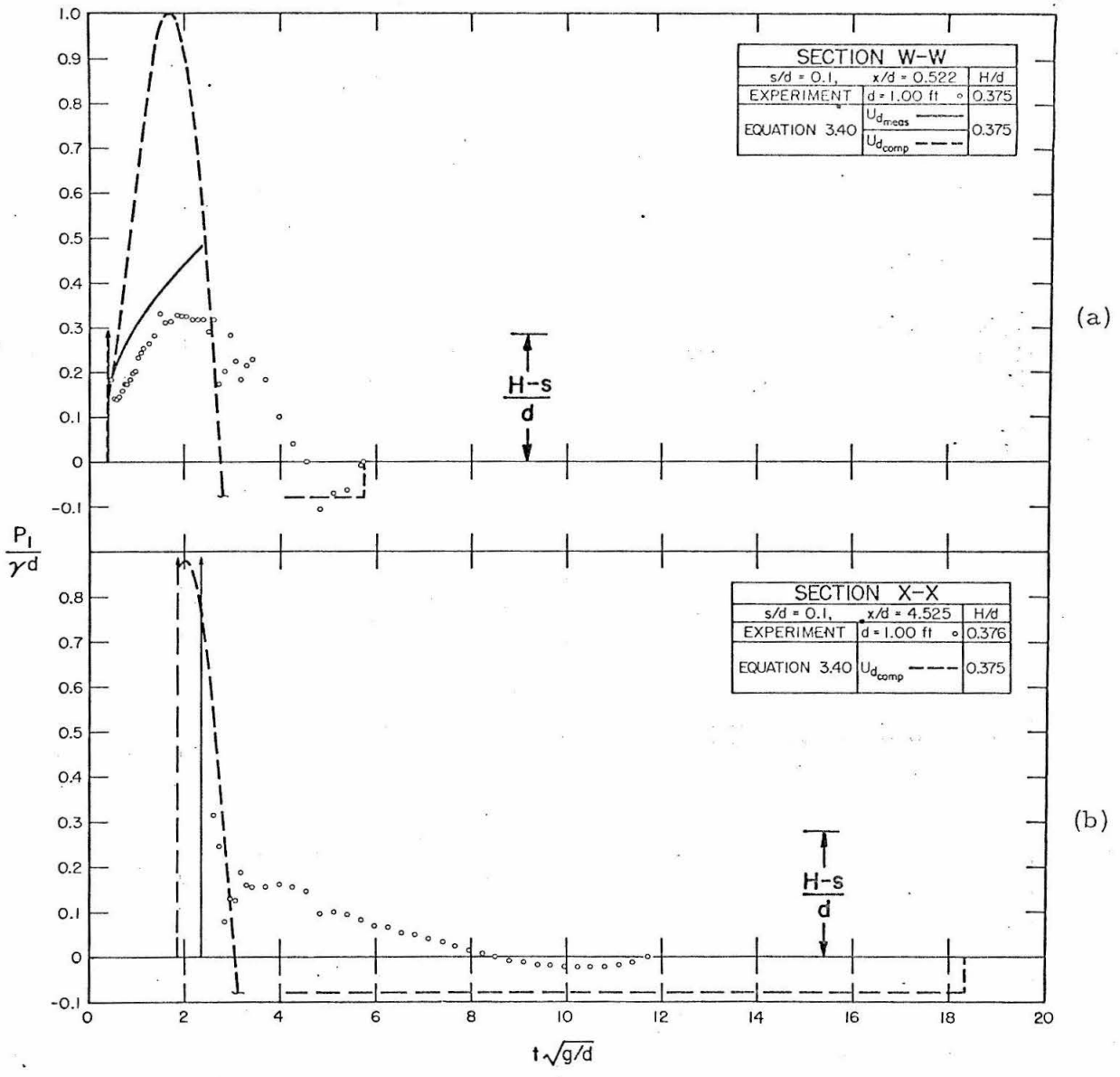

Figure 6.46. Pressure as a function of time for s/d = 0.1, H/d = 0.38.

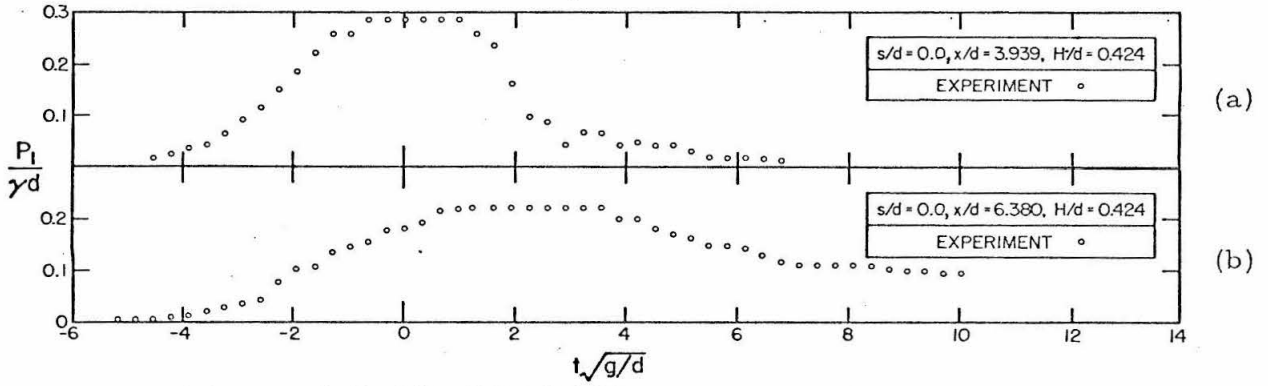

Figure 6.47. Pressure as a function of time for s/d = 0.0, H/d = 0.42.

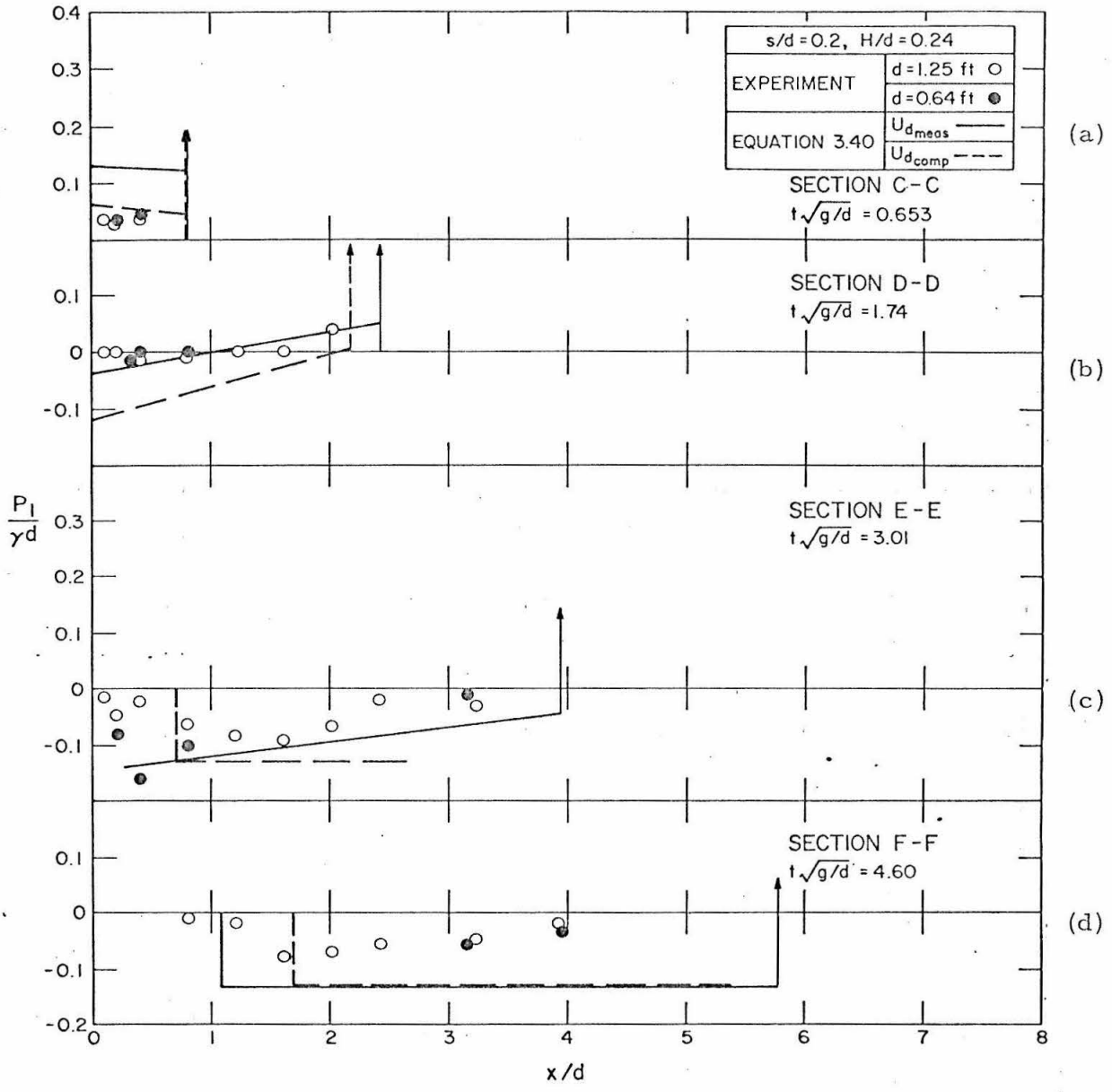

Figures 6.48. Pressure as a function of distance for s/d = 0.2, H/d = 0.24.

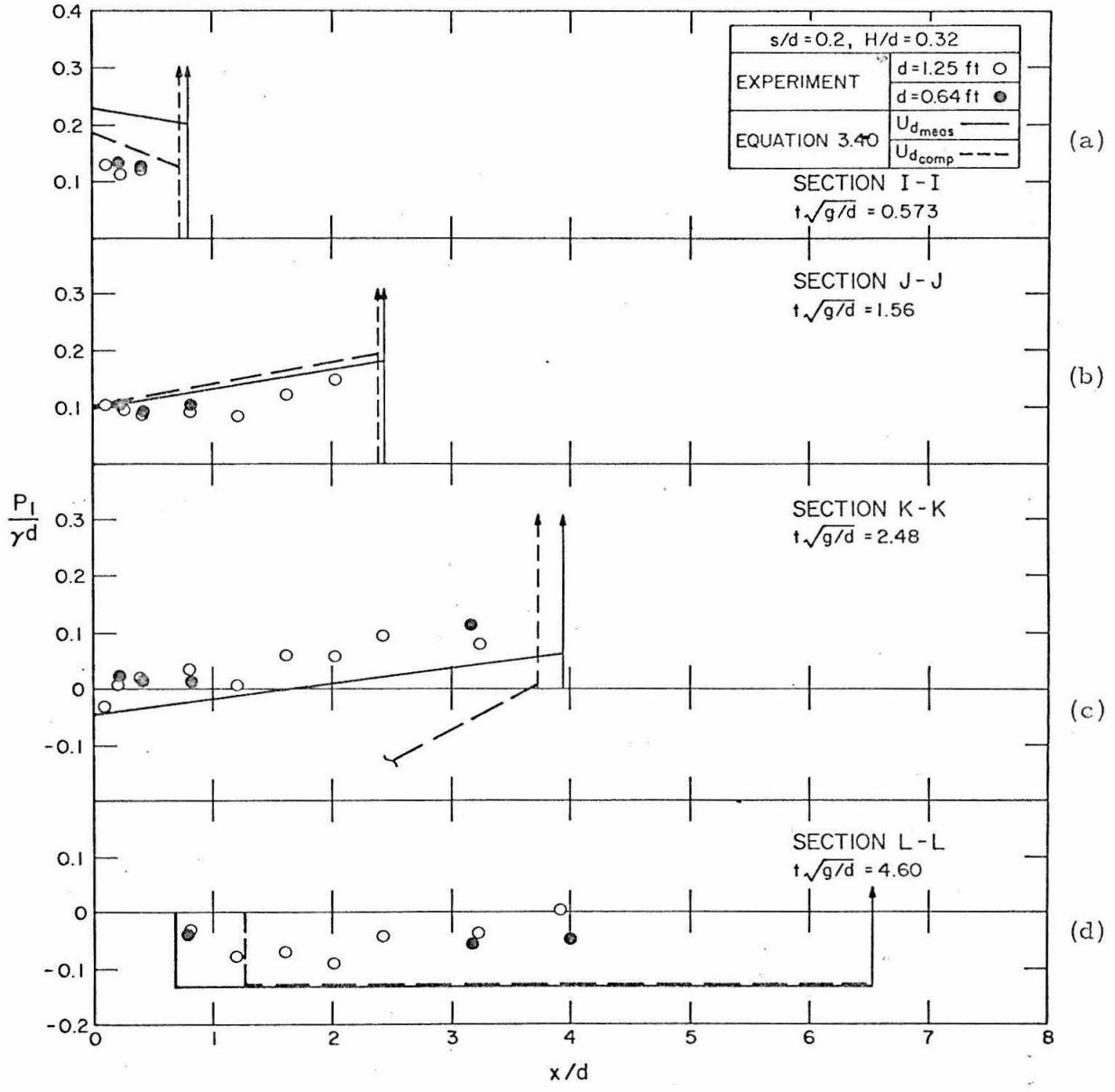

Figure 6.49. Pressure as a function of distance for s/d = 0.2, H/d = 0.32.

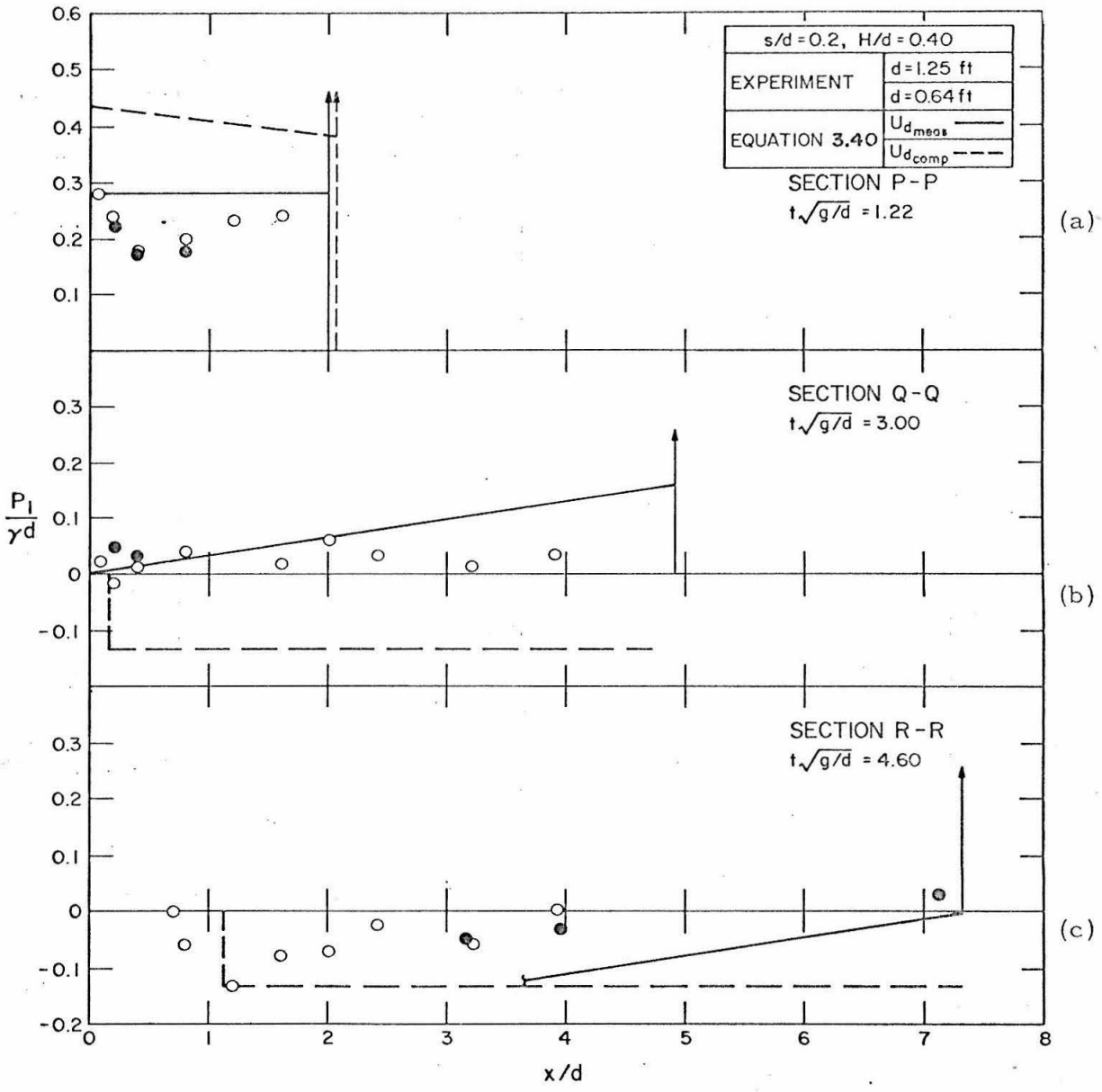

Figure 6.50. Pressure as a function of distance for s/d = 0.2, H/d = 0.40.

sufficiently close to the value $H/d = 0.24$ to illustrate the functional behavior of the slowly-varying pressure.

In Figures 6.41 through 6.47, solid curves indicate the normalized pressures $P_1 / \gamma d$ which are predicted by Equation 3.40 using measured values of the wave front celerity U_d (obtained from the solid curves fitted to the data in Figures 6.27 and 6.28), and using the associated measured values of x_d and dU_d/dt. Pressures derived from measured U_d (labeled, "$U_{d_{meas}}$" in the figures) are applied in the range of validity $0 < t < t_b$, as defined in Section 3.3. Long-dashed curves indicate normalized pressures predicated by Equation 3.40, but using values of x_d, dU_d/dt and U_d (labeled, "$U_{d_{comp}}$") computed from Equations 3.34 and 3.35. Pressures derived from computed U_d are presented for the range of validity $0 < t < t_a$, as defined in Section 3.3. Long-dashed curves also indicate the constant negative pressure in the specialized form of Equation 3.40 predicted by Equation 3.51 within the range of $t_a < t < t_c$, as defined in Section 3.3. The solid and dashed vertical arrows indicate the measured and predicted occurence, respectively, of peak pressure. (Peak pressure values, not shown in these figures, are presented in Section 6.6.)

Figures 6.41, 6.42, and 6.43, for relative soffit clearance $s/d = 0.2$, represent relative wave heights H/d of approximately 0.24, 0.32, and 0.40, respectively. In each figure, records are shown as obtained at relative locations $x/d = 0.816$ at both model scales, and at $x/d = 3.920$ at $d = 1.25$ ft and at $x/d = 3.938$ at $d = 0.64$ ft.

In addition, Figure 6.43 for $H/d = 0.40$ shows a record obtained at $x/d = 7.07$ at $d = 0.64$ ft. For $s/d = 0.1$, Figures 6.44, 6.45, and 6.46 represent relative wave heights H/d of 0.15, 0.31, and 0.38, respectively. The locations represented are the two locations at which data were obtained, $x/d = 0.522$ and $x/d = 4.525$. Similarly, Figure 6.47 for $s/d = 0.0$ shows data obtained from $x/d = 3.940$ and 6.380, the two locations at which pressures were measured, for a relative wave height of $H/d = 0.425$.

In each figure the time axes have been aligned so that at any given relative time, $t\sqrt{g/d}$, one may easily compare the pressures exerted at different transducer locations.

For $s/d = 0.2$ and $x/d = 0.816$, Figures 6.41a, 6.42a, and 6.43a show a period of time during which there are positive pressures following the arrival of the wave front. The pressure heads $P_1/\gamma d$ are at most approximately equal to $(H-s)/d$; this result suggests a simple hydrostatic relationship between incident wave height H and slowly-varying pressure head P_1/γ measured from a station located a distance s above the still water level.

These figures show that for relative transducer location $x/d = 0.816$, there is reasonably good agreement between the two scales for measured pressure over the full range of time from $t = t_d$ when the wave front arrives at the location, to $t = t_e$, when the principal wave of recession reaches the location. (It should be noted that the H/d for a record at one scale is never precisely equal to that at the other scale, and that the record with the greater relative pressures is

associated with the greater relative wave height. Therefore, the differences in measured pressure between the two scales during the period of positive uplift may be attributed in part to these small differences in incident wave height. A more definitive comparison of pressure values obtained at the two model scales will be presented later.)

Figures 6.41b, 6.42b, and 6.43b, for $s/d = 0.2$ and $x/d = 3.920$ at the depth $d = 1.25$ ft and for $x/d = 3.938$ at the smaller depth, $d = 0.64$ ft, show pressure functions where the duration of positive uplift pressures is very short, and the periods of negative pressure are correspondingly much longer than for $x/d = 0.816$. As mentioned previously, the ratio of durations of positive to negative pressure decreases with increasing x/d. In contrast with conditions at $x/d = 0.816$, there is poor agreement between scales at $x/d = 3.9$, except for values of relative time of wave front arrival $t_d\sqrt{g/d}$. The differences may be attributed to the difference in relative platform length, L/d. At $d = 0.25$ ft, the wave front reaches the shoreward end of the platform at $L/d = 4$ shortly after reaching the transducer located at $x/d = 3.920$. Pressures recorded by the transducer after the time t_b when the wave front reaches $L/d = 4$ reflect flow conditions influenced by the end of the platform: negative pressure values are not great, and the transducer location is shortly relieved of fluid from the wave by the secondary wave of recession. At $d = 0.64$ ft, the relative platform length $L/d = 7.81$ is sufficiently greater than the transducer location, $x/d = 3.938$, that fluid remains in contact with transducers until the

arrival of the principal wave of recession. Figures 6.35 through 6.37 show that the relative duration of negative pressures is considerably greater at $d = 0.64$ ft than at $d = 1.25$ ft. Figures 6.41b, 6.42b, and 6.43b show for these two scales that the negative pressures at $d = 0.64$ ft are somewhat greater than those measured than at $d = 1.25$ ft.

Figure 6.43c shows pressure as recorded at $x/d = 6.06$ for a depth of $d = 0.64$ ft and $s/d = 0.2$. (There is no record for $d = 1.25$ ft since for that scale the relative platform length is less than 7.07.) As it is, the location $x/d = 7.07$ is quite near the shoreward end of the platform (at $L/d = 7.82$) and the recorded pressures are therefore influenced by flow conditions at the end of the platform, as was the case for $x/d = 3.920$ at $d = 1.25$ ft. The most noticeable effects of this proximity to the trailing edge of the platform are that the values of negative pressure are less than those attained at smaller values of x/d, and the time of arrival of a wave of recession is less than $x/d = 3.928$.

For $s/d = 0.1$, Figures 6.44a, 6.45a, and 6.46a show slowly-varying pressures $P_1/\gamma d$ at $x/d = 0.522$ whose maximum values are equal to or slightly in excess of $(H-s)/d$. Figures 6.44b, 6.45b, and 6.46b show that at $x/d = 4.525$ values of positive pressure are less than at $x/d = .522$, and that the ratio of the durations of the positive to the negative pressure is less than at $x/d = 0.522$.

Figures 6.47 show pressure records obtained at zero soffit clearance at locations $x/d = 3.939$ and 6.380. As shown in Figure

6.32, the records at zero soffit clearance show only a slowly-varying increase and decrease in pressure, with no sudden increase or pressure peak and with no negative pressures. The records show that the maximum pressure attained for a given incident wave height decreases with increasing x/d, and that the time at which maximum pressure is recorded increases with x/d. The relative pressure head $P_1/\gamma d$ is everywhere less than the relative wave height H/d. However, one should note that pressures were sampled only at $x/d = 3.939$ and 6.380, and pressure amplitudes elsewhere, especially for lesser values of x/d, may be greater than those measured.

An interesting feature of the pressure records are irregular oscillations which appear to occur at the times t_a, when the principal wave of recession begins to form at the seaward end of the platform, and t_b, when the wave front reaches the shoreward end of the platform. The oscillations labelled, "secondary oscillations", are indicated on the sample record shown in Figure 6.20a. Because the oscillations were not the prime concern of this study, their form, amplitude, frequency, and cause were not studied in detail. In reducing the slowly-varying pressure data from records, the sampling frequency was usually less than the oscillation frequency, and therefore the oscillations do not always appear clearly in Figures 6.41 through 6.47. Yet Figure 6.43a shows oscillations occurring at $t\sqrt{g/d}$ for $H/d = 0.40$ and $s/d = 0.2$ (Figure 6.37; Figures 6.45a and 6.45b show oscillations at $t\sqrt{g/d} \simeq 2.9$, the approximate value of $t_a\sqrt{g/d}$ for $H/d = 0.31$ and $s/d = 0.1$ (Figure 6.39). Examination of certain

individual pressure records, not shown, shows that oscillations begin at both t_a and t_b, and that they appear at all transducer locations with little apparent dependence on location. The period of oscillation appears to be independent of wave height, but the amplitude is strongly dependent on relative wave height H/d.

Figures 6.41 through 6.43 for s/d = 0.2 show that positive uplift pressures computed by Equation 3.40 from measured values of U_d (solid curves) are generally greater than the measured pressures. However, the times of zero pressure indicated by these curves are in reasonably good agreement with measured values. For the duration of negative pressure, the values which are predicted by Equation 3.40 (in the specialized form expressed by Equation 3.51) are again greater in absolute value than measured values. In Figures 6.44 through 6.46, for x/d = 0.1, the measured celerity data are limited, which limits the time duration for which the pressure may be computed by Equation 3.40 using measured U_d. To the extent that data are available, however, the values predicted are again somewhat greater than measured pressure values.

Figures 6.41 through 6.46 show that the positive pressures, when computed from Equation 3.40 using analytical values of U_d, are much higher than measured values; the predicted time at which the pressure goes to zero is considerably less than the value indicated by experimental data; and negative pressures are much greater than measured. (In fact the maximum negative pressures predicted are not indicated on these figures due to their magnitude.)

Figures 6.41 through 6.46 show that the predicted negative pressure, derived from consideration of the wave of recession, is generally greater than is measured; yet Figures 6.41a, 6.42a and b, 6.43a and b, 6.44a, 6.45a, and 6.46a show measured pressures which at some time approach the predicted value. Where the transducer is mounted near the shoreward end of the platform (see Figures 6.41b, 6.42b, and 6.43b for $d = 1.25$ ft and Figure 6.43c for $d = 0.64$ ft) the measured negative pressures are much less than the predicted value.

For $s/d = 0.0$, Figure 6.47 shows no analytical values of pressure, simply because the analysis as derived cannot be applied to the case of zero soffit clearance, as stated in Section 3.2.

Relative pressure head $P_1/\gamma d$ is shown plotted as a function of relative location x/d for a soffit clearance of $s/d = 0.2$ in Figures 6.48, 6.49, and 6.50, for relative wave heights H/d of 0.24, 0.32, and 0.40, respectively. Figures such as these have not been developed for $s/d = 0.1$ or $s/d = 0.0$, since in these cases data were obtained at only two relative locations x/d, which is inadequate to show the functional dependence satisfactorily.) In each of Figures 6.48 through 6.50, the pressure distributions are shown for a number of relative times, $t\sqrt{g/d}$, representing periods of positive and negative uplift (see the corresponding time-distance diagrams in Figures 6.35 through 6.37).

In Figures 6.48 through 6.50, data have been taken from records obtained at several transducer locations. Values of H/d at

which waves were generated varied slightly from one transducer location to another. Therefore, in contrast to Figures 6.41 through 6.47 where data are plotted directly without interpolation, in Figures 6.48 through 6.50 it has been necessary to perform a simple interpolation in order to determine pressures at a common value of H/d at all locations for a particular time. At each relative transducer location, x/d, and at each value of normalized time represented, $t\sqrt{g/d}$, the measured pressure head P_1/γ is plotted against relative wave height H/d, and a curve is fitted to the data. Values from the curves at $H/d = 0.24$, 0.32, and 0.40 are then plotted in Figures 6.48 through 6.50 as a function of distance for the time of interest.

As in Figures 6.41 through 6.46, the pressure heads predicted by Equation 3.40 using measured values of U_d, x_d, and dU_d/dt are indicated by solid curves; positive pressure heads predicted by Equation 3.40 using analytical values of U_d, and negative pressure heads predicted by Equation 3.40, in the specialized form of Equation 3.51, are indicated by dashed curves. Again, solid and dashed vertical arrows indicate the measured and predicted location, respectively, of the wave front and of peak pressure.

For Figures 6.48a, 6.49a, and 6.50a, the relative times $t\sqrt{g/d}$ were chosen to show maximum values of slowly-varying pressure. In these figures, as well as in Figures 6.48b and 6.49b, values of relative pressure head $P_1/\gamma d$ approach or slightly exceed the value $(H-s)/d$, which was observed in pressure-time curves discussed earlier (see Figures 6.41 through 6.46). In no figure does relative

pressure head greatly exceed (H-s)/d.

There is fair to good agreement between data obtained at the two model scales (d = 1.25 ft and d = 0.64 ft) throughout Figures 6.48, 6.49, and 6.50, except in Figure 6.48c, for H/d = 0.24 and $t\sqrt{g/d} = 3.01$. Figure 6.35 shows that for this condition and relative time the wave front has traveled the relative distance x/d = 4, which is at the end of the platform for the scale defined by the depth d = 1.25 ft but not for the scale defined by d = 0.64 ft. As described earlier, oscillations in the pressure record have been noted to occur at time t_a when the principal wave of recession forms, and at time t_b, when the wave front reaches the shoreward end of the platform. In Figure 6.48c, it may be that at $t\sqrt{g/d} \simeq 3$ oscillations are occurring at d = 1.25 ft, for which $t_b\sqrt{g/d} = 3.01$, but are not occurring at d = 0.64 ft, for which $t_b\sqrt{g/d}$ has a value considerably different from 3.01; therefore a difference in measured relative pressure head between scales at $t\sqrt{g/d} = 3.01$ may be expected.

One may note that the dependence of pressure on relative distance, x/d, predicted by Equation 3.40 using measured values of U_d is in fair agreement with that shown by measured pressures; however, using analytical values of U_d in this expression, the dependence of pressures on x/d is much greater than actually observed. In Figures 6.48d, 6.49d, and 6.50c, measured pressures tend towards zero and towards positive values with increasing x/d, in contrast to the predicted constant negative value $P_1/\gamma d = 0.131$. (The discussion of the analysis will be continued in Section 6.5.4.)

For the benefit of the analysis of peak pressure to be undertaken in Section 6.6, it is important to determine the extent of agreement between relative slowly-varying pressure heads $P_1 / \gamma d$ measured at the two model scales defined by the depths $d = 1.25$ ft and $d = 0.64$ ft for similar values of s/d, x/d, and H/d. For comparison of slowly-varying pressure to be relevant to the peak pressure analysis, measurement should be made in a region near the wave front. Therefore, on from 12 to 32 records obtained for each wave height tested at both scales at $x/d = 0.816$, the slowly-varying pressure was obtained at a normalized time $t\sqrt{g/d} = t_d\sqrt{g/d} + 0.15$; i.e. the pressures measured were those recorded 0.15 dimensionless time units after the wave front (and peak pressure) had arrived at the relative transducer location 0.816. As may be determined from Figure 6.27 in Section 6.4, the normalized celerity $U_d / \sqrt{gd}$ of the wave front is of the order of 1.5 for all relative wave heights H/d for $s/d = 0.2$. Hence after an interval of 0.15 dimensionless time following the arrival of the wave front at the transducer, the wave front should be located at $x/d = 0.816 + 0.15(1.5)$, or 0.23 dimensionless units of distance shoreward of the transducer mounted at $x/d = 0.816$. Measurements obtained at 0.23 dimensionless distance units seaward of the wave front may be considered close enough to the wave front for relevant examination for dynamic similarity in slowly-varying pressure between scales, yet far enough from the wave front to avoid problems of measurement of the rapidly-varying peak pressure.

The average values of the relatively large samples of

slowly-varying pressure head P_1/γ obtained at each scale in the manner just described are presented in Figure 6.51, normalized with respect to the still water depth d and plotted against relative wave height H/d. The plotted values lie fairly close to a single curve, especially for the range $0.24 < H/d < 0.32$, indicating a fair degree of similitude in slowly-varying pressure in the positive uplift region neighboring the region of the wave front. It is assumed that similar agreement would be realized at other transducer locations x/d.

6.5.3 Uplift force, average uplift pressure, and center of uplift pressure.

For the larger model scale defined by d = 1.25 ft at the relative soffit clearance s/d = 0.2, the total uplift force per unit width, F, the average uplift pressure P_{av}, and the center of uplift pressure x_{cp} are computed from data similar to that presented in Subsection 6.5.2. The quantities F, P_{av}, and x_{cp} are also computed from considerations of wave front celerity U_d through Equations 3.53, 3.54, and 3.55, respectively, using both measured and computed values of wave front location x_d, wave front celerity U_d and wave front acceleration dU_d/dt. From considerations of the wave of recession, F, P_{av}, and x_{cp} are computed from Equations 3.56, 3.51, and 3.57, respectively. The maximum uplift force per unit width F_{max} and the center of maximum pressure x_{cmp} are compared with values obtained by El Ghamry (1963) for oscillatory waves.

The quantities F, P_{av}, and x_{cp} have been determined as functions of time for $0 < t\sqrt{g/d} < t_c\sqrt{g/d}$, where t_c is the time when

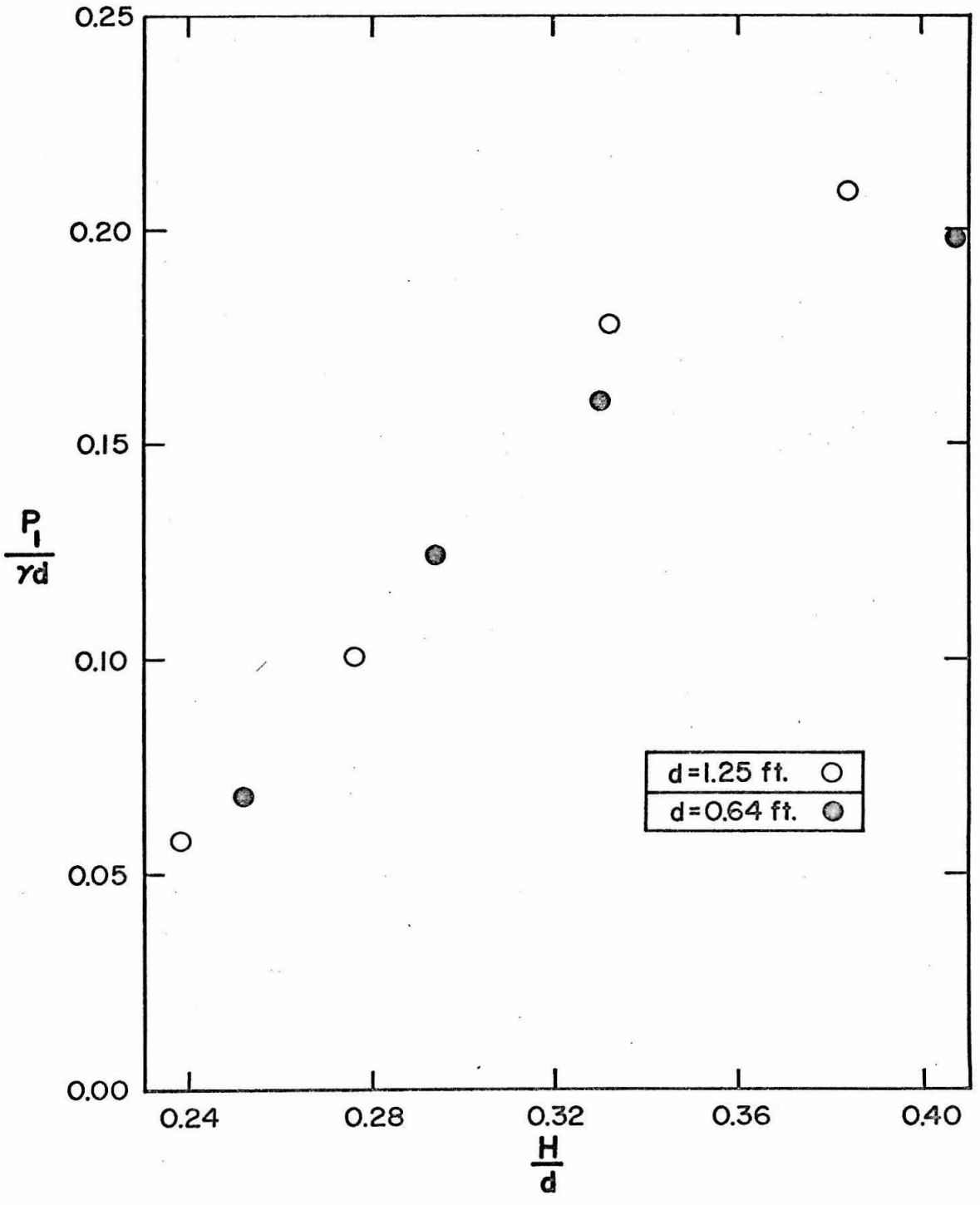

Figure 6.51. Comparison of normalized pressures obtained at two model scales. ($s/d = 0.2$, $x/d = 0.816$)

the wave is no longer in contact with the platform (Figures 3.5). Since the procedure involves a step-wise integration of the pressure data, as will be explained presently, the greatest accuracy is obtained where the number of transducer locations per unit length of platform is the greatest. Therefore, the case for $s/d = 0.2$, $d = 1.25$ft, with data available at 10 locations for a relative platform length of $L/d = 4$ (see Table 6.2), was the case chosen for study.

From data presented in Table B1 of Appendix B, values of time t are chosen at frequent intervals. For each chosen value of t, the pressure head P_1/γ at each transducer location is plotted as a function of relative wave height H/d, and a curve is fitted to these data. The pressure heads at relative wave heights: $H/d = 0.24$, 0.28, 0.32, 0.36, and 0.40, are then determined by interpolation from these curves. This procedure having been repeated for each of the ten transducer locations used at the model scale $d = 1.25$ ft, the location of the wave front x_d and of the wave of recession x_e are determined for each chosen value of t. (For $t < t_a$, when the wave of recession starts to form, $x_e = 0$; for $t > t_b$, when the wave front reaches the shoreward end of the platform, x_d equals the platform length L, or a smaller value estimated as the location of the secondary wave of recession.)

As a step-wise approximation of the pressure distribution the pressure $(P_1/\gamma)_i$ that is measured by transducer (i) located at x_i, where x_i is in the wetted region $x_e < x_i < x_d$, is assumed to be exerted uniformly at all points x in the wetted region $x_e < x < x_d$

that are nearer to transducer (i) than to any other transducer. One may therefore define a length of influence $(\Delta x)_i$ associated with each transducer (i) as the length of that part of the platform in the wetted region $x_e < x < x_d$ for which all point x are nearer to transducer (i) than to any other transducer.

With this approximation, the total force per unit width may be defined as the sum of the products of pressure head and length of influence:

$$\frac{F}{\gamma} = \sum \left(\frac{P_1}{\gamma}\right)_i (\Delta x)_i \, . \tag{6.10}$$

The average pressure is the force per unit width F divided by the wetted length of the platform $(x_d - x_e)$. The center of pressure x_{cp} is the first moment of the uplift force:

$$x_{cp} = \frac{\sum \left(\frac{P_1}{\gamma}\right)_i (\Delta x)_i \, y_i}{\frac{F}{\gamma}} \, , \tag{6.11}$$

where y_i is the distance from the seaward end of the platform to the center of the region of influence associated with transducer (i).

It should be mentioned that the characteristics of the secondary wave of recession for the depth $d = 1.25$ ft were not measured, so that the position and slope of the characteristic which describes it in Figures 6.35 through 6.37 are not precisely known (except for a value of t_e obtained for $x/d = 3.920$ at $d = 1.25$ ft). Therefore, values of force, average pressure, and center of pressure during the period of time when the secondary wave exists can only be estimated. In

figures presented in this subsection, no values are available for times greater than the value of $t_e\sqrt{g/d}$ for $x/d = 3.220$ (the greatest value of $t_e\sqrt{g/d}$ measured at $d = 1.25$ ft), although the actual value of $t_c\sqrt{g/d}$, when the platform is freed entirely of fluid, may be greater, as shown in Figures 6.35 through 6.37.

The uplift force F per unit width is presented in Figures 6.52. Normalized with respect to γd^2, where γ is the unit weight of water and d is the still water depth, the force per unit width is plotted as a function of relative time $t\sqrt{g/d}$ for relative wave heights: H/d = 0.24, 0.32, and 0.40. The normalized force computed from Equation 3.53 using measured values of U_d, x_d and U_d/dt are indicated by solid curves in Figure 6.52, for $0 < t\sqrt{g/d} < t_b\sqrt{g/d}$; the normalized force computed using analytical values of U_d, x_d, and dU_d/dt is indicated in these figures by dashed curves for $0 < t < t_a$. For $t_a < t < t_c$, the force is computed from Equation 3.56 (in which L/d is set equal to 4.0).

At all values of H/d the normalized force has an initial value of zero at $t\sqrt{g/d} = 0$; increases with time to a maximum; then decreases with time, reaching negative values; then returns slowly to zero.

As shown in the pressure record presented in Figure 6.20a and as mentioned in Subsection 6.5.2, "secondary oscillations" appear in the force computed from these pressures, indicating that oscillating pressures are exerted uniformly over the wetted length of the platform. These oscillations appear to have frequencies ranging from 3.6 cycles

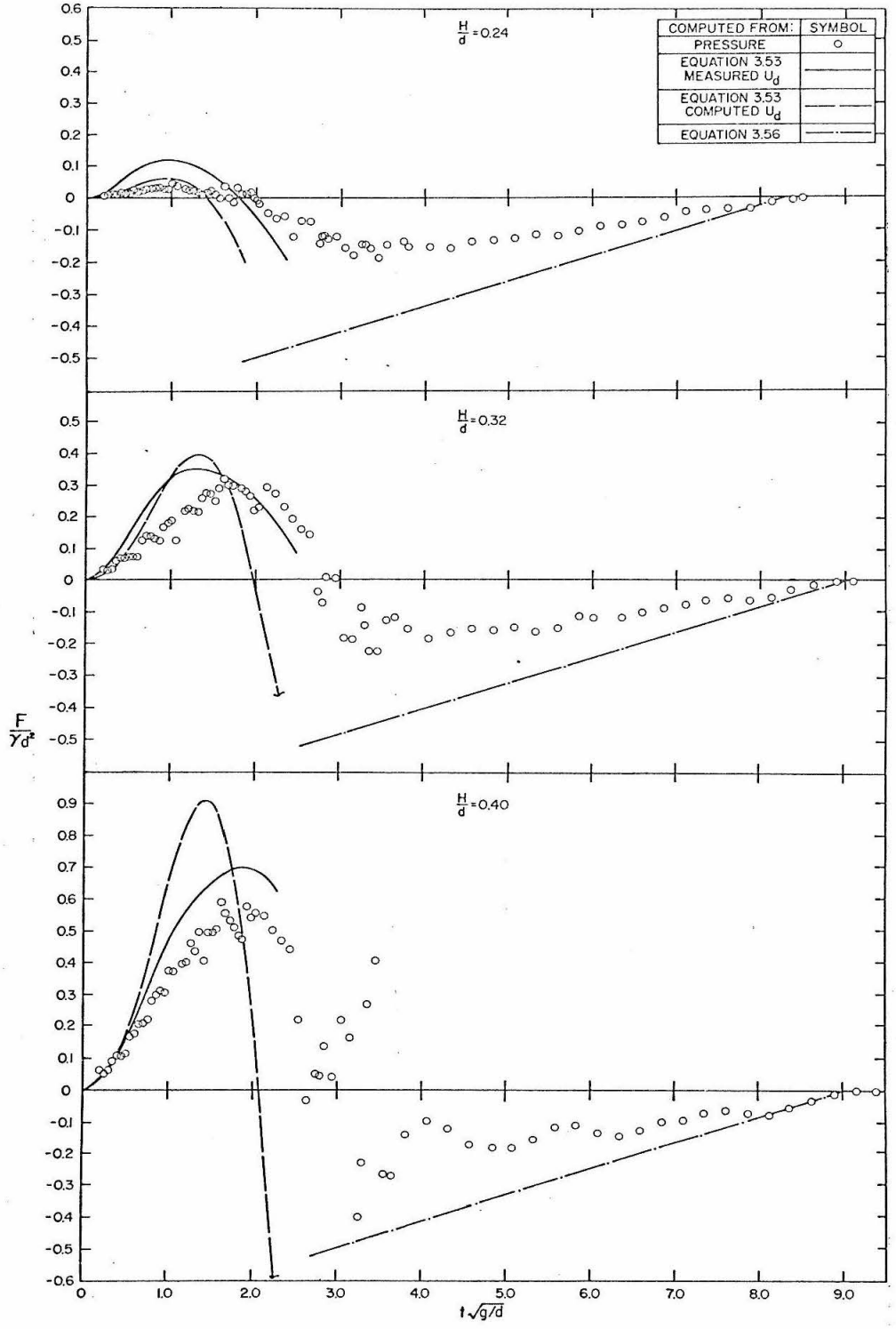

Figure 6.52. Normalized uplift force per unit width, for s/d = 0.2, L/d = 4.0.

per sec to 17 cycles per sec. The period of oscillation appears to be independent of wave height, but the amplitude of oscillation appears to be strongly dependent on wave height. As noted in the previous subsection, the oscillations occur at about the time the force becomes zero after having reached a maximum, and may be related to the time t_a when the wave of recession forms or the time t_b when the wave front reaches the shoreward end of the platform. As may be seen in Figures 6.52, the oscillations have an amplitude which may approach the value of maximum uplift force, and are therefore a phenomenon of some importance.

The values of force computed from pressure data indicate that maximum positive uplift force is strongly dependent on wave height, with the duration of the positive uplift force somewhat dependent on wave height. However, one may note that negative force as a function of time is nearly independent of wave height. The greatest negative value attained (apart from negative extrema of the oscillations) is approximately $F/\gamma d^2 = -0.15$, for all three values of relative wave height represented. The relative duration of negative force is about 6.3 dimensionless units of $t\sqrt{g/d}$, independent of H/d. Therefore, a wave of relatively small height may exert little upward force, but just as much negative or downward force as a considerably larger wave.

Values of positive force computed from measured values of the wave front celerity U_d appear to be generally greater than the force computed from measured pressure, especially at $H/d = 0.24$.

Agreement with values computed from the measured pressure improve with increasing H/d. In Figure 6.52a for H/d = 0.24, the time of zero force agrees well with the measured value. The time of maximum force agrees with the measured value for H/d = 0.24 and 0.40, but is less than the measured value for H/d = 0.32.

The maximum force computed from analytical values of U_d shows fair agreement with the value computed from pressure at H/d = 0.24; however, for H/d = 0.32 and 0.40, the predicted values are considerably higher than values from measured pressure. The computed time of zero force is consistently less than measured. The values of negative force derived from Equation 3.56 are generally about twice as great as values determined from measured pressure.

In Figure 6.53 the maximum value of normalized force per unit width $F_{max}/\gamma d^2$ is plotted as a function of (H-s)/d, where H is incident wave height, s is the soffit clearance, and d is the still water depth. Values derived from measured and computed values of wave front celerity U_d are compared with those derived from measured pressures. Values derived from measured wave front celerities U_d are generally slightly greater than the forces determined directly from the experimental pressures. The maximum normalized force derived from computed wave front celerities U_d shows good agreement with pressure-derived values for $(H-s)/d \leq 0.08$ (i.e., $H/d \leq 0.28$ for $s/d = .2$), but for larger wave-heights these predictions are considerably greater than pressure-derived values; this discrepancy can be noted also in Figures 6.52.

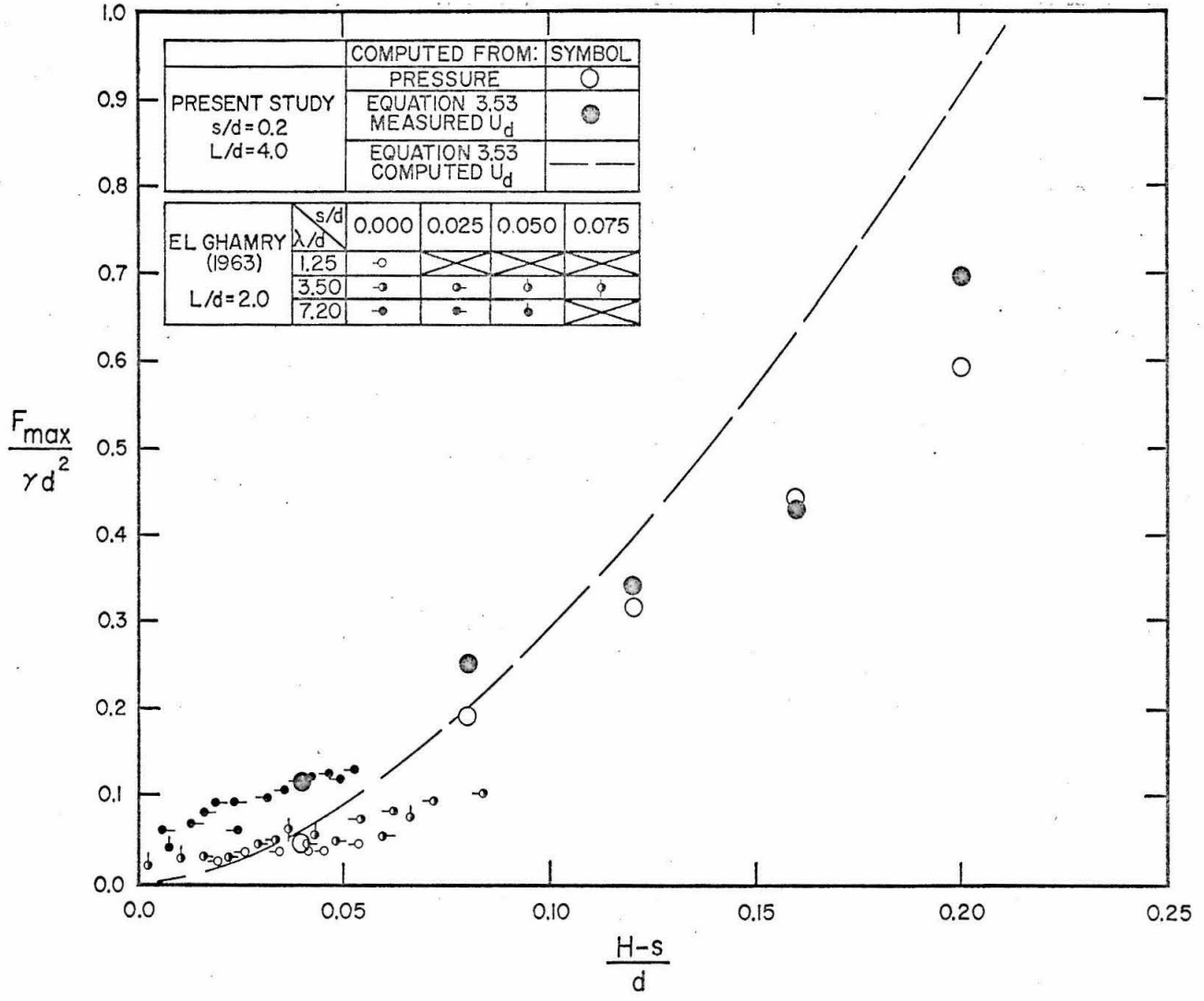

Figure 6.53. Maximum normalized uplift force per unit width, compared with values by El Ghamry (1963).

Maximum uplift forces measured by El Ghamry (1963) are included in Figure 6.53 for comparison. Before examining the data, however, one should note that experimental conditions used by El Ghamry differed from those used in the present study. As described in Section 2.3, El Ghamry studied the case in which periodic progressive waves in a wave tank 1 ft wide by 3 ft deep struck the underside of a 4 ft long horizontal platform. The platform, which had no vertical front face, extended nearly the width of the wave tank, but with a gap between the tank walls and the edge of the platform. Forces were measured directly by gauges mounted on the two platform supports. Tests were performed at values of relative incident wavelength λ/d ranging from 1 to 8 and relative soffit clearance s/d ranging from 0.0 to 0.1. Trough-to-crest wave heights were 0.262 times the still water depth, or smaller. The still water depth was 2.00 ft.

El Ghamry presents wave height data in terms of trough-to-crest wave height. However, in the present study the height H of a solitary wave is equal to its amplitude above still water level, and since the soffit clearance s in both El Ghamry's and the present study is defined with respect to the still water level, it is deemed most consistent to consider El Ghamry's data in terms of wave amplitude above still water level. If the waves are considered to be of small amplitude, the amplitude above still water level is one-half the trough-to-crest height. (According to the second-order progressive

wave theory of Miche, presented by Wiegel (1964), the error introduced by the assumption of small amplitude, for the experimental conditions considered, is less than 10%.) Therefore in Figure 6.53 the value of H for the El Ghamry data is taken as one-half the reported trough-to-crest height.

Plotted in Figure 6.53, the normalized El Ghamry data for maximum uplift force represent values of (H-s)/d ranging from zero to 0.084, and three values of relative incident wavelength λ/d ranging from 1.25 to 7.2. Values of $F_{max}/\gamma d^2$, which appear to increase with λ/d for constant (H-s)/d, generally do not exceed 0.15. At (H-s)/d = 0.04 the El Ghamry data are as much as twice as great as the values indicated from the present study; however these values are only 10% of the maximum force measured in this study at the largest values of (H-s)/d.

Figures 6.54 show relative average pressure $P'_{av}/\gamma d$ plotted as a function of relative time $t\sqrt{g/d}$ for H/d = 0.24, 0.32, and 0.40. Features such as periods of positive and negative uplift, with oscillations near the time of zero pressure, are qualitatively similar to those found in Figures 6.52 for $F/\gamma d^2$. As with the individual pressure records presented earlier, the maximum values indicated are equal to or slightly exceed (H-s)/d. The values predicted by Equation 3.54 using measured or analytical values of U_d are again greater than values determined from measured pressure. As with total force presented in Figures 6.52, the negative average pressure function appears to be independent of relative wave height H/d.

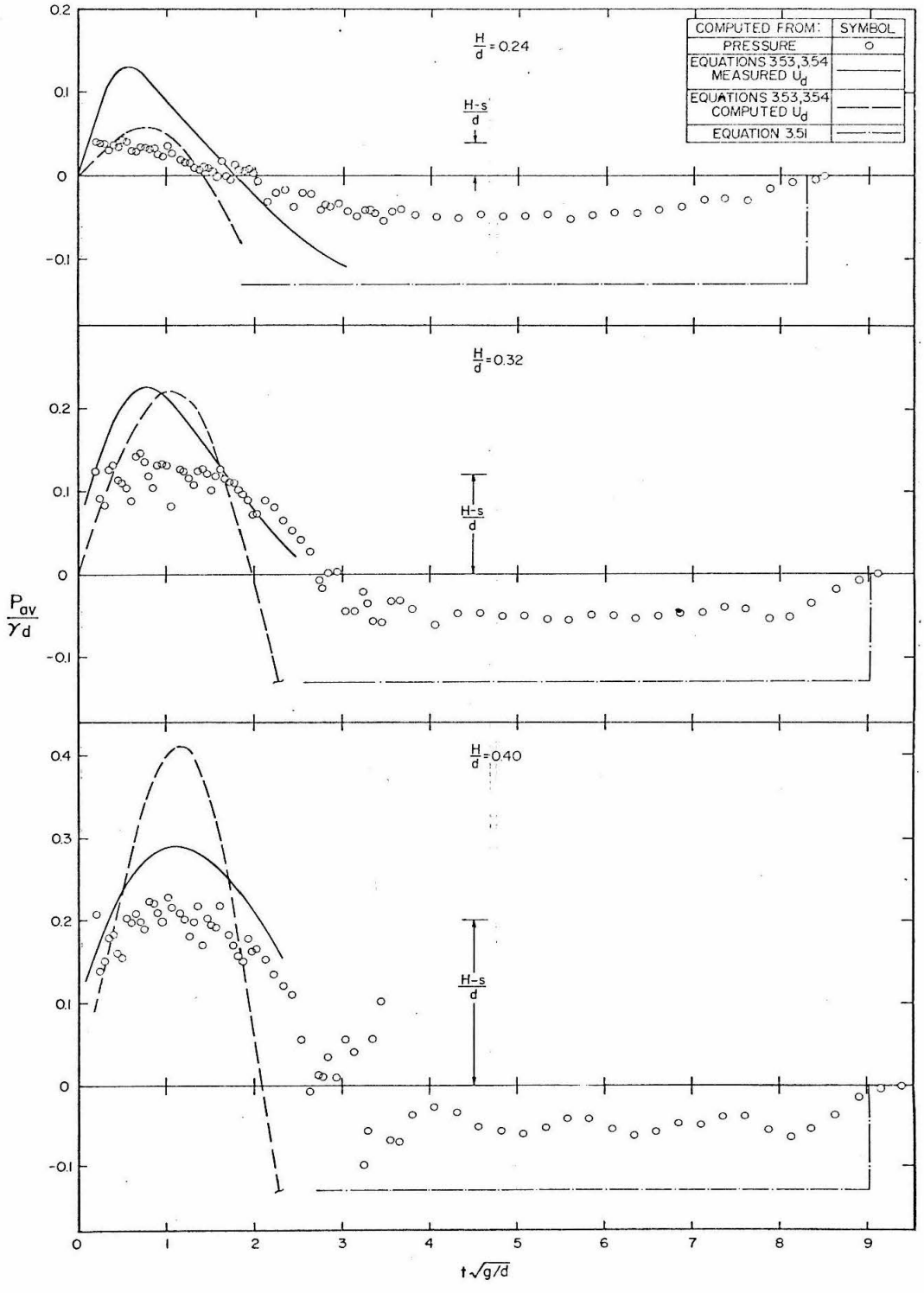

Figure 6.54. Normalized average uplift pressure, for s/d = 0.2, L/d = 4.0 (d = 1.25 ft).

Independence of negative pressure from H/d is predicted by Equation 3.51 from consideration of the wave of recession; yet the value of negative pressure is rarely more than half the value predicted by Equation 3.51.

The normalized center of uplift pressure x_{cp} is plotted in Figures 6.55 as a function of relative time $t\sqrt{g/d}$ for relative wave heights: H/d = 0.24, 0.32, and 0.40. The qualitative behavior of x_{cp}/d, as shown by data derived from measured pressure, is initially to increase with respect to $t\sqrt{g/d}$ at a rate which is approximately one-half the normalized wave front celerity $U_d/\sqrt{g\ d}$. (Comparison of Figures 6.55a, b, and c with Figures 6.35, 6.36, or 6.37, respectively, shows that for $t\sqrt{g/d} \leq 1$, approximately, the value of x_{cp}/d at a given value of $t\sqrt{g/d}$ is very nearly one-half the value of x_d/d, the wave front location, at that value of $t\sqrt{g/d}$.

Following this initial monotonic increase with time, it is difficult to define the center of pressure,due to the "secondary oscillations" of the force which are evident in Figures 6.52. Since x_{cp} is equal to a quantity divided by the total force per unit width F, it is to be expected that x_{cp} may diverge to infinity when F goes to zero. Since in the period of oscillations the force-time function derived from measured pressure crosses the zero axis repeatedly, large positive and negative values of x_{cp}/d may be expected in the period of oscillations.

Following the oscillations there is a period of monotonic increase of x_{cp} from zero or negative values to positive values; the

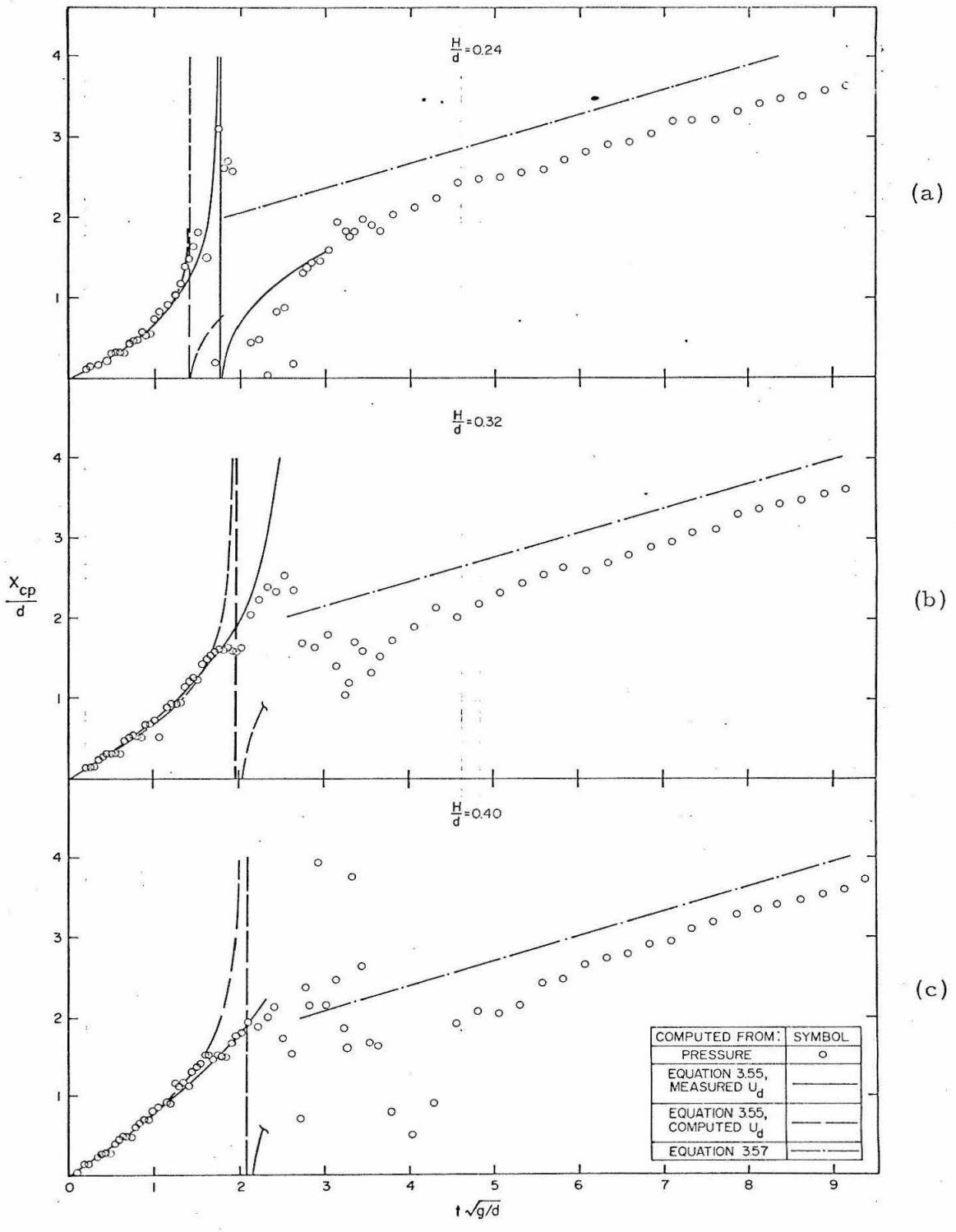

Figure 6.55. Normalized location of center of uplift pressure, for s/d = 0.2, L/d = 4.0 (d = 1.25 ft).

rate of increase of x_{cp}/d with $t\sqrt{g/d}$ appears to decrease with time, until at $t_c\sqrt{g/d}$, when the wave is no longer in contact with the platform, the final value of x_{cp}/d is the value of x/d where the principal and secondary waves of recession meet.

Values of x_{cp}/d predicted by Equation 3.55 using measured and analytical values of U_d, x_d and dU_d/dt are indicated for the ranges of validity $0 < t < t_a$ and $0 < t < t_b$, respectively. The two sets of predicted values show excellent agreement with values derived from measured pressure in the initial period of increase of x_{cp}/d with time. At the time of zero force (or zero average pressure), the curves diverge to $+\infty$, and with increasing time converge from $-\infty$ to finite positive values, equivalent to values derived from measured pressure in the period of monotonic increase of x_{cp} following the oscillations.

In Figure 6.55a for $H/d = 0.24$, the values of x_{cp}/d which were derived from the measured wave front celerity, U_d, appear to predict quite well the values determined from the measured pressure in the period following the time of zero force. For $H/d = 0.32$ and 0.40, values after the time of zero force are not available because the time t_b, beyond which the wave front is no longer defined (see Section 3.3), is less than the time of zero force. The time of zero force computed from analytical values of U_d is less than measured, and predicted values of x_{cp}/d following the time of zero force occur at smaller times than corresponding measured values.

Values of x_{cp}/d determined from Equation 3.57 from

consideration of the wave of recession, indicated in the range $t_a < t < t_c$, are generally greater than values derived from measured pressure. Neglect of the secondary wave of recession would tend to make computed values greater than measured values for the period during which the secondary wave of recession exists. It was indicated in Figures 6.30 in Section 6.4 that at a given location x_e, the computed time of arrival t_e is less than the measured value; correspondingly, at a given time t_c the computed location of x_e of the wave recession is greater than the measured location. This, too, causes computed values of x_{cp} to be greater than measured values. A third explanation for discrepancy between x_{cp} derived from measured pressure and that derived from Equation 3.57 is that in Equation 3.57, it is assumed that the pressure, as expressed in Equation 3.51, does not vary with respect to location x. However, Figures 6.48c, 6.48d, 6.49d, and 6.50c indicate that in fact negative pressure decreases with increasing x, so that the location of the center of pressure x_{cp} is smaller than it would be if pressure were uniformly distributed, as assumed in the derivation of Equation 3.57.

The normalized center of pressure x_{cmp}/d obtained at the time of maximum uplift force is presented in Figure 6.56, plotted against (H-s)/d. Values derived from measured pressure are compared with values derived from measured and analytical wavefront celerity, and with values obtained by El Ghamry for several relative wave lengths and soffit clearances.

Although Figures 6.55 showed excellent agreement between

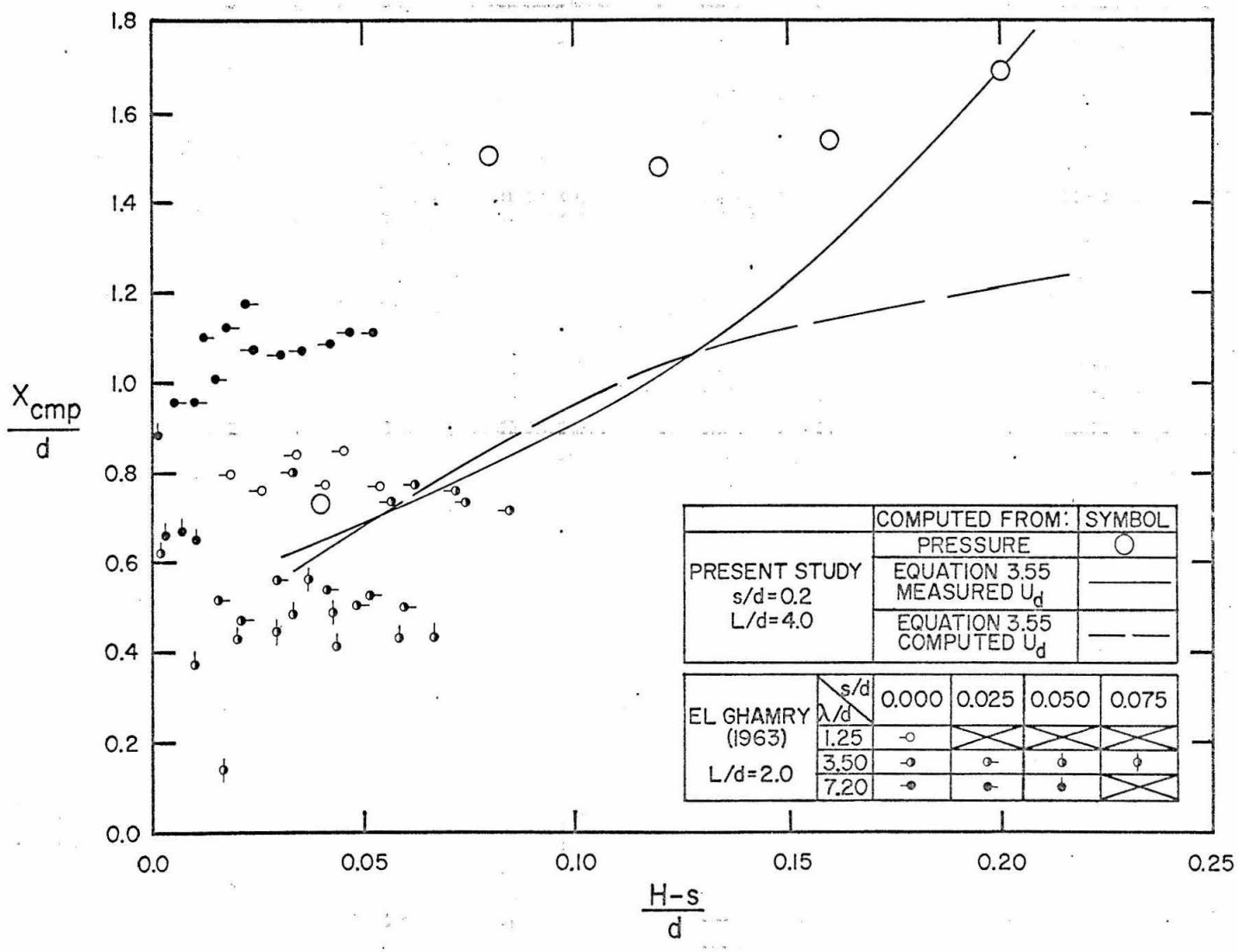

Figure 6.56. Normalized location of center of maximum uplift pressure, compared with values by El Ghamry (1963).

predicted and measured values of x_{cp}/d plotted against $t\sqrt{g/d}$, Figures 6.52 showed that the predicted time of maximum force did not always agree with the measured value. Hence there is poor agreement shown in Figure 6.56 between measured and predicted values of x_{cmp}/d at $(H-s)/d = 0.08$, 0.12, and 0.16. Agreement is good at $(H-s)/d = 0.04$ and 0.20.

For relative soffit clearance $s/d = 0.2$ and a relative wave height H/d ranging from 0.24 to 0.40, measured and predicted values of x_{cmp}/d range from 0.6 to 1.7, showing a general increase with $(H-s)/d$. Values measured by El Ghamry, for relative platform length $L/d = 2.00$ and relative wave lengths λ/d ranging from 1.25 to 7.2, ranged from 0.1 to 1.2, with most values being within the range 0.4 to 1.2. Although x_{cmp}/d appeared to vary with λ/d, it did not appear to vary significantly with $(H-s)/d$. Most values presented in Figures 6.56, from both El Ghamry's and the present study, therefore lie within the range $0.4 < x_{cmp}/d < 1.6$.

Measured and predicted values of slowly-varying pressure have now been presented and compared, with respect to individual pressure records as well as variables such as total force, average pressure, and center of force. Comparison of measured and predicted values permits one to reassess the validity of the assumptions underlying the analysis presented in Chapter 3.

6.5.4 Discussion of the analysis.

The performance of Equation 3.40 alone may be judged by comparison of measured values with values predicted from measured

U_d, x_d, and dU_d/dt. From comparison of measured values of pressure and force with values predicted from analytically derived U_d one may judge the performance of the complete analysis, Equation 3.40 and Equation 3.34. Since Equation 3.34 for the analytical value of U_d has already been discussed in Section 6.4, it will not be treated here. Attention will rather be concentrated on Equations 3.40 and 3.51 and the assumptions underlying them.

Equations 3.40 and 3.51 are based upon the following assumptions:

1. that the horizontal fluid velocity beneath the platform does not depend on depth at the location where pressure is measured;

2. that the surface profiles of the wave front and of the wave of recession are of unchanging form (although the wave celerity may change);

3. that effects of viscosity, surface tension, and air entrainment are negligible;

4. that the flow in the neighborhood of the wave front or of the wave of recession may be simply approximated as having a step form, as expressed by Equations 3.38.

As explained in Section 3.3, the assumption that fluid velocity is independent of depth should improve with increasing values of $(x_d - x_e)/(d + s)$, the ratio of wetted length of platform to distance from the platform to channel bottom, in that the flow pattern increasingly approaches that of uniform irrotational flow between parallel plates of infinite extent. For a given ratio of $(x_d - x_e)/(d + s)$,

the flow should be most uniform at points far from the "ends" of the parallel plate , such as either end of the platform, or the wave front or wave of recession.

At small values of relative time $t\sqrt{g/d}$ near the seaward end of the platform where $(x_d - x_e)/(d + s)$ is small, one may expect that the horizontal velocity distribution with depth would reflect that of the incident solitary wave, in which velocity at the surface is greater than at the bottom. Figures 6.48a and 6.49a, for $t\sqrt{g/d} \approx 0.6$ and $x_d/d < 1$, show considerable disparity between measured and predicted values of pressure. However, Figures 6.48b, 6.49b, and 6.50a, for which x_d/d is greater than 2, show better agreement between measured and predicted pressure. In Figures 6.54b and c, showing $P_{av}/\gamma d$ for $H/d = 0.32$ and 0.40, respectively, the improved agreement between measured and predicted values that occurs with increasing $t\sqrt{g/d}$ may be attributed in part to the increasing uniformity of fluid velocity. (However, in Figure 6.54a for $H/d = 0.24$, the predicted values are about three times as great as values derived from measured pressure for all values of $t\sqrt{g/d}$, and it is doubtful that part or any of this discrepancy may be attributed to the assumption of uniform velocity.)

The assumption of constant wave form may be considered valid as far as the wave front is concerned, if simply because examination of Figures 6.13 through 6.17 in Section 6.2 revealed no change in profile shape with respect to time.

However, Figures 6.13 through 6.17 do show an expected

change of profile shape for the wave of recession, especially at and immediately following the time $t = t_a$, when the wave is beginning to form. In Section 6.4, Figure 6.33 showed that despite variance in measured values of U_e at $s/d = 0.2$ (which may be due to problems of measurement), the average measured celerity is predicted well by Equation 3.49. In many of the Figures 6.41 through 6.50 the negative pressure is seen to approach the value predicted by Equation 3.51, at times shortly before t_e (as shown in Figures 6.42a, 6.42b, 6.43a, 6.43b, 6.44a, 6.45a, 6.46a) or at locations close to the wave of recession (as in Figures 6.48c, 6.49d, 6.50c). The last three figures mentioned show pressure increasing with distance in the shoreward direction (implying a deceleration of fluid beneath the platform), as predicted by Equation 3.40 from U_d for the period of negative pressure, rather than the constant, uniform pressure predicted by Equation 3.51. Therefore despite the changing profile observed, pressures approach the predicted value near the wave of recession; while the increase in pressure with distance reflects transient flow conditions which may be expected in the light of flow conditions at the wave-front. That average pressure shown in Figures 6.54 is never greater than about half the value predicted in Equation 3.51 is consistent with the pressure distributions shown in Figures 6.48c, 6.48d, and 6.50c, where pressures increase from the predicted value to zero.

The assumption that effects of viscosity and surface tension are negligible may be examined by evaluating the Reynolds number

and the Weber number, respectively. As indicated in Section 3.3, for considerations of pressure exerted over the entire wetted length of the platform, a meaningful Reynolds number may be defined as:

$$R_e = uL/\nu ,$$

where u is a characteristic fluid velocity, L is the platform length, and ν is the kinematic viscosity of the fluid. The platform length L was 5.0 ft; the kinematic viscosity of water at 70° F is given by Rouse (1950) as:

$$\nu = 1.05 \times 10^{-5} \text{ ft}^2/\text{sec.}$$

In Section 3.3 it was noted that the effects of viscosity are greatest for small Reynolds numbers; hence a conservative meaningful value of Reynolds number is one computed from the smallest value of fluid velocity u typical of experimental conditions. From Equation 3.32a, $u = U_d s/(d + s)$; for $s/d = 0.1$, $d = 1.00$ ft, and a conservative value $U_d\sqrt{gd} = 1.0$ obtained from Figures 6.28 for $H/d = 0.12$, $u = 8.524$ ft/sec may be taken as a conservative value of fluid velocity. The resultant Reynolds number is:

$$R_e = 2.5 \times 10^5 ,$$

which is sufficiently large that effects of viscous forces compared to other forces may be considered negligible.

To estimate the contribution of surface tension to slowly-varying pressure, i.e. to estimate the average pressure due to surface tension acting on the free surface shoreward of the wave front or seaward of the wave recession, one may consider the average radius of surface curvature as being approximately equal to half the soffit

clearance s. Therefore a meaningful Weber number may be defined as:

$$W_e = U_d \sqrt{\frac{\rho s}{2\sigma}} ,$$

where ρ is the fluid density and σ is the surface tension. For water at 70^o F, the fluid density and surface tension are given by Rouse (1950):

$$\rho = 1.94 \text{ slug/f}^3 ,$$

$$\sigma = 0.00497 \text{ lb/ft} .$$

As with the Reynolds number, it was noted in Section 3.3 that the effects of surface tension are greatest for small Weber number. The smallest non-zero value of s used in the experiments was 0.1 ft, for $s/d = 0.1$. With $s/d = 0.1$, $d = 1.00$ ft, and the conservatively small value $U_d\sqrt{gd} = 1.0$ obtained from Figures 6.28 for $H/d = 0.12$, the celerity U_d is 5.68 ft/sec, and the Weber number takes the value:

$$W_e = 25.1 .$$

In Equation 3.63 the term involving surface tension is $1/W_e^2$, which in this case takes the value 0.00159. This value is much less than that of the other terms in Equation 3.63, if it is assumed that they are of the order of unity; hence the effects of surface tension on slowly-varying pressure may be considered negligible.

Air entrainment may be partially responsible for measured pressures being less than predicted pressures, since the influence of entrained air is to reduce the amplitude of pressure, as noted in Section 3.3. Yet figures 6.13 through 6.17 indicate that the degree of

air entrainment increases with H/d; and since agreement between measured and predicted pressure values becomes better with increasing H/d, air entrainment can not be the principal reason for disparity between measured and predicted values of pressure.

The assumption of a simple step-form for the wave front, introduced to simplify the term $[(x_d - x)/(d+s)]\,(s/d)(\,dU_d/dt)$ in Equation 3.40, apparently introduces little error as far as the term in Equation 3.40 is concerned, since the rate of change of pressure with distance predicted by the term shows good agreement with the data in Figures 6.48a, b, and c, 6.49a, b, and c, and 6.50 a and c. (As stated earlier, Firgure 6.50b represents the time during which measured values may show considerable scatter due to oscillations.) In regions of the platform near the wave front or the wave of recession (Points 2 in the analysis in Section 3.2), the assumption may be considered to introduce error which could also be designated a violation of the assumption of a constant velocity with respect to depth. In these regions, fluid near the platform attains a velocity approaching the propagation celerity of the wave front or wave of recession, rather than the constant velocity assumed in Equation 3.38: viewed in a frame of reference moving with the wave celerity, the velocities approach zero, i.e. the Points 2 at the wave front and the wave of recession are stagnation points. Associated with these stagnation points of zero velocity relative to the wave front or wave of recession are regions of increased "stagnation" pressure, namely the peak pressure at the wave front and the smooth increase to zero

pressure at the wave of recession.

When based on measured values of U_d, x_d, and dU_d/dt, the analysis is qualitatively successful in predicting the form and duration of forces and pressure, and predicts the center of force well as a function of time. Predicted values of maximum force and pressure are greater than the values determined from measurements, but are sufficiently close to provide a conservative estimate of measured values. However, the simple hydrostatic relationship that appears to exist between incident wave height and maximum average pressure, $P_{av}/\gamma d \approx (H-s)/d$, is of attractive simplicity, although not accounted for in the analysis presented herein.

Negative pressures at a given location may approach but have not been observed to exceed greatly the value predicted analytically; average negative pressures have not been observed to exceed half the predicted value. The analysis thus provides a conservative estimate for negative pressures. Negative forces and pressures appear to be largely independent of relative wave height, but, as shown by Equation 3.51, are strongly dependent on relative soffit clearance s/d. As shown by Figures 6.35 through 6.37, the duration of negative force is dependent on relative platform length L/d. Therefore, for a long platform high above the still water level, a wave only slightly higher than the soffit will cause only a modest uplift pressure, but a negative pressure of considerable magnitude and duration.

6.6 The Peak Pressure

Measurements of the peak pressure amplitude P_2 and the peak pressure rise-time t_r are to be discussed in this section. The data are presented in Table B2 of Appendix B, showing P_2, t_r, and the wave height H for each wave, as well as the mean, standard deviation, and deviation of the mean of each quantity for each sample of recorded data. Unless otherwise indicated, all values of P_2 and t_r presented in this section are sample means.

6.6.1 Statistical Considerations

To examine the deviation inherent in measurements of peak pressure head P_2/γ, as obtained by the two transducers described in Section 4.4, data from individual waves, normalized with respect to the mean wave height H, have been plotted in Figure 6.57 on arithmetic probability paper in cumulative frequency diagrams for each of the samples of 16 to 32 waves generated at $x/d = 0.816$. In most cases the data in a sample may be fitted by a straight line, showing a normal distribution. For data obtained with the 1/8-in. transducer, the average ratio of sample standard deviation S_P to sample mean wave height H was 0.200. For data obtained with the 1/2-in. transducer, the average ratio was 0.0136. Figure 6.57 show that deviation for data measured with the 1/2-in. transducer was almost always less than for data measured with the 1/8-in. transducer.

Figure 6.58 shows the ratio of sample standard deviation S_P to sample mean $\overline{P}_2$ as a function of relative distance x/d, for all

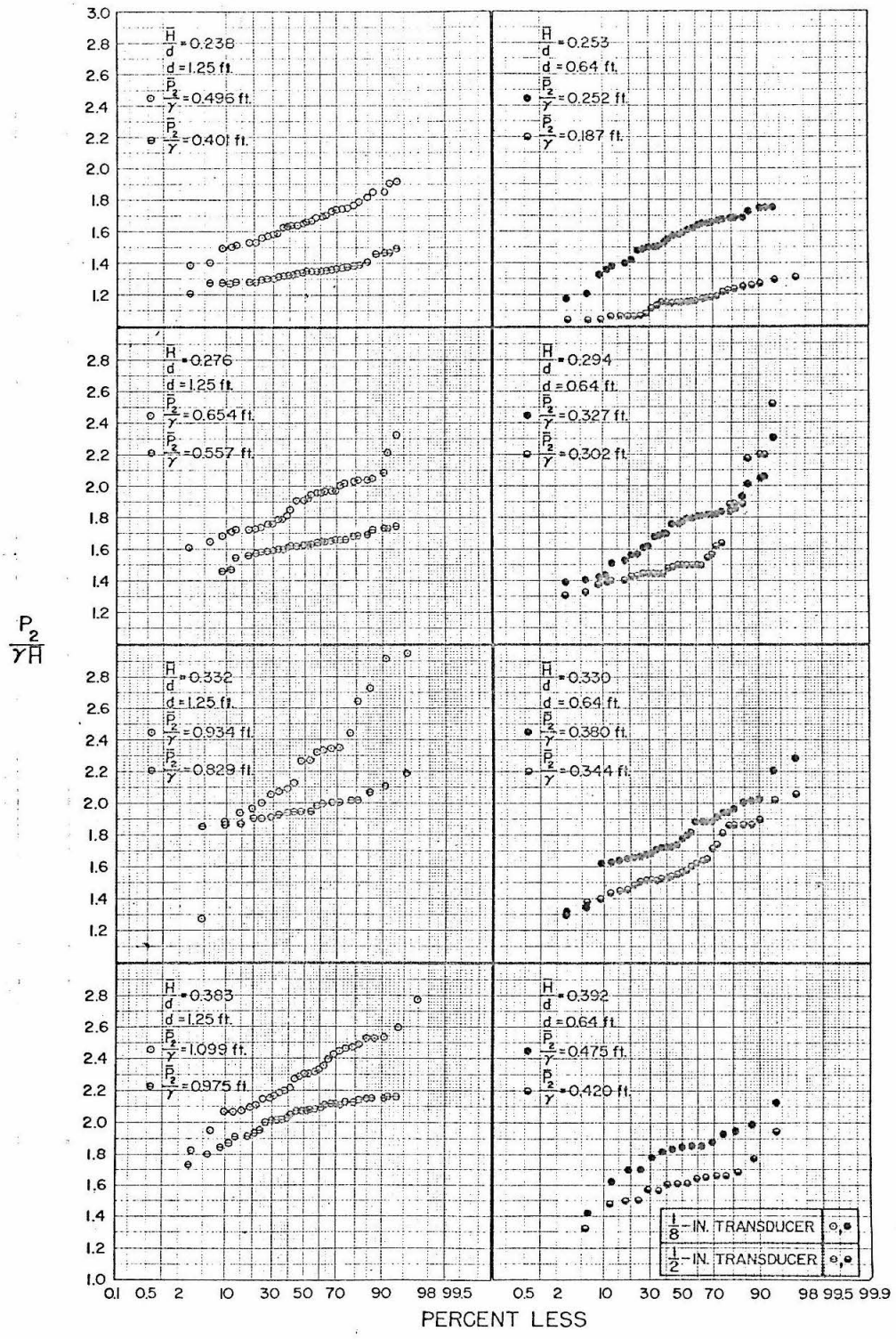

Figure 6.57. Cumulative frequency diagrams for normalized peak pressure $P_2/\gamma H$. (Uncorrected data obtained at $x/d = 0.816$, $s/d = 0.2$.)

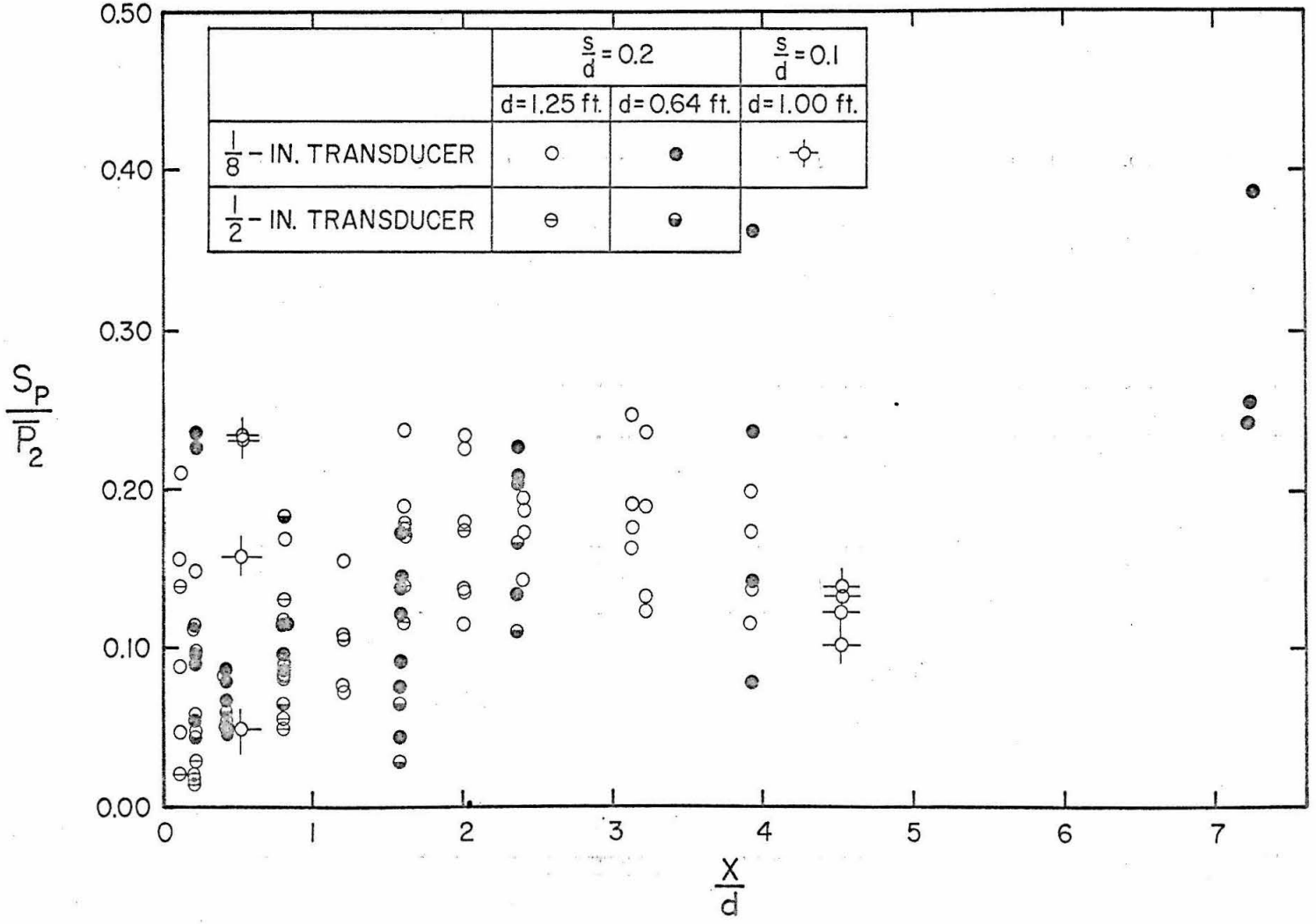

Figure 6.58. The ratio of standard deviation to mean in peak pressure, plotted against x/d. (Range of H/d is 0.15 to 0.46.)

values of H/d and relative soffit clearances s/d which were investigated and for both transducers. With a few exceptions, the values of $S_p/\bar{P}_2$ fall mainly within the range $0.025 < S_p/\bar{P}_2 < 0.25$. There is a tendency for $S_p/\bar{P}_2$ to increase with x/d. No distinct influence of scale size, choice of s/d, or choice of transducer is detectable.

Figure 6.59 shows cumulative frequency diagrams for the rise-time t_r, normalized by multiplication by $\sqrt{g/H}$, where H is the mean wave height for the sample. Again, the samples plotted are those obtained at x/d = 0.816. In most instances, the data appear to be normally distributed. For data obtained with the 1/8-in. transducer, the average ratio deviation to mean value of $t_r\sqrt{g/H}$ is 0.193; for data obtained with the 1/2-in. transducer, the ratio is 0.099.

Figure 6.60 shows the ratio of standard deviation to mean value of t_r, for samples obtained at several values of H/d, plotted against x/d. For $x/d < 2$, the ratio is always less than 0.30; for $x/d > 2$, the ratio increases to as much as 0.75.

In an investigation of the cause of the deviation in peak pressure, the peak pressure heads P_2/γ obtained in one 32-wave sample with the 1/8-in. transducer mounted at x/d = 0.816 (H/d = 0.238, d = 1.25 ft) were correlated respectively with the wave heights H, the peak pressure heads P_2/γ obtained simultaneously with the 1/2-in. transducer, and with the rise-times t_r obtained by the 1/8-in. transducer as shown in Figures 6.61. In each figure, the quantity plotted is the deviation from mean value, normalized with respect to the mean value.

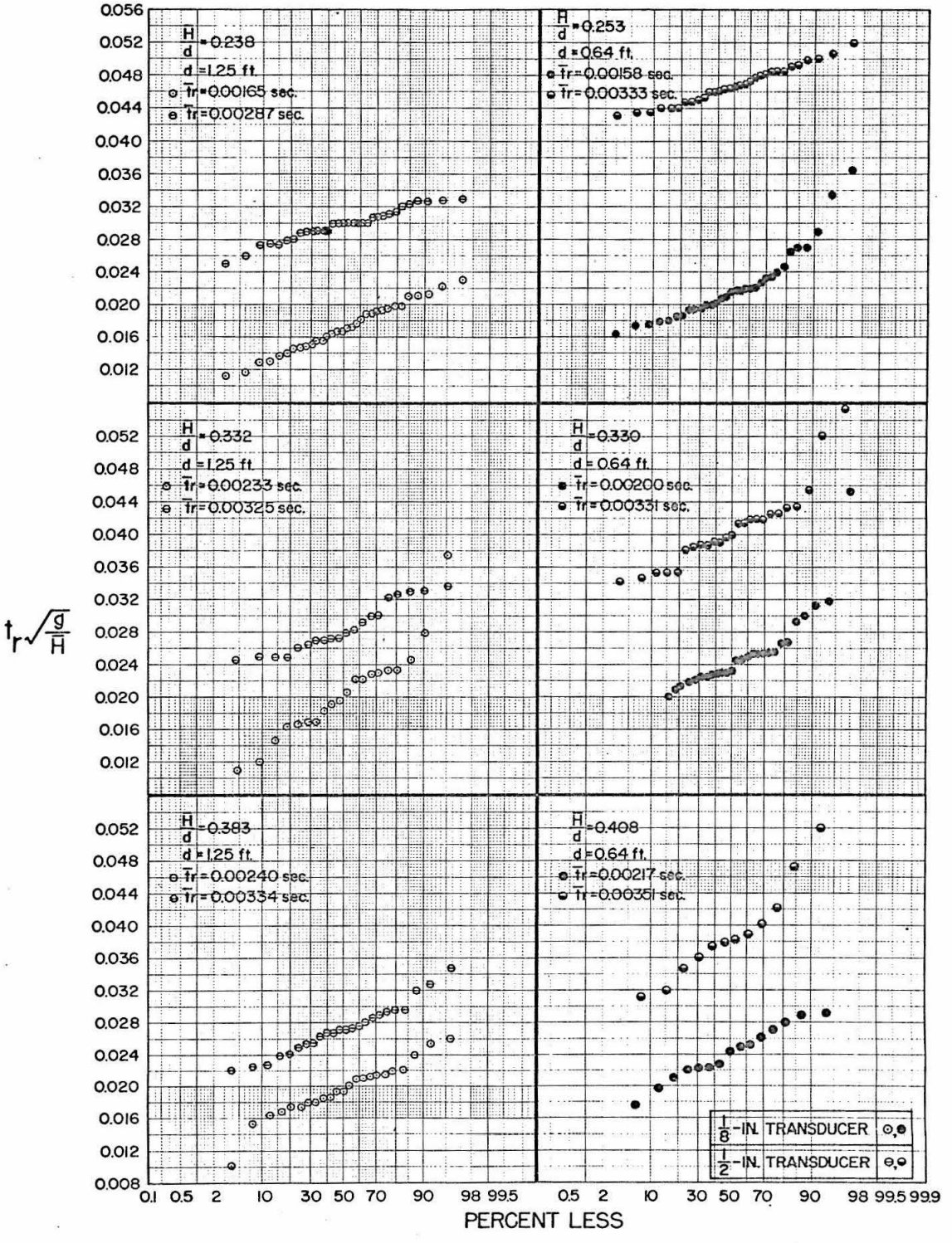

Figure 6.59. Cumulative frequency diagrams for normalized rise-time $t_r\sqrt{g/H}$. (Uncorrected data obtained at x/d = 0.816, s/d = 0.2.)

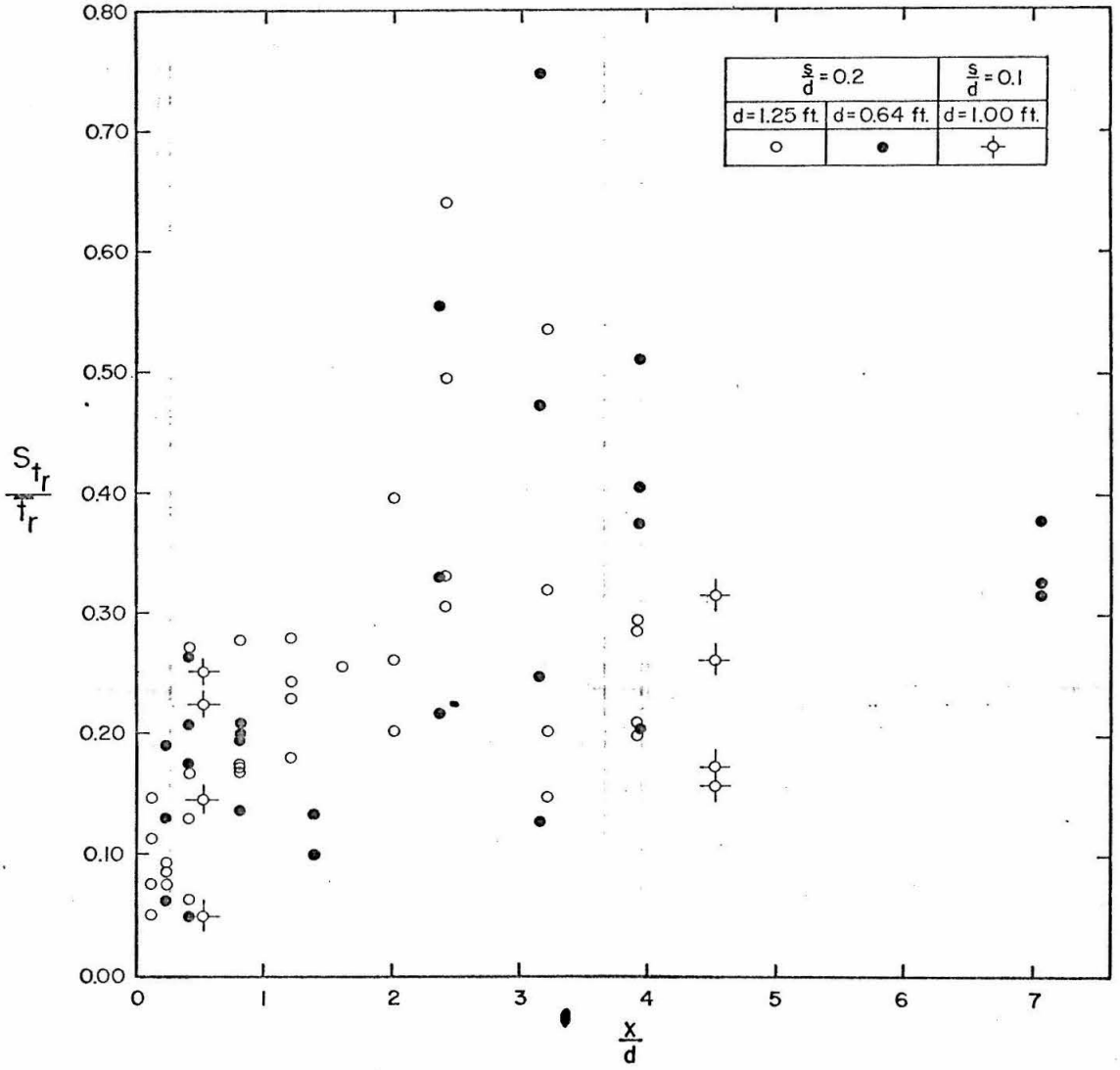

Figure 6.60. The ratio of standard deviation to mean in rise-time, plotted against x/d. (Range of H/d is 0.15 to 0.46.)

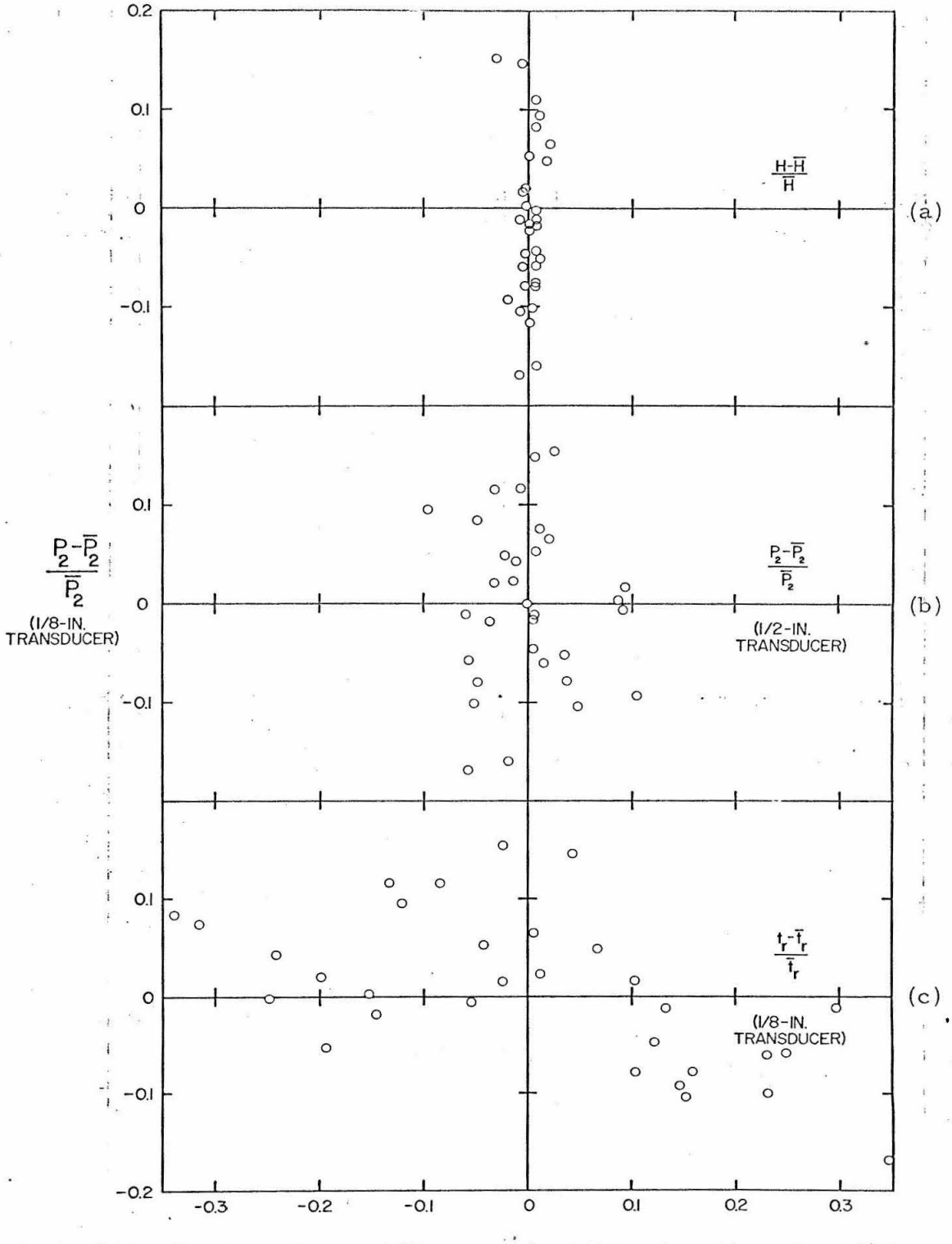

Figures 6.61. Correlation of quantities measured in a set of experiments made at $x/d = 0.816$, $s/d = 0.2$, $\bar{H}/d = 0.238$, $d = 1.25$ ft.

For example, in Figure 6.61a, $(P_2 - \bar{P}_2)/\bar{P}_2$ is plotted against $(H - \bar{H})/\bar{H}$, where P_2 is the peak pressure measured with the 1/8-in. transducer, H is the incident wave height, and the bars denote sample mean values.

In Figure 6.61a, there is no discernible correlation between the peak pressure P_2, as measured by the 1/8-in. transducer, and the wave height H; nor is there discernible correlation in Figure 6.61b between the peak pressure P_2 as measured by the 1/8-in. transducer and by the 1/2-in. transducer. However, in Figure 6.61c, a negative correlation is discernible (i.e. the plotted points lie mainly in the second and fourth quadrants of the graph) between the peak pressure P_2 and the rise-time t_r, both measured by the 1/8-in. transducer. The absence of correlation between wave height and peak pressure indicates that deviation in peak pressure is not attributable to deviation in the height of the incident wave. The absence of correlation between peak pressures measured simultaneously by two transducers mounted two inches apart (although at the same distance x from the seaward edge of the platform) indicates that the mechanism causing deviation in peak pressure not only is independent of the incident wave, but acts upon each transducer separately. It therefore appears reasonable to assume that the deviation is due to local inhomogeneity in fluid density caused by the spume and air entrainment generated at the wave front, shown in the photographs in Section 6.2.

The negative correlation shown between peak pressure and

rise-time in Figure 6.61c indicates that the uplift force in the peak, or the pressure integrated over the area of peak pressure, is a quantity of less deviation than either the peak pressure or rise-time alone. The fact that the 1/2-in. transducer shows less deviation in peak pressure and rise-time than the 1/8-in. transducer in Figures 6.57 and 6.59 is explained by the fact that the larger transducer is less sensitive to "details" of pressure distribution, and less readily distinguishes between pressure distributions of equal total impulse but of different rise-length and peak pressure, than does the 1/8-in. transducer.

6.6.2 Correction of peak pressure and rise-time.

The normalized peak pressure $P_2/\gamma d$ is presented in Figures 6.62, plotted as a function of relative wave height H/d, for each value of relative location x/d and for each relative soffit clearance s/d for which experiments were conducted. For $s/d = 0.2$, data from both model scales $d = 1.25$ ft and $d = 0.64$ ft are presented. Each set of data is presented twice. In the left hand part of the figures the sample mean values of $P_2/\gamma d$ are plotted against sample mean values of relative wave height H/d. Next to each point, a number in brackets (curved for $d = 1.25$ ft, square for $d = 0.64$ ft and for $d = 1.00$ ft) indicates the size of the sample. In the right hand column, the data corrected for the transducer size are plotted. Curves fitted to the data will be discussed presently. The rise-times t_r, normalized by multiplication by the ratio U_d/d of measured wave front celerity to still water depth, are presented similarly in Figures 6.63. The

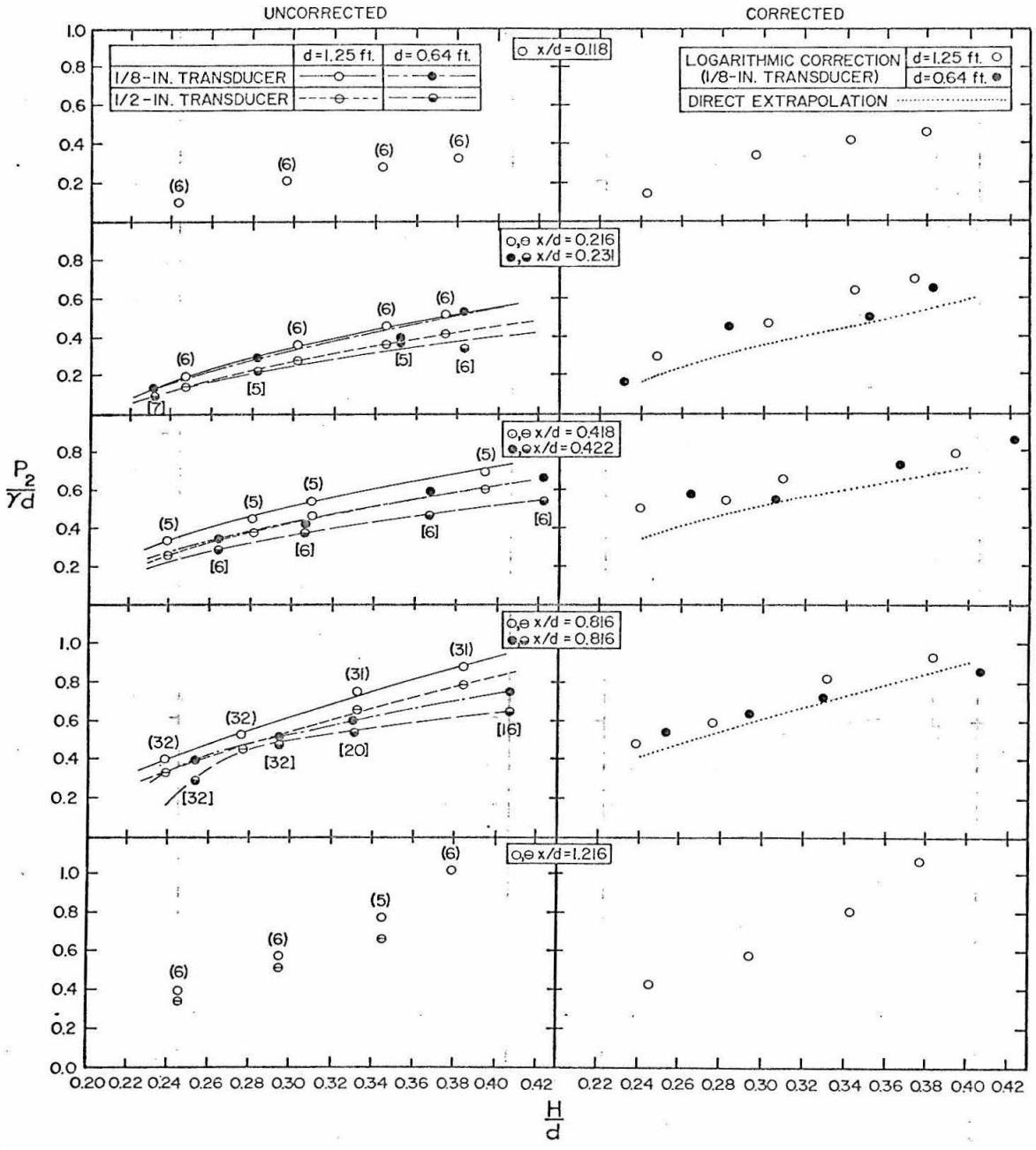

Figures 6.62. Uncorrected and corrected normalized peak pressure $P_2/\gamma d$, plotted as a function of H/d for several values of x/d. (s/d = 0.2).

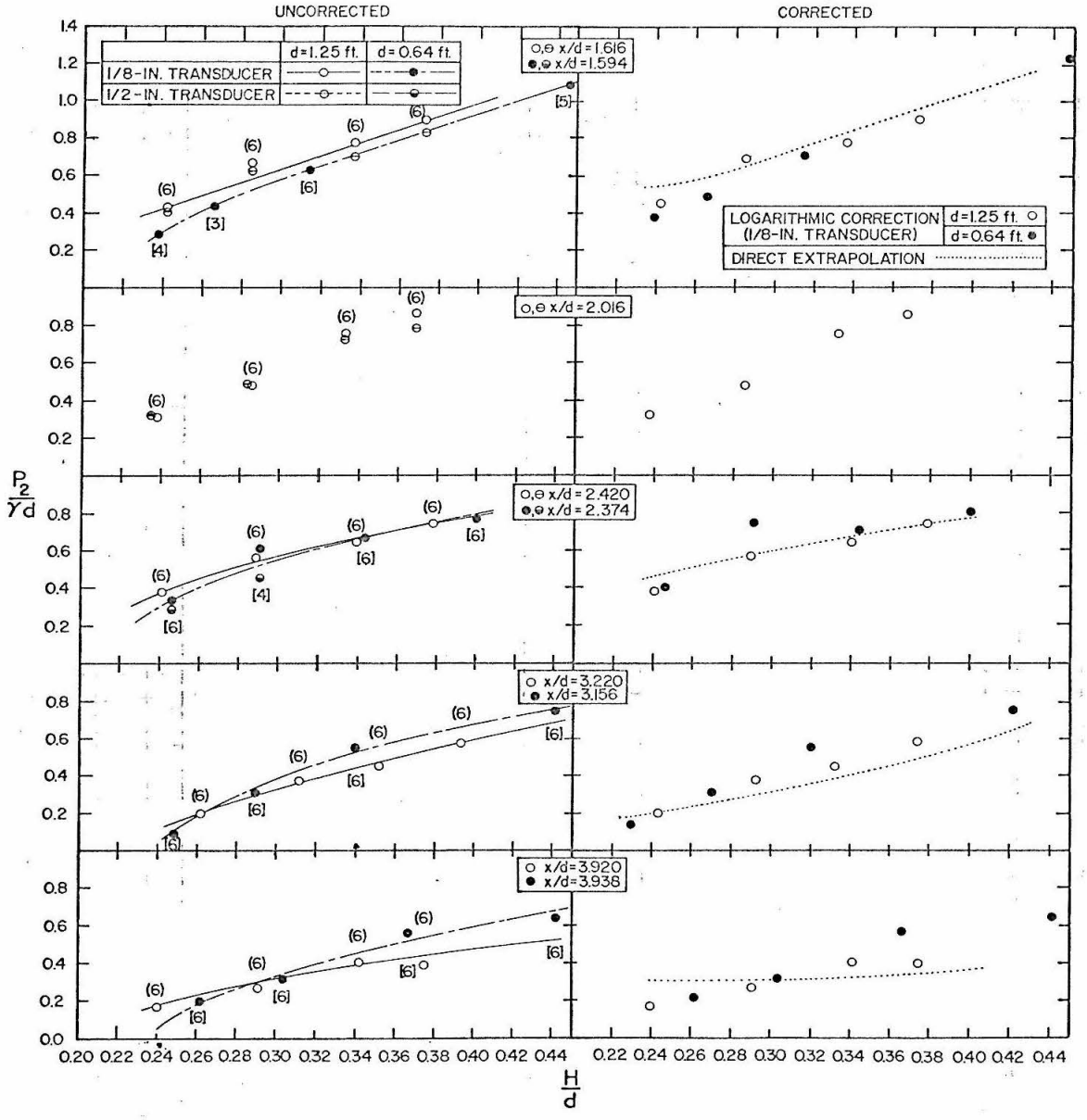

Figures 6.62 (continued). Uncorrected and corrected normalized peak pressure $P_2/\gamma d$, plotted as a function of H/d for several values of x/d. (s/d = 0.2.)

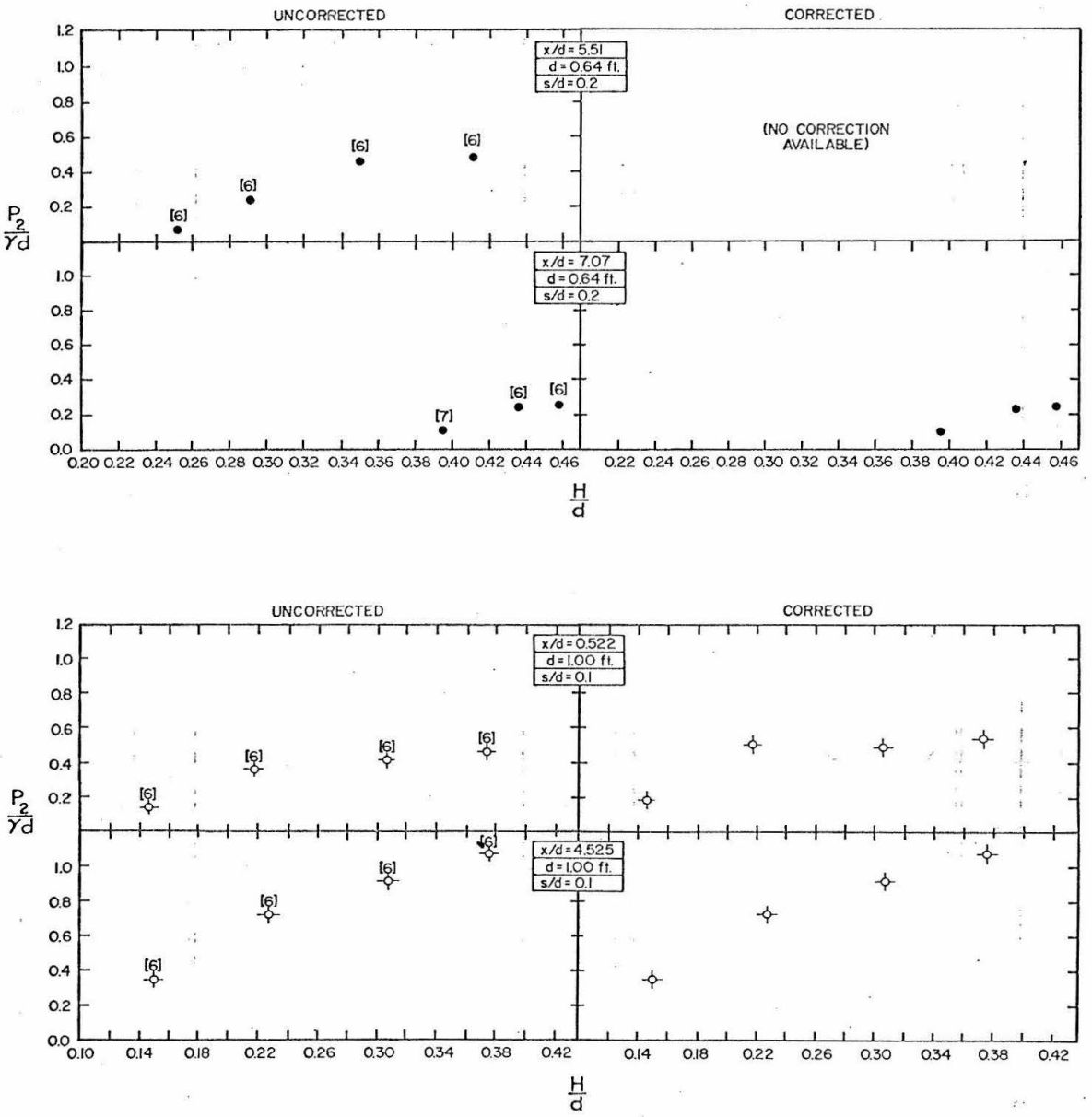

Figures 6.62 (concluded). Uncorrected and corrected normalized peak pressure $P_2/\gamma d$, plotted as a function of H/d for several values of x/d. (Upper frame: s/d = 0.2; lower frame: s/d = 0.1.)

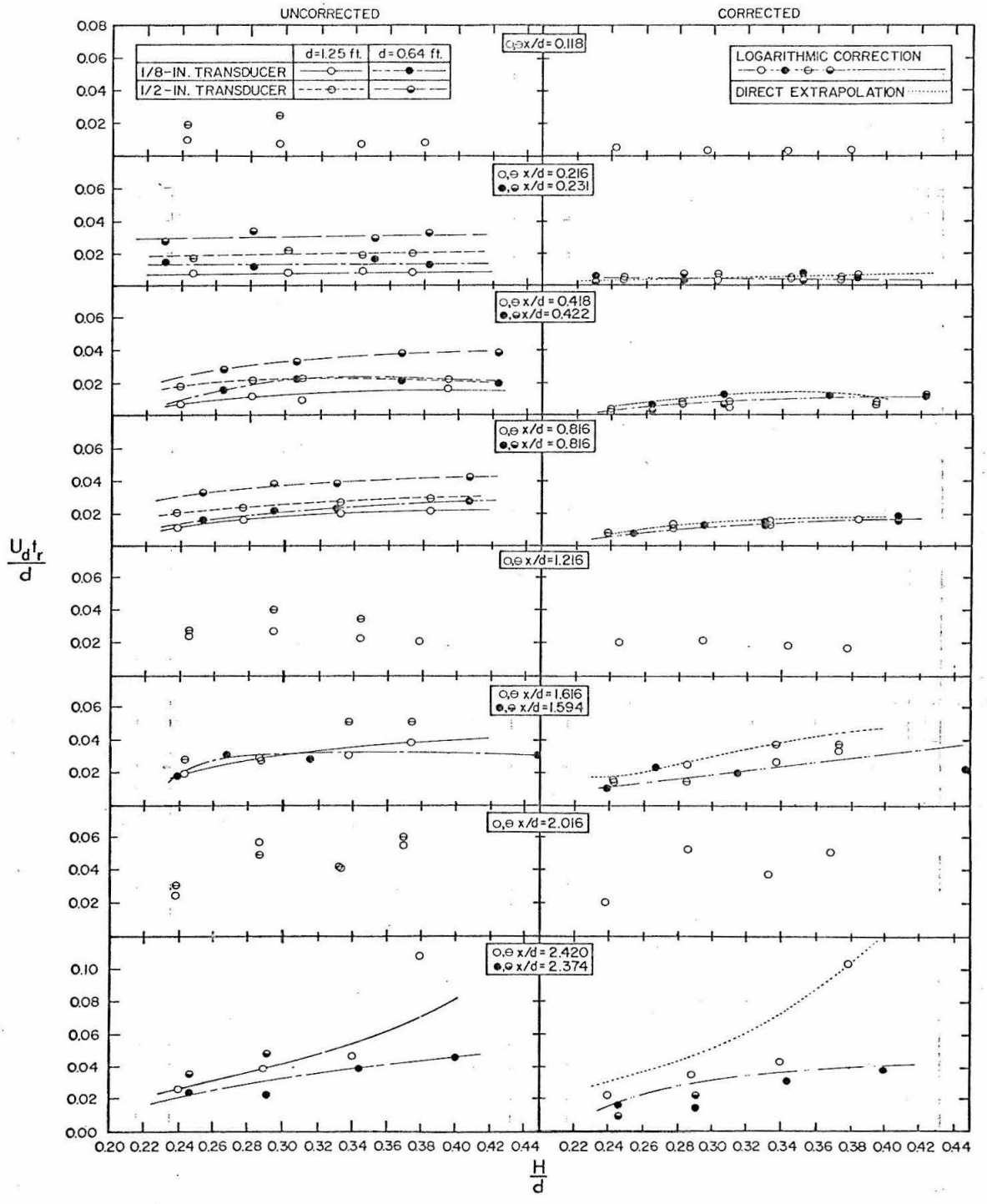

Figures 6.63. Uncorrected and corrected normalized rise-time $U_d t_r/d$, plotted as a function of H/d for several values of x/d. (s/d = 0.2. Corrected $U_d t_r/d$ is $b/d = (U_d t_r - a)/d$.)

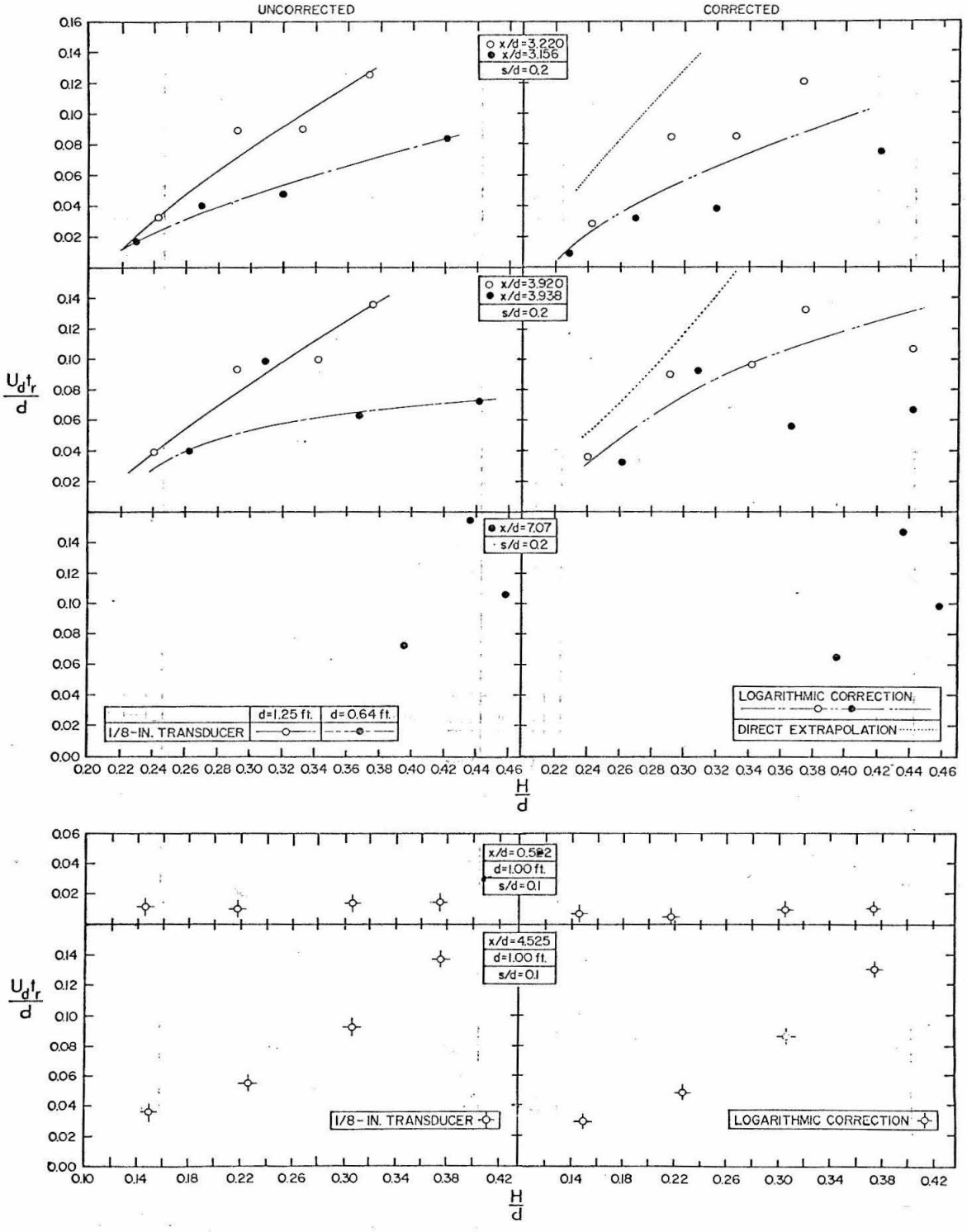

Figures 6.63 (concluded). Uncorrected and corrected normalized rise-time $U_d t_r/d$, plotted as a function of H/d for several values of x/d. (Upper frame: s/d = 0.2; lower frame: s/d = 0.1. Corrected $U_d t_r/d$ is b/d = $(U_d t_r - a)/d$.)

functional behavior of $P_2/\gamma d$ and $U_d t_r/d$ with respect to relative wave height H/d, relative location x/d and relative soffit clearance s/d will be discussed in Subsection 6.6.3. Figures 6.62 and 6.63 are presented in this subsection to illustrate the correction procedures. (Data obtained for $s/d = 0.2$ at the two model scales at comparable values of x/d are superimposed on one graph. For example, data obtained at $x/d = 0.231$ at $d = 0.64$ ft are presented with data obtained at $x/d = 0.216$ at $d = 1.25$ ft. For convenience, both sets of data may be termed collectively as data obtained at $x/d = 0.2$.)

The peak pressure amplitude and rise-time data are now to be corrected for transducer area defect. In Chapter 5 it was hypothesized that a transducer of finite sensitive area would record a pressure averaged over the area of sensitive surface, rather than record the pressure exerted at a single point. In the present case where a single propagating wave pulse sweeps past the transducer, the effect of finite area is to produce a record of time-dependent pressure in which the recorded pulse is of longer duration and of lesser amplitude than a record produced by a transducer of vanishingly small area, or even simply of somewhat smaller area. This loss of accuracy, termed "tranducer area defect", may be expected to increase with decreasing values of the ratio b/a, where b is the characteristic pulse length and a is the radius or other characteristic dimension of the sensitive transducer surface.

First, it should be determined whether there is evidence of transducer area defect. Examination of a single pressure record, such

as shown in Figure 6.20a, is not particularly useful, in that from the record it is impossible to tell the extent to which amplitude is decreased and duration is increased by the area effect. One needs rather to compare two or more records of pressure pulses generated under conditions mutually indentical in all respects except for the ratio b/a of pulse rise-length to transducer surface radius.

In the present study, such comparison may be made between the records produced with the 1/8-in. and 1/2-in. transducers, operating side-by-side, or between records produced with one transducer operating at the two different model scales for $s/d = 0.2$, $d = 1.25$ ft and $d = 0.64$ ft. One may first compare the data obtained with the two transducers operating side-by-side at a common scale. As shown in Section 4.4, the radius, a, of the 1/8-in. transducer is 0.0052 ft; the effective radius, a, of the 1/2-in. transducer is believed to be 0.016 ft. Therefore, provided that there was no lateral variation in wave front characteristics, including the pulse length b, the ratio b/a of pulse rise-length to transducer radius would be about three times as great for the 1/8-in. transducer as for the 1/2-in. transducer, for any given wave front. In Figures 6.62, for values of x/d where pressures obtained with both transducers are presented ($x/d = 0.2, 0.4, 0.8, 1.2, 1.6, 2.0$, and 2.4), the mean peak pressure head P_2/γ as recorded by the 1/2-in. transducer is consistently less than the mean value recorded by the 1/8-in. transducer, for which the values of b/a are greater. In Figures 6.63, for the same values of x/d, the rise-time t_r, multiplied by U_d/d, is consistently greater as measured by the

1/2-in. transducer than as measured by the 1/8-in. transducer. As hypothesized, recorded amplitudes are less and recorded rise-times are greater in the case for which b/a is less, i.e. for the 1/2-in. transducer.

One may object that lateral variations in wave front characteristics might cause pulses with different characteristics to propagate past the two transducers; but considerable effort was made to eliminate lateral variation in the wave tank, the wave generator, and the platform. (Random fluctuations in pressure due to spume and entraned air, described in Subsection 6.6.1, while contributing randomly to differences in transducer output, should not cause the peak pressure recorded by one transducer to be consistently greater than that recorded by the other transducer.)

It is also true that the internal structure and dynamic characteristics of one transducer differ from those of the other. Yet considerations of internal structure and of dynamic amplitude response both would indicate a greater response by the 1/2 in. transducer than by the 1/8-in. transducer: in the 1/2-in. transducer, the output is proportional to deflection of the center of the diaphragm; Figure 5.5 in Section 5.3 shows that where output is proportional to central deflection, as in the 1/2-in. transducer, one may expect less defect (i.e., a defect ratio R closer to unity) than in a case where output is proportional to average deflection, as in the 1/8-in. transducer. In Section 4.4, it was shown that the component frequencies of a typical recorded pressure pulse were 3000 cyc/sec or less, and that in the

range of frequencies from zero to 3000 cyc/sec the 1/2-in. transducer was susceptible to an amplitude considerably greater than unity, whereas the amplitude response of the 1/8-in. transducer was close to unity for that frequency range. Since considerations of internal structure and dynamic response both indicate that the 1/2-in. transducer should provide greater relative response to a given input excitation, and since it is found that it is rather the 1/8-in. transducer that provides greater response, the differences in transducer output may be attributed to differences in transducer size, which therefore result in differences in the ratio b/a of pulse rise-length to transducer radius.

Next, one may compare the values obtained with the 1/8-in. transducer operating at the two model scales. Experiments at the two scales were designed to be geometrically similar, as far as flow near the wave front was concerned (see Section 6.4). In Section 6.4 it was shown that there was kinematic similarity between the two scales, i.e., normalized values of wave front time of arrival t_d and of wave front celerity U_d showed the same dependence upon dimensionless parameters such as relative wave height H/d and relative location X/d at one scale as at another scale. In Section 6.5 it was demonstrated that there was dynamic similarity between the two scales in the normalized slowly-varying pressure $P_1/\gamma d$ measured a short distance behind (i.e. seaward of) the wave front. With geometric and kinematic similarity (and dynamic similarity for the slowly-varying pressure) established, the important remaining difference between

scales was the ratio of a characteristic scale size to the transducer radius a, which for both scales was 0.0052 ft. If the peak pressure rise-length b, defined in Chapter 5, is proportional to the geometric length scale, then the ratio b/a is similarly proportional to the geometric length scale, and will be about twice as great for d = 1.25 ft, as for d = 0.64 ft.

In Figures 6.62. for the seven values of x/d where pressures obtained with the 1/8-in. transducer at both model scales are compared (x/d = 0.2, 0.4, 0.8, 1.6, 2.4, 3.2, and 3.9; see Table 6.2 in Section 6.3), the normalized mean peak pressures $P_2/\gamma d$ recorded for d = 0.64 ft. are generally less than those for d = 1.25 ft. In Figures 6.63, for the same values of x/d, normalized mean rise-times $U_d t_r/d$ are generally greater for d = 0.64 ft than for d = 1.25 ft. Again, the effect of transducer size (diminished peak pressure, augmented rise-time) is greater for the smaller values of b/a (found at d = 0.64 ft). The same qualitative statements may be made concerning data obtained with the 1/2-in. transducer, where they are available.

For such a comparison there is no question of lateral variation or of different transducer characteristics; data from one transducer are compared at different scales, with ratios such as H/d, x/d, and s/d held reasonably constant, but with b/a allowed to vary. Now, however, there is the question of scale effects such as viscosity, surface tension, and air entrainment which may of themselves cause differences in $P_2/\gamma d$ and $U_d t_r/d$.

That significant differences due to scale have not been observed in incident wave form or in relative values of wave front travel time t_d, wave front celerity U_d, or slowly-varying pressure P_1 encourage one to believe that the peak pressure parameters P_2, t_r, and b may also be free of scale differences. Yet one must remember that the wave front beneath the platform is a region of particularly large pressure and velocity gradients, and free surface curvature; therefore, one must attempt to estimate the characteristics and extent of scale effects with respect to flow conditions at the wave front.

According to Prandtl's boundary-layer theory (Schlichting, 1960), pressure on the boundary is not directly affected by the viscous boundary layer, providing that the Reynolds number R_e is much greater than unity. For flow in the neighborhood of the wave front, a Reynolds number may be defined as:

$$R_e = \frac{U_d(U_d t_r)}{\nu},$$

where U_d is the wave front celerity, ν is the kinematic viscosity of the fluid, and $U_d t_r$ is a characteristic length approximately equal to the rise-length of the peak pressure distribution (see Chapter 5). The value of ν for water at 70°F is given by Rouse (1950):

$$\nu = 1.05 \times 10^{-5} \text{ ft}^2/\text{sec}.$$

In order to define a meaningful minimum Reynolds number, the following conservatively low values of the measured flow properties are used:

$$U_d \simeq 5 \text{ ft/sec},$$

$$t_r \simeq 6 \times 10^{-4} \text{ sec},$$

giving a Reynolds number of:

$$R_e = 1430 .$$

Since this is reasonably large one expects little influence on pressure due to viscosity. (The indirect influence of viscosity on pressures is to cause gross changes in flow patterns, such as flow separation. However, once such flow patterns are established, pressures are probably not affected further by viscosity.)

In Section 3.3 it was suggested that surface tension would act to reduce peak pressure by inhibiting the formation of the thin jet described in Section 3.2; and that the relative importance of surface tension could be estimated by evaluating the Weber number:

$$W_e = U_d \sqrt{\rho U_d t_r / \sigma} ,$$

where $U_d t_r$ is a characteristic length which may reasonably be assumed to be of the order of the maximum radius of free surface curvature in the neighborhood of the wave front. For water at 70°F, the surface tension and fluid density may be determined from Rouse (1950):

$$\sigma = 0.00497 \text{ lb/ft},$$

$$\rho = 0.94 \text{ slug/ft}^3 .$$

These values, combined with the values of U_d and t_r given previously, provide a conservatively small Weber number of 5.41.

The relative importance of surface tension is determined by comparing the magnitudes of the terms in Equation 3.63. By considering that a typical value of normalized peak pressure $P_2/\gamma d$ given in Figures 6.62 is 0.4, and that a typical value of $U_d/\sqrt{gd}$ given in Figures 6.27 in Section 6.4 is 1.5, the first term in Equation 3.63 may be evaluated as $P_2/\rho U^2$ approximately equal to 0.2. The term in Equation 3.63 involving surface tension is $1/W_e^2$, which, from the Weber number just derived, is evaluated as 0.034. The surface tension term, 17% as great as the pressure term, indicates that while surface tension effects are not predominant, they may be important.

In Section 3.3 it was indicated that the proportional amount of entrained air might be expected to increase with scale, and cause corresponding changes in relative pressure due to changes in average fluid density. However, the agreement as to the relative magnitude of slowly varying pressure P_1, despite the presence of entrained air as observed in many of the photographs in Section 6.2 (see Figures 6.13 through 6.17), suggests that for a scale ratio of approximately 1:2, as in the present study, any scale effect due to air entrainment is probably unimportant. Such a belief is supported by the laboratory experiments of Smetana (1938), in which no consistent dependence of air entrainment on scale was observed, even between models with a scale ratio as great as 1:10.

Since the quantative importance of surface tension has not been determined in these experiments, its consideration has been limited to

this discussion, and is not undertaken further.

The question of surface tension notwithstanding, the comparison of relative peak pressure amplitude and relative rise time as measured by two transducers and at two scales indicates the presence of a transducer area defect as predicted in Chapter 5, and the correction procedure presented therein may nowbe applied. First, however, the six assumptions upon which the procedure is based, presented in Section 5.3, must be discussed.

The first assumption was that the wave front celerity U_d is approximately constant for the time needed by the wavefront to cross the transducer, i.e.:

$$\frac{dU_d}{dx} \quad \frac{a}{U_d} \quad << 1 .$$

Figures 6.27 show that

$$\frac{dU_d}{dx}$$

is greatest, and U_d is least, when x_d/d is small. The smallest value of x_d/d for which tests were made is 0.118, where $x_d = 0.148$ ft, and $d = 1.25$ ft. For these values of x_d and d the quantity

$$\frac{dU_d}{dx} \quad \frac{a}{U_d} ,$$

computed for several values of H/d, has values ranging from 0.0013 to 0.0036, considerably less than one percent. The first assumption is therefore considered valid.

The second assumption was that the wave form does not vary in

the transverse direction over the transducer width. As stated previously, the tank, generator, and platform were carefully aligned to eliminate transverse variation. However, the deviation observed within a sample of peak pressures obtained in a series of similar experiments implies that spume and entrained air at the wave front cause the peak pressure to fluctuate from experiment to experiment, as noted in Subsection 6.6.1. It is also reasonable to suppose that spume and entrained air cause spatial fluctuations in pressure in any given wave front, implying a certain amount of transverse variation in pressure.

The third assumption was that the peak pressure distributions are similar for all conditions, and that they are time-dependent only as a wave form, i.e.:

$$P_{ac} = P_2 \, \phi\left(\frac{x-U_d t}{b}\right) \quad ,$$

where P_2 and b may vary, but ϕ depends solely on the value of $(x-U_d t)/b$. This assumption may be questionable because of the fluctuating nature of the pressure distribution at the wave front, just mentioned. Furthermore, it cannot be shown that the function ϕ is truly independent of such parameters as the relative wave height H/d, the relative location x/d, or the relative soffit clearance s.

The fourth assumption is that the maximum transducer output occurs when the actual pressure maximum is centered on the transducer center. It may be shown that this assumption is strictly valid only if the pressure is distributed symmetrically about the location of peak

pressure. For the somewhat asymmetric distribution shown schematically in Figures 5.1a and 5.1c, indicated as typical distributions by the pressure records shown in Figures 6.22, the peak recorded pressure will be obtained at a time shortly after the actual pressure peak (as shown in Figures 5.1a and 5.1c) has propagated past the center of the transducer center.

The fifth assumption, that the defect ratio R increases monotonically with b/a, is valid if the actual pressure function, within the range $-a < x < a$, has the form of a single symmetric or asymmetric pulse centered at the transducer center, and is nowhere negative. The spatial response function G(x) has no negative values for $-a < x < a$, for any of the five cases examined in Table 5.1. Therefore, if $P_{ac}(x)$ has no negative values, Equation 5.15 indicates that R will not be negative. If $P_{ac}(x)$ has the form of a single pulse, a simple increase in the ratio b/a of pulse half-width to transducer radius a (with the maximum value $P_{2_{ac}}$ held constant) would serve to increase or leave unchanged, but not decrease, values of $P_{ac}(x)$ within the range $-a < x < a$. Therefore, the integral on the left-hand side of Equation 5.15, and hence R on the right-hand side, would increase monotonically with b/a.

The sixth assumption, that of geometric, kinematic, and dynamic similarity between models at the two scales, has already been discussed in this section. The seventh assumption, that the dynamic properties of the transducer may be neglected in the analysis, is valid

for the 1/8-in. transducer, as shown in Section 4.4.

As outlined in Section 5.3, the first step of the correction procedure is to collect pairs of recorded values of relative peak pressures $P_{2_r}/\gamma d$ and relative rise-lengths b/d measured at two model scales with a common transducer of known radius a. Pairs of values of $P_{2_r}/\gamma d$ may be obtained from Figures 6.62, for seven relative locations of x/d: 0.2, 0.4, 0.8, 1.6, 2.4, 3.2, and 3.9, by fitting curves to the data obtained at each scale, as shown, and from the curves containing pairs of values of $P_{2_r}/\gamma d$ at common values of relative wave height H/d. (It is necessary to fit curves to the data to compare values of $P_{2_r}/\gamma d$ for constant H/d because of the practical difficulty of precisely reproducing relative wave heights H/d at one scale as produced at another.) When pairs of values of $P_{2_r}/\gamma d$ at several values of H/d, for the seven relative transducer locations x/d, have been tabulated, it is necessary to derive the rise-length b from Equation 5.16: $b = U_d t_r - a$. The normalized rise-length b/d may be considered a corrected normalized rise-time, i.e. a corrected version of $U_d t_r/d$, and is so presented in the right-hand column of Figures 6.63. (Rise-time data obtained with the 1/2-in. transducer, for which $a = 0.016$ ft, are corrected along with data obtained with the 1/8-in. transducer, for which $a = 0.0052$ ft.)

In Figures 6.63 for $x/d = 0.2$, 0.4, 0.8, and 1.6, the correction procedure has brought the data from both transducers at both scales into a common functional dependence on relative wave height H/d. The normalized quantity $b/d = (U_d t_r - a)/d$ appears to be

independent of geometric scale, indicating that peak pressure phenomena as well as slowly-varying pressure P_1 (as shown in Section 6.5) and wave front celerity U_d (as shown in Section 6.4) exhibit similarity between scales. (In Figures 6.63 for $x/d = 2.4$, 3.2, and 3.9, the agreement between sets of data is not as good; this is perhaps to be expected, since for larger values of x/d, the standard deviation in t_r is greater, as shown in Figure 6.60.) A curve (labeled "logarithmic correction" in the legend) is fitted to the plotted values of b/d in the right-hand column of Figures 6.63 for each of the seven values of x/d used: 0.2, 0.4, 0.8, 1.6, 2.4, 3.2, and 3.9. Values of b/d obtained from each curve for several values of H/d are tabulated, to correspond to the pairs of values of $P_{2_r}/\gamma d$ already tabulated.

Therefore, at each value of x/d, for each value of H/d, there is tabulated a pair of values $(P_{2_r}/\gamma d)_M$ and $(P_{2_r}/\gamma d)_m$, where the subscripts $(\,)_M$ and $(\,)_m$ refer to the scales represented by $d = 1.25$ ft and $d = 0.64$ ft, respectively; there is also a value b/d, common to both scales. It is now possible to compute the quantity Γ' for all values of x/d and H/d by reference to Equations 5.25 and 5.26:

$$\Gamma' = \frac{\log_{10}\left[\dfrac{(P_{2_r}/\gamma d)_M}{(P_{2_r}/\gamma d)_m}\right]}{\log_{10}\left[\dfrac{d_M}{d_m}\right]}, \qquad (6.12)$$

and the quantity β , by reference to Equation 5.28:

$$\beta = \log_{10}\left[\frac{b}{d}\,\frac{\sqrt{d_M d_m}}{a}\right]. \qquad (6.13)$$

When the values $d_M = 1.25$ ft, $d_m = 0.64$ ft, $a = 0.0052$ ft are substituted into Equation 6.13 the following relationship is obtained for β:

$$\beta = 2.188 + \log_{10}(b/d). \qquad (6.14)$$

The function Γ' is plotted against β in Figure 6.64 . From the assumption that the defect ratio R increases monotonically with b/a and approaches unity, one expects $\Gamma' = d(\log_{10}R)/d\left(\log_{10}(b/a)\right)$ to have the qualitative functional behavior shown schematically in Figure 5.6c.

The points plotted in Figure 6.64 do show a general decrease in Γ' with increasing β , but the functional dependence of Γ' on β is not too well defined. For β greater than 0.7, many values of Γ' are less than zero, not as predicted in Figure 5.6c. The scatter of points may be attributed in part to the deviation in peak pressure measurement, in part to inacurracy in fitting curves to the data in Figures 6.62 and 6.63, and in part to imperfect matching of values of x/d between scales (e.g. x/d = 0.216 at d = 1.25 ft is not precisely equal to x/d = 0.231 at d = 0.64 ft).

A curve having the general form shown in Figure 5.6c is fitted to the data in Figure 6.64. The function $\Gamma' = \Gamma'(\beta)$, defined by the curve, is then integrated numerically to give the function $\Gamma = \Gamma(\beta)$, using the integration condition that Γ approaches zero as Γ'

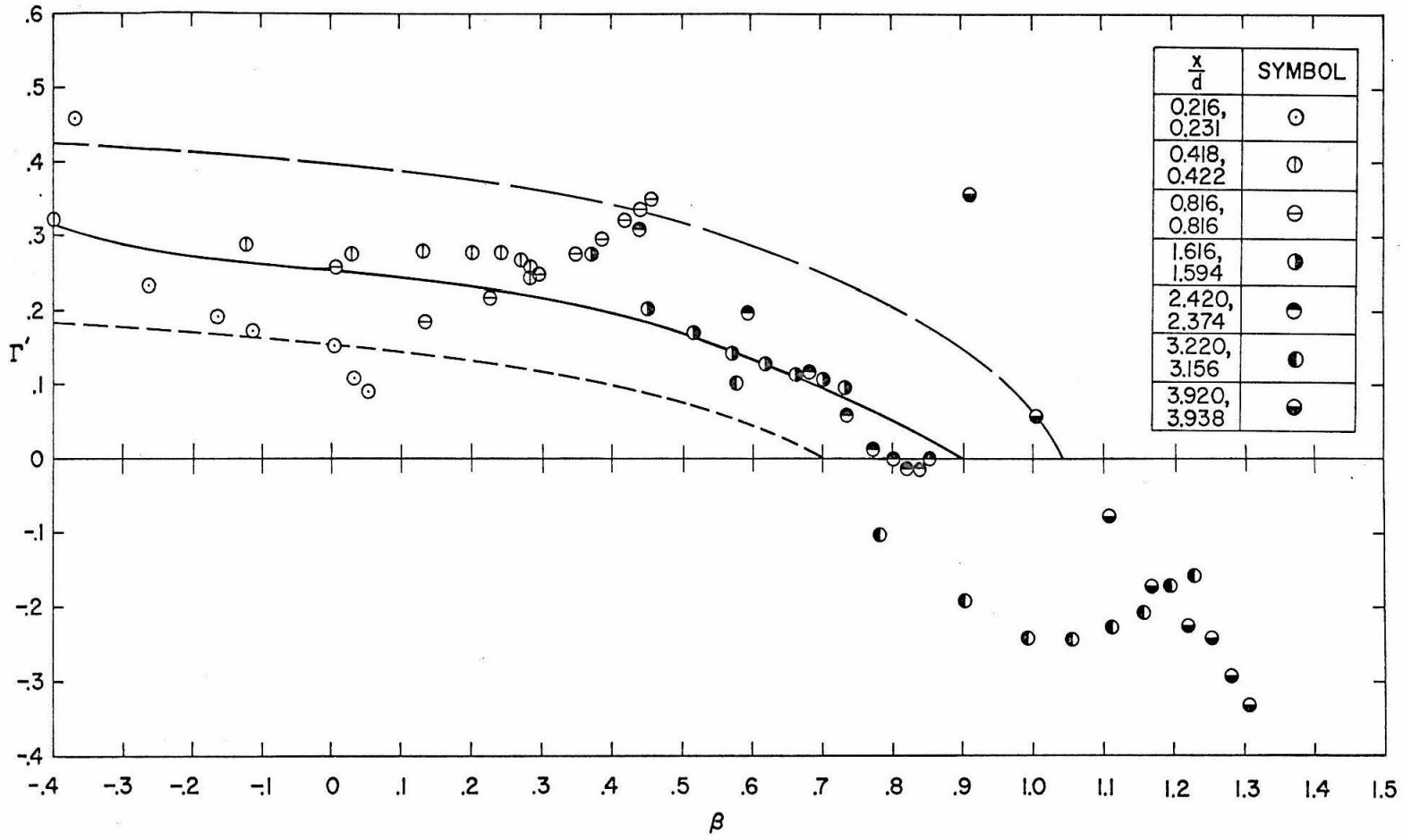

Figure 6.64. The function Γ' plotted as a function of β, used in the correction of recorded peak pressure.

approaches zero, as described in Section 5.3. The integrated function $\Gamma = \Gamma(\beta)$, shown by the solid curve in Figure 6.65, is the realized form of the function shown schematically in Figure 5.6b. Since $\Gamma = \log_{10} R$ and $\beta = \log_{10}(b/a)$, the next step is to map Γ and β into R and b/a, respectively. The function $R = R(b/a)$ thus derived is shown in Figure 6.66 in comparison with the expressions for R derived mathematically in Section 5.3 for several transducer models and several idealized input pressure functions.

To determine the importance of the deviation of plotted values of Γ' from the solid curve in Figure 6.64, two dashed curves are fitted to envelop most of the data in Figure 6.64. The dashed curves are similarly integrated numerically, as shown in Figure 6.66.

In Figure 6.66, the dashed curves indicate a range of values of the defect ratio R of from 0.35 to 0.85 for $b/a < 1$, of from 0.50 to 0.95 for $1 < b/a < 2$, of from 0.65 to 0.98 for $2 < b/a < 3$, and of from 0.75 to unity for $b/a > 3$. The fractional difference between the values of R indicated by the dashed curves and by the empirically derived function (the solid curve) is in approximate agreement with the mathematically derived function for any of the transducer models described in Table 5.1, for a triangular input pressure distribution. (For $b/a < 0.4$ the defect ratio is no longer empirically defined, because of a lack of data. However, in the present case R need not be defined for $b/a < 0.4$ since there are no values of $P_2/\gamma d$ to be corrected for which the corresponding value of b/a is less than 0.4.)

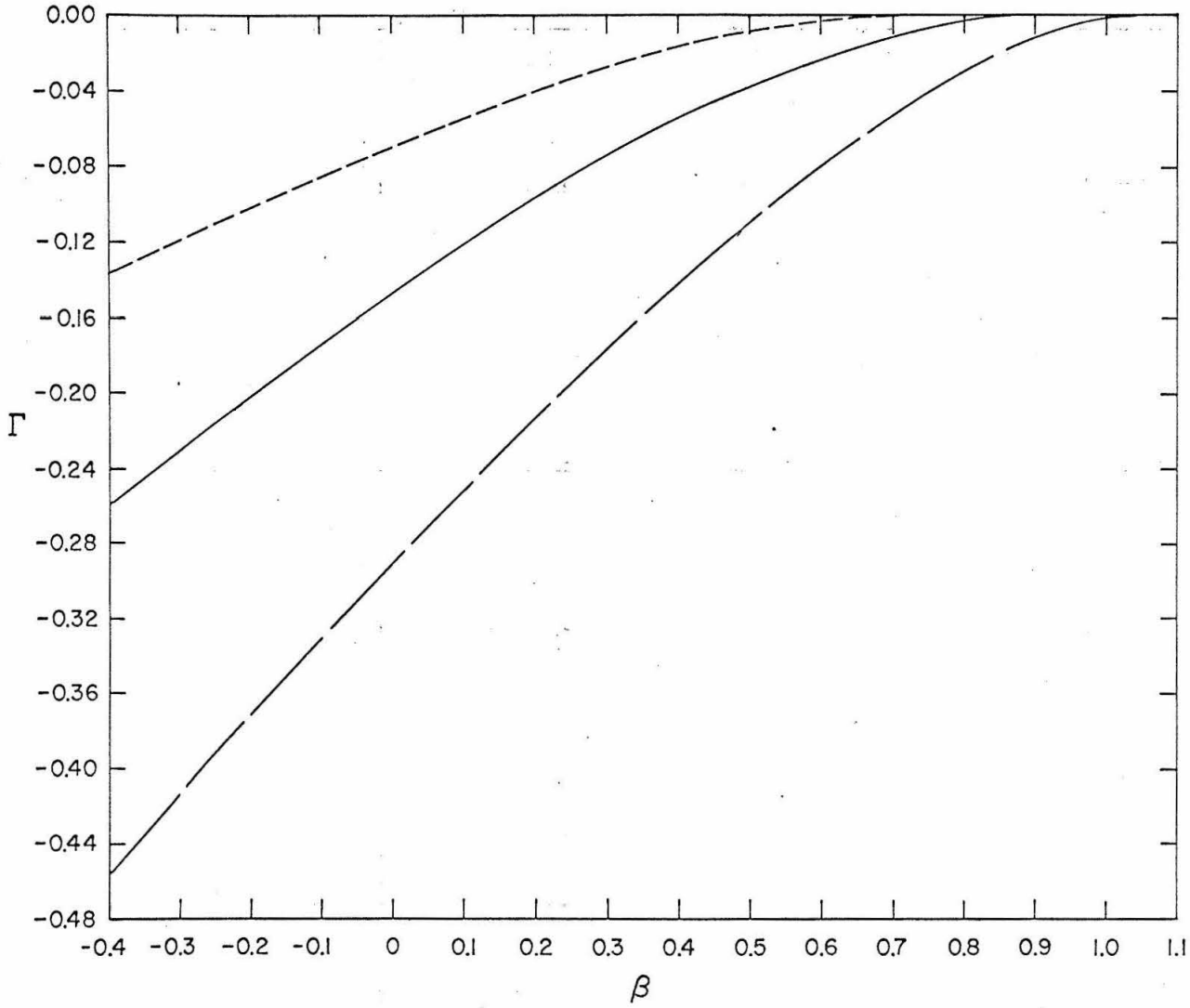

Figure 6.65. The function Γ plotted as a function of β, used in the correction of recorded peak pressure.

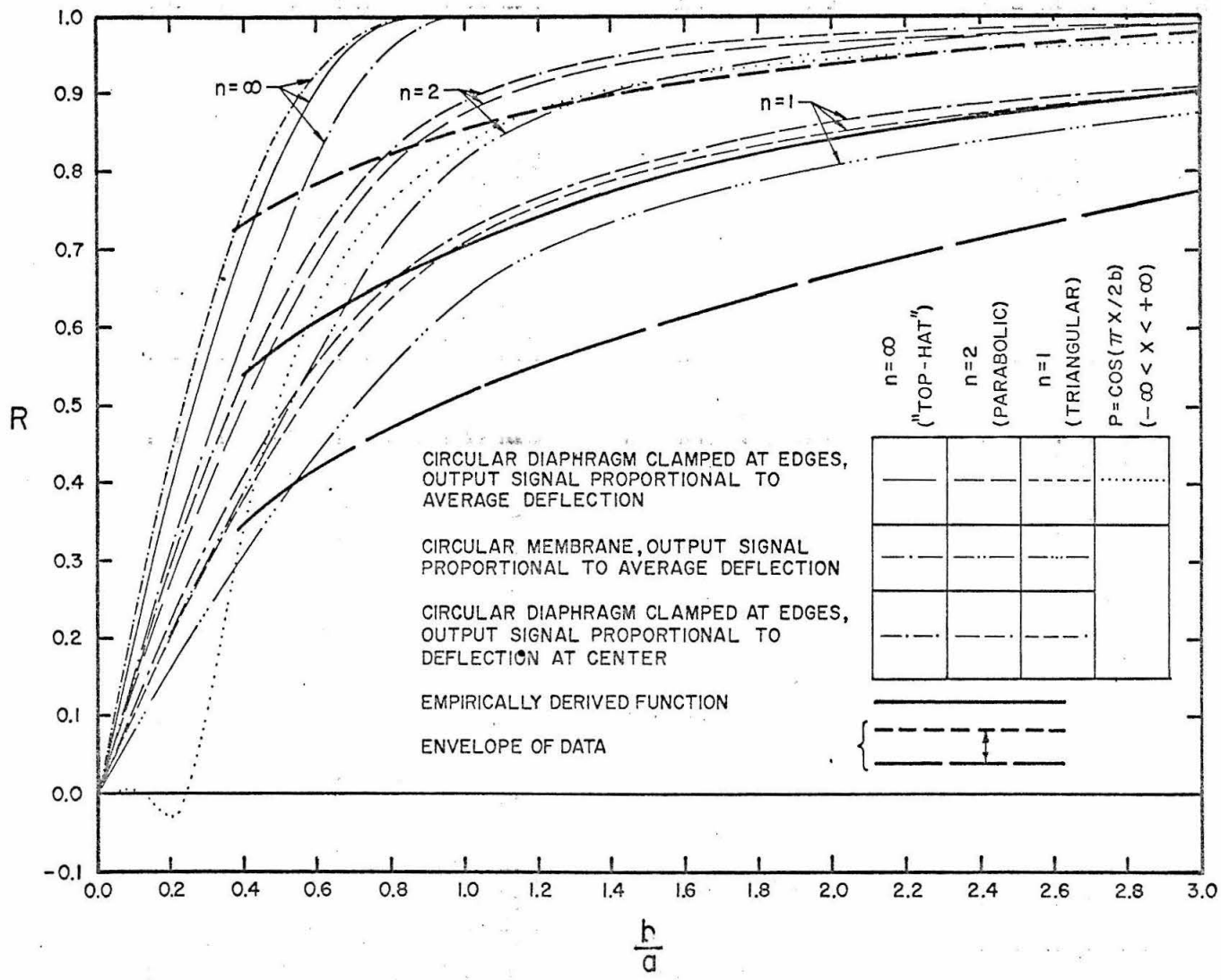

Figure 6.66. The empirically derived defect ratio R, a function of b/a, compared with mathematically derived values.

Each sample mean value of $P_2/\gamma d$ plotted in the left-hand column of Figure 6.62 is corrected by multiplication by $1/R$, where $R = R(b/a)$ is the empirically derived function in Figure 6.66 using the appropriate value of b/a obtained from the product of the ratio a/d of transducer radius to still-water depth and the corresponding value of b/a presented in the right-hand and portion of Figures 6.63. (Exceptions are values of $P_2/\gamma d$ at $x/d = 5.51$, which cannot be corrected because no rise-time data were obtained; hence no values of b are available for $x/d = 5.51$.) The corrected values of $P_2/\gamma d$ are then plotted in the right-hand portion of Figures 6.62. It was stated in Section 5.3 that two values of $P_{2_r}/\gamma d$ obtained for similar experimental conditions at the two model scales, after each value had been corrected, should yield the same value of $P_{2_{ac}}/\gamma d$, as indicated by Equation 5.18. For those values of x/d (0.2, 0.4, 0.8, 1.6, 2.4, 3.2, and 3.9) where data from the two scales may be compared, the corrected values in the right-hand column of Figures 6.63 indeed exhibit generally better agreement between scales than do the uncorrected values in the lef-hand column; for $x/d = 0.816$, the corrected values show an agreement between scales that is as good as that shown for slowly- varying pressure $P_1/\gamma d$ in Figure 6.51.

In the right-hand portion of Figures 6.62 for peak pressure and Figures 6.63 for rise-time, for $x/d = 0.2$, 0.4, 0.8, 1.6, 2.4, 3.2, and 3.9, corrected values obtained by the direct extrapolation procedure suggested by the work of Willmarth and Roos (1965) are also included

(dotted curves). In the direct extrapolation procedure, values of $P_2/\gamma d$ or $U_d t_r/d$ obtained with one or both transducers at the two model scales are obtained at a common value of relative wave height H/d from the curves fitted to the uncorrected data in the left-hand columns of Figures 6.62 or 6.63. Each set of values obtained at a common H/d is plotted against a/d, as shown in Figure 6.67, where a is the transducer radius and d is the still water depth. (Any other indicator of scale size, such as s, x, H, or b, could be used in place of d.) Graphs so plotted show the influence of relative transducer size a/d on the measured value of $P_2/\gamma d$ or $U_d t_r/d$. A straight line is fitted to the data points and extended to the ordinate axis, where $a/d = 0$, where the ordinate value provides an estimate of the output of an ideal, infinitesimal transducer.

In Figures 6.62 for $x/d = 0.2$, 0.4, and 0.8, values of $P_2/\gamma d$ corrected by direct extrapolation are 10% to 20% lower than those obtained by logarithmic extrapolation. For $x/d = 1.6$, 2.4, 3.2, and 3.9, there is fair agreement between values obtained by direct and logarithmic extrapolation. In Figures 6.63 for $x/d = 0.2$, 0.4, and 0.8, values of $U_d t_r/d$ corrected by direct extrapolation are in very good agreement with values obtained from the application of Equation 5.16. For $x/d = 1.6$, 2.4, 3.2, and 3.9, there is poor agreement between values obtained by direct extrapolation and by Equation 5.16, possibly because the disparity of the uncorrected data between scales is due to the large standard deviation shown for those values of x/d in Figures 6.60, hence high standard deviation in the

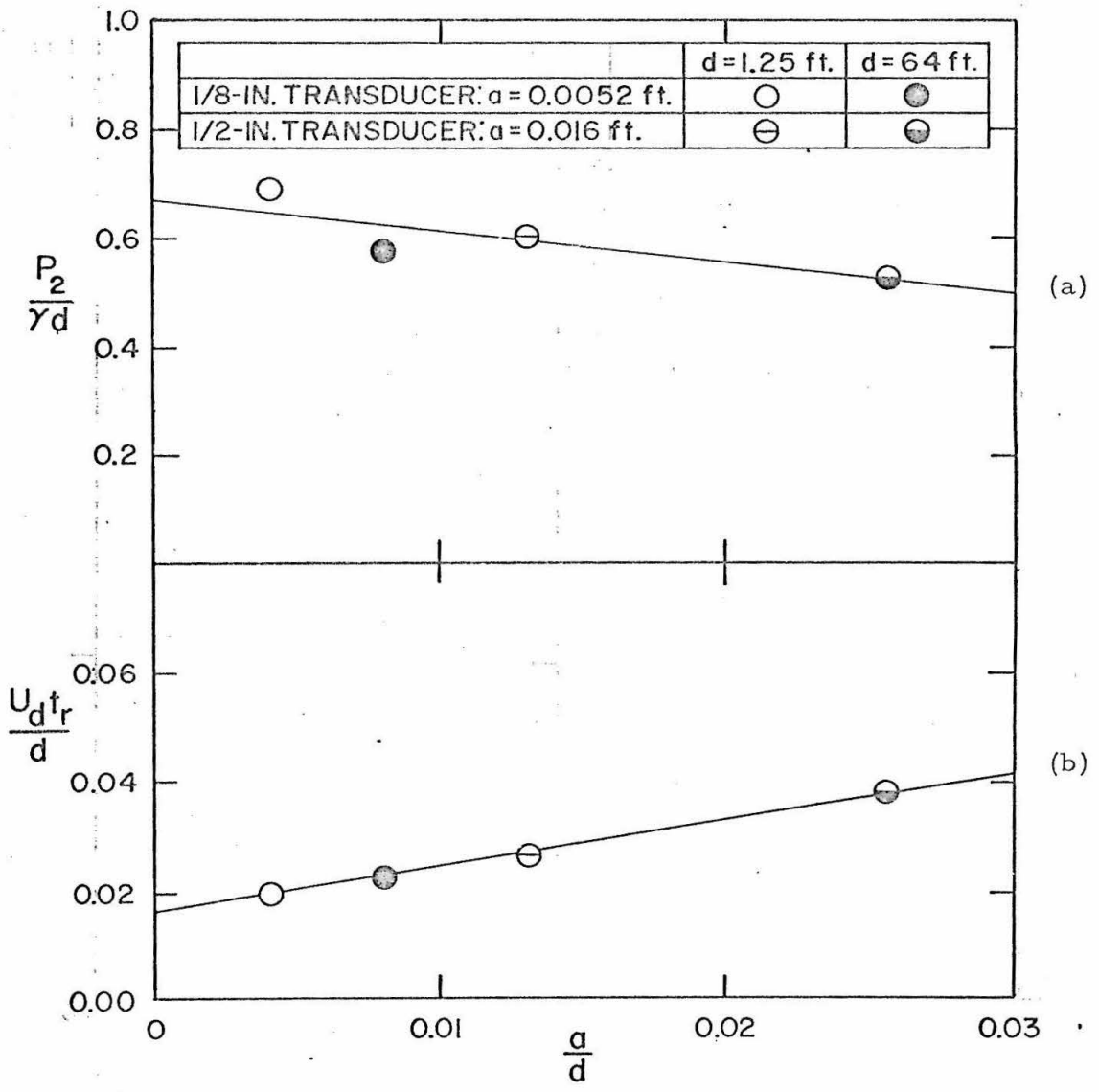

Figure 6.67. Two examples of direct extrapolation: (a) for peak pressure; (b) for rise-time. ($x/d = 0.816$, $s/d = 0.2$, $H/d = 0.32$.)

mean, rather than due to scale effects. The relative advantage of the logarithmic extrapolation procedure is that it involves a reasoned derivation of a correction function, which, once obtained, may be applied to any single peak pressure value, as long as the corresponding value of the argument b/a of the defect function R is known. For instance, it has been possible to correct all peak pressures presented in the left-hand portion of Figures 6.62 by the logarithmic procedure (except at $x/d = 5.51$, where b/a was not available), despite the fact that for only seven of the 14 values of x/d represented could data from similar experiments at two scales be compared.

The advantage of the direct extrapolation procedure is its simplicity. The disadvantages are that there is no appeal to analysis of the phenomena causing the defect; and that whereas the logarithmically derived correction function $R = R(b/a)$ is determined from many contributing pairs of peak pressure values, each direct extrapolation is subject to a set of at most four values. In Figures 6.63, for $x/d = 0.118$, 1.216, 2.016, etc., where values are not generated under similar geometric conditions at two (or more) model scales, no correction by direct extrapolation is possible; and for those values of x/d where values at two or more scales are available for comparison, random fluctuations in the values may cause unstably magnified fluctuations in the corrected value.

From the earlier discussion of the assumptions upon which the logarithmic correction procedure is based, from the presentation and discussion of Figure 6.64, and from the foregoing discussion of the

direct extrapolation procedure, it is apparent that the most serious obstacle to meaningful interpretation and correction of the data is the magnitude of the variations in measured peak. For both the logarithmic and the direct correction procedures, the large standard deviation within a sample of experimental values made it difficult to obtain meaningful mean values of peak pressure and rise-time. Within any single record, random fluctations rendered the reduction of peak pressure and rise—time data much more liable to human judgment than one would prefer. For the logarithmic procedure in particular, the superposition on the pressure record of random fluctuations due to spume and entrained air renders partially invalid the assumptions in Section 5.3 that the pressure distribution is a traveling wave of a form which is similar for all values of x/d, H/d, and s/d.

Because of the problem of fluctuations, and because of the general inconvenience of having to perform and establish confidence in a correction procedure, it is obviously well to avoid the necessity of correction. In Figure 6.66 the empirically derived defect function indicates that for b/a greater than 3, there may be less than 10% loss in measured peak pressure due to defect; it may therefore be established that to avoid transducer defect and the necessity of correction, one must use transducers of sufficiently small size so that the ratio b/a may be greater than 3, where b is half the characteristic length or width of the distribution being measure, and a is the transducer radius.

Yet in the present study there are many instances where b/a is less than 3; and with respect to these cases, the writer believes

that despite the uncertainties introduced by the pressure fluctuations and by the uncertain role of surface tension in scale effects mentioned earlier, application of the derived correction function $R = R(b/a)$ provides the best means at present available for estimating the mean values of actual peak pressure amplitude and rise-time. (It is also suggested that despite practical difficulties in application encountered in the present study, the correction procedure per se may remain of general interest.) In the following presentation and discussion of peak pressure data, the corrected values are those that are discussed. In most instances the uncorrected data are presented as well, however, so that results of the study may be studied independently of the correction procedure.

6.6.3 Functional behavior of peak pressure and rise-time.

Figures 6.62 presented in Subsection 6.6.2 in connection with the correction procedure indicate that normalized peak pressure $P_2/\gamma d$ increases with relative wave height H/d. The rate of increase of peak pressure head with wave height, $d(P_2/\gamma)/dH$, is approximately $1/4$ for all values of relative location x/d and both values of relative soffit clearance examined, $s/d = 0.2$ and $s/d = 0.1$.

Figures 6.63 indicate that for $x/d \leq 1.216$, for both $s/d = 0.2$ and $s/d = 0.1$, the normalized rise time $U_d t_r/d$ (or the normalized rise-length b/d) has practically no dependence on relative wave height H/d. For greater values of x/d, there is an increase of $U_d t_r/d$ with H/d. As noted in Subsection 6.6.2, there is also a marked increase in scatter, i.e. a lack of a common functional

pattern among the plotted points, for x/d greater than two at s/d = 0.2. However, for x/d = 4.525 at s/d = 0.1, the data appear to lie on a common curve. This observation as to the presence of scatter will be referred to later in this subsection.

Figures 6.68 show the dependence of peak pressure on relative location x/d and on relative soffit clearance s/d. Uncorrected mean values of peak pressure head P_2/γ, normalized with respect to the mean wave height H, are plotted against x/d in Figure 6.68a; corrected values of $P_2/\gamma H$ are presented in Figure 6.68b. (At any given x/d, values of $P_2/\gamma H$ representing all values of H/d are plotted undifferentiated, giving a multiplicity of values not due to scatter but due to an inconstancy of the ratio $P_2/\gamma H$ for different values of H/d.) In Figure 6.68a, for s/d = 0.2, data from the two transducers operating at both model scales are represented; for s/d = 0.1, only data from the 1/8-in. transducer are available. For s/d = 0.2, the data have been enveloped by solid curves; for s/d = 0.1, the data have been enveloped by dashed curves. The data for s/d = 0.2 show an initial increase of $P_2/\gamma H$ with increasing x/d, with a maximum attained at approximately x/d = 1.2. The data thereafter show a decrease with increasing x/d. The data for s/d = 0.1 are insufficient to indicate a detailed functional relationship, but also suggest an increase of $P_2/\gamma H$ with x/d. For both s/d = 0.2 and 0.1, the trend of $P_2/\gamma H$ with x/d is reminiscent of that of $U_d\sqrt{gd}$ with x/d, shown in Figures 6.27 and 6.28.

As shown in Subsection 6.6.1, the ratio of standard deviation to

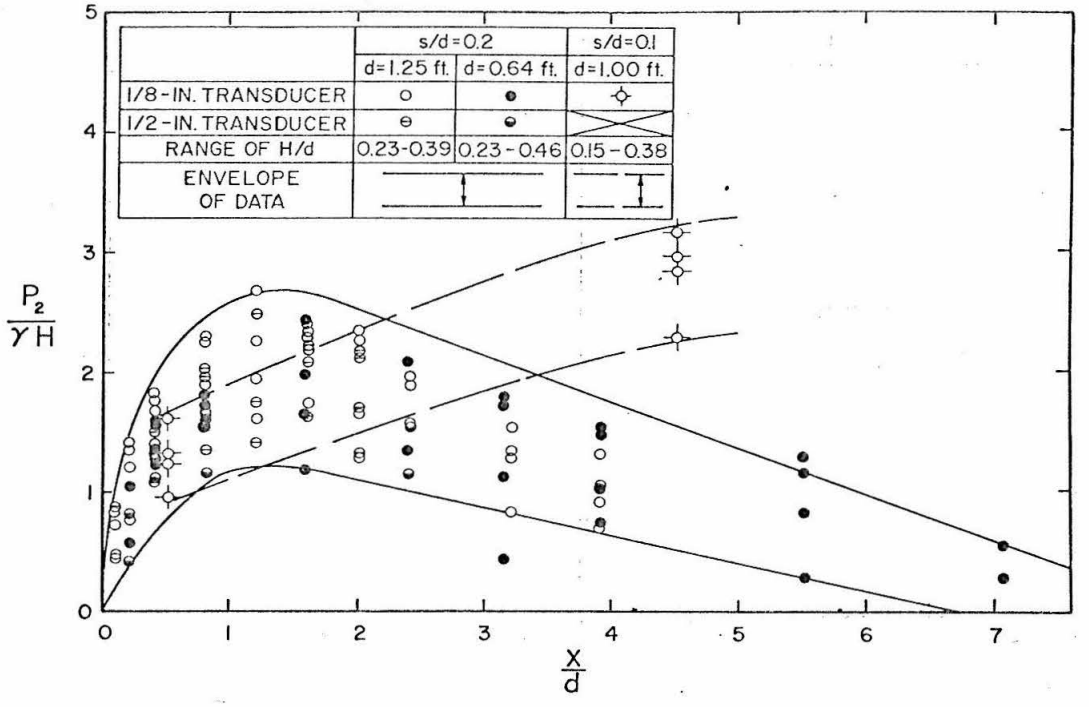

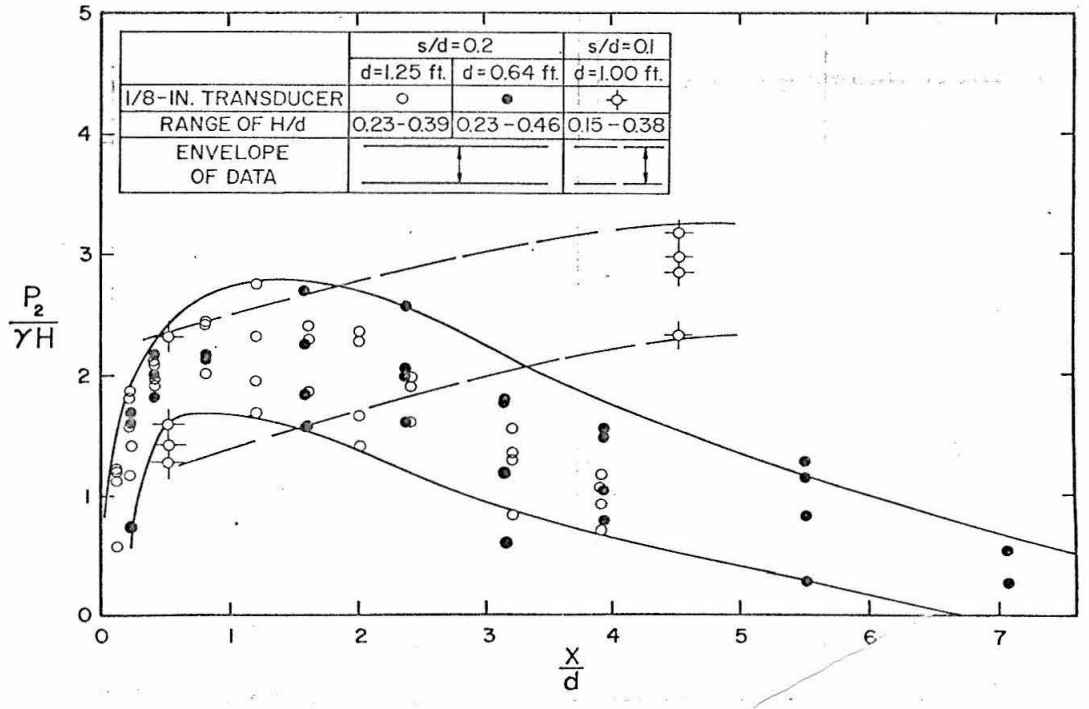

Figure 6.68. Normalized peak pressure $P_2/\gamma H$ plotted as a function of x/d. (a) Uncorrected mean values; (b) corrected values.

mean peak pressure generally did not exceed 0.25. According to the theory of normal distributions (Parratt, 1961, p.174), if a quantity is normally distributed about a mean m, with a standard deviation S, there is 98% probability that a single measurement will provide a value less than $m + 2S$. For a value of $S_p / \overline{P}_2 \leq 0.25$ as indicated by Figure 6.58, and for a maximum value $P_2/\gamma H = 3.1$ indicated in Figure 6.68b, there is therefore at least 98% probability that individual values of $P_2/\gamma H$ will be less than $3.1\ (1 + 2(0.25)) = 4.7$; i.e. there is at most 2% probability that the peak pressure head P_2/γ due to a wave will be greater than 4.7 times the incident wave height H, for the conditions of the present study.

In Figure 6.68b, data obtained with the 1/2-in. transducer do not appear, since only data obtained with the 1/8-in. transducer were corrected by the logarithmic procedure. Again the data for $s/d = 0.2$ are enveloped by solid curves, and the data for $s/d = 0.1$ are enveloped by dashed curves. There is little apparent difference between Figures 6.68a and 6.68b for the range $x/d > 1$. For $x/d < 1$, the data in Figure 6.68b indicate higher values of $P_2/\gamma H$ than in Figure 6.68a, and there is better agreement among data from the two model scales. As in Figure 6.68a, the data for $s/d = 0.2$ attain a maximum at approximately $x/d = 1.2$, whereas from the data for $s/d = 0.1$ one may only infer an increase in $P_2/\gamma H$ with increasing x/d. For $s/d = 0.2$, the maximum value indicated is $P_2/\gamma H = 2.75$; for $s/d = 0.1$ the maximum value obtained is $P_2/\gamma H = 3.17$, with the indication that greater values could be obtained at larger x/d.

In Figures 6.69, 6.70, and 6.71, the corrected peak-pressure data obtained in the present study are compared with peak pressures obtained by El Ghamry (1963) and Wang (1967). However, as mentioned in Section 6.5, it should be remembered that experimental conditions used by El Ghamry and by Wang differed from those used in the present study, and differed from each other.

As described in Section 2.3, El Ghamry studied the case in which periodic progressive waves in a wave tank 1 ft. wide by 3 ft. deep struck a 4-ft horizontal platform. The platform, which had no vertical front face, extended nearly the width of the wave tank, but with a gap between the tank walls and the edge of the platform. Pressure transducers were mounted at relative distances $x/d = 1$ and $x/d = 2$, where x was the distance from the seaward edge of the platform and d was the still water depth. Waves were generated at several wave lengths, but since it is reasoned that the wave of the greatest length is most comparable to a solitary wave, only the data generated at the greatest wave length (14.388 ft) has been included here for comparison. For tests conducted at this wavelength, the relative soffit clearance of the platform above still water level s/d ranged from 0 to 0.050, and the ratio of trough-to-crest wave height to still water depth ranged from 0.048 to 0.121. The still water depth was 2.00 ft. for all tests. The tank bottom was horizontal beneath the platform, for the data included here.

As explained in Section 6.5, it is deemed most consistent to consider El Ghamry's data in terms of wave height above still water

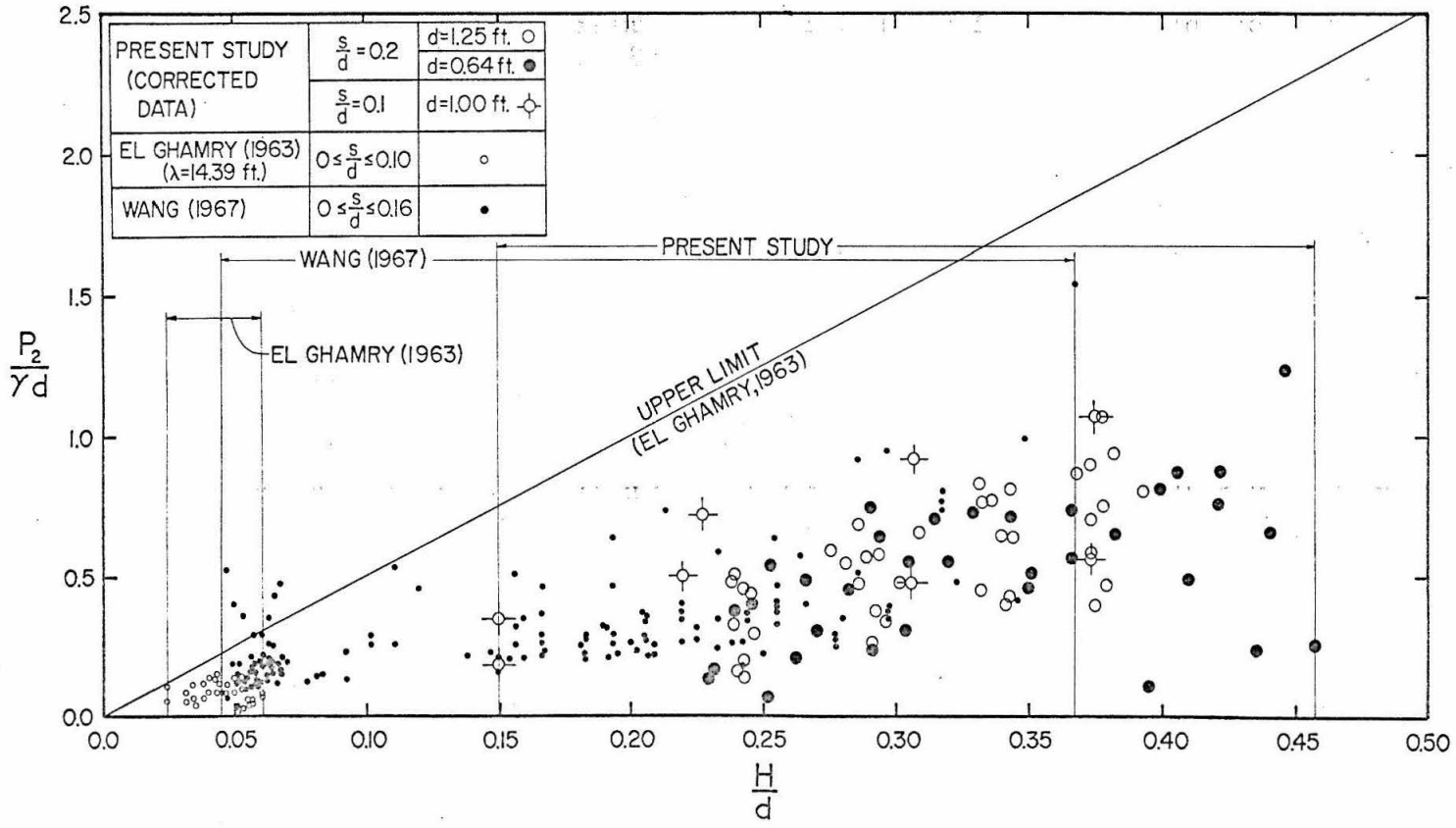

Figure 6.69. Normalized peak pressure $P_2/\gamma d$ plotted as a function of H/d, compared with values by El Ghamry (1963) and Wang (1967).

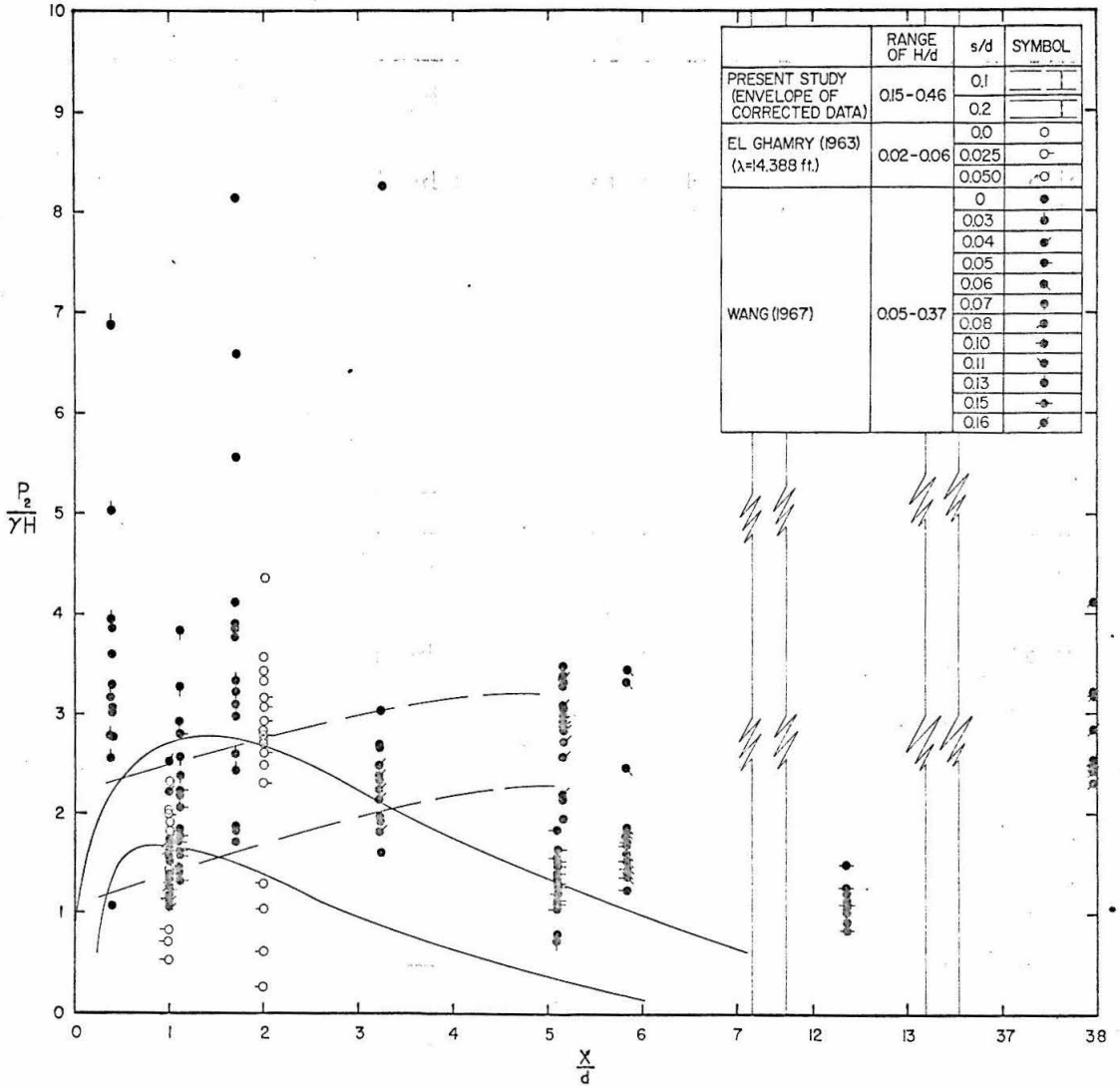

Figure 6.70. Normalized peak pressure $P_2/\gamma H$ plotted as a function of x/d, compared with values by El Ghamry (1963) and Wang (1967).

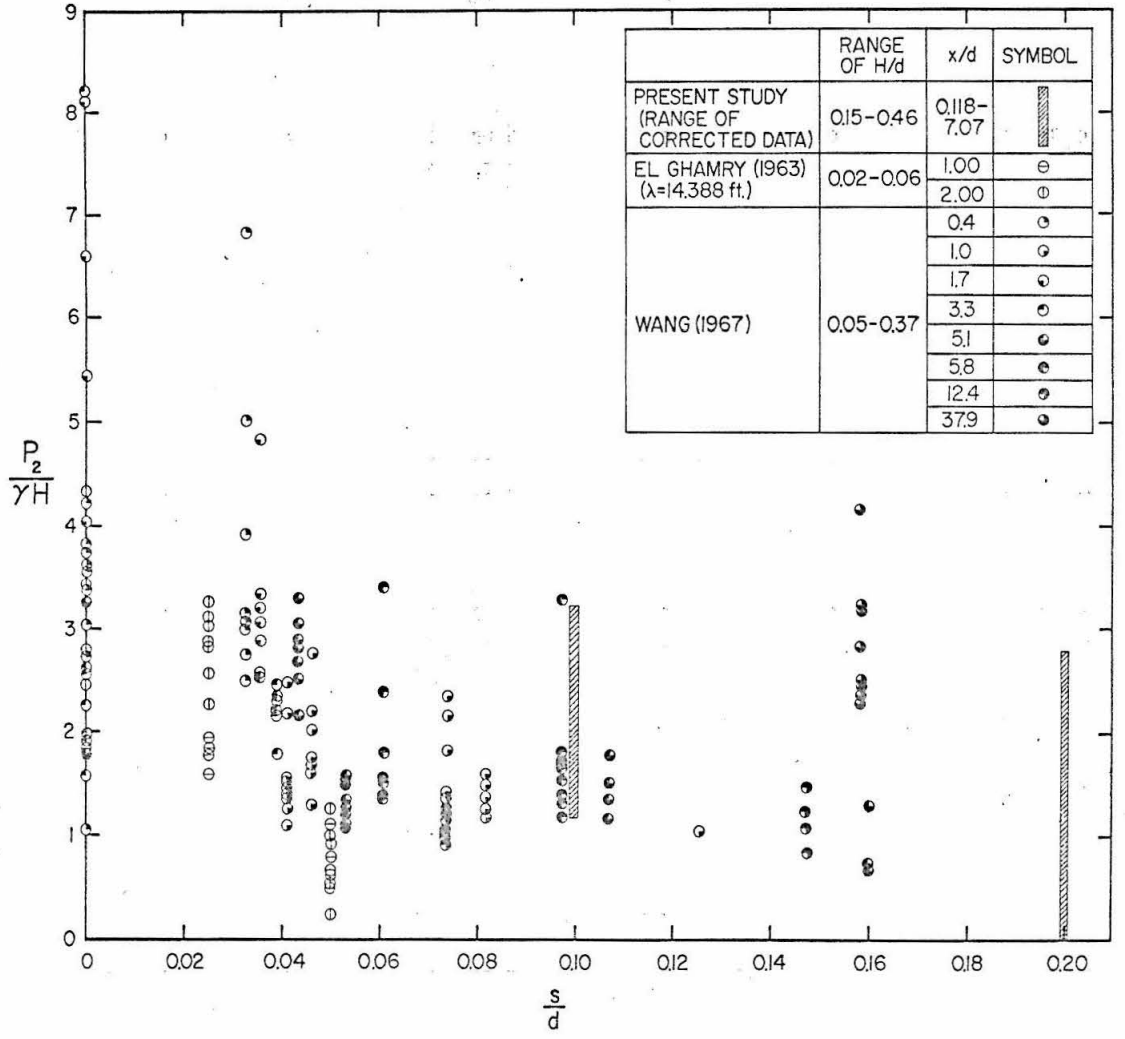

Figure 6.71. Normalized peak pressure $P_2/\gamma H$ plotted as a function of s/d, compared with values by El Ghamry (1963) and Wang (1967).

level, rather than of trough-to-crest wave height, as presented by El Ghamry. Defined in this way the wave height H above still water level is simply taken as one-half the trough-to-crest wave height. El Ghamry noted that peak pressure head never exceeded 2.5 times the trough-to-crest wave height; or in the terms of the present study, never exceeded 5 times the wave height above still water level.

Wang's (1967) experiments were performed on a model pier 1 ft wide and 6ft long located near a beach in a 92-ft. square wave basin. The pier, 1.5 inches thick, had no high vertical front face. The plunger-type generator produced a dispersive wave train, the leading wave of which was positive if the plunger was suddenly immersed, or negative if the plunger was suddenly withdrawn. Peak pressures and wave amplitudes generated by plunger withdrawal did not differ greatly from those generated by immersion; since most of the available data were for the case of withdrawal, data for the case of plunger immersion have not been included here. Only pressure generated by the first positive wave in the train of waves generated by plunger withdrawal have been included here for comparison. Pressures were measured at four transducer locations. Corresponding wave heights were measured with respect to still water level by wave gauges mounted alongside the pier at distances from the seaward edge equal to the distances of the transducers from the seaward edge. In the neighborhood of the pier, the bottom of the basin had a 1:14 slope for most tests. The still water depth d used in this discussion is the depth at the location of the transducer. (The depth at the

seaward end of the pier ranged from 8.2 in. to 30 in.) The relative distance x/d of the pressure transducers from the seaward edge ranged from 0.2 to 37.9; the relative clearance s/d of the soffit above still water level ranged from 0.0 to 0.16; and the relative wave height H/d ranged from 0.045 to 0.37.

El Ghamry's (1963) and Wang's (1967) experimental conditions thus differ in several ways from the conditions of the present study, in which a solitary wave in a 1.25-ft. wide wave tank with a horizontal bottom struck a horizontal platform with a high vertical front, with no clearance between the side walls and the platform; where for most tests $s/d = 0.2$, for a few tests $s/d = 0.1$ and $s/d = 0.0$; where H/d ranged from 0.15 to 0.46. Furthermore, the values presented in this subsection are mean values of data from five, six, or more similar experiments, corrected for transducer area defect, whereas values presented for El Ghamry and Wang are data from individual experiments.

In Figure 6.69, the peak pressure head P_2/γ, normalized with respect to the still water depth d, is plotted as a function of H/d, where H is the elevation of the wave crest measured with respect to the still water level. The El Ghamry and Wang data, together with data from the present study, indicate a general increase in peak pressure with wave height. El Ghamry's upper limit of P_2/γ less than or equal to 2.5 times the trough-to-crest wave height, or five times the height H above still water level, is exceeded by Wang's data in only a few instances, and is never exceeded by data from the present study. Furthermore, as explained in the discussion of Figures 6.68,

experiments indicate a probability of at least 98% that pressure head P_2/γ will not exceed 4.7, or approximately 5, times the wave height H.

Figure 6.70 shows the peak pressure head P_2/γ, this time normalized with respect to the wave height H, plotted as a function of relative distance x/d from the seaward end of the platform. Data from the present study are represented by the curves enveloping the range of data shown in Figure 6.68b. For all three studies, values of $P_2/\gamma H$ are less than 8.25, with all but a few values less than 5.0.

For the present study, the functional dependence of $P_2/\gamma H$ upon x/d has already been discussed. El Ghamry's data for s/d = 0.0 and s/d = 0.025 show an increase of $P_2/\gamma H$ with x/d, and a decrease with x/d for s/d = 0.050; yet since there are only two values of x/d, one cannot confidently discern a functional dependence of $P_2/\gamma H$ on x/d. Wang's data show no discernible dependence of $P_2/\gamma H$ on x/d, for any value of s/d. It may be that for Wang's study $P_2/\gamma H$ simply does not depend significantly on x/d because of the experimental conditions, which as stated earlier were considerably different from those of the present study; or it may be that due to the large deviation inherent in peak pressure measurements it is more difficult to detect functional trends from individual plotted data as provided by Wang than it is from data averaged from several similar experiments, as in present study.

Figure 6.71 shows the peak pressure head P_2/γ, again normalized with respect to the wave height H, plotted as a function of

relative soffit clearance s/d. For the data of El Ghamry which is presented in Figure 6.71, s/d ranges from 0.0 to 0.05; for the data of Wang, s/d ranges from 0.0 to 0.16. For $s/d = 0.1$ and 0.2, the range of corrected data from the present study are indicated. All three sets of data show a consistent trend indicating a general decrease of $P_2/\gamma H$ with increasing s/d. It may be noted that such a trend is predicted analytically in Equation 3.61: $P_2/\rho = \frac{1}{2}U_d^2 - gs$. For constant wave height H, the wave front celerity U_d in Equation 3.34 is inversely proportional to s/d, indicating a decrease in U_d (hence in $\frac{1}{2}U_d^2$) with increasing s/d. Furthermore, the second term $(-gs)$ on the right-hand side of Equation 3.61 acts directly to reduce P_2 as s increases. However, it should be remembered that the analysis as developed in this study is not necessarily applicable for experimental conditions such as used by El Ghamry or Wang. While Equation 3.61 per se may be considered applicable to conditions other than those of the present study, Equation 3.34 for U_d is restricted to the conditions of the present study. No attempt has been made to predict the wave front celerity U_d for the conditions of El Ghamry's or of Wang's study, nor was U_d measured in those studies.

Figures 6.69, 6.70, and 6.71 show that despite the differences in ranges of H/d and s/d, and the differences in experimental conditions, there is fair agreement among the El Ghamry study, the Wang study, and the present study as to the order of magnitude of $P_2/\gamma H$, the ratio of peak pressure head to incident wave height above still water level. El Ghamry's upper limit of $P_2/\gamma H \leq 5$ stands for

all measured data in the present study and for nearly all of Wang's data. The value of $P_2/\gamma H \leq 5$ is one to two orders of magnitude less than the ratios of impact pressure head to wave height due to waves breaking against vertical walls, as reported by Denny (1951), Ross (1954), or Garcia (1968). It is true that neither El Ghamry nor Wang considered the problem of transducer area defect, but as shown in the present study, neglect of area defect introduces error of the order of perhaps 50%, and hence does not affect an order-or-magnitude comparison of data values.

In Figures 6.72, the peak pressure data of the present study is compared with the values predicted in Equation 3.61. As the ordinate, the pressure head P_2/γ is normalized with respect to $(U_d^2/2g - s)$, where U_d is the local wave front celerity, g is the gravitational acceleration, and s is the soffit clearance. The abscissa is the relative distance x/d. The analytical value of $P_2/\gamma(U_d^2/2g - s)$, as expressed by Equation 6.1, is unity. Figure 6.72 a shows uncorrected sample means values; Figure 6.72b shows corrected values.

For $s/d = 0.2$, the corrected values shown in Figure 6.72b appear to be independent of x/d, for x/d less than 2, for the most part having values greater than 0.45 and less than 0.80. For x/d greater than 2, the values of $P_2/\gamma(U_d^2/2g-s)$ tend to decrease with x/d; this tendency will be discussed further following presentation of Figures 6.73. For $s/d = 0.1$, the values are approximately 0.4 at both values of x/d tested. It is not understood why values at

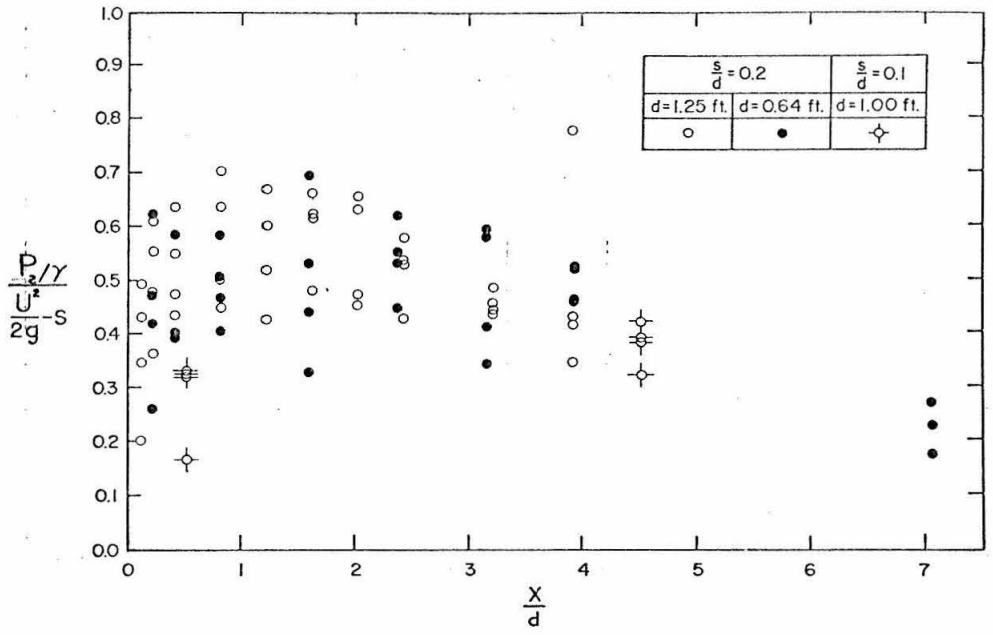

(a)

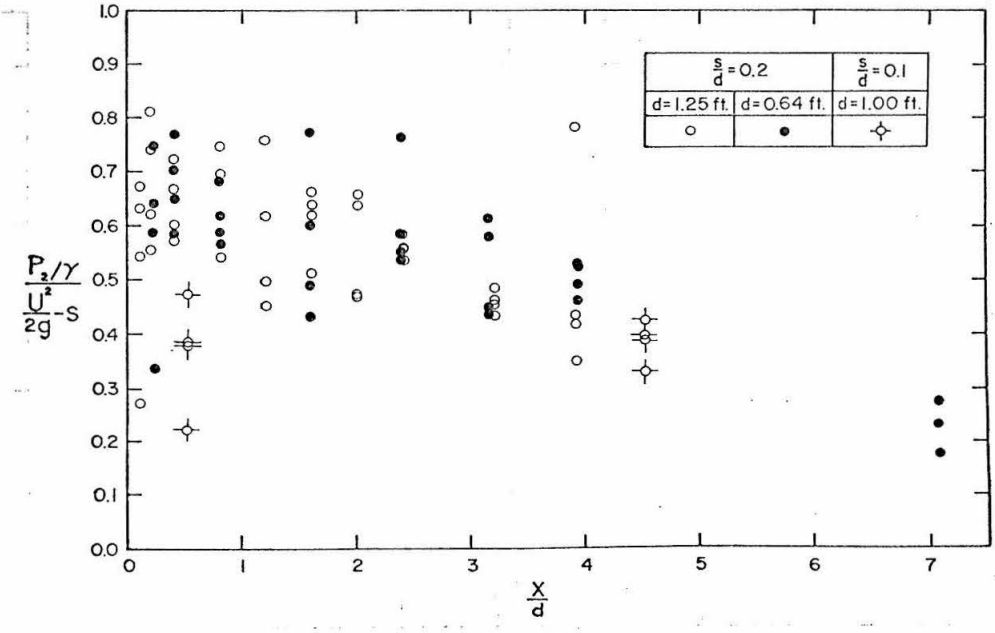

(b)

Figures 6.72. The ratio P_2/γ $(U_d^2/2g - s)$ plotted as a function of x/d. (a) Uncorrected mean values; (b) corrected values. (Range of H/d is 0.15 to 0.46.)

$s/d = 0.1$ should be generally less than the values at $s/d = 0.2$. The variety of values at a given value x/d reflects a tendency for $P_2/\gamma(U_d^2/2\,g\text{-}s)$ to increase with relative wave height H/d.

The assumptions underlying the derivation of Equation 3.61 were:

1. that the acceleration term $K\,d\,U_d/d_t$ in Equation 3.60 (or more generally, the term $\int_{x_2}^{x_3} du/dt\,dx$ in Equation 3.59) may be neglected;

2. that the form of the free surface in the neighborhood of the wave front remains approximately constant, although the wave celerity may change with time;

3. that the effect of surface tension, air entrainment, and boundary shear stress are negligible.

As for the first assumption, Figures 6.27 show that dU_d/dx, hence $dU_d/dt = U_d(dU_d/dx)$, is greatest for small x_d/d, and equal to zero at a relative location x_d/d approximately equal to 2, for all values of H/d shown. Since the coefficient K in Equation 3.60 is positive (for $\eta > 0$, as in the flow near the wave front), a positive contribution to peak pressure by the term $K\,dU_d/dt$ might be expected for small x_d/d, with no contribution at x_d/d approximately equal to 2. Hence if the term $K\,dU_d/dt$ is significant, values of $P_2/\gamma(U_d^2/2\,g\text{-}s)$ will be greater at small values of x_d/d than at $x_d/d = 2$. However, in Figure 6.72b, corrected values at small x_d/d are approximately equal to values at $x_d/d = 2$; and in Figure 6.72a, the uncorrected values of $P_2/\gamma(U_d^2/2g\text{-}s)$ are less, rather

than greater, at small x_d/d than at $x_d/d = 2$. It therefore appears that neglecting the acceleration term $K\, dU_d/dt$ Equation 3.61 does not introduce significant error.

As noted previously, the photographs presented in Figures 6.13 through 6.17 in Section 6.2 indicate little change in the form of the free surface near the wave front, except an increase with distance of spume thrown forward and of air entrained. The spume and entrained air do not affect the validity of the second assumption, which, since no change in surface profile is observed, apparently introduces little error into the analysis.

The entrained air, however, may affect the third assumption. As explained in Section 3.3, entrained air effectively reduces the average density of the fluid, and thereby reduces hydrodynamic pressure on the boundary. As described in Section 3.3, viscosity and surface tension may indirectly reduce peak pressure also by inhibiting the formation of the thin jet postulated for ideal flow. Thus, assuming that the procedure to correct transducer area defect has provided correct values of measured peak pressure, the difference between actual peak pressure and the value predicted in Equation 3.61 may be attributed to real fluid effects through the mechanisms described in Section 3.3.

The data from the present study have not been compared with values predicted by the analysis of Wang (1967) (see Section 2.3), because that analysis incorporates the vertical fluid velocity in the wave, and no suitable expression for the vertical fluid velocity was

obtained in the present study. Furthermore, while Wang's is derived from an analysis by von Karman (1929) for the transient total force on an obtuse wedge penetrating the water surface, the writer believes that the maximum of a pressure distribution cannot validly be derived from an analysis which is intended only to predict a total force, or an average pressure, over the entire surface, rather than the maximum value at one location.

It may be noted that peak pressure data for zero soffit clearance ($s/d = 0$) were obtained by El Ghamry (1963) and Wang (1967), but that in the present study no peak pressure was ever observed, as noted in Section 6.3. Peak pressure is associated with a wave front propagating into an empty or air-filled space, and for wave conditions where there are troughs in which the water level is less than still water level, the propagation of a trough beneath the platform will provide the condition for the generation of peak pressure with the advent of the next wave crest, even though the platform soffit is at the still water level. For the periodic progressive waves used by El Ghamry, and for wave trains used by Wang whose leading wave was negative, peak pressures could therefore be obtained even for zero soffit clearance. For solitary waves as used in the present study, no trough precedes the single positive wave, and there is thus no peak pressure for zero soffit clearance. (For wave trains in which the leading wave was positive, Wang, too, observed no peak pressure for the leading wave for zero soffit clearance.)

Figures 6.73 show the dependence of rise-time and rise length on relative location x/d. Figure 6.72a shows the uncorrected rise-time t_r, normalized by multiplication by $\sqrt{g/H}$, plotted as a function of relative distance x/d. For s/d = 0.2, data from the two transducers at the two model scales are included. The data obtained for s/d = 0.1, which are also included, are in functional agreement with the data for s/d = 0.2. The trend shown by the data indicates an increase in $t_r\sqrt{g/H}$ with x/d, with a marked increase in some values for x/d > 2.

Corrected values of $t_r\sqrt{g/H}$ plotted against x/d are presented in Figure 6.73b. Again, data from both transducers and both model scales, where available, have been included. Compared to Figure 6.73a, there is much better agreement between model scales and between transducers, corresponding to the improved agreement (for x/d < 2) provided by the correction procedure shown in Figures 6.63. Also shown is a range of rise-time values derived using a method proposed by Wang (1967), that the total duration of the pressure peak in milliseconds is 15 to 40 times the square root of the incident wave height measured in feet. If the rise-time t_r is taken as half the pressure peak duration, the proposed range, when normalized becomes:

$$0.043 < t_r \sqrt{g/H} < 0.114.$$

Many of the rise-time data from the present study fall within Wang's proposed range, but for values of x/d less than 2, the rise-times are less than indicated by the range, and for s/d greater than 3, there are several values of rise-time greater than indicated by the range.

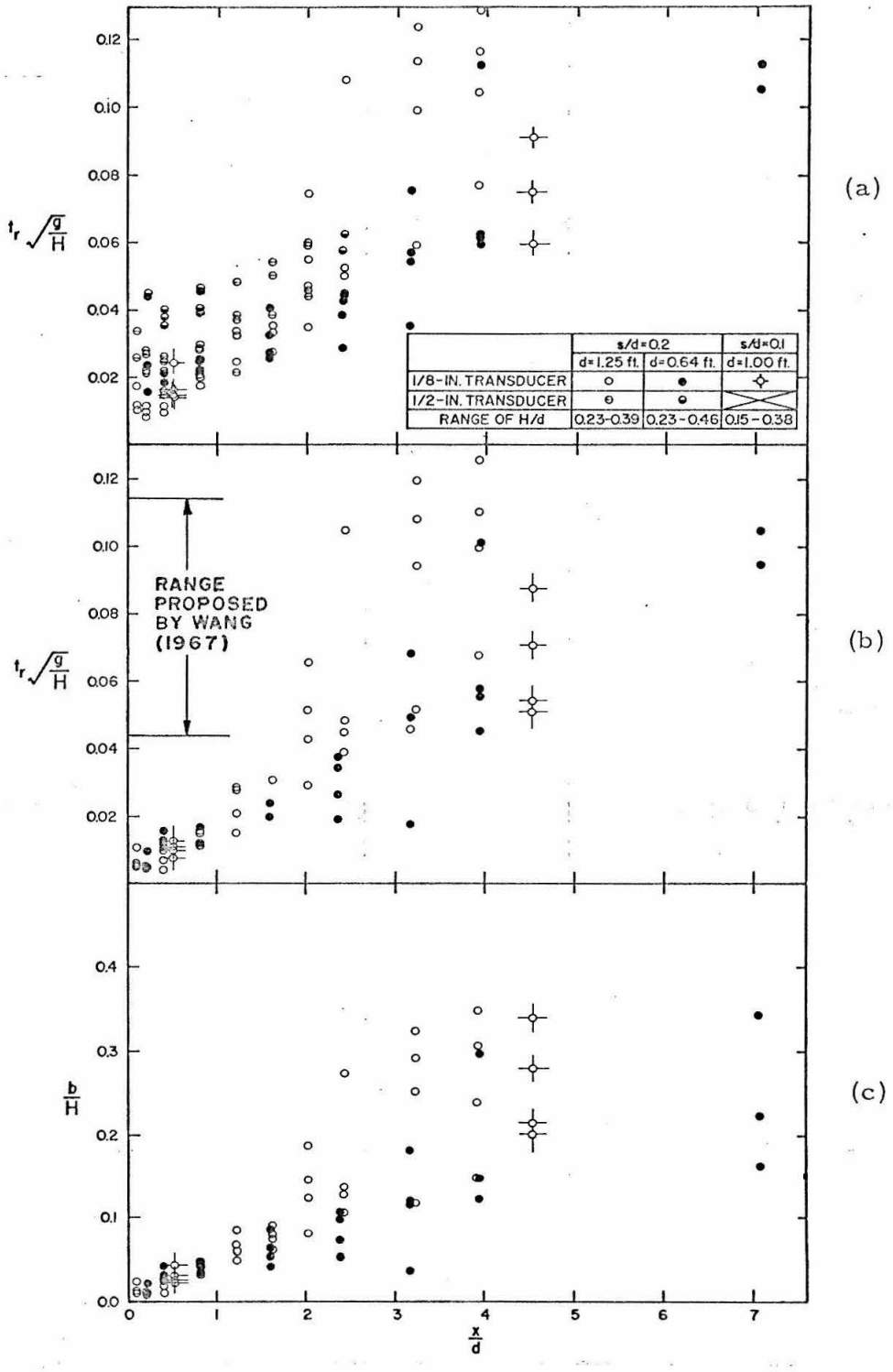

Figures 6.73. (a) Uncorrected normalized rise-time; (b) corrected normalized rise-time; (c) normalized rise-length; plotted as functions of x/d.

Figure 6.73c shows the computed rise length b, normalized with respect to the wave height H, plotted against x/d. (As explained in the discussion of the correction procedure: $b = U_d t_r - a$, where U_d is the measured wave front celerity, a is the transducer radius, and t_r is the uncorrected rise-time.) The qualitative appearance of the function b/H, as expected, is similar to that of the corrected function $t_r\sqrt{g/H}$, generally increasing with relative distance x/d.

Figures 6.73 show considerable variance in $t_r\sqrt{g/H}$ and in b/H, for constant x/d, for values of x/d greater than 2, especially for s/d = 0.2. In this connection it is noted that Figures 6.72 indicate a decrease in $P_2/\gamma(U_d^2/2g-s)$ for x/d > 2 at s/d = 0.2, that Figure 6.60 indicates an increase in the ratio $S_t/\bar{t}_r$ of standard deviation to mean rise-time for x/d > 2 at s/d = 0.2, and that, to a lesser extent, Figure 6.58 indicates an increase in the ratio S_p/P_2 of standard deviation to mean peak pressure at x/d = 0.2 for x/d > 2, particularly at x/d = 3.9 and 7.07.

It may also be noted that the photographs presented in Figures 6.13, 6.14, 6.16, and 6.17 in Section 6.2 show that the amount of spume and entrained air generated at the wave front increases as the wave propagates shoreward beneath the platform. An increase in the amount of spume and entrained air may be expected to increase the size of the region of activity at the wave front, hence increase the rise-time t_r and the rise-length b. By the assumption in Subsection 6.6.1 that deviations in peak pressure and rise-time are caused by inhomogeneities in fluid density due to spume and entrained air, an

increase in spume and entrained air could be expected to cause an increase in the ratios $S_p/\overline{P}_2$ and $S_t/\overline{t}_r$ of standard deviation to mean for peak pressure and rise-time, respectively. In Section 3.3 it was suggested that entrained air, by reducing the average fluid density, could cause a decrease in pressure exerted on the platform; therefore an increase in air entrainment may be the cause of the reduction in $P_2/\gamma\ (U_d^2/2g\text{-}s)$ noted for $x/d = 0.2$ in Figures 6.72.

Although the reasons for the increase in spume and entrained air that is observed with increasing x/d, especially for $x/d > 2$ at $s/d = 0.2$, have not been examined in detail in this study, it is conjectured that the fluid that in an ideal flow would be shot forward from the wave front as shown in Figure 3.4, in the real case simply falls to the fluid surface ahead of the wave front, entrapping air. As the wave propagates beneath the platform, the amount of fluid so involved accumulates, increasing in size with relative location x/d.

It may also be noted that for $x/d = 0.2$, Figures 6.27 in Section 6.4 indicate that the wave front celerity U_d attains a maximum at x/d approximately equal to 2. Furthermore, for $s/d = 0.1$, where the effects on t_r, b, $S_t/\overline{t}_r$, $S_p/\overline{P}_2$, and $P_2/\gamma(U_d^2/2g - s)$ have not been noted for $x/d > 2$, Figures 6.28 indicate that wave front celerity U_d generally attains a maximum only at x/d equal to values greater than three or four. Therefore, the increase in spume and entrained air may be in some way associated with the dynamics of deceleration of the wave-front.

If the pressure-time distribution in the pressure peak may be approximated by an isoceles triangle of height P_2 and base $2\,t_r$, then the product $P_2 t_r$ may be considered an approximate value of the upward impulse per unit area imparted to the platform in the vicinity of the wave front. Figure 6.74 a shows the normalized impulse $(P_2/\gamma\,H)\,(t_r\sqrt{g/H})$, where P_2/γ and t_r are uncorrected values of peak pressure head and rise-time, respectively, plotted as a function of x/d.

Figures 6.74b is similar, but for corrected values of P_2/γ and t_r. Since only data obtained with the 1/8-in. transducer were logarithmically corrected, data from the 1/2-in. transducer do not appear in Figure 6.74b. The main difference between Figure 6.74a and Figure 6.74b is evident for x/d less than 2, where the correction procedure reduces values and provides better agreement between data obtained at the two model scales. For $s/d = 0.2$, the normalized product $(P_2/\gamma\,H)\,(t_r\sqrt{g/H})$ is shown in Figure 6.74b to increase from a value approximately zero at $x/d = 0$ to a maximum value of 0.2 at approximately $x/d = 3$, thereafter decreasing with increasing x/d. For $s/d = 0.1$, there are again insufficient data to determine functional detail, except for a general increase in $(P_2/\gamma)\,(t_r\sqrt{g/H})$ between $x/d = 0.522$ and $x/d = 4.525$. The greatest measured value for $s/d = 0.0$ is 0.26 at $x/d = 4.525$.

The normalized values of uplift impulse per unit area may be compared with the impulse per unit area due to waves breaking against a vertical wall, as measured by Denny 1951), Ross (1954), and

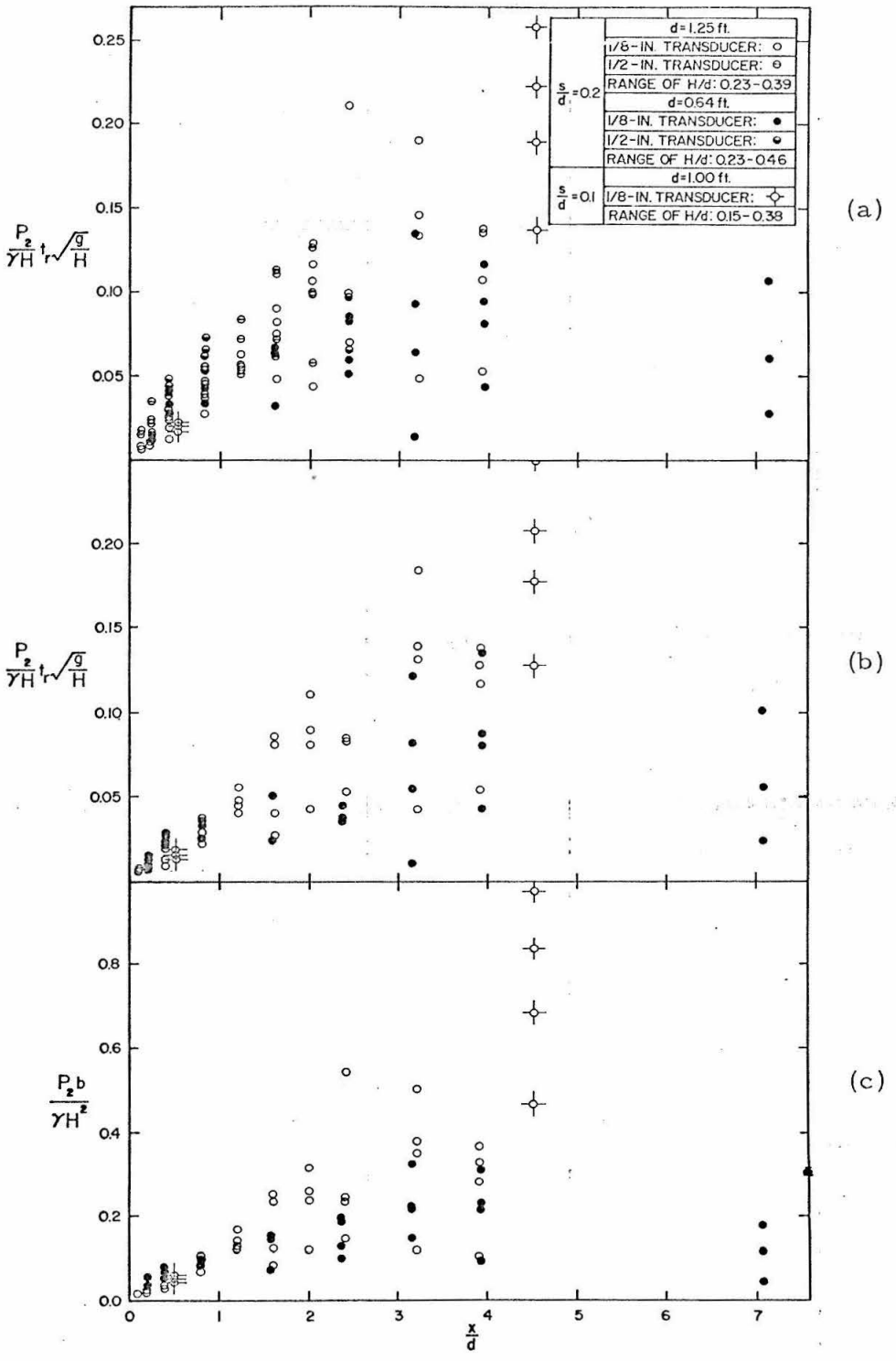

Figures 6.74. (a) Uncorrected measure of peak uplift impulse; (b) corrected measure of peak uplift impulse; (c) measure of uplift force per unit width at the peak; plotted as functions of x/d.

Garcia (1968). Values of $(I/\gamma H)\sqrt{g/H}$, where I is the impulse per unit area and H is the wave height, that may be obtained from Denny's * data range from zero to 0.71. For Ross's data, the range is 0.06 to 1.58. For Garcia's data, the range is 0.41 to 1.37. The largest values of uplift inpulse $(P_2/\gamma H)(t_r\sqrt{g/H})$ obtained in the present study (0.26 for s/d = 0.1 at x/d = 4.525) are therefore of the order of 20% of the largest measured impulses exerted horizontally against a vertical wall.

Figure 6.74c shows the product $P_2 b/\gamma H^2$ plotted as a function of x/d. As before, $b = U_d t_r - a$, where U_d is the wave front celerity, t_r is the uncorrected rise-time, and a is the transducer radius. By approximating the spatial distribution of peak pressure by an isosceles triangle of height P_2/γ and base 2b, one may define the product $P_2 b$ as the uplift force per unit width due to the pressure peak.

For x/d = 0.1, the value of $P_2 b/\gamma H^2$ at x/d = 0.522 is in close agreement with the data for s/d = 0.2, but at x/d = 4.525, for s/d = 0.1 this parameter is about twice as large as the corresponding value for x/d = 0.2, the greatest measured value of $P_2 b/\gamma H^2$ being 0.97. This behavior of $P_2/\gamma H$ shown in Figures 6.68.

---

* Denny presents his values for impulse in the normalized form $I/\rho U H$, where U is the wave celerity and ρ us the fluid density. If, following Denny, it is assumed that for breaking waves $U = \sqrt{gH(1+1/0.78)}$, Denny's data may be transposed into the normalized form $(I/\gamma H)\sqrt{g/H}$.

The total force per unit width imparted at the pressure peak may not be large compared to the total uplift force per unit width due to the slowly-varying pressure computed in Section 6.5. (For instance, at $H/d = 0.4$, $s/d = 0.2$, Figures 6.62 and 6.63 for $x/d = 0.816$ show typical values of $P_2/\gamma d$ and b/d to be 1.0 and 0.02, respectively, giving a normalized force per unit width of $P_2 b/d^2$ of 0.02, compared with a maximum value $F/\gamma d^2$ of 0.6, shown in Figure 6.52c.) However, to a structural engineer concerned with the stresses imposed on individual parts of the platform soffit whose length is of the order of 2b, the concentrated force in the pressure peak may be of greater importance than the more widely distributed force due to the slowly-varying pressure.

For the samples of data obtained at $x/d = 0.816$, cumulative frequency diagrams are presented for the impulse $P_2 t_r$ normalized with respect to the sample mean value, $\overline{P_2 t_r}$, in Figure 6.75. The values of P_2/γ and t_r are the uncorrected values obtained with the 1/8-in. transducer at both model scales for $x/d = 0.2$. As with the quantities H, P_2/γ and t_r, the product $P_2 t_r$ appears to be normally distributed; for the samples obtained at $x/d = 0.816$, the average value of standard deviation to mean value is $S_{pt}/\overline{P_2 t_r} = 0.174$.

Denny (1951), in a study of impact pressures and impulses due to waves breaking against vertical walls, found that whereas impact pressures tend to be normally distributed, the distribution of shock impulse per unit area tends to have a negative skewness; i.e. more than half the values in a sample are greater than the mean value,

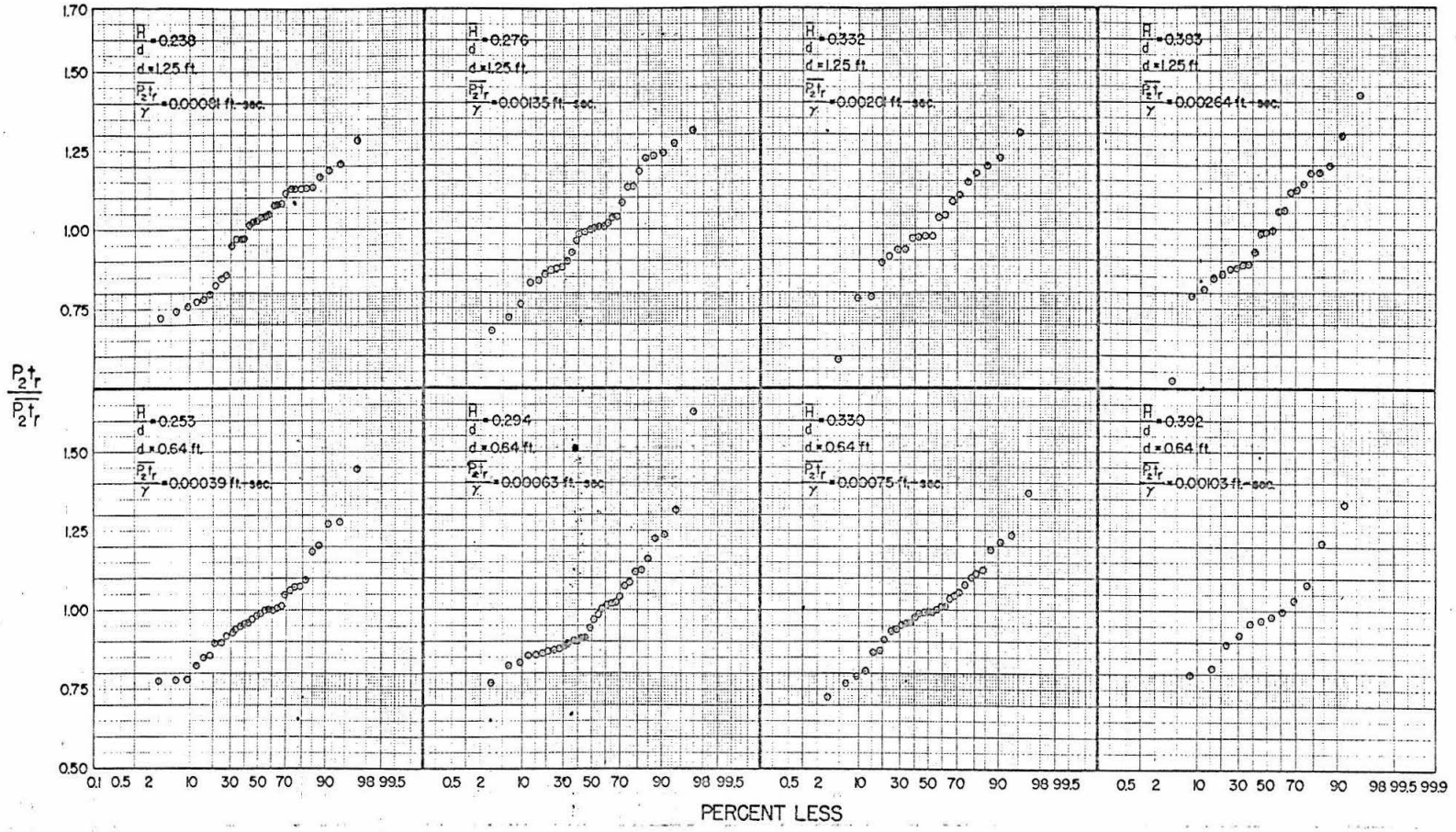

Figure 6.75. Cumulative frequency diagrams for uplift impulse P_2t_r. (Uncorrected data obtained at x/d = 0.816 with 1/8-in. transducer.)

but the majority of values with large deviations from the mean are less than the mean. Plotted on arithmetic probability paper such as used in Figures 6.75 and elsewhere in this study, data in a negatively skewed distribution would be fitted by a curve convex upward. The data from the present study plotted in Figures 6.75 show no consistent tendency towards lying on convex-upward curves; indeed, a more common tendency for samples not well-fitted by a straight line is to lie on a convex-downward curve, indicating positive skewness, in contrast to the trend found by Denny.

CHAPTER 7

CONCLUSIONS AND RECOMMENDATIONS FOR FUTURE STUDY

7.1 Conclusions.

The major objective of the present study has been to investigate in detail the basic nature of the flow beneath a pier or offshore platform, and the associated uplift pressures exerted on the platform, that result from the incidence of a solitary wave. Although there is a great variety and range of experimental conditions that may be studied, only a limited range of conditions in a geometrically simple two-dimensional model was examined.

While this range may not be broad, the investigation has been intensive. Peak pressures were examined in detail, with careful attention given to the measurement and recording capabilities and limitations of the pressure transducers and of the other components of the recording system. Since the peak pressure was found to be a highly variable quantity, the normal experimental procedure was to perform five, six, or as many as 32 similar experiments to obtain meaningful average values of peak pressure and of the rise-time, or characteristic duration of the peak pressure, for each value of relative wave height, soffit clearance, and transducer location examined. The distribution of slowly-varying pressure with respect to time and location was obtained for several values of relative wave height. Other quantities measured in detail were the celerity of the wave front and the celerity of the wave of recession. To aid in the general understanding of the flow process, numerous single-exposure and multiple-exposure photographs of the wave profile were taken, for the

range of conditions studied.

Although the study was two-dimensional, and limited to the geometrically simple configuration of a horizontal channel bottom and a flat horizontal platform, the conditions chosen for study are considered relevant to prototype conditions of interest. On the one hand, the solitary wave, used as a model incident wave, is considered a relevant model of ocean waves in shoal water, where piers or platforms are likely to stand. On the other hand, the values of parameters such as relative wave height and relative soffit clearance are considered representative of prototype cases of interest. Most of the experiments were performed at a relative soffit clearance s/d of 0.2, with a relative wave height H/d ranging from 0.2 to 0.4, and relative platform lengths L/d equal to 4.0 and 7.8. These conditions, would, for example, correspond to a prototype pier or platform 120 to 224 ft long situated six feet above the still water level, in water 30 ft deep, with incident waves six to twelve feet high. A few experiments were performed at a relative soffit clearance s/d = 0.1, with relative wave height H/d ranging from 0.15 to 0.38, which could correspond to an offshore platform standing in 100 ft of water, ten feet above the still water level, subjected to waves 15 to 38 ft high.

7.1.1 Correction of transducer defect.

With respect to the problems of measurement of peak pressure, it was found that:

1. A pressure distribution whose characteristic width is of the same order of size as the radius of the sensitive area of the transducer may be inadequately recorded by the transducer, due to a spatial averaging effect.

2. Theoretical analysis of the spatial response of pressure transducers mounted flush in a rigid boundary indicates that if the characteristic half-length of a pressure pulse is greater than about three times the transducer radius, the defect, i.e., the ratio of recorded maximum pressure to actual maximum pressure, will be reasonably close to unity, and areal effects of the transducer are relatively unimportant.

3. Although in certain cases it is possible to apply an analytical correction procedure (derived in Section 5.2), to retrieve the actual pressure distribution from the measured pressure distribution, it has been shown analytically that it is impossible to retrieve the Fourier components of the actual distribution for certain critical normalized frequencies $\omega a/U_d$ whose values depend on spatial resolution characteristics of the transducer. Practically, correction is possible only if the actual distribution has no frequency components greater than a certain critical value; yet such distributions by nature need little correction to begin with. Therefore the analytical correction procedure is of little practical value, at least as applied in this study.

4. When planning to measure pressures exerted non-uniformly on a surface, it is best to use a transducer of sufficiently small sensitive area that problems of spatial resolution may be avoided. (As indicated in Item 2, a "sufficiently small" transducer is one whose radius is less than one-third the characteristic half-width of the pressure distribution to be measured.)

5. In the present study, the problem of spatial resolution could not be avoided entirely, despite the use of the smallest commercially available strain-gauge-type transducer. Therefore an extrapolation

procedure based on the comparison of peak pressures measured under similar conditions but at two different model scales was devised (in Section 5.3) to correct values of rise-time and peak pressure. Although the procedure could not be applied with certainty, principally because of the randomly fluctuating nature of the peak pressure distribution, the corrected values appeared to be free of effects of scale attributed to problems of transducer resolution, and were in fair agreement with values corrected by a different procedure described by Willmarth and Roos (1965). Both correction procedures increased peak pressures from a few percent to as much as 50%.

7.1.2 Peak pressure and rise-time.

With respect to measured peak pressure P_2 and rise time t_r, it was found that:

1. Corrected values of peak pressure are generally 50% to 80% of the "stagnation pressure" predicted analytically from the measured wave front celerity and the soffit clearance. The discrepancy between measured values and the predicted value may largely be attributed to air entrainment and other real fluid effects. (Although air is entrained at the wave front in a region where the peak pressure is exerted, the air is not considered in the analysis, as it was in Bagnold's analysis (1939) of the considerably different case of waves breaking against a vertical wall.)

2. The greatest peak pressures are measured not at the seaward end of the platform, but at a location where wave front celerity is greatest. The functional dependence of peak pressure on distance is similar to the variation of wave front celerity with distance, as predicted by the analysis.

3. For relative locations x/d where the wave front is decelerating (see Subsection 7.1.4, Item 2), there is a notable decrease in peak pressure P_2, compared with the analytically predicted value; there is an increase in the rise-time t_r, hence in the rise-length b; and there is a notable increase in the ratio of standard deviation to mean for peak pressure and especially for rise-time. It is suggested that these concurrent phenomena may be in some way related to the deceleration of the wave front.

4. Corrected peak pressures obtained in the present study are of the same order of magnitude as those measured by El Ghamry (1963) and Wang (1967) for different incident wave systems, showing approximately the same increase with respect to waveheight and the same decrease with increasing soffit clearance. However, the dependence of peak pressure on distance from the seaward edge of the platform found in the present study is not definitively shown by data from the other studies.

5. All peak pressure data from the present study (and most data obtained by Wang) are less than the empirical upper limit of pressure head proposed by El Ghamry (1963), i.e., five times the incident wave height above still water level (2.5 times the trough-to-crest wave height for oscillatory waves).

6. Rise-times measured in the present study show approximately the same relationship to incident wave height as found by Wang.

7. This general agreement as to peak pressure and rise time measured in different studies exists despite considerable differences in experimental conditions, indicating that the form of the incident wave and of the platform may not be important variables in the rela-

tionship between peak pressure and wave height.

8. The normalized peak pressures were an order of magnitude less than the normalized maximum recorded shock pressures exerted by a breaking wave against a vertical wall reported in the literature.

9. The normalized peak impulse, or the normalized product of peak pressure and rise-time, was at most 20% of values reported for waves breaking against a vertical wall.

10. The peak pressure and the rise-time are found to be intrinsically subject to considerable variance, probably because of the spume and entrained air in the flow near the wave front. Despite a standard deviation in incident wave height of only about one percent of the mean height, the standard deviation in peak pressure and rise-time was as much as 30% or more of the mean value. Since the values obtained in the present study are average values, individual peak pressures may therefore exceed the analytically predicted values, or the empirical upper limit suggested by El Ghamry (1963).

7.1.3 Slowly-varying pressure.

With respect to the slowly-varying pressure P_1, it was found that:

1. A simple "one-dimensional" analysis relating slowly-varying pressure to wave front celerity and to celerity of the wave of recession predicts pressures that are usually greater than measured.

2. Although predicting pressures that are perhaps excessively conservative, the analysis provides a useful qualitative description of the hydrodynamics beneath the platform.

3. It was found that the maximum pressure head was equal to or slightly greater than the incident wave height less the soffit

clearance, suggesting a simple hydrostatic relationship between maximum pressure and wave height such as that suggested by Wang (1967) for the case of a narrow pier.

4. Whereas positive slowly-varying pressure depends strongly on wave height and soffit clearance, the negative slowly-varying pressure depends on soffit clearance, platform length, and location, with little dependence on wave height.

5. The positive uplift due to a wave only slightly higher than the platform may be insignificant, but the negative uplift will be as great, and of the same duration, as that due to a much higher incident wave.

6. At any given instant, the slowly-varying pressure distribution varies approximately linearly with respect to distance from the seaward edge of the platform, as predicted by the analysis, with variation apparently depending on acceleration or deceleration of the wave front.

7. For pressure measured at a particular location, the ratio of the durations of positive uplift pressure to negative uplift pressure decreases with increasing relative distance x/d from the seaward edge of the platform.

8. The ratio of the durations of positive to negative force per unit width on the entire platform decreases with increasing relative length L/d of the platform.

9. The normalized maximum uplift force per unit width on the platform, plotted as a function of wave height less soffit clearance, is in approximate agreement with values measured by El Ghamry (1963) for oscillatory waves.

10. The center of uplift pressure predicted by the analysis is in very good agreement with measured values for positive uplift pressure, and in fair agreement with measured values for negative uplift.

11. The oscillations in the pressure records (herein termed, "secondary oscillations") that appear to be associated with recession of the wave from the leading edge of the platform or with the arrival of the wave front at the shoreward edge of the platform may be of significant amplitude, i.e., comparable to the maximum positive uplift pressure.

7.1.4 Wave front and wave of recession: celerities and times of arrival.

Since in the course of the analysis both peak pressure and slowly-varying pressure are expressed in terms of the celerity of the wave front, and negative pressure is associated with flow conditions at the wave of recession, it was important to derive analytical expressions for the celerities and locations of the wave front and the wave of recession. It was found that:

1. A simple analysis provided values of wave front celerity U_d that were in fair agreement with measured celerity, and predicted wave front location x_d as a function of time that agreed well with measured values.

2. As a function of distance from the seaward end of the platform, the wave front celerity increases, attains a maximum value, then decreases, as predicted by the analysis. For a relative soffit clearance s/d of 0.2, the wave front celerity U_d attains its maximum value at a relative location x/d of approximately 2.0.

3. For the experimental conditions studied, it may be shown that an incident solitary wave can propagate beneath and in contact with a platform only for a finite distance from the seaward end of the platform, due to the condition of energy dissipation at the wave front and to the finite amount of energy associated with the incident wave. The distance beneath the platform that the wave may propagate in contact with the platform may be expected to increase with increasing incident wave height.

4. An analysis predicting the celerity U_e of the wave of recession, equivalent to an analysis by Benjamin (1968) for the propagation of gravity currents, provided values that on the average agreed well with measured values. As predicted, the measured celerity U_e of the wave of recession depends principally on the relative soffit clearance s/d, and little or not at all on incident wave height or on location.

5. The profile of the wave of recession, which may be considered a form of gravity current, resembles the profiles of other forms of gravity current, especially in the formation of its characteristic "head wave."

7.1.5 The incident solitary wave.

1. The form of the wave generated with the apparatus designed and built for this study was not measurably different from the forms of solitary wave profiles measured in a uniform rectangular channel by Daily and Stephan (1952) or by Perroud (1957) using different methods of generation.

2. The measured profiles are fitted best by the theoretical profile of Boussinesq (1872), at least in the region near the wave crest.

3. The measured celerity, in its dependence on incident wave height, was represented best by the theory of Laitone (1963).

4. The measured rate at which the solitary wave amplitude decreased with respect to distance travelled, though variable, was approximately that predicted by Keulegan (1948).

5. Although a decay of amplitude with respect to distance travelled was observed, the normalized profile of the solitary wave did not change measurably over these distances.

6. The wave generator designed and used in this study was capable of reproducing wave heights with a standard deviation of only about one percent of the mean wave height.

7. The solitary wave, reproducibly generated as in this study, may be considered a valuable tool for basic research on wave action on coastal structures. By practically eliminating variability in intial conditions, such as random disturbances on the water surface that are generated with a series of periodic progressive waves by reflection from the structure, it is possible to determine the extent of the innate variability of flow conditions, and to more easily determine meaningful measurements of pertinent quantities (such as peak pressure, in the present study). Furthermore, as stated at the beginning of this section, the solitary wave is a relevant model of ocean waves near shore.

7.1.6 Experimental techniques.

In the course of the present study, a number of experimental techniques have had to be developed that may be of general interest to those engaged in experimental fluid dynamics research. Among the items discussed in Chapter 4 are temperature insulation of the

pressure transducer, design of the solitary wave generator, cleaning of the free water surface, and single- and multiple-image photography of waves in a tank. Analysis of the spatial response problem of transducers and proposed correction procedures are presented in Chapter 5.

7.2. Recommendations for Future Study.

In the present study, uplift pressures due to a solitary wave incident on a horizontal platform have been studied in depth for a limited range of conditions. The qualitative behavior of peak pressure and slowly varying pressure may now be predicted by the analysis provided.

The case having been studied in depth, it is logical to suggest that the case next be studied in breadth. As noted in Chapter 6 and in Section 7.1, the peak-pressure, rise times, slowly-varying pressures, maximum uplift forces, and center of maximum uplift pressure as measured by El Ghamry (1963) and/or by Wang (1967) were all of the same order of magnitude and often showed the same functional behavior as comparable quantities measured in the present study, despite important differences in experimental conditions, such as type of incident wave, relative soffit clearance, platform length and width, and bottom slope. An aim of the suggested study in breadth would therefore be to determine the range of conditions for which the functional relationships derived in the present study and in the work El Ghamry and of Wang may validly be applied. Using a pressure transducer of sufficiently small sensitive area and of sufficient dynamic response capability, pressures could be recorded for a wide range of relative wave heights, soffit clearances, transducer locations along the platform, and platform lengths; for both the

"two-dimensional" case as examined in the present study, and for the "three-dimensional" or narrow-platform, case. In the latter instance, the ratio of platform width to still water depth could be varied. Bottom slope and platform slope could be varied. Several different classes of incident wave, such as solitary, dispersive, and periodic progressive, could be tested.

It would be of great interest to compare the experimental uplift measurements obtained in the laboratory with measurements made on prototype platforms. Instrumentation to measure uplift pressures on a pier or on an offshore platform, coupled with wave gauges to measure the incident wave conditions, would naturally provide the most complete and useful data. However, a survey of the damage sustained by platforms due directly to wave uplift forces (to be distinguished from damage inflicted by the horizontal wave forces on piles or by the surging of vessels lying alongside the platforms), when correlated with incident wave height and other parameters, would add important practical confirmation to the analysis and to the laboratory measurements of this and other studies.

Perhaps it would be interesting and useful to undertake a computer simulation of the transient flow beneath a platform due to an incident wave, as has been done for other flow conditions.

It is suggested that the solitary wave propagating into still water is a good tool for basic research in situations where good reproducibility of flow conditions from test to test is desirable. The solitary wave is a reasonable model of ocean waves near shore, as discussed in Section 2.4, and is therefore pertinent to coastal engineering wave research. Where the measured resultant quantity is subject to

considerable deviation, as was the peak pressure in the present study, use of the solitary wave, reproducibly generated, serves to reduce the amount of deviation in measurements, enabling a meaningful average value to be more easily obtained.

With respect to the available techniques for measurement of pressure on a wall, there is a need for further experimental research into the problem of spatial resolution of pressure distributions. The problem has been theoretically analyzed in this and other studies (see Chapter 5). One could therefore design an experiment to determine the accuracy and efficacy of the defect correction procedures derived in this study or in that of Willmarth and Roos (1965), using known, static experimental distributions rather than fluctuating (and basically unknown) travelling distributions, as dealt with in this study. The experiment could also check the criterion proposed in this study that loss in measured peak pressure will be only about 10% or less providing that the half-width of the pressure distribution is at least three times the transducer radius.

LIST OF REFERENCES

1. Bagnold, R. A., "Interim report of wave-pressure research", Journal of Institution Civil Engrs., (June 1939), pp. 202-26.
2. Bauer, W. J., "Turbulent Boundary Layer on Steep Slopes", Transactions ASCE, vol. 119, (1954), pp. 1212-1224.
3. Benjamin, T. B., "Gravity Currents and Related Phenomena", Journal of Fluid Mechanics, vol. 31, Part 2, (1968), pp. 209-248.
4. Boussinesq, J., "Theorie des ondes et des remous qui se propagent le long d'un canal rectangulaire horizontal, en communiquant au liquide contenu dans ce canal des vitesses sensibilement pareilles de la surface au fond". Journal des Mathematiques, 2nd Series, vol. 17, Paris, (1872).
5. Bronwell, Arthur, Advanced Mathematics in Physics and Engineering, N.Y.: McGraw-Hill Book Company, Inc., 1953, pp. 110-111.
6. Caldwell, Joseph M., "Reflection of Solitary Waves", U. S. Army Corps of Engrs., Beach Erosion Board, Technical Memorandum No. 11, (November 1949).
7. Daily, James W. and Stephan, Samuel, G., Jr., "The Solitary Wave", Proceedings 3rd Conference on Coastal Engineering, Cambridge, Mass., (October 1952), pp. 13-30.
8. Daly, Elton F., "Mounting Plate Glass in Sides of Flumes and Tanks", Civil Engineering, vol. 35, No. 6, (June 1965).

LIST OF REFERENCES (Continued)

9. Denny, D. F., "Further experiments on wave pressures", Journal of Institution Civil Engrs., London, No. 4, (February 1951), pp. 330-345.

10. El Ghamry, Osman, "Wave Forces on a Dock", University of California, Institute of Engineering Research, Technical Report HEL-9-1, Berkeley, California, (October 1963).

11. Friedrichs, K. O., "On the Derivation of the Shallow Water Theory", Appendix to "The Formation of Breakers and Bores", by J. J. Stoker, Communications on Pure and Applied Mathematics, vol. 1, (1948), pp. 81-85.

12. Friedrichs, K. O., "Water Waves on a Shallow Sloping Beach", Communications on Applied Mathematics, vol. 1, No. 2, (May 1948), pp. 109-134.

13. Friedrichs, K. O., and Hyers, D. H., "The existence of solitary waves", Communications on Pure and Applied Mathematics, vol. 7, (1954), pp. 517-550.

14. Friedrichs, K. O., and Lewy, Hans, "The Dock Problem", Communications on Applied Mathematics, vol. 1, No. 2, (May 1948), pp. 135-148.

15. Furudoi, Teruaki, and Murota, Akira, "Wave-Induced Up-Lift Forces Acting on Quay-Aprons", Reprinted from Technology Reports of the Osaka University, vol. 16, No. 734, Osaka, Japan, (1966).

LIST OF REFERENCES (Continued)

16. Garcia, W. J., Jr., "An Experimental Study of Breaking-Wave Pressures", U. S. Army Corps of Engrs., U. S. Army Engineer Waterways Experiment Station, Research Report H-68-1 (September 1968).

17. Hall, Jay V., Jr., and Watts, George M., "Laboratory investigation of the vertical rise of solitary wave on impermeable slopes", U. S. Army Corps of Engrs., Beach Erosion Board, Technical Memorandum No. 33 (March 1953).

18. Heins, Albert E., "Water Waves Over a Channel of Finite Depth With a Dock", American Journal of Mathematics, vol. 70, (1948), pp. 730-748.

19. Hsu, E. Y., "A Wind, Water-Wave Facility", Department of Engineering Technical Report No. 57, Stanford University, (October 1965).

20. Ippen, Arthur T., and Kulin, Gershon, "The Shoaling and Breaking of the Solitary Wave", Proceedings Fifth Conference Coastal Engineering, Berkeley, California, (1955), pp. 27-49.

21. Ippen, Arthur T., and Kulin, Gershon and Raza, Mir A., "Damping Characteristics of the Solitary Wave", MIT Hydrodynamics Laboratory Technical Report No. 16, (April 1955).

LIST OF REFERENCES (Continued)

22. Ippen, Arthur T. and Mitchell, Melvin M., "The Damping of the Solitary Wave from Boundary Shear Measurements", MIT Hydrodynamics Laboratory Technical Report No. 23, (June 1957).

23. Isaacson, Eugene, "Waves Against an Overhanging Cliff", Communications on Applied Mathematics, vol. 1, No. 2, (May 1948), pp. 201-210.

24. John, Fritz, "Waves in the Presence of an Inclined Barrier", Communications on Applied Mathematics, vol. 1, No. 2, (May 1948), pp. 149-200.

25. Keller, J. B., "The Solitary Wave and Periodic Waves in Shallow Water", Communications on Pure and Applied Mathematics, vol. 1, (1948), pp. 323-339.

26. Keulegan, G. H., "Gradual Damping of Solitary Waves", Research Paper RP 1895, Journal of Research of National Bureau of Standards, vol. 40, No. 6, (June 1948), p. 487.

27. Keulegan, G. H., "The Motion of Saline Fronts in Still Water", National Bureau of Standards, Report 5831 (1958).

28. Kishi, Isutonu and Saeki, Hiroshi, "The Shoaling, Breaking and Runup of the Solitary Wave or Impermeable Rough Slopes", Proceedings Tenth Conference on Coastal Engineering, Tokyo, Japan, (1966).

LIST OF REFERENCES (Continued)

29. Korteweg, D. J. and Vries, G. de, "On the change of form of long waves advancing in a rectangular canal and on a new type of long stationary waves", London, Dublin and Edinburgh Philosophical Magazine, Series 5, vol. 39, (1895), pp. 422-443.

30. Laitone, E. V., "Higher Approximation to Nonlinear Water Waves and the Limiting Heights of Cnoidal, Solitary, and Stokes' Waves", Beach Erosion Board Technical Memorandum No. 133, (February 1963), p. 106.

31. Lamb, Horace, Hydrodynamics, 6th ed., N. Y.: Dover Publications, 1945, pp. 423 and 456.

32. Leipmann, H. W., "Aspects of the Turbulence Problem", Z. Angew, Mathematics, Physics, vol. 3, (1952), p. 322.

33. McCowan, J., "On the solitary wave", London, Edinburgh, Dublin Philosophical Magazine Journal of Science, vol. 32, 5, (1891), pp. 45-58.

34. Middleton, G. V., "Experiments on Density and Turbidity Currents, Part 1, Motion of the Head", Canadian Journal of Earth Science, vol. 3, (1966), p. 523.

35. Milne-Thomson, L. M., Theoretical Hydrodynamics, 4th ed., N. Y.: The Macmillan Company, 1960, pp. 390 and 408.

LIST OF REFERENCES (Continued)

36. Minikin, R. R., Winds, Waves and Maritime Structures: Studies in Harbour Making and in the Protection of Coasts, London WC2: Charles Griffin and Company Limited, 1950.

37. Morse, Philip M., and Feshbach, Herman, Methods of Theoretical Physics, vol. 2, McGraw-Hill Book Company, N. Y., 1953.

38. Munk, Walter H., "The Solitary Wave Theory and its Application to Surf Problems", N. Y. Acad. Science Annals, vol. 51, (1948-51), pp. 376-425.

39. Nagai, S., "Shock Pressures Exerted by Breaking Waves on Breakwaters", Proceedings ASCE, vol. 86, No. WW2, (June 1960), pp. 1-38.

40. Parratt, L. G., Probability and Experimental Errors in Science: An Elementary Survey, N. Y.: John Wiley and Sons, 1961.

41. Perroud, Paul Henri, "The Solitary Wave Reflection Along a Straight Vertical Wall at Oblique Incidence", Institute of Engineering Research Wave Laboratory Technical Report, Series 99, Issue 3, Berkeley, California (September 1957).

42. Rayleigh, Lord, "On Waves", London, Edinburgh, Dublin Philosophical Magazine, Journal of Science, vol. 1, No. 4, (April 1876), pp. 257-79.

43. Romita, P. L., "Riflessione, Assorbimento e Transmissione di Onde Solitarie in Sequito All' Orto Contra una Barriera Permeabile", La Ricerca Scientifica, vol. 24, No. 1, (1954).

LIST OF REFERENCES (Continued)

44. Ross, C. W., "Shock pressure of breaking waves", Proceedings Fourth Conference on Coastal Engineering, Berkeley, California, (1954), pp. 323-332.

45. Rouse, Hunter, ed., Engineering Hydraulics, Iowa Institute of Hydraulic Research, 1949), N.Y.: John Wiley and Sons, Inc., (1950).

46. Rundgren, Lennart, "Water Wave Forces: A Theoretical and Laboratory Study", Royal Institute of Technology, Division of Hydraulics, Bulletin No. 54, Stockholm, Sweden, (1958).

47. Russell, J. Scott, "Report on Waves", Fourteenth Meeting Brit. Assoc. Advance. Sci., (1844), pp. 311-390.

48. Schlichting, Hermann, Boundary Layer Theory, Trans. by J. Kestin, 4th ed., N.Y.: McGraw-Hill Book Company, Inc., 1960.

49. Smetana, J., "Similitude of Hydraulic Phenomena in Which Water is Considerably Mixed With Air", Trans. by H. G. Dewey, Report on First Meeting of International Association of Hydraulic Structures Research, (1938), App. 4, pp. 97-103.

50. Stedman, C. K., "The Characteristics of Flat Annular Diaphragms", Statham Instrument Notes, Ch. 31, Statham Instruments, 12401 Olympic Blvd., Los Angeles, California, (June 1967).

LIST OF REFERENCES (Continued)

51. Stoker, J. J., "Surface Waves in Water of Variable Depth", Quarterly of Applied Mathematics, (April 1947), pp. 1-54.

52. Stoker, J. J., Water Waves, New York: Interscience Publishers, 1957, pp. 71 and 431-436 also p. 342.

53. Straub, L. G. and Anderson, A. G., "Self-Aerated Flow in Open Channels", Transactions ASCE, vol. 125, (1960), pp. 456-486.

54. Timoshenko, S., and Woinowsky-Krieger, S., Theory of Plates and Shells, McGraw-Hill Book Company, N. Y., 1959.

55. Uberoi, M. S. and Kovasznay, L. S. G., "On Mapping and Measurement of Random Fields", Quarterly of Applied Mathematics, vol. 10, (1953), p. 375.

56. von Karman, Theodore, "The Impact on Seaplane Floats During Landing", NACA Technical Note No. 321, Washington, (1929).

57. Wagner, H., "Über Stoss-und Gleitvorgänge an der Oberfläche von Flüssigkeiten", Zeitschrift für Angewandte Mathematische Mechanik, vol. 12, (August 1932), pp. 193-215.

58. Wagner, H., "Planing of Watercraft", Translated from the "Jahrbuch der Schiffbautechnik", vol. 34, (1933), NACA Technical Memorandum No. 1139, Washington, (April 1948).

59. Wang, Hsiang, "Estimating Wave Pressures on a Horizontal Pier", Technical Report R 546, Naval Civil Engineering Laboratory, Port Hueneme, California, (October 1967).

LIST OF REFERENCES (Continued)

60. White, Gifford, "Response Characteristics of a Simple Instrument", Statham Instrument Notes, Ch. 2. Statham Instruments, 12401 Olympic Blvd., Los Angeles, California (April-May 1948).

61. Wiegel, R. L., "Transmission of Waves Past a Rigid Vertical Thin Barrier", Journal of Waterways Harbors Division, Proceedings ASCE, vol. 86, WW1, Paper 2413, (March 1960).

62. Wiegel, R. L., Oceanographic Engineering, Englewood Cliffs, N. J.: Prentice Hall, 1964.

63. Willmarth, W. W. and Roos, F. W., "Resolution and Structure of the Wall Pressure Field Beneath a Turbulent Boundary Layer", Journal of Fluid Mechanics, vol. 22, (1965), pp. 81-94.

APPENDIX A

NOTATION

(Some subscripts are defined at the end of the table)

A	Area of the transducer surface.
a	Radius of the transducer surface.
B	Width of the wave channel.
B	Damping coefficient in dynamic analysis of recording system.
b	Rise-length of the peak pressure distribution.
c	Minimum distance of cam follower from center of cam wheel.
D	Wave generator stroke-length.
d	Still water depth.
E	Young's modulus.
F	Total uplift force per unit width.
F_{max}	Maximum total uplift force per unit width.
F, F_1	Functions proportional to transducer output due to a line load and to a point load, respectively.
F_2	Function proportional to deflection of diaphragm or membrane at one point due to a load at another point.
f	Excitation frequency.
f_n	Natural frequency of oscillation.
G, G_1	Spatial response functions for the transducer.
g	Gravitational acceleration.
h	Thickness of transducer diaphragm.
H	Height of the incident wave.
H_o	The first of two wave heights measured in determination of decay of height.

NOTATION (continued)

I	Impulse per unit area.
I	Integral representation of transducer spatial response function.
j	Applied forcing function.
K	Positive coefficient of acceleration in peak pressure analysis.
K'	Static proportionality constant in transducer analysis.
k	Stiffness of transducer diaphragm.
L	Platform length.
M	"Mass" of system considered in dynamic analysis of recording system.
m	Sample mean.
m'	"Universal" mean
m_d	Mass of transducer diaphragm.
m_f	Mass of oil in chamber of modified transducer.
n	Sample size.
P_{ac}	Actual pressure exerted at center of transducer area.
P_r	Pressure recorded by transducer.
P_1	Slowly-varying pressure.
P_2	Peak pressure.
P_{av}	Average uplift pressure.
Q	Proportionality constant in transducer defect analysis.
R	Maximum value of $r(\theta)$.
R	Transducer defect ratio.
R_e	Reynolds number

NOTATION (continued)

r	Radius.
$r(\theta)$	Distance of a point on the cam groove from the center of the cam wheel.
S, S'	Experimental and "universal" standard deviation.
S_m, S'_m	Experimental and "universal" standard deviation in the mean.
S	Standard deviation of quantity indicated by subscript.
s	Soffit clearance, or distance of the soffit (underside of the platform) above still water level.
t	Time (For t_a, t_b, t_c, t_d, t_e, see Figure 3.5, Section 3.3).
t_o	A constant.
t_r	Rise-time of peak pressure distribution.
U	Wave celerity.
U_d	Wave front celerity
U_e	Celerity of wave of recession.
U_o	Celerity of incident wave.
u	Horizontal fluid element velocity.
v	Vertical fluid element velocity.
W_e	Weber number.
x	Horizontal coordinate measured shoreward from the seaward end of the platform. (In defect analysis, measured from center of transducer area.)
x', x''	General horizontal limits of integration in analysis.
x_p	Position of wave generator piston.
x_{cp}	Center of uplift pressure.

NOTATION (continued)

x_{cmp}	Center of maximum uplift pressure.
Y_1, Y_2	Amplitudes of damped free oscillations of transducers.
y	Vertical coordinate measured from bottom of channel.
y	Transverse coordinate in transducer defect analysis, measured from center of transducer area.
α	Coefficient in solitary wave formula by Laitone.
β	Function equal to $\log_{10} b/a$ in transducer correction procedure.
Γ, Γ'	Functions in transducer correction procedure equal to $\log_{10} R$ and its derivative, respectively.
γ	Unit weight of fluid in wave.
δ	Boundary layer thickness.
δ	Elevation of point gauges above still water level.
ϵ	Phase-shift (radians), in dynamic analysis of recording system.
ζ	Damping ratio, in dynamic analysis of recording system.
η	Elevation of the free surface above still-water level.
η	Function of time in Equation 3.29.
θ	Angular coordinate measured with respect to a radius passing through the cusp on the cam wheel.
θ_o	Angular coordinate measured with respect to vertical radius passing through center of cam wheel.
λ	Wave length.
ν	Kinematic viscosity.

NOTATION (continued)

ξ	Abbreviated argument of pressure in transducer defect analysis.
π_{ac}, π_r	Fourier transforms of P_{ac}, P_r, respectively.
ρ	Density of fluid in the wave.
ρ_d	Density of the transducer diaphragm.
ρ_f	Density of oil in chamber of modified transducer.
σ	Surface tension per unit length.
φ	Velocity potential.
$\varkappa$	Poisson's ratio.
Ω	A measure of velocity of the wave generator piston.
ω	Angular velocity or frequency.
$( )_M$	Denotes larger model scale.
$( )_m$	Denotes smaller model scale.
$( )_s$	Denotes evaluation at the free surface.
$( )_1, ( )_2,$ $( )_3$	Denotes evaluation at Points 1, 2, 3 respectively.
$( )_d$	Denotes evaluation at the wave front.
$( )_e$	Denotes evaluation at the wave of recession.
$( )_x$	Denotes partial differentiation with respect to x.
"—"	(Overscore) Denotes mean value.
sgn	Symbol indicating that coefficient of "sgn" is to take the same algebraic sign as that of argument of "sgn".

APPENDIX B

TABLES OF DATA

Table B1. Slowly-varying pressure head P_1/γ(ft), tabulated as a function of time t and wave height H; time of arrival of wave of recession t_e(sec), tabulated as a function of wave height; for selected experiments.

d = 1.25 ft., s = 0.25 ft., x = 0.148 ft.				
H(ft)	.304	.303	.370	.370
t(sec)				
.02	0	0	0	0
.04	.052	.052	.116	.133
.05	.052	.052	.107	.123
.06	.048	.052	.107	.123
.07	.048	.049	.109	.138
.08	.048	.056	.123	.143
.09	.048	.052	.123	.112
.10	.050	.061	.124	.138
.11	.055	.061	.125	.143
.12	.048	.052	.120	.143
.13	.051	.052	.130	.148
.14	.048	.052	.138	.153
.15	.039	.052	.138	.148
.16	.044	.061	.127	.153
.17	.039	.057	.130	.145
.18	.044	.044	.131	.133
.19	.043	.043	.134	.133
.20	.040	.039	.143	.133
.21	.037	.035	.123	.133
.22	.033	.035	.121	.153
.23	.026	.026	.119	.153
.24	.019	.018	.120	.144
.25	.021	.017	.111	.133
.26	.017	.017	.104	.128
.27	.009	.013	.103	.118
.28	.005	.008	.094	.110
.29	0	0	.091	.105
.30	0	0	.090	.100
.31	-.017	-.008	.092	.100
.32	-.017	-.013	.082	.087
.33	-.022	-.017	.077	.087
.34	-.013	0	.077	.074
.35	-.022	0	.061	.082
.36	-.017	.026	.051	.077
.37	-.021	.048	.056	.066
.38	0	-.065	.056	.061
.39	-.061	-.130	.051	.052
.40	0	-.061	.046	.048
.42	-.035	-.0267	.026	.035
.44	-.026	-.0210	0	.017
.46	-.026	-.0174	-.051	-.026
.48	-.008	-.0131	-.051	-.031
.50	te = .50	te = .49	-.051	-.044
.52			0	.044
.54			-.051	-.102
.55			-.032	-.030
.56			te = .56	.008
.58				.002
.60				te = .59

d = 1.25 ft., s = 0.25 ft., x = 0.270 ft.					
H(ft)	.310	.310	.374	.383	.377
t(sec)					
.02	0	0	0	0	-.0084
.04	0	0	.346	.208	.3630
.05	.112	.141	.121	.125	
.06	.056	.061	.105	.107	.1180
.07	.048	.048	.105	.104	
.08	.052	.052	.097	.113	.0928
.09	.040	.049	.105	.101	
.10	.040	.043	.097	.115	.0885
.11	.048	.041	.105	.117	
.12	.044	.040	.105	.108	.1220
.13	.040	.040	.109	.120	
.14	.037	.040	.101	.117	.1220
.15	.038	.037	.103	.108	
.16	.040	.035	.108	.121	.1220
.17	.040	.035	.117	.121	
.18	.028	.036	.109	.121	.1220
.19	.036	.036	.121	.121	
.20	.032	.034	.109	.119	.1050
.21	.024	.032	.105	.119	
.22	.024	.032	.105	.117	.1180
.23	.020	.026	.105	.110	
.24	.016	.024	.093	.108	.1135
.25	.014	.016	.101	.106	
.26	0	.014	.097	.100	.1010
.27	0	.011	.097	.097	
.28	0	.005	.095	.093	.0925
.29	0	0	.0938	.091	.0968
.30	-.007	-.00807	.0938	.083	.0952
.31	-.016	-.01612	.0913	.071	.0926
.32	-.024	-.0121	.0830	.075	.0825
.33	-.028	-.01612	.0830	.075	.0800
.34	-.028	-.01612	.0745	.063	.0785
.35	-.028	-.024	.072	.050	
.36	-.028	-.026	.052	.050	.0546
.37	-.012	0	.040	.048	
.38	0	0	.045	.041	.0421
.39	0	.00807	.0523	.038	.0505
.40	-.0718	-.0242	.0415	.021	.0421
.42	-.0557	-.061	.0166	.020	.0378
.44	-.0639	-.0565	.0192	.015	.0169
.46	-.0718	-.0725	0	0	.0084
.48	-.0718	-.0725	0	-.016	0
.50	-.0319	-.0404	.0166	.016	.0169
.52	-.0279	te = .52	.0332	.067	.0757
.54	te = .54		-.105	-.083	
.55			-.072	-.050	-.0421
.56			-.0664	-.062	-.0926
.58			-.0747	-.054	-.0884
.60			-.041	-.054	-.0506
.62			-.005	-.042	
.64			te = .63	-.016	
.65				-.012	te = .65
.66				-.005	
.68				te = .67	

d = 1.25 ft. s = 0.25 ft. x = 0.270 ft.					
H(ft)	.428	.427	.462	.477	.307
t(sec)					
.02	0	0	0	0	
.04	.323	.298	.310	.4530	.180
.05	.149	.149	.185	.175	
.06	.136	.127	.172	.183	.0573
.07	.155	.145	.175	.188	.0573
.08	.166	.153	.202	.174	.573
.09	.149	.136	.181	.183	
.10	.157	.149	.172	.192	.0532
.11	.169	.157	.206	.210	
.12	.172	.153	.206	.205	.0409
.13	.180	.170	.218	.222	
.14	.174	.179	.220	.222	.0368
.15	.178	.168	.228	.222	
.16	.192	.178	.234	.237	.0409
.17	.187	.178	.236	.240	
.18	.195	.178	.234	.235	.0552
.19	.189	.178	.239	.231	
.20	.188	.178	.231	.235	.0450
.21	.188	.176	.232	.233	
.22	.192	.174	.229	.235	.0490
.23	.187	.170	.223	.226	
.24	.185	.170	.224	.226	.0450
.25	.180	.170	.224	.222	
.26	.172	.164	.211	.227	.0409
.27	.166	.157	.198	.200	
.28	.165	.149	.189	.192	.0409
.29	.157	.149	.1892	.192	
.30	.153	.145	.185	.196	.0327
.31	.145	.140	.1676	.179	
.32	.140	.136	.1548	.174	.0286
.33	.132	.115	.1460	.162	
.34	.123	.115	.1548	.170	.0123
.35	.128	.106	.142	.153	
.36	.123	.102	.138	.148	.0245
.37	.106	.102	.121	.131	
.38	.094	.093	.112	.131	.0492
.39	.098	.0935	.1204	.126	
.40	.085	.0850	.1032	.118	-.1310
.42	.081	.0680	.1032	.096	-.0745
.44	.077	.0680	.0903	.096	-.0204
.46	.056	.0595	.0860	.083	-.0370
.48	.042	.0362	.0731	.083	-.0245
.50	.021	.0323	.0731	.079	te = .50
.52	.017	.0170	.0258	0	
.54	0	.0298	-.0215	.013	
.55	.008	0	-.031	-.017	
.56	.025	.0850	-.0215	-.017	
.58	.102	.1222	.1301	.035	
.60	-.170	-.111	.345	.122	
.62	-.102	-.102	0	.114	
.64	-.076	-.068	-.155	-.262	
.65	-.068	-.059	-.138	-.096	
.66	-.051	-.042	-.086	-.084	
.68	-.042	-.008	-.064	-.062	
.70	-.020	te = .70	-.043	-.038	
.72			-.030		
.75	te = .73		-.017	te = .75	
.80			te = .77		

Table B1 for P_1/γ (ft) and t_e (sec).

d = 1.25 ft. s = 0.25 ft. x = .522 ft.

H(ft)	.300	.296	.382	.385	.351	.352	.427
t(sec)							
.02	0	0	0	0	0	0	0
.04	0	0	0	0	0	0	0
.05	0	0	0	0	0	0	0
.06	0	0	0	0	0	0	0
.07	.312	0	.223	.276	.256	.366	.270
.08	.114	.127	.172	.182	.162	.153	.240
.09	.084	.072	.137	.147	.119	.123	.170
.10	.063	.059	.137	.138	.102	.107	.170
.11	.059	.051	.129	.140	.102	.103	.178
.12	.051	.038	.120	.125	.094	.099	.171
.13	.048	.043	.138	.138	.102	.099	.179
.14	.042	.042	.129	.130	.094	.102	.171
.15	.042	.042	.129	.130	.094	.098	.166
.16	.042	.042	.138	.138	.094	.095	.179
.17	.038	.032	.121	.134	.094	.091	.179
.18	.038	.032	.124	.138	.089	.091	.184
.19	.036	.031	.129	.142	.094	.095	.183
.20	.034	.027	.121	.136	.085	.085	.178
.21	.025	.025	.129	.134	.085	.091	.184
.22	.025	.021	.129	.138	.085	.086	.183
.23	.017	.017	.121	.138	.085	.083	.171
.24	.017	.015	.121	.130	.085	.078	.175
.25	.008	.010	.116	.130	.077	.078	.171
.26	.006	0	.107	.121	.072	.078	.171
.27	.004	0	.112	.117	.072	.066	.162
.28	0	0	.103	.116	.068	.069	.154
.29	0	-.0127	.1031	.105	.0554	.061	.154
.30	0	-.0169	.1031	.104	.0596	.060	.145
.31	.00844	-.0169	.1031	.095	.0511	.0511	.136
.32	.00844	-.0212	.0946	.087	.0511	.0554	.128
.33	-.0253	-.0254	.0859	.087	.0426	.0511	.128
.34	-.0169	-.0297	.0859	.087	.0383	.0426	.119
.35	-.020	-.034	.086	.087	.030	.034	.119
.36	-.030	-.042	.081	.082	.026	.034	.119
.37	-.030	-.025	.073	.078	.017	.021	.111
.38	-.020	-.021	.060	.074	.017	.021	.119
.39	-.00844	-.00848	.03864	.069	.01705	.01705	.102
.40	-.0253	-.0254	.0473	.061	.01705	.01705	.098
.42	-.076	-.0764	.0344	.052	0	-.00852	.089
.44	-.0675	-.0764	.0344	.043	-.00852	-.0213	.085
.46	-.0675	-.0594	.0172	.035	0	.00852	.068
.48	-.1100	-.1100	0	.017	.0213	.0298	.051
.50	-.0844	-.0933	-.00859	0	-.081	-.094	.042
.52	-.0760	-.0509	.00859	.026	-.0767	-.0672	.030
.54	-.0844	-.0765	.0516	.078	-.0767	-.0767	-.030
.55	-.072	-.076	0	0	-.072	-.068	0
.56	-.0760	-.0678	-.172	-.260	-.0852	-.0939	.013
.58	-.0591	-.0594	-.102	-.086	-.1278	-.1449	.076
.60	-.025	-.030	-.069	-.069	-.111	-.094	-.171
.62	-.017	-.017	-.013	-.095	-.076	-.064	-.107
.64	-.005	-.007	-.012	-.131	-.076	-.060	-.085
.65	te = .65	te = .65	-.129	-.138	-.061	-.052	-.068
.66			-.103	-.112	-.042	-.025	-.068
.68			-.069	-.086	-.007	te = .68	-.145
.70			-.056	-.069	te = .69		-.128
.72			-.007	-.026			-.085
.75			te = .73	te = .74			-.041
.80							te = .79

d = 1.25 ft. s = 0.25 ft. x = 1.020 ft.

H(ft)	.487	.482	.344	.347	.303	.304	.423	.412
t(sec)								
.10	0	0					0	
.11	.978	.980	0	0			.830	0
.12	.374	.402	.753	.572	0	0	.314	.863
.13	.301	.333	.340	.172	.432	.399	.260	.374
.14	.274	.304	.261	.143	.157	.140	.233	.269
.15	.252	.277	.209	.122	.102	.106	.166	.251
.16	.244	.286	.188	.117	.082	.082	.197	.224
.17	.244	.290	.178	.098	.079	.068	.188	.215
.18	.242	.278	.177	.094	.079	.066	.188	.197
.19	.236	.286	.172	.091	.075	.049	.188	.202
.20	.232	.273	.157		.074	.049	.161	.188
.21	.228	.277	.151	.079	.059	.045	.172	.188
.22	.228	.278	.157	.079	.063	.041	.175	.197
.23	.224	.273	.151	.079	.065	.037	.161	.187
.24	.224	.282	.149	.073	.059	.033	.175	.193
.25	.224	.273	.141	.075	.047	.027	.175	.188
.26	.220	.256	.136	.072	.039	.025	.157	.179
.27	.212	.252	.126	.068	.039	.021	.171	.179
.28	.208	.244	.123	.068	.039	.017	.157	.171
.29	.2040	.243	.115	.057	.038	.010	.157	.175
.30	.2040	.243	.104	.057	.037	.008	.134	.171
.31	.1955	.243	.115	.061	.035	0	.143	.170
.32	.1873	.241	.107	-.065	.032	0	.143	.174
.33	.1710	.214	.104	.061	.022	-.044	.134	.148
.34	.1710	.213	.100	.057	.018	-.008	.134	.157
.35	.1710	.210	.098	.053	.015	-.008	.130	.139
.36	.1750	.213	.089	.057	.021	-.017	.126	.134
.37	.1630	.205	.078	.049	.017	-.025	.117	.139
.38	.1510	.197	.073	.045	.012	.017	.108	.125
.39	.1384	.188	.078	.041	.015	.0	.103	.1170
.40	.1304	.167	.073	.040	0	-.008	.098	.1160
.42	.1304	.171	.052	.033	-.039	-.058	.090	.1200
.44	.1220	.158	.042	0	0	-.066	.090	.1080
.46	.1059	.137	.052	.016	-.039	-.041	.081	.0800
.48	.114	.128	.063	.033	-.051	-.083	.067	.0800
.50	.1018	.149	-.026	0	-.021	-.091	.050	.0640
.52	-.0815	.017	-.052	-.045	-.051	-.062	.036	.0560
.54	0	.020	-.026	-.041	-.056	-.082	0	.0400
.55	.00815	.026	0	-.021	-.039	-.098	0	.0080
.56	.0490	.085	-.037	-.041	-.039	-.090	.041	.0400
.58	.0320	.030	-.131	-.123	-.063	-.079	0	.0560
.60	.0040	.051	-.120	-.123	-.067	-.094	-.094	-.067
.62	.0620	.094	-.056	-.061	-.059	-.095	-.120	-.126
.64	0	0	-.104	-.106	-.079	-.097	-.064	0
.65	-.1420	-.086	-.130	-.115	-.076	-.098	-.072	-.026
.66	-.1470	-.145	-.104	-.110	-.063	-.105	-.134	-.080
.68	-.1470	-.120	-.063	-.070	-.047	-.091	-.165	-.154
.70	-.0490	-.023	-.094	-.082	-.039	-.090	-.094	-.089
.75	-.1500	-.128	-.078	-.074	0	-.058	-.099	-.099
.80	-.1510	-.120	-.042	-.057	te = .76	-.025	-.094	-.081
.85	-.114	-.077	te = .83	te = .85		te = .79	-.040	-.027
.90	-.049	-.002					te = .88	te = .87
.95	te = .94	te = .91						

d = 1.25 ft. s = 0.25 ft. x = 1.520 ft.

H(ft)	.431	.306	.370	.471
t(sec)				
.14	0			
.15	.402			0
.16	.309		0	.781
.17	.257		.405	.462
.18	.217	0	.230	.358
.19	.203	.179	.188	.328
.20	.179	.099	.153	.325
.21	.175	.082	.137	.283
.22	.166	.064	.127	.277
.23	.166	.055	.114	.255
.24	.157	.046	.110	.255
.25	.157	.037	.105	.244
.26	.153	.027	.105	.255
.27	.148	.023	.092	.233
.28	.143	.023	.088	.233
.29	.139	.018	.087	.233
.30	.129	.014	.079	.222
.31	.125	0	.072	.220
.32	.116	0	.067	.209
.33	.112	0	.067	.193
.34	.107	0	.063	.198
.35	.098	0	.058	.198
.36	.094	0	.058	.176
.37	.089	-.005	.054	.176
.38	.085	-.005	.054	.176
.39	.080	0	.049	.187
.40	.080	0	.045	.165
.42	.067	-.075	.036	.137
.44	.062	-.057	.027	.148
.46	.053	-.028	.005	.132
.48	.030	-.094	.008	.110
.50	.030	-.075	.036	.110
.52	.062	-.061	.027	0
.54	-.027	-.094	-.067	-.055
.55	0	-.094	-.081	-.027
.56	.058	-.085	-.0 1	0
.58	-.089	-.085	-.063	.055
.60	-.196	-.108	-.099	.038
.62	-.072	-.094	-.117	0
.64	-.046	-.103	-.094	-.137
.65	-.152	-.118	-.090	-.176
.68	-.161	-.094	-.113	0
.70	-.081	-.094	-.090	-.132
.72	-.165	-.104	-.090	-.436
.75	-.116	-.094	-.094	-.127
.80	-.130	-.094	-.104	-.148
.85	-.125	-.080	-.095	-.143
.90	-.112	-.033	-.090	-.138
.95	-.082	te = .92	-.067	-.110
1.00	-.020		-.022	-.077
1.05	te = 1.01		te = 1.02	te = 1.05

Table B1 for P_1/γ (ft) and t_e (sec).

d = 1.25 ft., s = 0.25 ft., x = 2.020 ft.

H(ft)	.305	.306	.357	.357
t(sec)				
.21			0	0
.22	0		.342	.294
.23	.426	0	.279	.402
.24	.161	.174	.214	.245
.25	.112	.129	.179	.196
.26	.0878	.087	.1620	.172
.27	.0682	.069	.1460	.147
.28	.0545	.055	.1269	.128
.29	.0487	.0433	.1170	.1350
.30	.0439	.0368	.1111	.1175
.31	.0248	.0359	.1060	.1095
.32	.0183	.0221	.1060	.1076
.33	.0137	.0138	.0915	.0970
.34	.0137	.0092	.0818	.0930
.35	0	0	.087	.088
.36	0	0	.082	.078
.37	0	0	.079	.078
.38	0	0	.077	.074
.39	.0092	0	.0626	.0685
.40	.0041	0	.0626	.0636
.42	-.069	-.0462	.0482	.0587
.44	-.023	-.0323	.0434	.0441
.46	-.037	-.0184	.0337	.0245
.48	-.092	-.0830	.0308	.0470
.50	-.041	-.0368	.0434	.0392
.52	-.064	-.0783	.0337	.0441
.54	-.092	-.0783	-.0723	-.0587
.55	-.069	-.064	-.106	-.078
.56	-.064	-.0664	-.1060	-.0656
.58	-.092	-.0967	-.0578	-.0392
.60	-.109	-.110	-.097	-.082
.62	-.078	-.092	-.144	-.123
.64	-.092	-.106	-.087	-.098
.65	-.110	-.115	-.073	-.068
.66	-.092	-.092	-.096	-.098
.68	-.082	-.092	-.121	-.118
.70	-.100	-.110	-.088	-.082
.72	-.083	-.083	-.092	-.102
.75	-.090	-.099	-.097	-.102
.80	-.075	-.099	-.097	-.111
.85	-.080	-.097	-.097	-.097
.90	-.080	-.097	-.102	-.097
.95	-.080	-.090	-.107	-.097
1.00	-.060	-.060	-.097	-.087
1.05	-.025	-.030	-.078	-.077
1.10	te = 1.08	te = 1.07	-.058	-.048
1.15			0	0
1.20			te = 1.15	te = 1.15

d = 1.25 ft., s = 0.25 ft., x = 2.020 ft.

H(ft)	.415	.418	.46'	.46'
t(sec)				
.19			0	0
.20	0	0	.775	.097
.21	.712	.920	.557	.725
.22	.405	.396	.381	.445
.23	.305	.309	.319	.362
.24	.261	.256	.275	.304
.25	.237	.217	.251	.275
.26	.217	.212	.242	.267
.27	.198	.193	.237	.236
.28	.189	.187	.227	.232
.29	.183	.1840	.213	.226
.30	.183	.1741	.203	.208
.31	.1645	.1645	.203	.198
.32	.1645	.1530	.198	.198
.33	.1560	.1490	.198	.1885
.34	.1510	.143	.179	.1935
.35	.135	.140	.169	.183
.36	.135	.135	.164	.169
.37	.125	.125	.174	.164
.38	.125	.116	.160	.159
.39	.1335	.126	.1645	.1597
.40	.1132	.1130	.1540	.1550
.42	.1200	.1015	.1354	.1480
.44	.1035	.0910	.1354	.1296
.46	.0929	.087	.1298	.1120
.48	.0813	.0842	.1162	.1160
.50	.0706	.0638	.0872	.0950
.52	.0619	.0435	-.0097	-.0242
.54	-.0300	-.0290	-.0194	-.0290
.55	-.029	-.039	0	0
.56	-.0194	-.0145	.0339	.0406
.58	.0600	.0532	.0387	.0484
.60	-.116	-.096	.024	.009
.62	-.116	-.164	0	.039
.64	-.039	0	-.154	-.097
.65	-.000	-.020	-.173	-.183
.66	-.106	-.097	-.145	-.194
.68	-.174	-.193	0	0
.70	-.029	-.077	-.116	-.067
.72	-.065	-.095	-.092	
.75	-.082	-.111	-.067	-.048
.80	-.101	-.106	-.067	-.082
.85	-.105	-.087	-.082	-.096
.90	-.101	-.077	-.096	-.101
.95	-.101	-.077	-.106	-.116
1.00	-.094	-.077	-.106	-.111
1.05	-.086	-.077	-.096	-.106
1.10	-.072	-.063	-.082	-.087
1.15	-.034	-.039	-.058	-.048
1.20	te = 1.18	te = 1.20	te = 1.20	te = 1.20

Table B1 for P_1/γ (ft) and t_e (sec).

d = 1.25 ft. s = 0.25 ft. x = 2.50 ft.				
H(ft)	.293	.293	.356	.361
t(sec)				
.26			0	0
.27			.472	.250
.28	0	0	.346	.346
.29	.183	.200	.230	.214
.30	.174	.190	.175	.1610
.31	.113	.1114	.152	.152
.32	.172	.074	.129	.1240
.33	.061	.060	.115	.1135
.34	.0418	.0435	.102	.1050
.35	.031	.022	.093	.092
.36	.026	.013	.083	.078
.37	.013	.011	.078	.074
.38	.017	.013	.074	.074
.39	.0174	.0174	.076	.0647
.40	.0174	.0131	.065	.0647
.42	-.0392	-.0348	.046	.0462
.44	-.0087	.0087	.042	.0416
.46	0	0	.034	.0277
.48	-.074	-.0697	.018	.02305
.50	-.0218	-.0436	.037	.0406
.52	-.0435	-.0348	.042.	.0415
.54	-.0783	-.0870	-.055	-.0876
.55	-.061	-.061	-.069	-.102
.56	-.0435	-.0653	-.065	-.0832
.58	-.0653	-.0697	-.046	-.0507
.60	-.087	-.074	-.083	-.102
.62	-.070	-.061	-.102	-.125
.64	-.096	-.087	-.083	-.078
.65	-.123	-.083	-.074	-.078
.66	-.109	-.070	-.074	-.083
.68	-.074	-.048	-.102	-.115
.70	-.091	-.078	-.088	-.088
.72	-.087	-.057	-.083	-.088
.75	-.087	-.074	-.092	-.097
.80	-.074	-.079	-.097	-.097
.85	-.078	-.077	-.102	-.106
.90	-.083	-.079	-.106	-.111
.95	-.087	-.070	-.110	-.116
1.00	-.087	-.070	-.110	-.125
1.05	-.083	-.070	-.110	-.125
1.10	-.074	-.064	-.110	-.120
1.15	-.065	-.044	-.102	-.116
1.20	-.035	-.021	-.092	-.111
1.25	te = 1.25	te = 1.24	-.065	-.092
1.30			-.028	-.030
1.35			te = 1.33	te = 1.33

d = 1.25 ft. s = 0.25 ft. x = 2.50 ft.				
H(ft)	.415	.416	.461	.462
t(sec)				
.24			0	0
.25	0	0	.329	.652
.26	1.06	.971	.656	.616
.27	.378	.369	.425	.389
.28	.284	.281	.329	.328
.29	.225	.1975	.301	.298
.30	.215	.224	.255	.263
.31	.1845	.192	.2523	.252
.32	.1660	.181	.237	.227
.33	.1615	.1615	.217	.212
.34	.1467	.1524	.207	.202
.35	.138	.138	.182	.197
.36	.133	.129	.192	.187
.37	.120	.129	.187	.182
.38	.115	.120	.177	.177
.39	.1144	.1310	.1718	.162
.40	.1070	.1200	.1718	.158
.42	.0945	.1014	.1444	.157
.44	.1015	.1082	.1414	.143
.46	.0823	.0980	.1363	.137
.48	.0720	.0739	.1212	.116
.50	.0628	.0657	.1110	.101
.52	.0314	.0554	.0101	0
.54	-.0462	-.0277	.0606	-.051
.55	-.046	-.056	-.032	0
.56	-.0322	-.0296	-.0202	-.023
.58	-.0527	.0618	.0465	-.029
.60	-.092	-.079	.025	-.032
.62	-.189	-.194	.025	.025
.64	0	0	-.101	-.126
.65	.040	.056		-.228
.66	-.046	0	-.202	-.152
.68	-.185	-.208	0	.040
.70	-.083	-.046	-.051	-.101
.72	-.046	-.023	-.197	-.192
.75	-.138	-.015	-.045	0
.80	-.111	-.012	-.101	-.076
.85	-.092	-.088	-.101	-.101
.90	-.083	-.083	-.116	-.111
.95	-.092	-.083	-.116	-.121
1.00	-.092	-.092	-.121	-.121
1.05	-.102	-.106	-.121	-.106
1.10	-.106	-.106	-.132	-.111
1.15	-.106	-.120	-.121	-.102
1.20	-.102	-.102	-.111	-.102
1.25	-.074	-.092	-.111	-.086
1.30	-.041	-.051	-.068	-.051
1.35	te = 1.33	-.005	-.020	te = 1.35
1.40		te = 1.36	te = 1.37	

Table B1 for P_1/γ(ft) and t_e (sec).

d = 1.25 ft , s = 0.25 ft x = 3.025 ft				
H(ft)	.302	.306	.362	.361
t(sec)				
.29			0	0
.30			.0246	.031
.31			.307	.478
.32	0		.417	.307
.33	.0607	0	.294	.233
.34	.485	.288	.215	.208
.35	.242	.197	.184	.184
.36	.167	.136	.169	.153
.37	.121	.106	.153	.141
.38	.117	.085	.147	.126
.39	.115	.073	.138	.129
.40	.0757	.066	.133	.138
.42	.0727	.054	.113	.1197
.44	.0303	0	.0970	.1265
.46	.0545	.031	.0859	.1265
.48	.0121	0	.0767	.1197
.50	-.0121	-.031	.0883	.0952
.52	.0206	0	.0982	.092
.54	.0061	-.024	-.0859	-.0982
.55	-.006	-.031	-.0740	-.046
.56	-.0121	-.036	-.0215	-.0202
.58	0	-.015	.0424	.0454
.60	-.021	-.031	-.046	-.061
.62	-.054	-.073	-.086	-.068
.64	-.003	-.045	-.006	.015
.65	0	-.031	-.012	0
.66	-.015	-.036	0	-.031
.68	-.045	-.067	-.067	-.077
.70	-.021	-.042	0	0
.72	-.015	-.039	0	-.015
.75	-.031	-.061	-.061	-.049
.80	-.058	-.067	-.080	-.086
.85	-.055	-.067	-.074	-.077
.90	-.055	-.076	-.061	-.061
.95	-.057	-.079	-.074	-.080
1.00	-.060	-.085	-.086	-.093
1.05	-.060	-.085	-.092	-.080
1.10	-.070	-.091	-.092	-.086
1.15	-.076	-.085	-.095	-.086
1.20	-.076	-.082	-.100	-.092
1.25	-.073	-.082	-.098	-.086
1.30	-.063	-.063	-.098	-.086
1.35	-.042	-.031	-.089	-.061
1.40	-.015	te = 1.38	-.058	-.031
1.45	te = 1.43		-.015	-.010
1.50			te = 1.48	te = 1.49

d = 1.25 ft. s = 0.25 ft. x = 3.025 ft.				
H(ft)	.425	.416	.472	.472
t(sec)				
.27			0	0
.28	0	0	.216	.0616
.29	.076	.042	.308	.650
.30	.660	.570	.524	.493
.31	.444	.437	.462	.400
.32	.330	.330	.357	.339
.33	.300	.300	.308	.308
.34	.300	.270	.277	.277
.35	.240	.231	.246	.259
.36	.216	.207	.231	.234
.37	.204	.205	.222	.222
.38	.195	.180	.210	.220
.39	.192	.186	.203	.2155
.40	.186	.168	.1417	.2155
.42	.168	.156	.1355	.1910
.44	.156	.144	.1724	.1850
.46	.150	.138	.1724	.1970
.48	.150	.126	.1724	.1724
.50	.120	.114	.0677	.0738
.52	.0420	.0240	-.0062	.0123
.54	0	-.0180	.0554	.0677
.55	.054	.030	.0740	.0830
.56	.084	.076	.0768	.0554
.58	.102	.102	.0493	.0493
.60	-.090	-.150	.059	.083
.62	-.060	-.031	.062	0
.64	.072	.102	-.154	-.123
.65	.060	.030	-.046	0
.66	-.038	-.081	0	.062
.68	-.080	-.012	.049	.031
.70	.038	.042	-.131	-.154
.72	0	-.030	-.062	-.031
.75	-.060	-.045	-.031	-.049
.80	-.090	-.102	0	.031
.85	-.078	-.084	0	.031
.90	-.045	-.060	-.055	-.018
.95	-.072	-.060	-.061	-.049
1.00	-.039	-.060	-.063	-.055
1.05	-.069	-.078	-.061	-.049
1.10	-.090	-.084	-.056	-.056
1.15	-.081	-.090	-.065	-.074
1.20	-.090	-.090	-.092	-.086
1.25	-.096	-.096	-.092	-.086
1.30	-.090	-.090	-.086	-.092
1.35	-.090	-.084	-.068	-.083
1.40	-.060	-.066	-.056	-.065
1.45	-.030	-.015	-.005	-.031
1.50	te = 1.49	te = 1.50	te = 1.47	te = 1.47

Table B1 for $P_1/\gamma(ft)$ and t_e (sec).

d = 1.25 ft., s = 0.25 ft., x = 4.025 ft.							
H(ft)	.303	.305	.366	.415	.414	.467	.467
t(sec)							
.37				0	0	0	0
.38				0	0	0	0
.39			0	.2755	.2755	.4415	.6120
.40			0	.398	.429	.453	.428
.42	0	0	.2108	.2706	.337	.288	.275
.44	0	0	.1685	.2140	.233	.2265	.2140
.46	.289	.325	.1325	.153	.1725	.1960	.1840
.48	.0782	.0842	.0782	.1410	.147	.153	.135
.50	.0331	.0313	.0842	.0918	.1100	.0550	.0184
.52	.02108	.02108	.0812	.0124	.0184	-.0124	-.0306
.54	-.0060	-.0090	-.1204	-.0490	-.0245	.0306	.0368
.55	-.015	-.012	-.081	-.033	.018	.037	.034
.56	-.0181	-.0181	-.0482	.0490	.0490	.0428	.0245
.58	-.0090	0	-.0060	.0490	.0734	.0276	.0061
.60	-.046	-.036	-.063	-.151	.092	.015	0
.62	-.061	-.061	-.091	0	.031	.058	.046
.64	-.046	-.042	-.021	.060	.046	-.128	-.134
.65	-.034	-.036	-.012	-.031	-.061	-.061	-.098
.66	-.043	-.039	-.030	-.090	-.083	-.012	0
.68	-.061	-.057	-.069	-.060	0	-.073	-.089
.70	-.033	-.042	-.030	-.039	.043	-.061	-.092
.72	-.037	-.033	-.022	-.054	-.046	-.061	-.092
.75	-.049	-.045	-.060	-.0	-.024	0	0
.80	-.049	-.054	-.063	-.057	-.027	.031	-.037
.85	-.055	-.051	-.060	-.060	-.031	0	-.024
.90	-.049	-.060	-.060	-.048	-.031	-.040	-.064
.95	-.055	-.057	-.066	-.033	-.028	-.046	-.067
1.00	-.058	-.060	-.072	-.045	-.029	-.043	-.071
1.05	-.061	-.063	-.078	-.060	-.040	-.049	-.061
1.10	-.071	-.072	-.072	-.060	-.046	-.049	-.061
1.15	-.071	-.075	-.075	-.063	-.040	-.052	-.055
1.20	-.076	-.075	-.090	-.063	-.049	-.061	-.071
1.25	-.076	-.081	-.090	-.081	-.064	-.086	-.089
1.30	-.076	-.075	-.097	-.078	-.061	-.080	-.086
1.35	-.073	-.081	-.099	-.078	-.064	-.088	-.092
1.40	-.071	-.075	-.090	-.085	-.071	-.092	-.092
1.45	-.061	-.066	-.090	-.083	-.064	-.089	-.095
1.50	-.055	-.060	-.090	-.078	-.061	-.089	-.092
1.55	te = 1.68	te = 1.68	te = 1.77	te = 1.81	te = 1.79	te = 1.85	te = 1.80

d = 1.25 ft. s = 0.25 ft. x = 4.90 ft.			
H(ft)	.300	.366	.468
t(sec)			
.40			0
.42			0
.44			.0545
.46		0	.2060
.48		.0300	.4120
.50		.3540	.1330
.52		.030	.045
.54		.082	.031
.55		.0300	.0364
.56		.082	.033
.58	0	0	.027
.60	.0900	-.0120	.0273
.62	0	.033	.061
.64	.009	.033	-.031
.65	0	0	.030
.66	0	0	.030
.68	-.006	.044	.058
.70	0	.0270	0
.72	.009		
.75	-.0090	.0150	.0303
.80	-.0090	.0180	.0273
.85	-.0210	0	.0182
.90	-.0210	0	.0061
.95	-.0240	-.0180	0
1.00	-.0210	-.0180	0
1.05	-.009	-.038	0
1.10	te = 1.10	-.044	0
1.15		-.027	0
1.20		te = 1.20	-.031
1.25			-.036
1.30			-.030
1.35			-.018
1.40			te = 1.37

d=0.64 ft., s=0.128 ft., x=0.148 ft.								
H(ft)	.177	.147	.153	.195	.193	.247	.245	.226
t(sec)								
.02	0	0	0	.035	.0282	.021	.0424	.042
.04	.059	.067	.0730	.085	.0917	.117	.1130	.106
.05	.064	.024	.020	.071	.071	.099	.106	.113
.06	.050	.013	.0199	.065	.0706	.113	.1130	.106
.07	.059	.013	0	.070	.078	.121	.113	.120
.08	.062	.010	0	.073	.0706	.113	.1200	.114
.09	.053	.010	0	.079	.071	.147	.134	.133
.10	.066	.010	0	.080	.0706	.127	.1340	.130
.11	.066	0	.006	.071	.071	.141	.137	.134
.12	.066	0	.0199	.078	.0706	.141	.1410	.127
.13	.066	0	.013	.071	.071	.134	.141	.127
.14	.059	0	.0132	.073	.0847	.155	.1410	.134
.15	.055	0	0	.083	.078	.144	.127	.144
.16	.061	0	0	.073	.0706	.141	.1410	.139
.17	.053	0	-.013	.084	.085	.150	.127	.136
.18	.057	0	0	.071	.0706	.127	.1270	.124
.19	.048	0	0	.063	.085	.141	.120	.127
.20	.040	0	0	.057	.0706	.134	.1200	.120
.21	.0571	-.0146	-.013	.0537	.071	.1130	.099	.1215
.22	.0465	-.0159	0	.0396	.0706	.1130	.1060	.1160
.23	.040	0	-.026	.057	.064	.106	.092	.106
.24	.040	0	-.0132	.051	.0692	.106	.0917	.099
.25	.0306	-.0212	-.033	.0396	.056	.1017	.085	.1002
.26	.030	-.027	-.0265	.042	.0565	.071	.0776	.095
.27	.022	-.013	-.027	.035	.049	.092	.064	.078
.28	.013	-.020	-.0265	.028	.0424	.064	.0635	.085
.29	.013	-.013	-.027	.028	.043	.059	.056	.078
.30	.011	-.023	-.0133	.028	.0353	.071	.0565	.078
.31	0	-.020	-.027	.021	.035	.057	.049	.078
.32	0	-.027	-.398	.014	.0282	.057	.0494	.071
.33	-.0066	-.0598	-.040	0	.021	.0636	.042	.0565
.34	0	-.046	-.0305	0	.0141	.042	.0353	.071
.35	-.0198	-.0650	-.013	-.0099	0	.0593	.028	.0508
.36	0	-.033	-.0398	.007	0	.042	.0282	.064
.37	0	-.026	0	0	.014	.035	.021	.056
.38	0	-.017	-.0265	.021	0	.049	.0141	.049
.39	0	-.013	-.007	0	.017	.021	0	.043
.40	-.013	-.006	0	-.014	.0565	.014	0	.035
.42	-.0664	te=.42	te=.42	-.0282	-.0282	.0141	0	.0226
.44	-.060			-.056	-.0353	0	.0635	.106
.46	-.040			-.028	-.0425	-.212	-.0989	-.127
.48	-.007			te=.48	-.0141	-.120	-.0565	-.021
.50	te=.50				te=.50	-.0468	-.0494	-.0374
.52						-.035	-.021	te=.52
.54						te=.54	-.007	
.55							te=.55	

Table B1 for P_1/γ(ft) and t_e (sec).

d = 1.25 ft., s = 0.25 ft., x = 0.148 ft.				
H(ft)	.304	.303	.370	.370
t(sec)				
.02	0	0	0	0
.04	.052	.052	.116	.133
.05	.052	.052	.107	.123
.06	.048	.052	.107	.123
.07	.048	.049	.109	.138
.08	.048	.056	.123	.143
.09	.048	.052	.123	.112
.10	.050	.061	.124	.138
.11	.055	.061	.125	.143
.12	.048	.052	.120	.143
.13	.051	.052	.130	.148
.14	.048	.052	.138	.153
.15	.039	.052	.138	.148
.16	.044	.061	.127	.153
.17	.039	.057	.130	.145
.18	.044	.044	.131	.133
.19	.043	.043	.134	.133
.20	.040	.039	.143	.133
.21	.037	.035	.123	.133
.22	.033	.035	.121	.153
.23	.026	.026	.119	.153
.24	.019	.018	.120	.144
.25	.021	.017	.111	.133
.26	.017	.017	.104	.128
.27	.009	.013	.103	.118
.28	.005	.008	.094	.110
.29	0	0	.091	.105
.30	0	0	.090	.100
.31	-.017	-.008	.092	.100
.32	-.017	-.013	.082	.087
.33	-.022	-.017	.077	.087
.34	-.013	0	.077	.074
.35	-.022	0	.061	.082
.36	-.017	.026	.051	.077
.37	-.021	.048	.056	.066
.38	0	-.065	.056	.061
.39	-.061	-.130	.051	.052
.40	0	-.061	.046	.048
.42	-.035	-.0267	.026	.035
.44	-.026	-.0210	0	.017
.46	-.026	-.0174	-.051	-.026
.48	-.008	-.0131	-.051	-.031
.50	te = .50	te = .49	-.051	-.044
.52			0	.044
.54			-.051	-.102
.55			-.032	-.030
.56			te = .56	.008
.58				.002
.60				te = .59

d = 1.25 ft., s = 0.25 ft., x = 0.270 ft.					
H(ft)	.310	.310	.374	.383	.377
t(sec)					
.02	0	0	0	0	-.0084
.04	0	0	.346	.208	.3630
.05	.112	.141	.121	.125	
.06	.056	.061	.105	.107	.1180
.07	.048	.048	.105	.104	
.08	.052	.052	.097	.113	.0928
.09	.040	.049	.105	.101	
.10	.040	.043	.097	.115	.0885
.11	.048	.041	.105	.117	
.12	.044	.040	.105	.108	.1220
.13	.040	.040	.109	.120	
.14	.037	.040	.101	.117	.1220
.15	.038	.037	.103	.108	
.16	.040	.035	.108	.121	.1220
.17	.040	.035	.117	.121	
.18	.028	.036	.109	.121	.1220
.19	.036	.036	.121	.121	
.20	.032	.034	.109	.119	.1050
.21	.024	.032	.105	.119	
.22	.024	.032	.105	.117	.1180
.23	.020	.026	.105	.110	
.24	.016	.024	.093	.108	.1135
.25	.014	.016	.101	.106	
.26	0	.014	.097	.100	.1010
.27	0	.011	.097	.097	
.28	0	.005	.095	.093	.0925
.29	0	0	.0938	.091	.0968
.30	-.007	-.00807	.0938	.083	.0952
.31	-.016	-.01612	.0913	.071	.0926
.32	-.024	-.0121	.0830	.075	.0825
.33	-.028	-.01612	.0830	.075	.0800
.34	-.028	-.01612	.0745	.063	.0785
.35	-.028	-.024	.072	.050	
.36	-.028	-.026	.052	.050	.0546
.37	-.012	0	.040	.048	
.38	0	0	.045	.041	.0421
.39	0	.00807	.0523	.038	.0505
.40	-.0718	-.0242	.0415	.021	.0421
.42	-.0557	-.061	.0166	.020	.0378
.44	-.0639	-.0565	.0192	.015	.0169
.46	-.0718	-.0725	0	0	.0084
.48	-.0718	-.0725	0	-.016	0
.50	-.0319	-.0404	.0166	.016	.0169
.52	-.0279	te = .52	.0332	.067	.0757
.54	te = .54		-.105	-.083	
.55			-.072	-.050	-.0421
.56			-.0664	-.062	-.0926
.58			-.0747	-.054	-.0884
.60			-.041	-.054	-.0506
.62			-.005	-.042	
.64			te = .63	-.016	
.65				-.012	te = .65
.66				-.005	
.68				te = .67	

d = 1.25 ft. s = 0.25 ft. x = 0.270 ft.					
H(ft)	.428	.427	.462	.477	.307
t(sec)					
.02	0	0	0	0	
.04	.323	.298	.310	.4530	.180
.05	.149	.149	.185	.175	
.06	.136	.127	.172	.183	.0573
.07	.155	.145	.175	.188	.0573
.08	.166	.153	.202	.174	.573
.09	.149	.136	.181	.183	
.10	.157	.149	.172	.192	.0532
.11	.169	.157	.206	.210	
.12	.172	.153	.206	.205	.0409
.13	.180	.170	.218	.222	
.14	.174	.179	.220	.222	.0368
.15	.178	.168	.228	.222	
.16	.192	.178	.234	.237	.0409
.17	.187	.178	.236	.240	
.18	.195	.178	.234	.235	.0552
.19	.189	.178	.239	.231	
.20	.188	.178	.231	.235	.0450
.21	.188	.176	.232	.233	
.22	.192	.174	.229	.235	.0490
.23	.187	.170	.223	.226	
.24	.185	.170	.224	.226	.0450
.25	.180	.170	.224	.222	
.26	.172	.164	.211	.227	.0409
.27	.166	.157	.198	.200	
.28	.165	.149	.189	.192	.0409
.29	.157	.149	.1892	.192	
.30	.153	.145	.185	.196	.0327
.31	.145	.140	.1676	.179	
.32	.140	.136	.1548	.174	.0286
.33	.132	.115	.1460	.162	
.34	.123	.115	.1548	.170	.0123
.35	.128	.106	.142	.153	
.36	.123	.102	.138	.148	.0245
.37	.106	.102	.121	.131	
.38	.094	.093	.112	.131	.0492
.39	.098	.0935	.1204	.126	
.40	.085	.0850	.1032	.118	-.1310
.42	.081	.0680	.1032	.096	-.0745
.44	.077	.0680	.0903	.096	-.0204
.46	.056	.0595	.0860	.083	-.0370
.48	.042	.0362	.0731	.083	-.0245
.50	.021	.0323	.0731	.079	te = .50
.52	.017	.0170	.0258	0	
.54	0	.0298	-.0215	.013	
.55	.008	0	-.031	-.017	
.56	.025	.0850	-.0215	-.017	
.58	.102	.1222	.1301	.035	
.60	-.170	-.111	.345	.122	
.62	-.102	-.102	0	.114	
.64	-.076	-.068	-.155	-.262	
.65	-.068	-.059	-.138	-.096	
.66	-.051	-.042	-.086	-.084	
.68	-.042	-.008	-.064	-.062	
.70	-.020	te = .70	-.043	-.038	
.72			-.030		
.75	te = .73		-.017	te = .75	
.80			te = .77		

Table B1 for P_1/γ (ft) and t_e (sec).

d = 0.64 ft. s = 0.128 ft. x = 0.270 ft.				
H(ft)	.167	.196	.234	.270
t(sec)		0	0	0
.05	0	.085	.145	.1330
.06	.062	.0845	.1180	.1122
.07	.052	.069	.111	.106
.08	.0416	.0745	.0980	.1144
.09	.0500	.0765	.1156	.1270
.10	.0333	.0639	.1111	.1250
.11	.042	.064	.111	.133
.12	.042	.074	.111	.127
.13	.026	.064	.106	.138
.14	.031	.075	.111	.130
.15	.0291	.0595	.1269	.1400
.16	.0312	.0745	.1111	.1340
.17	.1364	.0639	.1230	.136
.18	.021	.152	.111	.122
.19	.018	.050	.101	.127
.20	.018	.050	.101	.106
.21	.0187	.0532	.1047	.1166
.22	.0146	.0659	.1025	.1080
.23	0	.037	.078	.106
.24	.011	.053	.083	.089
.25	.0094	.0394	.0824	.0763
.26	.011	.048	.067	.078
.27	.011	.048	.067	.078
.28	0	.032	.065	.073
.29	0	.037	.056	.078
.30	0	.042	.056	.078
.31	-.007	.026	.056	.063
.32	0	.025	.051	.073
.33	-.0104	0	.0556	.0476
.34	-.011	0	.044	.045
.35	-.0135	0	.0467	.0445
.36	-.062	0	.039	.078
.37	-.031	.016	.028	.073
.38	-.011	.009	.033	.078
.39	-.041	.016	.011	.073
.40	-.041	0	0	.057
.42	-.0803	-.0585	.0133	.0201
.44	-.036	-.042	.028	.045
.46	-.036	-.053	.138	.052
.48	-.031	-.059	.016	0
.50	-.0208	-.0700	-.0666	-.0424
.52	te = .52	-.047	-.100	-.048
.54		te = .545	-.061	-.062
.55			-.0722	-.0742
.56			-.033	-.068
.58			-.055	-.047
.60			te = .59	-.021
.62				-.055
.64				te = .63

d = 0.64 ft. s = 0.128 ft. x = 0.522 ft				
H(ft)	.261	.162	.188	.208
t(sec)				
.07	0			
.08	.347		0	0
.09	.1690	0	.180	.145
.10	.1350	.0673	.0937	.1086
.11	.135	.053	.086	.087
.12	.135	.035	.077	.087
.13	.135	.027	.063	.082
.14	.135	.025	.068	.078
.15	.1350	.0230	.0564	.0805
.16	.1300	.023	.1564	.0795
.17	.1254	.0248	.0537	.0747
.18	.125	.008	.055	.078
.19	.116	.015	.045	.068
.20	.116	.009	.050	.072
.21	.1184	.0115	.0409	.0679
.22	.1166	.0106	.0428	.0698
.23	.096	0	.036	.058
.24	.092	.011	.036	.053
.25	.0838	0	.0382	.0534
.26	.092	0	.029	.049
.27	.087	0	.032	.043
.28	.082	0	.027	.041
.29	.089	0	.023	.039
.30	.072	0	.018	.039
.31	.067	0	.013	.040
.32	.072	0	.011	.037
.33	.0588	-.0266	.0091	.0252
.34	.058	-.021	.007	.022
.35	.0 78	-.0310	.0009	.0155
.36	.067	-.017	0	.018
.37	.058	-.026	0	.020
.38	.062	-.027	0	.029
.39	.058	-.035	0	.019
.40	.048	-.026	-.046	.024
.42	.0298	-.045	-.0364	-.0291
.44	.048	-.044	-.046	0
.46	.019	-.044	-.063	-.049
.48	-.048	-.044	-.046	-.043
.50	-.0193	-.0398	-.0534	-.0714
.52	-.102	-.040	-.050	-.048
.54	-.077	-.040	-.050	-.063
.55	-.0868	-.0310	-.0534	-.0570
.56	-.087	-.035	-.055	-.048
.58	-.058	-.019	-.045	-.047
.60	-.0675	-.007	-.0364	-.0427
.62	-.039	te = .62	-.034	-.037
.64	-.039		-.0137	-.0238
.65	-.0386		-.007	-.019
.66	-.019		te=.66	-.009
.68	-.009			te = .678
.70	te = .70			

d=0.64 ft., s=0.128 ft., x=2.020 ft.								
H(ft)	.146	.146	.173	.172	.205	.267	.271	.208
t(sec)								
.25						0	0	
.26						.214	.175	
.27						.278	.308	
.28					0	.199	.226	0
.29					.136	.151	.181	.259
.30			0		.167	.111	.167	.175
.31			.061	0	.121	.099	.139	.121
.32			.124	.154	.088	.105	.133	.091
.33			.075	.087	.061	.077	.129	.078
.34			.062	.058	.061	.074	.127	.072
.35			.050	.043	.056	.071	.115	.067
.36		0	.025	.025	.052	.077	.109	.057
.37	0	.033	.048	.042	.045	.057	.103	.054
.38	.021	0	.012	.015	.056	.062	.114	.054
.39	0	0	.006	0	.036	.054	.112	.042
.40	-.015	-.012	.006	.006	.043	.056	.099	.051
.42	-.024	-.021	0	0	-.021	.039	.091	0
.44	-.024	-.024	0	-.015	.042	.048	.091	0
.46	-.027	-.024	0	-.012	0	.031	.082	.018
.48	-.027	-.024	-.009	-.012	.024	-.072	-.031	-.036
.50	-.030	-.024	-.012	-.024	0	0	.042	0
.52	-.027	-.027	-.018	-.021	-.036	-.061	-.031	-.031
.54	-.030	-.026	-.021	-.024	-.015	-.061	0	-.015
.55	-.030	-.027	-.021	-.024	-.021	-.030	0	-.027
.56	-.030	-.030	-.024	-.031	-.039	-.061	-.018	-.032
.58	-.030	-.027	-.027	-.030	-.024	-.075	-.027	-.018
.60	-.034	-.033	-.028	-.032	-.039	-.048	0	-.031
.62	-.038	-.034	-.029	-.032	-.031	-.001	-.037	-.031
.64	-.040	-.034	-.032	-.040	-.043	-.056	-.013	-.036
.65	-.040	-.035	-.035	-.037	-.043			-.031
.66	-.040	-.037	-.037	-.037	-.046	-.081	-.037	-.033
.68	-.040	-.037	-.037	-.042	-.050	-.068	-.028	-.039
.70	-.043	-.038	-.037	-.044	-.050	-.074	-.026	-.036
.72	-.043	-.039	-.037	-.043	-.053	-.074	-.026	-.039
.75	-.045	-.042	-.036	-.039	-.051	-.091	-.045	-.042
.80	-.048	-.039	-.045	-.045	-.045	-.085	-.033	-.048
.85	-.048	-.042.	-.048	-.051	-.067	-.078	-.039	-.051
.90	-.048	-.042	-.054	-.051	-.067	-.082	-.042	-.057
.95	-.043	-.048	-.054	-.048	-.072	-.084	-.051	-.054
1.00	-.061	-.054	-.056	-.054	-.069	-.078	-.054	-.054
1.05	-.031	-.036	-.056	-.054	-.067	-.078	-.061	-.051
1.10	-.018	-.031	-.063	-.060	-.060	-.072	-.063	-.054
1.15	-.012	-.024	-.039	-.042	-.054	-.063	-.054	-.045
1.20	-.007	-.012	-.009	-.006	-.030	-.042	-.052	-.030
1.25	te=1.21	te=1.24	te=1.22	te=1.21	te=1.25	-.007	-.024	-.007
1.30						te=1.26	-.006	te=1.26
1.35							te=1.32	

Table B1 for P_1/γ (ft) and t_e (sec).

d = 0.64 ft., s = 0.128 ft., x = 2.520 ft.

H(ft)	.153	.194	.235	.281
t(sec)				
.30				0
.31			0	.056
.32			.0186	.1055
.33			0	.328
.34			.0372	.2380
.35			.264	.204
.36		0	.1860	.1765
.37		.015	.149	.151
.38		.1300	.1210	.1425
.39		.099	.105	.139
.40		.0960	.0900	.1300
.42		.0124	.0620	.1175
.44	0	.0341	.0745	.0990
.46	0	.0062	.0310	.0960
.48	-.0122	-.0105	.0031	.0960
.50	-.0183	0	.0248	.-.0434
.52	-.0183	-.0248	-.0031	-.0240
.54	-.018	-.018	0	0
.55	-.018	-.027	0	-.025
.56	-.021	-.027	-.031	0
.58	-.021	-.027	-.012	0
.60	-.0183	-.0248	-.0279	-.0150
.62	-.018	-.031	-.022	-.007
.64	-.021	-.031	-.031	-.012
.65	-.0214	-.0372	-.0310	-.0060
.66	-.024	-.036	-.033	
.68	-.024	-.039	-.031	-.017
.70	-.0244	-.0435	-.0341	-.0120
.72	-.031	-.043	-.037	-.031
.75	-.0305	-.0435	-.0403	-.0360
.80	-.0305	-.0495	-.0557	-.0240
.85	-.0336	-.0537	-.0496	-.0150
.90	-.0336	-.0557	-.0465	-.0090
.95	-.0366	-.0620	-.0496	te = .95
1.00	-.0336	-.0620	-.0589	
1.05	-.055	-.059	-.058	
1.10	-.0244	-.0682	-.0620	
1.15	-.039	-.071	-.061	
1.20	-.0305	-.0714	-.0683	
1.25	-.018	-.068	-.068	
1.30	te = 1.30	-.0605	-.0620	
1.35		-.056	-.047	
1.40		-.0279	-.0217	
1.50		te = 1.45	te = 1.45	

d = 0.64 ft. s = 0.128 ft. x = 4.525 ft.

H(ft)	.254	.252	.295	.294
t(sec)				
.54			0	0
.55			.0096	.0479
.56			.070	.105
.58			.107	.108
.60		0	.0543	.0512
.62	0	.029	.032	.027
.64	.038	.041	.022	.019
.65	.0192	.0192	.0128	0
.66	.019	.009	0	-.012
.68	0	0	-.019	-.013
.70	0	-.0160	-.0096	-.0064
.72	0	-.019	-.016	-.016
.75	-.0159	-.0319	-.0096	-.0064
.80	-.0064	-.0255	-.0096	0
.85	-.0065	-.0224	-.0128	-.0064
.90	-.0095	-.0319	-.0191	-.0095
.95	-.0128	-.0319	-.0224	-.0160
1.00	-.0191	-.0383	-.0256	-.0191
1.05	-.023	-.038	-.029	-.025
1.10	-.0224	-.0398	-.0319	-.0287
1.15	-.025	-.039	-.035	-.028
1.20	-.0255	-.0383	-.0383	-.0287
1.25	-.025	-.041	-.038	-.035
1.30	-.0271	-.0383	-.0415	-.0383
1.35	-.027	-.035	-.043	-.038
1.40	-.0275	-.0319	-.0447	-.0383
1.50	-.0191	-.0319	-.0383	-.0319
1.60	te = 1.52	te = 1.59	-.0256	-.0160
			te = 1.67	te = 1.64

Table B1 for P_1/γ (ft) and t_e (sec).

d = 1.00 ft., s = 0.10 ft., x = .522 ft.								
H(ft)	.217	.215	.138	.145	.307	.303	.373	.375
t(sec)								
.06							0	0
.07		0			0	0	.247	.193
.08	0	.138			.162	.176	.228	.183
.09	.152	.103	0		.141	.148	.176	.141
.10	.124	.086	.043	0	.135	.127	.152	.138
.11	.117	.083	.045	.058	.133	.123	.169	.145
.12	.107	.079	.048	.069	.130	.113	.172	.158
.13	.107	.083	.045	.055	.137	.134	.186	.173
.14	.117	.079	.038	.041	.144	.131	.187	.173
.15	.124	.090	.038	.042	.165	.148	.207	.183
.16	.114	.083	.038	.048	.158	.155	.215	.197
.17	.131	.093	.048	.048	.176	.169	.225	.202
.18	.121	.103	.034	.048	.176	.176	.234	.232
.19	.134	.113	.045	.040	.179	.172	.248	.243
.20	.130	.113	.041	.048	.194	.194	.260	.253
.22	.138	.113	.048	.053	.211	.197	.283	.264
.24	.145	.124	.045	.041	.222	.211	.299	.282
.26	.134	.124	.052	.041	.243	.236	.313	.330
.28	.148	.134	.052	.052	.246	.232	.334	.310
.30	.148	.138	.055	.052	.261	.246	.331	.313
.32	.166	.141	.062	.045	.254	.246	.338	.327
.34	.155	.138	.045	.048	.268	.257	.338	.324
.36	.155	.145	.048	.048	.254	.257	.331	.324
.38	.152	.141	.052	.057	.264	.257	.324	.317
.40	.157	.143	.048	.048	.264	.257	.317	.317
.42	.159	.145	.041	.037	.258	.256	.317	.317
.44	.152	.145	.036	.034	.254	.254	.317	.290
.46	.152	.145	.038	.034	.250	.244	.303	.317
.48	.142	.138	.034	.034	.236	.240	.183	.173
.50	.140	.138	.028	.028	.176	.201	.204	.202
.52	.131	.128	.022	.014	.172	.155	.275	.282
.54	.138	.138	.019	.014	.194	.169	.234	.224
.56	.048	.038	0	0	.197	.194	.183	.183
.58	.069	.059	0	0	.170	.147	.211	.215
.60	.114	.110	0	-.007	.158	.144	.240	.229
.65	.038	.032	-.034	-.035	.113	.113	.183	.183
.70	0	0	-.033	-.028	.085	.078	.117	.101
.75	0	0	-.034	-.050	.034	.020	.055	.041
.80	-.034	-.041	-.045	-.059	-.014	-.035	0	0
.85	-.052	-.060	-.052	-.055	-.049	-.067	-.085	-.106
.90	-.050	-.055	-.045	-.048	-.053	-.063	-.070	-.070
.95	-.041	-.048	-.032	-.040	-.046	-.060	-.056	-.063
1.00	-.028	-.032	te=.99	te=1.00	-.031	-.034	-.014	-.007
1.05	te=1.04	te=1.03			te=1.02	te=1.03	te=1.01	te=1.01

d = 1.00 ft., s = 0.10 ft., x = 4.525 ft.								
H(ft)	.306	.308	.230	.227	..19	.150	.376	.377
t(sec)								
.40							0	0
.42	0	0					.810	.612
.44	.537	.468					.518	.498
.46	.360	.387	0	0			.315	.175
.48	.256	.297	.374	.405			.246	.188
.50	.137	.150	.228	.281			.078	.026
.52	.006	.056	.187	.250			.130	.087
.54	.078	.093	.093	.151	0	0	.126	.084
.56	.099	.093	0	0	.163	.227	.188	.130
.58	.166	.172	.041	.053	.105	.107	.159	.130
.60	.087	.131	.087	.109	.085	.094	.156	.113
.65	.097	.128	.047	.081	0	-.023	.156	.117
.70	.087	.141	.093	.116	0	0	.162	.143
.75	.084	.131	.093	.119	.026	.032	.156	.113
.80	.084	.113	.062	.078	.032	.026	.144	.081
.85	.066	.116	.062	.087	.013	.016	.094	.068
.90	.056	.100	.068	.093	.009	.013	.100	.174
.95	.050	.084	.057	.078	0	.010	.094	.081
1.00	.037	.072	.041	.062	0	.013	.081	.058
1.05	.028	.062	.032	.053	0	0	.068	.052
1.10	.022	.056	.032	.041	-.013	0	.065	.045
1.15	.014	.044	.032	.037	-.013	-.006	.052	.032
1.20	.007	.037	.028	.031	-.019	-.010	.049	.026
1.25	0	.031	.012	.018	-.026	-.016	.039	.019
1.30	-.007	.028	.012	.012	-.029	-.013	.032	.016
1.35	-.014	.018	.007	0	-.029	-.016	.023	.006
1.40	-.019	.009	0	-.007	-.026	-.019	.013	.003
1.45	-.027	0	-.007	-.012	-.026	-.019	.006	-.006
1.50	-.028	0	-.012	-.019	-.032	-.023	0	-.006
1.55	-.035	-.007	-.016	-.034	-.029	-.026	-.010	-.013
1.60	-.037	-.011	-.018	-.031	-.029	-.023	-.013	-.019
1.65	-.042	-.016	-.025	-.031	-.026	-.026	-.019	-.019
1.70	-.040	-.018	-.028	-.031	-.019	-.019	-.020	-.026
1.75	-.046	-.025	-.031	-.031	-.013	-.010	-.023	-.026
1.80	-.044	-.025	-.031	-.037	-.007	.006	-.023	-.026
1.85	-.046	-.028	-.032	-.031	te=1.81	te=1.82	-.023	-.026
1.90	-.041	-.034	-.032	-.031			-.023	-.026
1.95	-.049	-.034	-.021	-.018			-.019	-.016
2.00	-.035	-.031	te=2.00	te=2.00			-.013	-.006
2.05	-.031	-.017					.019	te=2.04
2.10	te=2.08	te=2.10					te=2.06	

Table B1 for P_1/γ (ft)
(concluded)

d = 0.768 ft, s = .000 ft, x = 3.025 ft.					
H(ft)	.326	.322	.240	.233	.125
t(sec)					
-.80					0
-.75	0	0	0	0	.011
-.70	.013	.010	.010	.014	.015
-.65	.019	.019	.013	.015	.019
-.60	.028	.020	.022	.019	.021
-.55	.033	.028	.028	.033	.028
-.50	.049	.047	.041	.037	.037
-.45	.070	.065	.056	.052	.039
-.40	.089	.075	.067	.070	.056
-.35	.117	.111	.088	.089	.057
-.30	.144	.140	.107	.107	.069
-.25	.170	.169	.126	.126	.075
-.20	.199	.196	.141	.145	.089
-.15	.199	.209	.159	.164	.094
-.10	.220	.215	.163	.168	.099
-.05	.220	.215	.168	.170	.103
0	.220	.209	.170	.170	.107
.05	.220	.205	.170	.170	.107
.10	.220	.196	.170	.170	.107
.15	.220	.224	.159	.164	.101
.20	.199	.196	.150	.156	.094
.25	.182	.178	.131	.145	.090
.30	.126	.131	.103	.117	.078
.35	.075	.078	.078	.107	.072
.40	.067	.075	.065	.070	.060
.45	.033	.037	.049	.051	.052
.50	.052	.047	.047	.051	.041
.55	.050	.039	.037	.033	.037
.60	.033	.034	.029	.033	.037
.65	.037	.037	.028	.033	.028
.70	.033	.032	.028		.024
.75	.033	.023	.028		.019
.80	.024	.023	.019		.019
.85	.015	.019	.013		.019
.90	.014	.019	.010		.015
.95	.014	.013	.010		.010
1.00	.013	0	0		.010
1.05	.010				0
1.10	0				

d = 0.768 ft, s = 0.000 ft, x = 4.900 ft.					
H(ft)	.326	.322	.240	.233	.125
t(sec)					
-.90		.017		.006	
-.85	0	.023		.006	
-.80	.005	.023		.006	
-.75	.005	.014		.011	
-.70	.005	.014	0	.011	
-.65	.009	.017	.009	.014	
-.60	.011	.023	.009	.014	0
-.55	.017	.029	.011	.020	.011
-.50	.023	.031	.017	.026	.017
-.45	.029	.034	.023	.029	.020
-.40	.034	.046	.029	.031	.026
-.35	.060	.057	.031	.035	.026
-.30	.080	.057	.051	.054	.029
-.25	.083	.074	.057	.057	.040
-.20	.105	.089	.071	.072	.052
-.15	.113	.111	.086	.086	.057
-.10	.120	.117	.095	.092	.063
-.05	.137	.137	.111	.111	.080
0	.140	.143	.114	.114	.083
.05	.149	.151	.122	.123	.086
.10	.166	.157	.134	.133	.083
.15	.169	.172	.140	.140	.090
.20	.171	.172	.143	.143	.094
.25	.174	.172	.143	.143	.094
.30	.172	.172	.143	.143	.097
.35	.172	.172	.143	.143	.095
.40	.172	.172	.143	.140	.100
.45	.171	.168	.140	.140	.086
.50	.171	.168	.137	.137	.086
.55	.171	.160	.123	.126	.086
.60	.160	.143	.120	.120	.086
.65	.157	.143	.114	.103	.086
.70	.140	.138	.114	.109	.083
.75	.132	.120	.105	.097	.080
.80	.126	.117	.095	.092	.080
.85	.115	.114	.086	.086	.071
.90	.114	.112	.083	.085	.066
.95	.110	.100	.083	.080	.066
1.00	.100	.092	.079	.074	.060
1.05	.090	.080	.079	.069	.057
1.10	.086	.063	.057	.066	.057
1.15	.086	.072	.057	.063	.054
1.20	.086	.080	.057	.069	.054
1.25	.086	.080	.057	.060	.051
1.30	.084	.080	.057	.063	.049
1.35	.080	.080	.057	.063	.040
1.40	.077	.072	.057	.057	.040
1.45	.077	.066	.057	.057	.040
1.50	.074	.069	.057	.057	.040
1.55	.074		.057	.057	.040
1.60			.057	.057	.040

Table B2. Wave height H, peak pressure head P_2/γ, rise-time t_r, wave front time of arrival t_d tabulated for individual experiments.

d = 1.25 ft, s = 0.25 ft, X = 0.148 ft						
		Statham Pressure Transducer		Modified Schaevitz-Bytrex Pressure Transducer		
Exp. No.	H(ft)	$\frac{P_2}{\gamma}$ (ft)	t_r(m sec)	$\frac{P_2}{\gamma}$ (ft)	t_r(m sec)	t_d(sec)
1	.302	.165	3.47	.137	1.10	.02578
2	.305	.143	3.12	.125	1.25	.02720
3	.304	.118	3.44	.125	1.25	.02718
4	.303	.122	3.15	.125	.95	.02717
5	.305	.122	3.00	.131	---	.02620
6	.305	.161	3.64	.125	1.29	.02718
mean	.304	.139	3.30	.128	1.68	.02679
standard deviation	.001	.019	.23	.005	.13	.00058
deviation of mean	.001	.008	.09	.002	.06	.00023
1	.369	.261	2.89	.271	1.28	.02398
2	.368	.276	2.42	.249	1.36	.02425
3	.370	.266	2.27	.247	1.36	.02345
4	.371	.271	3.12	.246	1.32	.02378
5	.370	.261	3.06	.305	1.29	.02417
6	.372	.266	2.81	.292	.94	.02393
mean	.370	.267	2.76	.268	1.26	.02394
standard deviation	.001	.005	.32	.023	.15	.00026
deviation of mean	.001	.002	.13	.0010	.04	.00011

d = 1.25 ft, s = 0.25 ft, X = 0.148						
		Statham Pressure Transducer		Modified Schaevitz-Bytrex Pressure Transducer		
Exp. No.	H(ft)	$\frac{P_2}{\gamma}$ (ft)	t_r(m sec)	$\frac{P_2}{\gamma}$ (ft)	t_r(m sec)	t_d(sec)
1	.433	---	---	.259	1.21	.02210
2	.428	---	---	.420	1.11	.02265
3	.427	---	---	.336	1.14	.02233
4	.430	---	---	.336	1.28	.02196
5	.427	---	---	.400	1.15	.02246
6	.432	---	---	.403	1.20	.02250
mean	.430	---	---	.359	1.18	.02233
standard deviation	.002	---	---	.055	.06	.00024
deviation of mean	.001	---	---	.023	.02	.00010
1	.477	---	---	.541	1.19	.02169
2	.479	---	---	.541	.97	.02172
3	.474	---	---	.318	1.51	.02092
4	.474	---	---	.425	1.15	.02150
5	.478	---	---	.375	1.43	.02127
6	.467	---	---	.324	1.43	.02190
mean	.475	---	---	.421	1.28	.02150
standard deviation	.004	---	---	.092	.19	.00033
deviation of mean	.002	---	---	.038	.08	.00013

Table B2 (continued).

d = 0.640 ft, s = 0.128 ft, X = 1.020 ft						
		Statham Pressure Transducer		Modified Schaevitz-Bytrex Pressure Transducer		
Exp. No.	H(ft)	$\frac{P_s}{\gamma}$ (ft)	t_r(m sec)	$\frac{P_s}{\gamma}$ (ft)	t_r(m sec)	t_d(sec)
1	.153	---	---	.170	1.41	.17169
2	.153	---	---	.174	2.16	.17505
3	.153	---	---	.191	1.96	.17463
4	.155	---	---	.192	2.00	.17407
5	.153	---	---	---	---	.17700
6	.153	---	---	---	---	.17351
mean	.153	---	---	.182	1.88	.17485
standard deviation						
deviation of mean						
1	.171	---	---	.283	4.32	.16258
2	.171	---	---	.279	2.07	.16211
3	.171	---	---	.282	2.53	.16198
mean	.171	---	---	.281	2.97	.16245
standard deviation						
deviation of mean						

d = 0.640 ft, s = 0.128 ft, X = 1.020 ft						
		Statham Pressure Transducer		Modified Schaevitz-Bytrex Pressure Transducer		
Exp. No.	H(ft)	$\frac{P_s}{\gamma}$ (ft)	t_r(m sec)	$\frac{P_s}{\gamma}$(ft)	t_r(m sec)	t_d(sec)
1	.199	---	---	.358	2.88	.15119
2	.202	---	---	.408	2.59	.15124
3	.202	---	---	.392	2.34	.15169
4	.203	---	---	.408	2.78	.15089
5	.199	---	---	.378	2.96	.15280
6	.204	---	---	.458	1.94	.15175
mean	.202	---	---	.400	2.58	.15159
standard deviation	.002	---	---	.031	.35	.00062
deviation of mean	.001	---	---	.013	.14	.00025
1	.285	---	---	.649	2.50	.13608
2	.286	---	---	.690	2.48	.13503
3	.286	---	---	.690	2.15	.13554
4	.285	---	---	.720	2.26	.13630
5	.291	---	---	.736	2.88	.13626
mean	.287	---	---	.697	2.45	.13584
standard deviation	.002	---	---	.030	.25	.00049
deviation of mean	.001	---	---	.013	.11	.00022

Table B2 (continued).

d = 1.25 ft, s = 0.25 ft, X = 0.270 ft							
			Statham Pressure Transducer		Modified Schaevitz-Bytrex Pressure Transducer		
Exp. No.	H(ft)	U_o(ft/sec)	$\frac{P_s}{\gamma}$ (ft)	t_r(m sec)	$\frac{P_s}{\gamma}$ (ft)	t_r(m sec)	t_d(sec)
1	.310	7.04	.184	2.72	.238	1.06	.04469
2	.307	7.03	.177	2.72	.384	1.04	.04476
3	.310	7.05	.185	2.69	---	---	---
4	.312	7.01	.194	2.72	.221	1.28	.04532
5	.306	7.05	.179	2.72	.221	1.12	.04472
6	.307	7.20	.184	2.89	.238	1.12	.04468
mean	.309	7.06	.184	2.74	.240	1.12	.04483
standard deviation	.002	.06	.005	.07	.023	.08	.00024
deviation of mean	.001	.03	.002	.03	.010	.04	.00011
1	.382	7.18	.345	2.81	.505	.94	.03829
2	.376	7.18	.351	2.90	.499	1.13	.03829
3	.374	7.15	.353	2.79	.383	.93	.03747
4	.383	7.16	.349	3.16	.342	1.11	.03789
5	.377	7.17	.343	2.88	.476	1.20	.03820
6	.377	7.18	.362	2.98	.522	.97	.03834
mean	.378	7.17	.351	2.92	.455	1.05	.03808
standard deviation	.003	.01	.006	.12	.067	.10	.00031
deviation of mean	.001	.01	.003	.05	.028	.04	.00013

d = 1.25, s = 0.25, X = 0.270						
		Statham Pressure Transducer		Modified Schaevitz-Bytrex Pressure Transducer		
Exp. No.	H(ft)	$\frac{P_s}{\gamma}$(ft)	t_r(m sec)	$\frac{P_s}{\gamma}$ (ft)	t_r(m sec)	t_d(sec)
1	.434	.467	2.32	.557	1.33	.03583
2	.433	.470	2.58	.595	1.05	.03605
3	.428	.463	2.50	.549	1.09	.03617
4	.433	.446	2.58	.604	1.10	.03612
5	.427	.455	2.61	.567	1.23	.03620
6	.430	.450	2.72	.624	1.05	.03618
mean	.431	.459	2.55	.583	1.14	.03609
standard deviation	.008	.009	.12	.027	.10	.00013
deviation of mean	.001	.004	.05	.011	.04	.00005
1	.471	.522	2.58	.676	1.06	.03490
2	.465	.516	2.80	.649	1.20	.03516
3	.463	.538	2.26	.679	.97	.03484
4	.462	.537	2.67	.578	1.13	.03495
5	.470	.537	2.42	.679	.97	.03498
6	.477	.532	2.74	.690	1.01	.03512
mean	.468	.530	2.58	.658	1.06	.03499
standard deviation	.005	.008	.19	.038	.08	.00011
deviation of mean	.002	.003	.08	.016	.03	.00005

Table B2 (continued).

d = 1.25 ft, ε = 0.25 ft, X = 1.52 ft						
		Statham Pressure Transducer		Modified Schaevitz-Bytrex Pressure Transducer		
Exp. No.	H(ft)	$\frac{P_2}{\gamma}$ (ft)	t_r(m sec)	$\frac{P_2}{\gamma}$ (ft)	t_r(m sec)	t_d(sec)
1	.369	.625	5.56	.657	2.67	.16735
2	.369	.578	5.50	.864	2.75	.16758
3	.370	.537	7.64	.754	3.34	.16817
4	.370	.665	4.67	.669	3.67	.16830
6	.367	.729	3.30	.638	4.08	.16802
mean	.368	.643	5.17	.715	3.48	.16788
standard deviation	.002	.066	1.34	.0766	.63	.00036
deviation of mean	.001	.027	.55	.031	.26	.00016
1	.478	1.019	---	1.181	3.37	---
2	.478	---	---	1.328	1.56	.15519
3	.471	---	---	1.160	1.71	.15556
4	.471	1.343	2.56	1.198	3.20	.15617
5	.471	---	---	1.380	2.54	.15595
6	.467	---	---	1.371	3.14	.15716
mean	.473	1.176	2.56	1.2697	2.57	.15601
standard deviation	.004	---	---	.092	.72	.00067
deviation of mean	.0016	---	---	.0376	.30	.00030

d = 1.25 ft, ε = 0.25 ft, X = 1.52 ft						
		Statham Pressure Transducer		Modified Schaevitz-Bytrex Pressure Transducer		
Exp. No.	H(ft)	$\frac{P_2}{\gamma}$ (ft)	t_r(m sec)	$\frac{P_2}{\gamma}$ (ft)	t_r(m sec)	t_d(sec)
1	.429	.753	4.61	.780	3.50	.15964
2	.430	---	---	---	---	---
3	.431	.909	4.11	.864	3.80	.15992
4	.431	.905	5.00	1.090	2.03	---
5	.431	.800	4.31	.955	2.77	.15897
6	.428	.827	3.44	1.187	2.19	.15993
mean	.430	.839	4.29	.972	2.86	.15962
standard deviation	.001	.061	.52	.151	.70	.00039
deviation of mean	.000	.027	.23	.067	.31	.00020
1	.312	.436	3.22	---	---	---
2	.312	.467	3.37	---	---	---
3	.309	---	---	---	---	---
4	.310	.482	4.33	---	---	---
5	.306	.438	4.80	.505	4.37	.18203
6	.303	.433	3.53	.529	2.57	.18165
7	.301	.427	2.67	.416	3.33	.18234
8	.300	.422	3.22	.523	2.42	.18316
9	.304	---	---	.480	4.21	---
10	.304	.365	4.92	.492	2.88	.18034
mean	.306	.434	3.76	.491	3.30	.18904
standard deviation	.004	.032	.77	.037	.76	.00093
deviation of mean	.001	.011	.27	.015	.31	.00041

Table B2 (continued).

d = 1.25 ft, s = 0.25 ft, X = 2.525 ft						
		Statham Pressure Transducer		Modified Schaevitz-Bytrex Pressure Transducer		
Exp. No.	H(ft)	$\frac{P_2}{\gamma}$ (ft)	t_r(m sec)	$\frac{P_2}{\gamma}$ (ft)	t_r(m sec)	t_d(sec)
1	.474	---	---	1.067	---	---
2	.471	---	---	1.067	---	---
3	.473	---	---	1.195	---	---
4	.467	---	---	1.110	---	---
5	.463	---	---	.875	---	---
6	.467	---	---	1.071	---	---
mean	.469	---	---	1.064	---	---
standard deviation	---	---	---	---	---	---
deviation of mean	---	---	---	---	---	---
1	.305	---	---	.426	---	---
2	.300	---	---	.431	---	---
3	.307	---	---	.420	---	---
4	.303	---	---	.430	---	---
5	.304	---	---	.311	---	---
6	.303	---	---	.346	---	---
mean	.304	---	---	.394	---	---
standard deviation	---	---	---	---	---	---
deviation of mean	---	---	---	---	---	---
Note: Dock is turned around. This test is to compare with X = 2.520.						

Table B2 (continued).

d = .64, s = .128, $\bar{X}$ = 4.525						
		Statham Pressure Transducer		Modified Schaevitz-Bytrex Pressure Transducer		
Exp. No.	H(ft)	$\frac{P_2}{\gamma}$ (ft)	t_r(m sec)	$\frac{P_2}{\gamma}$ (ft)	t_r (m sec)	t_d (sec)
1	.258	---	---	.1011	5.75	---
2	.254	---	---	.0535	5.00	---
3	.252	---	---	.0420	16.00	---
4	.252	---	---	.1011	10.00	---
5	.245	---	---	.0459	7.41	---
6	.255	---	---	.0382	9.00	---
7	.255	---	---	.0764	12.00	---
mean	.253	---	---	.0655	9.31	---
standard deviation	.044	---	---	.0253	3.53	---
deviation of mean	.001	---	---	.0096	1.34	---
1	.289	---	---	.1165	7.88	---
2	.295	---	---	.1796	8.93	---
3	.294	---	---	.1395	18.40	---
4	.293	---	---	.2100	9.37	---
5	.293	---	---	.1950	9.78	---
6	.295	---	---	.1031	10.00	---
mean	.293	---	---	.1573	10.73	---
standard deviation	.004	---	---	.0400	3.50	---
deviation of mean	.0008	---	---	.0163	1.43	---

d = .64, s = .128, $\bar{X}$ = 4.525						
		Statham Pressure Transducer		Modified Schaevitz-Bytrex Pressure Transducer		
Exp. No.	H(ft)	$\frac{P_2}{\gamma}$ (ft)	t_r(m sec)	$\frac{P_2}{\gamma}$ (ft)	t_r (m sec)	t_d (sec)
1	.280	---	---	.1210	19.00	---
2	.279	---	---	.1844	10.00	---
3	.278	---	---	.1500	30.00	---
4	.278	---	---	.2036	16.00	---
5	.278	---	---	.1152	18.40	---
6	.283	---	---	.1114	19.00	---
mean	.279	---	---	.1476	18.73	---
standard deviation	.002	---	---	.0355	5.93	---
deviation of mean	.0007	---	---	.0145	2.42	---

Table B2 (continued).

d = .64, s = .128 X = 2.520

Exp. No.	H(ft)	Statham Pressure Transducer $\frac{P_s}{\gamma}$ (ft)	Statham Pressure Transducer t_r(m sec)	Modified Schaevitz-Bytrex Pressure Transducer $\frac{P_s}{\gamma}$ (ft)	Modified Schaevitz-Bytrex Pressure Transducer t_r (m sec)	Modified Schaevitz-Bytrex Pressure Transducer t_d (sec)
1	.168	---	---	.202	2.31	.40482
2	.166	---	---	----	----	------
3	.168	---	---	.139	5.45	.40445
4	.169	---	---	.066	7.20	.40489
5	.169	---	---	.088	4.98	.40153
6	.167	---	---	.101	3.42	.40355
7	.168	---	---	.136	2.46	.40218
mean	.168	---	---	.122	4.30	.40357
standard deviation	.001	---	---	.044	1.75	.00130
deviation of mean	.000	---	---	.017	.71	.00053
1	.194	---	---	.240	3.08	.37507
2	.195	---	---	.187	11.00	.37894
3	.194	---	---	.178	11.27	.37698
4	.194	---	---	.238	8.40	.37730
5	.194	---	---	.205	6.24	.38212
6	.196	---	---	.165	12.70	.38061
mean	.195	---	---	.202	8.78	.37850
stardard deviation	.0008	---	---	.029	3.31	.00235
deviation of mean	.000	---	---	.012	1.35	.00096

d = .64, s = .128, X = 2.520

Exp. No.	H(ft)	Statham Pressure Transducer $\frac{P_s}{\gamma}$ (ft)	Statham Pressure Transducer t_r(m sec)	Modified Schaevitz-Bytrex Pressure Transducer $\frac{P_s}{\gamma}$(ft)	Modified Schaevitz-Bytrex Pressure Transducer t_r (m sec)	Modified Schaevitz-Bytrex Pressure Transducer t_d(sec)
1	.232	---	---	.382	5.77	.34819
2	.235	---	---	.530	3.24	.34445
3	.236	---	---	.372	5.62	.34676
4	.235	---	---	.310	6.80	.34381
5	.235	---	---	.281	4.78	.34646
6	.237	---	---	.288	5.27	.34946
mean	.235	---	---	.361	5.25	.34652
stardard deviation	.002	---	---	.085	1.09	.00196
deviation of mean	.0006	---	---	.035	.44	.00080
1	.285	---	---	.354	11.68	.32654
2	.281	---	---	.408	4.82	.32431
3	.281	---	---	.417	3.18	.32482
4	.282	---	---	.461	2.73	.32240
5	.281	---	---	.433	5.52	.32219
6	.281	---	---	.404	7.00	.32434
mean	.282	---	---	.413	5.82	.32410
stardard deviation	.002	---	---	.032	2.98	.00149
deviation of mean	.0006	---	---	.013	1.22	.00060

Table B2 (continued).

d = 0.64 ft, s = 0.128 ft, X = 0.522 ft							
			Statham Pressure Transducer		Modified Schaevitz-Bytrex Pressure Transducer		
Exp. No.	H(ft)	U_o(ft/sec)	$\frac{P_2}{\gamma}$ (ft)	t_r(m sec)	$\frac{P_2}{\gamma}$ (ft)	t_r(m sec)	t_d(sec)
1	.211	5.214	.308	3.55	.354	2.10	.08253
2	.207	5.165	.393	---	.484	1.87	.08247
3	.207	5.218	.304	3.40	.411	1.47	.08242
4	.210	5.227	.321	4.51	.284	2.38	---
5	.212	5.117	.394	3.17	.398	2.07	.08250
6	.210	5.210	.392	3.12	.349	1.87	---
7	.212	5.198	.435	---	.278	3.68	.08125
8	.214	5.218	.347	2.88	.384	1.82	.08159
9	.212	5.181	.332	3.13	.365	.148	.08281
10	.212	5.181	.348	3.40	.425	1.98	.08258
11	.211	5.198	.319	2.81	.343	2.43	.08233
12	.213	5.210	.343	3.17	.375	2.08	.08169
13	.214	5.198	.315	3.70	.346	2.06	.08160
14	.212	5.227	.339	.288	.399	1.44	.08225
15	.213	5.181	.368	---	.364	2.54	.08248
16	.217	5.202	.333	2.88	.361	2.06	.08240
17	.212	5.214	.330	3.09	.380	1.70	.08260
18	.209	5.185	.321	3.52	.367	1.61	.08195
19	.210	5.185	.292	3.38	.401	1.84	.08280
20	.213	5.185	.362	---	.357	2.17	.08254
21	.209	5.173	.400	---	.411	1.74	.08286
22	.208	5.210	.274	4.24	.401	1.82	.08284
23	.210	5.190	.381	3.13	.429	1.88	.08230
24	.210	5.223	.305	2.78	.427	1.85	.08321
25	.211	5.202	.320	3.45	.416	1.80	---
26	.208	5.210	---	---	---	---	---
27	.208	5.198	.296	3.38	.352	2.15	.08206
28	.206	5.210	.323	.339	.344	2.58	.08219
29	.208	5.214	.326	3.22	.351	2.00	.08285
30	.202	5.214	.427	---	.365	2.03	.08269
31	.204	5.210	.325	3.24	.405	1.77	.08265
32	.209	5.231	.394	3.44	.467	1.62	.08262
mean	.211	5.202	.344	3.31	.380	2.00	.08240
standard deviation	.003	---	.040	.40	.044	---	.00044
deviation of mean	.001	---	.007	.08	.008	---	.00008

d = 0.64 ft, s = 0.128 ft, X = 5.22 ft							
			Statham Pressure Transducer		Modified Schaevitz-Bytrex Pressure Transducer		
Exp. No.	H(ft)	U_o(ft/sec)	$\frac{P_2}{\gamma}$ (ft)	t_r(m sec)	$\frac{P_2}{\gamma}$ (ft)	t_r(m sec)	t_d(sec)
1	.264	5.368	.410	3.40	.509	2.36	.07717
2	.260	5.303	.433	2.80	.490	2.03	.07742
3	.264	5.346	.430	3.44	.370	2.62	.07766
4	.262	5.363	.392	---	.520	2.19	---
5	.264	5.337	.462	3.79	.505	2.00	.07694
6	.259	5.346	.438	---	.422	2.62	.07777
7	.260	5.355	.429	2.88	.485	2.52	.07736
8	.259	5.390	.345	4.68	.475	1.90	.07674
9	.260	5.355	.391	3.50	.465	2.05	---
10	.259	5.355	.510	---	.555	1.58	.07750
11	.259	5.355	.386	---	.443	1.77	.07697
12	.261	5.294	.419	4.25	.483	2.27	.07658
13	.260	5.324	.419	3.36	.485	2.44	.07730
14	.261	5.355	.419	3.13	.445	1.98	.07711
15	.259	5.328	.434	3.63	.479	2.24	.07719
16	.262	---	.410	3.24	---	---	---
mean	.261	5.345	.420	3.508	.475	2.17	.07705
standard deviation	.002	---	.0348	.51	.042	.30	.00033
deviation of mean	.000	---	.0087	.148	.0109	.077	.00009

Table B2 (continued).

d = 1.25 ft, s = 0.25 ft, X = 1.020 ft							
			Statham Pressure Transducer		Modified Schaevitz-Bytrex Pressure Transducer		
Exp. No.	H(ft)	U_o(ft/sec)	$\frac{P_s}{\gamma}$ (ft)	t_r(m sec)	$\frac{P_s}{\gamma}$ (ft)	t_r(m sec)	t_d(sec)
1	.415	7.30	.794	3.68	.781	2.60	.10970
2	.410	7.26	.762	2.97	.945	2.66	.11000
3	.412	7.27	.825	2.86	.805	2.54	.10931
4	.412	7.26	.829	2.79	.885	2.62	.11036
5	.412	7.30	.834	3.02	.834	2.80	---
6	.412	7.24	.807	3.75	.817	2.34	---
7	.412	7.28	.792	3.84	.940	2.08	---
8	.423	7.24	.834	3.33	.860	3.17	---
9	.418	7.25	.794	3.12	.854	2.19	---
10	.416	7.27	.789	3.78	.867	1.89	---
11	.423	7.27	.834	3.44	.964	2.66	---
12	.426	7.28	.798	2.86	.530	4.28	---
13	.416	7.24	.778	3.08	1.100	1.85	---
14	.416	7.31	.860	3.22	1.014	1.93	---
15	.411	7.24	.805	3.07	.969	2.54	---
16	.411	7.23	.807	3.71	1.130	1.93	---
17	.411	7.25	.910	2.86	.973	1.27	---
18	.412	7.26	.771	3.17	1.224	1.67	---
19	.412	7.27	.874	3.11	.975	2.22	---
20	.412	7.26	.836	3.36	1.212	1.36	---
mean	.415	7.26	.817	3.25	.934	2.33	---
standard deviation	.004	---	.036	---	.157	---	---
deviation of mean	.001	---	---	---	---	---	---

d = 1.25 ft, s = 0.25 ft, X = 1.020 ft							
			Statham Pressure Transducer		Modified Schaevitz-Bytrex Pressure Transducer		
Exp. No.	H(ft)	U_o(ft/sec)	$\frac{P_s}{\gamma}$ (ft)	t_r(m sec)	$\frac{P_s}{\gamma}$ (ft)	t_r(m sec)	t_d(sec)
1	.472	7.39	1.018	---	1.004	---	---
2	.480	7.48	1.013	3.27	1.100	1.25	.10700
3	.484	7.41	.965	3.44	1.182	2.62	.10754
4	.485	7.37	1.013	2.74	.989	2.29	---
5	.485	7.43	.970	---	1.050	---	---
6	.487	7.38	.990	3.22	1.166	2.71	.10726
7	.480	7.36	.863	3.12	1.130	2.60	---
8	.487	7.39	1.000	3.64	1.150	2.27	---
9	.481	7.38	.895	3.13	---	---	---
10	.477	7.41	1.035	4.25	.989	2.62	.10776
11	.485	7.34	.994	3.90	1.181	2.22	.10707
12	.493	7.36	.927	3.35	1.104	2.08	.10685
13	.481	7.39	.965	2.92	1.089	2.15	---
14	.479	7.39	1.026	3.50	.878	3.18	.10772
15	.489	7.40	1.019	3.27	1.028	2.38	.10742
16	.482	7.39	.990	3.39	.994	2.15	.10782
17	.488	7.36	.830	3.62	1.109	2.67	.10700
18	.485	7.39	1.012	3.54	1.209	2.57	.10700
19	.485	7.38	.913	2.78	1.039	2.01	.10696
20	.487	7.43	.995	3.05	1.331	2.56	.10668
21	.484	7.41	.935	4.00	1.030	2.92	.10764
22	.470	7.39	.916	3.32	1.172	2.37	.10727
23	.483	7.40	1.012	3.30	.933	2.47	.10800
24	.479	7.39	.885	3.60	1.209	3.11	.10788
25	.482	7.30	.961	2.70	1.052	2.22	.10731
26	.473	7.39	.959	2.96	1.193	1.87	.10645
27	.474	7.40	.980	---	1.104	---	---
28	.477	7.40	1.031	---	1.120	---	---
29	.477	7.39	1.029	---	1.062	---	---
30	.470	7.46	1.033	---		---	10670
31	.473	7.46	1.031	---	1.217	---	---
32	.474	7.38	.990	---	1.217	---	---
mean	.480	7.39	.975	3.34	1.100	2.40	.1073
standard deviation	.01	---	.053	.38	.098	.41	.00043
deviation of mean	.002	---	.009	.08	.018	.09	.00010

Table B2 (continued).

d = 1.25 ft, ε = 0.25 ft, X = 1.020 ft							
			Statham Pressure Transducer		Modified Schaevitz-Bytrex Pressure Transducer		
Exp. No.	H(ft)	U_o(ft/sec)	$\frac{P_2}{\gamma}$ (ft)	t_r(m sec)	$\frac{P_2}{\gamma}$ (ft)	t_r(m sec)	t_d(sec)
1	.350	7.11	.567	3.75	.763	2.19	.11437
2	.348	7.10	.551	---	.606	---	---
3	.348	7.08	.563	2.50	.705	1.64	.11530
4	.347	7.12	.551	2.88	.659	1.70	.11793
5	.348	7.11	.559	2.93	.674	2.01	.11832
6	.347	7.12	.602	2.31	.658	1.39	.11776
7	.344	7.12	.504	3.66	.677	1.67	.12013
8	.347	7.14	.548	2.90	.637	1.61	.11823
9	.348	7.12	.533	2.55	.590	2.70	.11580
10	.349	7.10	.557	2.88	.556	2.40	.11748
11	.335	7.13	.408	---	.601	---	---
12	.340	7.16	.537	2.50	.596	2.34	---
13	.340	7.13	.561	2.88	.708	1.76	.11869
14	.347	7.11	.541	3.28	.802	1.90	---
15	.342	7.13	.587	2.95	.618	2.48	.11881
16	.348	7.13	.545	3.22	.701	1.93	.11953
17	.346	7.14	.596	3.16	.697	2.46	.11750
18	.346	7.12	.571	3.25	.680	2.60	.11835
19	.347	7.14	.561	3.13	.624	2.66	.11825
20	.347	7.11	.506	3.46	.680	1.73	.11869
21	.352	7.14	.584	2.71	.606	2.20	.11882
22	.346	7.12	.547	3.26	.595	2.45	.11877
23	.342	7.09	.571	3.22	.619	2.26	.11871
24	.352	7.15	.596	3.30	.595	1.97	.11877
25	.348	7.17	.412	3.03	.570	2.12	.11740
26	.342	7.15	.588	2.88	.675	1.92	.11762
27	.340	7.14	.588	3.44	.720	1.64	.11766
28	.340	7.14	.588	3.12	.580	2.34	.11862
29	.350	7.09	.609	3.18	.680	1.43	.11712
30	.344	7.12	.584	3.10	.708	2.33	.11841
31	.342	7.15	.594	3.03	.694	1.91	.11813
32	.344	7.11	.600	3.30	.663	2.07	.11931
mean	.345	7.13	.557	3.06	.654	2.06	.118
standard deviation	.004	---	.046	.33	.057	.36	.00121
deviation of mean	.001	---	.008	.06	.010	.066	.00023

d = 1.25 ft, ε = 0.25 ft, X = 1.020 ft							
			Statham Pressure Transducer		Modified Schaevitz-Bytrex Pressure Transducer		
Exp. No.	H(ft)	U_o(ft/sec)	$\frac{P_2}{\gamma}$ (ft)	t_r(m sec)	$\frac{P_2}{\gamma}$ (ft)	t_r(m sec)	t_d(sec)
1	.300	6.96	.388	3.17	.553	1.43	.12605
2	.300	7.00	.393	3.03	.417	1.51	.12701
3	.300	7.01	.381	2.66	.537	1.09	.12610
4	.298	6.98	.403	3.10	.488	1.61	.12900
5	.296	6.97	.407	2.50	.466	2.03	.12640
6	.300	6.98	.437	2.81	.493	1.56	---
7	.292	6.78	.443	2.68	.450	1.89	---
8	.296	7.00	.438	2.88	.504	1.82	.12863
9	.298	7.01	.404	2.85	.522	1.58	.12553
10	.300	7.01	.378	2.86	.467	2.06	.12647
11	.303	6.99	.392	2.88	.520	1.76	.12679
12	.297	6.98	.388	2.64	.506	1.32	.12767
13	.295	6.99	.378	2.86	.412	2.22	.12827
14	.300	7.03	.400	2.80	.495	1.24	.12865
15	.295	7.00	.377	2.86	.490	2.14	.12863
16	.300	7.02	.396	2.81	.517	1.21	.12900
17	.300	6.97	.386	2.66	.487	1.41	.12812
18	.300	7.01	.381	2.72	.457	1.82	.12950
19	.297	6.99	.380	2.97	.446	2.03	.12986
20	.298	7.00	.395	3.00	.507	1.67	.12986
21	.298	7.00	.398	2.42	.553	1.51	.12894
22	.300	7.00	.405	2.80	.533	1.13	.12919
23	.296	7.00	.404	2.81	.569	1.72	.12969
24	.298	7.01	.411	2.90	.572	1.61	.12968
25	.301	7.02	.362	2.90	.543	1.45	.12607
26	.297	7.02	.416	3.18	.457	1.91	.12718
27	.297	7.00	.403	2.78	.473	1.85	.12755
28	.301	7.03	.415	3.16	.470	1.33	.12840
29	.295	7.00	.403	3.12	.490	1.87	.12866
30	.295	7.02	.420	3.16	.444	1.90	.12816
31	.297	6.99	.436	2.95	.497	1.40	.12815
32	.304	7.09	.409	3.01	.528	1.66	.12860
mean	.298	7.00	.401	2.87	.496	1.65	.12806
standard deviation	.003	---	.019	.10	.041	.29	.00110
deviation of mean	.001	---	.003	.02	.007	.05	.00020

Table B2 (continued).

d = 1.25, s = 0.25, X = 4.90						
		Statham Pressure Transducer		Modified Schaevitz-Bytrex Pressure Transducer		
Exp. No.	H(ft)	$\frac{P_3}{\gamma}$ (ft)	t_r(m sec)	$\frac{P_3}{\gamma}$ (ft)	t_r (m sec)	t_d(sec)
1	.305	---	---	.229	6.97	
2	.297	---	---	.238	6.40	
3	.297	---	---	.161	6.06	
4	.302	---	---	.179	12.30	
5	.302	---	---	.264	5.89	
6	.300	---	---	.158	7.00	
mean	.301	---	---	.205	7.44	
standard deviation	.003	---	---	.041	2.21	
deviation of mean	.001	---	---	.017	.90	
1	.366	---	---	.315	----	
2	.362	---	---	.408	9.70	
3	.364	---	---	.308	15.40	
4	.363	---	---	.266	9.20	
5	.362	---	---	.374	14.30	
6	.366	---	---	.328	13.50	
mean	.364	---	---	.333	12.42	
standard deviation	.002	---	---	.046	2.50	
deviation of mean	.0007	---	---	.019	1.20	

d = 1.25, s = .25, X = 4.90						
		Statham Pressure Transducer		Modified Schaevitz-Bytrex Pressure Trandsucer		
Exp. No.	H(ft)	$\frac{P_3}{\gamma}$ (ft)	t_r(m sec)	$\frac{P_3}{\gamma}$ (ft)	t_r (m sec)	t_d (sec)
1	.429	---	---	.493	14.20	---
2	.427	---	---	.497	7.12	---
3	.427	---	---	.611	7.62	---
4	.427	---	---	.473	12.60	---
5	.426	---	---	.513	16.10	---
6	.426	---	---	.415	14.60	---
mean	.427	---	---	.500	12.04	---
standard deviation	.001	---	---	.0585	3.46	---
deviation of mean	.000	---	---	.0239	1.41	---
1	.468	---	---	.477	13.20	---
2	.467	---	---	.424	19.20	---
3	.470	---	---	.368	14.50	---
4	.470	---	---	.633	10.45	---
5	.468	---	---	.522	20.00	---
6	.474	---	---	.535	16.50	---
mean	.470	---	---	.493	15.64	---
standard deviation	.002	---	---	.085	3.32	---
deviation of mean	.0009	---	---	.035	1.36	---

Table B2 (continued).

d = 0.640 ft, s = 0.128 ft, X = 1.520 ft						
		Statham Pressure Transducer		Modified Schaevitz-Bytrex Pressure Transducer		
Exp. No.	H(ft)	$\frac{P_2}{\gamma}$ (ft)	t_r(m sec)	$\frac{P_2}{\gamma}$ (ft)	t_r(m sec)	t_d(sec)
1	.157	.196	4.47	.208	2.98	.24502
2	.157	.160	3.93	.165	3.03	.24378
3	.157	.168	5.05	.313	1.42	.24440
4	.157	.215	3.39	.186	3.09	.24417
5	.158	.185	3.63	.188	3.03	.24436
6	.157	.159	3.75	.204	2.66	.24519
mean	.157	.181	4.04	.211	2.70	.24449
standard deviation	.000	.020	.56	.048	.59	.00048
deviation of mean	.000	.008	.23	.019	.24	.00020
1	.186	.241	5.30	.426	1.87	.22431
2	.185	.222	7.27	.407	1.97	.22484
3	.189	.334	4.25	.300	3.04	.22551
4	.185	.334	3.43	.424	1.87	.22423
5	.185	---	4.38	---	---	.22414
6	.187	.312	4.00	---	---	.22428
mean	.186	.289	4.76	.389	2.19	.22455
standard deviation	.002	.048	1.25	.052	.49	.00048
deviation of mean	.0006	.021	.51	.026	.24	.00020

d = 0.640 ft, s = 0.128 ft, X = 1.520						
		Statham Pressure Transducer		Modified Schaevitz-Bytrex Pressure Transducer		
Exp. No.	H(ft)	$\frac{P_2}{\gamma}$ (ft)	t_r(m sec)	$\frac{P_2}{\gamma}$ (ft)	t_r(m sec)	t_d(sec)
1	.223	---	---	.475	2.53	.20966
2	.223	---	---	.390	4.96	.21005
3	.220	---	---	.395	3.00	.20959
4	.220	---	---	.360	3.30	.21015
5	.218	---	---	.598	2.10	.21103
6	.218	---	---	.352	5.27	.21126
mean	.220	---	---	.428	3.53	.21029
standard deviation	.002	---	---	.086	1.17	.00064
deviation of mean	.001	---	---	.035	.48	.00026
1	.259	---	---	.367	8.25	.20280
2	.257	---	---	.440	2.32	.20012
3	.261	---	---	.585	1.98	.20032
4	.255	---	---	.454	4.35	.20062
5	.255	---	---	.665	2.12	.20003
6	.251	---	---	.440	4.92	.20142
mean	.256	---	---	.492	3.99	.20089
standard deviation	.003	---	---	.101	2.22	.00097
deviation of mean	.001	---	---	.041	.90	.00040

Table B2 (continued).

d = 1.25 ft, s = 0.25 ft, X = 2.020 ft						
		Statham Pressure Transducer		Modified Schaevitz-Bytrex Pressure Transducer		
Exp. No.	H(ft)	$\frac{P_1}{\gamma}$ (ft)	t_r (m sec)	$\frac{P_2}{\gamma}$ (ft)	t_r (m sec)	t_d (sec)
1	.305	.485	4.37	.653	1.88	.23259
2	.306	.402	4.68	.412	3.12	.23362
3	.306	.633	3.55	.446	3.55	.23395
4	.303	.498	3.22	.743	1.68	.23322
5	.304	.484	3.22	.535	2.42	.23204
6	.299	.478	3.43	.410	3.43	.23502
mean	.304	.497	3.75	.533	2.68	.23341
standard deviation	.002	.069	.57	.126	---	.00096
deviation of mean	.001	.028	.23	.052	---	.00039
1	.357	---	---	.780	3.04	.21428
2	.358	.700	3.46	.828	3.46	.21634
3	.357	.637	4.03	.986	2.91	.21645
4	.359	.927	3.48	.685	5.70	.21760
5	.357	.957	2.70	1.059	4.11	---
6	.360	.685	3.87	.665	3.23	---
mean	.358	.781	3.51	.834	3.74	.21617
standard deviation	.001	.133	.46	.146	.96	.00120
deviation of mean	.000	.060	.21	.059	.39	.00060

d = 1.25 ft, s = 0.25 ft, X = 2.020 ft						
		Statham Pressure Transducer		Modified Schaevitz-Bytrex Pressure Transducer		
Exp. No.	H(ft)	$\frac{P_1}{\gamma}$ (ft)	t_r (m sec)	$\frac{P_2}{\gamma}$ (ft)	t_r (m sec)	t_d (sec)
1	.428	.802	8.75	.905	3.69	.20737
2	.418	.830	5.26	.935	3.28	---
3	.426	1.061	5.84	1.188	3.99	.20746
4	.423	.942	3.57	.824	3.40	.20816
5	.422	.917	5.31	.872	4.37	.20772
6	.418	.753	8.70	1.104	3.94	.20834
mean	.423	.884	6.24	.971	3.78	.20781
standard deviation	.003	.185	1.59	.213	---	.00096
deviation of mean	.001	.076	.65	.087	---	.00043
1	.467	.820	7.50	1.050	3.78	---
2	.467	.904	7.70	1.326	1.55	.20158
3	.467	.912	6.93	1.082	3.83	.20154
4	.466	1.275	6.25	.890	6.37	.20191
5	.475	1.300	3.25	1.480	3.68	.20178
6	.464	1.023	4.78	.920	7.83	.20409
mean	.468	1.039	6.07	1.125	4.51	.20218
standard deviation	.003	.185	1.59	.213	---	.00096
deviation of mean	.001	.076	.65	.087	---	.00043

Table B2 (continued).

d = 0.640 ft, s = 0.128 ft, X = 0.148 ft						
		Statham Pressure Transducer		Modified Schaevitz-Bytrex Pressure Transducer		
Exp. No.	H(ft)	$\frac{P_s}{\gamma}$ (ft)	t_r(m sec)	$\frac{P_s}{\gamma}$(ft)	t_r(m sec)	t_d(sec)
1	.175	.149	3.28	.218	1.19	.03274
2	.177	.146	3.82	.168	1.28	.03223
3	.189	.154	3.49	.178	1.21	.03251
4	.178	.135	3.18	.184	1.06	.03237
5	.181	.151	3.07	.192	1.06	.03256
mean	.180	.147	3.37	.188	1.16	.03248
standard deviation	.005	.007	.27	.017	.09	.00017
deviation of mean	.002	.003	.12	.008	.04	.00008
1	.148	.053	3.20	.064	1.15	.04084
2	.150	.061	3.03	.092	1.73	.04032
3	.147	.066	2.97	.089	1.88	.04020
4	.145	.066	3.28	.089	1.62	.04054
5	.153	.072	2.90	.072	1.55	.04003
6	.144	.066	2.80	.062	1.70	.04053
7	.150	.051	2.81	.121	1.56	.03986
mean	.148	.062	2.99	.084	1.60	.04033
standard deviation	.003	.007	.17	.091	.21	.00031
deviation of mean	.003	.003	.07	.007	.08	.00012

d = 0.640 ft, s = 0.128 ft, X = 0.148 ft						
		Statham Pressure Transducer		Modified Schaevitz-Bytrex Pressure Transducer		
Exp. No.	H(ft)	$\frac{P_s}{\gamma}$ (ft)	t_r(m sec)	$\frac{P_s}{\gamma}$(ft)	t_r(m sec)	t_d(sec)
1	.246	.226	3.42	.300	1.25	.02780
2	.242	.253	2.80	.327	1.40	.02789
3	.245	.233	2.80	.529	.72	.02740
4	.245	.238	2.88	.319	1.21	.02825
5	.249	.184	3.31	.300	1.30	.02813
6	.240	.212	3.60	.308	1.41	.02811
mean	.245	.224	3.15	.347	1.22	.02793
standard deviation	.003	.022	.32	.082	.23	.00028
deviation of mean	.001	.009	.13	.033	.10	.00011
1	.228	.206	3.11	.256	1.56	.02873
2	.226	.219	3.40	.270	1.41	.02888
3	.226	.266	2.70	.261	1.58	.02907
4	.223	.233	2.36	.235	1.71	.02858
5	.222	.276	2.27	.273	1.51	.02908
mean	.225	.240	2.77	.259	1.55	.02887
standard deviation	.002	.027	.43	.014	.10	.00019
deviation of mean	.001	.012	.00	.006	.04	.00009

Table B2 (continued).

d = 0.64 ft, s = 0.128 ft, X = 0.522 ft							
			Statham Pressure Transducer		Modified Schaevitz-Bytrex Pressure Transducer		
Exp. No.	H(ft)	U_o(ft/sec)	$\frac{P_2}{\gamma}$ (ft)	t_r(m sec)	$\frac{P_2}{\gamma}$ (ft)	t_r(m sec)	t_d(sec)
1	.158	5.101	.203	3.27	.257	1.49	.09393
2	.155	5.050	.205	3.55	.283	1.25	.09610
3	.157	5.069	.212	3.13	.215	1.44	.09529
4	.160	5.081	.197	3.32	.241	1.39	.09648
5	.164	5.058	.187	3.18	.226	1.67	.09651
6	.162	5.097	.188	3.70	2.84	1.39	.09679
7	.162	5.046	.179	3.21	.195	2.39	---
8	.162	5.073	.170	3.30	.251	1.57	---
9	.165	5.058	.169	3.18	.256	1.27	.09668
10	.163	5.054	.201	3.06	.190	1.61	.09531
11	.163	5.062	.173	3.33	.240	1.66	.09908
12	.162	5.046	.173	3.22	.244	1.55	.09708
13	.161	5.073	.172	3.44	.254	1.56	.09652
14	.161	5.085	.173	3.10	.243	1.54	.09662
15	.161	5.058	.169	3.56	.220	2.59	.09712
16	.163	5.085	.175	3.14	.223	1.88	.09612
17	.165	---	.204	3.27	.272	1.56	.09472
18	.162	---	.183	3.42	.273	1.55	.09438
19	.163	---	.186	3.40	.269	1.31	.09623
20	.161	4.974	.186	3.43	.280	1.41	.09667
21	.163	4.936	.186	3.51	.274	1.32	---
22	.162	4.992	.188	3.34	.271	1.75	.09676
23	.160	4.985	.186	3.28	.243	1.70	.09711
24	.161	4.985	.186	3.28	.248	2.03	.09717
25	.164	4.962	.191	3.49	.284	1.29	.09663
26	.162	4.955	.191	3.45	.268	1.38	.09618
27	.159	4.958	.183	3.59	.274	1.41	.09691
28	.160	4.970	---	3.29	.230	1.88	.09625
29	.162	4.958	.187	3.45	.262	1.16	.09606
30	.160	4.947	.173	---	.267	1.26	.09700
31	.161	4.974	.209	3.11	.265	1.47	.09700
32	.164	4.970	.190	3.37	.261	1.92	.09670
mean	.162	5.022	.187	3.33	.252	1.58	.09639
standard deviation	.002	---	.012	.16	.024	.31	.00096
deviation of mean	.000	---	.002	.03	.004	.06	.00018

d = 0.640 ft, s = 0.128 ft, X = 0.522 ft							
			Statham Pressure Transducer		Modified Schaevitz-Bytrex Pressure Transducer		
Exp. No.	H(ft)	U_o(ft/sec)	$\frac{P_2}{\gamma}$ (ft)	t_r(m sec)	$\frac{P_2}{\gamma}$ (ft)	t_r(m sec)	t_d(sec)
1	.191	5.161	.282	3.75	.318	1.80	.08675
2	.188	5.181	.273	3.52	.435	2.35	.08680
3	.188	5.161	.278	3.72	.342	1.60	---
4	.188	5.169	.355	3.99	.261	2.70	.08667
5	.190	5.129	.273	3.34	.340	2.43	.08671
6	.189	5.161	.250	3.69	.320	2.00	.08728
7	.193	5.125	.273	3.31	.333	1.70	.08698
8	.193	5.153	.246	3.95	.331	2.04	.08741
9	.191	5.113	.273	3.53	.320	1.72	.08667
10	.191	5.137	.309	3.03	.296	1.82	.08522
11	.189	5.125	.264	3.44	.331	1.56	.08681
12	.187	5.153	.296	4.09	.388	1.65	---
13	.187	5.153	.262	3.13	.270	2.33	.08611
14	.188	5.101	.268	3.50	.343	1.80	.08648
15	.189	5.133	.282	3.48	.288	2.53	.08620
16	.189	5.097	.282	3.31	.338	1.64	.08584
17	.192	5.153	.264	3.34	.294	1.64	.08584
18	.187	5.109	.305	3.40	.283	2.31	.08694
19	.188	5.141	.291	3.37	.267	2.88	.08661
20	.188	5.141	.355	3.00	.264	2.58	.08597
21	.189	5.141	.259	3.49	.346	1.51	.08669
22	.186	5.145	.410	4.24	.386	1.65	.08606
23	.185	5.129	.280	3.71	.349	1.55	.08717
24	.183	5.161	.282	3.18	.338	1.59	.08598
25	.189	5.137	.268	3.55	.346	2.03	.08665
26	.185	5.137	.282	3.38	.316	2.46	.08785
27	.183	5.149	.353	3.87	.305	1.87	.08577
28	.184	5.141	.473	---	.377	1.50	.08627
29	.188	5.157	.273	3.47	.303	1.80	---
30	.187	5.137	.414	---	.364	1.54	.08600
31	.184	5.149	.282	3.16	.340	1.64	.08612
32	.189	5.125	.414	2.99	.342	1.73	.08616
mean	.188	5.141	.302	3.50	.327	1.94	.08651
standard deviation	.003	---	.055	.31	.038	.39	---
deviation of mean	.000	---	.010	.06	.007	.07	---

Table B2 (continued).

d = 0.64 ft, s = 0.128 ft, X = 0.270 ft						
		Statham Pressure Transducer		Modified Schaevitz-Bytrex Pressure Transducer		
Exp. No.	H(ft)	$\frac{P_s}{\gamma}$ (ft)	t_r(m sec)	$\frac{P_s}{\gamma}$ (ft)	t_r(m sec)	t_d(sec)
1	.171	.198	2.65	.227	1.32	.05397
2	.166	.178	2.33	.215	1.31	.05403
3	.166	.169	2.96	.241	1.25	.05421
4	.167	.179	2.92	.208	2.00	.05485
5	.168	.192	3.16	.195	1.58	.05421
6	.176	.198	2.86	.244	1.74	.05437
mean	.169	.186	2.81	.228	1.53	.05427
standard deviation	.004	.011	.26	.018	.27	.00029
deviation of mean	.002	.005	.107	.007	.11	.00012
1	.196	.232	2.97	.268	1.88	.05005
2	.198	.236	3.10	.270	1.87	.04983
3	.195	.230	2.98	.258	2.06	.04986
4	.200	.268	3.33	.294	2.12	.04983
5	.193	.241	3.37	.260	1.96	.05012
6	.194	.241	3.13	.254	1.88	.05059
mean	.196	.241	3.15	.267	1.96	.05005
standard deviation	.002	.013	.16	.013	.10	.00027
deviation of mean	.001	.005	.06	.005	.04	.00011

d = 0.640 ft, s = 0.128 ft, X = 0.270 ft						
		Statham Pressure Transducer		Modified Schaevitz-Bytrex Pressure Transducer		
Exp. No.	H(ft)	$\frac{P_s}{\gamma}$ (ft)	t_r(m sec)	$\frac{P_s}{\gamma}$ (ft)	t_r(m sec)	t_d(sec)
1	.234	.287	3.18	3.66	1.53	.04647
2	.230	.293	3.13	.366	2.25	.04638
3	.246	.300	3.57	.398	1.37	.04596
4	.236	.334	3.87	.401	1.24	.04588
5	.233	.278	3.12	.328	2.59	.04645
6	.230	.289	3.13	.375	1.87	.04657
mean	.235	.297	3.33	.372	1.81	.04628
standard deviation	.005	.018	.29	.024	.48	.00027
deviation of mean	.002	.007	.12	.010	.20	.00011
1	.276	.327	3.44	.359	1.88	.04272
2	.270	.346	3.38	.410	1.23	.04305
3	.274	.335	3.65	.458	2.03	.04302
4	.263	.341	2.95	.399	1.99	.04371
5	.267	.342	2.81	.465	1.19	.04357
6	.274	.379	3.41	.430	1.55	.04320
mean	.271	.345	3.27	.420	1.66	.04321
standard deviation	.005	.016	.29	.036	.34	.00034
deviation of mean	.002	.007	.12	.015	.14	.00014

Table B2 (continued).

d = 0.640 ft, ε = 0,128 ft, X = 2.020						
		Statham Pressure Transducer		Modified Schaevitz-Bytrex Pressure Transducer		
Exp. No.	H(ft)	$\frac{P_2}{\gamma}$ (ft)	t_r(m sec)	$\frac{P_2}{\gamma}$ (ft)	t_r(m sec)	t_d(sec)
1	.147	---	---	.074	2.48	.36575
2	.146	---	---	.059	2.80	.37482
3	.146	---	---	.052	2.00	.36874
4	.147	---	---	.064	1.91	.36256
5	.146	---	---	.078	2.49	.36175
6	.146	---	---	.044	2.45	.37299
mean	.146	---	---	.062	2.36	.36777
standard deviation	.0005	---	---	.012	.31	.00492
deviation of mean	.000	---	---	.005	.13	.00200
1	.176	---	---	.182	4.57	.31124
2	.173	---	---	.158	6.17	.31308
3	.172	---	---	.195	3.42	.31368
4	.172	---	---	.174	3.97	.31168
5	.172	---	---	.202	4.23	.31261
6	.173	---	---	.267	2.81	.31112
mean	.173	---	---	.196	4.20	.31224
standard deviation	.001	---	---	.035	1.05	.00096
deviation of mean	.0006	---	---	.014	.43	.00039

d = .640 ft, ε = .128 ft, X = 2.020						
		Statham Pressure Transducer		Modified Schaevitz-Bytrex Pressure Transducer		
Exp. No.	H(ft)	$\frac{P_2}{\gamma}$ (ft)	t_r(m sec)	$\frac{P_2}{\gamma}$(ft)	t_r(m sec)	t_d (sec)
1	.208	---	---	.240	6.06	.28981
2	.206	---	---	.288	5.72	.28877
3	.205	---	---	----	----	------
4	.207	---	---	.481	1.71	.28908
5	.202	---	---	.386	3.59	.28937
6	.202	---	---	.428	1.86	.29035
7	.200	---	---	.281	6.94	.29046
mean	.204	---	---	.351	4.31	.28964
stardard deviation	.003	---	---	.087	2.05	.00063
deviation of mean	.001	---	---	.035	.84	.00026
1	.273	---	---	.404	1.82	.26207
2	.267	---	---	.486	3.33	.26205
3	.271	---	---	.413	4.24	.26069
4	.267	---	---	.422	14.33	.26627
5	.267	---	---	.555	14.00	.26136
6	.272	---	---	.615	3.77	.26360
mean	.270	---	---	.483	6.92	.26267
standard deviation	.003	---	---	.079	5.18	.00184
deviation of mean	.001	---	---	.032	2.11	.00075

Table B2 (continued).

d = 1.25, s = .25, X = 4.025						
		Statham Pressure Transducer		Modified Schaevitz-Bytrex Pressure Transducer		
Exp. No.	H(ft)	$\frac{P_s}{\gamma}$ (ft)	t_r(m sec)	$\frac{P_s}{\gamma}$ (ft)	t_r(m sec)	t_d(sec)
1	.303	---	---	.162	5.00	.45863
2	.305	---	---	.343	4.75	.46118
3	.303	---	---	.231	5.31	---
4	.307	---	---	.258	4.75	---
5	.301	---	---	.205	6.70	---
6	.301	---	---	.292	7.90	---
mean	.303	---	---	.249	5.74	.45991
standard deviation	.002	---	---	.059	1.18	---
deviation of mean	.001	---	---	.024	.48	---
1	.363	---	---	.442	10.00	---
2	.366	---	---	.509	11.36	.42170
3	.369	---	---	.421	14.70	.42400
4	.362	---	---	.436	12.45	---
5	.362	---	---	.427	14.00	---
6	.362	---	---	.587	10.00	---
mean	.364	---	---	.469	12.09	.42285
standard deviation	.003	---	---	.058	1.82	---
deviation of mean	.001	---	---	.024	.74	---

d = 1.25, s = .25, X = 4.025						
		Statham Pressure Transducer		Modified Schaevitz-Bytrex Pressure Transducer		
Exp. No.	H(ft)	$\frac{P_s}{\gamma}$ (ft)	t_r(m sec)	$\frac{P_s}{\gamma}$ (ft)	t_r (m sec)	t_d(sec)
1	.415	---	---	.609	8.75	.39970
2	.414	---	---	.529	8.38	.39979
3	.414	---	---	.480	18.00	---
4	.418	---	---	.663	7.75	---
5	.414	---	---	.468	10.90	---
6	.414	---	---	.619	13.70	---
mean	.415	---	---	.561	11.25	.39975
standard deviation	.002	---	---	.073	3.62	---
deviation of mean	.0006	---	---	.030	1.48	---
1	.467	---	---	.565	11.50	.38493
2	.467	---	---	.753	18.20	.38751
3	.462	---	---	.889	10.30	---
4	.466	---	---	.537	30.00	---
5	.467	---	---	.873	4.27	---
6	.470	---	---	.702	15.10	---
mean	.467	---	---	.720	14.90	.38622
standard deviation	.002	---	---	.136	8.01	---
deviation of mean	.001	---	---	.056	3.27	---

Table B2 (continued).

d = 1.25 ft, s = 0.25 ft, X = 0.522 ft							
			Statham Pressure Transducer		Modified Schaevitz-Bytrex Pressure Transducer		
Exp. No.	H(ft)	U_o(ft/sec)	$\frac{P_s}{\gamma}$ (ft)	t_r(m sec)	$\frac{P_s}{\gamma}$ (ft)	t_r(m sec)	t_d(sec)
1	.300	---	.326	2.54	.438	.96	.07293
2	.300	7.011	.324	---	.359	---	---
3	.300	6.991	.333	2.33	.449	.83	.07388
4	.296	6.991	.318	2.30	.427	.96	.07384
5	.297	7.011	.320	2.30	.421	.98	.07381
mean	.299	7.001	.324	2.37	.419	.93	.07362
standard deviation	.002	.010	.005	.00	.031	.06	.0004
deviation of mean	.001	.005	.002	.00	.014	.03	.0002
1	.387	7.201	.580	3.66	.707	1.33	.06407
2	.382	7.199	.564	2.26	.685	1.21	.06427
3	.385	7.201	.575	2.64	.629	1.40	.06425
4	.385	7.194	.573	3.38	.662	1.03	.06342
5	.391	7.196	.602	2.47	.685	1.32	.06413
mean	.386	7.198	.579	2.88	.674	1.26	.06403
standard deviation	.003	.003	.013	.54	.027	.13	.00031
deviation of mean	.001	.001	.006	.24	.012	.06	.00014

d = 1.25 ft, s = 0.25 ft, X = 0.522 ft							
			Statham Pressure Transducer		Modified Schaevitz-Bytrex Pressure Transducer		
Exp. No.	H(ft)	U_o(ft/sec)	$\frac{P_s}{\gamma}$ (ft)	t_r(m sec)	$\frac{P_s}{\gamma}$ (ft)	t_r(m sec)	t_d(sec)
1	.347	7.117	.469	3.03	.508	1.82	.06656
2	.351	7.104	.465	2.74	.633	1.22	.06713
3	.352	7.126	.452	2.49	.627	.94	---
4	.353	7.115	.469	2.95	.573	2.13	.06735
5	.353	7.089	.469	2.51	.597	1.57	---
mean	.351	7.110	.465	2.74	.588	1.54	.06701
standard deviation	.002	.013	---	.00	.045	.42	.00033
deviation of mean	.001	.006	---	.00	.020	.19	.00015
1	.499	7.437	.750	---	1.028	---	---
2	.500	7.407	---	---	.909	1.97	.05976
3	.499	7.433	.686	2.78	.895	1.56	---
4	.483	7.417	.788	---	.843	---	---
5	.486	7.399	.742	2.54	.818	2.36	.05972
mean	.493	7.419	.742	2.66	.899	1.96	.05974
standard deviation	.007	.015	.036	.12	.073	.33	.00002
deviation of mean	.003	.007	.018	.08	.033	.19	.00001

Table B2 (continued).

d = 1.25 ft, s = 0.25 ft, X = 2.520 ft						
		Statham Pressure Transducer		Modified Schaevitz-Bytrex Pressure Transducer		
Exp. No.	H(ft)	$\frac{P_2}{\gamma}$ (ft)	t_r(m sec)	$\frac{P_2}{\gamma}$ (ft)	t_r(m sec)	t_d(sec)
1	.293	.458	3.27	.429	2.45	.29114
2	.293	.331	4.35	.423	3.70	.29148
3	.298	.331	4.32	.355	4.32	.29184
4	.300	.358	5.13	.471	3.53	.29196
5	.302	.436	3.77	.266	---	---
6	.295	.436	4.56	.344	2.70	.29196
mean	.297	.392	4.23	.381	3.34	.29162
standard deviation	.003	.053	.59	.068	.68	.00029
deviation of mean	.001	.022	.24	.028	.31	.00013
1	.356	.628	5.16	.489	7.90	.26917
2	.357	.619	4.42	.501	10.00	.27157
3	.357	.481	7.43	.648	5.30	---
4	.356	.887	5.09	.612	9.55	.26949
5	.361	.495	9.00	.781	4.84	.26745
6	.354	.531	6.25	.518	6.88	.26946
mean	.357	.607	6.23	.592	7.41	.26943
standard deviation	.002	.137	1.57	.103	1.95	.00131
deviation of mean	.001	.056	.64	.042	.80	.00059

d = 1.25 ft, s = 0.25 ft, X = 2.520 ft						
		Statham Pressure Transducer		Modified Schaevitz-Bytrex Pressure Transducer		
Exp. No.	H(ft)	$\frac{P_2}{\gamma}$ (ft)	t_r(m sec)	$\frac{P_2}{\gamma}$ (ft)	t_r(m sec)	t_d(sec)
1	.415	1.080	5.21	.785	3.70	.25725
2	.416	.970	4.50	1.291	4.50	.25675
3	.418	.692	4.71	.900	4.40	---
4	.417	.960	5.02	.655	10.00	.25824
5	.417	.818	6.45	.857	5.32	.25630
6	.413	.908	5.35	1.239	4.25	.25648
mean	.416	.905	5.21	.946	5.36	.25700
standard deviation	.002	.123	.63	.221	2.13	.00070
deviation of mean	.001	.050	.26	.090	.87	.00031
1	.457	1.261	3.92	1.223	7.30	.25045
2	.461	.858	10.00	1.060	6.50	.25079
3	.461	.914	10.00	.993	8.00	---
4	.461	.900	6.55	1.133	6.25	.24904
5	.465	1.004	4.87	.871	7.62	.24918
6	.462	.949	7.55	1.218	3.93	.24943
mean	.461	.981	7.15	1.083	6.61	.24978
standard deviation	.002	.133	2.32	.125	1.35	.00071
deviation of mean	.001	.054	.95	.051	.55	.00032

Table B2 (continued).

d = 1.25, s = .250, X = 3.025						
		Statham Pressure Transducer		Modified Schaevitz-Bytrex Pressure Transducer		
Exp. No.	H(ft)	$\frac{P_2}{\gamma}$ (ft)	t_r(m sec)	$\frac{P_2}{\gamma}$ (ft)	t_r (m sec)	t_d(sec)
1	.302	---	---	.382	6.39	.34129
2	.295	---	---	.542	1.35	.34228
3	.301	---	---	.461	2.61	---
4	.295	---	---	.331	7.18	.34419
5	.300	---	---	.502	5.67	---
6	.300	---	---	.601	2.90	.34399
mean	.300	---	---	.470	4.35	.34294
standard deviation	.004	---	---	.097	2.16	.00121
deviation of mean	.001	---	---	.038	.88	.00060
1	.362	---	---	.876	5.57	.31647
2	.361	---	---	.592	7.97	.31793
3	.363	---	---	.877	2.71	.31625
4	.360	---	---	.577	4.68	.31735
5	.360	---	---	.621	6.35	.31810
6	.363	---	---	.721	4.52	.31693
mean	.362	---	---	.711	5.30	.31717
standard deviation	.001	---	---	.126	1.63	.00069
deviation of mean	.0005	---	---	.051	.67	.00028

d = 1.25, s = .25, X = 3.025						
		Statham Pressure Transducer		Modified Schaevitz-Bytrex Pressure Transducer		
Exp. No.	H(ft)	$\frac{P_2}{\gamma}$ (ft)	t_r(m sec)	$\frac{P_2}{\gamma}$ (ft)	t_r (m sec)	t_d(sec)
1	.425	---	---	.791	4.82	.29973
2	.416	---	---	.981	4.17	.30104
3	.425	---	---	.634	7.60	.30066
4	.425	---	---	.910	5.25	.30042
5	.425	---	---	.785	9.79	.30323
6	.431	---	---	.718	4.60	.30033
mean	.425	---	---	.803	6.04	.30090
standard deviation	.004	---	---	.115	2.01	.00111
deviation of mean	.002	---	---	.047	.82	.00045
1	.472	---	---	.627	32.00	.29518
2	.472	---	---	.970	8.28	.29103
3	.470	---	---	.880	10.10	---
4	.478	---	---	1.201	10.30	.29143
5	.475	---	---	.880	9.08	.29263
6	.474	---	---	1.021	8.99	.29158
mean	.474	---	---	.930	13.13	.29237
standard deviation	.003	---	---	.173	8.47	.00150
deviation of mean	.001	---	---	.071	3.46	.00067

Table B2 (continued).

d = 1.0 s = 0.1 X = .522						
		Statham Pressure Transducer		Modified Schaevitz-Bytrex Pressure Transducer		
Exp. No.	H(ft)	$\frac{P_s}{\gamma}$(ft)	t_r(m sec)	$\frac{P_s}{\gamma}$(ft)	t_r(m sec)	t_d(sec)
1	.151	---	---	.136	1.35	.10327
2	.138	---	---	.160	1.18	.10114
3	.145	---	---	.109	1.77	.09971
4	.151	---	---	.149	1.82	.10104
5	.145	---	---	.168	1.32	.10130
6	.149	---	---	.115	1.56	.10016
mean	.147	---	---	.140	1.50	.10110
standard deviation	.005	---	---	.022	.24	.01123
deviation of mean	.002	---	---	.009	.10	.00459
1	.220	---	---	.419	1.06	.08175
2	.217	---	---	.439	.95	.08409
3	.215	---	---	.434	.82	.08340
4	.217	---	---	.322	1.28	.08432
5	--	---	---	.258	1.32	.08164
6	.222	---	---	.242	1.60	.08315
mean	.218	---	---	.352	11.72	.08306
standard deviation	.003	---	---	.082	2.59	.00104
deviation of mean	.001	---	---	.034	1.06	.00043

d = 1.0 s = 0.1 X = .522						
		Statham Pressure Transducer		Modified Schaevitz-Bytrex Pressure Transducer		
Exp. No.	H(ft)	$\frac{P_s}{\gamma}$(ft)	t_r(m sec)	$\frac{P_s}{\gamma}$(ft)	t_r(m sec)	t_d(sec)
1	.380	---	---	.447	1.56	.06967
2	.373	---	---	.430	1.54	.07000
3	.375	---	---	.472	1.55	.06804
4	.374	---	---	.499	1.56	.07182
5	.370	---	---	.450	1.51	.06910
6	.371	---	---	.450	1.76	.06978
mean	.374	---	---	.458	1.58	.06974
standard deviation	.003	---	---	.022	.08	.00113
deviation of mean	.001	---	---	.009	.03	.00046
1	.309	---	---	.582	1.11	.07400
2	.307	---	---	.285	2.27	.07298
3	.303	---	---	.434	1.13	.07534
4	.307	---	---	.400	1.56	.07307
5	.306	---	---	.392	1.84	.07491
6	.305	---	---	.330	1.61	.07434
mean	.306	---	---	.404	1.59	.07411
standard deviation	.002	---	---	.093	.40	.00087
deviation of mean	.001	---	---	.038	.16	.00036

Table B2 (concluded).

d = 1.0 ε = .1 X = 4.525						
		Statham Pressure Transducer		Modified Schaevitz-Bytrex Pressure Transducer		
Exp. No.	H(ft)	$\frac{P_s}{\gamma}$(ft)	t_r(m sec)	$\frac{P_s}{\gamma}$ (ft)	t_r (m sec)	t_d(sec)
1	.150	---	---	.358	4.55	---
2	.149	---	---	.379	3.12	---
3	.150	---	---	.315	4.15	---
4	.150	---	---	.379	3.75	---
5	.150	---	---	.283	5.31	---
6	.150	---	---	.347	3.61	---
mean	.150	---	---	.344	4.08	---
standard deviation	.000	---	---	.035	.71	---
deviation of mean	.000	---	---	.014	.29	---
1	.380	---	---	1.180	4.76	---
2	.376	---	---	1.149	11.14	---
3	.377	---	---	1.020	8.75	---
4	.377	---	---	.833	14.30	---
5	.377	---	---	1.035	10.30	---
6	---	---	---	1.225	---	---
mean	.377	---	---	1.074	9.85	---
standard deviation	.001	---	---	.130	3.12	---
deviation of mean	.0006	---	---	.053	1.40	---

d = 1.0 ε = .1 X = 4.525						
		Statham Pressure Transducer		Modified Schaevitz-Bytrex Pressure Transducer		
Exp. No.	H(ft)	$\frac{P_s}{\gamma}$(ft)	t_r(m sec)	$\frac{P_s}{\gamma}$(ft)	t_r(m sec)	t_d(sec)
1	.308	---	---	1.112	9.06	---
2	.306	---	---	.850	.850	---
3	.308	---	---	.850	7.10	---
4	.307	---	---	.732	5.31	---
5	.307	---	---	.896	8.10	---
6	.307	---	---	1.032	6.77	---
mean	.307	---	---	.912	7.33	---
standard deviation	.0007	---	---	.126	1.16	---
deviation of mean	.000	---	---	.051	.48	---
1	.224	---	---	.601	6.67	---
2	.230	---	---	.825	4.44	---
3	.227	---	---	.660	6.50	---
4	.227	---	---	.640	5.31	---
5	.227	---	---	.710	4.46	---
6	.227	---	---	.710	4.46	---
mean	.227	---	---	.719	5.03	---
standard deviation	.002	---	---	.101	1.32	---
deviation of mean	.0007	---	---	.041	.54	---

Table B3. Normalized force $F/\gamma d^2$, average pressure $P_{av}/\gamma d$, and center of pressure x_{cp}/d for $s/d = 0.2$, $L/d = 0.4$.

$F/\gamma d^2$

$t\sqrt{g/d}$ \ H/d	0.24	0.28	0.32	0.36	0.40
0.203	0.00907	0.01778	0.03326	0.05013	0.06240
0.254	0.01120	0.01760	0.02990	0.04038	0.05134
0.305	0.01304	0.02289	0.03290	0.05905	0.06687
0.355	0.01225	0.02429	0.05773	0.07597	0.09288
0.406	0.01723	0.03345	0.06950	0.08822	0.10980
0.457	0.01393	0.03600	0.06880	0.08960	0.10647
0.508	0.02404	0.04318	0.07256	0.09365	0.11541
0.558	0.02506	0.04612	0.07421	0.13666	0.16903
0.609	0.02038	0.08687	0.07035	0.14287	0.17853
0.660	0.02212	0.10128	0.12342	0.16581	0.20975
0.711	0.02862	0.10891	0.13829	0.17527	0.21528
0.761	0.03020	0.09442	0.13798	0.17355	0.22278
0.812	0.03151	0.08498	0.12969	0.22226	0.28198
0.863	0.03428	0.10332	0.12335	0.22715	0.29847
0.914	0.02907	0.10495	0.16539	0.23779	0.30741
0.964	0.02761	0.13955	0.17879	0.25492	0.30697
1.015	0.04485	0.12952	0.18653	0.25776	0.37613
1.066	0.03674	0.11122	0.12404	0.29077	0.37399
1.167	0.02858	0.13496	0.21548	0.30748	0.39849
1.218	0.02481	0.14123	0.22158	0.30426	0.40416
1.269	0.02434	0.14577	0.21599	0.32961	0.46259
1.320	0.01568	0.10712	0.21382	0.34823	0.43653
1.370	0.01300	0.16120	0.25661	0.35308	0.49680
1.421	0.01828	0.16997	0.27402	0.33847	0.40578
1.472	0.01650	0.17431	0.27057	0.36382	0.49523
1.523	0.01128	0.15593	0.24724	0.38132	0.49777
1.573	-0.00073	0.13227	0.28874	0.36502	0.50657
1.624	0.03730	0.19389	0.31743	0.40768	0.59280
1.675	-0.00038	0.16915	0.29705	0.40604	0.55596
1.726	-0.01175	0.16910	0.29631	0.43757	0.53406
1.776	0.03111	0.18442	0.30107	0.40587	0.51159
1.827	0.01477	0.17854	0.28623	0.39880	0.48566
1.878	0.01476	0.17003	0.27650	0.37667	0.47505
1.929	0.01828	0.16361	0.26415	0.37064	0.57746
1.979	0.00661	0.13920	0.21736	0.40585	0.54398
2.030	-0.01762	0.11834	0.22705	0.41203	0.56290
2.132	-0.09064	0.08485	0.29110	0.41053	0.54897
2.233	-0.06172	0.11867	0.27262	0.41322	0.50350
2.335	-0.05553	0.12521	0.22868	0.34425	0.47031
2.436	-0.12362	0.07863	0.19054	0.36035	0.44162
2.538	-0.07106	0.07512	0.15790	0.24845	0.22389
2.639	-0.07440	0.05296	0.10438	0.06769	-0.02722
2.741	-0.14293	-0.10324	-0.03666	0.01256	0.05354
2.791	-0.12076	-0.16332	-0.07379	0.01317	0.04627
2.842	-0.12971	-0.07191	0.00640	0.09170	0.13799
2.944	-0.12134	-0.14556	0.00480	0.08692	0.04016
3.045	-0.15540	-0.19502	-0.18340	-0.08587	0.22285
3.147	-0.17805	-0.21866	-0.18563	-0.05474	0.16527
3.248	-0.14611	-0.17181	-0.08870	-0.20093	-0.39808
3.299	-0.14572	-0.16112	-0.14242	-0.16277	-0.23048
3.350	-0.15982	-0.16841	-0.22401	-0.19368	0.22719
3.451	-0.18942	-0.17713	-0.22634	-0.15340	0.40699
3.553	-0.14561	-0.12820	-0.12761	-0.12688	-0.26688
3.654	-0.13633	-0.10619	-0.11906	-0.21172	-0.27052
3.807	-0.15188	-0.17234	-0.15260	-0.11815	-0.13667
4.060	-0.15319	-0.17618	-0.18419	-0.15980	-0.09428
4.314	-0.15368	-0.16711	-0.16205	-0.15034	-0.11749
4.568	-0.13549	-0.34527	-0.15453	-0.14982	-0.17183
4.822	-0.13208	-0.16529	-0.15822	-0.16146	-0.18095
5.075	-0.12611	-0.16256	-0.14892	-0.15725	-0.18358
5.329	-0.11454	-0.15536	-0.15411	-0.13869	-0.15405
5.583	-0.11972	-0.15307	-0.14947	-0.12899	-0.11416
5.837	-0.10379	-0.13568	-0.12585	-0.11142	-0.10687
6.091	-0.08982	-0.13071	-0.11840	-0.13203	-0.13336
6.344	-0.08436	-0.10248	-0.11787	-0.13995	-0.14303
6.598	-0.07353	-0.09890	-0.10275	-0.11800	-0.12473
6.852	-0.06045	-0.09180	-0.08894	-0.09997	-0.09642
7.106	-0.04200	-0.07291	-0.07833	-0.08194	-0.09034
7.359	-0.03540	-0.05040	-0.06073	-0.05930	-0.06645
7.613	-0.03300	-0.05100	-0.05688	-0.04739	-0.06000

P_{av}/d

$t\sqrt{g/d}$ \ H/d	0.24	0.28	0.32	0.36	0.40
0.203	0.03942	0.08080	0.12320	0.16711	0.20800
0.254	0.03862	0.06520	0.09362	0.10915	0.13877
0.305	0.03726	0.07154	0.08226	0.13419	0.15199
0.355	0.02988	0.06566	0.12551	0.14612	0.17862
0.406	0.03665	0.07965	0.13113	0.14952	0.18299
0.457	0.03317	0.07501	0.11466	0.13576	0.16131
0.508	0.04146	0.07996	0.10995	0.12655	0.15596
0.558	0.03678	0.07952	0.10307	0.16269	0.20365
0.609	0.02912	0.09871	0.08793	0.15874	0.19836
0.660	0.02836	0.10661	0.14186	0.16919	0.20975
0.711	0.03467	0.10677	0.14557	0.16535	0.19933
0.761	0.03355	0.08583	0.13528	0.14961	0.19041
0.812	0.03089	0.07082	0.11790	0.17640	0.22380
0.863	0.03234	0.08200	0.10366	0.17079	0.22109
0.914	0.02506	0.07774	0.13126	0.16629	0.21855
0.964	0.02281	0.09827	0.13342	0.16882	0.19933
1.015	0.03477	0.08635	0.13136	0.16110	0.22935
1.066	0.02624	0.07039	0.08161	0.17308	0.21618
1.167	0.01880	0.07756	0.12675	0.16531	0.20863
1.218	0.01560	0.07760	0.12379	0.15683	0.20208
1.269	0.01493	0.07672	0.11550	0.16237	0.18141
1.320	0.00891	0.05410	0.10691	0.16426	0.19933
1.370	0.00718	0.07825	0.12457	0.16049	0.21789
1.421	0.00962	0.07942	0.12686	0.14780	0.17050
1.472	0.00842	0.07887	0.12133	0.15287	0.20296
1.523	0.00561	0.06780	0.10476	0.15501	0.19520
1.573	-0.00036	0.05581	0.11882	0.14371	0.19261
1.624	0.01695	0.07979	0.12697	0.15501	0.21794
1.675	-0.00017	0.06686	0.11469	0.14928	0.19785
1.726	-0.00506	0.06454	0.11056	0.15628	0.18353
1.776	0.01313	0.06856	0.10948	0.14093	0.17053
1.827	0.00608	0.06469	0.10150	0.13428	0.15768
1.878	0.00577	0.05987	0.09502	0.12310	0.15033
1.929	0.00703	0.05603	0.08864	0.11766	0.17823
1.979	0.00223	0.04767	0.07150	0.12526	0.16385
2.030	-0.00638	0.03855	0.07254	0.12411	0.16507
2.132	-0.03147	0.02643	0.08875	0.11763	0.15334
2.233	-0.02051	0.03564	0.08418	0.11357	0.13535
2.335	-0.01730	0.03629	0.06660	0.09012	0.12121
2.436	-0.03761	0.02172	0.05178	0.09009	0.11040
2.538	-0.02131	0.01993	0.04133	0.06211	0.05597
2.639	-0.02187	0.01358	0.02609	0.01692	-0.00680
2.741	-0.04143	-0.02598	-0.00916	0.00314	0.01339
2.791	-0.03447	-0.04137	-0.01845	0.00329	0.01157
2.842	-0.03709	-0.01834	0.00160	0.02293	0.03450
2.944	-0.03385	-0.03763	0.00120	0.02173	0.01004
3.045	-0.04290	-0.05111	-0.04585	-0.02183	0.05571
3.147	-0.04918	-0.05811	-0.04648	-0.01410	0.04132
3.248	-0.04095	-0.04630	-0.02253	-0.05246	-0.09952
3.299	-0.04114	-0.04373	-0.03643	-0.04278	-0.05762
3.350	-0.04546	-0.04604	-0.05772	-0.05125	0.05680
3.451	-0.05469	-0.04913	-0.05918	-0.04115	0.10288
3.553	-0.04269	-0.03609	-0.03387	-0.03451	-0.06848
3.654	-0.04059	-0.03034	-0.03208	-0.05840	-0.07048
3.807	-0.04630	-0.05038	-0.04208	-0.03329	-0.03644
4.060	-0.04864	-0.05356	-0.05285	-0.04672	-0.02616
4.314	-0.05091	-0.05292	-0.04846	-0.04566	-0.03399
4.568	-0.04692	-0.11409	-0.04825	-0.04734	-0.05191
4.822	-0.04809	-0.05710	-0.05168	-0.05317	-0.05720
5.075	-0.04839	-0.05883	-0.05100	-0.05406	-0.06086
5.329	-0.04665	-0.05902	-0.05546	-0.04988	-0.05368
5.583	-0.05173	-0.06198	-0.05668	-0.04863	-0.04192
5.837	-0.04775	-0.05878	-0.05042	-0.04413	-0.04148
6.091	-0.04419	-0.06061	-0.05050	-0.05509	-0.05489
6.344	-0.04459	-0.05112	-0.05424	-0.06169	-0.06266
6.598	-0.04199	-0.05336	-0.05132	-0.05591	-0.05839
6.852	-0.03777	-0.05427	-0.04858	-0.05094	-0.04847
7.106	-0.02878	-0.04734	-0.04749	-0.04541	-0.04903
7.359	-0.02685	-0.03656	-0.04109	-0.03580	-0.03942
7.613	-0.02832	-0.04157	-0.04354	-0.03163	-0.03950

x_{cp}/d

$t\sqrt{g/d}$ \ H/d	0.24	0.28	0.32	0.36	0.40
0.203	0.11546	0.11000	0.13500	0.15035	0.15000
0.254	0.14720	0.12015	0.14074	0.14237	0.14425
0.305	0.16081	0.15412	0.14997	0.21217	0.19846
0.355	0.16422	0.15396	0.23841	0.24705	0.24262
0.406	0.23559	0.20791	0.27358	0.27653	0.27574
0.457	0.21474	0.24730	0.30616	0.30321	0.29392
0.508	0.31000	0.27226	0.30548	0.29745	0.29356
0.558	0.31489	0.29130	0.30861	0.42097	0.40939
0.609	0.31124	0.52166	0.30755	0.44902	0.45106
0.660	0.31175	0.55722	0.47670	0.48078	0.48776
0.711	0.42515	0.58598	0.51225	0.50097	0.49121
0.761	0.46726	0.56118	0.53435	0.50235	0.49551
0.812	0.47158	0.53855	0.52059	0.62505	0.62206
0.863	0.57943	0.67153	0.50165	0.65610	0.67234
0.914	0.52831	0.68207	0.66099	0.71042	0.71238
0.964	0.54191	0.81570	0.69359	0.73456	0.71752
1.015	0.73379	0.75720	0.72021	0.72466	0.82773
1.066	0.82453	0.75140	0.50498	0.83938	0.87310
1.167	0.91440	0.95640	0.89074	0.90640	0.92822
1.218	0.91414	1.02414	0.93906	0.89993	0.91650
1.269	1.03264	1.04638	0.92877	1.03268	1.17200
1.320	1.17790	0.81093	0.94125	1.08574	1.13941
1.370	1.38465	1.25369	1.14778	1.13650	1.18383
1.421	1.48995	1.31048	1.20871	1.15550	1.14283
1.472	1.63914	1.39310	1.25914	1.20881	1.31711
1.523	1.80660	1.33840	1.22160	1.33072	1.38244
1.573	-14.97093	1.35579	1.42972	1.38831	1.42319
1.624	1.50600	1.50029	1.48067	1.43261	1.53460
1.675	-21.79080	1.67607	1.53272	1.47318	1.53166
1.726	0.18702	1.74906	1.57948	1.53724	1.48793
1.776	3.09924	1.74653	1.60474	1.59241	1.53257
1.827	2.60471	1.72031	1.59920	1.55686	1.51814
1.878	2.70017	1.79194	1.62319	1.57561	1.51509
1.929	2.57125	1.77891	1.59892	1.51462	1.69610
1.979	6.60607	1.84368	1.57963	1.78455	1.78611
2.030	-1.76663	1.95361	1.62876	1.82724	1.81966
2.132	0.43611	2.20253	2.04393	1.95916	1.97236
2.233	0.47484	2.65754	2.22322	2.09727	1.91254
2.335	0.02445	2.97025	2.39090	2.19471	2.03287
2.436	0.81517	3.37289	2.32566	2.30226	2.14618
2.538	0.86783	3.41674	2.53623	2.50364	1.76270
2.639	0.16509	4.14009	2.35047	1.98449	1.54698
2.741	1.30690	1.25469	1.68203	0.49792	0.72529
2.791	1.36336	1.68247	1.62408	1.91816	2.39047
2.842	1.43490	0.20153	17.09433	2.65335	2.17787
2.944	1.44729	1.25883	31.63733	2.44840	3.96265
3.045	1.59054	1.57336	1.78433	1.21342	2.17720
3.147	1.93600	1.93558	1.38805	-0.36412	2.48192
3.248	1.82068	1.18936	1.03121	1.69206	1.89646
3.299	1.76997	1.42049	1.18529	1.57525	1.63004
3.350	1.81428	1.60776	1.69886	1.59443	3.77227
3.451	1.97006	1.88000	1.58054	1.36646	2.66245
3.553	1.89471	1.57504	1.31372	1.91212	1.71581
3.654	1.82046	1.82503	1.51860	1.63377	1.66796
3.807	2.03877	1.92293	1.71318	1.31394	0.80615
4.060	2.11923	2.05500	1.88755	1.57567	0.52494
4.314	2.23250	2.19069	2.12396	1.71058	0.91953
4.568	2.41583	1.63534	2.01007	2.00895	1.94905
4.822	2.47651	2.35410	2.17765	2.21585	2.09689
5.075	2.48823	2.45347	2.31170	2.29210	2.06338
5.329	2.55229	2.53379	2.43231	2.31499	2.17170
5.583	2.59493	2.62857	2.53959	2.42241	2.43217
5.837	2.71877	2.73122	2.62713	2.53964	2.49620
6.091	2.80045	2.66855	2.59507	2.73204	2.67313
6.344	2.89400	2.83418	2.69156	2.77553	2.75164
6.598	2.93821	2.90861	2.78949	2.84394	2.80104
6.852	3.03779	2.92548	2.88385	2.92816	2.93788
7.106	3.19500	3.02374	2.95394	2.94669	2.96797
7.359	3.19500	3.19500	3.06738	3.10217	3.11640
7.613	3.19500	3.19500	3.11093	3.17233	3.19500

APPENDIX C

DERIVATION OF UNDAMPED NATURAL FREQUENCY OF OSCILLATION OF 1/8-IN. TRANSDUCER IN OIL CHAMBER

For purposes of thermal insulation, the 1/8-in. transducer was recessed behind a cylindrical oil chamber 1/8 in. in diameter and 1/8 in. long, as shown in Figure 4.22b. The inner end of the chamber is formed by the circular stainless steel diaphragm of the original transducer, which in its unmodified state has a rated natural freqency f_{nd} of 60.0 kilocyc/sec. The outer end of the chamber is formed by a piece of polyethylene adhesive tape, whose mass and stiffness are neglected in this analysis. The chamber is filled with oil having a density ρ_f approximately equal to 1.55 slug/ft^3, or 7.5×10^{-5} lb-sec^2/in.^{4}

It is assumed that the system behaves as a single-degree-of-freedom harmonic oscillator, whose undamped natural frequency is:

$$f_n = \frac{1}{2\pi} \sqrt{\frac{k}{m}} \quad , \qquad \text{C1}$$

where in this case k is the stiffness of the damped circular diaphragm of the original transducer and m is the mass m_d of the diaphragm of the original transducer plus the mass m_c of the oil in the chamber.

The mass and stiffness of the diaphragm may be derived as follows: the stiffness k of a clamped circular diaphragm is related to the diaphragm dimensions by the equation:

$$k = \frac{192\,\pi E h^3}{a^2\ 12(1 - \nu^2)} \quad , \qquad \text{C2}$$

where E is Young's modulus, h is the diaphragm thickness (as yet unknown, in this case), a is the transducer radius, and ν is Poisson's ratio. (Equation C2 was derived from Timoshenko and Woinowsky-Krieger, 1959, pp. 5, 55.) The diaphragm mass is simply

$$m_d = \rho_d \pi a^2 h \quad , \tag{C3}$$

where ρ_d is the density of stainless steel.

Since the natural frequency of the original transducer f_{nd} is known, it is useful to apply Equation C1 to the diaphragm alone:

$$f_{nd} = \frac{1}{2\pi} \sqrt{\frac{k}{m_d}} \quad . \tag{C4}$$

Equations C2, C3, and C4 may be combined to obtain h:

$$h = \frac{\pi a^2}{2} f_{nd} \sqrt{\frac{\rho_d}{E} (1 - \nu^2)} \quad . \tag{C5}$$

The stiffness and mass of the diaphragm may now be obtained from Equations C2 and C3, respectively. For $E = 30 \times 10^6$ lb/in.^{2}, $\nu = 0.3$, $\rho_d = 0.735 \times 10^{-3}$ lb-sec^2/in.^{4}, and a = 1/16 in.,

$$h = 0.00174 \text{ in.},$$

$$k = 2228 \text{ lb/in.},$$

$$m_d = 1.57 \times 10^{-8} \text{ lb-sec}^2/\text{in.}$$

The mass of the oil is:

$$m_f = \rho_f \pi a^2 \ell \quad , \tag{C6}$$

where ρ_f is the density of the oil, and ℓ is the length of the chamber.

For $\rho_f = 7.5 \times 10^{-5}$ lb-sec^2/in.^{4}, and $\ell = 1/8$ in.:

$$m_f = 1.15 \times 10^{-7} \text{ lb-sec}^2/\text{in.}$$

By Equation C1, in which $m = m_d + m_f$:

$$f_n = 20.8 \text{ kilocyc/sec},$$

the computed value of natural frequency that appears in Table 4.1.